POLITECNICO DI MILANO
Facoltà di Ingegneria

Dipartimento di Ingegneria Idraulica, Ambientale,
Infrastrutture viarie, Rilevamento
Sezione Ambientale

Dottorato di Ricerca in

Ingegneria Sanitaria-Ambientale

XXIII Ciclo

CONTAMINANT VAPOUR EMISSIONS FROM POLLUTED SOIL AND GROUNDWATER

Tutor: Prof. Luca Bonomo

Relatore: Dott. ssa Sabrina Saponaro

Coordinatore del dottorato: Prof. Roberto Canziani

Tesi di Dottorato di:

Sara PURICELLI

Matr. 724095

2008-2010

ACKNOWLEDGMENTS

To my two families: my husband Davide and my parents Gianfri and Bruno with my sister Laura…
…for all their strength, understanding, patience, faith, support and true love in particular over these three Ph.D. years.

A sincere thank you to Sabrina and Elena, who guided my initial steps into Soil Remediation and taught me so much;
many thanks to David and Khaled, who assisted me during experimental activity at Newcastle University, and for their friendship that I hope will carry on;
all my thanks to Julia for her kind efforts in suggesting me proper English forms;
thanks to Claudia, Ivana, Alessandro, Agazio and again to Elena who supported me during my field activities;
a special thank you to Laura, Paul and Barney who introduced me to a deeper knowledge of chemical analytical processes.

"… and if the road we WANT to travel along is hard,
we will face it with the right CONVICTION…"

Sara

INDEX

INTRODUCTION AND AIM OF THE WORK *1*

1 SANITARY RISK ASSESSMENT *3*

1.1 Law aspects **3**

1.2 Risk analysis **4**

1.3 Exposure and vapour concentration in air **6**

2 BEHAVIOUR OF CHEMICAL COMPOUNDS IN THE ENVIRONMENT *9*

2.1 Volatile compounds **9**

2.2 Principles of volatile compounds behaviour **11**
- 2.2.1 Solubility 12
- 2.2.2 Vapour pressure 12
- 2.2.3 Henry’s law 13
- 2.2.4 Adsorption 14
- 2.2.5 Diffusion 16
- 2.2.6 Indications for common volatile pollutant compounds 16

3 VOLATILISATION OF VOLATILE COMPOUNDS *19*

3.1 General concepts **19**

3.2 Soil system **20**
- 3.2.1 Degree of saturation and soil pressure 20
- 3.2.2 Soil properties affecting volatilization 22
  - 3.2.2.1 Water content 22
  - 3.2.2.2 Gaseous permeability 23
  - 3.2.2.3 Bulk density 23
  - 3.2.2.4 Organic matter content 24
  - 3.2.2.5 Vegetative transport 24

3.3 Flux and transport volatilisation processes **24**
- 3.3.1 Flux equations 24
- 3.3.2 Transport equations 25

3.4 Models **32**
- 3.4.1 Numerical models 33
  - 3.4.1.1 Basic models 33
  - 3.4.1.2 Improved models 34
  - 3.4.1.3 Models also considering NAPL 37
- 3.4.2 Analytical models 39
  - 3.4.2.1 Only gas diffusion 40
  - 3.4.2.2 Gas advection, diffusion and biodegradability 40

4 VOLATILISATION FLUX DETERMINATION *47*

4.1 Techniques of measurements **47**
- 4.1.1 Aerodynamic methods 47
  - 4.1.1.1 Aerodynamic method 48
  - 4.1.1.2 Energy Balance method 48
  - 4.1.1.3 Eddy correlation method 49
  - 4.1.1.4 Integrated Horizontal Flux method 49
  - 4.1.1.5 Concentration-profile 50
  - 4.1.1.6 Transect technique 50

4.1.1.7 Theoretical profile shape method 50
4.1.2 Enclosure methods 51

4.2 Flux chamber 52
4.2.1 Operating conditions 53
4.2.1.1 Non- steady state systems 53
4.2.1.2 Steady state systems 54
4.2.2 Advective conditions 55
4.2.3 General common indications 55
4.2.4 Design considerations 58
4.2.4.1 Chamber geometry 58
4.2.4.2 Material 62
4.2.4.3 Structure 63
4.2.4.4 Positioning of the FC 64
4.2.4.5 Injection system 65
4.2.4.6 Mixing 68
4.2.4.7 Vent 69
4.2.4.8 Interference factors 71
4.2.4.8.1 Temperature 72
4.2.4.8.2 Pressure 73
4.2.4.8.3 Wind 75
4.2.4.8.4 Rain 75
4.2.5 Sampling 75
4.2.5.1 Direct-reading method 77
4.2.5.2 Whole air collection techniques 78
4.2.5.3 Tubes 79
4.2.6 Flux estimation 80
4.2.6.1 Non-steady state chambers 80
4.2.6.2 Steady state chambers 85

5 SETUP DEFINITION 87

5.1 Introduction 87

5.2 Materials and methods 87
5.2.1 Source and sampling system 87
5.2.2 Commercial FC with sweep air injection via a tube 90
5.2.2.1 Reaching stationary conditions 92
5.2.2.2 Mixing test 93
5.2.2.3 Purge duration 94
5.2.3 Commercial FC equipped with distribution ring 95
5.2.3.1 Tests with ring A 96
5.2.3.1.1 Blank 96
5.2.3.1.2 Reaching stationary conditions 96
5.2.3.1.3 Mixing test 97
5.2.3.2 Tests with ring B 99
5.2.3.2.1 Reaching stationary conditions 99
5.2.3.2.2 Mixing test 99
5.2.3.3 Rings A and B used simultaneously 100
5.2.3.3.1 Mixing test 100
5.2.3.4 Absorption test on Plexiglass 102
5.2.4 Modifications to the commercial FC: setup equipped with steel tube 102
5.2.4.1 Mixing test 105
5.2.5 FC final setup 105
5.2.5.1 Mixing test 106
5.2.5.2 Purge duration 108

5.3 Results 110
5.3.1 Ethanol source 110
5.3.2 Commercial FC with sweep air injection via a tube 110
  5.3.2.1 Reaching stationary conditions 110
  5.3.2.2 Mixing test 111
  5.3.2.3 Purge duration 112
5.3.3 Commercial FC equipped with distribution ring 114
  5.3.3.1 Tests with ring A 114
    5.3.3.1.1 Blank 114
    5.3.3.1.2 Reaching stationary conditions 114
    5.3.3.1.3 Mixing test 117
  5.3.3.2 Tests with ring B 123
    5.3.3.2.1 Reaching stationary conditions 123
    5.3.3.2.2 Mixing test 124
  5.3.3.3 Rings A and B used simultaneously 128
    5.3.3.3.1 Mixing test 128
  5.3.3.4 Adsorption tests on Plexiglass 131
5.3.4 Modifications to the commercial FC: setup equipped with steel tube 132
  5.3.4.1 Ambient air treatment by adsorption on activated carbon 132
  5.3.4.2 Mixing test 133
5.3.5 FC final setup 134
  5.3.5.1 Mixing test 134
  5.3.5.2 Purge duration 139

5.4 Conclusions 141

6 FIELD APPLICATION: CASE STUDY 143

6.1 Introduction 143

6.2 Materials and methods 144
6.2.1 The site general information 144
6.2.2 Site characterization: specific contaminated part of the site 144
  6.2.2.1 Local geology and hydrogeology 145
  6.2.2.2 Contamination 146
    6.2.2.2.1 Groundwater monitoring 147
    6.2.2.2.2 Soil gas monitoring 148
    6.2.2.2.3 Open air monitoring 156
6.2.3 Flux chamber monitoring 157
  6.2.3.1 Field equipment 158
  6.2.3.2 FC measurements 160
  6.2.3.3 Recording physical parameters 163
6.2.4 Fluxes from modelling 163
  6.2.4.1 Transport from groundwater 164
  6.2.4.2 Transport from soil gas 164
6.2.5 Fluxes from flux chamber measurements 164
6.2.6 Ambient air measurements from modelling 164
6.2.7 Risk calculation 165

6.3 Results 166
6.3.1 Flux chamber measurements 166
  6.3.1.1 Physical parameters recording 172
    6.3.1.1.1 Temperature 172
    6.3.1.1.2 Humidity 179
    6.3.1.1.3 Pressure difference 183
6.3.2 Fluxes from modelling 188
  6.3.2.1 Transport from groundwater 188

6.3.2.2 Transport from soil gas 189
6.3.3 Fluxes from flux chamber measurements 192
6.3.4 Comparison between modelled and calculated fluxes 194
6.3.5 Ambient air measurements from modelling 204
6.3.6 Risk calculation 207

6.4 Conclusions 207

7 A REMEDIATION TECHNIQUE: BIOCHAR-AMENDED SOIL 209

7.1 Introduction 209
7.1.1 Biochar 209

7.2 Materials and methods 214
7.2.1 Pollutant mixture 214
7.2.2 Material Characterization 218
7.2.2.1 Material Origin 218
7.2.2.2 Biochar petrography and screening carbon fingerprint 219
7.2.2.3 Grain size distribution 219
7.2.2.4 Soil porosity 220
7.2.2.5 Soil and biochar density 220
7.2.2.6 Moisture 220
7.2.2.7 Organic carbon content 220
7.2.2.8 pH 221
7.2.2.9 Nutrient content 221
7.2.2.10 Microbiological analysis 221
7.2.3 Chemical analysis 221
7.2.4 Laboratory batch microcosm experiments 223
7.2.4.1 Blank vials 224
7.2.4.2 Sorption tests 224
7.2.4.3 Biodegradation tests 225
7.2.5 Laboratory column experiments 228
7.2.5.1 Experimental apparatus 228
7.2.5.2 Filling up 229
7.2.5.3 VOC Source 231
7.2.5.4 Column monitoring 231
7.2.5.5 Modelling code 232

7.3 Results 235
7.3.1 Material Characterization 235
7.3.1.1 Biochar petrography and screening carbon fingerprint 235
7.3.1.2 Soil grain size distribution 236
7.3.1.3 Soil porosity 238
7.3.1.4 Soil and biochar density 238
7.3.1.5 Soil and amended soil moisture 239
7.3.1.6 Soil organic carbon content 239
7.3.1.7 Natural/amended soil and biochar pH 240
7.3.1.8 Nutrient content 240
7.3.2 Laboratory batch microcosm experiments 241
7.3.2.1 Blank vials 241
7.3.2.2 Sorption test 243
7.3.2.3 Biodegradation test 251
7.3.2.4 Conclusions 256
7.3.3 Laboratory column experiments 258
7.3.3.1 VOC Source 258
7.3.3.2 Tracer tests 260
7.3.3.3 Background conditions 264

7.3.3.4 Open boundary conditions 266
7.3.3.4.1 Biological parameters 266
7.3.3.4.2 VOC monitoring 268
7.3.3.5 Closed boundary conditions 279
7.3.3.5.1 Biological parameters 279
7.3.3.5.2 VOC monitoring 281
7.3.3.5.3 Matrix final conditions 293

7.4 Conclusions 294

CONCLUSIONS 295

BIBLIOGRAPHY 297

APPENDIX 1 MEASURING INSTRUMENTS 319

A1.1 Instruments used for experimentation at Politecnico di Milano and for FC field activity (§ 5 and § 6) 319
A1.1.1 Instruments for physical parameter determination 319
A1.1.1.1 Multifunction digital micro manometer DC 100^{PRO} (WÖHLER) 319
A1.1.1.2 Multifunction measuring instrument Testo – 435 Probe 320
A1.1.1.3 Temperature probe Checktemp-1 (Hanna Instruments) 320
A1.1.1.4 Digital thermo-igrometer (TFA) 320
A1.1.2 Instruments for air flow regulation 320
A1.1.2.1 SKC AirCheck XR 5000 Sample Pump 320
A1.1.2.2 Ego Plus TT (Zambelli) Sample Pump 320
A1.1.2.3 Thermal mass flow controller Model 80D-10 (McMillan Company) 321
A1.1.2.4 Mass flow controller (ALBORG) 321
A1.1.2.5 Rotameters 321

A1.2 Instruments used for experimentation at Newcastle University (§ 7) 322
A1.1.1 Instruments used for matrices characterization 322

APPENDIX 2 ANALYTICAL METHODS 323

A2.1 Gas chromatography 323

A2.2 Chemical analysis performed at DIIAR laboratory (Politecnico di Milano) 324
A2.2.1 GC configuration for Ethanol determination 324

A2.3 Chemical analysis performed at Civil and Geotechnical laboratory (Newcastle University) 326
A2.3.1 air VOC analyses 326
A2.3.2 CO_2, O_2 and SF_6 analyses 327
A2.3.2 Liquid VOCs analyses 327

APPENDIX 3 MEASURING UNCERTAINTY 329

APPENDIX 4 NUMERICAL CODE DESCRIBING VOC VAPOURS IN COLUMN TESTS 331

INTRODUCTION AND AIM OF THE WORK

The Soil Framework Directive, discussed by the European Council of Ministers and the European Parliament, and in Italy, the Legislative Decree 152/2006, affirm the centrality of Risk Assessment for long-term exposure of humans in order to identify contaminated sites and their remediation target limits (Chapter 1).

Exposure pathways often involve inhalation of Volatile Organic Compounds (VOCs) (Chapter 2). These compounds, which partition easily into air (Chapter 3), are major soil and groundwater contaminants at many polluted sites. To evaluate exposure to them, assessments or measurements of their concentration in air are necessary.

Traditional approaches involve application of transport modelling tools starting from concentrations in the secondary source or in soil gas, but their results are not very representative because they are based on non site-specific hypotheses and simplified conceptual models. Both analytical and numerical transport models are available in literature (Chapter 3). Another common approach is sampling ambient air, bypassing the modelling step, which however may be affected by background values, local sources, wind speed for outdoor measurements, and air conditioning/heating for indoor measurements. Finally, a more recent approach is the measuring of emission flow at ground surface, but it is still generally used only at experimental scale for VOC applications.

Consolidated micro-meteorological techniques are elective only for extensive sites and are often not valid at ground surface; enclosure devices, therefore, such as flux chambers (FC) or wind tunnels, seem to be the proper methods (Chapter 4). They measure the vapour flux emitted through the soil towards the atmosphere, isolating a volume of air layering over the surface without causing perturbations; this gives the input term for dispersion models to define vapour concentration in air required by Risk Analysis.

Flux measurements allow all the contributions from soil to be evaluated without needing prior deep knowledge of soil; however, they cannot be applied indoors where critical permeable zones (cracks, conducts, walls junctions/corners) are difficult to enclose within the covered structure. Therefore, FC application is still controversial and requests further studies in order to define proper device configuration and monitoring protocols. Available commercial FCs are often built without a detailed study on critical issues.

The experimental part of the work of this Ph.D. thesis started thanks to a research grant given by Politecnico di Milano and the Region of Lombardy ("Human Health Risk Assessment: site characterization, monitoring and modelling of subsurface contaminant vapour emissions from soil both outdoors and into enclosed spaces"). It entailed the project and the execution of tests to study a dynamic FC with the aim to obtain an ideal FC setup to monitor emissions of volatile compounds from contaminated soils. A number of tests were performed at DIIAR Laboratory of Politecnico di Milano, both on a commercial apparatus and a new arranged setup, to evaluate the FC technical characteristics and main operative parameters, such as mixing conditions, purge duration and inertness of material (Chapter 5). Furthermore, a system to treat environmental air as sweep gas, sampling line and proper analytical methods were defined.

This defined configuration was used to carry out FC measurements at a site located in the North of Italy potentially contaminated by petroleum hydrocarbons. Three seasonal campaigns were performed, and data of groundwater, soil gas, and ambient air monitoring were also provided thanks to collaboration with the regional environmental Agency. The field activity (Chapter 6) gave the opportunity to compare results from different approaches used to evaluate vapour inhalation pathway for Risk Assessment: air concentrations assessed from both FC measurements fluxes and modelled fluxes (by using concentrations in groundwater and soil gas), and air measurements.

Finally, a non-conventional remediation technique to treat soil contaminated with VOCs was assessed through laboratory tests performed at Civil and Environmental Laboratory of Newcastle University –UK- (Chapter 7). Biochar-amended soil was compared to natural soil (both by batch and column tests) to study the effects on vapour transport, in particular as far as biodegradation and adsorption were concerned. A numerical code was written in Matlab to describe vapour transport in the test-specific conditions and geometry and to interpret the experimental results.

1

SANITARY RISK ASSESSMENT

1.1 Law aspects

Soil contamination is a hazard which may be a source of risk if toxic substances reach receptors by various pathways (Ferguson et al., 1998). Risk assessment (RA) is a tool promising a rational and scientific basis for priority setting and decision-making. Technical standards for the application of human health environmental RA at contaminated sites have been available at US and EU level since early ’90s and were subsequently improved (D’Aprile et al., 2008).

Risk-based methodology to define cleanup levels or guidelines has officially entered in thirty-two states of the USA (Liptak et al., 1996), among which Alabama, Alaska, Arkansas, California, Florida, Indiana, Massachusetts, New Jersey have their own guidance. Other states use the federal guidance or other state guidance documents, such as Hawaii, Idaho and Washington, Wisconsin (ITRC, 2008).

In Europe, the policy to preserve soil quality is linked to a draft of the Soil Framework Directive, discussed by the European Council of Ministers and European Parliament in September 2006, without having reached a common agreement until now. This document, derived from the Sixth Community Environment Action Program and amending the previous Directive 2004/35/EC, aims to protect natural resources and promote a sustainable use of soil by establishing common actions.

Considering the principle according to which the polluter has to pay and following the indications for remedying environmental damages, this decision underlines the importance of following a coherent soil protection regime. The document restates the centrality of risk concept, also used to define a contaminated site as a place “where there is a confirmed presence, caused by man, of dangerous substances of such a level that Member states consider they pose a significant risk to human health or the environment” (Chapter III, Section one, Article 10). It admits that different RA methodologies are currently being applied in Member states, leading to their homogenization and to a further improvement of risk assessment based on eco-toxicological methodologies (CECOM, 2006).

The main criticisms of the draft Directive that have slowed down its issue are that it would impose strong administrative and cost burdens on both public authorities and businesses, and that it is unnecessary as it duplicates soil protection already provided under existing EU and national environmental legislation.

Section V "Reclamation of contaminated sites", Chapter Four of the Legislative Decree (L.D.) nr. 152 that substitutes the Ministerial Decree 471/99 on "Regulations containing criteria, procedures and modalities for the environmental security, reclamation and recovery of polluted sites" has been in force in Italy since 29 April 2006. The new normative uses the same definition as the European draft guide and indicates a polluted site if the concentrations of contaminants in different soil matrices give risk for a potential receptor on the site.

The technical procedure for the application of human health RA was issued by the National Environmental Agency and Technical Services (APAT) of Italy, in collaboration with many Italian scientific institutes (ISS, ISPESL and ICRAM) and with several Italian Regional Environmental Agencies (ARPA), on the basis of the ASTM (American Society for Testing and Materials) approach, and was summarized in the manual "Methodological criteria for the application of absolute risk analysis at contaminated sites" (APAT, 2008a).

1.2 Risk analysis

Risk analysis is preliminary based on health-based investigation levels (HILs) that are the first considerations in assessing the potential for health effects from sites contaminated through the use of exposure assessment models (Schmidt et al., 1998b). According to D.L. 152/2006 these threshold contamination concentrations are called CSC ("Concentrazione Soglia di Contaminazione").

The highly influential report on the definition of RA structure was processed by the US National Research Council (NRC) describing four distinct stages in the procedure (NRC, 1983). Official risk-based guides, which are most followed today, were developed by the ASTM; they are called Guides for Risk-Based Corrective Action (RBCA) at Petroleum Release Sites, composed of a three-tiered approach (see Fig. 1.1), aiming to incorporate RA into the corrective action process (ASTM 1739, ASTM PS-104, ASTM, 2004).

The first stage is hazard identification, that is the definition of the preliminary site conceptual model (SCM), and consists in a deep characterization of the source, by acquiring historical information, and by performing investigation (to define geology, hydrogeology and meteorological data), sampling, chemical analysis and quality control. It involves the selection of the contaminant agents that may cause adverse effects, based on their physical-chemical properties, and the definition of the source geometry (that may be in surface soil, deep soil and/or groundwater) giving, at last, the connection between source-pathway-receptor elements.

The second step is the definition of dose-response relationships to estimate the link between exposures (or doses) and adverse effects, using laboratory experiments or epidemiological studies. In Italy these values are reported in ISS/ISPESL [1] Italian Institutes database (DB) (ISS/ISPESL, 2010).

The third step is the exposure analysis that is “the process of estimating or measuring the magnitude, frequency, and duration of exposure to an agent, along with the number and characteristics of the population exposed” (IPCS, 2004), depending on context and site specific features (including several physical parameters). The pollutants originally present in the contamination source may reach potential receptors through different migration pathways, based on the transport and fate of contaminants in surface soil, vadose and saturated zone, indoor and outdoor air and surface water.

The final step is the risk characterization: the description of the distribution of risk in exposed population derived from the previous steps (NRC, 1983; ITRC, 2008) considering all the contaminants and ways of exposure, as dermal contact, accidental ingestion, dust inhalation in outdoor or indoor space, and vapour outdoor or indoor inhalation.

For a long time volatilisation has received comparatively little attention in scientific literature, probably due to the general belief that it was not a significant transport process relative to other processes (Tillman et al., 2004), but now it is recognized that, apart from direct ingestion of contaminated groundwater, inhalation is often the dominant exposure and the most sensitive pathway for human intake of volatile contaminants arising from underground sources and capable of entering dwellings (Lowell et al., 2004, Turczynowicz et al., 2007).

Vapour intrusion is a controversial current topic and a problem of rising public concern (Pasteris et al., 2002). This theme has direct health, social and therefore political implications. Until the early 1990s, the most discussed themes concerned radon and methane; more recently the attention has been posed on volatile organic compounds (VOCs), semi-volatile organic compounds (SVOCs), and in some cases metals (e.g., mercury) (Pennel et al., 2009).

Fig. 1.1 is a sketch of the tier-level approach proposed by the ASTM, which is a useful instrument to guide remediation strategies and the basis of decision supporting systems to define priority sites. In details, Fig. 1.1 gives indication about RA procedure followed for inhalation risk specific case. It underlines the dependence of risk on the specific use (residential/recreational or industrial) of the site; if this prevents receptor exposure (in Italy if concentrations are lower than CSCs), no further investigation is needed, otherwise a tier-1 screening assessment has to be conducted. This step starts with obtaining knowledge of chemicals present at the site, in order to determine whether they are sufficiently volatile and toxic to pose a potential threat. A generic screening prediction of air concentration with conservative default algorithm assumptions is then performed by using values of secondary source concentrations (Lowell et al., 2004; Tillman et al., 2005).

---

[1] ISS is the Italian Institute for Public Health and Hygiene; ISPESL is the Italian Institute for prevention and safety on working places

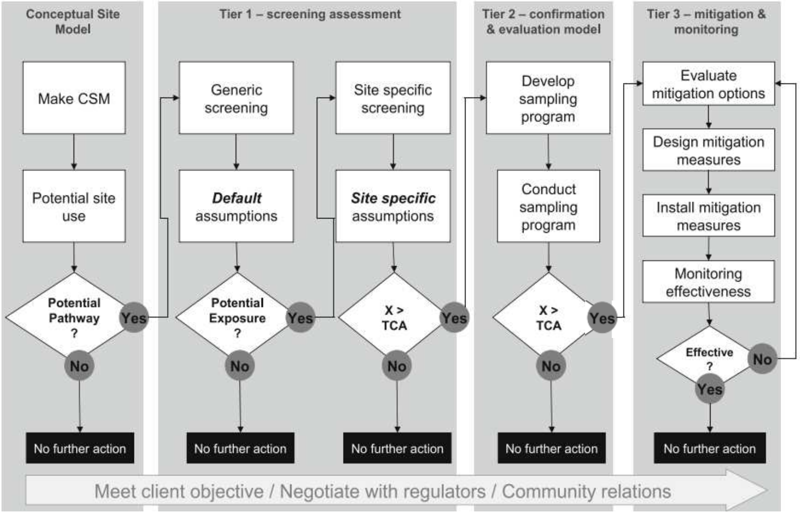

***Fig. 1.1**: general sketch to manage Risk-Site Assessment focused on inhalation risk; CSM: conceptual site model, TCA: tolerable concentration in the air (Provoost et al., 2009b).*

The following step, tier 2 assessment, aims to confirm the exceeding of tolerable concentration in air. Due to the uncertainty associated with models for volatilisation pathway, direct field sampling is often required to validate model predictions (Hers et al., 2001). Sampling may be carried out in the soil air and/or directly collecting air at ground level to detect the concentrations at exposure point. Sampling should take into account spatial and temporal variation. A further step, tier 3, includes mitigations and monitoring activities that prevent exposure to contaminants of concern or involves numerical site-specific model simulations (Provoost et al., 2009a, Provoost et al., 2009b).

1.3 Exposure and vapour concentration in air

The impact of vapour inhalation is directly proportional to the pollutant concentration in the air inhaled indoors (C_{in}) or outdoors (C_{out}); this evaluation is performable through four different approaches (as indicated in Fig. 1.2), requiring different monitoring techniques and often also the application of specific models based on chemical analyses of soil/ groundwater and of parameters due to the local conditions (Roffman et al., 1995; Rinklebe et al., 2010). Nowadays the use of only models for site-screening purposes is diminishing because the poor correlation between measured and model predicted concentrations has been seen, especially for chlorinated hydrocarbon sites, which is why Environmental Agencies more often request site specific measurements (Lahvis, 2010).

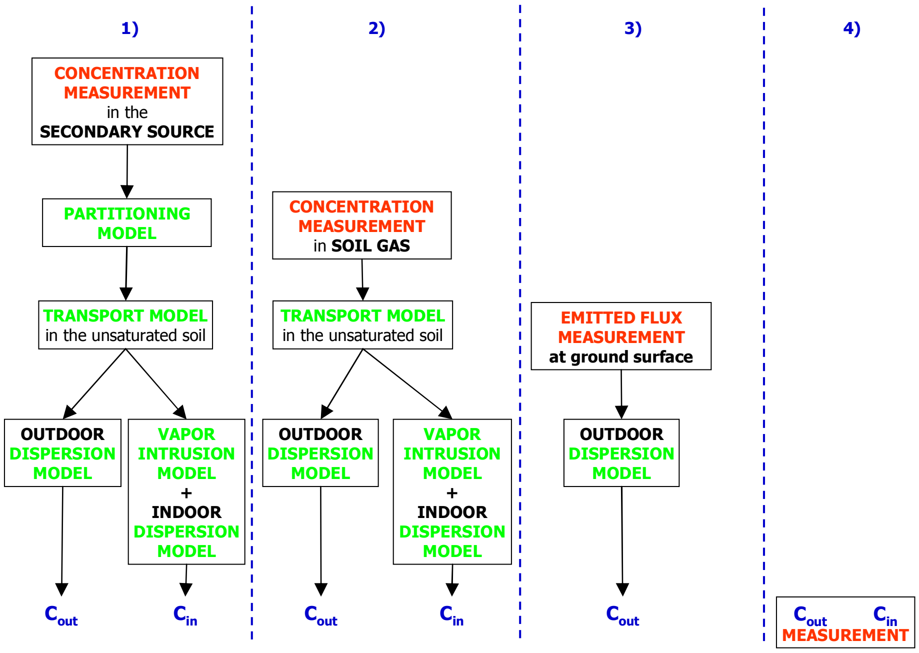

***Fig. 1.2**: different approaches applied to estimate pollutant air concentration for risk assessment (Puricelli et al., 2010).*

The first approach is based on the pollutant concentration measurement in the secondary source (vadose or saturated zone) and then requires the application of analytical repartition laws between different phases of soil matrix, transport in the unsaturated soil, up to the ground surface or building foundations. Then, the flux (the amount of pollutant emitted per unit area and unit time) is mixed with the ambient air (outdoors or indoors), and dispersion models are applied to calculate C_{in} or C_{out} (Schmidt et al., 1998b). Soil, building cracks and ambient air are usually described by simplifying assumptions and approximations, resulting in not very representative models (ASTM, 1998). Values for many input parameters are, in fact, not measured at the site, so that site-specific values are replaced by default values from literature, resulting in conservative estimates (regarding up to 74-160 times the direct measured fluxes (Schmidt et al., 1998b)). Critical conditions, greatly affecting vapour transport are: the thickness of the capillary fringe, the real moisture content in soil throughout most of the vadose zone, the presence of preferential path and lateral diffusion of vapours in the subsurface (Schmidt et al., 1998b; Fisher et al., 1996). Another problem is the definition of the biodegradation parameter that often is not included in RA guidelines following precautionary principles.

The second approach implies the direct measurement of soil potential contaminant as vapour in the soil gas, cutting the first step of repartition modelling. This measurement is not affected by the uncertainties due to the partitioning model, but it is strongly affected by the choice of proper soil profile features (Schmidt et al., 1998a; Schmidt et al., 1998b; Hutchinson et al., 2002) and environmental factors such as soil moisture, temperature, and atmospheric pressure (DTSC, 2004; MDNR, 2005).

The third approach implies direct measurements of vapour flux evaporated from the ground surface, and requires only dispersion models (Lonati, 2010) to obtain the concentration at the receptor point (Schmidt et al., 1998a), such as box model for outdoor air taken from the American Society of Testing and Materials (ASTM, 2002). In this way fewer uncertainties are involved in parameter definition and fluxes from all sources underlying the surface are considered, such as soil and groundwater; furthermore it does not require any hypothesis on the depth from which flux occurs (Carlsen et al., 2010). As a result, direct soil flux measurements more realistically represent true VOC flux but as far as indoor measurements are concerned, some problems arise in locating pavement cracks (USEPA, 1986; DTSC, 2004).

The last option, finally, is the direct sampling of the ambient air, bypassing completely the modelling tools. In this case, results may be affected by background values, local sources not ascribable to the secondary sources below ground surface, wind speed and presence or absence of small currents of air for outdoor measurements, and air conditioning/heating for indoor measurements (Schmidt et al., 1998b; Hers et al., 2001; Davidson et al., 2002; Hers et al., 2003; McHugh et al., 2004).

2

BEHAVIOUR OF CHEMICAL COMPOUNDS IN THE ENVIRONMENT

2.1 Volatile compounds

Contaminants of concern in vapour transport are typically VOCs and SVOCs respectively, although vapours emanating from inorganic sources such as mercury vapour may be involved as well.

There are different definitions of VOC in literature. It is defined as an organic compound having a vapour pressure (§ 2.2.2) greater than 0.1 Torr (0.013 kPa) at 25°C (298 K) and 760 mm Hg (101.3 kPa) (USEPA, 1999), or on the basis of its Henry constant (§ 2.2.3), that has to be higher than 10^{-5} atm m^3 mol^{-1} with a molecular weight lower than 200 g mol^{-1} (OEHHA, 2004; Tillman et al., 2005; NPI, 2006). For Italian law, eventually, it is an organic compound with pressure higher or equal to 0.01 kPa at a temperature of 293.15 K (Art. 268, Chapter One, Section V of L.D. 152/2006).

VOCs represent all the compounds tending to easily evaporate at environmental conditions. Examples of VOCs, related to impacted environmental systems, include chlorinated solvents such as carbon tetrachloride, tetrachloroethylene, and trichloroethylene (TCE), and their degradation compounds, solvents, fuel aromatic hydrocarbons such as benzene, toluene, ethylbenzene and orto (o), meta (m), para (p)-xylenes (called altogether BTEXs), alcohols (as ethanol, propanol, butanol), esters, ketons and aldehydes, as well as volatile pesticides such as chlordane, aldrin and lindane.

The U.S. Environmental Protection Agency has drawn up a list of 107 compounds whose toxicity and volatility produce a potentially unacceptable inhalation risk to receptors (USEPA, 2004). In fact there is evidence that volatilization towards atmosphere is one of the major loss processes by which VOCs may reach receptors at soil surface (Gao et al., 1997).

Inorganic compounds, are also involved into soil-atmosphere interchanges, such as carbon dioxide (CO_2), nitrous oxide (N_2O) and some metals (Hg), and also sulfur dioxide, hydrogen sulfide, fluorine, chlorine, bromine, and iodine (McCarthy, 1972).

In particular CO_2 is due to metabolic activity of soil microbes and plant root zone and plays a relevant role into terrestrial carbon cycle (Lund et al., 1999).

N_2O is given by the nitrogen fertilization in landfarming that evaporates increasing greenhouse effect and reducing stratospheric ozone layer (Matthias et al., 1980).

Mercury is present in different oxidation forms that change over time due to anthropic processes or geological transformations. The dominant form of mercury in the atmosphere (~ 98%) (Poissant et al., 1998) is gaseous elemental mercury (Hg^0) (Lindberg et al., 1995; Lindberg et al., 1999), having relatively high vapour pressure at environmental temperature (0.26 Pa) and high adimensional Henry constant value ($4.67\ 10^{-1}$) (ISS/ISPESL, 2010). These features explain the tendency of Hg^0 to migrate from water or soil to air phase, becoming a serious problem for human health because of its strong toxicity (Roffman et al., 1995).

Anthropogenic substances may enter the soil due to accidental chemical spills, chemical waste burials, leaking storage tanks (in particular leaking underground storage tanks –LUSTs-) or improper surface applications, generally as a separate phase. During their movement into unsaturated soil, a fraction of their mass is trapped in porosity due to capillary forces, obtaining a residual saturation of about 2-20 % v/v of the vacuum space (Falta et al., 1989, Jury et al., 1990, Karapanagioti et al., 2003). Some of these contaminated locations may contain considerable chemical mass, which may potentially volatilize for years.

The behaviour of a volatile compound in the unsaturated zone depends on its physical and chemical properties and on the characteristics of the matrix. In particular, its fate is due to its degree of evaporation and transport in the aqueous phase, and to possible chemical or biological reactions, which determines its presence in the soil as a separate phase, as adsorbed material to the organic matter, as dissolve phase into water inside porosities of soil or as gas phase in equilibrium with all the previous phases. The transported vapours and this aqueous phase may also reach the saturated zone where they dissolve into groundwater (Provoost et al., 2009b).

Knowing gas-phase transport processes and/or monitoring soil gases fluxes are main points to detect contaminant plumes and quantify potential risks of exposure pathways due to vapours flowing toward soil surface and groundwater (USEPA, 1986; Nazaroff et al., 1987; Batterman et al., 1995; Choi et al., 2002; Pennel et al., 2009). At landfill and land treatment sites, they are detected to define the path of a toxic constituent in soil gas towards its release to the atmosphere and to estimate basic parameters necessary in biodegradation processes (like CO_2 or O_2), or for polluted sites to monitor remediation techniques to remove VOCs, such as natural remediation or extraction/ venting strategies. Generally, in fact, VOCs constitute health hazards and at certain petroleum hydrocarbon sites, they may give cases of fires and explosions, and noxious odours (Moseley et al., 1992; Little et al., 1992; Turner et al., 2005).

In conclusion, due to both public health concerns and potential financial liability, a better understanding of how vapours migrate from source is required today supported by systematic scientific investigation, in order to remove uncertainty from the policy debate (Ririe et al., 2002). Knowing precisely both the properties of these compounds and description of soil aspects, at the basis of vapour transport, becomes therefore necessary.

2.2 Principles of volatile compounds behaviour

A contaminant may be present in the soil in three different phases (see Fig. 2.1):

- as solute dissolved in liquid phase present as interstitial water (w)
- as adsorbed layer attached to solid phase (s)
- as gas phase (g) in free pores.

In particular conditions some compounds may be present as non aqueous phase liquid form, called generally as NAPL.

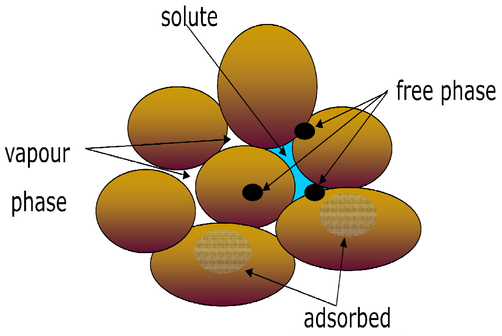

Fig. 2.1: *sketch of the four possible forms in which a chemical compound is present in soil (Sbaffoni, 2007).*

The behaviour of a compound in the environment is primarily controlled by its chemical and physical properties governing its partitioning between different phases present in the soil (water, solid and air) and in general its flow and transport. Fig. 2.2 is a sketch with the relationships between different soil phases and the properties linking them, as described in the following paragraphs.

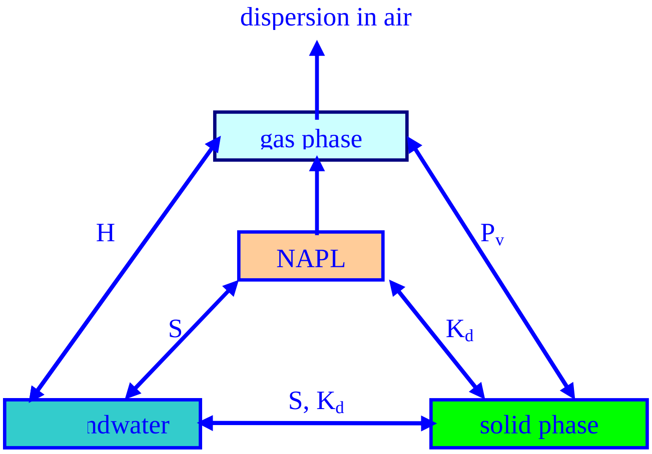

Fig. 2.2: *relationships between environmental compartments in which contaminants are spread and symbols of physical laws describing them (Sbaffoni, 2007, modified).*

All the above described properties depend on temperature; they are generally indicated for room temperature and some thermodynamic relations, containing empirical variables, are used to calculate their values for soil temperature, (Karapanagioti et al., 2003).

2.2.1 Solubility

Solubility (S_i, for the compound i) is the maximum quantity of a compound, called solute, that may dissolve in a certain quantity of solvent (for environmental scopes it is almost always water) giving a homogeneous solution; it therefore represents the specific compound concentration when it reaches dynamic equilibrium in liquid phase. It depends on the nature of the solute, temperature (an increase in the temperature of the solution increases generally the solubility of a solid/liquid solute), pressure (especially for gaseous solute) and the rate of mixing between different components (Schwarzenbach et al., 1993). The presence of a mass of a liquid compound higher than the maximum soluble in water determines the presence of a NAPL phase.

2.2.2 Vapour pressure

Volatilization is the transfer process of a compound from liquid to gas phase. Vapour pressure or partial pressure is the measure of the pressure of a vapour in thermodynamic equilibrium with its pure liquid phase in a closed system ($P^0_{v,i}$). The maximum reachable value is the saturation vapour pressure ($P^0_{v,\ sat,i}$) that is an indication of the tendency of a liquid to evaporate, thus the higher the value is and the more volatile the substance is. This property is effective for NAPL phase, it is strongly dependent on temperature according to the non-linear Clausius-Clapeyron relation and it represents the maximum gas phase concentration at a given temperature (Schwarzenbach et al., 1993).

Pollutants are commonly not present as pure compounds but as mixtures of different compounds and this has an effect on the availability of previous properties because of reciprocal competition, especially as for adsorption (Yaron et al., 1996). Partial vapour pressure of each component i ($P_{v,sat,i}$) is, in this case, described by Raoult's law. $P_{v,sat,i}$ in a mixture is proportional to saturated vapour pressure of pure component at that temperature according to its mole fraction in the mixture (X_i), expressed by:

$$P_{v,sat,i} = X_i * P^0_{v,sat,i} \tag{2.1}$$

where

$$X_i = \frac{n_i}{\sum_{j=1}^{N_c} n_j} \tag{2.2}$$

n_i being the mole number and N_c the number of the compounds in the solution.

Fig. 2.3.a presents ranges of value of $P^0_{v,\ sat,i}$ for various classes of organic compounds (according to classification at § 2.2.6).

2.2.3 Henry's law

Henry's law describes the relationship between the vapour pressure of a gas above its aqueous solution and the concentration in solution. It is valid under typical field moisture conditions and for dilute concentrations (i.e. mole fraction less than 0.001) (Evans et al., 2002).

The air to water partitioning, of the generic compound i, is generally expressed by the constant H_i indicated as $[(M_i\,L^{-3}{}_{gas})\,(M_i\,L^{-3}{}_{water})^{-1}]$ and expressed by the relationship:

$$C_{ig} = H_i * C_{iw} \tag{2.3}$$

where C_{ig} and C_{iw} are respectively the concentrations of i as gas phase $[M_i/L^3{}_{gas}]$ and liquid phase $[M_i\,L^{-3}{}_{water}]$

In other cases the same expression is written as:

$$C_{iw} = H`_i * C_{ig} \tag{2.4}$$

where $H`_i$ is H_i^{-1} $[\,(M_i\,L^{-3}{}_{water})\,(M_i\,L^{-3}{}_{gas})^{-1}]$.

Concentration into the gas phase is sometimes expressed as a pressure considering perfect gas law and therefore H may be expressed as $[P_{gas}\,(M_i\,L^{-3}{}_{water})^{-1}]$.

Henry's law constants may be generally estimated from the ratio of contaminant vapour pressure to its aqueous solubility or, experimentally, by measuring the vapour pressure and/or solubility for a system in equilibrium.

This relationship is also available between saturated vapour density and the compound solubility, and therefore for a wide range of concentrations (Jury et al., 1983).

There are only a few peer-reviewed papers comparing predicted values reached from Henry's law and measured gas concentrations, but it has been suggested that there is a poor correlation between them; this is due to both difficulties in proper gas investigation inside soils and the unlikelihood that soil, water and gas phases reach equilibrium between them in interconnected pores (Fischer et al., 1996; Roggemans et al., 2001). It has been quantified that this approach gives estimations of gas concentrations ten times higher than directly measurable values (Jeffries et al., 2008).

Fig. 2.3.b presents ranges of value of H for various classes of organic compounds (according to classification at § 2.2.6).

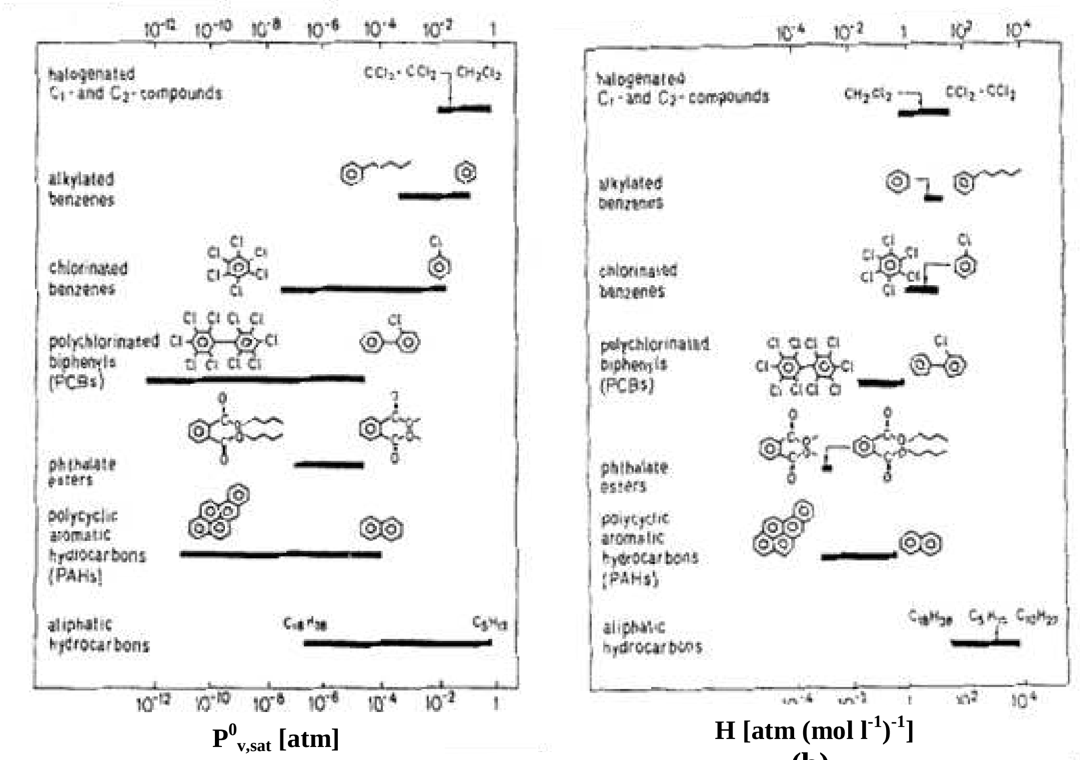

(a) **(b)**

Fig. 2.3: *range of values of saturated vapour pressure (a) and dimensional Henry's constant (b) and for different families of organic compound (Schwarzenbach et al., 1993).*

2.2.4 Adsorption

Soil grains are assumed always to be covered with a continuous film of water and therefore only partitioning between water and solid phase is assumed, without admitting direct transformation between gas and solid ones (Mendoza et al., 1990). Partitioning depends on chemical features, temperature and soil properties (such as mineralogical composition, texture, pH, organic material content, moisture). Adsorption of neutral, non-polar molecules (like most VOCs) onto soil surfaces is influenced by soil moisture: at low moisture content VOCs are highly adsorbed to soil whereas, when soil moisture content increases, VOCs are displaced from their adsorption sites due to competition with polar water molecules on the polar mineral surface (Poe et al., 1988).

The relationship between solid properties and isotherm shape is given by the mass of chemical i adsorbed per unit mass of soil, C_{is} $[M_i\,M^{-1}_{soil}]$, and C_{iw}.

Various theories describing adsorption have been found in literature, but it is still not perfectly understood (Farrel et al. 1994). The most complete ones imply nonlinear desorption processes and also take into account slow desorption kinetics, and/or mass transfer limitations, thus fitting laboratory and field data better. One of them is BET equation (Brauner, Emmett and Teller`s theory), that is a function dependent on: number of adsorbed layers existing on the surface, heat of adsorption and liquefaction of vapour, pressure, saturation pressure and as well as a monolayer adsorption capacity (Poe et al., 1988). For a single layer it may be reduced to a modified Langmuir isotherm. The latter is based on the concept of constant adsorption energy, characterized by a “b” coefficient, and a maximum sorption capacity, $C_{is,0}$, following the expression:

$$C_{is} = (C_{is,0} * b * C_{iw}) / (1 + b * C_{iw}) \tag{2.5}$$

It presents linear adsorption at low surface coverage, but becomes nonlinear as adsorption sites approach saturation.

Another famous model, that of Freundlich, is based on the theory of adsorption energies resulting from surface heterogeneities: adsorption preferentially occurs in the highest energy sites, and as surface coverage is increased, lower energy sites become successively occupied. This law is expressed by a nonlinear isotherm:

$$C_{is} = K_F * C_{iw}^{1/n} \tag{2.6}$$

where K_F is related to the sorption capacity and n to energy distribution of the adsorption sites.

These models seem particularly suitable for soils with low organic content (Farrel et al., 1994). In general, however, local equilibrium conditions are expressed as linear adsorption isotherms (Waitz et al., 1996), based on a linear sorption model between dissolved and solid phases, that may be derived from (2.6) by posing n=1:

$$C_{is} = K_{d,i} * C_{iw} \tag{2.7}$$

$K_{d,i}$ is the distribution coefficient given by partitioning into any natural organic matter $[(M_i\, M^{-1}_{soil})\, (M_i\, L^{-3}_{water})^{-1}]$ which does not take in consideration the adsorption onto mineral surfaces. However, it seems insignificant since non-polar compounds correlate mostly with natural organic matter. Another linear expression found in literature is (Jury et al., 1980):

$$C_{is} = \alpha * C_{iw} + \beta \tag{2.8}$$

where α and β are two empirical constants.

The relationship between K_d and the organic content (oc) of the soil, f_{oc} (§ 3.2.2.4), defines the organic matter partitioning coefficient K_{oc} $[L^3_{water}\, M^{-1}_{oc}]$,

$$K_{oc} = K_d * f_{oc}^{-1} \tag{2.9}$$

It expresses the tendency of a compound to be kept by solid matrix as an inner molecular property, and may be derived by the octanol-water partition coefficient K_{ow}. Tab. 2.1 indicates ranges of values of K_{oc} for different behaviours of mobility of chemicals in soil.

Tab. 2.1*: mobility into soil of chemicals as a function of organic matter partitioning coefficient* K_{oc} *(Teggi, 2008).*

Mobility in soil	K_{oc} [l kg^{-1}]
very high	0-50
high	50-150
middle	150-500
low	500-2,000
very low	2,000-5,000
immobile	> 5,000

On the contrary, sorption from gas phase to the solid phase is important only at very low moisture contents and for compounds with low solubility (Karapanagioti et al., 2003).

2.2.5 Diffusion

Molecular diffusion is the spreading out of compounds from random collisions resulting from thermal motion of atoms. These collisions may occur between the molecules themselves or between molecules and their surroundings. It is a slow process, dependent on chemical gradient, temperature and viscosity of transport medium (Jeffries et al., 2008).

It is described by diffusion coefficient (D) which is a factor of proportionality representing the amount of substance diffusing across a unit area through a unit concentration gradient in unit time, assuming compound- and medium-specific values.

Diffusion transport mechanism is particularly important for volatile compounds, considering that D for the gas phase (D_i^g) is in the order of 10^{-2} - 10^{-1} ($cm^2\ s^{-1}$) compared to diffusivity in the aqueous phase one (D_i^w) that is in the order of 10^{-6}-10^{-4} ($cm^2\ s^{-1}$) (Karapanagioti et al., 2003). This is due to the strengths that keep liquid molecules closer to each other, limiting movement among them.

D_i^β depends only on temperature and viscosity of the fluid β, and is typically measured at 25°C. Increased temperature T (in K) produces an increased free-air diffusion coefficient, leading to a greater rate of diffusion relative to the same system at lower temperature, which may be calculated by (Bird et al., 1960):

$$D_i^\beta = D_{i,25°C}^\beta * (T/298)^{1.5} \qquad (2.10)$$

For most petroleum compounds D^g ranges from 0.05 to 0.1 $cm^2\ s^{-1}$ (Johnson et al., 1998).

2.2.6 Indications for common volatile pollutant compounds

As a general prompt, aliphatic hydrocarbons depend on the carbon chain length that determines their molecular weight: the higher it is, the less volatile and soluble they are, while they become more absorbable. They are subdivided into three different classes by Massachusetts Department of Environmental Protection (MADEP): from 5 to 8 atoms of carbon (group C5-C8) they present poor leaching and strong volatilization behaviour; group C9-C18 is both poor soluble and volatile and heavier ones (C19-C36) are stable and motionless (MADEP, 2002).

As for BTEX they present high solubility, volatility and biodegradation, whereas polycyclic aromatic hydrocarbons (PAHs), especially among group C11-C22, have low volatility, solubility and tend to stay more adsorbed to solid phase by adsorption. Heters are generally very volatile and soluble in water and methyl-tert butyl heter (MTBE) is the best known, whereas phenols are well soluble in water, biodegradable, and may be dissociated.

As for aliphatic and aromatic chloride compounds, their behaviour depends on the number of Cl atoms they contain, and as a thumb rule, the higher the chlorination is, the lower their volatility, solubility and aerobic biodegradation are, whereas adsorption and anaerobic biodegradation increase (as happens for PCBs) (Bonomo, 2005).

Behaviour of inorganic compounds depends on their chemical form, influencing their environmental mobility. The most widespread and troublesome one, mercury, in particular, may be present both as an organic form (dimethylmercury) and as an inorganic one, giving mercuric sulfide (HgS), very stable, or/and the volatile elemental Hg^0.

The DB of reference in Italy containing physical and chemical properties, is that of ISS/ISPESL (ISS/ISPESL, 2010). Properties of substances that are not included in the document are available in a summarizing document prepared by Politecnico di Milano and ARPA (Politecnico di Milano et al., 2010).

3

VOLATILISATION OF VOLATILE COMPOUNDS

3.1 General concepts

Emissions of contaminated vapours at ground level are not determined by mixed planetary boundary layer due to pressure and air density-driven advection (Livington et al., 1995); they are influenced by several factors: vapour source type (e.g., soil or groundwater), its concentration, depth and position (and in the case of indoor intrusion its proximity to the building) (Batterman et al., 1995); chemical behaviour of the contaminant and in particular its biodegradability; many site properties like physical characteristics of the soil (the most important of which are air permeability, moisture and porosity) (Hers at al., 2003; Koblizková et al., 2009; Provoost et al, 2009a), its homogeneity and isotropy; groundwater level (Kliest et al., 1989), fluctuations in the water table -called “pumping effect”- (Kreamer et al., 1988); distribution and concentration of oxygen in the soil (Roggemans et al., 2001); environmental parameters, such as atmospheric pressure fluctuations (Thortestenson et al., 1989; Massmann et al., 1992; Chen et al., 1995; Lindberg et al., 1995; Choi et al., 2002; Tillman et al., 2001), that may also cause horizontal transport in heterogeneous systems (Massmann et al., 1992); meteorological conditions (Roffman et al., 1995), such as temperature, speed of wind causing surface wind turbulence, with high-frequency pressure fluctuations (Livingston et al., 1995) and finally precipitation (Koblizková et al., 2009; USEPA, 1986; Jeffries et al., 2008).

For indoor intrusion[2] also building construction and foundation characteristics are meaningful, such as the building air exchange rate, indoor-outdoor temperature difference (causing stack effect) and the presence of heating, ventilation, and air-conditioning –HVAC- systems (Jury et al., 1980; Hers et al., 2001; Abreu et al., 2005; Tillman et al., 2005). Different building construction techniques may have different impacts and behave in different way: semi-pervious concrete (e.g., basement, slab-on-grade), foundation with crawl-space ventilation, foundation bedding layer, foundation cracks and openings). They may actually influence vapour

---

[2] “Vapour intrusion” is the gas migration of the volatile compounds from the subsurface into overlying buildings (ITRC, 2007).

intrusion: buildings with basements generally have more surface area through which vapours may move inside and they stay closer to subsurface sources than slab-on-grade ones (Hers et al., 2001; Provoost et al., 2009b).

Mathematical description of vapour movement inside soil requires a flux and a transport model. This may be quite complicated because transport phenomena must be coupled with phase change and reaction processes. Both liquid phases inside soil are involved: gas and water ones which are expressed by multiphase theory. According to it air and water are assumed to flow as a continuum in soil and relative permeability of each soil phase depends on its degree of saturation in soil (EOLBNL, 1999).

Flux model governs vapour-phase pressure distribution into the soil and thus provides soil gas velocity field. This equation is coupled with a chemical transport equation describing different chemical-physical phenomena as diffusion and/or advection, and/or biodegradation.

Solution of the systems joining them, gives three-dimensional pressure field, soil gas velocity, and chemical concentration fields. This information is used to derive the soil gas flow rate at ground surface, or into/out of the building in case of indoor vapour intrusion and, from a transport point of view, the emission rate of chemicals (Abreu et al., 2005).

Dissertations on modelling determination of C_{in} and C_{out} (§ 1.3) of chemical pollutants are often treated separately in literature. For both cases however volatilisation is originated by the same phenomena and their transport from subsoil to the surface follows the same processes; difference consists in transport from the surface to receptor’s position (Jeffries et al., 2008).

The following paragraphs present the most important factors influencing volatilisation from soil: soil features, position of the source and environmental variables (Steinberg et al., 1993).

3.2 Soil system

3.2.1 Degree of saturation and soil pressure

A soil system is composed of three phases β: solid (β = s), liquid (β = w, the wetting phase) and gas (β = g, the non-wetting phase). The degree of saturation of the mobile phases, S_β [-], is defined as the fraction between phase β volume, V_β, and vacuum volume, V_f:

$$S_\beta = \frac{V_\beta}{V_\beta} \tag{3.1}$$

Along a vertical soil profile direction, at equilibrium, a static distribution of S_β is noticeable:

- water table that is by definition the locus of points at which water is at atmospheric pressure: under it soil is saturated, pores are fully occupied by liquid phase and liquid pressure P_w [M L^{-1} t^{-2}] increases with depth because of the weight of water column above it;

- an unsaturated zone, called vadose zone, where pores are partially filled by water and partially by air;
- an intermediate zone of transition, called capillary fringe (with thickness h_{cap} [L] of about a few centimetres for coarse sands to several meters for clays (Narasimhan et al., 1977; Berkowitz et al., 2004)) where $S_w \leq 1$ and P_w is below the air pressure P_g due the interfacial forces pushing water through pores (called suction pressure) (Corey, 1986).

As a general indication the following constitutive relation applies:

$$S_g + S_w = 1 \tag{3.2}$$

Some values of S_β are noteworthy:

- S_{ws} and S_{gs} are respectively saturated liquid and gas saturation;
- S_{wr} is residual liquid saturation defined as S_w at which "water is immobile or water flow is negligible on the time scale of importance for the evaluation of flow properties" (Moseley et al., 1996; Cornelis et al., 2005; Byrnes, 2010) or the value at which the gradient (dS_w / dh) becomes zero (Van Genuchten, 1980). It happens because connecting films become so thin that liquid phase stays adsorbed to solid phase and it does not follow suction forces (Luckner et al., 1989);
- S_{gr} is residual gas saturation that represents the gas saturation below which the gas phase is discontinuous and then it flows no more (Luckner et al., 1989; Moseley et al., 1996). Experimentally it is determined as gas saturation found when a threshold pressure achieves first detectable gas flow.

The reciprocal relationships of previous definitions are indicated in Fig. 3.1, expressed as volumetric phase content:

$$\theta_\beta = f * S_\beta \tag{3.3}$$

where f denotes soil total porosity [-], that is

$$f = V_f/V_{tot} \tag{3.4}$$

and it usually varies from 0.3 to 0.5 (Sanders et al., 1997).

The effective porosity, f_e, is lower than f, as is defined as the ratio of the part of V_f where water may drain by gravity, from a saturated sample of the soil, to V_{tot} (Argonne, 2010).

As for capillary fringe, close relations exist between liquid volumetric content ($\theta_{w,cap}$) or saturation ($S_{w,cap}$) and capillary pressure head (h_{cap}) called soil-water characteristic curve, or soil-water retention curve.

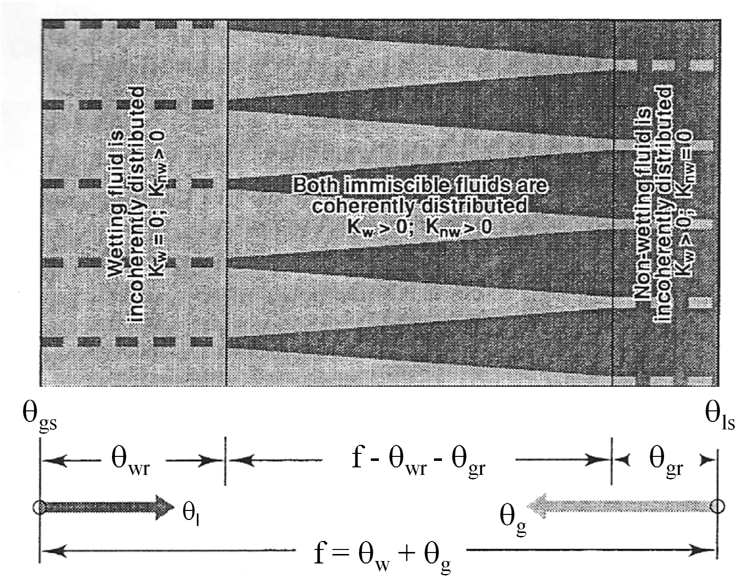

Fig. 3.1*: distribution of two immiscible phases, expressed as water or gas volumetric phase content, in a porous medium.*

3.2.2 Soil properties affecting volatilization

3.2.2.1 Water content

The level of wetness of the soil may also be expressed as soil moisture w [%]:

$$w = M_w/M_s*100 \quad (3.5)$$

The water content in soil is generally highly variable, both spatially due to soil heterogeneity and temporally due to rainfall. It changes, in fact, for precipitation and percolating, that directly affect transport by physically moving air in soil both vertically and laterally; this causes temporally disordered displacement of contaminants, thus giving them local and transient sources or sinks.

It acts indirectly, too: it influences unsaturated zone vapour transport since the presence of water determines the ratio of air-filled porosity to total porosity in soil, and moreover it changes vapour partitioning with soil-water. Wetting soil reduces its real effective diffusion D_g (§ 3.3.2), thus rapidly precluding advective transport and reducing molecular diffusion (Farmer et al., 1980; Livingston et al., 1995; Gan et al., 1996).

Moisture content is particular meaningful across the capillary zone of sandy soils, where it may sharply change along the depth, giving effective diffusion coefficients that may vary by several orders (Choi et al., 2002; Hers et al., 2003).

In fine soils, wetting reduces the continuity between pore spaces with a rate higher than the reduction of discontinuous gas phase (Focht, 1992); gas transport therefore diminishes significantly long before all the θ_g reaches θ_{gr}. In coarse-textured soil, on the contrary, wetting affects in a minor way gas transport because continuity between pore spaces is persistent over a large range of θ_w (Livingston et al., 1995).

As for transport forces in general, for very low moisture contents, like desert areas (w less than 2%), there is the direct interaction between soil surface and the contaminant, reducing the effective contaminant vapour pressure and therefore the vapour transport too. For moist soils (w between 2 and 4%) the competition for adsorption sites increases as water molecules form a layer on mineral and organic surfaces; in contrast, VOC adsorption in wet soils (w higher than 4%) mostly occurs on the organic matter due to the hydrophobic behaviour of many organic compounds (Sanders et al., 1997; USEPA, 1996b).

Another important effect is on the microbial activity. The optimal soil moisture content should be between 75 to 90% of field capacity, whereas if it falls below 50% of field capacity biological processes stop (Evans et al., 2002).

3.2.2.2 Gaseous permeability

For the generic phase β the scalar value of the permeability in the β phase, k_β, is given by:

$$k_\beta = k_{r,\beta} * k \tag{3.6}$$

where k $[L^2]$ is the intrinsic permeability of soil and $k_{r,\beta}$ is the relative β phase permeability [-] (EOLBNL, 1999; Rannaud et al., 2009). The relative permeability of water ($k_{r,l}$) and air ($k_{r,g}$) is generally calculated by Van Genuchten-Mualem model (Van Genuchten, 1980):

$$k_{r,l}(h) = \frac{1-(\alpha h)^{n-2}\left[1+(\alpha h)^n\right]^{-m}}{\left[1+(\alpha h)^n\right]^{2m}} \tag{3.7}$$

$$k_{r,g} = 1 - k_{r,l} \tag{3.8}$$

where α, n and m are numerical parameters and h [L] is the pressure head.

k_g in particular varies by several orders of magnitude according to dimensions, shapes, direction and water content of soil porous spaces.

This parameter defines the air movement in soil and gives indications of potential effect of pressure changes in soil (Gao et al., 1998) and also of oxygen availability in the unsaturated zone, directly influencing the biodegradation of potentially biodegradable compound (Davis et al., 2009).

3.2.2.3 Bulk density

Bulk density, ρ_b $[M\,L^{-3}]$ is defined as:

$$M_s/V_t, \tag{3.9}$$

and is linked to total porosity of soil f through solid density ρ_s:

$$f = 1 - \rho_b/\rho_s \tag{3.10}$$

so lower is ρ_b and higher free space is available among the soil matrix (Farmer et al., 1980; Sanders et al., 1997).

3.2.2.4 Organic matter content

The organic matter of soil is generally expressed as f_{oc}, the ratio of organic carbon to total dry solid phase. Due to its direct involvement in adsorption phenomenon (§ 2.2.4), the higher it is, the lower the free vapour phase of the contaminant, while adsorption increases (Glotfelty et al., 1984; Dupont et al., 1986).

Soils with high organic carbon content may also request higher amount of oxygen only because of natural soil respiration, and this may represent a critical sink which is antagonistic to contaminant biodegradation (DeVaull, 2007).

3.2.2.5 Vegetative transport

Vegetation heavily influences gas exchange across the ground-atmosphere layer by phenomena of gas production, consumption and transport across roots and leaves. In particular rhizospheric environment hosts microbial communities giving biodegradation transformations (Livingston et al., 1995).

3.3 Flux and transport volatilisation processes

3.3.1 Flux equations

Flux model requires three equations: i) an equation of motion; ii) an equation of state and iii) a continuity equation (Massmann, 1989). Their solution results in air pressure P_g and air saturation S_g in soil, both dependent on space and time.

As for equation of motion i), in general flow of gases due to pressure gradients is different from flow of liquids because the velocity at the pore walls cannot generally be assumed to be zero; another term should be added, called “slip flow" or "drift flow”, in Darcy's law (3.11) which governs the flow of liquids in porous media. This term depends on average pore radius and is meaningful only for pore radii greater than approximately 10^{-3} mm, such as in clay materials. For transport in silt, sand, and gravel soils, under laminar flow conditions for both fluids, this term is negligible and the equation of motion for gas flow has the same form as Darcy's law (Dullien, 1979).

$$\mathbf{q}_\beta = -\frac{k_{r\beta}\mathbf{k}}{\mu_\beta}\left(\nabla P_\beta - \rho_\beta g \mathbf{e}_z\right) \tag{3.11}$$

where not above mentioned symbols denote: $\mathbf{q}_\beta$ [L t^{-1}] is Darcy velocity of phase β, μ_β [M L^{-1} t^{-3}] is its viscosity, **k** is II rank tensor of k intrinsic permeability (§ 3.2.2.2), and $\mathbf{e}_z$ is an unitary vector in z direction of a Cartesian coordinate system originating at the bottom of the domain and increasing upwards.

The equation of state ii) is required to convert potentials into pressures. Water density may be assumed as a constant value, whereas the gas phase may be modelled as an ideal gas dependent only upon pressure (Falta et al., 1989; Massman, 1989) due to the range of pressures and temperatures involved in soil theory (both in unperturbed conditions and with vapour extraction systems). The relationship between pressure and density for an ideal gas is given by the Boyle-Mariotte law:

$$P_g = \frac{\rho_g}{\omega_g} RT \tag{3.12}$$

where ω_g [M mol^{-1}] is gas molecular weight, R [M L^2 t^{-2}mol^{-1}T^{-1}] is the universal gas constant and T is the temperature.

The continuity equation iii), that expresses the mass conservation, may be written as:

$$\frac{\partial(f\rho_\beta S_\beta)}{\partial t} = \nabla \bullet \left(\frac{\rho_\beta k_{r\beta}\mathbf{k}}{\mu_\beta} (\nabla P_\beta - \rho_\beta g \mathbf{e}_z) \right) + \Gamma_\beta \tag{3.13}$$

where Γ_β [M L^{-3} t^{-1}] are sinks or sources.

3.3.2 Transport equations

Each chemical i is assumed to be in equilibrium between all three phases: g, w and s, according to the relationship (Jury et al., 1980; Jury et al., 1990):

$$C_i = \theta_g C_{ig} + \theta_w C_{iw} + C_{is} \rho_b \tag{3.14}$$

Linear expressions are commonly used to relate concentrations between the three phases, following relations (§ 2.2.3 and § 2.2.4). This hypothesis is always posed, but statistical analysis showed that in nature there is lack of equilibrium in repartition (Kliest et al., 1989). During transport chemicals will continue to partition between different phases, and over time they will tend to reach equilibrium concentrations in all of them (Davis et al., 2009).

The transport of a chemical i inside an unsaturated soil is generically given by:

$$\frac{\partial C_i}{\partial t} + \nabla F_i + \Xi_i = 0 \tag{3.15}$$

where C_i is the total concentration in the soil [M_i L^{-3}_{soil}], F_i is the mass flux vector [M_i L^{-2}_{area} t^{-1}], and Ξ_i is the net loss rate of chemical i due to reaction [M_i L^{-3}_{soil} t^{-1}].

F_i is the sum of all the aspects of transport involved that cause the movement of chemical i. It is provided by (Jury et al., 1980; Abreu et al., 2005):

$$F_i = \Sigma_\beta C_{i\beta} * q_{i\beta} + \Sigma_\beta F_{i\beta\_diff} \tag{3.16}$$

where β are obviously just the mobile phases g and w.

The first addendum of (3.16) explains fluxes due to advection and the second flux due to diffusion, that are linearly added together (Provoost et al., 2009b).

The term $q_{i\beta}$ is calculated from (3.11). This component, which is often neglected, is actually very important because ever weak atmospheric pressure changes may induce gas flow in the unsaturated zone (Choi et al., 2002), and the flux linked to this phenomenon may be greater than diffusion (Massmann et al., 1992). Barometric pressure changes usually have an inverse influence on volatile transport: when pressure decreases, volatile flux from the soil to the atmosphere increases because of air-pumping and vice-versa (Chen et al., 1995; Tillman et al., 2004).

Advection is the most important driving force for soil gas intrusion into buildings because building under-pressurizations may vary from 0 to 50 Pa (Nazaroff et al., 1985), with typical values ranging among 2-10 Pa (Waitz et al., 1996, Hers et al., 2001, Olson et al., 2001). It depends also on soil temperature as expressed through (3.12): an increase in temperature gives a faster movement of vapours because of expansion of soil gas, causing a higher ΔP and therefore an advection movement (Rannaud et al., 2009).

Gas phase advection may also be due to gas density ($\rho_{i,g}$) gradients too. They occur in the presence of dense vapours (like chlorinated solvents) (Sleep et al., 1989, Mendoza et al., 1990a) or in general because the density of a gas in contact with the liquid is different from ambient soil gas; this creates a gradient which, under certain conditions, may become the most dominant aspect in transport (Falta et al., 1989).
In this specific case the Darcy velocity for gas phase, $q_{g,d}$ is given by an expression similar to (3.11):

$$\mathbf{q}_{g,d} = -\frac{k_{rg}\mathbf{k}}{\mu_g}\left(\rho_{i,g} - \rho_{air}\right) = -\frac{k_{rg}\mathbf{k}\,gP}{\mu_g RT}\left(\omega_{i,g} - \omega_{air}\right) \tag{3.17}$$

The density-driven gas flow may be upward ($\omega_{i,g} < \omega_{air}$) or downward ($\omega_{i,g} > \omega_{air}$), due to molecular weight of the evaporating chemical i,

Diffusion is, instead, the most important component when there is any suction forcing gas movement; in the unsaturated-zone it is much greater than in groundwater owing to the larger diffusion coefficient (§ 2.2.5) (Choi et al., 2002; Pasteris et al., 2002). As a general indication, for soil with higher gas permeability/ porosity or well-drained, advection transport dominates gas transport, reaching values several times higher than diffusion; in cases with k_g low (such as for fine-textured soils), the opposite is true (Livingston et al., 1995).

Diffusion is due to a concentration gradient (Antony et al., 1995; Webb et al., 2003), causing net movement of molecules from high to low concentration. It includes two components.
One, called Knudsen flow, describes situations in which gas molecules collide more frequently with flow boundaries than with other gas molecules. It is therefore relevant in situations involving very small length scales and/or very low gas density, when the mean free path of gas molecules is of the same order as the characteristic length scale of the flow field (Thortestenson et al., 1989; Massmann et al., 1992; Fuel Cell Knowledge, 2010).
The second component is molecular diffusion process, which explains that molecules can collide only with other gas molecules, and depends only on molecular weights and temperatures of the gases.
In presence of common soil pore sizes and permeability, Knudsen diffusion, is negligible (Kreamer et al., 1988; Choi et al., 2002) and molecular diffusion prevails. Numerically flux due to diffusion for the β phase, $F_{i\beta\_diff}$, is generically explained by Fick`s first law:

$$F_{i\beta\_diff} = -D_{i\beta} * \nabla C_{i\beta} \tag{3.18}$$

where $D_{i\beta}$ [$L^2\ t^{-1}$] is the effective porous media diffusion coefficient or diffusivity in soil, that is derived from the molecular diffusion coefficient of i in β phase (§ 2.2.5, D_i^{β}). D_{ig} is generally estimated by Millington and Quirk relationship (Millington et al., 1961):

$$D_{i\beta} = D_i^{\beta} * \tau_\beta \tag{3.19}$$

where the corrective factor τ_β is equal to (with symbols indicated in § 3.2.1):

$$\tau_\beta = f * \theta_\beta^{1/3} * S_\beta^{7/3} \tag{3.20}$$

or to the equivalent form

$$\tau_\beta = \theta_\beta^{10/3} / f^2 \tag{3.21}$$

It considers the reduced cross-sectional flow area and increased path length of diffusing gas molecules (Jury et al., 1983; Jury et al., 1984).

Some researchers have found that this relationship often underestimates chemical diffusivity, especially in the presence of high soil moisture content (Evans et al., 2002).

Another expression used in literature, only for gas diffusivity, is (Kliest et al., 1989):

$$D_{ig} = D_i^{g} * \frac{\theta_g - 0.1}{\sqrt{3}} \tag{3.22}$$

In both these ways the diffusion coefficient does not vary either according to concentration or over time.

Especially for effective gas-phase diffusivity, Werner et al. (2004) presented a deep analysis of several different models proposed in literature and defined that in situ measurements should be conducted, since this parameter depends deeply on soil and chemical properties. As a useful indication, Moldrup`s relation was considered the best predictor for several tested soils (Werner et al., 2004):

$$D_{ig} = D_i^{g} * \theta_g^{2.5} / f \tag{3.23}$$

Another relationship derives from Fick's first law and a mass balance describing how diffusion causes the concentration field to change over time. It is Fick's second law expressed as:

$$\frac{\partial C_i}{\partial t} = D_{ig} * \nabla^2 C_{ig} \tag{3.24}$$

The validity of both above laws (3.18) and (3.24) seems valid only in open spaces, not in porous media. Other ways to describe diffusion are Stefan–Maxwell equations which are considered extensions of Fick’s laws for a multi-component mixture. Recently new interpretations have been presented. One of them is the dusty-gas model (DGM) including effect of the porous media as a `dusty gas` component, an ensemble of large molecules, within gas mixture. This allows the coupling effects between diffusion and advection to be assessed, and fits experimental data better (Thortestenson et al., 1989; Webb et al., 2003).

It does not appear opportune to enter into details at this point, since none of the models presented below (§ 3.4) implements this theory.

As a general consideration, diffusion in the aqueous phase is negligible as compared with that in the gaseous one, especially for highly volatile compounds (Mendoza et al., 1990), whereas gas dispersion is negligible due to its weak velocities (Massmann et al., 1992; Batterman et al., 1995).

Fick’s first law generally gives (3.18) reasonably accurate results for steady state fluxes (excluding stagnant gases such as N_2 and Ag), whereas it is not well understood if Fick’s second law (3.24) is valid, since it employs diffusion coefficients that are constant over time (Jury et al., 1980; Thortestenson et al., 1989).

Diffusion is not an instantaneous process but it takes some time depending on the compound distance from the soil surface. Therefore, at initial conditions, for deep sources under a clean shallow layer, the initial vapour flux through the surface can be null. Since equilibrium in the matrix is reached, and stationary conditions achieved, vapour flux is constant over time till the source depletion (USEPA, 1986).

As an example, Jury et al. followed the evaluation of benzene vapours, spread in a 30 cm thick source layer, varying the boundary condition of the amount of soil covering the source. They used a thickness of the soil cover varying from 0 to 1.5 m and monitored gas volatilization for 1000 days after the beginning of the test (Fig. 3.2). The thicker the cover, the less vapours are spread; considering for example the maximum clean layer, only a small amount of benzene is diffused after 100 days and only 30% of source mass reaches the surface after 1000 days (Jury et al. 1990), because of adsorption and biodegradation phenomena.

Attention has to be paid in case of contaminated soil surface, because this alters the gradient of concentration along depth.

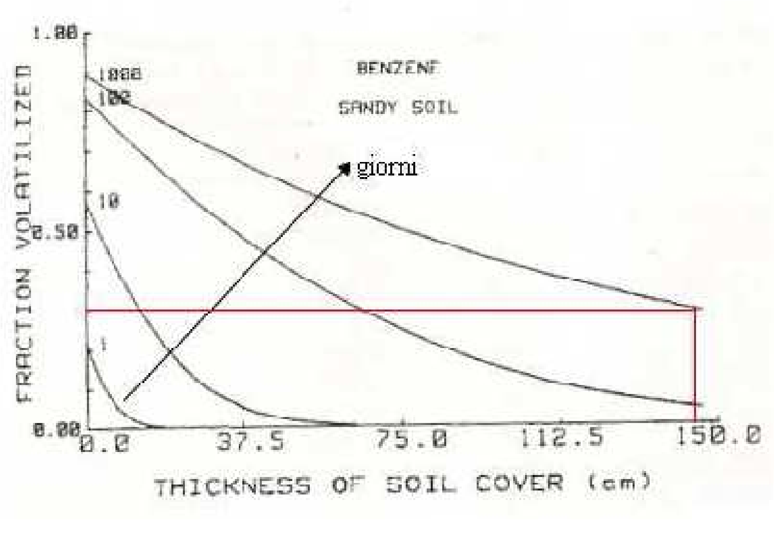

Fig. 3.2: *volatilization of benzene in sandy soil, depending on time and thickness of the clean cover on the source (Jury et al. 1990).*

The other term in (3.15), Ξ_i, is the component considering possible reduction of the mass of the component i due to biodegradation by biomass present in soil.
This term may be described by different kinds of kinetic expressions (including zero-order, first-order or Monod), depending on the behaviour of degradation of the specific chemical.
In detail, the zero-order kinetic is given by:

$$\Xi_i = K_{0,i} * \theta_w \tag{3.26}$$

the first-order kinetics by :

$$\Xi_i = K_{1,i} * \theta_w * C_{iw} \tag{3.27}$$

the Monod kinetic by:

$$\Xi_i = K_{max,i} * \theta_w * \frac{C_{iw}}{\lambda_i + C_{iw}} \tag{3.28}$$

where $K_{o,i}$ is the zero-order reaction rate [M_i t^{-1} L^{-3}_{water}], $K_{1,i}$ is the first-order reaction rate [t^{-1}], $K_{max,i}$ is the maximum contaminant utilization rate [M_i t^{-1} L^{-3}_{water}], λ_i is the half-saturation constant [M_i L^{-3}_{water}], all chemical i -specific. Degradation constants are difficult to determine and influenced by site-specific factors, therefore biodegradation tests should be carried out (Lahvis, 2010)

Biodegradation has been proved to be a significant process, in particular at sites with low-level concentrations in soil and groundwater (Davis, 2009). Literature reports that, where oxygen content is higher than 0.23% by volume, the microbial transformation is rapid (Roggemans et al., 2001) and concentrations decrease rapidly (till to several orders of magnitude) over relatively short vertical distances (lower than 1 m) (Fischer et al., 1996; Hers et al., 2002; Davis, 2006; Patterson et al., 2009).

Substituting eq.s (3.14), (3.16) and (3.19) into eq. (3.15) yields to the overall transport equation a function of the variable C_{ig}:

$$a_i \frac{\partial C_{ig}}{\partial t} = -\nabla \cdot (C_{ig} * \mathbf{q}_g) - \nabla \left(\frac{C_{ig}}{H_i} \mathbf{q}_w \right) + \nabla \cdot (D_i \nabla C_{ig}) - \Xi_i \tag{3.29}$$

where

$$a_i = \left(\theta_g + \frac{\theta_w}{H_i} + \frac{K_{oc} f_{oc} \rho_b}{H_i} \right) \tag{3.30}$$

a_i expresses the gas-phase retardation coefficient that increases with water and organic contents of soil.

The hypothesis subdued to all above mentioned differential equations are that gas density does not depend upon gas pressure. This is a likely condition if the maximum pressure difference between any two points in the flow field is less than approximately 0.5 atm. Equations become therefore linear and the same equations used to model groundwater flow may be used (Massmann, 1989). As a note, in general, the soil properties θ_{β}, f, ρ_b and f_{oc} are also assumed to be constant in space and time (Jury et al., 1990).

Tab 3.1 presents a summary of common assumptions subdued to modelling used to represent vapour transport, with references to limitations of application field.

***Tab.3.1**: General assumptions and limitations at the base of flux and transport models (Massmann, 1989, modified).*

Assumption	**Limitation**
The equation of motion for gas transport is ascribable to an equation similar to Darcy's law	Valid approximation for flow in not fine-grained materials, like sands and gravels
Vapour behaves as ideal gas	Valid approximation for temperature and pressure conditions typical of environmental conditions (also for vapour extraction systems)
Constant and uniform porosity	In real world porosity changes over time and with location due especially to temporal and spatial variations in moisture content
Molecular weight is uniform	Molecular weight changes with reactions happening on gas; variations are generally small for organic vapour
Gravitational effects are negligible	Valid assumption quite always for common VOC (not for chlorinates ones)
Compressibility of the porous media is negligible	Valid assumption quite always valid
Gas transport may be modelled using the equation for incompressible flow	Valid assumption for pressure variations on order of 0.5 atm
There is no immiscible phase	Not available near source boundary

When the emission of vapours from the subsoil to the surface is acknowledged, models calculating transport of chemicals inside an indoor space may be applied. They are based on a steady state mass balance inside the enclosed space, giving indoor air concentration C_{ig}^{indoor} as:

$$C_{ig}^{indoor} = \frac{E_s + V_b * A_{ex} * C_{i,amb}}{V_b * A_{ex} * Q_s} \tag{3.31}$$

where:

Q_s is the soil gas flow rate entering into the enclosed space [L^3 t^{-1}], dependent on crack length and the soil gas flow rate per unit length of crack (Q_{ck}, [L^3gas t^{-1} L^{-1}]);

V_b is the enclosed space/building volume [L^3];

A_{ex} is the enclosed space air exchange rate [t^{-1}];

$C_{i,amb}$ is the concentration of compound i in ambient air entering the enclosed space [M L^{-3}];

E_s is the emission of chemical i into enclosed space [M t^{-1}], dependent on crack width, foundation thickness and effective diffusion coefficient for transport into the crack [L^2 t^{-1}].

Fig. 3.3 is a sketch explaining the processes involved in vapour flux from a source and transport through soil, including the case of transport in indoor spaces.

Vapour concentrations in indoor air are assumed, in all models, to be uniform and well mixed, but field measurements have shown that they may be strongly variable both within a room and throughout a building (ECA, 1989; USEPA, 2008).

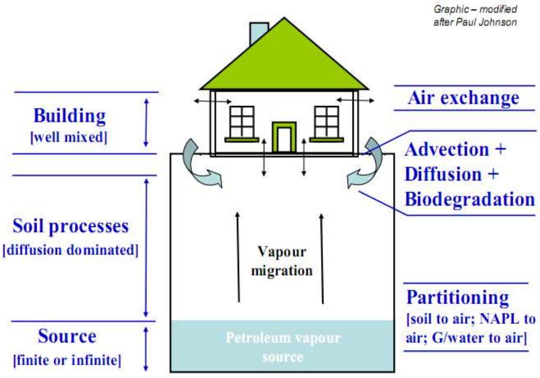

***Fig. 3.3**: simplified sketch of zones of interest for vapour flux and transport, including vapour intrusion (Davis et al., 2009).*

The solution of eq.s (3.29) and (3.30), also describing situation of Fig. 3.3, in a domain (Ω) depends on: i) the initial conditions (i.c.), which define the values for the variables at time t = 0 in Ω; ii) the boundary conditions (b.c.), specifying the values for the variables along Ω boundary (Dirichlet b.c.) or the air, water and mass flow rates through Ω boundary (Neumann b.c.).

No presence of the chemical i is posed as boundary condition at the ground surface for solutions of almost all models found in literature (presented in § 3.4). This implies that the concentration in the layer above ground surface has a thickness equal to zero, and thus maximizes the rate of mass transfer to the atmosphere due to diffusion.

In short, during most of modelling approaches, no presence of immiscible phase, like NAPL (§ 2.2), within Ω is assumed (even if in reality it could exist near the source), but this hypothesis is coherent with the use of modelling for RA. According to indications of Italian Regulatory Organism, ISPRA (ex-APAT), in fact, RA has to be applied only for secondary sources because all primary sources (like NAPL) are supposed to be removed immediately to solve emergencies (APAT, 2008(a); APAT, 2008(b)). A long-lasting source, made up of residual chemicals, should otherwise be considered, giving a three-phase system (including an air-water-oil phases) and partitioning of VOCs between all them: gas-aqueous, gas-NAPL, aqueous-NAPL, gas-solid, and aqueous-solid. Complexity is inside the fact that concentrations of each component moving from the NAPL source depend on their mole fraction in the NAPL phase (according to Raoult's law, § 2.2.2); these last change over time and depend on all the other compounds (Karapanagioti et al., 2003). Moreover, moisture inside porosities is contaminated because of phase partitioning, and may be transported towards groundwater for precipitations or groundwater fluctuations, and this makes the system become extremely complicated (Mendoza et al., 1990a).

3.4 Models

Mathematical bases of vapour models came from models enveloped to study radon vapour intrusion within the subsurface developed since 1980s (Abreu et al., 2005) with simple diffusive and/or pressure-driven flow analytical models (Nazaroff, 1985; Nazaroff, 1987). New volatile compounds models differ from previous ones for a localized source and they often include chemical/biological reactions.

There are two kinds of available models: analytical and numerical ones.

Analytical models, often describing only one-dimensional transport, are suitable instruments to define a site-screening RA and to help in definitions of remedial decisions (USEPA, 2002; USEPA 2004). They are useful if their application is preceded by deep understanding of their hypothesis, limits, field of application and knowledge of uncertainties. In most cases they have been used improperly or with non site-specific key parameters, and therefore many Regulatory Agencies have now limited their use only to site-screening purposes, imposing the use of default parameters to obtain conservative results. In many American states, Regulators have chosen to deepen analysis by further assessment (COMEOEA, 2002; MADEP, 2009; NYSDOH, 2006; NJDEP, 2005; NJDEP, 2009). In fact these simplified tools describe only a part of all the elements that play a role in determining whether vapour intrusion does or does not pose a risk at a particular site, and cannot adequately accommodate site-specific conditions (Choi et al., 1995).

Previous models have led to the development of more complicated and exhaustive computational fluid dynamic (CFD) models, useful to predict the effects of various site features on vapour transport. Their complexity, necessary to describe site-specific transport in soil properly, requires numerical solution. They belong to an ongoing research area, because they are still being validated and need to be applied to different cases in order to increase their proper and realistic description of vapour transport complexity (Abreu et al., 2005). Till now, no model in current commercial use has been completely field verified and modelling therefore is considered only as a theoretical guide or a screening tool to define the necessity of additional site investigations (Turczynowicz et al., 2007; Pennel et al., 2010).

As for model geometry, in general 1-D models are simpler to understand, require less memory effort, may be solved simply but cannot capture the full range of effects happening in real vapour transfer. They are preliminary indications before a 3-D analysis. In general they tend to over-predict vapour transport, especially for indoor intrusion, because they neglect dilution effects related to lateral air movement flow (Hers et al, 2002). They are potentially used before, during, and after vapour investigations (for example to inform sampling plan details), also after the application of a remediation technology or as decision support tool to define future modifications in site features (Pennel et al., 2010).

Particular attention has to be paid to:

- field validation of all input parameters;
- presence of biodegradation and aerobic degradation;
- diffusion, advection, and preferential pathways;

- influence of water tables;
- partitioning characteristics of phase-separated hydrocarbons;
- soil heterogeneity
- as for indoor migration, linking of subsurface transport pathways to above ground dwellings and dwelling influences in general (Turczynowicz et al., 2007).

Literature presents several papers about the comparison between different models (Evans et al., 2002; Tillman et al., 2005; Walden, 2005; Turczynowicz et al., 2007; Davis et al., 2009; Provoost et al., 2009; Pennel et al., 2010; Lahvis, 2010) and generally achieved conclusions affirm that vapour concentrations at ground level could differ by more than an order (Evans et al., 2002) (up to three orders (Walden, 2005)) of magnitude for equivalent applications and model input. Defining the best choice is difficult, because none of the models has demonstrated to be more accurate than any other. Attention is therefore placed on understanding limits and hypothesis of most common simulators.

3.4.1 Numerical models

The use of numerical codes as tools for gaining a better understanding of vapour pathway began with studies on radon, starting with two-dimensional, steady state models; they were based on theory of fluid flow through porous media, developed by both finite element (Garbesi et al., 1989) and finite difference theory (Mowris et al., 1988 in Abreu, 2005). Three-dimensional models were also produced, as for example Loureiro`s steady state finite-difference one, coupling soil gas flow equation with that of transport, and describing both diffusive and convective transport processes through the use of an interactive code (Loureiro et al. 1990) or its reformulation to cylindrical coordinates (Revzan et al., 1991). These two models, in particular, left free choice in an irregular subdivision of spatial grid. Another numerical model, created to study radon transport indoors, was based on CFD theory and simulated the effects on transport of fan systems, various pressure gradients, changes in temperature and wind speed/direction (Wang et al., 2002). As a general consideration, implementing these 3-D models showed that the quantitative prediction of a gaseous compound requires accounting for a multitude of effects and variables, and, especially for indoor intrusion, some considerable sophistication in geometry modelling (Pennel et al., 2009).

3.4.1.1 Basic models

One of the simplest models used for VOC is that of Jury (Jury et al., 1982) (created to study N_2O emissions in a 2-D field) that uses a very simple finite difference method (alternating direction implicit) only to solve gas diffusion, without any advection, both for open and closed cover boundary condition at the top of the column of soil.

Another model considering diffusion in the gas phase and aqueous-phase mechanical dispersion in a one-dimensional domain, using finite difference technique, is that of McCarthy (1992). It describes only one compound and omits biodegradation processes. Gas concentrations are not used as variables, but have to be calculated from the aqueous phase concentration output and (2.3). The author verified model results with data from a set of laboratory tests and, furthermore, he compared it with a 2-D advection-diffusion model based on random walk theory: he obtained that simple 1-D approximation offered a good estimation of vertical transport across the capillary fringe (McCharthy et al., 1993).

Another simple numerical model, for 1-D field, considering both gas diffusion (but no dispersion) and advection, neglecting transfer between soil and water and biodegradation, is that of Choi (written in FORTRAN). Pressure gradient along vertical direction in (3.11) is solved through a linearized flow equation. It consists of two parts: the first simulates gas flow while the other simulates contaminant transport solved using a finite difference scheme. As i.c. the model has a linear concentration gradient (starting with zero value at land surface) and as b.c. no chemical presence above the soil surface (C_g equal to zero at the top boundary) (Choi et al., 2002).

As regards indoor intrusion, Olson and Corsi found that many models contain numerous parameters needing idoneous fitting, subjected to meaningful uncertainty. They created a new two-compartment model: the upper one including the space from the basement to the first floor, and the bottom one from the source to the ground level. They observed in fact that gas pressure difference between soil and basement may be significantly lower than that between the basement and ambient (Olson et al., 2001). The model is based on a mass balance given by a system of ordinary differential equations solved numerically; solution is time dependent because of the transient nature of most indoor sources. Various transport phenomena are included, such as advection for ventilation system, diffusion through cracks in the foundation or through the foundation itself, volatilization from water (involving gas-liquid mass transfer), chemical and physical reactions (e.g. adsorption and desorption) (Olson et al., 2002), and, as in Ferguson's analytical one (Ferguson et al., 1995), contribution of other indoor materials.

Another simple numerical model, used as screening algorithms by Dutch Environmental Agencies, is CSoil (§ 3.4.1.3). It was created by National Institute of Public Health and the Environment (RIVM) and is based on equilibrium partitioning and stationary transport equations, considering vapours due to diffusion into a homogeneous vadose zone according to Jury's theory (Jury, 1984b). It may estimate vapour concentration both outdoors (considering dilution by aeration flux as in SOILRISK approach) and indoors, especially for typical Dutch single-family dwelling, with crawl space floor (Van den Berg, 1994). It also contains an algorithm to calculate human exposure to soil pollutants and an user-friendly version of this model is available as Risc-Human (version 3.1) (VHBC, 2010). However, it does not include biological degradation and only considers inexhaustible source (Rikken et al., 2001; Provoost et al., 2009a).

3.4.1.2 Improved models

One of the first complete numerical models was VLEACH, an one-dimensional finite difference code derived from a code used to predict water contents and fluxes (LEACHP). It considers a non equilibrium partitioning of one VOC in different soil phases and describes only the vadose zone-leaching; it simulates vertical advection and dispersion in the aqueous phase and only diffusion of the gaseous components, neglecting biodegradation process. The domain is subdivided into numerous cells that may differ in soil properties, recharge rate, and depth of the water table. Constant concentration, no-flow conditions and finite sources can be chosen to describe the two b.c.s (Chen et al., 1995; USEPA, 1996a; Ravi et al., 1997).

Talimcioglu and Korfiatis created a 2-D numerical model, Integrated Moisture Plus Contaminant Transport (IMPACT), to simulate the effect of day-to-day and seasonal variations in soil moisture content and advection, in particular inside unsaturated zone on the volatilization pathway. It assumes equilibrium partitioning, diffusion, biodegradation only in the liquid phase (according (3.27)), as well as hydrodynamic dispersion too, giving an equation in terms of aqueous concentration, solved through a fully implicit difference technique (Sanders et al., 1997).

Another well-known code used to simulate outdoor or indoor intrusion is that of Turczynowicz and Robinson, involving the coupling of VOC migration in the soil to the crawl space (through a thin stagnant boundary layer at the soil surface) and a 1-D well-mixed box model, dependent on dwelling features to define fluxes in closed spaces. The source may be indicated in whatever discrete space interval inside the soil, and defined as finite in time to avoid undue conservatism. From the original 1-D diffusion modelling version (Turczynowicz et al., 2001 in Robinson et al., 2005), the authors derived a 3-D code, but maintained the simplified assumption of no VOC variations along the horizontal planes. Thus means that the potential house overlaps the source completely and that the model works in an axisymmetric restrictive geometry. The model does not involve NAPL, considers biodegradation (using (3.27), both in soil and in crawl-space), homogeneous soil, gas advection and diffusion as described by (3.29), and aqueous advection, but it neglects the influence of vertical waver of the water table (Davis et al., 2009). The equations are solved imposing an initial distribution of VOC inside a known buried layer and, as b.c., on the top, a stagnant boundary layer of air. Above it there is either no house or a house with a crawl space. In the former case VOC concentration in air is zero, whereas in the latter, two differing flux conditions are posed, for both crawl and for dwelling spaces transportation (Robinson et al., 2005).

The absolutely new evolution of numerical models, considering specific features of organic compounds, was introduced by Abreu and Johnson who created a 3-D numerical code for multi-component transient transport. It simultaneously solves equations for diffusion, advection and biodegradation, and also transport into indoor environments through foundation cracks.

As for Ξ_i term, it makes it possible to choose between a range of biodegradation kinetic expressions, (3.26), (3.27) and (3.28) and also a dual-Monod considering dependence also on another dissolved reactant. The space geometry is non-symmetrical and it is therefore suitable for studying lateral transport towards a building. It is able to simulate heterogeneous soil lithology, transient indoor and

atmospheric pressure (P) variations and it allows for spatially distributed foundation cracks (Abreu et al., 2005; Abreu et al., 2006). P, in particular, is allowed to change over time and follows a periodic function; the soil gas flow rate flowing through the cracks in the foundations is given by the same algebraic expressions used in some models for Radon (Loureiro et al. 1990).
As regards the determination of the indoor concentration, the model assumes rapid mixing of the indoor air, no indoor emission sources, no indoor reactions and no entrance of i-compound from the ambient air.

Another computation 3-D fluid dynamic is that of Pennel et al., which is based on a commercially available package, Comsol Multiphysics; it is characterized by a user-friendly approach and uses finite elements, allowing more flexibility in choosing complex geometries and also treating simple geological heterogeneities (Bozkurt et al., 2009). This model considers diffusion in both liquid and gas phase, but advection only for gas phase, so q_w is = 0. It deals with indoor intrusion too, assessing the chemical transport across building foundations dependent on an user-defined disturbance P at the foundation-soil interface. The model implements a domain with a boundary far enough from the structure not to have perdurbed b.c., and therefore uses no-flow boundary conditions at the edges of the domain. The lower horizontal domain boundary is given by water, considered as a no-soil gas-flow and as an infinite contaminant source; at the top of the domain a reference pressure is imposed and the contaminant concentration is defined as null (although this value may be changed to simulate elevated atmospheric concentrations). However, by changing boundary conditions, this model which is a numerical code, is able to follow diminishing sources, periodic pressure fluctuations, other transient and spatially variable conditions and biodegradation sinks. As usual the model solves soil gas continuity equation in advance and then couples it with the chemical transport equation (since the contaminant species represent only a small fraction of the soil gas concentration) (Bozkurt et al., 2009; Pennel et al., 2009; Pennel et al., 2010).

All the models presented so far do not consider advection due to density gradient.

The first model that considered advection due to (3.17) is that of Sleep and Sykes (Sleep, 1998), in two dimensions and solved through finite elements. It shows the real importance of this aspect for chlorinated solvents. Another important model, considering all gas transport components, is that of Falta, who used a modified version of TOUGH (Transport of unsaturated groundwater and heat) (EOLBNL, 1999), a 3-D numerical code using an integral finite difference method, to follow the behaviour of a VOC in liquid and gas phases. The model uses some simplifying assumptions for water: it is immobile and present only as a liquid phase. Other impositions (homogenous and isotropic soil, uniform soil properties, immobile liquid VOC phase, 2-D geometry, no VOC gas phase at ground level) were given by the authors only for the purposes of their runnings, but can adapted to other site-specific conditions (Falta et al., 1989).

Falta et al. indicated that considering the effect of density-driven flow is necessary for chlorinated compounds and benzene, whereas for others, such as ethylbenzene, toluene, xylene, napthalene, phenol and chlorobenzene it is negligible.

They underlined the interdependence between diffusion and density-driven flow that cannot be isolated by using numerical models.

3.4.1.3 Models also considering NAPL

In literature models describing the presence and, in some cases, also the transport, of non-aqueous phase liquid which implies high levels of VOCs are available too.

The simplest application of a NAPL phase in a model (present as a flowing layer over water table) was performed by Baehr who derived a numerical solution for a radially symmetric geometry, considering the com-presence of different compounds, as an extension of the analytical formula (3.33). The model employs both paved surface and free layer as b.c. at the surface; it gives the solution of (3.29), when q_g and Ξ_i are null, by an algorithm reapplied for each constituent inside the VOC mixture. At each interior spatial node and each time step, differences to approximate the derivatives are used in the modified eq. (3.29), following a two-step procedure: a first-order approximation followed by an iterative refinement (Baehr, 1987).

Another model, considering multi-component NAPL phase, is Park's, a steady state screening numerical model specific for total petroleum hydrocarbons (TPH). It is based on instantaneous, reversible, and linear equilibrium between contaminants in the four possible phases: NAPL, water, air, and soil (adsorbed) (§ 2.2). Laws ruling the equilibrium are (2.3) and (2.1). The equilibrated mole fraction of each i-compound is obtained by solving a series of mass balance equations simultaneously; an iterative spreadsheet routine built in MS EXCEL^{TM} Solver is employed for this purpose. The physical processes involved in gas transport towards indoor spaces are advection and diffusion, using a modified J&E model (Johnson et al., 1991) as well as temperature adjustment, too (both for equilibrium partitioning and diffusion coefficient). The results are given as attenuation coefficients (Park, 1999).

Mendoza's model is more complex and was created to follow the behaviour of high vapour pressure and molecular weight pollutants (like dichloromethane, chloroform and in general chlorinated compounds). It considers, in the unsaturated zone, repartition between different soil phases according to linear equilibrium, and various transport processes such as diffusion, advection due to both density gradients and vapour mass released by vaporization of the source (being therefore a function of soil moisture content due to relative gas permeability term as in eq.(3.11)), infiltration towards groundwater, not diffusion in the aqueous phase neither biodegradation depletion. The top of the domain may be represented as a stagnant air layer by a concentration-dependent mass transfer, as proposed by Jury et al (1983). It is written in axisymmetric coordinates (to follow the spreading of the vapour in all directions from the source), uses triangular finite elements and solves interdependent and nonlinear flow and transport equations (Mendoza et al., 1990a; Mendoza et al., 1990b).

Another very common model, used by the Dutch Public Health and the Environment Agency, is VolaSoil, the evolution of CSoil (§ 3.4.1.1), which was developed by RIVM and also contains RA module. The model considers equilibrium between different contaminant phases, diffusive and convective transport, the presence of a limiting stagnant layer; it may accept site-specific data to define the source, including contaminant concentrations in groundwater, both dissolved and as NAPL, solid or soil gas, and follows gas behaviour inside the vertical capillary boundary profile. A sketch of vapour transport is indicated in Fig. 3.4. As for indoor transport, it describes vapour intrusion through different kinds of compartments: crawl space, concrete basement and slab-on-grade. Regards model limitations, it does not consider gas advection and has the same features as CSoil: exclusion of biological degradation, infinite source, homogeneous soil and no consideration of lateral transport or leaching (Waitz et al., 1996; Van Wijnen et al., 2006; Provoost et al., 2009a).

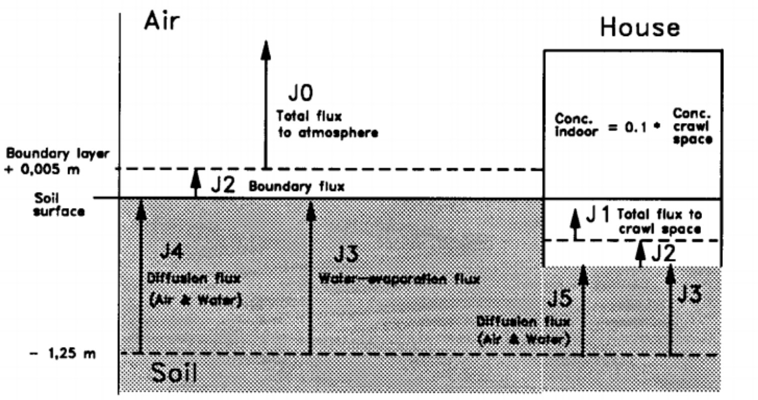

***Fig. 3.4**: sketch of transport fluxes of volatile compound considered by VolaSoil, from soil compartment to both outdoors and indoors (Waitz et al., 1996).*

A more complex and complete model is VENT2D (a finite difference code), that considers multi-phase (vapour, dissolved, adsorbed, NAPL) distribution of a multi-component (up to 60 constituents), and NAPL only as a contaminant source, without considering its flux. The code considers only vapour as mobile phase and describes (in unsaturated soil and in a two dimensional domain) vapour phase diffusion and also advection due to a pressure gradient, as well as to a soil vapour extraction plant. It contains utility programs translating SURFER grids to ASCII maps and vice-versa for fast contouring. As boundary conditions it imposes constant pressure and zero concentration (Benson, 1994).

Another model considering only NAPL and not its flow is R-UNSAT, coded by the US Geological Survey and of public domain. It is a finite difference algorithm, for 1 or 2 dimensional axisymmetric domains, describing transport in unsaturated soil (without a saturated zone at the bottom of the domain). It is written in FORTRAN and now there is a Visual Basic code that uses a Microsoft Excel application for data entry and output processor.

The model follows up to seven components, which may be expressed as constant concentrations at one of the boundaries or as a definite source zone inside the domain. The transport processes dealt with are: gas diffusion, aqueous vertical advection and dispersion, sorption and biodegradation (considering zero, first or Monod kinetics, as well as oxygen limited degradation). Calculations are performed regarding the gas phase. It has been largely used to quantify the biodegradation and volatilization rates at a gasoline spill site and is useful for natural attenuation estimation (Lahvis e al., 1998).

A complete public domain American model, MOFAT, developed by Katyal et al., describes a multiphase flow and multi-component transport, including three fluid phases (w, NAPL, and g) and treats up to five different compounds. It is a two-dimensional (with planar or radially vertical symmetric geometry) finite element program (with linear rectangular elements). NAPL is neglected if it is not present, while either equilibrium or kinetically controlled mass transfer between different phases are considered at the source. It is a complete transport model, including advection, dispersion, diffusion, sorption and biodegradation (only using (3.27)) in all phases, both in unsaturated and saturated zones, with an availability of several steady or transient boundary conditions, and freedom in defining spatially variable soil properties. The governing equations are solved, in space, using an efficient upstream-weighed finite element scheme, whereas nonlinear time integration in the flow analysis is handled using a Newton-Raphson method (Katyal et al., 1991).

Another public domain EPA model, able to describe flux and transport in 1, 2 and 3 dimensions and regarding transport in saturated, capillary fringe and unsaturated zones is NAPL, written in FORTRAN 77. Like the previous one, it considers three fluid phases (w, NAPL, and g), behaving according to a rate-limited partition law, but it includes only one constituent inside NAPL. Flow equations are written for all three phases and those regarding transport include processes of diffusion, sorption into the solid phase (only for the water phase dissolved contaminants) and biodegradation in both water and gas phase (according to (3.27)). Only constant-property boundary conditions are allowed. The set of partial differential balance equations, describing the above mentioned physical phenomena in space and time, is numerically solved using an implicit-in-time finite element method to generate the systems of algebraic equations including nonlinear terms. The code is also available with a commercially graphical user interface to help output understanding (Guarnaccia et al., 1997).

3.4.2 Analytical models

Analytical modelling has been developed largely since the early 1990s and has been applied by Control Institutions to define regulatory screening criteria and decide site-specific target levels for remediation and mitigation, especially for cases with few available data. Nowadays its benefits are questioned because experience has shown poor correlation between their results and measured data, due to: application of simple mathematical algorithms to solve complex space-temporal phenomena; use of over simplified approaches, like simple parameter reference tables (Johnson, 2002b); inadequate or limited model validation; uncertainties in the conceptual model or model parameters/inputs; poor knowledge of model attributes and uncertainty (Hers et al., 2003); exclusion of biodegradation in transport modelling as for biodegradable compounds (as petroleum hydrocarbons) (Ririe et al., 2002; Davis, 2006; Davis, 2009). Literature presents models considering a wide range of transport conditions, including steady state or time-dependent transport, finite sources, variable soil types and moisture saturations, unsaturated-zone transport processes, and different types of building construction. Some of them also include simultaneous sorption and biodegradation too (Lahvis et al., 2010).

3.4.2.1 Only gas diffusion

A famous analytical model for diffusion is that of Baehr (Baehr, 1987), in 1-D field described by spatial coordinate x. It considers, for one only substance, transient gas diffusion with phase partitioning directly inside (3.24) (joined with (3.19) and (3.21)), by dividing it for the gas phase retardation factor R_g derived from (3.30):

$$R_g = a/\theta_g \tag{3.32}$$

It considers a semi-infinite case with an infinite source located at the bottom of the column and as for initial time, the rest of the domain is clean.

Another well-known model considering both diffusions and only liquid advection is that of Jury, in a 1-D domain and for only one substance (Jury et al., 1980). The model solves equation (3.29) where q_g and R_g are null. I.c. is a uniform distribution of C_g throughout the domain, and b.c.s are represented by an infinite source at the bottom of the soil and by no C_g at the top of soil.

As for evaluation in indoor spaces, Little et al. determined a transient solution for the diffusion of a volatile organic compound through an adsorbing unsaturated porous medium in a building. The cases they considered were two: an infinite plane source placed at a finite distance (inside clean soil) from a building (using a series of transient terms) and a limited source with a paved area over it (Little et al., 1992).

3.4.2.2 Gas advection, diffusion and biodegradability

One of the most wide-spread models, suggested directly by USEPA, is RTI model, developed by Clark Allen of Research Triangle Institute (USEPA, 1994). It was initially created to follow emissions from land treatment operations, but it is also available for diffusion of VOCs from the surface of porous media due to a contamination in shallow soil.

It is based on Fick's second law of diffusion (3.24) applied to a flat slab (Crank, 1970), and considers an overall mass transfer coefficient from the surface to wind, depending on molecular diffusion characteristics of VOC, size of contamination and wind-speed (McKay et al., 1973), including both resistance of the soil and the resistance at the wind-porous solid interface. This is given by:

- a term considering partitioning of volatile constituents between the vapour space, adsorbent solids and liquids in the soil, in the hypothesis of reached water-gas equilibrium at all times, following (3.14);

- effective diffusion coefficient (calculated as (3.19));
- a gas-mass transfer coefficient (k_g [L t^{-1}], function of D_i^g);
- (3.27) to estimate biological degradation in involved surfaces.

It contains both a complete solution for long-term emissions, and a simpler one valid for short-term ones. This model does not consider any form of advection transport, imposes that chemical concentration in gas phase at soil surface is much lower than that in soil and follows only upward diffusion, neglecting diffusion into the soil beneath the contaminated zone.

Another famous analytical model, Jury`s (for only one compound), is used to assess gaseous and liquid diffusion, convective fluxes and also first-order biological/chemical degradation (3.27), but does not take hydrodynamic dispersion into account (Farmer et al., 1980; Jury et al., 1983; Jury et al., 1984; Jury et al., 1990). This model was born as a screening procedure to classify different types of pesticides. The volatilization towards the atmosphere, at ground level, is assumed to occur for diffusion through a stagnant air boundary layer of thickness d; above which chemical concentration is zero. A low value of d corresponds to a well-mixed surface condition, due to high wind velocity, that increases depletion of contaminants from the soil (Jury et al., 1983).

The authors obtained solutions for both a case with a uniform source placed from surface down to depth L, and one with chemicals incorporated at uniform concentration in a finite buried layer covered by a clean soil stratum.

Generally speaking, this model explains why volatilization flux decreases as water content, organic carbon fraction and evaporation increase (Jury et al., 1984).

One of the simplest models considering depletion of source via volatilization and degradation (using (3.27)) is that of Sanders and Stern, derived from a modified Jury’s model (Jury et al., 1983) with a finite thickness of contaminated soil and extended to allow calculation of time-dependent intrusion into indoor spaces, using a rate of diffusion into zone of influence of the building. This model directly calculates dose of exposure of target populations and defines the cleanup criteria to protect them (Sanders et al., 1994).

Labieniec et al. (1996) developed a transient, computationally efficient, analytical screening model. Using integration of different modules, it simulates a uniformly contaminated layer in the unsaturated zone over a shallow, horizontal, and unconfined aquifer. The first module, the unsaturated zone one, based on Jury model (Jury et al., 1983; Jury et al., 1990), considers 1-D vertical contaminant concentration profile over time and long-term depletion of contaminant mass due to volatilization towards the atmosphere through a stagnant boundary, leaching into the saturated zone and degradation causes. The unsaturated zone is assumed uniform and homogeneous with steady state infiltration. It is available for both buried contaminated layers, and for contamination up to ground surface.

The other modules, 2-D saturated zone (assuming that once the contaminant mass has moved below water level it is instantaneously mixed into the groundwater), air dilution/dispersion (by respectively box and a simplified Gaussian models) and dust generation ones (following EPA indications), provide long-term average contaminant concentrations in environmental media.

There are also exposure and risk modules to estimate chronic exposure and carcinogenic risk directly. Together these packages are called SoilRisk, which is one of the first RA models (Labieniec et al., 1996).

Lin and Hildemann developed a 1-D non-steady state analytical model predicting VOC emissions from hazardous or sanitary landfills, and considering gas and aqueous diffusion, leachate flow downward and vertical gas advection, first order degradation of the chemicals into other compounds, and mass transfer limitations through the top soil cover. As top b.c. the model assumes that, at the bottom, the concentration drops to zero. The contamination is supposed to begin with a contaminated layer thick from the ground surface to a known depth, or to be due to an instantaneous release from a plane source. The solution uses Laplace transformation and gives analytical solution for concentration at whatever time and depth as a function of the concentration gradient within the landfill (Lin et al., 1995).

Jeng et al. (1996) developed a series of time-dependent diffusion models to determine the diffusive vapour flux moving through a homogeneous geology between a hydrocarbon and source a building, also including a first-order degradation applied to the aqueous phase (Turczynowicz, 1997; Hers, 2002).

Other models find steady state solutions directly.

The Johnson and Ettinger (J&E) model is currently the most-known and referenced model, suggested also as a screening tool by U.S. Environmental Protection Agency (USEPA, 1996a; USEPA, 1996b; USEPA, 2002a) and it is available as a Microsoft Excel™ spreadsheet prepared by USEPA itself (Johnson, 2005). It has been developed for heuristic purposes on the basis of Nazaroff model (Nazaroff et al., 1987) and has been officially judged as predictive and quite conservative model, but in the original version cannot consider any temporal feature changes or VOC degradation because it is a steady state model. It couples diffusion from an infinite planar source (dissolved in groundwater or as soil gas) to vapour intrusion into basements (through cracks in the foundation/floor) of buildings (located at an arbitrary distance from it) via advection and diffusion processes. Diffusion (within vapour and soil moisture phases) is considered dominant in soil whereas advection due to pressure differentials prevails within close proximity of the foundation. The hypotheses of this 1-D model are: homogeneous soil, instantaneous and linear equilibrium between different phases, as in (3.14), advection described by (3.11), diffusion due to (3.18), and the conservative assumptions of absence of chemical or biological reactions. All vapours originating directly below the basement will enter it, unless the floor and walls are perfect vapour barriers. In general, however, the unsaturated soil zone may be composed of distinct soil layers which give an overall diffusivity calculated similarly to resistors linked in series. A crack area is needed to determine the building contaminant entry rate (Q_{soil}, generally ranging from 1 to 10 l min^{-1} for houses on coarse-grained soils (Hers et al., 2003)) using a mass transport balance approach; a further steady state mass balance is used to produce an expression for indoor air concentration. In order to be precautionary, the model, presumes that the building structure is directly above the source and is small relative to the source extension (Devaull et al., 2002). It is suitable for both a constant and infinite source and a depleting one, where the concentration decreases initially near the layers closest to the building floor and walls, thus reaching, in that case, a quasi-steady state solution (Johnson et al., 1991).

Field validation of the J&E model by assessment of attenuation factors (predicted versus measured levels of volatiles in soil gas and indoor air expressed as a ratio) was undertaken by various investigators (Fitzpatrick et al., 2002; Roggemans et al., 2001; Devaull et al., 2002; Johnson et al., 2002b; Hers at al., 2003), finding over-prediction by models of several orders of magnitude for biodegradable compounds, whereas the model seems to fit well when biodegradation is insignificant (Johnson et al., 2002a).

The model has, in fact, been changed over time by the authors to include biodegradation too. Initially a first order biodegradation process was introduced, describing reactions occurring in soil moisture, and based on soil column experiments, then a "dominant layer model" was presented, where biodegradation is confined into a layer bordered by two zones without reactions (Johnson et al., 1998). Then Devaull added (for a multi-component mixture of VOCs) a limited oxygen availability, based on a set of conservation equations, including diffusion and oxidation reaction of chemicals due to oxygen. This model is solved by iteratively varying the aerobic depth of a sort of "dominant layer" to match oxygen demand to oxygen supply (Devaull, 2007). Another evolution of the model contains a sensibility analysis package based on Monte Carlo technique in order to place certainty bounds on the model results (Mills et al., 2007).

Various kinds of software for RA contain J&E transport model. The most famous commercial softwares are RISC (RISC, 2010) and RBCA, both by GroundwaterSoftware.com. The former joins multiple available applications of J&E model, as described in Tab.3.2.

***Tab.3.2**: different J&E model versions available in RISC Software (from Davis et al., 2009).*

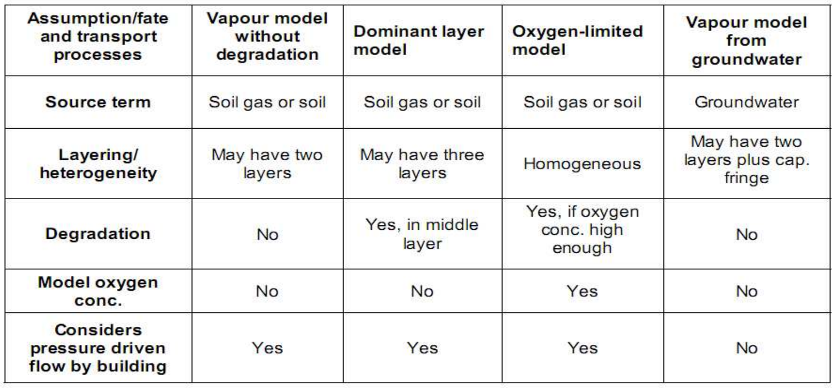

Assumption/fate and transport processes	Vapour model without degradation	Dominant layer model	Oxygen-limited model	Vapour model from groundwater
Source term	Soil gas or soil	Soil gas or soil	Soil gas or soil	Groundwater
Layering/ heterogeneity	May have two layers	May have three layers	Homogeneous	May have two layers plus cap. fringe
Degradation	No	Yes, in middle layer	Yes, if oxygen conc. high enough	No
Model oxygen conc.	No	No	Yes	No
Considers pressure driven flow by building	Yes	Yes	Yes	No

in the United Kingdom, Ferguson et al. developed a simple screening steady state analytical model of vapour intrusion from an infinite soil source directly beneath the dwelling in the case of a typical semi-detached house. The model is based on contaminant equilibrium partitioning into the soil-vapour phase (3.14), diffusion (3.18), involved also in indoor intrusion, biodegradation by (3.27), suction flow using (3.11), and building ventilation as a function of ingoing and outgoing air fluxes through holes, cracks and open doors and windows. It may also take into account air contaminant contributions from other sources (e.g. stack emissions, road traffic, smoking in the living space and volatilization of certain domestic chemicals inside the house). The model considers both houses with ground-bearing concrete slabs (called also slabs-on-ground) (Ferguson et al., 1995) and ones with subfloor voids with a structure available also for monolithic concrete raft foundations and clean cover systems (Krylov et al., 1998).

Ririe et al. evaluated gas diffusion from a slice of contaminated soil considering biodegradation. Its kinetic was calculated considering that oxygen replenishment is the limiting factor controlling the rate of the biodegradation reaction and that oxygen concentration gradient can be evaluated for steady state conditions. Thus they calculated an α factor, relating attenuation and diffusive transport, to adjust 1-D Orange County Health Care Agency (OCHCA) Vapour Diffusion Model which had only considered diffusion before (Ririe et al., 2002).

Parker presented a complex model to simulate emission towards indoor space from contaminated soil, groundwater or NAPL finite sources. In the last case, initial vapour concentration near the source is given by repartition and Raoult’s laws (§ 2.2.2). Transport phenomena are described by a modified J&E model, considering advection for pressure variations, vertical diffusion, biodegradation including an oxygen-limited kinetic (due to limiting oxygen diffusive-dispersive or advective transports towards the building) (Parker, 2003).

A further step in the analytical approach to understand vapour intrusion is given by Lowell et Eklund model, that evaluates the effect of the distance from the side of the house to the contamination source, considering only diffusive transport. The simple solution is based on a Fourier series approach and is expressed as a decreasing exponential function (Lowell et al., 2004).

Tab. 3.3 presents a summary of the features of the transport model cited above, as what gas phase is concerned. Another useful table with information only on analytical and semi-analytical models is available in Lahvis (2010).

***Tab. 3.3**: summary (in alphabetical order) of comparison between numerical and analytical models cited in § 3.4; num-fd: numerical at finite difference; num-fe: numerical at finite elements; an: analytical; NAPL: already implemented for cases with NAPL; y: yes; n: not; *: advection due to gas density is considered, too; #: contribution of other indoor material is considered, too.*

Model	**type**	**domain**	**gas diffusion**	**gas-phase advection**	**biodegra-dation**	**time variable**	**indoor**	**NAPL**	**source**
Abreu and Johnson	num-fd	3D	y	Y	y	y	y	n	Abreu et al., 2005; Abreu et al., 2006
Baehr	num-fd	2D	y	N	n	y	n	y	Baehr, 1987
Baehr	an	1D	y	N	n	y	n	n	Baehr, 1987
Choi	num-fd	1D	y	Y	n	y	n	n	Choi et al., 2002
Comsol Multiphysics	num-fe	3D	y	Y	y	y	y	n	Bozkurt et al., 2009; Pennel et al., 2009; Pennel et al., 2010
Csoil of RIVM	num-fd	1D	y	N	n	y	y	n	Van den Berg, 1994
Dominant layer model	an	1D	y	Y	y	n	y	n	Johnson et al., 1998
EPA-97	num-fe	1/2/3 D	y	Y	y	y	n	y	Guarnaccia et al., 1997
Ferguson et al	an	1D	y	Y	y	n	y	n	Ferguson et al., 1995; Krylov et al., 1998
IMPACT	num-fd	2D	y	N	y	y	n	n	Sanders et al., 1997
Jeng	an	1D	y	N	y	y	y	n	Turczynowicz, 1997; Hers, 2002
Johnson and Ettinger -91	an	1D	y	Y	n	n	y	n	Johnson et al., 1991
Jury	num-fd	2D	y	N	n	y	n	n	Jury et al., 1982
Jury -80	an	1D	y	N	n	y	n	n	Jury et al., 1980
Jury-83	an	1D	y	Y	y	y	n	n	Farmer et al., 1980; Jury et al., 1983; Jury et al., 1984; Jury et al., 1990
Lin and Hildemann	an	1D	y	Y	y	y	n	n	Lin et al., 1995
Little	an	1D	y	N	n	y	y	n	Little et al., 1992
Lowell et Eklund	an	2D	y	N	n	n	y	n	Lowell et al., 2004

Tab. 3.3*: continued.*

McCarthy	num-fd	1D	y	n	n	y	n	n	McCharthy et al., 1993
Mendoza	num-fe	2D	y	y*	n	y	n	y	Mendoza et al., 1990a; Mendoza et al., 1990b
MOFAT	num-fe	2D	y	y	y	y	n	y	Katyal et al., 1991
Olson and Corsi	num-fd	2D	y	y	y	y	y#	n	Olson et al., 2001
oxygen limited layer	an	1D	y	y	y	n	y	n	Devaull, 2007
Park	num-fd	1D	y	y	n	y	y	y	Park, 1999
Parker	an	1D	y	y	y	y	y	y	Parker, 2003
Ririe	an	1D	y	n	y	n	n	n	Ririe et al., 2002
RTI	an	1D	y	n	y	y	n	n	USEPA, 1994
R-UNSAT	num-fd	1/2D	y	y	y	y	n	y	Lahvis e al., 1998
Sanders and Stern	an	1D	y	n	y	y	y	n	Sanders and Stern
Sleep and Sykes	num-fe	2D	y	y*	y	y	y	n	Sleep, 1998
SoilRisk	an	1D	y	n	y	y	n	n	Labieniec et al., 1996
SoilRisk	an	2D	y	n	y	y	n	n	Labieniec et al., 1996
TOUGH	num-fd	3D	y	y*	y	y	n	n	EOLBNL, 1999
Turczynowicz and Robinson	num-fd	3D	y	y	y	y	y	n	Turczynowicz et al., 2001
VENT2D	num-fd	2D	y	y	n	y	y	y	Benson, 1994
VLEACH	num-fd	1D	y	n	n	y	n	n	Chen et al., 1995; USEPA, 1996a; Ravi et al., 1997
VolaSoil of RIVM	num-fd	2D	y	y	n	y	y	y	Waitz et al., 1996; Van Wijnen et al., 2006; Provoost et al., 2009a

4

VOLATILISATION FLUX DETERMINATION

4.1 Techniques of measurements

Protocols for air sampling are not widely used and often limited to soil gas acquisition, whereas an effort must be made to develop uniform guidelines based on information reached from previous field tests (Hers et al. 2001).

As § 1.3 has already presented, direct measurements may be influenced by environmental back values or local point sources, where problems of accuracy and representativeness may arise. The direct quantification of volatilization flux determinations is most of all suggested, especially for outdoor spaces (where there are no local preferential paths or sources located along vertical walls) (Politecnico di Milano et al., 2010), even if it may sometimes be expensive and time-consuming (Lin et al., 1995). With this approach background concentrations are taken off and no transport model, with its uncertainty and poor site-specific description, is necessary.

As for vapour intrusion, indoor air direct measurements and sub-slab foundation field measurements are the only proper methods to perform (Hartman, 2004). There are, however, still problems, linked to these techniques, due to background sources and/or spatiotemporal variability (Hers et al., 2001; Tillman et al., 2005; Folkes et al., 2009).

The present dissertation will only focus on outdoor measurements, which may be managed by aerodynamic or closed chambers methods.

4.1.1 Aerodynamic methods

Micrometeorological (called also aerodynamic) methods include several techniques used to quantify vapour flux. They are based on the theory that the transfer of any conservative entity from a surface to the atmosphere is governed by atmospheric turbulence, which is due to wind moving over the surface. The vertical fluxes may be expressed as flux gradient equations of wind, temperature, and contaminant concentrations in the air above the soil (Zhang et al., 2002).

These methods are advantageous because the surface of emission is not influenced directly by measurements, provide large areal average of fluxes, and do not require any dispersion model to be applied afterwards (Lindberg et al., 1995; Rayment et al., 1997).

All fluxes are characterized by equations (Chen et al., 1995, Majewski et al., 1990) and the best known ones are:

- aerodynamic (AD) vertical profile technique;
- energy balance-Bowen ratio (EB);
- eddy correlation (EC) method;
- integrated horizontal flux (IHF) method;
- theoretical profile shape (TPS) method based on a trajectory simulation;
- concentration-profile (C-P) technique ;
- transect technique.
- model of turbulent dispersion.

4.1.1.1 Aerodynamic method

Aerodynamic (AD) method is based on Thornthwaite-Holzman theory, containing the hypothesis of logarithmic wind vertical profile. The contaminant flux F emitted from the soil is given by:

$$F = \frac{k^2 * \Delta C * \Delta u}{\varphi_m * \varphi_c * \left(\ln \frac{z_2}{z_1} \right)^2} \tag{4.1}$$

where k is a constant (generally posed equal to 0.4), ΔC [M L^{-3}] and Δu [L t^{-1}] are respectively average differences of gas concentrations and horizontal wind speeds between heights z_1 and z_2 [L], φ is the stability correction function for the vapour momentum (φ_m) and the compound (φ_c) obtained by empirical expressions, which depend on ambient temperature T and vertical gradient of T and v (Majewski et al., 1990).

The theory of this method is well documented (Glotfelty et al., 1984) and has been used for years; it needs relatively simple instrumentation but requires a large and uniform surfaced area, an upwind distance (fetch) of at least 100 times the height of the instruments, ensuring in this way that the fluxes are constant at that height (Yates et al., 1997). Furthermore it requires a high degree of accuracy in the gradient measurements and may fail during low-wind situations. Besides k is very difficult to define well.

4.1.1.2 Energy Balance method

Energy Balance (EB) method, called also Bowen Ratio method, is based on an energy balance, between the net radiation (R_n), the soil heat flux (G), the sensible heat flux (H) and the latent heat flux (LE):

$$R_n + G + H + LE = 0. \tag{4.2}$$

R_n and G are measured directly; the ratio H/LE (called Bowen ratio), is proportional to the ratio of sensible to latent heat flux and to air temperature and water vapour pressure gradients along vertical direction. H is derived from (4.2), and using dT/dz, the specific heat of dry air at constant pressure (C_d) and the air density (ρ_a), the turbulent exchange coefficient for sensible heat (K_H) is achieved with:

$$K_H = H/[\rho_a * C_d * (dT/dz)] \tag{4.3}$$

and finally F is obtained as:

$$F = - K_H * (dC/dz) \tag{4.4}$$

where the negative sign indicates vapour movement away from the surface (Majewski et al., 1990).

A modified Bowen Ratio is used too; based on the assumption that the transport characteristics for heat and scalars are equal, it therefore uses temperature and a trace gas vertical gradient (such as water vapour or carbon dioxide) to define the flux of the interested chemical (Lindberg et al., 1995; Meyers et al., 1996; Poissant et al., 1998). It is suitable for the same conditions of AD method, but is applicable for any surface roughness and also in cases with low wind because the horizontal wind speed is not a critical measurement.

Problems sometimes arise when measurements are performed in the afternoon/evening with the minimum evaporation, and in general, for fluxes measured downwind that are actually influenced by the soil contamination outside the examined area.

4.1.1.3 Eddy correlation method

Eddy correlation or covariance (EC) method is based on the theory that, due to atmospheric turbulence, all measured parameters (w) have fluctuations (w’) as for their mean value ($\overline{w}$).

The mean vertical flux F is proportional to the time-averaged mean of product between the instantaneous deviations of vertical wind velocity (u’) and of the contaminant volumetric gas concentration (C’):

$$F = \rho_a * \overline{u'C'} \tag{4.5}$$

The difficulty linked to this method is due to the necessity to collect C data with a very high frequency, with fast-response sensors, and it is only suitable for vapour fluxes at some height above the ground, typically 1-2 m (Norman et al., 1997; Poissant et al., 1999).

4.1.1.4 Integrated Horizontal Flux method

Integrated Horizontal Flux method (IHF) is based on a time-averaged mass balance technique, and the flux is calculated as:

$$F = \frac{1}{x\int_0^\infty \overline{u} * \overline{C}\, dz} \tag{4.6}$$

where x is the upwind distance to the leading edge of the source, and $\overline{u}$ and $\overline{C}$ are the averaged wind speed and air concentration at height Z.

This method neither requires atmospheric stability corrections, and neither a long fetch, it requires only single-point measurement therefore reducing the numbers of samples and the analysis time, but it is not suitable in very low wind conditions, and it is limited to bare surfaces (Yates et al., 1997).

4.1.1.5 Concentration-profile

The concentration-profile (C-P) technique was developed by Thibodeaux and predicts F upon experimental measurements of wind velocity and direction, temperature profile above the involved site, VOC concentration (located in six logarithmic intervals and requiring very low detection limit for dilution in the atmosphere), water temperature and its sampling, according to the relationship:

$$F = \left(\frac{D^g}{D^g_{H2O}} \right)^n \frac{S_V S\, K^2}{\varphi^2_m S_c} \tag{4.7}$$

where D^g_{H2O} is the molecular diffusivity in air of water vapour, K is a constant, S_V is the logarithmic slope of the air velocity profile, n is exponent diffusivity ratio, S is the logarithmic slope of the contaminant concentration profile, Φ_m is wind shear parameter, S_c is turbulent Schmidt number, and the products of the two last terms represent a correction factor influenced by atmospheric stability (Balfour et al., 1987).

4.1.1.6 Transect technique

The transect technique uses horizontal and vertical arrays of samplers to define i-concentrations within the effective cross-section of the fugitive emission plume emitted from areal and line sources.

It is based on the integration of the measured concentrations over the assumed plume area, the surface area of emitting source (A), u, C (corrected for upwind background) at each point (h, w) inside the effective cross-sectional area of plume (A_p), that extends along h and w directions, according to the relationship:

$$F = \frac{u \int\int_{A_p} C_i\,(h, w)\; dh\; dw}{A} \tag{4.8}$$

During the sampling period also meteorological parameters are monitored (Balfour et al., 1987).

4.1.1.7 Theoretical profile shape method

Theoretical profile shape (TPS) technique does not require many experimental data and it is based on a two-dimensional trajectory simulation model describing a contaminant flux from a circular source. A single measurement of horizontal u and C taken above the centre of the source plot is enough. The flux is given by the ratio between measured data and normalized horizontal flux predicted by the model (Majewski et al., 1990).

4.1.2 Enclosure methods

Although micrometeorological techniques allow net gas exchange rates to be quantified, there are many sites and logistical aspects to consider where they are not appropriate (Livingston et al., 1995). They in fact are: elective for extensive sites, often not valid at ground surface, dependent on rates of exchange from the soil to atmosphere and therefore highly variable in space and time. They generally have poor resolution and furthermore need suitable sensors or sampling mechanisms that are often not available or too costly (Woodrow et al., 1991; Rayment et al., 1997, Hutchinson et al., 2002; Reichman et al., 2002).

F is therefore more often evaluated using a nonintrusive closed method like flux chamber or wind tunnel (Reinhart et al., 1992) that have been applied to measure soil respiration for many decades, starting with preliminary applications in the '30s (Davidson et al., 2002). As a note, wind tunnels are similar to chambers, but i) have a completely horizontal development of air flowing inside the tunnel, ii) require higher sweeping air (generally above 1800 l min^{-1}) giving a velocity between 0.7 and 1.3 m sec^{-1} and iii) are mostly applied to odour monitoring; in fact, due to dilution given from these flow rates they would necessitate too low analytical detection limits for VOC application (Jiang et al., 1996; Capelli et al., 2009).

The aim of enclosure methods is to isolate a volume of air layering over a surface (ground or liquid) without perturbing either the natural F across that surface, or consumption or transport of the analyzed substances (Batterman et al., 1992). Any net emission or uptake inside the enclosed system may be measured as a concentration change.

To sum up, flux measurement provides a direct method for obtaining the input term needed in dispersion models (such as box model, § 1.3), and is therefore indicated in different points of RA, such as assessing the extent of subsurface contamination during characterization phase or monitoring the behaviour of remedial actions (Batterman et al., 1992; Bohme et al., 2005). This technique is relatively low-cost, simple to operate, versatile (Schwartzkopf, 1978), requests minimal manpower as compared to methods in § 4.1.1, possesses great intrinsic sensitivity (if coupled with proper sampling/analytical techniques, § 4.2.5), permits simple data elaboration, is less affected by environmental factors than meteorological techniques and provides discrete information on different space and time scales (Eklund et al., 1985, USEPA, 1986; Xiao et al., 1991; Reinhart et al., 1992; Kim et al., 1995; Livingston et al., 1995; Hutchinson et al., 2002).

Enclosure techniques are not applicable in all situations because of their inherent limitations (Trevitt et al., 1988; Baldocchi et al., 1991) and offer both advantages and disadvantages for dealing with spatial heterogeneity of fluxes. Where site variation is known, they may be displaced to measure the importance of specific variability (Allaire et al., 2002); on the other hand, since identifying heterogeneity is very hard, proper decision on how many chambers are needed to adequately estimate the mean and variance of vapour fluxes (§ 4.2.3) is difficult to define (Yates et al., 1996; Wang et al, 1997; Davidson et al., 2002; Reichman et al., 2002). In particular, they may not be applied in closed spaces, where flux critical permeable zones (cracks, conducts, walls junctions/corners) are difficult to close by a covered structure. Furthermore they are unsuitable in basements or any other subterranean enclosures, because the lateral underground surfaces (that are not object of measurements) could also be a source of vapour flux.

Their use to predict fluxes in future structure is in discussion too: on the one hand, the measured flux could be over-estimated because there is no building foundation preventing the flux, whereas, on the other hand, it could be under-estimated, for example for the lack of pressure inducing advective flow (Hartman, 2003).

However enclosure methods represent a cost-effective technique suitable for many different survey objectives, on many spatial and temporal scales.

4.2 Flux chamber

Flux chamber (FC) instrument was designed originally to calculate emissions of biogenic inorganic gases (Mosier et al., 1991; Eklund, 1992) in the oceanographic, soil science, and natural resource exploration (Hartman, 2003). In the early 80’s U.S. Environmental Protection Agency, in collaboration with Radian Corporation, started to look at this apparatus to measure F over contaminated soils from different kinds of sources. U.S.EPA identified the flux chamber as a recommended method to apply on Superfund sites (Eklund, 1992) and elaborated a protocol (that has no value as regulatory guidance) useful in designing, building and using this instrument. A parallel branch of research implemented its application over liquid surfaces and produced a specific monitoring guide (Eklund, 1992).

There are various types of chambers, different in geometry, material and the scope of their application. They are classified on the basis of i) the operating conditions that are performed during measurements (Hutchinson et al., 2002) and ii) the advective conditions under the chamber (Hutchinson et al., 1981; Livingston et al., 1995; Hutchinson et al., 1993); there are strong differences in advantages, limitations, assumptions and complexity for the different kinds of design.

In Fig. 4.1 there is a sketch to classify enclosure configurations: along vertical axis there are i) possibilities; in particular where there is an accumulation of pollutant mass inside the chamber a recirculation may be applied or not. Along the horizontal axis there is classification in vented or non-vented systems, according to ii) classification. As it is reasonable, steady state systems using mixing flow by definition are inherently open because of their open-path circulation (Livingston et al., 1995).

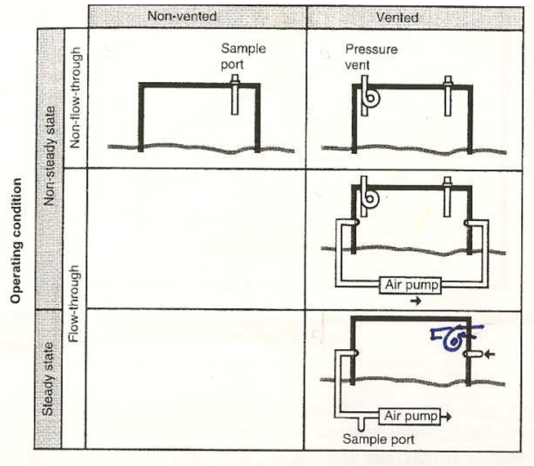

Fig. 4.1*: classification of enclosure configurations according to parameters i) (along vertical axis) and ii) (along horizontal axis) used in the text (Livingston et al., 1995, modified).*

4.2.1 Operating conditions

As regards i), molecular diffusion inside the chamber may be stable (in steady state conditions) or not.

4.2.1.1 Non- steady state systems

Non-steady state systems are really easy to apply, since it is enough to put the chamber over the interested area for a meaningful time (from about 5 hours to 10-12 days (Rayment et al., 1997; Frez et al., 1998; Hutchinson et al., 2002) and sample, collecting small volumes (Nay et al., 1994) at different times or better one at the end of the deployment in order to avoid disturbances (Hutchinson et al., 2001). There is no introduction of gas into the chamber during the incubation period, so the contaminant vapours accumulate in the trapped stagnant chamber volume, making their concentration build up over time (Hartman, 2003). This alters diffusion gradients with the soil profile, pushes vapours to diffuse laterally and to escape from the soil outside the chamber base (Davidson et al., 2002), making the concentration F_{ig_diff} decrease (Denmead, 1979; Davidson et al., 2002; Hartman, 2003; Pumpanen et al., 2004) – that may be in part corrected by proper data treatment (§ 4.2.6).

Enclosure dimensions and sampling time have to be properly selected for each application and data have to be treated according to proper functions presented in literature. These systems are also called static or closed.

Non-steady state apparatus is suitable for short periods of measurements (Hutchinson et al., 1981; Gao et al., 1998), for rapid flux changes (whereas the other kind of chambers tend to moderate them) (De Mello et al., 1994) and to quantify low exchange rates because there is no additional mixing flux that makes the measured concentrations decrease (Hartman, 2003). It is cheap, simple because it does not need technological devices (whereas the dynamic one needs inner re-circles (§ 4.2.4.6)) and allows to use several chambers at the same time. Minimizing the time that the chamber is on the soil may reduce the artefacts caused by altering the vapour concentration gradient within the soil profile and between the soil-atmosphere and the chamber headspace (Davidson et al., 2002; Hartman, 2003); for some authors this technique, if well applied, gives the same results as steady state FC (Valente et al., 1995) whereas for others it gives underestimation of 4-14 % (Pumpanen et al., 2004) to half of real flux (Norman et al., 1997).

A similar apparatus, called gas suck chamber, is used for preliminary estimates, which consists in a non vented chamber connected, through a sample port, to a suck system for 1-6 hours, involving also air from soil adjacent to the chamber (Bohme et al., 2005).

4.2.1.2 Steady state systems

In steady state systems (Fig. 4.2) the gas concentration gradient, giving F_{ig_diff} (3.18) is assumed constant after an initial transitional adjustment period (Gao et al., 1997). This condition may be given by introducing an absorptive surface under the chamber, in closed passive[3] FC (Batterman et al., 1992; Norman et al., 1992) and leaving it enough time (several days) to collect sufficient material for accurate analysis (Brown, 1993).

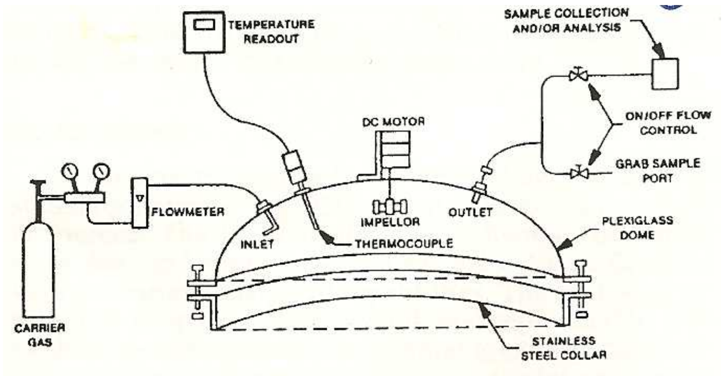

***Fig. 4.2**: Generic sketch of dynamic state chamber (Eklund et al., 1985).*

Another possibility is to operate a sweep inside the chamber, at a flow Q_{in}, by performing an open path circulating system with a constant injected air flow with known features. The same effect may be reached by a close inner re-circle where outflow is sucked on sorbent tubes trapping the chemical vapours and then flushed again inside the FC (Smith et al., 1996; Jellali et al., 2003; Tillman et al., 2004). Sweep gas may therefore be achieved by a positive pumping force or by a negative suction one (Sanders et al., 1985; Sartin et al., 2000).

---

[3] Passive chambers are different from simply burying adsorbent tubes into the cracks of the slab, utility conduits, or room edges, that adsorb also environmental air and do not give quantitative results because it is unknown the volume of air that passes through the adsorbent while it is emplaced (Hartman, 2003).

Sufficient time has to be spent in order to reach a new equilibrium between soil and covering apparatus (Denmead, 1979); it is evaluated as the amount of time required to obtain negligible changes of the researched compound; for this scope an in-line sensor to monitor in real time could be suitable (Jury et al., 1982) or some shut off test tracer gas may be performed (Eklund et al., 1985). It is however generally reached after 3-7 hydraulic retention time, HRT (Denmead, 1979; Schmidt et al., 1983; Eklund et al., 1985; Dupont et al., 1986; Batterman et al., 1992; Eklund, 1992; Hartman, 2003), that is defined as the ratio between the volume of the chamber to Q_{in}. Literature values are generally included between 2 and 20 min (Tab. 4.3), with an average value of 10 min. The measurements start therefore directly in stationary conditions (Gao et al., 1998), because, after the initial flushing, the vapour concentration flowing outside the chamber is the same as under it. A well mixed reactor guaranteeing a sufficient turbulence is thence necessary to reach perfect homogeneity of concentrations and therefore a meaningful sampling.

Perturbations of the original flux are minimized by optimizing the flow-rate and the system of introduction of the mixing flow (§ 4.2.4.6), obtaining higher precision than with static chamber (Fang et al., 1998). Since this system uses a flow gas it is also called dynamic or open chamber. It allows data to be collected in dynamic conditions, as really happens in natural systems and it is difficult to apply with other techniques (Xiao et al., 1991). It is in fact indicated for monitoring fixed locations over extended or repeated time periods and it has been demonstrated to induce smaller changes in the subsurface gas concentration gradient than non-steady state one (Denmead, 1979; Gao et al., 1997; Norman et al., 1997; Hutchinson et al., 2002). Disadvantages include the fact that it is more complicated to perform because it needs additional apparati (sweep gas tanks, flow controller, connections, …) and sweep gas may perturb natural vapour emissions; it may in particular give a pumping effect increasing the estimation, or move gas towards the soil, especially for permeable soils, reducing the flux estimation (Cooper et al., 1994; Hutchinson et al., 2002).

4.2.2 Advective conditions

As for ii) point, advective transport inside the system is allowed to happen if there are vented enclosures to communicate atmospheric pressure changes and fluctuations inside the enclosed environment, and perturbing less, in this way, the natural mass flow across soil-atmosphere interface. In not-vented systems this natural advective transport is suppressed.

4.2.3 General common indications

Chamber artefacts and biases may cause serious errors in flux measurements, but they are well described in the literature and may be minimized or avoided with proper chamber designs, data analyses, and spatial and temporal sampling regimes (Davidson et al., 2002). Fixing detailed plans defining site-specific conditions and positions to sample is important to perform a monitoring campaign with FC correctly.

After having located the equipment instruments, the chamber is emptied to purge from pollutant environmental air in order to measure only the contribution from soil; for stationary chambers it is done directly by the sweep gas used to reach stationary conditions.

A good practical law is to execute a “blank” measurement, before and after monitoring, consisting in measuring the flux when the chamber is put on an inert clean surface (such as a Teflon layer), far from areas of known contamination on test site, in order to check possible releases of pollutant only due to the system (Eklund et al., 1985; U.S.EPA, 1986; Matthews, 1987; Schmidt, 1991; Xiao et al., 1991; Eklund, 1992; Carpi et al., 1998; Poissant et al., 1998; Poissant et al., 1999; Wallschläger et al., 1999). Cleaning the whole employed apparatus to remove any contaminant residuals is in fact suggested. In literature there are various suggestions according to the pollutant behaviour: using a commercial dish-washing product, followed by a laboratory one and then rinsing with a solution of HNO_3 and water (1%) (Roffman et al., 1995; Poissant et al., 1998); using an acid or an alkaline detergent and then drying (-for mercury- Kim et al., 1995; Wallschlager et al., 1999); simply fluxing some clean air or nitrogen on the walls (De Mello et al., 1994; Hartman, 2003) or washing with some water and then drying (USEPA, 1986). Storing the chamber in a clean room and transporting it onto the field in clean plastic bags is suggested in order to lower field blanks (Poissant et al., 1999; Magarelli et al., 2005). Particular attention should be paid to not leaving the chamber at ambient air in particularly contaminated places, to avoid cross-contamination (Wallschlager et al., 2002).

The measurements have to be repeated as a minimum twice a year, in the wet and dry seasons at least (Davidson et al., 2002; Parkin et al., 2003), better seasonally (Folkes et al., 2009), in order to consider the effect of different factors influencing vapour flux (§ 3.1) and obtain a full idea of the potential exposure on the site (Politecnico di Milano et al., 2010).

A preliminary survey of the site is always suggested in order to avoid local anomalies, and to define the right number and position of sampling points necessary to note special variability and heterogeneities (Cropper et al., 1985; Batterman et al., 1992; Davidson et al., 2002; Parkin et al., 2003); the area covered by a chamber influences the number of chambers needed. According to the scope of the sampling campaign, possible approaches may be to adopted: a systematic random sampling, entailing a plot grid and a random number table, (Schmidt et al., 1983; Eklund et al., 1985; Dupont et al., 1986; Schmidt et al., 1998b); selection of expected centres of contamination (Roffman et al., 1995) or again a method, guided by known chemical distribution, to maximize the between-zone variability and minimize the within-zone one (USEPA, 1986).

According to this indication, U.S.EPA suggested a relationship to define the number of units of grid to be sampled in a zone of area A_{zone} (expressed in m^2) (USEPA, 1986):

$$n_{grid} = 6 + 0.15\sqrt{A_{zone}} \qquad (4.9)$$

To estimate the number (n) of individual flux measurements needed for various degrees of precision at various confidence levels, Davidson et al., suggest performing a large sampling numbers (N), and testing the data population for normality. Then the following relationship is applied:

$$n = \left(\frac{t * s}{\text{range}/2} \right)^2 \tag{4.10}$$

where t the t-statistic for a given confidence level and degrees of freedom, s the standard deviation of the full population of N measurements, and range is the width of the desired interval of the full population mean in which a smaller sample mean is expected to fall. For example, from Davidson et al.'s experience, six flux measurements gave a mean that fell within ± 20% of the full population (N=36) mean with 80-90% confidence, and within ± 30% with 95% confidence (Davidson et al., 2002)

Once the flux (§ 4.2.6) in each field zone has been calculated (F_j), the mean exchange rate F_{mean} for the total area is given by:

$$F_{mean} = \sum_{j=1}^{m} \alpha_j * F_j \tag{4.11}$$

where α_j is the fractional area where F_j has been measured. Its variance $V(F_{mean})$ is similarly computed by:

$$V(F_{mean}) = \sum_{j=1}^{m} \alpha^2{}_j * V(F_j) \tag{4.12}$$

where
$$V(F_j) = s_j^2 / n_j \tag{4.13}$$

from s_j that is the variance from n samples taken in zone j (Livingston et al., 1995). N should be a great number (higher than 20-30), otherwise classical descriptive statistics are not proper.

Literature indicates that distribution of chamber-based estimates are probably often log-normal or at least strongly positively skewed, (because they derive from stratified sampling approach on a very variable space, where F may vary from one to two orders of magnitude across a distance less than a meter) (Hutchinson et al., 1993), and therefore other data summaries are suggested (Livingston et al., 1995).

During the measurements some data are suggested to be recorded, such as data of time, sweep gas and sampling flow rate, inner and outside chamber air temperature by some thermocouples or thermistors (Matthias et al., 1980; Cropper et al., 1985; Eklund et al., 1985; Norman et al., 1992; Wang et al, 1997; Wallschläger et al., 1999; Pumpanen et al., 2004; Martins, 2010) and humidity (De Mello et al., 1994), surface soil temperature (at -1 ÷ -6 cm below ground surface) adjacent to the chamber, by using for example thermocouples probes (Dupont et al., 1986; Eklund, 1992; Norman et al., 1992; Carpi et al., 1998; Wallschläger et al., 1999; Parkin et al., 2003), gas pressure, possibly pressure difference between inside and outside FC with micro differential pressure sensor/transducer/transmitter (Lund et al., 1999; Widen et al., 2003; Pumpanen et al., 2004), wind speed and direction (Eklund, 1992), and general indications on soil physical aspects (Dupont et al., 1986) and weather data (Yates et al., 1997; Wallschläger et al., 1999; Parkin et al., 2003), for the reasons that are explained in the next few paragraphs (USEPA, 1986, Livingston et al., 1995;

Poissant et al., 1999; Magarelli et al., 2005; Bahlman et al., 2006). The instruments should be checked and calibrated routinely (Schmidt et al., 1983).

As a general indication, the ideal monitoring device would be simple, low cost, accurate, portable and self-contained, permitting easy deployment and good areal coverage (Batterman et al., 1992). Next paragraphs will deal with the specific aspects of a flux chamber.

4.2.4 Design considerations

For the same kind of chamber, different design features can be defined, varying for chamber geometry, fabrication material, deployment, sweep gas introduction, temperature control, monitoring of vapour concentrations, mixing system and sampling line (Eklund, 1992). There is not a general indication, but the measurement system in toto should be designed according to the site features and magnitude of exchange rates, remembering that these devices can perform the representativeness of the measure (Gao et al., 1997); some authors have employed numerical simulations to see the effect of different possible configurations in order to minimize errors (Hutchinson et al., 2001; Zhang et al., 2002).

4.2.4.1 Chamber geometry

Some simple fluid-dynamic simulations have been performed to define the effect of FC geometry on measured F. Chambers are classified according to their volume to basal area ratio (H=V/A): the lower H is, the more rapidly the chamber responds to concentration gradients influencing molecular diffusion across the surface; the less constant the rate of concentration is, change in time and perturbations due to sampling line the stronger are (Matthias et al., 1980; Zhang et al., 2002); as an advantage however they require shorter sampling times to obtain concentration differences and they are more easily homogeneously mixed (in case of not extreme conditions, where width is more than 2 orders of magnitude than other measures (Wallschlager et al., 2002)).

As a general indication, for non-steady state FC, H should be large enough to minimize disturbance of the enclosed surface (especially for measurements with vegetative field), but small enough to avoid vertical gradients, to allow measurements of concentration changes in the shorter feasible time of measurements (getting a clearer idea of F over time), and to reach wanted sensitivity (Wallschläger et al., 1999; Davidson et al., 2002).

H may differ widely in cases reported in literature, from 2.5 to 170 cm, with an average value of 15-20 cm (Tab. 4.1; Parkin et al., 2003). In particular for dynamic chamber, H is linked to sweep flux to allow for time required to achieve stationary conditions before starting to sample (Eklund, 1992).

The ideal geometry of the chamber should not create dead volumes or corners or inhibit mixing inside it (Eklund, 1992; Cooper et al., 1994). Cross-section is generally rectangular or circular with area typically ranging from 175 cm^2 to 1 m^2, with preferential values of 300-900 cm^2 (Tab. 4.1; Davidson et al., 2002; Hutchinson et al., 2002). Smaller chambers are easier to transport, simple to fabricate, allow shorter time to reach steady state, ensure better uniformity under enclosed spaces, ever with smaller sweep flows, but areas perturbed by chamber walls are a higher percentage than in bigger FC (Eklund, 1992; Lund et al., 1999) and are representative only of the specific point of measurements, requiring more sampling positions to define spatial variability properly (Sanders et al., 1985). In fact they are most of all used for studies along huge special horizontal gradient all around a point of interest. Bigger FCs need greater sweep flow to guarantee homogeneity under them which however may cause unwanted overpressure.

The cover can be planar or hemispheric; the standard U.S.EPA chamber was in fact a dome superimposed on a cylinder, but a systematic study to define the best FC geometry approved a cylinder with flat top (Adams et al., 1980 in Eklund, 1992).

***Tab. 4.1**: geometry, dimensions and material of FC found in literature; (-*: omitted datum).*

Geometry	**FC Type**	**A [m^2]**	**H [m]**	**V [m^3]**	**Material**	**Chemical**	**Reference**
Circular	Steady state	0.200	0.1-0.4	0.02-0.08	Stainless steel covered by Teflon-FEP	Hg	Bahlmann et al., 2006
Circular	Steady state	0.069	0.298	0.021	Polycarbonate covered by Teflon-PFA	CS_2 and COS	Castro et al.,1991
Circular	Steady state	0.053	0.300	0.016	Hemisphere in Plexiglass	CO_2	Cropper et al., 1985
Circular	Non-steady state	0.071	0.180	0.013	Steel base covered with hemisphere in Plexiglass	N_2O	Denmead, 1979
Circular	Steady state	0.132	0.227	0.030	Steel base with covered with acrylic dome	VOC	Eklund, 1992
Circular	Non-steady state, closed	0.018	0.175	0.003	Galvanized steel	chlorates	Frez et al., 1998
Circular	Steady state	0.012	0.035	0.0004	Glass	MeBr	Gan et al., 1996
Circular	Steady state	0.132	0.180	0.030	Steel base with covered with acrylic hemisphere	VOC	Gholson et al., 1991
Circular	Non-steady state, closed	0.011	0.136	0.002	Steel base with external surface in PVC	generic, N_2O	Hutchinson, et al., 1981
Circular	Non-steady state, closed	0.071	0.200	0.014	-*	generic	Hutchinson, et al., 2001
Circular	Steady state	0.283	0.350	0.096	Steel	VOC	Lin et al., 2003
Circular	Steady state	0.067	0.180	0.011	Polycarbonate	Hg	Lindberg et al., 2002
		0.045	0.090	0.002	Acrylic		
		0.029	0.035	0.001	Polycarbonate		
		0.024	0.110	0.002	Polycarbonate		
Circular	Non-steady state	0.071	0.05 -1	0.004 – 0.071	-*	CO_2	Livingstone t al., 2006

Tab. 4.1: *continued.*

Circular	Steady state	0.322	1.000	0.322	Hemisphere in polyethylene	CO_2	Lund et al., 1999
Circular	Steady state	0.122	0.178	0.027	Similar to USEPA, 1986	generic	Martins, 2010
Circular	Steady state	0.608	0.170	0.103	Metal	N_2O	Matthias et al., 1980
Circular	Non-steady state	0.035	0.200	0.007	PVC	CO_2	Nay et al., 1994
Circular	Non-steady state open dynamic	0.004	0.182	0.0008	Base in PVC	CO_2	Norman et al., 1992
Circular	Dynamic non-steady state (LI-6200 system)	0.008	0.125	0.001	Base in PVC	CO_2	Norman et al., 1997
	Closed non-steady state (Crill system)	0.250	0.284	0.071	-*		
	Closed non-steady state (Savage system)	0.041	0.195	0.008	-*		
	Dynamic non-steady state (Striegl system)	0.114	0.301	0.034	-*		
	Steady state (Rayment system)	0.070	-*	-*	-*		
Circular	Steady state	0.13	-*	0.01	Teflon	Hg	Poissant et al., 1998
Circular	Dynamic non-steady state	0.007	-*	0.001	PVC	CO_2	Pumpanen et al., 2004
Circular	Steady state	0.062	0.150	0.009	Steel collar and acrylic flat lid	CO_2	Rayment et al., 1997
Circular	Steady state	0.397	0.305	0.121	Stainless steel	CH_4	Reinhart et al., 1992
Circular	Dynamic non-steady state	0.01	-*	-*	Steel cylinder + glass chamber	Hg	Rinklebe et al., 2009
Circular	Steady state	0.126	-*	-*	Hemisphere in Plexiglass	Hg	Roffman et al., 1995

Tab. 4.1*: continued.*

Circular	Steady state	0.11	-*	0.055	Tedlar	VOC	Sadek et al., 1998
Circular	Steady state, dynamic with passive sorber	0.025	0.600	0.015	Stainless steel	Thichlor oethene	Smith et al., 1996
Circular	Steady state	0.061	0.150	0.0092	Polycarbonate	Hg	Song et al., 2005
Circular	Steady state	0.049	0.025	0.001	Stainless steel covered by Teflon	TCE	Tillman et al., 2004
Circular	Steady state	0.13	0.230	0.030	Steel base with covered with acrylic hemisphere, inlet and outlet in Teflon	VOC	USEPA, 1986
Circular	Closed, non-steady state	0.007	-*	0.001	-*	CO_2	Widen et al., 2003
Square	Closed non-steady State	0.010	0.15	0.002	galvanised metal internally covered by TFE		Gao et al., 1998
Square	Steady state	0.090	0.3	0.027	Teflon-FEP	dimethyl sulfide	Morrison et al., 1990
Square	Non-steady state, closed	0.093	0.043	0.004	Metal	CO_2	Norman et al., 1992
Square	Steady state	0.090	0.300	0.027	Teflon-PFA supported by a stainless steel structure	NO	Valente et al., 1995
Square	Non-steady state, closed	0.348	0.203	0.071	Teflon supported by an steel structure		
Rectangular	Steady state	0.120	0.200	0.024	Teflon-FEP supported by a stainless steel structure	Hg	Carpi et al., 1998
Rectangular	Steady state	0.350	0.059	0.021	Glass	VOC	De Bortoli et al., 1999
Rectangular	Steady state	0.050	0.035	0.002	Aluminium	Hg	Di Francesco et al., 1998
Rectangular	Steady state	0.16	0.095	0.015	galvanised metal internally covered by TFE	MeBr	Gao et al., 1997
Rectangular	Steady state	0.040	0.05	0.002	galvanised metal covered by TFE	MeBr	Gao et al., 1998

***Tab. 4.1**: continued.*

Rectangular	Steady state	0.680	0.340	0.231	Transparent Perspex	H_2O, CO_2	Iritz et al., 1997
Rectangular	Steady state, with inner recircle	0.06	0.3	0.018	High density polyethylene	TCE	Jellali et al., 2003
Rectangular	Steady state	0.120	0.200	0.024	FEP Teflon supported by a steel structure	Hg	Kim et al., 1995
Rectangular	Steady state	0.099	0.25	0.035	Glass	Organochlorine pesticides	Koblizková et al., 2009
Rectangular	Steady state	0.120	0.20	0.024	Teflon	Hg	Lindberg et al., 2002
		0.030	0.10	0.003			
Rectangular	Steady state	0.12	0.2	0.024	Acrylic	Hg	Magarelli et al., 2005
Rectangular	Steady state	7.147	1.7	12.15	ETFE foil on a stainless steel frame	MTBE, benzene	Reiche et al., 2010
Rectangular	Steady state	0.270	0.104	0.028	Plexiglass	Hg (FC of FGS)	Wallschlager et al., 1999
		0.120	0.200	0.024	Teflon	Hg (FC of GKSS)	
		0.120	0.200	0.024	Teflon	Hg (FC of GU)	
Rectangular	Steady state	0.300	0.15	0.045	Hemisphere in Plexiglass	Hg	Wallschlager et al., 2002
Rectangular	Steady state	0.6	0.3	0.18	-*	CO_2	Widen et al., 2003
Rectangular	Steady state	0.160	0.200	0.032	Stainless Steel	Hg	Xiao et al., 1991

Line length should be as short as possible, for both the inlet and the outlet, tubes about 2-3 m long with small diameter (about 6 mm), because they have strong influence on the magnitude of possible pressure deficits (§ 4.2.4.8.2) (USEPA, 1986; Eklund, 1992; Gao et al., 1998).

4.2.4.2 Material

The basic feature of a good chamber is to be built in an inert material, including sealing parts and all the inner part in contact with the gas flow (Schmidt et al., 1983; Eklund, 1992; Cooper et al., 1994; Allaire et al., 2002; Hutchinson et al., 2002), such as non permeable, non reactive and not a source or sink for the compounds of interest, which do not give memory effects (Sartin et al., 2009).

Possible materials are aluminium, stainless steel (Eklund et al., 1985) (not good for mercury (Wallschläger et al., 1999), Teflon (slightly permeable to non-polar organic compounds), FEP (Fluorinated ethylene propylene) Teflon (Morrison et al., 1990; Kim et al., 1995), transparent PFA (perfluoralkoxy) Teflon (Valente et al., 1995) or glass (Bohme et al., 2005); some plastics, such as Plexiglass, polycarbonate or ETFE (copolymer of ethylene and tetrafluoroethylene), are useful only for non-reactive gases, like CH_4, CO_2, CS_2/COS (carbonyl sulfide) and N_2O (Denmead, 1979; Cropper et al., 1985; Castro et al., 1991; Lindberg et al., 2002; Reiche et al. 2010), that may also be covered with adhesive Teflon coating (Bytac) (Morrison et al., 1990; Tillman et al., 2004).

The inert nature of an apparatus should always be confirmed by adsorption and diffusion laboratory tests. Diffusion, by the way, is particularly important for application with strong wind blowing outside the chamber, which, while reducing contaminant concentration locally, makes concentration gradient increase through the cover, causing lateral losses through it. Control tests on recovery of FC, due to adsorption and bad mixing, are performed with multi-component standard gas (Eklund et al., 1985).

The same attention has to be paid to all the connections, pipes and in general all the devices, in order to avoid cross-contamination between different monitoring points/campaigns, that are generally built in Teflon (Batterman et al., 1992), Tygon (Schmidt et al., 1983; Morrison et al., 1990; Hartman, 2004), nylon or stainless-steel (Hartman, 2004) or more expensive PEEK (polyetheretherketone) (Hartman, 2006).

Chambers generally have rigid structures (Gao et al., 1997), but they may also be built of films supported by rigid structures (suitable for large spaces to cover) (Reichman et al., 2002) or again not supported by any frames, such as some Teflon bags (they increase however risk of pressure or subsurface concentration gradient perturbations) (Fried at al., 1993, Reiche et al. 2010).

The enclosures should be shaded (Dupont et al., 1986; Norman et al., 1992; De Mello et al., 1994; Valente et al., 1995; Frez et al., 1998; Roffman et al., 1995) or made in opaque material -such as Teflon-(Matthias et al., 1980; Schmidt et al., 1983; Dupont et al., 1986; Lindberg et al., 1999), reflective (Gao et al., 1997; Reichman et al., 2002), such as mylar (Hutchinson et al., 1981; Parkin et al., 2003) and aluminium foils (Cropper et al., 1985; Woodrow et al., 1991; Yates et al., 1996; Wang et al, 1997or insulating material (like polyurethane foam - Matthias et al., 1980; Batterman et al., 1992; Hutchinson et al., 1992; Hutchinson et al., 1993; Parkin et al., 2003), or again covered with the local soil itself (Smith et al., 1996; Wallschläger et al., 1999) or some straw (Yates et al., 1996) in order to avoid direct solar heating.

If vegetal physiological activity has to be studied (for CO_2 absorption/production or phytoremediation studies) transparent material is suggested.

4.2.4.3 Structure

The chamber may have a single- or multi-component construction.

The formers are more economical to fabricate, are deployed in a single step which increases the risk of error: any physical disturbance of the measurement site during the placement will give direct bias in the measurements (Hutchinson et al., 2002).

The latters are applied on the site in two steps which decreases such errors: the first step is to seal an open base to the surface previously to measurement time (at least 30-60 minutes (Norman et al., 1997; Davidson et al., 2002) better 24 h before (Parkin et al., 2003)), after which the enclosure is applied without directly disturbing the soil. The two pieces have to be well sealed in order to avoid diffusion of gas through the junction (Hutchinson et al., 2001). They are joined by air-tight overlapping -a sort of metal band that encircles the collar and the chamber (Matthias et al., 1980) - or otherwise an abutting joint, such as a Teflon frame (Rinklebe et al., 2009) or a compressible foam gasket, pressed by the weight of the cover (Norman et al., 1992; Nay et al., 1994; Carpi et al., 1998), or again by some foam tape (Fang et al., 1998). This design is appropriate for repeated observations at fixed locations and moreover, changing the ring at the basis, they may be suitable for different situations (vegetation height on soil or measurements on water by a flotation collar) (Klinger et al., 1994), but a two-component chamber for non-steady state is not recommended (Pumpanen et al., 2004).

4.2.4.4 Positioning of the FC

The base of the chamber has to be sealed to the soil. According to the specific compound that has to be analyzed, surface vegetation has to be removed (Rinklebe et al., 2010), cut or has not (Reiche et al., 2010).

One choice is by inserting its sharp walls, for a depth variable from a few millimetres (in very wet with low D_g (§ 3.3.2) soils) to 10-20 cm (for well-drained soils or dumps), minimizing vapour lateral diffusion but causing a potential alteration of F (Tab. 4.2) (Denmead, 1979; Matthias et al., 1980; Reinhart et al., 1992; Rayment et al., 1997; Hutchinson et al., 2001; Davidson et al., 2002). In order to avoid perturbations on ρ_b, the insertion should not be forced but an incision trace should be prepared to set the boundary of the chamber (Poissant et al., 1998). For deeper collocations (> 15 cm), a pre-excavation of the soil trying not to disturb it is allowed; the chamber is placed in it for almost all its height; in this way the pressure deviation between inside and outside chamber space is reduced, because wind effect (§ 4.2.4.8.3) is negligible (Smith et al., 1996).

In general inserting depth is higher for dry and porous soils, with required values of 9 cm as usual (Davidson et al., 2002), and depends also on sampling length; for compact or fine soil it should be less than 5 cm (Hutchinson et al., 2002), whereas U.S.EPA suggests depth values of 2- 3 cm (USEPA, 1986; Eklund, 1992), and however as small as possible (Parkin et al., 2003).

As other alternative, chamber and soil can be sealed together by applying fine wet clean sand (Woodrow et al., 1991), caulk (Eklund, 1992; Poissant et al., 1998) or bentonite (Livingston et al., 1995) all around the foot of the device; other strategies consist in using weighed flexible non permeable skirts applied to the basis of the chamber and fixed all around it (for cases where surface wind is negligible) (Matthias et al., 1980; Iritz et al., 1997) or put some heavy materials on the enclosures (Castro et al., 1991; Kim et al., 1995; Poissant et al., 1998).

The placing of the chamber itself, even if it is vented (§ 4.2.4.7), can trap air elevating pressure within the chamber headspace for several seconds, that has to be considered for short time sampling (Davidson et al., 2002).

Tab. 4.2*: FC inserting depth from literature.*

FC inserting depth [cm]	FC Type	Reference
2	Closed steady state	Batterman et al., 1992
2.5 for moderate porous soil	Open/closed non-steady state	Davidson et al., 2002
9 for high porous soil		
10	Open/closed steady state	Denmead, 1979
2.5	Steady state	Eklund, 1992
2.5	Non-steady state	Frez et al., 1998
10	Steady state	Gao et al., 1997
5	Closed non-steady state	Gao et al., 1998
3	Non-steady state	Hutchinson et al., 1981
5	Non-steady state	Hutchinson et al., 2002
10 – 20	Non-steady state	Klinger et al. 1994
5 – 10	Non-steady state	Livingston et al., 2006
3	Steady state	Lund et al., 1999
2.5	Open/closed non-steady state	Nay et al., 1994
1 – 3	Dynamic non-steady state	Norman et al., 1992
2	Dynamic non-steady state (LI-6200 system)	Norman et al., 1997
10	Closed non-steady state (Savage system)	
6 – 10	Dynamic non-steady state (Striegl system)	
20	Steady state (Rayment system)	
4 - 15	Dynamic non-steady state	Pumpanen et al., 2004
0.2 - 1.4	Static Non-steady state	
1.6 - 8.9	Steady state	Reinhart et al., 1992
10	Dynamic non-steady state	Rinklebe et al., 2009
15 in excavated soil	Steady state	Smith et al., 1995
2.5	Steady state	Tillman et al., 2004
10	Steady state	Valente et al., 1995
0.5 – 5	Dynamic non-steady state	Widen et al., 2003
0.5	Open/closed non-steady state	Woodrow et al.,1991

4.2.4.5 Injection system

Injection air is used only in stationary state chambers.

U.S. EPA suggests using dry clean gas, without any researched compounds (Dupont et al., 1986; Morrison et al., 1990; Eklund, 1992). Nitrogen at atmospheric pressure is generally used, or, as another possibility, purified (by proper cleaning systems, such as adsorption on activated carbon for hydrocarbons) and dried air (on silica gel, magnesium perchlorate (Norman et al., 1992) or anhydrous $CaSO_4$ (Rayment et al., 1997) or again using an impinger left in a cold bath) (Lin et al., 2003; Eklund, 1992).

For long sampling (more than 24 hours) constant humidity is recommended, especially for vapour fluxes influenced by biological activity, also because a decrease in water vapour pressure in the FC gives a lower resistance to vapour transfer resulting in a higher F (Iritz et al., 1997); for shorter periods, tests have revealed that there is no difference in emissions in using humidified or non-humidified fluxes. For easy oxidative substances, it may be suitable to use oxygen-free sweep air (Eklund, 1992).

The flow has to be guaranteed constant using mass flow controller (Morrison et al., 1990; Kim et al., 1995; Hutchinson et al., 2002) or mechanical devices, such as calibrated rotameter (Eklund, 1992; Castro et al., 1991) or micro-valve flow controller (Dupont et al., 1986), and frequently checked by flow-meter, micro-manometer (Fang et al., 1998) or turbine-wheel gas flow sensor (Gao et al., 1997).

Air can be both flowed inside and sucked outside the chamber. Some FCs, in literature, use the same fan applied for mixing in order to such environmental air from outside and recirculate it through a return channel (De Bortoli et al., 1999).

The choice of air flow rate is a compromise between the need to achieve rapid equilibrium and analytical sensitivity for researched compound concentration (Denmead, 1979); typical values of Q_{in} are in the range of 0.15-30 l min^{-1}, with suggested values of 5-10 l min^{-1} (USEPA, 1986; Morrison et al., 1990; Eklund, 1992), giving an optimum ratio of Q_{in} on A in the range 0.1-0.3 cm s^{-1} (Gao et al., 1998).

Some authors attest that flushing flow rate has no impact on F (Cropper et al., 1985; Fried et al., 1993; Di Francesco et al., 1998; Edwards et al., 1973 in Fang et al., 1998), whereas others say the opposite (Schwartzkopf, 1978; Eklund, 1992; Sakamoto et al., 1988 in Iritz et al., 1997; Gao et al., 1997; Lindberg et al., 1999; Lund et al., 1999; Wallschläger et al., 1999; Lindberg et al., 2002; Widen et al., 2003; Bahlman et al., 2006; Rinklebe et al., 2009): low Q_{in} takes longer to reach stationary conditions at the beginning of the measurements, and even if the flux continues to flow inside the chamber, it causes an accumulation of contaminant concentration causing a decrease of sampled F (Gao et al., 1998; Wallschläger et al., 1999; Lindberg et al., 2002; Zhang et al., 2002). A high flow reduces relative humidity in the chamber with risk of moisture (giving an effect similar to § 4.2.4.8.1) (Eklund, 1992; Gao et al., 1998 - this evaporation rate may be experimentally calculated (Di Francesco et al., 1998)), but minimizes emission reduction due to concentration gradient between the chamber and the soil, till to give an opposite effect (Davidson et al., 2002; Lindberg et al., 2002). That is why some researchers have suggested not using sweep air containing a zero concentration of the researched compound, if the atmosphere in the chamber reaches concentrations lower than atmospheric conditions at steady state: this could locally increase flux from soil (Castro et al., 1991; Fried et al., 1993; Cooper et al., 1994; Rayment et al., 1997; Wallschläger et al., 1999). This technique, however, has higher detection limit due to analytical uncertainties on both inlet and outlet carrier gas stream (Castro et al., 1991; Eklund, 1992).

Tab. 4.3 indicates the most common Q_{in} found in literature, with indication HRT (§ 4.2.1.2) and its relationship with sampling flow (§ 4.2.5).

***Tab. 4.3**: Indications from literature about sweep inflow Q_{in}, hydraulic retention time HRT and ratio between sampling flow, Q_s, and Q_{in} (-*: omitted datum).*

Type of sweep gas	Q_{in} [l min^{-1}]	Q_s [l min^{-1}]	Volume [l]	HRT (V/Q_{in}) [min]	Q_s/Q_{in}	Compound	Reference
Dried, cleaned, environmental air	0.85	0.85	1.6	1.9	1.0	Toluene	Batterman et al.., 1992
Environmental air	5	0.4	24.0	4.8	0.1	Hg	Carpi et al., 1998
Environmental air	1, 4 and 8	-*	16.0	16, 4 and 2	-*	CO_2	Cropper et al., 1985
Environmental air	14	-*	20.8	1.5	-*	COV	De Bortoli et al., 1999
Environmental air	1 - 3	-*	12.7	12.5 - 4.2	-*	N_2O	Denmead, 1979
Cleaned, environmental air	3	0.15	27	9	0.05	Compounds with S	De Mello et al., 1994
Inner recirculate	0.7	-*	1.8	2.5	-*	Hg	Di Francesco et al., 1998
Environmental air	11	11	225	20.5	1.0	COS	Fried et al., 1993
Environmental air	0.15	0.15	0.4	2.9	1.0	MeBr	Gan et al., 1996
Environmental air	7.4	0.1	15.0	2.0	0.01	MeBr	Gao et al., 1997
Environmental air	3 - 132	3 - 132	2.0	0.015 - 0.66	1.0	CH_2Cl_2	Gao et al., 1998
Environmental air	5	0.4	24.0	4.8	0.1	Hg	Kim et al., 1995
Environmental air	5	5	96.0	19.2	1.0	COV	Lin et al., 2003
Environmental air	3 - 9	0.25	27	3-9	0.08 - 0.03	Compounds with S	Morrison et al., 1990
Environmental air	0.25 - 0.5 - 0.75 - 1	0.25 - 0.5 - 0.75 - 1	9.2	36.8 - 18.4 - 12.3 - 9.2	1	CO_2	Rayment et al., 1997
Environmental air	4	0.01 - 0.012	-*	-*	0.003	Hg	Roffman et al., 1995
Dry clean air	2.5 - 20	2.5 - 20	55	2.75 - 22	1	VOC	Sadek et al., 1998
Inner loop with treated clean air	0.03	0.03	15.2	508.8	1	Trichloroethene	Smith et al., 1995
Environmental air	23	-*	9.2	0.4	-*	Hg	Song et al., 2005
Environmental air	15.6 - 1.5	1.5	28.0	1.8 - 18.7	0.1 - 1	Hg (FC of FGS)	Wallschläger et al., 1999
	1.5	1.5	24.0	16.0	1.0	Hg (FC of GKSS)	
	1.5	0.9	24.0	16.0	0.6	Hg (FC of GU)	
Environmental air	15	15	19.0	1.3	1.0	Pesticide	Woodrow et al.,1991
Environmental air	20	0.1	-*	-*	0.01	MeBr	Yates et al., 1996
Environmental air or no S air	2	0.04 - 0.06	21.0	10.5	0.02 - 0.03	COS, CS_2	Castro et al., 1991
Dry clean air	16.3 - 18.4	-*	121	7.4 - 6.6	-*	CH_4	Reinhart et al., 1992
Dry clean air	4	1	27.0	6.8	0.25	NO	Valente et al., 1995
Dry no VOC air	5	2	30.0	6.0	0.4	VOC	USEPA, 1986

***Tab. 4.3**: continued.*

Dry no VOC air	3	3	27	9.0	1	VOC	Martins, 2010 (FC modified from USEPA, 1986)
Treated air, inner loop	0.125	0.125	1.2	9.8	1	TCE	Tillman et al., 2004
Nitrogen or dry clean air	5	-*	30.0	6.0	-*	VOC	Eklund, 1992
Nitrogen or dry clean air	2, 5 and 10	0.15	30.0	15, 5 and 3 respectively	0.075, 0.03 and 0.015	VOC	Gholson et al., 1991

The injection is performable by a simple holed tube, or by a more complicated system allowing a more homogeneous distribution, such as holed ring/spiral where distance from the covering, distance between different holes (generally equidistant) and the diameter of each perforation (Sanders et al., 1985; Reinhart et al., 1992; Sadek et al., 1998) and flow direction (generally toward FC centre) have to been defined properly (Castro et al., 1991; Eklund, 1992; Gholson et al., 1991; Rinklebe et al., 2009).

Q_{in} influences turbulence inside the chamber that should simulate as much as possible natural turbulence in the atmosphere (Eklund, 1992; Reinhart et al., 1992; Reichman et al., 2002). Sweep gas can have also vertical components, both upwards and downwards, causing negative or positive pressure (§ 4.2.4.8.2) on soil surface that exerts local advection forces (Reinhart et al., 1992; Gao et al., 1997; Fang et al., 1998; Wallschläger et al., 1999; Wallschlager et al., 2002). It would be better to apply a system giving just horizontal forces, parallel to the covered soil surface (Gao et al., 1997; Davidson et al., 2002; Reichman et al., 2002); for example a chamber where the inlet has the same size as cross-section of the chamber itself has been created (Iritz et al., 1997).

4.2.4.6 Mixing

Mixing is of critical importance because F computation is based on the assumption that chamber effluents are representative of a completely mixed chamber volume (Dupont et al., 1986; Reinhart et al., 1992; Gao et al., 1997).

For non-steady state (close) deployments mixing circulation happens in an inner close loop (Denmead, 1979; Norman et al., 1992; Nay et al., 1994; Norman et al., 1997; Di Francesco et al., 1998), or by pumping and releasing inner gas with a syringe, before collecting the sample (Norman et al., 1997); for steady state ones it is rather represented by the sweep flow system itself or the suction used for sampling (Kanemasu et al., 1974) (or again by an inner loop, after having treated the recirculated air with on-line adsorbent tubes (Jellali et al., 2003)). Their turbulence is useful to simulate the effect of exchange rates of wind stress.

Attention has to be paid to the dimensions of both air entry and exit ports, that have to be large enough to avoid pressure alterations (also P difference of 1 Pa may induce a significant alteration of gas exchange rate (Rayment et al., 1997)), and located in such a way as not to allow direct passage between them, without filling the chamber (Cropper et al., 1985; Gao et al., 1997). The pump inducing the air flow has to be located outside the chamber, and be inert in order not to adsorb or release compounds in the isolated environment (as for example Teflon pump or metal bellow).

Some mechanical mixing systems can be used as an alternative consisting in simple deflection vanes/baffles/obstacles (Denmead, 1979; Iritz et al., 1997; Gao et al., 1997; Wang et al, 1997; Reichman et al., 2002; Widen et al., 2003; Song et al., 2005; Capelli et al., 2009) or in a structure of horizontal and vertical tubes to inject sweep into the FC (Lin et al., 2003). Holes for flowing air are located in order that air flows parallel to soil and do not perturb F (Lin et al., 2003).

Another possibility indicated in literature is not focused on homogeneity, but on collecting samples from different points in the chamber (§ 4.2.5).

Also some fans, covered by inert material, such as Teflon (to avoid false negatives) (Schmidt et al., 1983; Gustin et al., 1999; Lin et al., 2003; Parkin et al., 2003; Martins, 2010) or flow-through circulation systems may be used, avoiding stagnation zones and uncontrolled induction of vertical components of air flow, also in closed non-steady state chambers (Gao et al., 1997; Gao et al., 1998; De Bortoli et al., 1999; Lund et al., 1999; Reichman et al., 2002; Bahlman et al., 2006; Capelli et al., 2009). They have to be controlled since they may have influences on F (Norman et al., 1992; Fang et al., 1998; Hutchinson et al., 2000; Davidson et al., 2002; Lin et al., 2003; Widen et al., 2003; Pumpanen et al., 2004; Bahlman et al., 2006), whereas other experiments have highlighted that they have no strong effects on flux measurements (Xiao et al., 1991; Norman et al., 1997; Poissant et al., 1998). The increased turbulence regime or air velocity however seem not give a sufficient mixing alone (Matthias et al., 1980; De Bortoli et al., 1999), and therefore they are not recommended (Eklund, 1992).

Appropriate tracer test with dense smoke (for example produced from burning vegetable oil) can be carried out for visual inspection of the chamber (Schwartzkopf, 1978; Eklund, 1992; Gao et al., 1997; Allaire et al., 2002; Reiche et al. 2010) or anemometric probes may be placed at different positions inside the chamber to obtain profiles of air velocity and turbulence (De Bortoli et al., 1999). Other tests are performed directly by using a known source of vapour and taking air samples for analytical analysis or using on-line devices (§ 4.2.5.1) (Schmidt et al., 1983; Dupont et al., 1986; Kreamer et al., 1988; Gholson et al., 1991; Nay et al., 1994; Di Francesco et al., 1998; Gao et al., 1998; De Bortoli et al., 1999; Reichman et al., 2002; Widen et al., 2003; Pumpanen et al., 2004; Tillman et al., 2004; Allaire et al., 2002; Bahlman et al., 2006).

4.2.4.7 Vent

The application of pressure vents is suggested to compensate for air sample withdrawal and possible reduction in chamber volume during sampling, which could perturb the measurement (Hutchinson et al., 2001; Hutchinson et al., 2002;

Hutchinson et al., 2003). Vents may be represented by simple holes on the coverage (USEPA, 1986) of the FC of by properly designed open tubes.
Unvented designs can result in development of pressure differentials caused by circulating gases or by cooling or warming of chamber air (Davidson et al., 2002).

Guidelines and analytical relationships have been defined to calculate their dimensions appropriately (length and diameter, see Fig. 4.3) according to chamber volume and wind speed (Hutchinson et al., 1981); they have to be large enough to minimize resistance of air flow to changes of atmospheric pressure and to minimize the advection force driving air exchange between the closed system and outdoor atmosphere (Hutchinson et al., 1981; Fang et al., 1998).

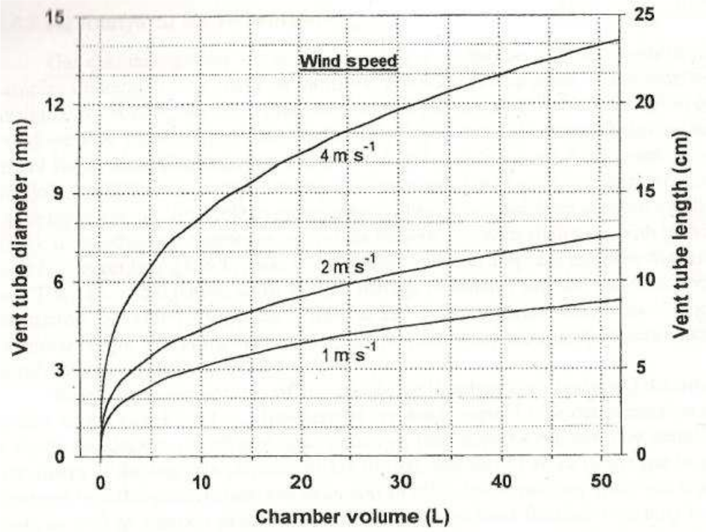

Fig. 4.3: *Optimum vent tube and diameter as a function of wind speed and enclosure volumes (Hutchinson et al., 2002).*

As a general indication vents are between 2 and 10 mm in diameter and between 5 and 30 cm long (Tab. 4.4) (Parkin et al., 2003), in order to contain air expelled from FC due to temporal perturbations, and then to return it in the closure (Hutchinson et al., 2003). It should be mounted near ground surface to minimize wind speed, separated from the chamber's sampling port to avoid unwanted interactions with outlet pointing downwind and horizontally (Hutchinson et al., 2001; Hutchinson et al., 2002). Diffusion through the vent tube is commonly assumed negligible.

Tab. 4.4: *Vent dimensions found in literature (-*: omitted datum).*

FC Type	**Vent Diameter [mm]**	**Vent tube length [cm]**	**Reference**
Non-steady state state, static	10	16	Conen et al., 1998
	4	4.9	
Dynamic non-steady state, closed	2.16	-*	Davidson et al., 2002

Dynamic non-steady state state, closed	2	30	Norman et al., 1992
Steady state	18	-*	Eklund, 1992
Steady state	6.3	Just to connect with a sampling bottle	Matthias et al., 1980
Non-steady state state, static	8	300	Pumpanen et al., 2004
Non-steady state state, closed	4.8	10	Parkin et al., 2003

Vented systems are especially necessary when the underlying soils are strongly permeable or the pollutant source is located in shallow soil, which is when F is directly influenced by barometric conditions. Windy sites are critical, because wind could give a Venturi effect of drawing vapours through vent tubes, with fluxes higher than five times those measured in FC without vent (Conen et al., 1998).

Using a dynamic non-vented chamber involves greater risk than using a static one, because gas overpressure may be produced inside the chamber, giving a downward advection flux towards the soil and therefore reducing the measured value (see Fig. 4.4).

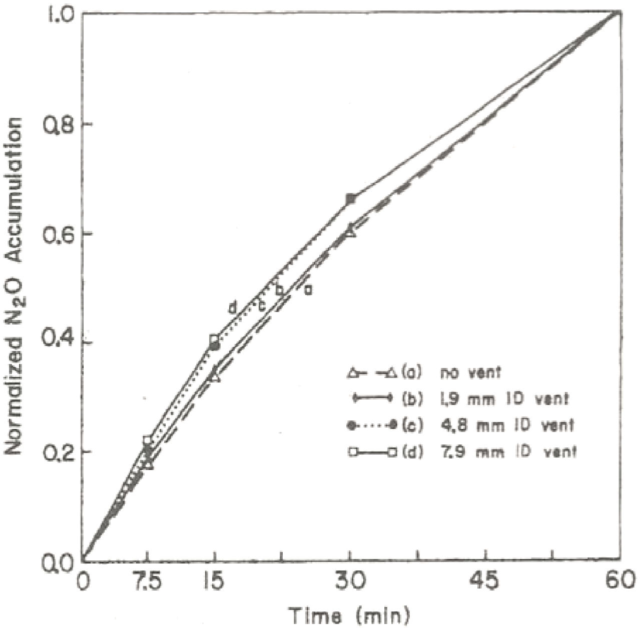

Fig. 4.4*: influence of vent diameter for a non-steady chamber (Hutchinson et al. 1981).*

4.2.4.8 Interference factors

Care must be taken in order to avoid all possible perturbations: operators should not compact soil or walk all around the enclosure, preferring remote controls and operations, and also minimizing the disturbance of vegetation inside and around the enclosure system, which heavily effects volatilization processes, especially for greenhouse gases, on which light intensity and humidity also count a great deal (Hutchinson et al., 1993; Livingston et al., 1995; Rayment et al., 1997; Fang et al., 1998).

Generally speaking, the FC is effectively isolated from most external environmental conditions (Eklund, 1992), but some boundary conditions are affected by its presence (Wang et al, 1997; Yates et al., 1997), such as soil temperature, air pressure at ground level, wind presence and soil moisture.

4.2.4.8.1 **Temperature**

The enclosure system should avoid changes in net energy flux (such as avoiding greenhouse effect) at the sampling location due to FC presence (Eklund, 1992; Pumpanen et al., 2004), preserve the same mean ambient temperature, and in particular the difference between air and superficial soil temperature (the heat flux into soil is rapidly attenuated with depth). Matthias et al. indicate that the difference between soil temperature at 2 cm below ground surface under the chamber and that of the same depth, outside the chamber, if this is placed just for 20 minutes, is no more than 1°C, with an average of 0.4°C (Matthias et al., 1980). Other authors indicate that in general temperature inside their chamber was ± 2 °C as a reference with outside temperature (Denmead, 1979; De Mello et al., 1994), but in literature greater differences have also been reported as is summarized in Tab. 4.5.

***Tab. 4.5**: Difference (ΔT) between inside and outside flux chamber temperature.*

FC temperature [°C]	**Air temperature [°C]**	**ΔT [°C]**	**Reference**
Air temperature ± 2	3 – 29,3	2	De Mello et al., 1994
Air temperature + 9 (after 30 min) and 30 after (2.5 h)	28	9-30	USEPA, 1986
Air temperature ± 1÷3	12.2 ± 2.5 (day) – 9.4 (night)	1-3	Fried et al., 1993
Air temperature ± 1÷3	22.7 ± 2.4 (day) 20.8 ± 1.8 (night)	1-3	
11 - 31 (night)	11 - 31 (night)	0	Sanders et al., 1985
17 - 31 (morning)	12 - 23 (morning)	5-8	
27 - 34 (afternoon)	25 (afternoon)	2-9	
In a year changes from 8.7 to 25	From 91 to 140 % of outdoor temperature	From -1.1 to 5.5	Reiche et al., 2010
a) Air temperature + 5 b) Air temperature + 15	a) early morning b) early afternoon	5-15	Yates et al., 1996

Its alterations are mostly due to solar heating that make the inner T increase according to the specific material thermal conductivity, length of deployment and presence of insulation material (Fig. 4.5). To avoid perturbations, chambers should be built in suitable material (§ 4.2.4.2), kept in the shade during monitoring (Morrison et al., 1990; Tillman et al., 2003) and temperature monitoring of both outdoor and enclosure air is required. As short measurements as possible should be preferred since soil temperature reaches the same as that of air only after quite a long time (Hutchinson et al., 1993).

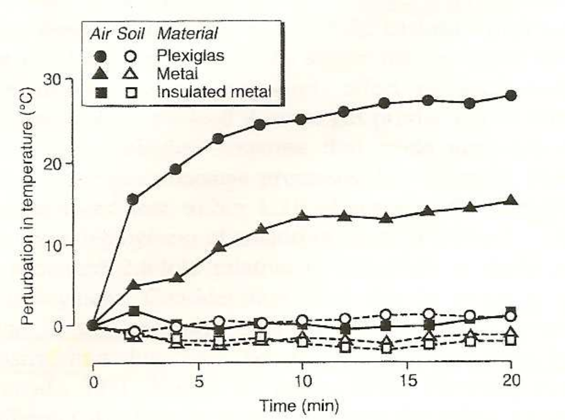

***Fig. 4.5**: alteration of enclosure temperature, as difference compared to that of environment, for different chamber construction materials and deployment time (Matthias et al., 1980).*

It is particularly important to know this difference for some compounds, such as mercury, whose flux depends heavily on temperature, in order to be able to define some analytical relationships between these two variables (Matthias et al., 1980; USEPA, 1986; Xiao et al., 1991; Eklund, 1992; Poissant et al., 1998). For really wet soils a temperature increase can induce condensation of water vapour on chamber walls, causing increase in moisture and potentially dissolution of vapours, affecting the sampling (Xiao et al., 1991; Carpi et al., 1998; Parkin et al., 2003). This is why in literature there are chambers with heating/cooling devices outside them: some examples include a high sweep air flowing around it added to a ring of cold water flowing outside the chamber (Eklund, 1992), a wire surrounding its external wall (to keep the temperature of the wall surface at 0.5-1°C higher than the internal temperature (Poissant et al., 1998)), a heating lamp (Roffman et al., 1995) or again a thermostated box (Xiao et al., 1991) to impose constant artificial boundary conditions. UV radiation, for some compounds, is also significant and influences F (Schroeder, 1995; Rabideau et al., 1996; Bahlmann et al., 2006).

4.2.4.8.2 **Pressure**

The pressure difference (ΔP) between inside and outside environment of FC influences heavily vapour emissions, especially for dry, porous, high permeable soils (Hutchinson et al., 1993; Rayment et al., 1997; Lund et al., 1999; Reichman et al., 2002) and really volatile compounds (Woodrow et al., 1991): a negative ΔP as a reference to atmospheric pressure causes a pumping effect from the soil, inducting an overestimation of F; where the opposite sign may give an underestimation (Hutchinson et al., 1981). The difference is due, for open chambers, to the way and magnitude by which its injection flow is performed (suction or blowing) (Kanemasu et al., 1974; Eklund, 1992; Dupont et al., 1986; Fang et al., 1998; Gao et al., 1998), and the length and the section of inlet air tube (Hutchinson et al., 1993). To minimize this perturbation it is possible to pump and suction with the same flow rate (Cropper et al., 1985; Lund et al., 1999; Martins, 2010).

It has been demonstrated that a pressure increase of only 0.5 Pa reduces measured fluxes by 20–70%, whereas an increase of 6 Pa gives a reduction of flux of 70–90% (Lund et al., 1999). An under-pressurization of the chamber can result in overestimation of fluxes due to suction out of the soil; a difference of only a 0.2 Pa and 2 Pa can cause a factor of 2 and 20 respectively in overestimation of F (Fang et al., 1998); others say that a difference of - 1.2 Pa causes 20% increase in measured flux (Reichman et al., 2002); it has therefore been suggested keeping ΔP to values lower than ± 0.2 Pa (Fang et al., 1998).

Other causes of over-pressure are due to small dimensions of the vent, or in general of gas ports. Examples are when outlet port is smaller than inlet one (Davidson et al., 2002; Fang et al., 1998), or the particular case in which outside wind is low compared to sweep air speed inside the chamber, giving a sort of Venturi effect that makes F increase (Gao et al., 1997; Reichman et al., 2002).

For non-stationary chambers (closed ones) increase in temperature under the chamber gives positive pressure, whereas decrease in temperature or air sampling gives negative pressures and lower F. Fig. 4.6 indicates the effects of the change of pressure (due to various reasons) under the chamber to F, normalised on a non perturbed emission, F_0, and the time they take to disappear (Hutchinson et al., 2001).

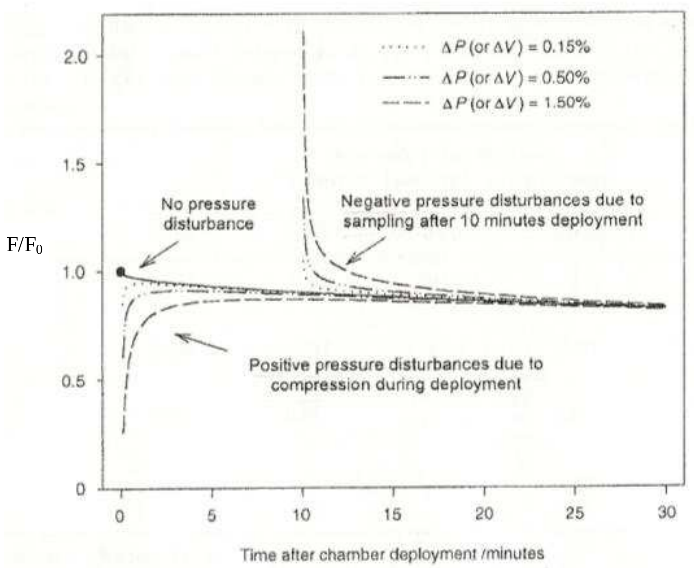

Fig. 4.6*: pressure gradient influence on flux F as a reference to a non perturbed emission flux F_0 (Hutchinson et al., 2001).*

To reduce ΔP Tillman et al. have suggested using a covering with a flexible membrane on it, that expands according to barometric pressure changes (Tillman et al., 2004). For closed dynamic chambers, with inner closed loop, the position of the chemical adsorbent also influences the pressure deficit (Denmead, 1979).

4.2.4.8.3 **Wind**

Another natural element, wind, affects vapour emission, too, and since the chamber is a closed structure, may be submitted to different conditions compared to outside (Sanders et al., 1985; Schroeder, 1995; Rabideau et al., 1996; Wang et al, 1997; Wallschläger et al., 1999; Wallschlager et al., 2002 Widen et al., 2003); however a strong correlation with wind was measured (Woodrow et al., 1991; Poissant et al., 1998). For open chambers (especially where sweep gas is induced by suction) it is advisable to apply a wind shield or baffle to reduce the velocity of air, prevent Venturi effect (toward the outside of FC as indicated by Bernouilli law (Norman et al., 1992; Reinhart et al., 1992; Hutchinson et al., 2001)) and air from blowing into the chamber (Denmead, 1979; Cooper et al., 1994). In very windy areas, in particular, wind reduces diffusion resistance and thus makes F increases; some authors suggest reproducing wind speed by a fan (Iritz et al., 1997), or managing sweep gas in order to simulate environmental conditions (0.4-0.6 m sec^{-1} (Schwartzkopf, 1978; Iritz et al., 1997). For typical continental monitoring, where wind is often low, minimizing pressure fluctuation due to wind effect (generally in the range between -0.7 and +0.9 Pa) is recommended (Davidson et al., 2002) because flowing on the chamber vents, it induces a local depression compared to inside space (called Venturi effect) that causes local and temporal emission increases (Norman et al., 1992; Reinhart et al., 1992; Poissant et al., 1998; Pumpanen et al., 2004). Some simple windbreaks extending from the top of the chamber to the soil surface are sometimes used (Matthias et al., 1980; Parkin et al., 2003).

4.2.4.8.4 **Rain**

Rain also has direct influence on F, because it decreases air-filled porosity of soil, limits diffusion (§ 3.2.2.1), displaces natural fluxes of soil vapours, dissolves VOCs, and creates a sort of “cap” above the soil (Hartman, 2002), leading to smaller F (Smith et al., 1996). Trace precipitations (< 0.25 mm) have no effect, whereas more consistent (7-10 mm) ones do (USEPA, 1986; Eklund, 1992; Yates et al., 1997; Hartman, 2003). Other scientists have seen that a small addition of water has the opposite effect on F: it decreases VOC sorption and leads to an increased volatilization (Steinberg et al., 1993; Rinklebe et al., 2010); in the case of mercury in particular emissions after a rain event are greatly increase (if w is lower than 15%), because of its reactive nature (Wallschläger et al., 1999; Wallschlager et al., 2002; Song et al., 2005).

When the effects of each of these phenomena are studied, some corrective factors may be defined, in order to check flux biases (Yates et al., 1996).

4.2.5 Sampling

The overall accuracy and precision of a FC depend on the biases and variability due to emission source, sampling method and analytical method (Eklund, 1992).

In closed non-flow through (static) chambers sampling may occur on chemical adsorbent materials left under the enclosure. Another alternative is to use a sampling port for removal of discrete gas sampling, for example sampling by a syringe through a self-sealing septum. In these cases sample withdraw is compensated by pressure venting, in order not to make the flux increase artificially. For closures with high H, a tube perforated along its length is used in order to obtain an average sample, representative of all the system.

In steady state apparatus, the sampling system may be constituted by a simple holed tube, or by a system holed in different positions to achieve an average concentration under the chamber (Reinhart et al., 1992; Livingston et al., 1995; Di Francesco et al., 1998; Wallschlager et al., 2002; Lin et al., 2003). This system is particularly useful if the sampling port is next to a vent, if the chamber has high H or for vegetative soils where conditions under FC are perturbed by plant presence (Hutchinson et al., 2002).

The outflow lines are connected to suction forces (pumps, personal air check, depression due directly to sampling system (§ 4.5.2)) located generally after the collecting system (in order not to perturb it (Batterman et al., 1992)). Sometimes they are used directly to create mixing inside the chamber (§ 4.2.4.6), without using any sweep gas, but this gives strong pressure deficit (§ 4.2.4.8.2).

Obviously the sampling flow, Q_s, has to be less than Q_{in} to avoid negative pressure inside the chamber drawing air from outside. The ratio of Q_s to Q_{in} is subject to change inside the range 0.01-1 (Tab. 4.3).

Monitoring details have to be defined to perform the proper sampling technique, in particular information such as analytes of interest, adequate detection limits (d.l.) for the work purpose, location and number of samples required to depict site conditions properly, time duration and frequency of the monitoring events, the impact of topographic, meteorological and physical/chemical parameters on the sampling plan, the logistics of the site and the time of storage (Romele et al., 2010).

The overall precision, due to sampling and analytical phases, is determined to be ± twice the standard deviation of the mean (Parkin et al., 2003).

The duration of sampling depends on the chosen/possible technique of collecting samples linked to applicable analytical techniques, scope of the monitoring and kind of FC. If the emission is assumed constant (for open systems) or the concentration rate is supposed to be constant over time (for closed ones) measurements generally last 20-40 minutes, useful to give imminent risk for personnel on the site. When collecting for RA purposes (§ 1.2) it is suggested to conduct flux monitoring for a time representative of the exposure of the receptor and to avoid short-length sampling (Batterman et al., 1992); monitoring duration of a half-day is enough to approximate a 24 h mean flux (Davidson et al., 2002). This is because obtaining an average sample is more meaningful than it is not affected by temporal changes of environmental conditions. Perturbations on natural F are however to be avoided by not prolonging measuring times in excess (§ 4.2.3) (Eklund, 1992; Gustin et al., 1999; Parkin et al., 2003).

As a general rule, rigorous protocols have to be established and followed for the collection, transport, storage and analysis, and it is advisable to take minimum 10% of the sampling points as duplicates (USEPA, 1986; Schmidt, 1991; Eklund, 1992; Smith et al., 1995). These consecutive measurements have to be performed at the same locations at appropriate intervals in order to avoid perturbations from previous deployments, even if initial flush is applied; typically the flux tends to increase at each measurement (Hutchinson et al., 2001).

Gas standards, with known concentration, should be handled, stored and analyzed regularly in the same way as the real sample and, as an indication, air samples can easily give artefacts, in terms of adsorption or reaction on the walls of sample container, leaks, dissolution in water, or react chemically, biologically or photochemically inside the same sampling device (Dupont et al., 1986; Livingston et al., 1995; Hutchinson et al., 2002).

Outflowing fluxes may be monitored by on-line sampling and or collected for later analysis at the laboratory (Fig. 4.7). In this case they can be poured into proper devices or made to flow through proper "pre-concentration" devices, such as sorbent media or cold traps to trap chemicals by freezing, adsorption or chemical reactions.

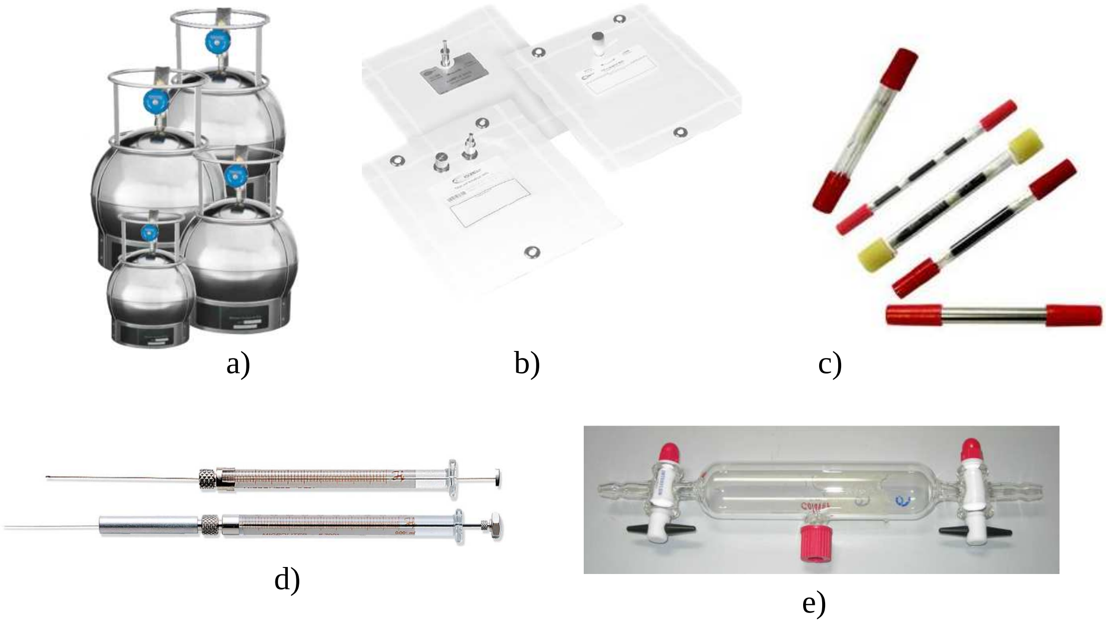
a) b) c)

d) e)

Fig. 4.7: *sampling devices suitable for analyses of compounds in gas flow: a) canister, b) Tedlar bag, c) tubes, d) gas tight syringes, e) glass sampling bulb.*

4.2.5.1 Direct-reading method

When it is not necessary to preserve the sample, real-time on site detection and quantification of chemical compounds may be performed (Eklund et al., 1985). These measurements may provide both qualitative and quantitative data, because there are specific devices for each family of compounds. These systems are useful especially for non-steady state closed devices, where there is no sweep flux that dilutes the flux coming out the soil, or in general to monitor compound concentration over time.

Common hand-held Flame-Ionization Detector (FID) and Photo-Ionization Detector (PID) analyzers cannot reach low d.l. (generally ppmv), and the use of a field portable gas chromatograph, equipped with the same type of devices as laboratory instruments, would be required. There are also portable mass spectrometers, with sensitivity up to a few ppbv, but they give an indication in terms of classes of volatile compounds. For some gases, such as carbon dioxide (Davidson et al., 2002), methane, oxygen (Eklund et al., 1998) or elemental mercury, portable gas analyzers are also available, but they usually have a narrow dynamic range (because they are subjected to memory effects).

4.2.5.2 Whole air collection techniques

These techniques consist in collecting a sufficient quantity of air into suitable containers such as bottles, polymer bags or canisters that may preserve the sample with the researched compounds (still in the gas matrix) in it, until the completion of the analysis. This technique is suitable for chemicals with a high volatility level, in order to avoid their condensation in the sampler. You can just collect a ‘grab’ sample or use a time weighed average (TWA) samples using calibrated flow controllers to fill at a constant, controlled flow rate over time. It is simple, does not need any refrigeration or special handling until they are analyzed, does not depend on chemical concentration (such as the case of tubes where there is the risk of breakthrough) and moreover it allows to carry out replicate analysis on multiple aliquots of the same sample.

Gas tight syringes and glass sampling bulbs/pipes are suitable for instantaneous sampling, to analyze gas soon after its collection, directly on site (Frez et al., 1998) or however for short storage time, by portable gas chromatography device, and are in general applied for laboratory studies. The first ones may contain from microlitre to some litres of capacity, and gas is collected manually or by a pump; the second ones generally have volumes lower than one litre, and have an inlet and an outlet with Teflon tops to help sampling procedure.

The most known devices are polymer bags in Tedlar, aluminized Tedlar, Teflon or Nalophan (with volume from 500 ml to 100 l), available for limited storage period (< 24/48 h) because of risk of chemical adsorption on organic material.

Other possibilities are steel canisters (with volume from 1 to 32 l) that are often treated to be chemically inert using electropolishing process and passivation to increase chemical inertness (ensuring stability for many VOCs over periods of up to 30 days). These systems are prepared and cleaned directly by the laboratory. The sampling belongs under the direct driving force of the canister that is kept under vacuum (<13 Pa): a bellow valve regulates the inlet flow and seals off the canister once the sample has been collected. These systems are suitable for both polar and not polar VOCs, including also reactive species such as mercaptanes and carboniles. They are quite expensive devices but do not need any sample preparation step directly since are attached directly to the instruments for the analytical determinations (Romele et al. 2010).

4.2.5.3 Tubes

Pre-concentration systems are consolidated and objects of official methods approved by NIOSH, OSHA or U.S. EPA. They are based on different commercially available ad-sorbent tube/as-sorbent media, applicable to different kinds of compounds with various volatility ranges. They are small sealed glass tubes containing one or two different adsorbent materials, divided in two parts: the bigger one is the sampling one, whereas the second, separated by a polyurethane set, is called backup and is used as a check control: if it contains a mass higher than 25% of what was adsorbed, it is an index of a breakthrough phenomenon an therefore the sampling is not representative of the total mass collected on sampling line.

To collect on a tube, it has to be opened at the ends, attached to a suction pump regulated at an imposed flow (generally lower than 1.5-2 l min^{-1}). The inflow is suggested to pass through a dehumidifier system aiming to collect the humidity inside the flux separately and avoid compromising the tube or induce gas dissolution in it. It is performed by making air pass through hydrophobic membranes (Nafion (Castro et al., 1991; Eklund et al., 1998), Teflon) or cold-impingers (Morrison et al., 1990). At the sampling end, tubes are closed by proper caps and taken to the laboratory where the compounds are desorbed by thermal (TD) or chemical extraction (CE) (Brown, 2002), and then transferred into the analytic device, which is often a gas chromatography (GC), equipped with either mass spectrometer (MS) or flame ionization (FID) detectors, or a high performance liquid chromatography (HPLC) system.

Breakthrough can occur if the sorbent surface gets saturated with the compound, or the compounds have no enough time to interact sufficiently with the sorbent surface (e.g. when the flow rate through it is too high) or the retained compounds is eluted in the ongoing sampling procedure due to changes in environmental conditions.

As a general indication extensive quality control measures (such as duplicates, field blanks, lab blanks) are required to avoid artefacts due to passive unwanted adsorption of VOCs. The choice of the sorbent material depends on affinity with the target VOCs (influencing not only the chemical uptake during the sampling but also the desorption efficiencies for the analysis), the characteristics of gas flow to sample (moisture, presence of reactive substances) and, also, available extraction technique (Politecnico di Milano et al., 2010). A rough classification might be based on three broad categories: porous polymer-based sorbents, carbon-based sorbents and inorganic materials (see details in Tab. 4.6) (Romele et al. 2010).

Passive devices can also be found on the market, which are used for closed steady state chamber (§ 4.2.1.2), but their performance is strongly dependent on temperature cycling and high humidity; furthermore they need long exposure time (more than 2 days) to make the mass collected during initial period (affected by environmental air under the chamber) negligible as compared to that collected at steady state (Batterman et al., 1992; Brown, 1993).

Particular attention has to be paid to the choice of the method, because more common protocols, used for working place controls, do not reach sufficient sensible detection limits according to RA point of view. Tab. 4.7 indicates a summary of the most common measurements and matched analytical methods for chemicals in gas flow (Politecnico di Milano et al., 2010).

4.2.6 Flux estimation

As a general indication, taking replicate observations especially for instantaneous or short time sampling is a good practice. At the sampling end, a good data analysis is necessary to avoid statistical outliers (Skoog et al., 1992 in Kim et al., 1995) and to verify or adjust samples of chamber blanks.

4.2.6.1 Non-steady state chambers

In non-steady state systems F changes over time because of modified accumulation of compound C under the cover, which modifies F due to diffusion.

This protocol has to be followed: i) define a model that correlates concentration in enclosure chamber and time; ii) fit it to concentration data, iii) calculate F at the moment of deployment (t=0) and iv) verify the credibility of the prediction (examining for example in a plot actual versus predicted concentrations over time), evaluating its significance by using proper statistical tests (Livingston et al., 1995).

When the compound vapours react with the other gases closed under the chamber (for example ambient O_3), it is advisable to use concentrations collected after a certain lag time, when all the reactive gases have been adsorbed or destroyed.

Both linear and non-linear correlations are used in literature. The former is suitable for short deployment periods, and considers a constant exchange rate over time:

$$F = \frac{V}{S}\frac{\Delta C_g}{\Delta t} \tag{4.14}$$

where $\frac{\Delta C_g}{\Delta t}$ is the variation of concentration over time observed under the chamber (De Mello et al., 1994; Livingstone et al., 1995; Frez et al., 1998; Gao et al., 1998; Widen et al., 2003).

Rayment argues that there is an intrinsic error in (4.14) because the “effective volume” of the chamber is larger than the chamber itself and includes some of the pore spaces within the soil (Rayment, 2000). It has been evaluated that for a 10–20 cm tall chamber, the error for using non-steady state systems with (4.14) data elaboration ranges from negligible to 15% underestimation, depending on soil texture and water content (Davidson et al., 2002).

One way to solve artefacts due to concentration change under the chamber is to extrapolate C values at initial time (t = 0), or collect samples soon after the closure of the chamber (De Mello et al., 1994).

***Tab. 4.6:** Properties of some solid sorbents according (Uhde, 2009 in Romele et al. 2010).*

Type	**Structure**	**Surface area [m^2 g^{-1}]**	**Products**	**Desorption**	**Compounds tested**	**Polarity**	**Thermal stability**	**Water affinity**
Inorganic	Silica gels	1 – 30	Volasphere, Florisil	Solvent	PCBs, pesticides	High	400 °C	High
	Aluminium oxides	300	Alumina F1	Solvent	Hydrocarbons	High	300 °C	High
	Cupper and manganese oxides	-	Hopcalite/ Anasorb C300	Acid digestion	Mercury	High	-	High
	Gold trap				Mercury	High		
Carbon based	Activated Charcoal	800 – 1200	ORBO	Solvent	Non - polar and slightly polar VOCs (> 50 ° C)	Medium	> 400 °C	High
	Carbon molecular Sieves	400 – 1200	Carbosieve, Ambersorb, Spherocarb Carboxen	Solvent/ Thermal	Non - polar and slightly polar VOCs (>-80 °C)	Low	> 400 °C	Low - medium
	Graphitized carbon blacks	12 – 100	Carbotrap, Carbopack, Carbograph	Thermal	Non - polar VOCs (> 60 °C)	Low	> 400 °C	Low
Porous polymers	Styrene, divinylbenzene or polyvinylpyrrolidone polymers	300 – 800	Porapak Q/N, Chromosorb 106/102	Thermal/ solvent	Non - polar and moderately polar VOCs (> 40 °C)	Variable	< 250 °C	Low
	Phenylphenylen oxide polymers	20 – 35	Tenax	Thermal	Non - polar VOCs (> 60°C)	Low	< 350 °C	Low
	PU- Foams	-	-	Solvent	Pesticides and other semivolatile compounds	Low	< 200 °C	Low
	Polystyrene,/divinylbenzene	300	XAD-2	Solvent	Semivolatile compounds (eg. PAH and chlorinated pesticides)	Low	< 200 °C	Low

Remarks: Tenax® is a registered trademark of Buchem B.V., NV, NL; Carbotrap®, Carbopack®, Carbograph®, Carbosieve® and Carboxen® are registered trademarks of Sigma - Aldrich Co., USA; Chromosorb® is a registered trademark of Johns - Manville Corp, USA; Porapak® is a registered trademark of Waters Associates Inc., USA; Spherocarb® is a registered trademark of Analabs Inc., USA.; Volasphere® of E.Merck KGaA, Germany; Florisil® is a registred trademark of U.S. Silica Co., USA.

***Tab. 4.7**: Main sampling/analytic methods for air flow (Politecnico di Milano et al., 2010, modified).*

Method	**Compound [1]**	**Sampling system**	**Analytical technique**	**Detection limit**	**Reference**
TO-1	VOC	Tenax	DT-GC/MS	0.02-200 µg m^{-3} (0.01-100 ppbv)	USEPA, 1999
TO-2	VVOC	Molecular sieve	DT- GC/MS	0.2-400 µg m^{-3} (0.1-200 ppbv)	USEPA, 1999
TO-3	Non-polar VOC	*Canister*, Tedlar bags	GC/FID/ECD	0.2-400 µg m^{-3} (0.1-200 ppbv)	USEPA, 1999
TO-12	Non-methanic hydrocarbons	*Canister*	GC/FID	0.2-400 mg m^{-3} (0.1-200 ppmv)	USEPA, 1999
TO 14A	Non-polar VOC	*Passivated canister*	GC/MS	0.4-20 µg m^{-3} (0.2-2.5 ppbv)	USEPA, 1999
TO-15	VOC	*Passivated canister*	GC/MS	0.4-20 µg m^{-3} (0.2 -2.5 ppbv)	USEPA, 1999
TO-15A	VOC	*Passivated canister*	GC/MS/SIM	0.005-0.02 µg m^{-3} (0.002-0.04 ppbv)	USEPA, 2000
TO-17	VOC	Single or multi-layer adsorbent	DT-GC/MS, FID	0.4-20 µg m^{-3} (0.2-2.5 ppbv)	USEPA, 1999
TO-23	VOC	Molecular sieve	DT-GC/MS	0.2-400 µg m^{-3} (0.1-200 ppbv)	USEPA, 1999
ASTM D5466	VOC	*Canister*	GC/MS	0.1-1.0 ppbv	ASTM, 2001 (confirmed 2007)
ASTM D6196	VOC	Adsorbent Tube	DT + proper analytical technique	>0.1 µg m^{-3}	ASTM, 2003 (confirmed 2009)

***Tab. 4.7**: continued.*

ISO 16017-1	VOC	Adsorbent Tube	DT-GC/FID/PID/MS	>0.5 μg m^{-3}	ISO, 2000
ISO 16017-2	VOC	Adsorbent Tube	DT-GC/FID/PID/MS	>2 μg m^{-3}	ISO, 2003
UNI EN 14662-4	Benzene	Adsorbent Tube	DT-GC/FID or others	>0.5 μg m^{-3}	UNI, 2005
OSHA 7	VOC	Adsorbent material	CE-GC/MS, FID	1-20 μg m^{-3} (0.4-2.5 ppbv)	OSHA, 2000
M.U. 1386	VOC (traction hydrocarbon)	Chromosorb	GC/MS	-	UNICHIM, 1999
ISO16200-1	VOC and SVOC	Adsorbent material	CE- GC/MS	1 mg m^{-3}	ISO, 2001
ISO16200-2	VOC	Adsorbent Tube	CE-GC/MS, FID, ECD	1 mg m^{-3}	ISO, 2000
MADEP APH 2008	C5-C8, C9-C12 aliphatic hydrocarbon C9-C10 aromatic hydrocarbon	*Canister*	GC/MS	>2 μg m^{-3}	MADEP ,2008
NIOSH 1550	Hydrocarbon fractions	Adsorbent material	CE-GC/FID	100-400 μg m^{-3}	NIOSH, 2005
NIOSH 1501	BTEX	Activated carbon	CE-GC/FID	> 0.01 mg m^{-3}	NIOSH, 2003
UNI EN 14662-5	Benzene	Adsorbent Tube	CE-GC/FID or other	>0.5 μg m^{-3}	UNI, 2005
M.U. 1576	Benzene and chlorinated hydrocarbon	Tubes	DT-GC/MS	-	UNICHIM
NIOSH 1615	MTBE	Activated carbon	CE-GC/FID	> 0.2 μg m^{-3}	NIOSH, 1994
TO-13A	PAH	PU- Foams or XAD2	CE-GC/MS	0.5-500 μg m^{-3} (0.6-600 ppbv)	USEPA, 1999
NIOSH 5506	PAH	XAD2	CE-HPCL/FL/UV	> 5 ng m^{-3}	NIOSH, 1998
NIOSH 5515	PAH	XAD2	CE-GC/FID	> 1 μg m^{-3}	NIOSH, 1994
TO-9A	Poli-chlorurates and bromates Br- e Cl- PCDD/PCDF	PU- Foams	CE-GC/HRMS	0.25-5000 pg m^{-3}	USEPA, 1999

Tab. 4.7*: continued.*

TO-4	Pesticides and PCB	PU- Foams	CE-GC/MS/ECD	0,2 pg m^{-3}- 200 ng m^{-3}	USEPA, 1999
TO-10A	Pesticides and PCB	PU- Foams	GC/MS/ECD	1-100 ng m^{-3}	USEPA, 1999
ASTM 4861	Pesticides and PCB	PU- Foams, PU-Foams+XAD2	GC/ECD	<0.001 µg m^{-3}	ASTM, 2005
NIOSH 2533	tetraethyl lead	XAD2	GC/PID	> 10 µg m^{-3}	NIOSH,1994
NIOSH 1022	Trichloroethylene	Activated Carbon	CE-GC/FID	0.3-10 mg m^{-3}	NIOSH, 1994
TO-11A	formaldehyde and other aldehyde	DNPH on adsorbent	CE-HPLC-UV	0.5-100 ppbv	USEPA, 1999
ISO 16000-4	Formaldehyde	DNPH on adsorbent	CE-HPLC-UV	> 1 µg m^{-3}	ISO, 2004
TO-8	fenol and cresol	NaOH in bubbler	HPLC-UV	1-250 ppbv	USEPA, 1999
NIOSH 2017	Aniline, p-toluidine, Nitrobenzene	Silica gel	CE-GC/FID	> 0.02 mg m^{-3}	NIOSH, 2003
NIOSH 2002	aromatic anilines	Silica gel	CE-GC/FID	> 1 mg m^{-3}	NIOSH, 1994
MDHS62	p-phthalic acid	Tenax	CE-HPLC-UV	> 4 µg m^{-3}	HSE (UK), 2002
NIOSH 1600	carbon sulfure	Activated carbon	CE-GC/FPD	> 1 mg m^{-3}	NIOSH, 1994
IO-5	Mercury	Golden misture	CVAFS	45 pg m^{-3}	USEPA, 1999
NIOSH 6009	Mercury	Hopcalite	CE-CVAAS	> 0.01 µg m^{-3}	NIOSH 1994

1) VOC = volatile organic compounds, VVOC, very volatile organic compounds, SVOC = semi-volatile organic compounds, PAH = polycyclic aromatic hydrocarbon, PCB = polychlorobiphenyl, PCDD/PCDF = dioxins and furans.

When measuring time is longer, due to analytical limitations (for example when there are low exchange rates, or for situations in which source is very near the surface), F is no longer constant with measuring time and therefore non-linear models have to be applied (Hutchinson et al., 1993; Hutchinson et al., 2001; Davidson et al., 2002). Hutchinson et al., defined a model under the hypothesis that contaminant concentration increases linearly with depth in a uniform layer of soil, which is suitable when observations are available over two successive time periods:

$$F = \frac{V * (C_1 - C_0)^2}{S\,(t_1 - t_0)(2C_1 - C_2 - C_0)} \ln\left[\frac{C_1 - C_0}{C_2 - C_1}\right] \tag{4.15}$$

for $t_2=2t_1$, $\frac{C_1 - C_0}{C_2 - C_1} > 1$ and subscript 0 defines ambient conditions. The results depend heavily on the single measurement precision, and therefore the model is little robust (Hutchinson et al., 1981).

Pedersen at al. introduced a stochastical evolution of (4.15), without any limits on numbers of samples and or equidistance in time (Pedersen at al., 2000).

4.2.6.2 Steady state chambers

In open steady state systems, once it has reached stationary conditions, F is defined as:

$$F = \frac{Q_{in} * (C_{g,out} - C_{g,in})}{A} \tag{4.16}$$

where $C_{g,out}$ and $C_{g,in}$ are concentrations of the observed analyte in outgoing and incoming sweep air (Zhang et al., 2002; Eklund et al., 1985; Castro et al.,1991; De Mello et al., 1994; Kim et al., 1995; Carpi et al., 1998; Poissant et al., 1998; Bahlman et al., 2006), as indicated in Fig. 4.8. Precision of F is derived from replicate C observations over time.

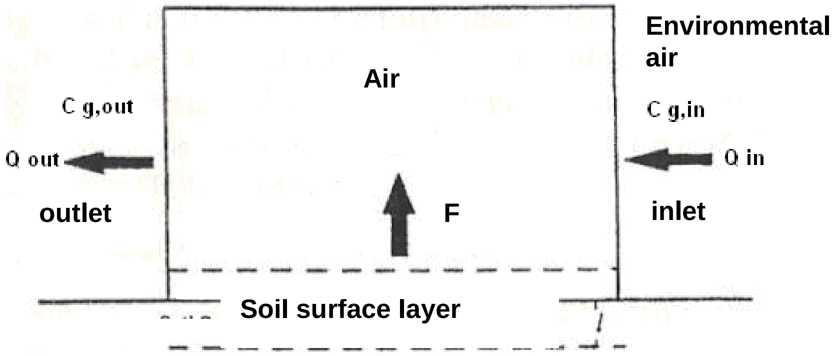

***Fig. 4.8**: steady state chamber (Zhang et al., 2002, modified).*

When clean injection air is used, $C_{g,in}$ is posed equal to zero (USEPA, 1986; Eklund, 1992). Furthermore, when sorbent tubes are applied for sampling, there is often a repartition of out-flowing gas and just a part (Q_{sampl}) is adsorbed on the sampling cartridge for a time Δt. The analytical results are expressed as mass of compounds adsorbed on the tube, M_{sampl}, which is used in a mass balance to give (Gao et al., 1997):

$$F = \frac{Q_{in} * M_{sampl}}{A * \Delta t * Q_{sampl}} \tag{4.17}$$

In open static steady state systems, gas is collected on a passive sampler and F is given by:

$$F = \frac{(M_{sampl} + M_{wall})}{A * \Delta t} \tag{4.18}$$

where M_{sampl} and M_{wall} are the mass absorbed on passive sampling elements and chamber wall respectively; since the latter cannot be measured, it is calculated through numerical models (Batterman et al., 1992). That is why these devices are not used so often for field application, considering the problems indicated in (§ 4.2.5.3).

5

SETUP DEFINITION

5.1 Introduction

This chapter describes the execution and the results of the tests carried out to define stationary state and mixing conditions and the evaluation of the purge time, in order to obtain an ideal chamber setup to monitor emissions of the volatile compounds from contaminated soils. These conditions were verified with a chamber purchased from a supplier, and later by varying the vector gas emission system. On the basis of the results obtained using these configurations, the chamber structure was modified, improving the negative aspects of the previous configuration. This made it possible to obtain a more appropriate chamber setup.

The tests were carried out at DIIAR laboratory as well as outside, while the samples were analyzed exclusively at the DIIAR laboratory.

5.2 Materials and methods

5.2.1 Source and sampling system

The main tracer used to test the Flux Chamber’s (FC) behaviour was ethanol, specifically commercial denatured ethyl alcohol (90%). This choice was made since it is an organic volatile substance, with low toxicity, easily obtainable, and easy to use and analyze. It also samples to be taken instantly, without needing to be accumulated on absorbent material. This analyte, however, has the disadvantage of being less significant when compared to other pollutants found in soil contamination cases, for both its chemical and physical properties and the high concentrations needed to quantify it by the analytical method available in the DIIAR laboratory. As it is in liquid form at room temperature, it was brought to vapour state by fluxing air through a drechsel bottle and making it become saturated by the alcohol. The flows were controlled and measured with a flow meter.

At the beginning of each test, the source parameters were measured; in particular the air inflow moving towards the drechsel bottle (Q_{source}) was recorded (by a bobble glass flowmeter for lower flows) and the concentration of ethanol at its exit (C_{source}) was measured.

The system, used to inject the ethanol-saturated air into the chamber, was a diffuser made of 2 glass Ys linked together by metal and Teflon fittings, ending in 4 PTFE tubes. This device was placed in the centre of the base of the FC and was created in order to have as uniform a source as possible at the bottom planar section of the chamber (Fig. 5.1). The flux emitted by the diffuser was tangential and close to ground level, and therefore best simulated emissions from the soil.

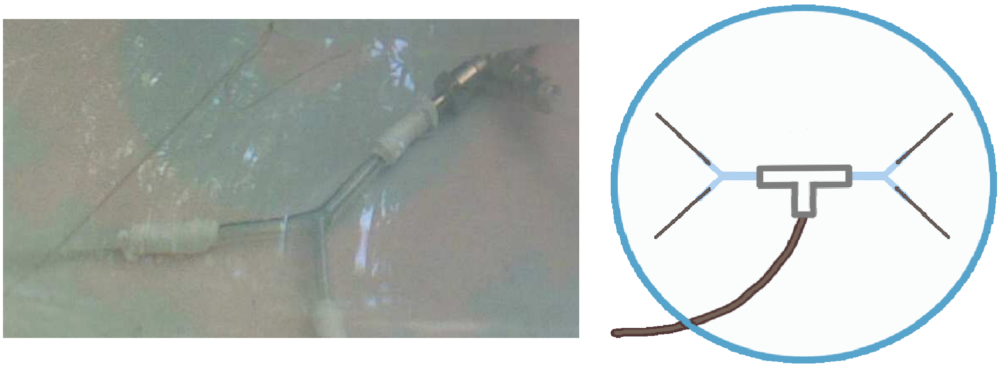

***Fig. 5.1**: device for ethanol source inlet under the Flux Chamber.*

The second used type of source was several coloured tracers produced by smoke candles. As the direct lighting of the smoke bomb under the chamber could have released too much heat, it was lit in a separate reactor, linked to a pneumatic pump emitting environmental air at a pressure of 1-1.5 bar ($1 \bullet 10^5$ - $1.5 \bullet 10^5$ Pa).

The coloured tracer input system consisted of a tube linking the reactor outlet with the FC: it entered below the FC buried in the sand surrounding the base of the chamber (Fig. 5.2).

Fig. 5.2: *device for coloured tracer inlet inside the Flux Chamber.*

Samples of the ethanol-contaminated air were taken using glass sampling bulbs (Fig. 5.3.a) with PFTE taps (§ 4.2.5.2), from which it was possible to extract the sample, by piercing the Teflon septum with a Gas Chromatography (GC) syringe. The sample was taken by linking the bulb, with open taps, to the sampling port and letting the air from the chamber flow through it long enough time to allow multiple complete exchanges of the inner capacity of the bulb (110 ml). According the kind of test, the sampling was carried either with or without suction. In the case of suction, the exit of the bulb was linked to an SKC personal sampler or a suction compressor (§ A1.1.2) (guarded by active carbon cartridges placed between the sampling bulb and the pump). Once the sampling was done, the taps were closed (first the one outside, then the one inside the glass bulb).

Once the sample had been analyzed (§ A2.2.1), the bulb was cleaned by fluxing repeatedly compressed air through it and substituting the septum with an intact one. Preliminary tests had verified that this was enough: by analyzing the content of a bulb cleaned following this procedure, the ethanol concentration resulted inferior to the detection limit (d.l., equal to 0.07 mg l^{-1}).

Just for two final tests a PID (Phocheck Plus) for field activity (§ A1.1.3) was rented to detect directly ethanol concentration during real time measurements. The instrument was filled inside a holed PTFE septum closing glass bulb, which was connected to the sampling line as already described (Fig. 5.3.b).

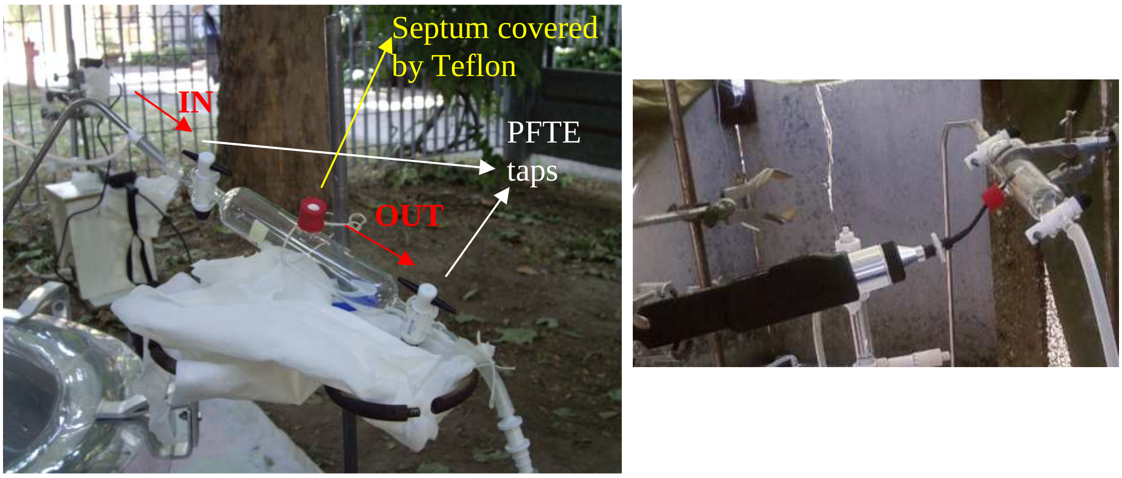

Fig. 5.3*: ethanol-contaminated air sampling device: glass bulb (a) and PID, sampling on line through PTFE septum of glass bulb (b).*

The instrument output results as TPH (total petroleum hydrocarbon) concentrations (x), and therefore an initial calibration phase was performed to convert them in ethanol concentrations, by injecting known amounts of ethanol into airtight bottles, giving concentration (y) inside the measure range. Results of calibration are indicated in Fig. 5.4. C_{source} could not be analysed by this method because beyond its maximum detectable value.

The resulting calibration, with a R^2 coefficient equal to 0.952, was:

$$y = -0.0875\,x^2 + 1.3582\,x - 0.3861 \qquad (5.1)$$

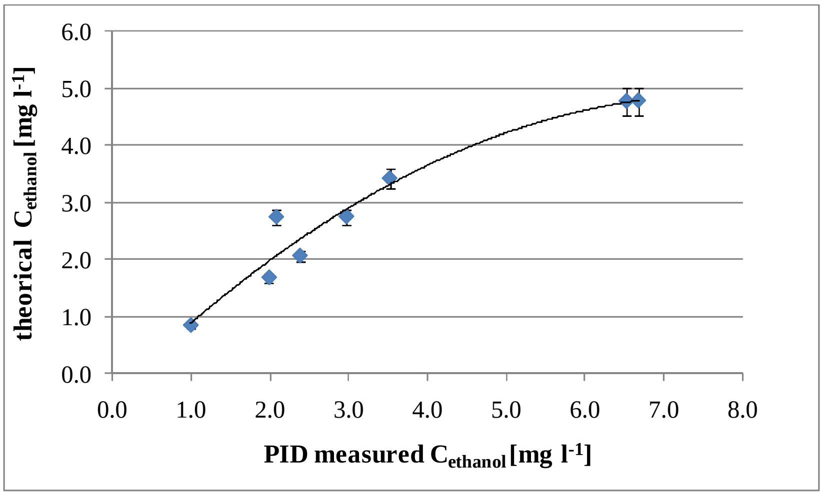

***Fig. 5.4**: calibration curve to set PID instrument.*

With the coloured tracer, the test results were evaluated by visual examination of the behaviour of the gas inside the chamber.

5.2.2 Commercial FC with sweep air injection via a tube

The Flux Chamber used for the first phase of the experiment was bought from Zambelli s.r.l, a company manufacturing and marketing air-quality check equipment. The chamber was manufactured according to EPA guidelines. It was therefore made of an aluminium cylinder, with no base, and an over-mounting circular crown, on which it rests a Plexiglass hemispheric dome, sealed to the crown with a spongy sealing gasket and silicon paste. The dome features three opening vents (VENT), a vector gas intake port (IN) and a sampling port (OUT) (Figs. 5.5 and 5.6). It is also equipped with two steel tubes, one as a sweep gas distribution system and the other for sampling. The size of the chamber is summarized in tab. 5.1.

***Tab. 5.1**: geometrical features of the commercial FC.*

Aluminium cylinder inner diameter	cm	60.8
Aluminium cylinder external diameter	cm	67.0
Height of the aluminium cylinder	cm	25.4
Bottom basis of the cylinder	cm^2	2902
Volume of the cylinder	cm^3	73707
Crown external diameter	cm	72.2
Plexiglas dome external diameter	cm	81.6
dome height	cm	12.0
Total volume	cm^3	92023

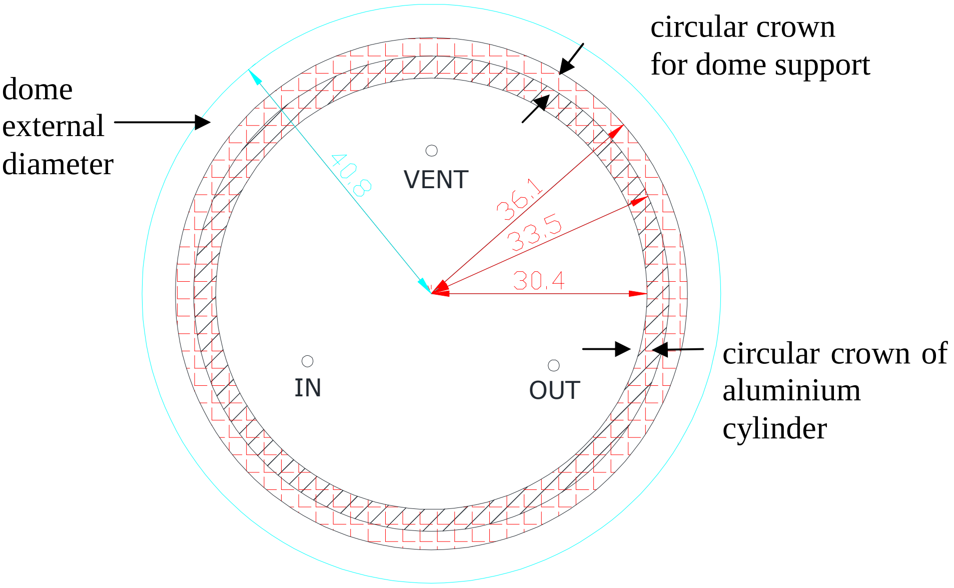

***Fig. 5.5**: planar section of commercial flux chamber.*

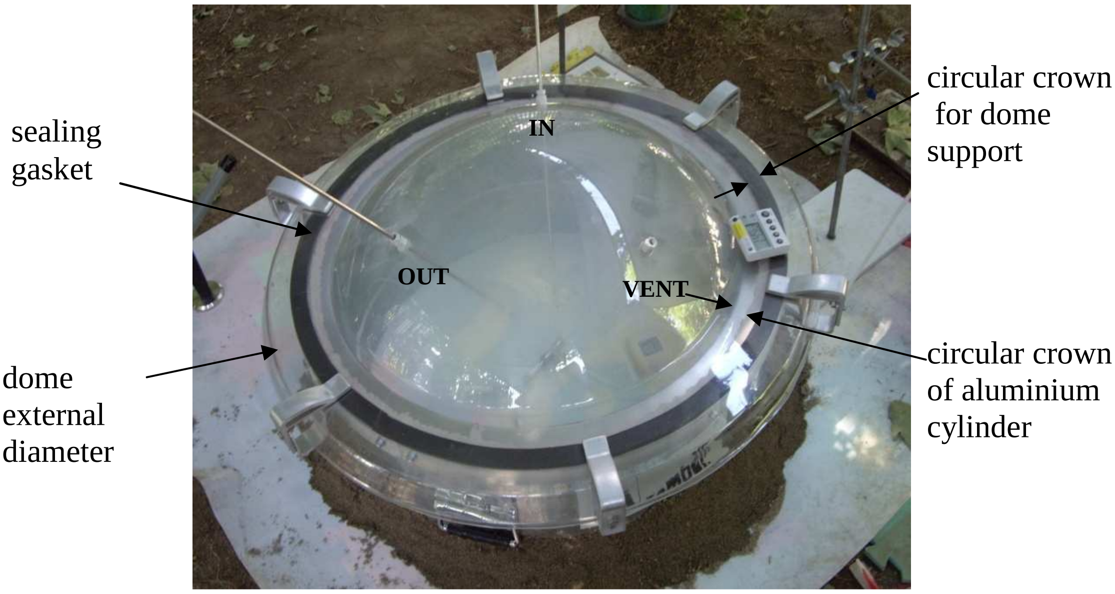

***Fig. 5.6**: picture of commercial flux chamber.*

The chamber was used as an open dynamic FC (§ 4.2.1.2).

In each test it was placed on a Teflon sheet (1 m x 1 m) (produced by Setecs Engineering, MI – I) and sealed at the base with fine wet sand (Fig. 5.7). As sweep gas nitrogen from a pressurized cylinder (Tecnogas S.r.l., MI –I) equipped with a bistadium pressure gauge was used, and the flow was managed and controlled by a mass flow controller (§ A1.1.2.4), ensuring also that the internal pressure was just above the external atmospheric pressure. The sweep gas injection system initially used was the provided steel tube (Fig. 5.7). For these tests, both ethanol and coloured tracers were used.

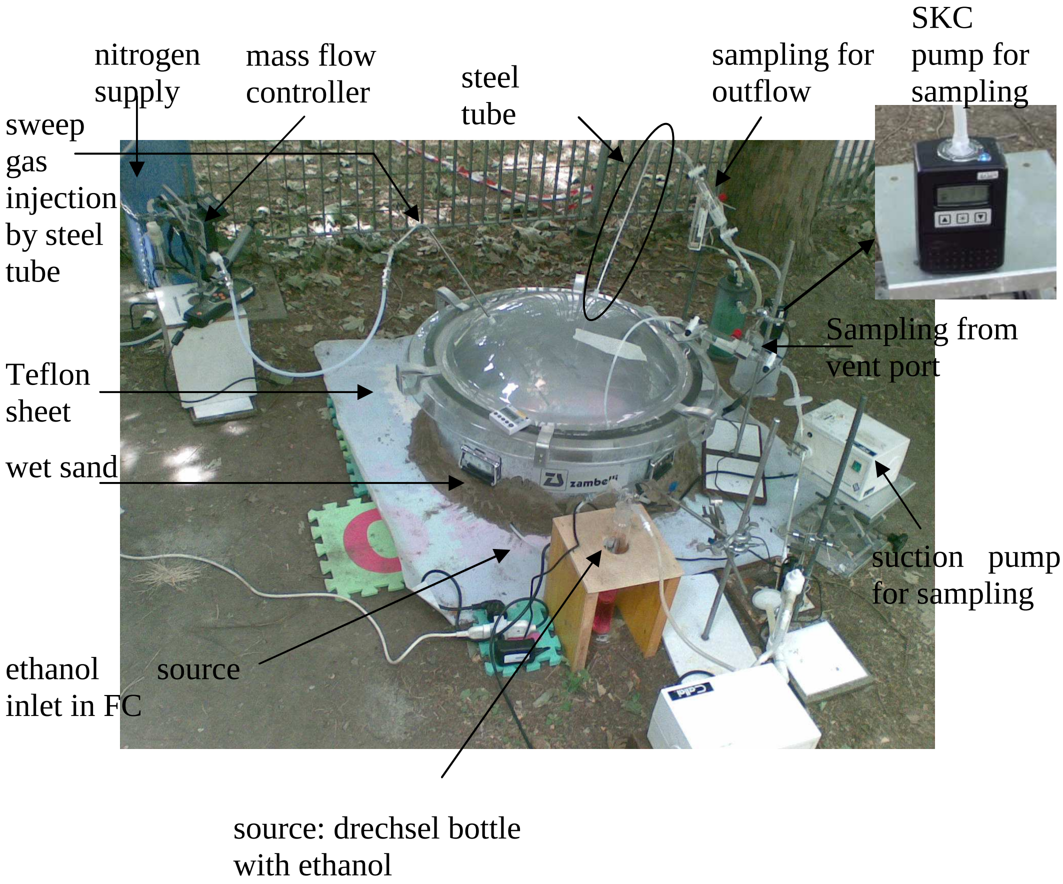

***Fig. 5.7**: elements of test arrangements used for texts with commercial flux chamber.*

With the ethanol source, according to the test, the sample from the FC was taken from the OUT sampling port and/or from the VENT one. In the former case, the inner air from the FC was suctioned through the steel tube inserted into the FC and driven to a glass bulb linked to the SKC personal sampler (§ A1.1.2.1) set to a flow rate of 1.0 ± 0.1 l min^{-1}. In the latter case, a Teflon tube, linked to a bulb (free or linked to a suction pump) was used.

Teflon tubes were used to link the various parts of the system, except for the linking/junction points, where a softer plastic material was used (silicone or tygon).

This configuration was used for three kinds of tests: a) to evaluate the time needed to reach stationary conditions (with ethanol), b) mixing tests (with both ethanol and coloured tracer) and c) measuring the purge time (with coloured tracer). Temperature and humidity data were collected too.

5.2.2.1 Reaching stationary conditions

The aim of this kind of test was to evaluate the time needed to reach stationary conditions inside the chamber, that was how long the concentration of the pollutant (ethanol) took to reach a constant value, and therefore to define the starting sampling time.

The first test (**test 1**) was carried out by injecting ethanol with the “double Y” system (Q_{source} = 0.2 ± 0.2 l min^{-1} and C_{source} = 92 ± 14 mg l^{-1}). The nitrogen injection tube (Q_{in} = 5.00 ± 0.01 l min^{-1}, HRT (§ 4.2.1.2) = 18 min) was inserted 30 cm into the FC and the sampling was done both from the OUT port, with the tube inserted 30 cm (Q_{out} = 1 ± 0.1 l min^{-1}), and from the VENT too, with a PTFE tube inserted 5 cm and linked to a suction compressor, with a flow set to Q_{vent} = 250 ± 7 ml min^{-1}.

The samples were taken 2 hours after the source was switched on, then again, to verify the stability, after 6 hours and 30 min (Fig. 5.8).

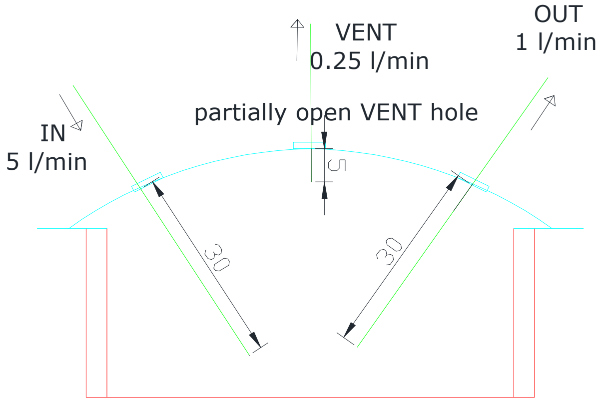

***Fig. 5.8**: test 1 configuration.*

5.2.2.2 Mixing test

The aim of these tests was to verify the complete mixing of the volume enclosed in the FC, that was the complete absence of dead space or preferential paths, and therefore to evaluate that the gas vector injection system via a tube was adequate. The configuration used for this test (**test 2**) was the same as the first test one, with an added sampling point, by pumping from the OUT port through the tube inserted 17 cm into the chamber (Fig. 5.9). Sampling was done simultaneously via VENT and OUT, waiting 90 min between measurements with rods at 17 cm and 30 cm from the dome. Later, two samples were taken from VENT (at 5 cm) and from OUT with tube at 17 cm, doubling the suction flow from VENT (Q_{vent} = 490 ± 5 ml min^{-1}).

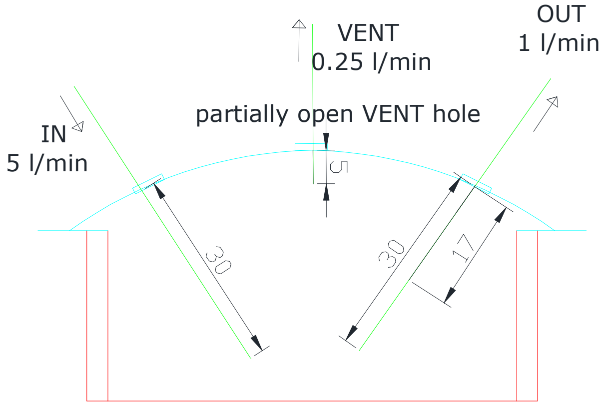

***Fig. 5.9**: test 2 configuration.*

During test 2 physical parameters were measured with the instruments indicated in Tab. 5.2 (details in Appendix 1).

Tab. 5.2*: Instruments used for physical parameters monitoring.*

Parameter	**Inside FC (in)**	**Outside FC (out)**
Temperature (T)	Termoigrometer (Oregon Scientific)	Testo - 435
Humidity (H)	Termoigrometer (Oregon Scientific)	Testo - 435

A third test was also carried out (**test 3**) using an orange tracer to detect the nitrogen inflow path ($Q_{in} = 5.00 \pm 0.01$ l min^{-1}, HRT = 18 min). Nitrogen was driven toward a closed tank containing tracer test; one port was used for inflow and a second one as outflow of coloured gas. In this case, after accurate cleaning, the chamber was filled with white smoke to create an opaque environment to highlight the contrast given by the traced sweep gas.
A suction pump ($Q_{out} = 1.0 \pm 0.5$ l min^{-1}) protected by active carbon, was used for sampling (via tube) (Fig. 5.10).

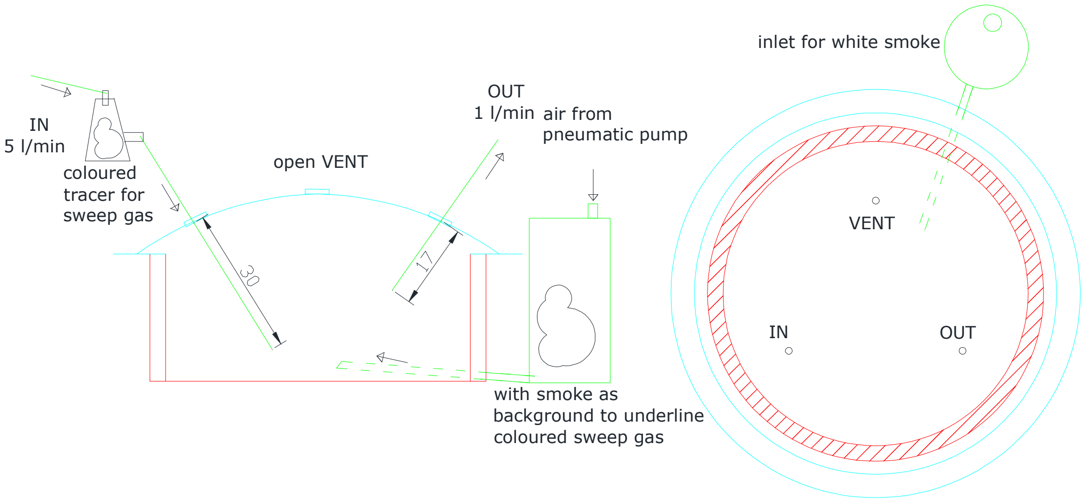

Fig. 5.10*: test 3 configuration.*

5.2.2.3 Purge duration

The aim of these tests was to evaluate the time needed to purge the chamber of environmental background content of the worth compound through sweeping gas injection, verifying that the analyte concentration reached asymptomatically a concentration lower than the d.l.. Specifically, when coloured tracers were used (tests 4 and 5) the length of the time was determined by the disappearance of the smoke.

In **test 4** a pink tracer was injected with the setup described in § 5.2.1. When the injection finished, the nitrogen was introduced via steel tube at $Q_{in} = 5.00 \pm 0.01$ l min^{-1} (HRT = 18 min), regulated by mass flow controller.

A duplicate of previous test (**test 5**) was carried out after having cleaned the chamber from test 4, by injecting orange tracer and simulating the sampling method used in test 3.

5.2.3 Commercial FC equipped with distribution ring

Following the unsatisfactory results of the tests performed by steel tube, an alternative injection system was considered, via perforated ring (as suggested in literature, see § 4.2.4.5), while all the other chamber components remained the same (§ 5.2.2).

The tests were carried out using two different types of ring (A and B, see Tab. 5.3), made in Teflon (PTFE), which were placed at different heights and with the holes facing in different directions, according to the performed test.

Tab. 5.3: *features of rings used for sweep gas injection.*

	ring A	**ring B**
diameter [cm]	60.8	16.0
number of holes	6	74

Initially ring A was used, fixed to the FC by using some fishing line slid between the dome and the gasket; the vector gas was injected into the ring through a steel tube rod inserted into the IN port. Following negative results from the test with ring A, injection by using ring B was tested, with the ring attached directly to the tube. Finally, gas injection was evaluated using both rings simultaneously.

With ring A, three kinds of tests were carried out: a) blank, b) defining the time to reach stationary conditions, and c) evaluating complete mixing tests. With ring B, tests evaluated were: a) verifying the time for reaching stationary conditions, and b) evaluating complete mixing. With both rings together, mixing only was tested.

The sweep gases used were: a) nitrogen (Tecnogas S.r.l., MI-I), or b) treated environmental air when there were nitrogen supply problems (also aiming to test an alternative configuration for application where no cylinders are available for FC measurements). Treated air was sucked by a suction pump (KNF Laboport), then filtered at 0.45 μm (Aperx Instruments) to remove particulate (which, in the long term, would damage the machine), dehumidified on silica gel (Carlo Erba) and purified on two in sequence tubes containing activated carbon (a.c.) (tubes “1” and “2”) (Sigma Aldrich). Two tubes of a.c. were used just for security reasons. A parallel test, performed by sampling ambient air on an a.c. tube, linked to a personal sampler (1.5 ± 0.1 l min^{-1}) for 8 h, showed on “sampling part a” a mass of ethanol lower than the d.l. (< 0.5 μg); thus demonstrating that the ethanol concentration in ambient air was irrelevant for the research aims.

In all the tests, the pollutant source applied was ethanol. The samples from the FC were collected, according to the test, from the sampling port OUT and/or from VENT (§ 5.2.2).

During some tests, temperature, humidity and pressure data were also collected.

Finally, an ethanol adsorption test was carried out on Plexiglass to evaluate the consistency of the occurrences.

5.2.3.1 Tests with ring A

5.2.3.1.1 Blank

The aim of this test (**test 6**) was to verify that the chamber did not give any memory effect that is the presence of residuals of past contamination, kept during a monitoring, that could interfere with following measurements. In this experimental apparatus (Fig. 5.11) ring A (in blue in the figure), placed half way up the cylinder, with the holes facing the centre of the FC, was used and the sampling tube (OUT) was inserted 30 cm into the chamber.

After the chamber had been placed on the sheet, nitrogen (Q_{in} = 5.00 ± 0.01 l min^{-1}) flowed for 120 min, corresponding to 6.5 times the HRT, in order to ensure a complete exchange of the full capacity of the FC. A sample of air from the FC was taken by a glass bulb at the initial moment, when the FC was placed on the Teflon sheet (before the vector gas flow started) and another one 120 min after the sweep gas was switched on. During test 6, some physical parameters were measured using the same instruments indicated in Tab. 5.2.

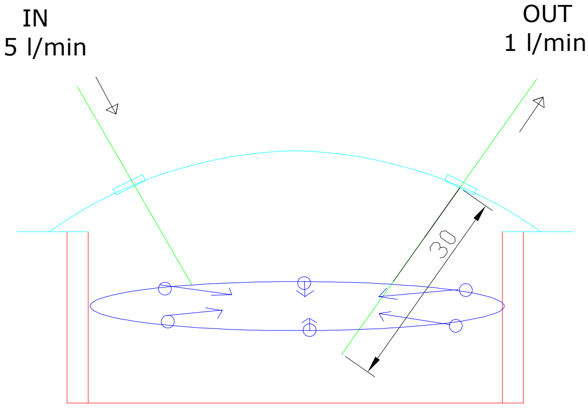

Fig. 5.11: *test 6 configuration.*

5.2.3.1.2 Reaching stationary conditions

To evaluate the reaching of stationary conditions, two tests were carried out (**test 7** and **8**) with the same configuration as used in § 5.2.3.1.1. The ethanol was injected into the chamber using the 4-ways system described in § 5.2.1, with different flow rates according to differently performed tests (Tab.5.3). In test 7, carried out soon after the end of the blank test, samples were taken 15 min, 60 min, 90 min and 120 min after the source was turned on; in the replicate, test 8, just after 30 min and 150 min, to verify previous data. During both tests, temperature and humidity were measured with the same instruments as indicated in Tab. 5.2.

Tab.5.3: *source features for tests 7 and 8. Symbols are introduced at § 5.2.1.*

	Q_{source} [l min^{-1}]	**C_{source} [mg l^{-1}]**
test 7	0.152 ± 0.008	119 ± 18
test 8	0.152 ± 0.008	101 ± 15

5.2.3.1.3 Mixing test

In order to evaluate the mixing with ring A, three tests were carried out (9, 10 and 11) using the flow rates described in Tab.5.4 to generate the source, with indications of ethanol concentrations measured at the drechsel bottle outflow (C_{source}).

***Tab.5.4:** source features for tests 9, 10 and 11. Symbols are introduced at § 5.2.1.*

	Q_{source} [l min^{-1}]	C_{source} [mg l^{-1}]
test 9	0.152 ± 0.008	101 ± 15
test 10	0.152 ± 0.008	142 ± 21
test 11	0.56 ± 0.05	69 ± 10

In **test 9** nitrogen gas was injected using ring A, placed half way up the cylinder, with the holes facing the centre of the FC, with a flow rate of Q_{in} = 5.00 ± 0.01 l min^{-1} (HRT = 18 min). After having reached stationary conditions, the samples were collected from sampling port OUT at three different distances from the dome (9 cm, 17 cm, 30 cm from the dome) as well as from VENT (Fig. 5.12). The samples taken at different heights were collected 60 min after the previous one to allow the system to re-stabilize after the disturbance caused by the tube position change.

During the test, temperature and humidity were measured with the instruments indicated in Tab. 5.2.

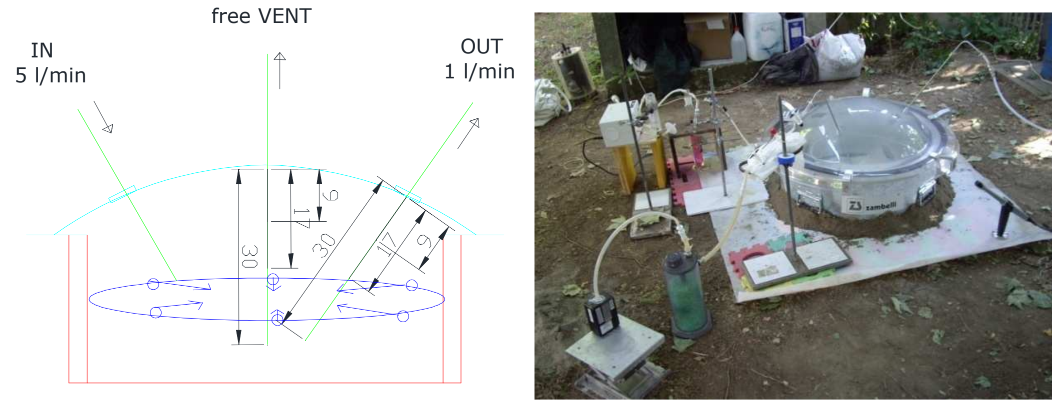

***Fig. 5.12**: test 9 configuration.*

Test 10 was carried out according to the same procedure as test 9, but with a higher nitrogen flow (Q_{in} = 10.00 ± 0.07 l min^{-1}, HRT = 9 min) to evaluate any possible improvements on the chamber's internal mixing. Unlike previous test, another sampling point through VENT was added, by inserting the PTFE tube also at 3 cm inside the dome (Fig. 5.13). During this test temperature and humidity were also measured with the instruments indicated in Tab. 5.2.

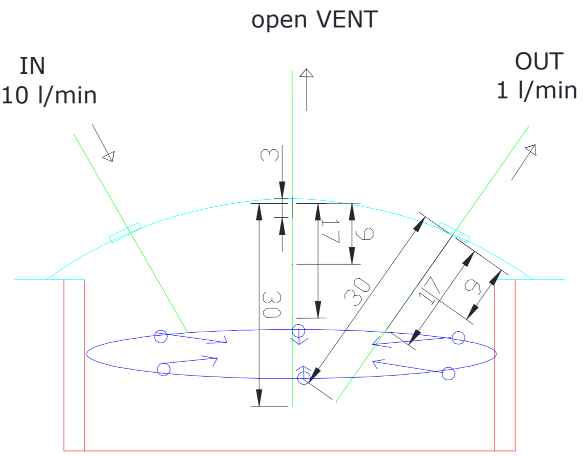

***Fig. 5.13**: test 10 configuration.*

In **test 11** ambient air purified on two vials of a.c. in series (§ 4.2.2) was used, as sweep gas. The air was injected with $Q_{in} = 5.5 \pm 0.2$ l min^{-1} (HRT = 17 min) via ring A placed at ¾ of the cylinder's height, with the holes facing the centre. The samples were taken from an additional position through OUT port, placed at 37 cm from the dome, close to the Teflon sheet, whereas only one was taken at 17 cm through VENT.

Finally, a fan (generally used for personal computer aeration), placed in the central part of the dome, was switched on. The sample was taken from OUT port with the tube at 17 cm (Fig. 5.14).

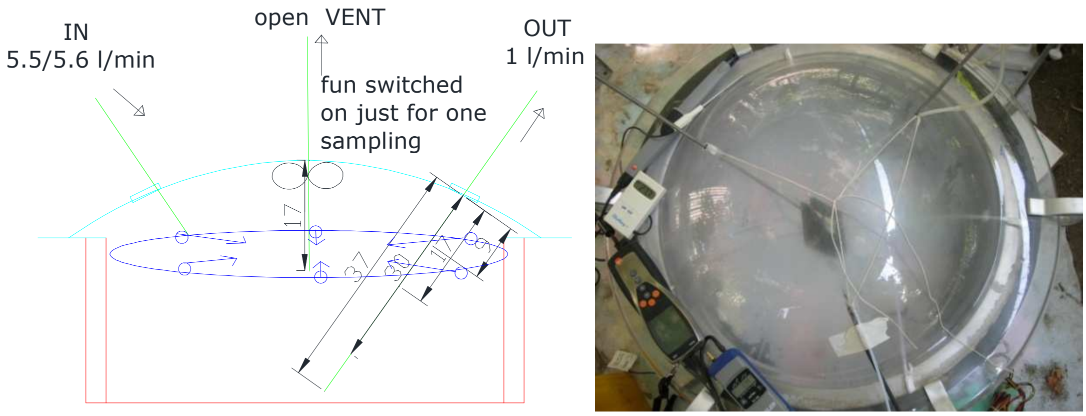

***Fig. 5.14**: test 11 configuration.*

During test 11, temperature and humidity were measured with the same instruments as indicated in Tab. 5.2. The pressure difference between the inside and the outside of the chamber ($\Delta P = P_{in} - P_{out}$) was also measured, at different distances from the dome (0 cm, 13 cm, 25 cm, 31 cm and 37 cm from ground level) by using Micro-manometer DC 100^{PRO} probe (§ A1.1.1.1).

5.2.3.2 Tests with ring B

5.2.3.2.1 Reaching stationary conditions

Only one test was carried out to define the time necessary to reach stationary conditions with ring B configuration: **test 12**. The ring was placed at 13 cm from the dome, with holes facing downwards and nitrogen was injected with $Q_{in} = 5.00 \pm 0.01$ l min^{-1} (HRT = 18 min). Ethanol was injected through the 4-way system, with $Q_{source} = 0.56 \pm 0.05$ l min^{-1} and $C_{source} = 76 \pm 11$ mg l^{-1}. The samples were taken at 60 min and 290 min via a tube inserted 17 cm into the chamber (Fig. 5.15).

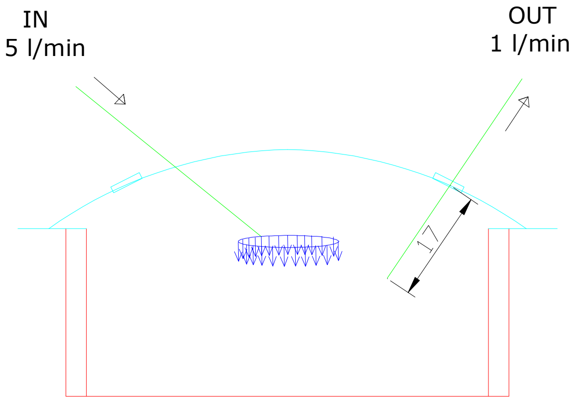

***Fig. 5.15**: test 12 configuration.*

5.2.3.2.2 Mixing test

Two mixing tests were carried out with ring B (test 13 and test 14) and as source the ethanol was injected via the “double Y” system. Tab. 5.5 shows the flows entering the drechsel bottle and the source concentrations.

***Tab.5.5**: source features for tests 13 and 14. Symbols are introduced at § 5.2.1.*

	Q_{source} [l min^{-1}]	**C_{source} [mg l^{-1}]**
test 13	0.56 ± 0.05	76 ± 11
test 14	0.56 ± 0.05	52 ± 8

For **test 13** ring B was placed at 13 cm from the dome, holes facing downwards, injecting nitrogen at $Q_{in} = 5.00 \pm 0.01$ l min^{-1} (HRT = 18 min). From the OUT port, sampling was taken also at 37 cm from the dome, whereas from VENT the sampling was done without suction, at 3 cm from the dome, while it was performed sampling from OUT at 17cm (Fig. 5.16). During this test temperature and humidity were also measured with the instruments in Tab. 5.2.

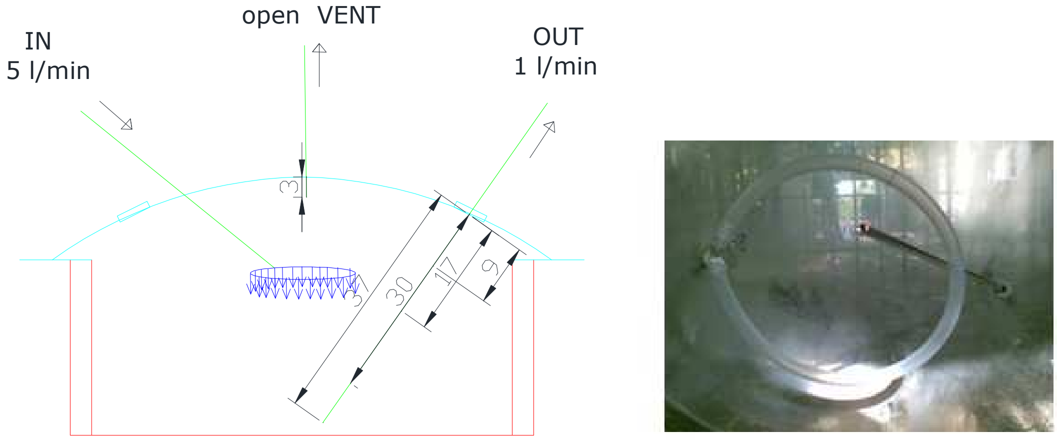

a) **b)**

Fig. 5.16*: test 13 configuration (a) and detail of ring B facing downwards (b).*

In **test 14**, nitrogen was injected through ring B at 2 cm from ground level, with holes facing upwards, with a flow rate of $Q_{in} = 5.00 \pm 0.01$ l min^{-1} (HRT = 18 min) (Fig. 4.17). For OUT port, sampling took place through a tube placed at different distances (from the dome) inside FC (9 cm, 17 cm and 30 cm), whereas for VENT samples were taken at 3 cm from the dome with and without suction (250 ± 7 l min^{-1}). During the test, temperature and humidity were measured with the instruments indicated in Tab. 5.2.

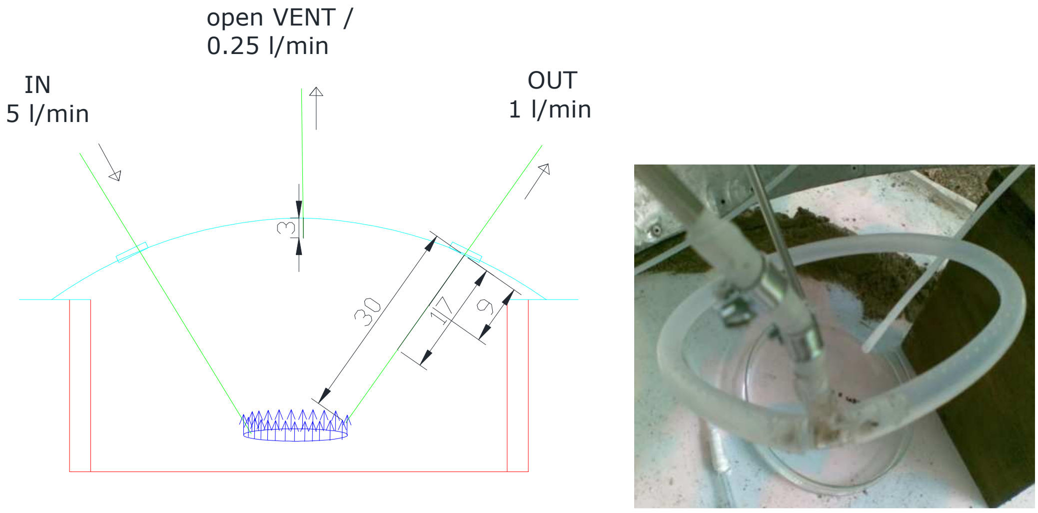

a) **b)**

Fig. 5.17*: test 14 configuration (a) and detail of ring B facing upwards (b).*

5.2.3.3 Rings A and B used simultaneously

5.2.3.3.1 Mixing test

Two tests were carried out with both rings (test 15 and test 16) to evaluate any possible improvement in the mixing. For both tests the vector gas used was purified ambient air (§ 5.2.2) on two vials of a.c. in series. For both tests the airflow flowing through the drechsel, Q_{source}, was 0.56 ± 0.05 l min^{-1} and the outgoing source ethanol concentration C_{source} was 85 ± 13mg l^{-1}.

For **test 15,** ring A ($Q_{in,A}$ = 2.5 ± 0.2 l min^{-1}) was placed as in test 11, whereas ring B ($Q_{in,B}$ = 3 ± 1 l min^{-1}) was placed at 1 cm from ground level (close to the source) with the holes facing upwards. The total flow rate of vector gas was 5.5 ± 1.0 l min^{-1} (HRT = 17 min). The samples were taken only from the OUT port, at 4 different distances from the dome (9 cm, 17 cm, 30 cm, and 37 cm) to evaluate the vertical mixing (Fig. 5.18). Physical parameters were also measured (temperature, humidity and pressure), such as in test 11 (§ 5.2.3.1.3).

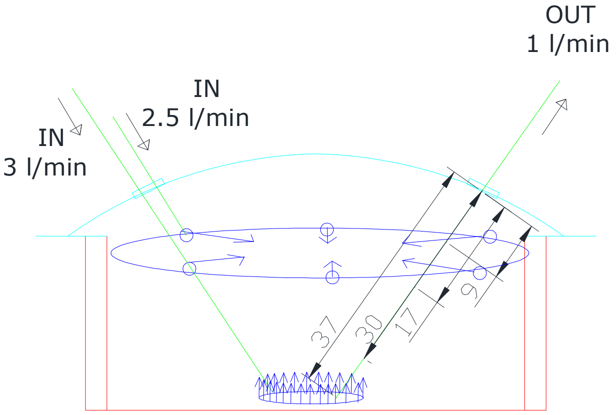

Fig. 5.18: *test 15 configuration.*

In **test 16**, a follow-up to test 15, the fan was switched on (Fig. 5.19). During this test, temperature and humidity were measured, using the instruments in Tab. 5.2.

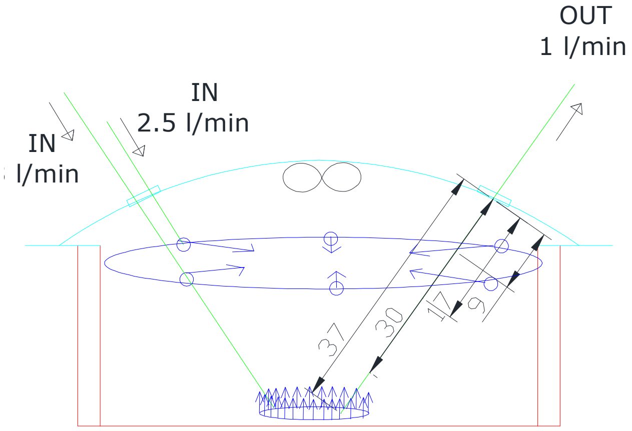

Fig. 5.19: *test 16 configuration.*

5.2.3.4 Absorption test on Plexiglass

In order to verify the entity of the absorption on the material of which the dome was made in its original configuration (Plexiglass), an absorption test with ethanol was carried out.

For this test, four glass reactors were used (A, B, C, D) (Fig. 5.20). A and B contained a piece of Plexiglass suspended using a staple (to allow the entire piece to be exposed to the ethanol), C contained only the staple, for the blank test (to test reactors perfect tightening), and D was left empty.

***Fig. 5.20**: reactors used for adsorption test on Plexiglass.*

Ethanol (32 μl, equivalent to a concentration of 19 ± 3 mg l^{-1}) was added inside A, B and C reactors. The quantity was defined with the aim of testing the same strain undergone during previous tests, with an analogous ratio of ethanol per surface unit. After contacting for 24 h, some gas samples were taken from reactors A and C, whereas the reactor B content was moved into D reactor, and then placed in an oven at 35 °C for 3 h 45 min to evaluate any leak from the strained Plexiglass.

5.2.4 Modifications to the commercial FC: setup equipped with steel tube

On the basis of the results obtained with the commercial FC, its original structure was modified. The main modification consisted into the substitution of the Plexiglass dome with a flat PTFE cover (produced by Setecs Engineering, MI – I). The new cover was equipped with 4 holes (VENT 1, VENT 2, IN, OUT) with airproof joints (Fig. 5.21). The non-inert rubber gasket and the silicon paste were removed, and replaced with a PTFE gasket (with a lining of BA-U R 200[4]) (produced by Setecs Engineering, MI – I). The cover was secured to the cylinder with clamps.

The dimensions of the new setup are indicated in Tab. 5.6.

---

[4] BA-U R 200 is a strong gasket material with special metal reinforcement, made by aramide and inorganic fibers, suitable for high pressure, high temperature and stressed surface applications. 1.5 mm thick sheet was used.

Regarding the sweep gas injection system, tests were initially made using the provided steel tube. The sweep gas was ambient air, purified with activated carbon, with a flow rate of $Q_{in} = 7.5 \pm 0.5$ l min^{-1} (HRT = 10 min). This higher flow rate was chosen to guarantee a lower purge length (helped also by lower FC volume) and directly to test a configuration that would be used for future field application, where different tubes in parallel could be connecting at outflow to sample different analytes, allowing however a positive pressure difference between the inside and the outside of the FC (§ 4.2.4.8.2).

Tab. 5.6: *geometrical features of the commercial FC.*

PTFE cover thickness	cm	1.5
PTFE gasket width	cm	4.8
Inner diameter of the aluminium cylinder	cm	60.8
External diameter of the aluminium cylinder	cm	67.0
Height of the aluminium cylinder	cm	25.4
Surface (A) of the cylinder base	cm^2	2901.9
Total volume	cm^3	73707.3

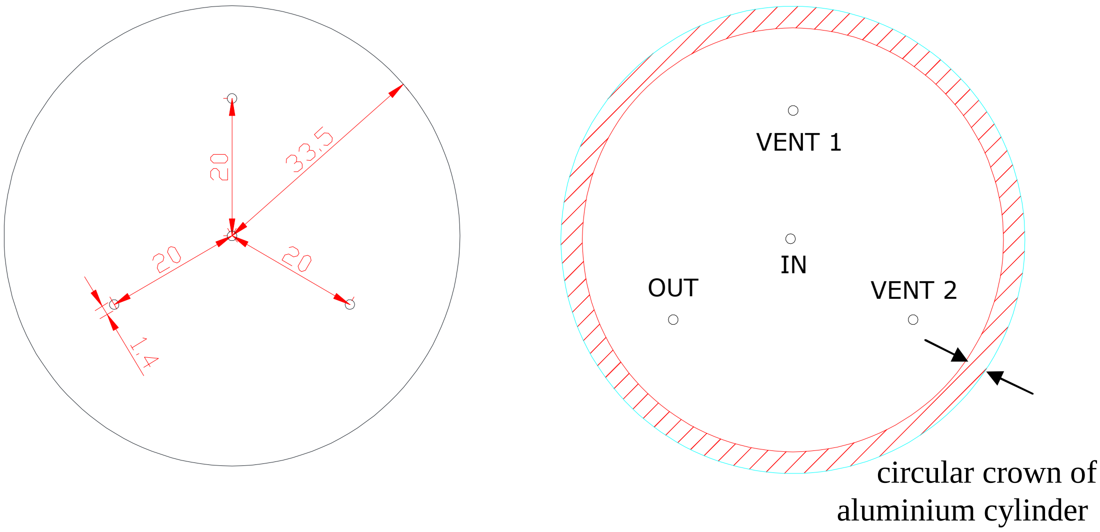

Fig. 5.21*: final FC configuration: planar section.*

New tests were carried out to choose the proper type of activated carbon (a.c.) suited to purify the air for a sampling of 8 h at this flow rate, both for treatment of ethanol to perform tests with the FC new configuration device and for other VOCs treatment for future application at field scale (§ Chapter 6). Three types of activated carbon were tested: GAC 830, NORIT 1 mm and NORIT 3 mm. As is shown in Fig. 5.22, ambient air was sucked (by a pump), after having flowed through a 45 µm filter, then dehumidified on silica gel, and therefore forced through a U shaped container with the a.c.. Sampling to verify the absence of ethanol, as well as the BTEX (with a view to activity at Chapter 6), was carried out by absorbing on a.c. tubes (Sigma Aldrich) (§ 4.2.5.3) with a sampling flow of 1 l min^{-1} after 24 h and 16

h. For the chosen carbon and verified length of treatment, its treatment capacity also for other compounds was verified. In particular chemicals researched during field activity presented at § 6 were analysed: light hydrocarbons (C5 aliphatic, C6-C8 aliphatics, C9-C12 aliphatics, C9-C10 aromatics and MTBE -§ 2.2.3-) sampled on a.c. (Sigma Aldrich) and heavy hydrocarbons (C13-C18 aliphatics, C19-C36 aliphatics, C11-C22 aromatics, naphthalene) on XAD2 (Sigma Aldrich) (§ 4.2.5.3), where C indicates the number of carbon atoms contained in the molecule as indicated in § 2.2.3. The analytical methods, also performed at DIIAR laboratory, were modified MADEP APH (MADEP, 2009b) and MADEP EPH (MADEP, 2004) methods (Tab. 4.7; d.l. indicated at § A2.2.4).

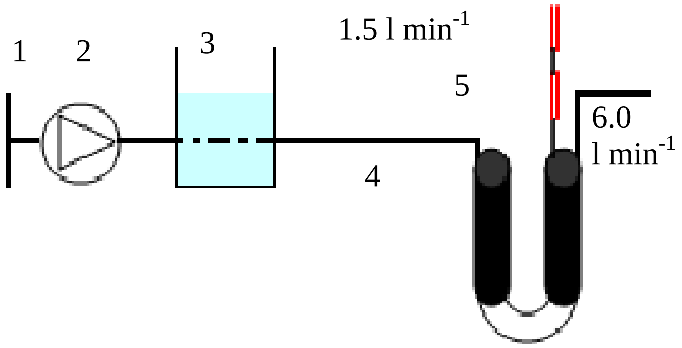

***Fig. 5.22**: environmental air treatment line; 1: particulate filter 45 µm; 2: suction pump; 3: silica gel; 4: U shaped container filled with activated carbon; 5: activated carbon sampling tubes (sampling flow rate = 1.5 l min^{-1}).*

A technique to regenerate the a.c. chosen for the air treatment was also verified. First it was placed in a ventilated muffle at 200°C, with suction system switched on (to remove desorbed contaminated vapours) for 4 h 30 min, allocated in aluminium tanks resistant to that temperature. Then it was left for 2 h in another preheated oven at 150°C, in order to continue the thermal desorption in the final tank (at safe temperature for its glass material). This step was in fact necessary to avoid an abrupt temperature decrease which could have caused air pollutant to be adsorbed on cold carbon. The carbon was placed in an airtight tank (left open) that was already pre-cleaned by leaving it at 150°C for 3 h. Finally the carbon was left to cool in the turned off oven for 2 h.

Because the new Teflon cover was no longer transparent, it was not possible to use cheap qualitative coloured tracers, and therefore all tests were carried out by using ethanol.

Only mixing was tested with the new configuration. The reaching of stationary conditions was not tested, because reducing the volume of the FC and increasing the intake flow, the previous results were deemed valid.

5.2.4.1 Mixing test

To test mixing with the tube as sweep gas injection device, a test **(test 17)** was carried out with the tube placed in centred position (Fig. 5.23). After the chamber was perfectly cleaned, washed and purged, the sweep flow and the ethanol source were switched on simultaneously ($Q_{source} = 400 \pm 100$ ml min^{-1}, $C_{source} = 43 \pm 6$ mg l^{-1}). The sampling, which started 2 hours later to ensure stationary conditions had been met, was performed through OUT port at three different distances (4 cm, 13 cm, and 21 cm from the cover). The top of the steel tube was linked to a Y, whose branches were connected to two SKC personal samplers ($Q_{out} = 1.5 \pm 0.1$ l min^{-1}) protected by a.c. tubes; along one line, before the pump, a glass sampling bulb was placed. Double exit line was applied to simulate parallel sampling on two different devices at the same time (for example also in case of parallel collection of a double sample). During this test, the difference in pressure (ΔP) between the inside and the outside of the chamber was measured by using the same instrument as test 11 (§ 5.2.31.3).

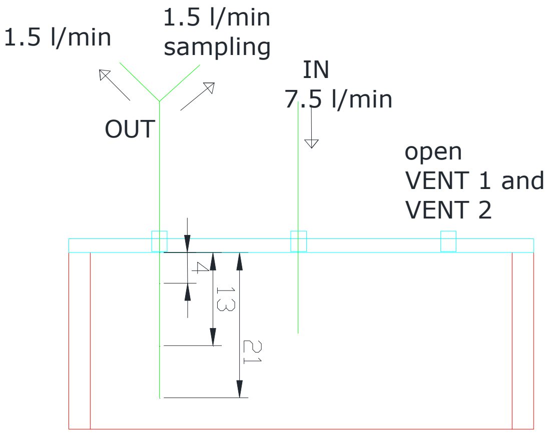

Fig. 5.23: *test 17 configuration.*

5.2.5 FC final setup

Following the unsatisfactory results obtained with the gas injection system through tube (§ 5.2.4), new tests were made using a distribution system consisting of a Teflon spiral, developed along the whole cylinder height, creating one complete coil, with a diameter equal to cylinder one (Fig. 5.24). The coil features 6 equidistant holes, facing the centre of the chamber, characterized by slightly increasing diameters from the air inlet point to the terminal point (sealed).

The used sweep gas was ambient air, purified with a.c. (§ 5.2.4), with a flow of $Q_{in} = 7.5 \pm 0.5$ l min^{-1} (HRT = 10 min).

With the new setup, two tests were carried out using ethanol as a tracer: a) mixing and b) measuring of purge duration.

Fig. 5.24: *final FC setup, with a detail of the Teflon spiral used as sweep air distribution system.*

5.2.5.1 Mixing test

For **test 18**, the sweep gas was injected through IN port (Fig. 5.25) using the spiral system linked to the provided injection tube. The source was injected via the “double Y” system, with a flow of Q_{source} of 400 ± 100 ml min^{-1} and $C_{source} = 43 \pm 6$ mg l^{-1}. The sampling was done via OUT port, such as in test 17.

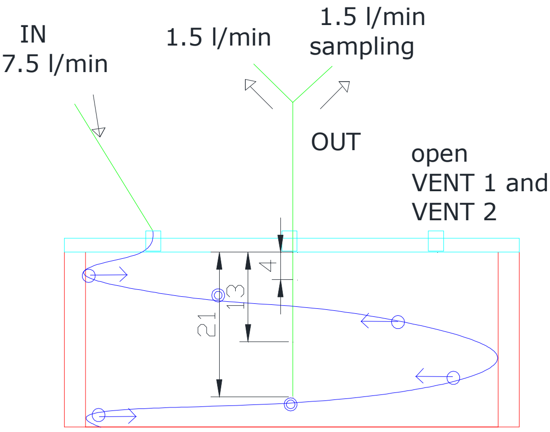

Fig. 5.25: *test 18 and test 19 configuration.*

At the end of test 18, the source was switched off and the OUT port was sealed. Then, the ΔP were measured, half way up the cylinder, to define the influence of the sampling flow, by using the probe described at § 5.2.3.1.3. The sweep gas flow was set to $Q_{in} = 7.5 \pm 0.5$ l min^{-1}. One set of data was acquired by inserting the probe into VENT 1 and sucking air out from VENT 2 with increasing flow rates ($Q_{out} = 0$; 1.0 ± 0.1; 3.0 ± 0.1; 5.0 ± 0.1; 7.5 ± 0.1 l min^{-1}). A second set of data was collected by inverting VENT 1 and 2. For each point 3 measurements were taken.

Test 19 was carried out similarly to test 18, with $C_{source} = 36 \pm 5$ mg l^{-1}. ΔP still half way up way up the cylinder, was also measured, in triplicate for each point, both in VENT 1 and in VENT 2 (with the probe described at § 5.2.3.1.3).

Another test (**test 20**) was carried out in the same way as test 18, but with additional samplings, taken at 3 different distance from the cover (4, 13 and 21 cm) both through OUT port (via the steel tube and Q_{out}=1.5 ± 0.1 l min^{-1}), and both through the two VENTs ports (via a PTFE tube, without suction) (Fig. 5.26). In this case the source was injected with a flow rate of Q_{source} of 800 ± 100 ml min^{-1} and C_{source} = 12 ± 2 mg l^{-1}.

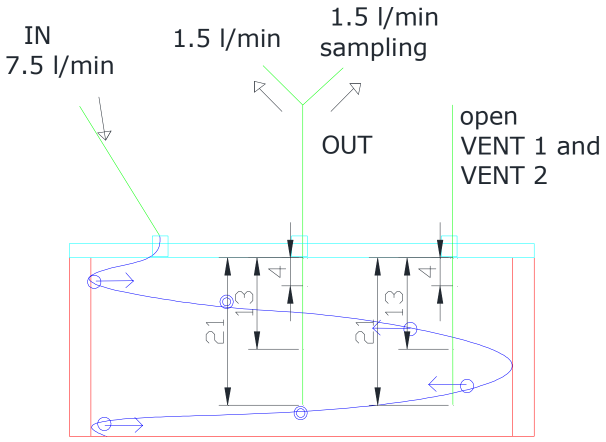

Fig. 5.26*: test 20 configuration.*

A similar test (**test 21**) was carried out, in exactly the same way as test 20, but taking replicates from each sampling point (in triplicate from OUT and in duplicate from VENTs ports), at the same sampling distances from the cover (4, 13 and 21 cm) and in all the ports via the steel tube and Q_{out}=1.5 ± 0.1 l min^{-1} (Fig. 5.27). In this case the source was injected with a flow rate of Q_{source} of 38 ± 1 ml min^{-1} and C_{source} = 160 ± 13 mg l^{-1}.

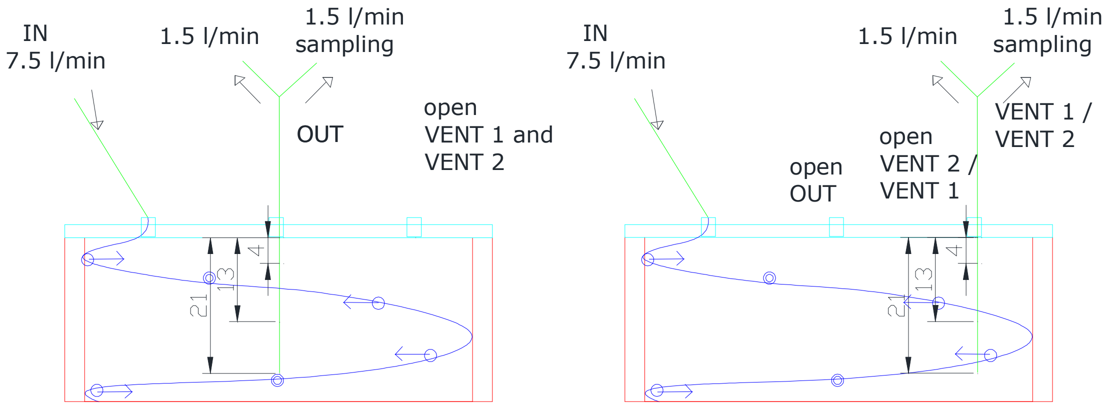

Fig. 5.27*: different phases of test 21 configuration.*

A final mixing test (**test 22**) was performed by sampling directly on line through field-using FID, to check ethanol concentration in OUT, VENT 1 and VENT 2 ports, at the usual sampling distances from the cover (4 cm, 13 cm and 21 cm). Samples were taken at three different suction flows: a) 3.0 ± 0.1 l min^{-1}, b) 1.5 ± 0.1 l min^{-1} and c) 0.22 ± 0.01 l min^{-1}. For a) and b) the FID sampling tip was inserted into a glass bulb which was connected to the steel tube and SKC pump as in previous tests. For c) the samples were taken directly by inserting the FID tip inside the FC at the right distance; in this case the internal pump of the instrument was used for sucking (Fig. 5.28). In this case the source was injected with a flow rate of Q_{source} of 200 ± 10 ml min^{-1}. Each datum was the average of 7 data collected in 10 minutes, thanks to the short duration of analysis, and for each position 8 replicates were performed. TPH concentrations, returned by FID, were transformed into ethanol ones by 5.1.

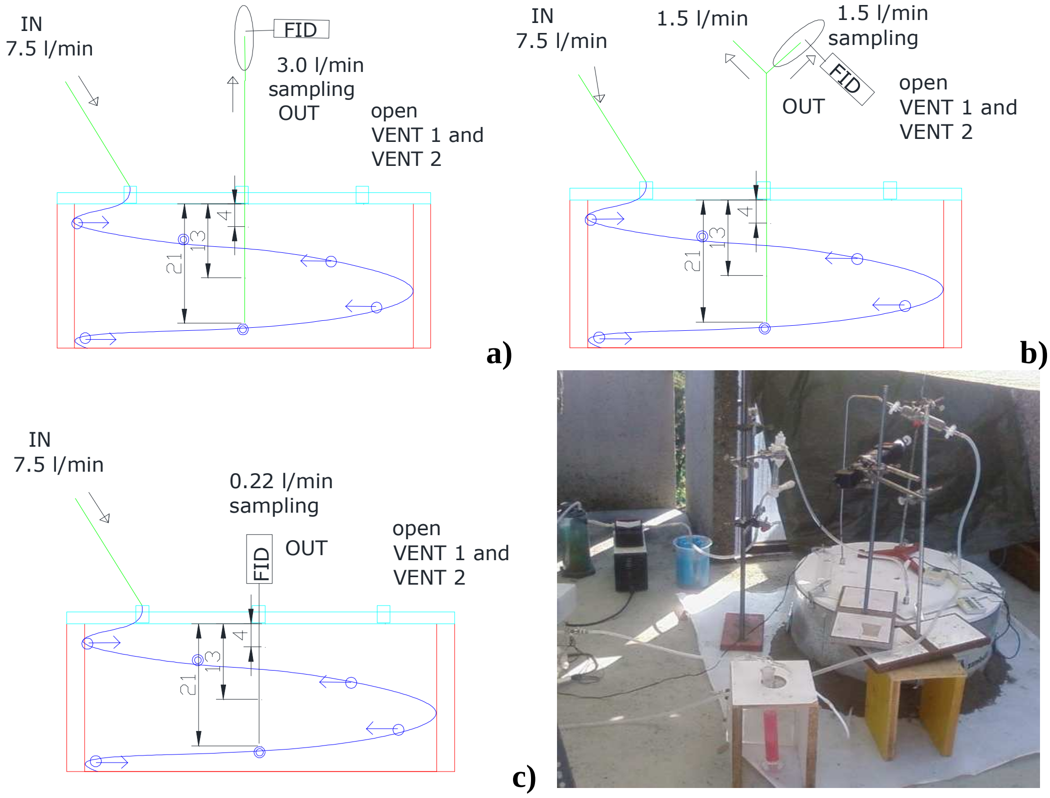

Fig. 5.28*: different phases of test 22 configuration: shown sketch only for OUT port for different suction flows: a) 3.0 ±0.1 l min^{-1}, b) 1.5 ±0.1 l min^{-1} and c) 0.22 ±0.01 l min^{-1}. d) is a picture for sampling from VENT 1.*

5.2.5.2 Purge duration

In the purge duration test (**test 23**), the injection system was configured analogously to test 20. After cleaning the FC (with compressed air) and the PTFE sheet, the source was switched on at Q_{source} = 4.0 ± 0.1 l min^{-1} for 20 min. Sampling occurred from VENT 2 (Fig. 5.29), with the steel tube placed approximately 15 cm below the PTFE cover. The first sample was taken at 0.5 ± 0.1 l min^{-1} for 1 min soon after the source was switched off and the sweep gas started to flow; following samples were taken, with Q_{out}= 1.5 ± 0.1 l min^{-1}, 30 min, 90 min, 150 min and 870 min after the sweep gas was turned on (having verified that the results were not influenced by the two different sampling flow rates).

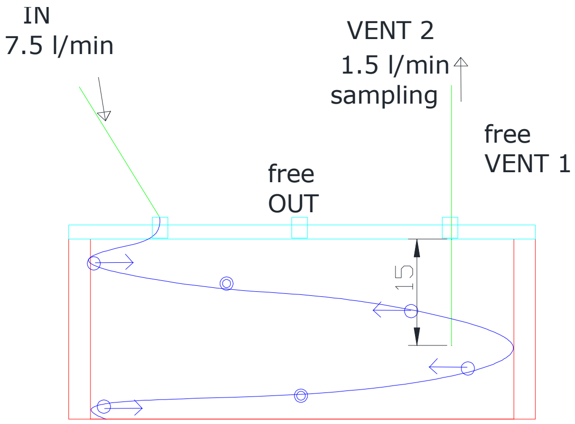

Fig. 5.29: *test 23 configuration.*

Another purge duration test (**test 24**) was performed by using FID analysis. After having cleaned the FC (similarly to procedure followed for test 23) and measured background values, the source was switched on at $Q_{source} = 1.0 \pm 0.1$ l min^{-1} for 1.5 min to obtain an initial concentration inside the detection range of the instrument. Sampling occurred from OUT (Fig. 5.30), with the steel tube regulated approximately 15 cm below the PTFE cover. Samples were taken by placing FID tip into a glass bulb connected to SKC pump regulated at $Q_{out} = 0.15 \pm 0.1$ l min^{-1} (similarly to test 22.b), first at shorter and then at longer intervals, according to test behaviour. The test was performed in triplicate and lasted respectively 135, 155 and 138 min after the source was switched off, when stable values were reached.

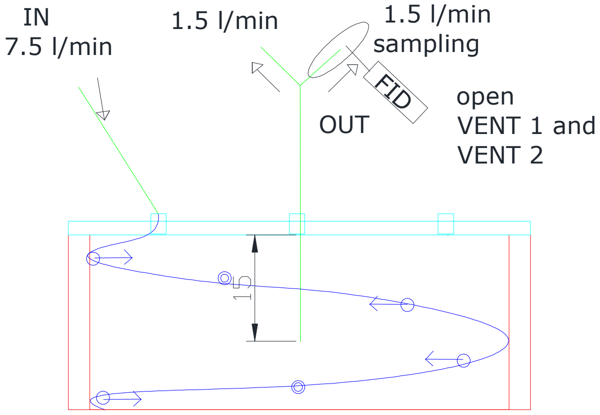

Fig. 5.30*: test 24 configuration.*

5.3 Results

5.3.1 Ethanol source

Fig. 5.31 shows the trend of the ethanol concentration measured in the differently generated sources, according to the amount of air injected into the drechsel bottle.

When the flow grows, the concentration of the ethanol in the outlet flow (used as source inside the FC) decreases, due to a reduced contact time between the air entering the drechsel bottle and the liquid ethanol within it.

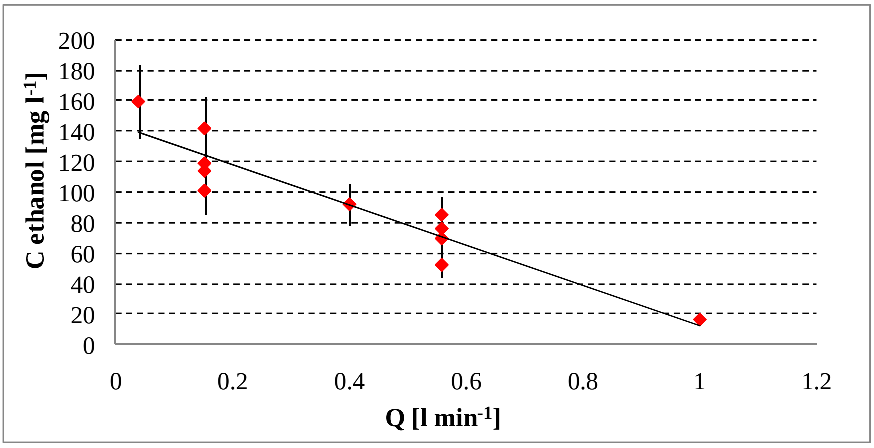

***Fig. 5.31**: ethanol concentration [mg l^{-1}](used as pollutant source for FC tests) as a function of air flowing through the drechsel bottle [l min^{-1}], interpolated by linear regression. Error bars indicate analytical error (VC: 15%, see § A2.2.1).*

5.3.2 Commercial FC with sweep air injection via a tube

5.3.2.1 Reaching stationary conditions

The ethanol concentrations measured during **test 1**, from the two sampling points (OUT and VENT), 2 h and 6 h 30 min after the source had been switched on, are summarized in Tab. 5.7.

***Tab. 5.7:** ethanol concentration [mg l^{-1}] from OUT and VENT ports (test 1); s.d.: standard deviation.*

Time	**$C_{ethanol}$** **L_{OUT} = 30 cm**	**$C_{ethanol}$** **L_{VENT} = 5 cm**
min	**mg l^{-1}**	**mg l^{-1}**
120	3.1	3.1
390	3.8	3.5
average ± s.d.	3.5±0.4	3.3±0.2

The results show how, for a given sampling port, there is no meaningful difference (considering the analytical variation coefficient for the used method: 15%) between the two measuring times, which indicates that the necessary time to reach stable conditions is less than 2 h. Furthermore, there is no significant difference between the results on the samples taken from OUT and from VENT (considering the average values), which further indicates the possible interchange of the two ports.

5.3.2.2 Mixing test

The results of the mixing test via steel tube (**test 2**) are indicated in Tab. 5.8. The agreement between the samples taken from OUT at 17 and 40 cm, as well as the agreement between VENT at 5 cm, show that, with this setup, there was a good level of vertical mixing in the chamber.

Tab. 5.8*: ethanol concentration [mg l^{-1}] from OUT and VENT ports (test 2); s.d.: standard deviation.*

Sampling distance from the dome	**$C_{ethanol}$ OUT**	**$C_{ethanol}$ VENT**
cm	**mg l^{-1}**	**mg l^{-1}**
5	-	3.9 3.1
17	3.9	-
30	3.1	-
average ± s.d.	3.5±0.4	3.5±0.4

Doubling the sampling flow rate from VENT, the found results were lined up with previous ones, as from OUT (at 17 cm) the ethanol concentration was 3.6 mg l^{-1} while from VENT (at 5 cm) it was 3.2 mg l^{-1}.

Fig. 5.32 shows the values of the temperature inside (T_{in}) and outside (T_{out}) the FC, taken during test 2. It is clear the temperatures had a parallel trend, with $\Delta T = T_{out} - T_{in}$ constant for the entire test, with an average ($\Delta T_{average}$) value of 3.4 °C.

Fig. 5.33 shows the humidity levels measured during the test, inside (H_{in}) and outside (H_{out}) the FC: although it followed the same trend as the external humidity, the internal humidity was lower, which may have been because the test was performed on the Teflon sheet and, therefore, not influenced by ground moisture.

Test 3, with the orange tracer, did not confirm the good mixing that resulted from test 2. After injecting the traced nitrogen, coloured threads were visible close to the gasket, where they seemed to be escaping from the contact point between dome and base, highlighting that the system was not airtight. This test also showed that the dome tip was not involved by the nitrogen flow and that the end of the injection tube was the vertex of upside down cone of air.

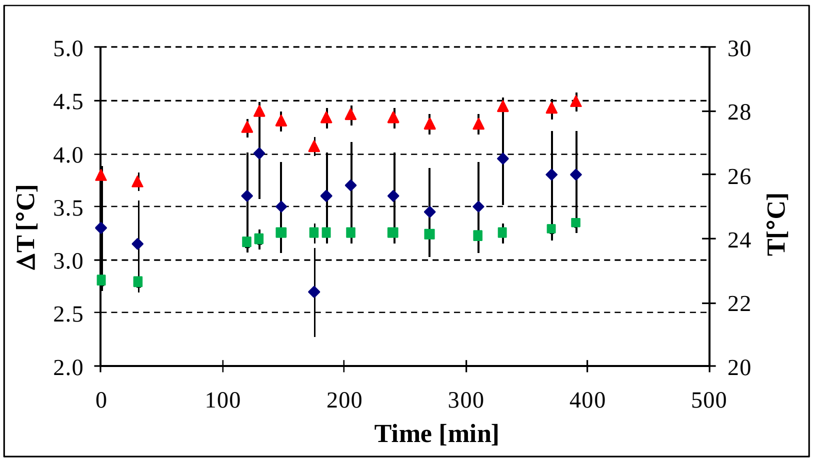

***Fig. 5.32**: temperature measured outside (red triangles) and inside (green squares) the FC (read on right axis), and their difference (blue lozenges) (read on left axis) (test 2). Error bars indicate instrumental error or its propagation on temperature difference.*

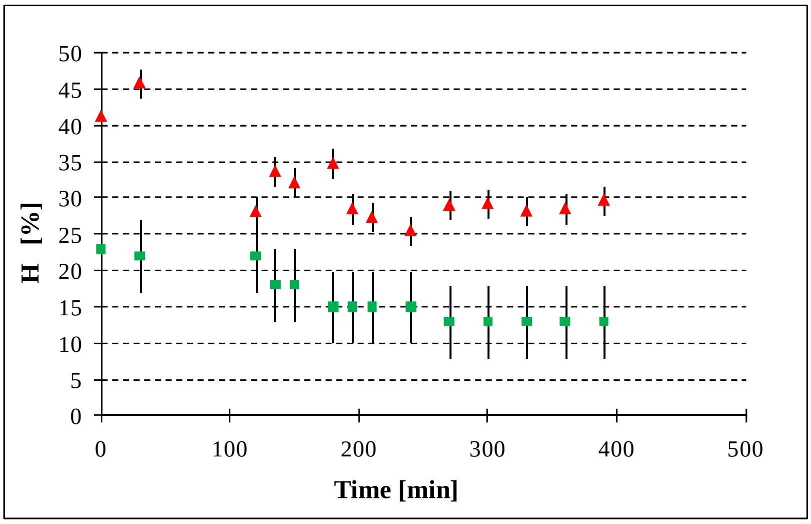

***Fig. 5.33**: humidity measured outside (red triangles) and inside (green squares) the FC (test 2). Error bars indicate instrumental error.*

5.3.2.3 Purge duration

Fig. 5.34 shows the reduction of intensity of the pink tracer over time, inside the FC, due to continuous injection of sweep gas (**test 4**). 3 hours were not enough to purge the chamber completely of the coloured smoke; it was noticed that, after 2 hours, the situation was almost unvaried, possibly due to the dead zones in the FC.

This was confirmed also by the pictures in Fig. 5.35, showing the orange tracer trend over time during **test 5**. Also in this case, in fact, 2 hours were not long enough to purge the chamber completely of the smoke.

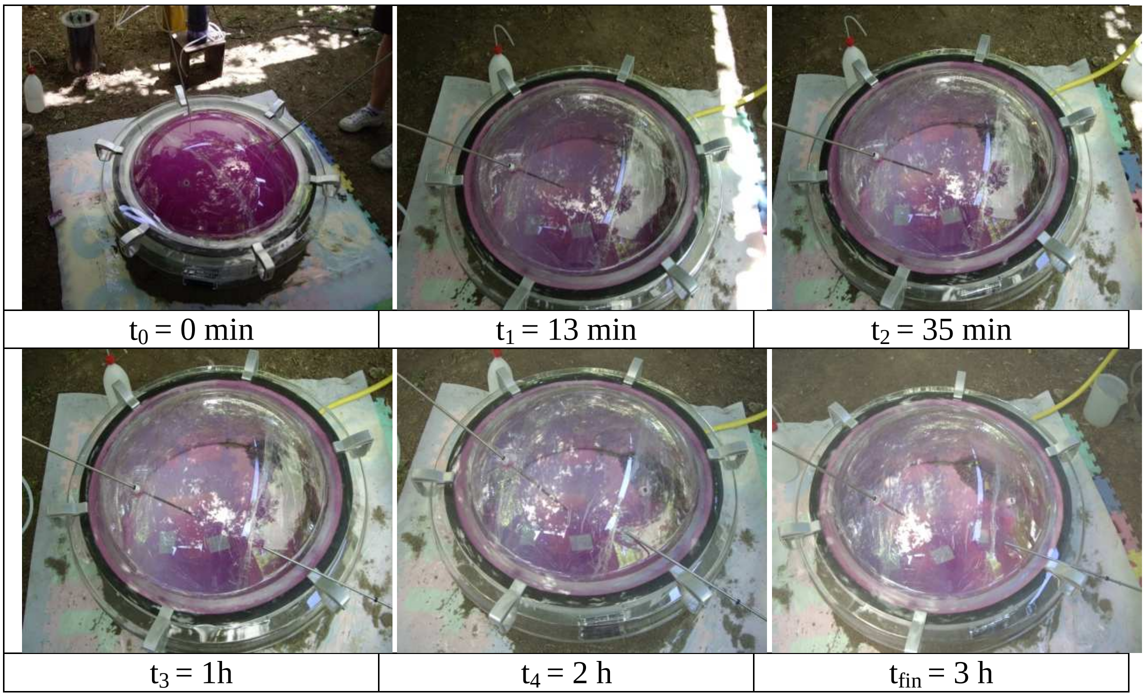

t_0 = 0 min | t_1 = 13 min | t_2 = 35 min

t_3 = 1h | t_4 = 2 h | t_{fin} = 3 h

***Fig. 5.34**: purge duration (test 4); t_0 was seen soon after the tracer injection.*

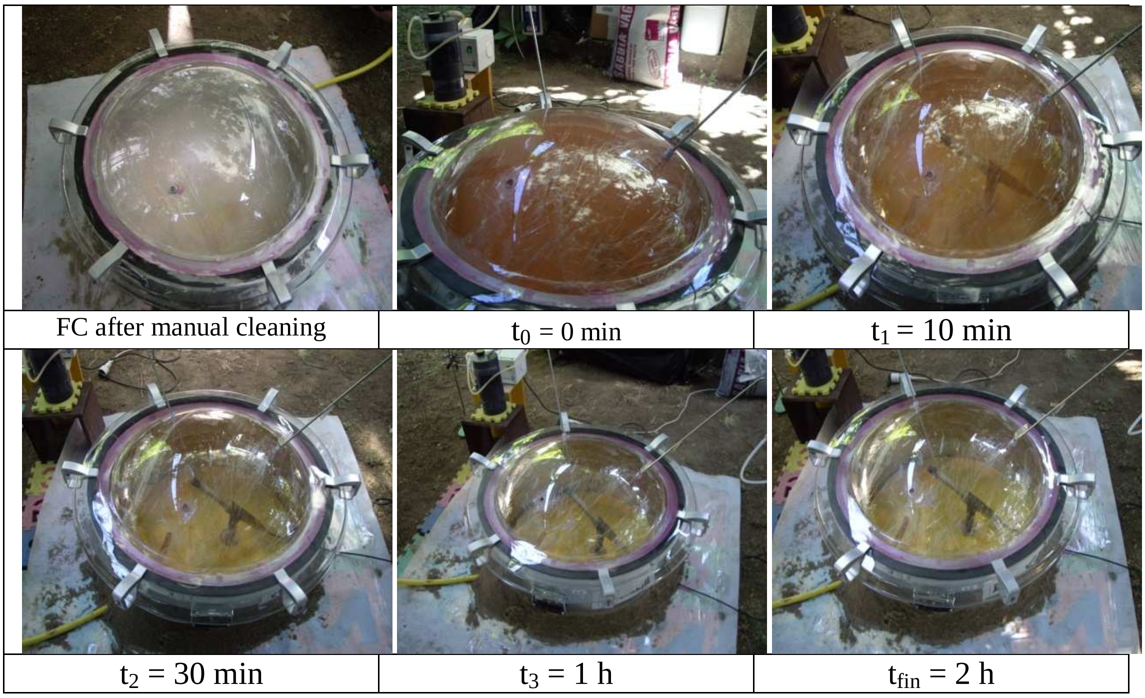

FC after manual cleaning | t_0 = 0 min | t_1 = 10 min

t_2 = 30 min | t_3 = 1 h | t_{fin} = 2 h

***Fig. 5.35**: purge duration (test 5); t_0 was seen soon after the tracer injection.*

5.3.3 Commercial FC equipped with distribution ring

5.3.3.1 Tests with ring A

5.3.3.1.1 Blank

During **test 6**, both the sample taken immediately after the chamber was placed on the Teflon sheet and the one taken hours after 2 the sweep gas had been switched on, revealed ethanol concentrations lower than the d.l. (0.07 mg l^{-1}, Appendix 2). This result demonstrated the absence of a deposit of the analyte inside the FC.

5.3.3.1.2 Reaching stationary conditions

The results of **test 7** (in Tab. 5.9 and Fig. 5.36) show that, already after 1 hour, the chamber equipped with ring A had met stationary conditions, as the ethanol concentration stayed constant.

Tab. 5.8*: ethanol concentration [mg l^{-1}] in the FC versus time after source switching on (test 7); s.d.: standard deviation due to analytical error.*

Time	**min**	15	60	90	120
$C_{ethanol}$ average ± s.d.	**mg l^{-1}**	1.2 ± 0.2	2.9 ± 0.4	2.9 ± 0.4	2.9 ± 0.4

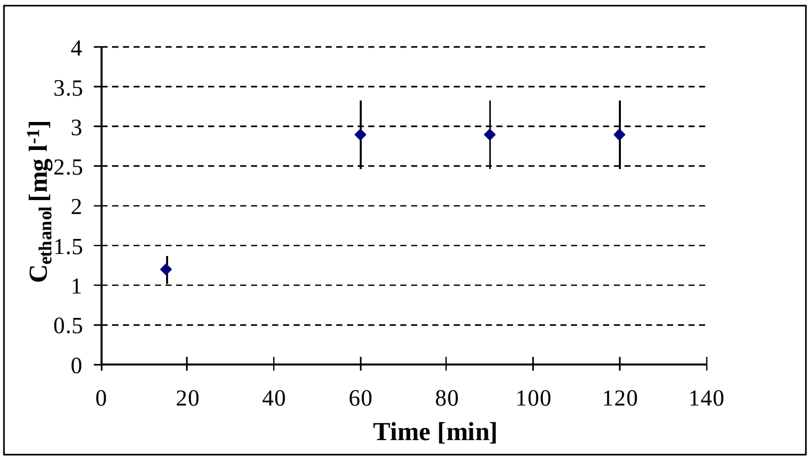

Fig. 5.36*: ethanol concentration [mg l^{-1}] in the FC versus time after source switching on (test 7, Tab. 5.8); error bars indicate analytical error.*

Figs. 5.37 and 5.38 show temperature and humidity trends (internal and external to the FC) observed during tests 6 and 7 (120 min is the starting time of test 7). During test 6, the internal temperature (T_{in}) was initially higher than the external one (T_{out}). This was due to the overheating of the FC positioning surface before it was placed over it, which occurred during the warmest hours of the day (12 a.m.). During test 7 the internal and external temperature had contrasting trends, and T_{in} was always lower than T_{out}; $\Delta T_{average}$ was 1.3 °C.

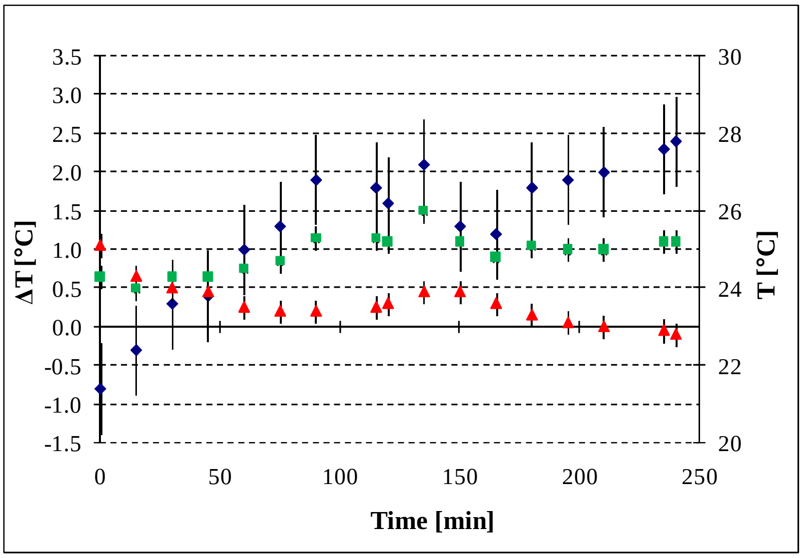

Fig. 5.37*: temperature measured outside (red triangles) and inside (green squares) the FC (read on right axis), and their difference (blue lozenges) (read on left axis) (test 6 and 7). Error bars indicate instrumental error or its propagation on temperature difference.*

During both tests, the internal humidity was lower to the external one; which was because the chamber was placed on a Teflon sheet and was therefore not affected by ground moisture. After 50 minutes, moreover, the internal humidity remained constant due to the influence of dry sweeping flow.

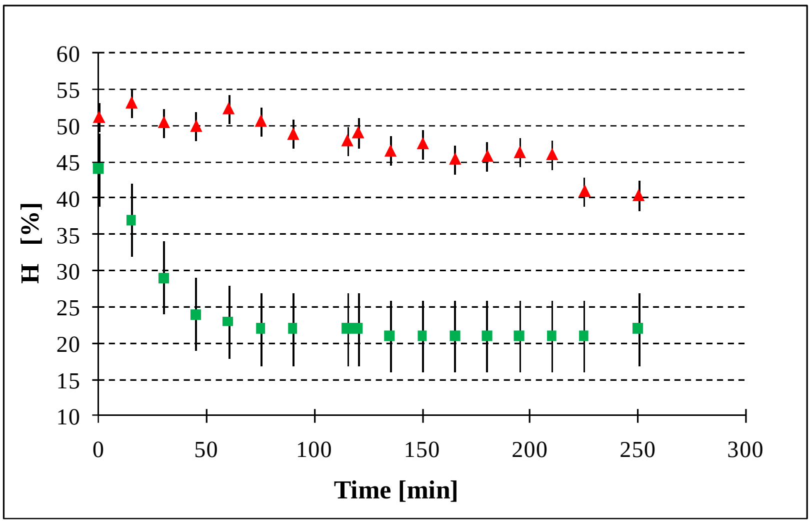

Fig. 5.38*: humidity measured outside (red triangles) and inside (green squares) the FC (test 6 and 7). Error bars indicate instrumental error.*

Results of **test 8** are shown in Tab. 5.10. The ethanol concentrations at the two sampling times were similar, confirming that after 30 min the chamber had reached stationary conditions. To operate under safe conditions, however, the samples of following tests were taken 2 hours after the source had been switched on.

***Tab. 5.10**: ethanol concentration [mg l^{-1}] from OUT port (test 8); s.d.: standard deviation.*

Time	**$C_{ethanol}$ L_{OUT}= 30 cm**
min	**mg l^{-1}**
30	2.8
150	2.7
average ± s.d.	2.75±0.05

Figs. 5.39 and 5.40 show respectively the trend over time of temperature (both inside and both outside the FC, and their difference) and of humidity (inside and outside the FC) recorded during test 8. The internal temperatures was always lower than external ones and followed a parallel trend, proved by a stable $\Delta T_{average}$ value equal to 1.4 °C ± 0.1°C (as standard deviation).

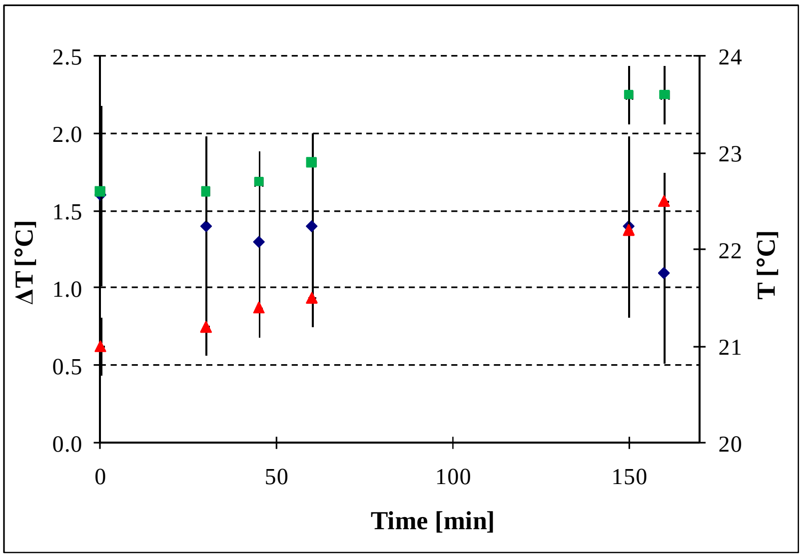

***Fig. 5.39**: temperature measured outside (red triangles) and inside (green squares) the FC (read on right axis), and their difference (blue lozenges) (read on left axis) (test 8). Error bars indicate instrumental error or its propagation on temperature difference.*

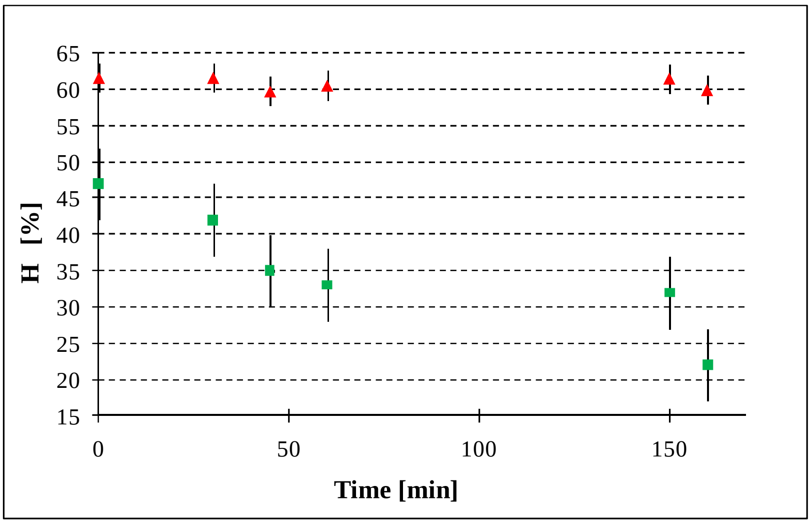

Fig. 5.40: *humidity measured outside (red triangles) and inside (green squares) the FC (test 8). Error bars indicate instrumental error.*

5.3.3.1.3 Mixing test

Ethanol concentrations sampled during **test 9** through OUT and VENT ports are indicated in Tab. 5.11 and shown in Fig. 5.41.

Comparing the concentrations along the verticality of VENT, the FC equipped with ring A showed a good level of mixing. On the contrary, along the verticality of OUT, the chamber resulted poorly mixed, highlighting an accumulation of the analyte in the central distance (17 cm). As for horizontal mixing, the comparing between samples from OUT and VENT depends on the distance; a good agreement is shown at the distances of 17 and 30 cm, whereas at the highest part of the chamber (9 cm from the dome) there is a meaningful difference among the two positions.

Tab. 5.11: *ethanol concentration [mg l^{-1}] from OUT and VENT ports (test 9); s.d.: standard deviation.*

Sampling distance from the dome	**$C_{ethanol}$ OUT**	**$C_{ethanol}$ VENT**	**Average ± s.d. on horizontal position**
cm	**mg l^{-1}**	**mg l^{-1}**	**mg l^{-1}**
9	2.6	3.6	3.1 ± 0.5
17	4.0	3.5	3.8 ± 0.3
30	2.7	3.3	3.0 ± 0.3
average ± s.d. on vertical position	3.1 ± 0.6	3.5 ± 0.1	

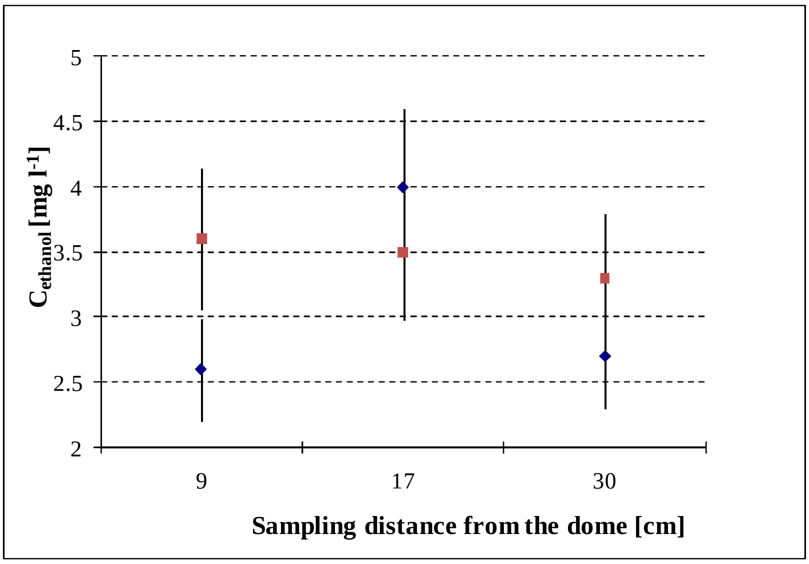

***Fig. 5.41**: ethanol concentration [mg l^{-1}] in the FC from mixing test 9 (Tab. 5.11); in OUT (blue lozenges) and VENT (pink squares); error bars indicate analytical error.*

Figs. 5.42 and 5.43 indicate respectively the temperature (T_{in} and T_{out}) and humidity (H_{in} and H_{out}) values observed during test 9. Temperatures followed the same trend observed for test 8, with $\Delta T_{average}$ being 2.4 ± 0.2 °C (as standard deviation). Similarly, humidity showed the same trend as the other tests performed on the Teflon sheet, U_{in} being lower than U_{out}.

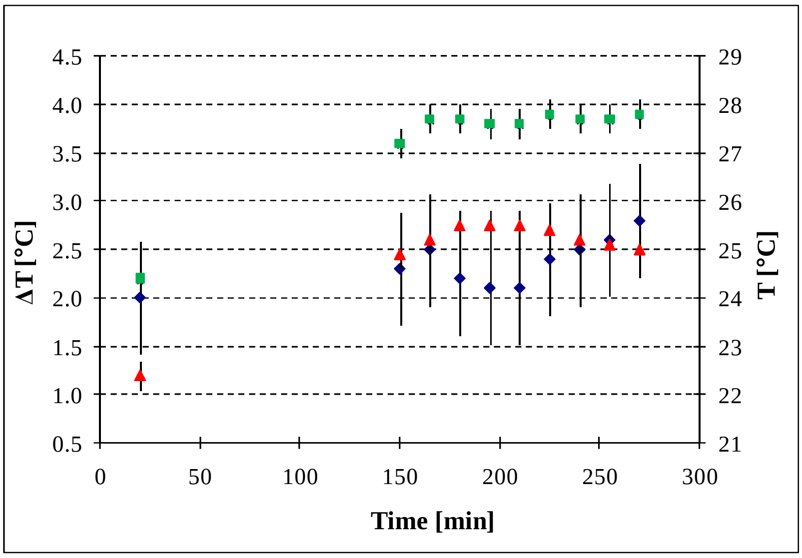

***Fig. 5.42**: temperature measured outside (red triangles) and inside (green squares) the FC (read on right axis), and their difference (blue lozenges) (read on left axis) (test 9). Error bars indicate instrumental error or its propagation on temperature difference.*

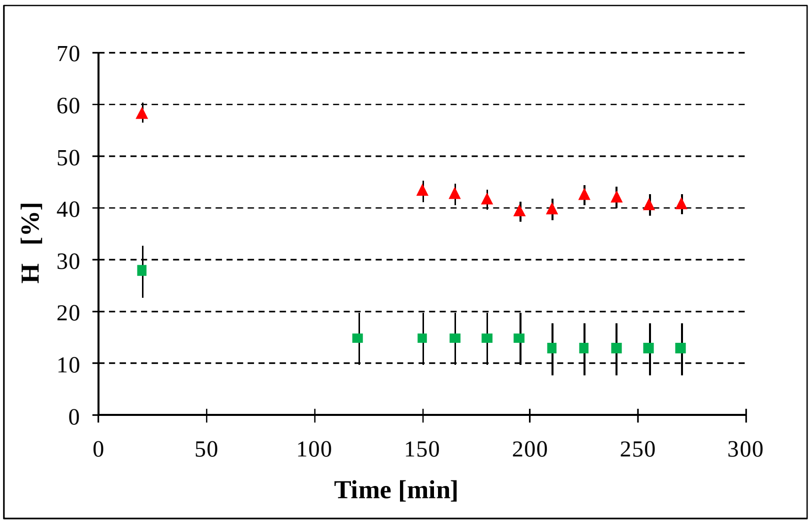

Fig. 5.43: *humidity measured outside (red triangles) and inside (green squares) the FC (test 9). Error bars indicate instrumental error.*

Results from **test 10**, with a higher nitrogen flow rate compared to test 9, are indicated in Tab. 5.12 and shown in Fig. 5.44. Comparing ethanol concentrations at different distances sampled in OUT port, the mixing did not seem homogeneous as the central part of the chamber had a lower concentration than in other points. The same conclusion was true for VENT port, too, $C_{ethanol}$ differing significantly at different distances. Comparing samples from different ports at the same distance, however, a good level of horizontal mixing was observed.

However, the mixing tests with ring A placed half way up way up the cylinder did not provide overall, satisfactory results.

Tab. 5.12: *ethanol concentration [mg l^{-1}] from OUT and VENT ports (test 10); s.d.: standard deviation.*

Sampling distance from the dome	**$C_{ethanol}$ OUT**	**$C_{ethanol}$ VENT**	**Average ± s.d. on horizontal position**
cm	**mg l^{-1}**	**mg l^{-1}**	**mg l^{-1}**
3	-	0.9	-
9	1.9	1.7	1.8 ± 0.1
17	1.0	1.0	1.0 ± 0.0
30	1.7	1.7	1.7 ± 0.0
average ± s.d. on vertical position	1.5 ± 0.4	1.3 ± 0.4	

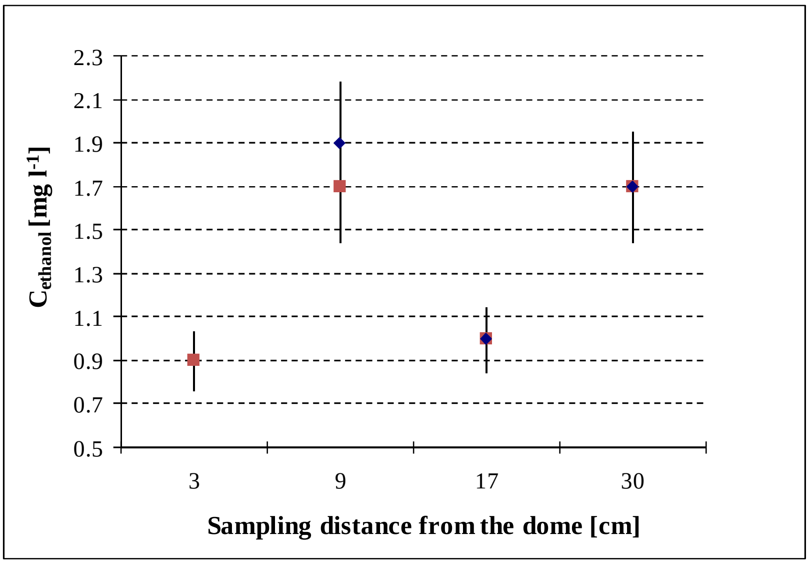

Fig. 5.44*: ethanol concentration [mg l^{-1}] in the FC from mixing test 10 (Tab. 5.12); in OUT (blue lozenges) and VENT (pink squares); error bars indicate analytical error.*

Figs. 5.45 and 5.46 show respectively the trend over time of temperature (both inside and both outside the FC, and their difference) and of humidity (inside and outside the FC) recorded during test 10. T_{out} and T_{in} increased over the entire test, according to a parallel trend, with $\Delta T_{average}$ being 2.9 ± 0.5 °C (as standard deviation). The internal humidity followed the trend of the external one, remaining constant during the whole test (with the exception of a single anomalous datum).

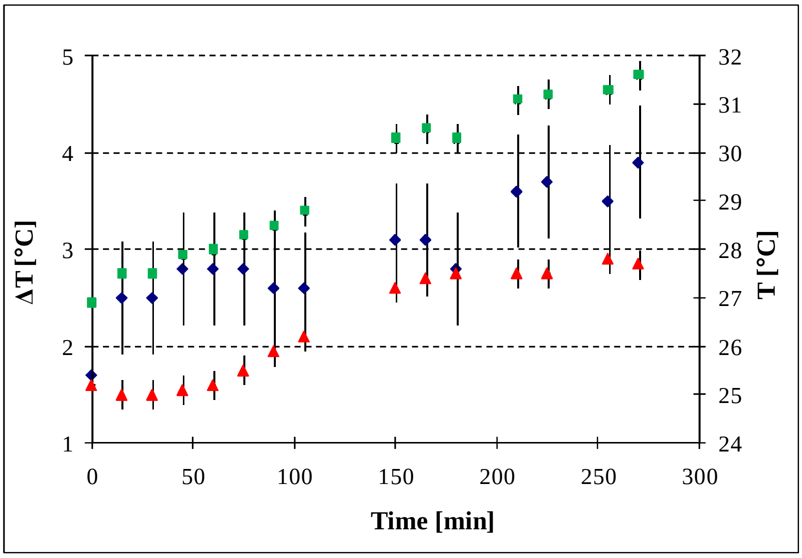

Fig. 5.45*: temperature measured outside (red triangles) and inside (green squares) the FC (read on right axis), and their difference (blue lozenges) (read on left axis) (test 10). Error bars indicate instrumental error or its propagation on temperature difference.*

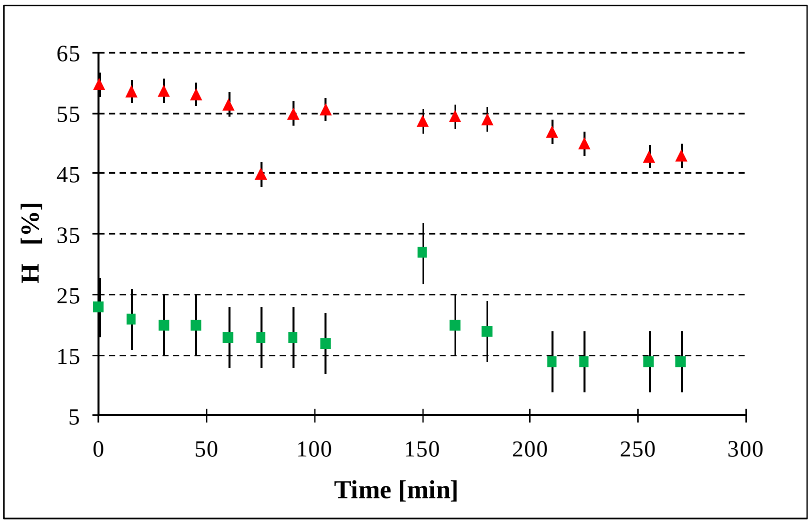

***Fig. 5.46**: humidity measured outside (red triangles) and inside (green squares) the FC (test 10). Error bars indicate instrumental error.*

Results obtained by changing the position of ring A (**test 11**) are shown in Tab. 4.13 and Fig. 5.47, in which the concentration measured in OUT when the fan was switched on, at the end of the test (indicated by a "F" in the table) is also indicated. Despite changing the ring A position, the central part of the chamber still showed poor mixing, as sample taken from OUT at 17 cm from the dome was significantly lower than ones at other distances. Comparing ethanol concentrations from the samples taken at 17 cm through OUT and VENT, it was clear that the chamber was insufficiently mixed also horizontally. The introduction of the fan caused an increase in the concentration measured from OUT at half way up the chamber (17 cm), due to some ethanol accumulation in the centre of the FC, and therefore index of poor mixing.

***Tab. 5.13:** ethanol concentration [mg l^{-1}] from OUT and VENT ports, with and without fan (F) switching on (test 11); s.d.: standard deviation.*

Sampling distance from the dome	**$C_{ethanol}$ OUT (no F)**	**$C_{ethanol}$ VENT (no F)**	**$C_{ethanol}$ OUT (F)**
cm	**mg l^{-1}**	**mg l^{-1}**	**mg l^{-1}**
9	3.8	-	-
17	2.5	5.5	5.4
30	3.9	-	-
37	3.7	-	-
average ± s.d. on vertical position	3.5 ± 0.6		

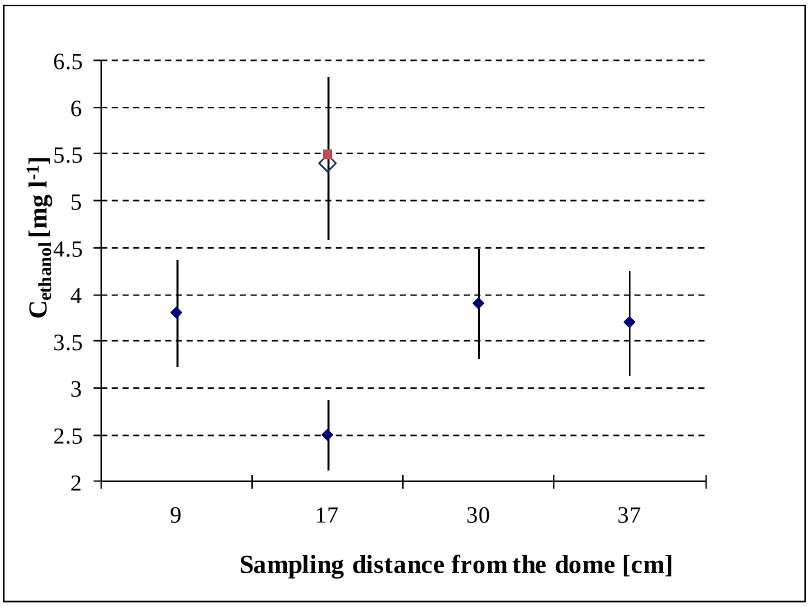

***Fig. 5.47**: ethanol concentration [mg l^{-1}] in the FC from mixing test 11 (Tab. 5.13); in OUT, without fun (full blue lozenges) and with fun switched on (empty blue lozenge), and in VENT (pink squares); error bars indicate analytical error.*

Figs. 5.48 and 5.49 show temperature and humidity levels observed during the test. Tab. 5.14 indicates the average ΔP values at different distances.

The internal temperature followed the same trend as the external one ($\Delta T_{average}$ = 2.0 ± 0.5 °C, as standard deviation), become stable after 200 min. The internal humidity was constant throughout the test (with the test beginning exception), and lower than outside the FC. All the ΔP values were positive, showing that the chamber was slightly pressurized.

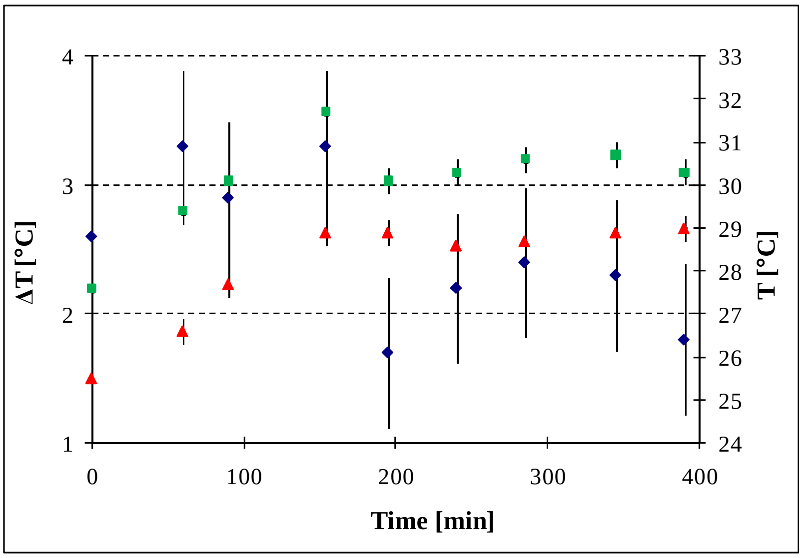

***Fig. 5.48**: temperature measured outside (red triangles) and inside (green squares) the FC (read on right axis), and their difference (blue lozenges) (read on left axis)*

(test 11). Error bars indicate instrumental error or its propagation on temperature difference.

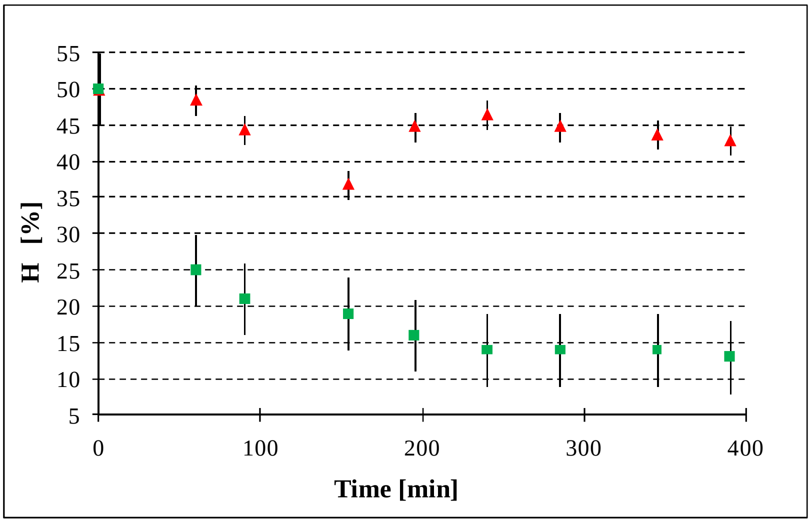

Fig. 5.49: *humidity measured outside (red triangles) and inside (green squares) the FC (test 11). Error bars indicate instrumental error.*

Tab. 5.14: $\Delta P_{average}$ values at different distances (test 11).

distance from the dome	**$\Delta P_{average}$**
cm	**Pa**
0	0.7± 0.2
13	0.7± 0.1
25	0.7± 0.2
31	0.8± 0.2
37	0.5± 0.1

5.3.3.2 Tests with ring B

5.3.3.2.1 Reaching stationary conditions

The results of **test 12** are shown in Tab. 5.15. Since sampled ethanol concentrations at 60 min and 290 min after the source had been switched on were similar, it was deduced that 1 h was enough to reach stationary conditions in ring B configuration tests.

Tab. 5.15: *ethanol concentration [mg l^{-1}] from OUT port (test 12); s.d.: standard deviation.*

Time	**$C_{ethanol}$** **L_{OUT}= 17 cm**
min	**mg l^{-1}**
60	4.6
290	3.9
average ± s.d.	4.3 ± 0.4

5.3.3.2.2 Mixing test

The ethanol concentrations observed in the chamber during **test 13**, where ring B position was changed and the holes were facing downwards, are summarized in Tab. 5.16 and presented in Fig. 5.50. This test showed that, even if the sweep gas flowed downward, it did not limit the ethanol diffusion at the lower part of the chamber; the concentration at ground level (sample taken at 37 cm from the dome), was similar to that at 30 cm. Despite changing the ring position and the orientation of the holes, the FC still showed poor vertical mixing along OUT. On the contrary values measured contemporaneously at 17 cm and exiting through VENT (as in test 13) were similar.

Tab. 5.16*: ethanol concentration [mg l^{-1}] from OUT with tube inserted for different distance and from VENT, at 3 cm inside the FC, taken when tube in OUT was at 17 cm from the dome (test 13); s.d.: standard deviation.*

Sampling distance from the dome	$C_{ethanol}$ OUT	$C_{ethanol}$ VENT distance: 3 cm from the dome
cm	**mg l^{-1}**	**mg l^{-1}**
9	2.6	-
17	4.6	4.6
30	3.2	-
37	3.3	-
average ± s.d.	3.4 ± 0.7	

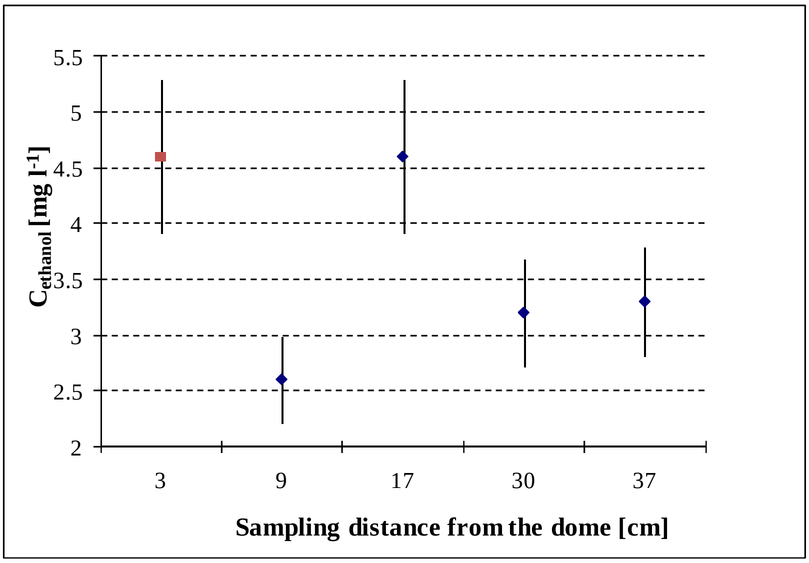

Fig. 5.50*: ethanol concentration [mg l^{-1}] in the FC from mixing test 13 (Tab. 5.16); in OUT (blue lozenges) and in VENT (pink squares); error bars indicate analytical error.*

Figs. 5.51 and 5.52 respectively show temperature and humidity values collected during the test. T_{in} was lower than T_{out} and followed its trend, with $\Delta T_{average}$ being 4.3 ± 0.7 °C. Unlike the other tests, the internal humidity was sometimes higher than the external one, despite the fact that the FC was placed on a Teflon sheet.

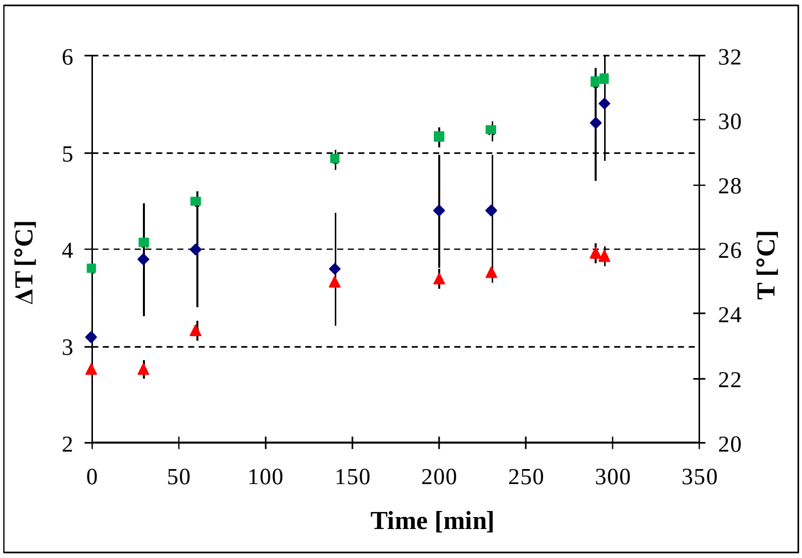

Fig. 5.51: *temperature measured outside (red triangles) and inside (green squares) the FC (read on right axis), and their difference (blue lozenges) (read on left axis) (test 13). Error bars indicate instrumental error or its propagation on temperature difference.*

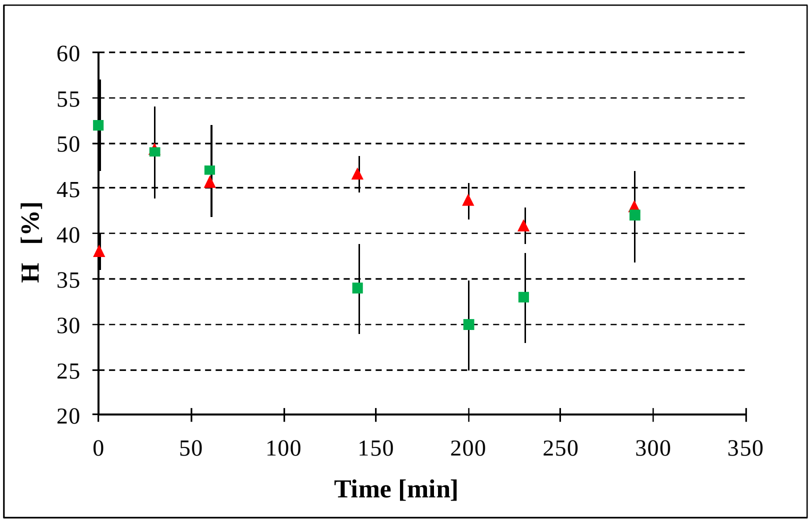

Fig. 5.52: *humidity measured outside (red triangles) and inside (green squares) the FC (test 13). Error bars indicate instrumental error.*

Results of **test 14**, with sampling from OUT and VENT without and with pump suction (indicated respectively by “no P” and “P” in the table), while pump in OUT was active, are reported in Tab. 5.17 and shown in Fig. 5.53 Comparing ethanol concentration values at three different distances through OUT, poor vertical mixing was deduced. Furthermore, as concentration sampled from the same distance (3 cm) through VENT, without pump, were significantly different, it was deduced that the area around free VENT was unstable. This happened because the airflow naturally escaping through VENT (without external suction forces) was affected by the suction forces operating in OUT port; these depended on distance of the tube inserted into the FC. In addition a difference between measurements from OUT and from VENT was noticed.

Tab. 5.17*: ethanol concentration [mg l^{-1}] from OUT with tube inserted for different distance; sampling from VENT (at 3 cm inside the FC) without (no P) and with (P) suction pump indicated next to the OUT position when sample was taken (test 14); s.d.: standard deviation.*

Sampling distance from the dome	**$C_{ethanol}$ OUT (P)**	**$C_{ethanol}$ VENT distance: 3 cm from the dome**	
Cm	**mg l^{-1}**	**(no P) mg l^{-1}**	**(P) mg l^{-1}**
9	3.6	1.8	-
17	2.7	3.1	2.6
30	1.7	2.6	2.7
average ± s.d.	2.7 ± 0.8	2.5 ± 0.5	2.65 ± 0.05

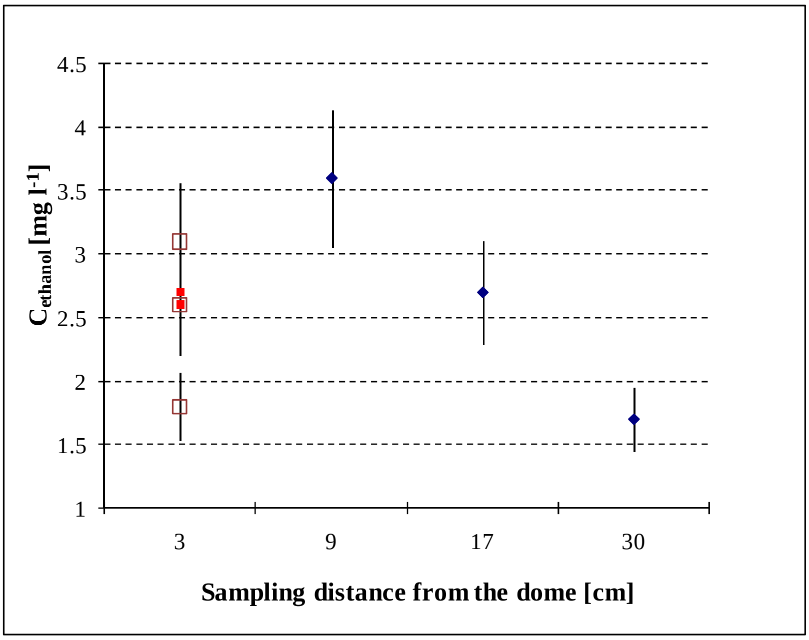

Fig. 5.53*: ethanol concentration [mg l^{-1}] in the FC from mixing test 14 (Tab. 5.17); in OUT (blue lozenges) and in VENT (squares), collected without (empty symbols) and with (filled signs) suction pumps; error bars indicate analytical error.*

The ethanol concentration values acquired from VENT with suction are similar to those sampled without suction from the same port; the measured ethanol concentration was therefore independent from the flow rate (Q_{vent}), similarly to the results obtained with ring A.

Figs. 5.54 and 5.55 show respectively external and internal temperature trends and the humidity values collected during the test. Both parameters followed the same trends seen in test 9, with $\Delta T_{average} = 4.9 \pm 0.5$ °C.

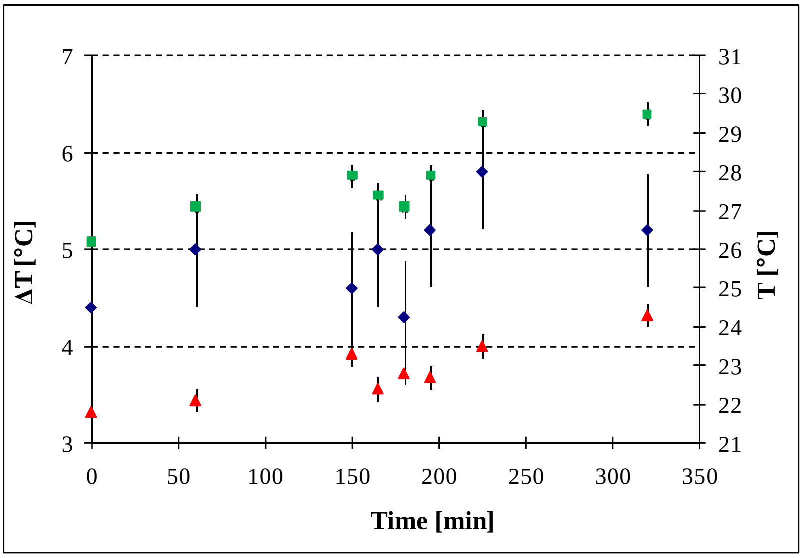

***Fig. 5.54**: temperature measured outside (red triangles) and inside (green squares) the FC (read on right axis), and their difference (blue lozenges) (read on left axis) (test 14). Error bars indicate instrumental error or its propagation on temperature difference.*

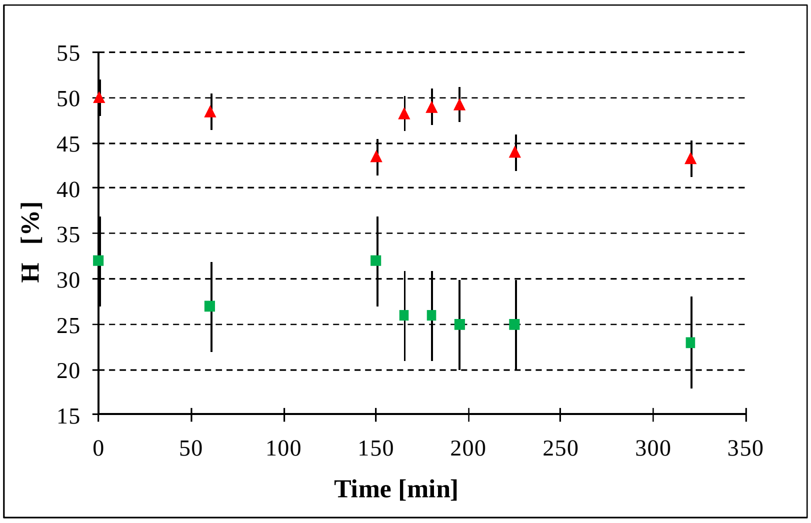

***Fig. 5.55**: humidity measured outside (red triangles) and inside (green squares) the FC (test 14). Error bars indicate instrumental error.*

5.3.3.3 Rings A and B used simultaneously

5.3.3.3.1 Mixing test

Results obtained using both rings as injection system (**test 15**) are shown in Tab. 5.18 and in Fig. 5.56. Comparing ethanol concentrations from samples acquired through OUT at four different distances, poor vertical mixing was observed. This setup gave the worst results of all the tests, as the lower part of the chamber (L=30 cm and L=37 cm), near ground level, does not seem to have been involved in the mixing.

***Tab. 5.18:** ethanol concentration [mg l^{-1}] from OUT with tube inserted for different distance from the dome (test 15); s.d.: standard deviation.*

Sampling distance from the dome	**$C_{ethanol}$ OUT**
cm	**mg l^{-1}**
9	5.8
17	6.8
30	4.0
37	8.4
average ± s.d.	6 ± 2

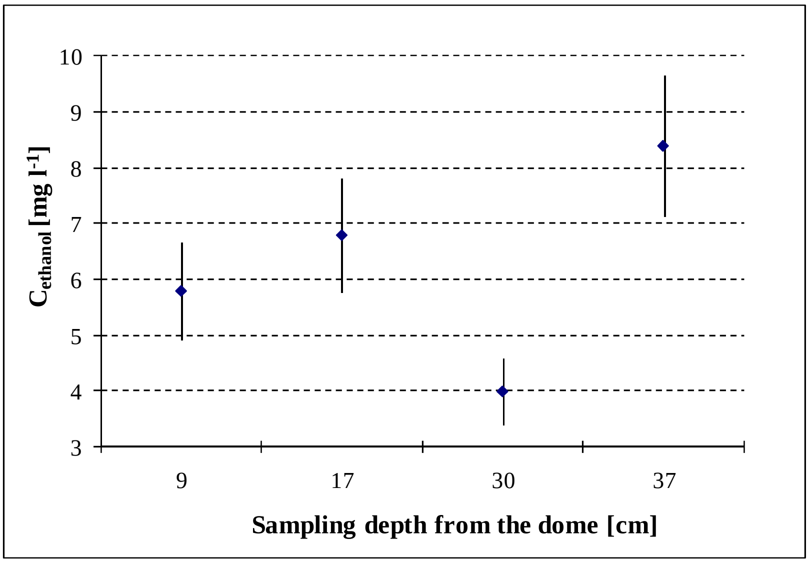

***Fig. 5.56**: ethanol concentration [mg l^{-1}] in the FC from mixing test 15 (Tab. 5.18); in OUT; error bars indicate analytical error.*

Results for the final mixing test (**test 16**), when the fan was switched on, are indicated in Tab. 5.19 and shown in Fig. 5.57. In this case, too, the chamber presented poor mixing, since the results at different heights are not comparable. Although the fan moved the gas from ground level to 30 cm distance from the dome, its application was no longer investigated, as this device is made of plastic, not easily covered by inert material, and requires electrical supply.

Tab. 5.19: *ethanol concentration [mg l^{-1}] from OUT with tube inserted for different distance from the dome (test 16); s.d.: standard deviation.*

Sampling distance from the dome	**$C_{ethanol}$ OUT**
cm	**mg l^{-1}**
9	7.4
17	6.3
30	10.8
37	4.9
average ± s.d.	7 ± 2

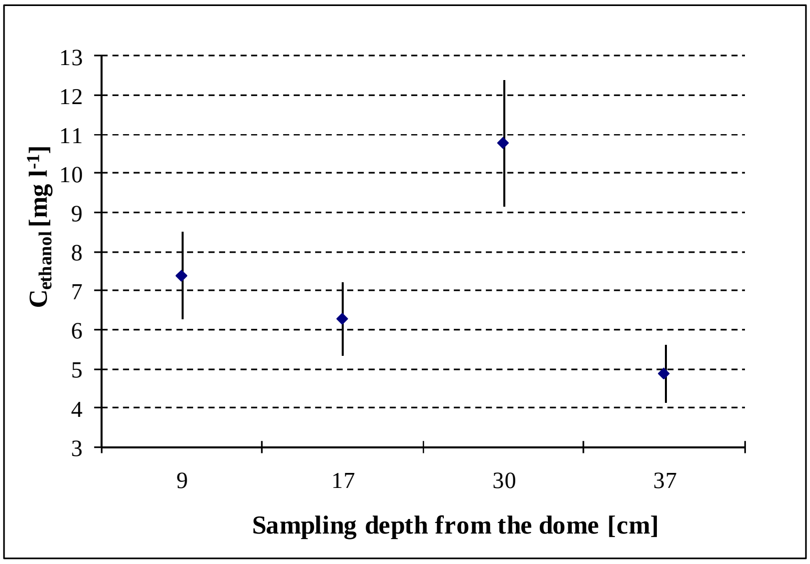

Fig. 5.57*: ethanol concentration [mg l^{-1}] in the FC from mixing test 16 (Tab. 5.19); in OUT; error bars indicate analytical error.*

Figs. 5.58 and 5.59 show temperature and humidity trends for, both inside and outside the FC, recorded during test 15 (that lasted 285 min, coincident with initial time of test 16) and test 16. Tab. 5.20 shows the average values of ΔP at different distances.

T_{in} did not follow T_{out}, and stayed constant 200 min after the test began; internal humidity remained constant throughout both tests, and lower than the external one. Finally ΔP was positive during both tests, showing that the chamber operated under slight pressure.

Fig. 5.60 shows the average values of ΔP s a function from p.c. from ground level for tests 11, 15 and 16. The ΔP values, being constantly positive, confirmed that the FC worked (correctly) at slightly pressurized condition, without sucking environmental air. Furthermore ΔP values at different distances were similar each other and slightly lower near VENT port, because it was the connection with external environment.

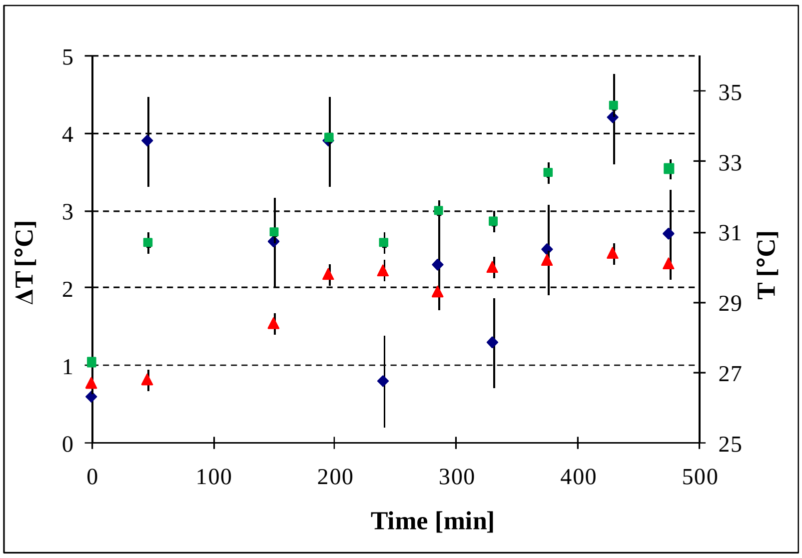

Fig. 5.58: *temperature measured outside (red triangles) and inside (green squares) the FC (read on right axis), and their difference (blue lozenges) (read on left axis) (tests 15 and 16, starting at 330 min). Error bars indicate instrumental error or its propagation on temperature difference.*

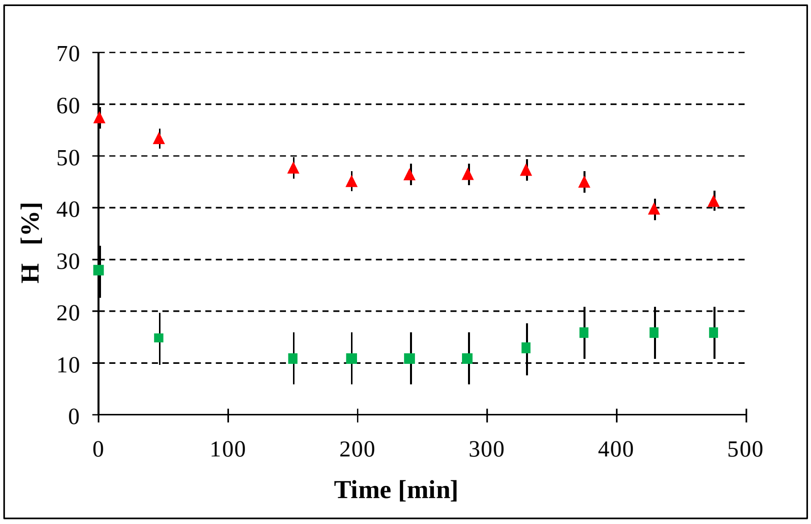

Fig. 5.59: *humidity measured outside (red triangles) and inside (green squares) the FC (tests 15 and 16, starting at 330 min). Error bars indicate instrumental error.*

Tab. 5.20: $\Delta P_{average}$ values at different distances (*tests 15 and 16*).

Distance from the dome	**$\Delta P_{average}$**
cm	**Pa**
0	0.9± 0.3
13	0.7± 0.2
25	0.6± 0.2
31	0.7± 0.2
37	0.4± 0.1

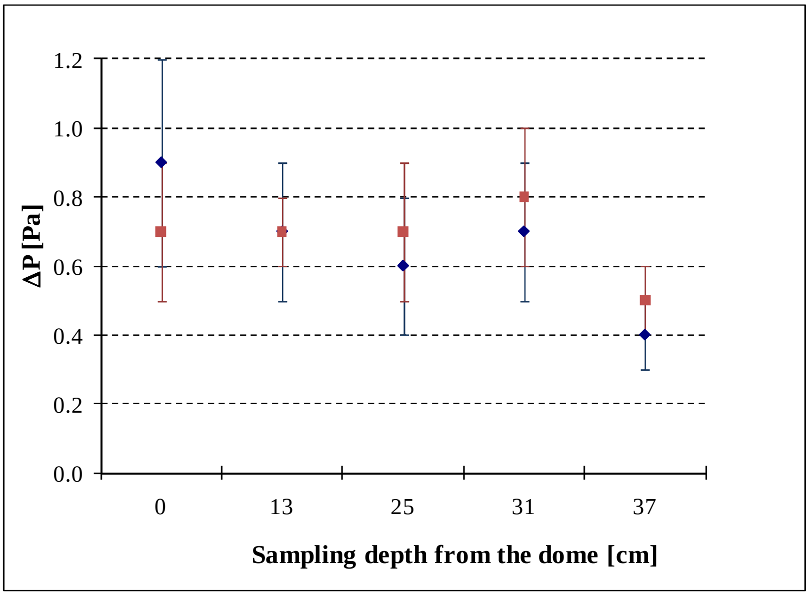

Fig. 5.60*: average pressure difference ΔP [Pa] as a function of sampling distance from the dome measured during test 11 (pink squares) and tests 15 and 16 (blue lozenges); error bars indicate standard deviation of average values.*

5.3.3.4 Adsorption tests on Plexiglass

The ethanol concentrations observed in reactors A, C and D are indicated in Tab. 5.21.

Tab. 5.21*: ethanol concentrations observed in reactors for adsorption tests on Plexiglass.*

Reactors	**A**	**C**	**D**
$C_{ethanol}$ [mg l^{-1}]	39 ± 6	21 ± 3	0.8 ± 0.1

The used reactors resulted airtight, as the concentration measured in C was consistent with that taken at the beginning of the test (19 ± 3 mg l^{-1}). In reactor A the concentration increased by factor 2 compared to the initial value, due to releases of ethanol adsorbed by the piece of Plexiglass. Finally, the concentration detected in reactor D shows that Plexiglass released actually some ethanol, although in small quantities, probably because most of the ethanol had been released in reactor B.

5.3.4 Modifications to the commercial FC: setup equipped with steel tube

5.3.4.1 Ambient air treatment by adsorption on activated carbon

Activated carbon type Norit 1 mm was suitable to remove ethanol, as in "sampling part a" (§ 4.2.5.3) of the first tube the measured mass was lower than d.l. (0.5 µg), for a test length of 8 h.

Results of the tests carried out on GAC 830 and Norit 1 mm to establish the ability to keep BTEX over 24 h are shown in Tabs. 5.22 and 5.23. The mass of the checked analytes adsorbed on activated carbon tubes placed at the outlet of environmental air treatment is indicated.

Tab. 5.22*: BTEX mass detected on activated carbon tubes placed at the outlet of environmental air treatment with GAC 830, time length: 24 h. In bold type values higher than d.l..*

benzene	**toluene**	**ethylbenzene**	**p-xylene**	**m-xylene**	**o-xylene**
µg	**µg**	**µg**	**µg**	**µg**	**µg**
1.6	< 0.45	<0.45	**0.47**	**0.47**	<0.45

Tab. 5.23*: BTEX mass detected on activated carbon tubes placed at the outlet of environmental air treatment with Norit 1 mm, time length: 24 h. In bold type values higher than d.l..*

benzene	**toluene**	**ethylbenzene**	**p-xylene**	**m-xylene**	**o-xylene**
µg	**µg**	**µg**	**µg**	**µg**	**µg**
<0.45	<0.45	<0.45	**0.52**	<0.45	<0.45

Both types were unsuitable, in the used quantities, for a proper BTEX removal over a 24 h treatment length.

Results of shorter test length (16 h), however suitable for future field scale applications, are indicated in Tab. 5.24, both for Norit 1 mm and for Norit 3 mm. Both types of carbon proved suitable to treat ambient air for the checked time.

Tab. 5.24*: BTEX mass detected on activated carbon tubes placed at the outlet of environmental air treatment with Norit 1 mm or Norit 3 mm, time length: 16 h. Part a: tube sampling part, part b: tube backup (§ 4.2.5.3).*

	benzene	**toluene**	**ethylbenzene**	**p-xylene**	**m-xylene**	**o-xylene**
	µg	**µg**	**µg**	**µg**	**µg**	**µg**
Tube – part a	<0.3	<0.3	<0.3	<0.3	<0.3	<0.3
Tube – part b	<0.1	<0.1	<0.1	<0.1	<0.1	<0.1

The thinner Norit a.c. was chosen because of its higher specific surface and lower porosity left after filling the air treatment reactor. Results of further analysis on light and heavy hydrocarbons collected at the outlet of air treatment for 16 h are indicated in Tab. 5.25.

Tests performed on regenerated a.c. confirmed previous results and therefore Norit 1 mm was considered suitable to treat ambient air as sweep gas, also for further field activities (§ 6).

Tab. 5.25*: light and heavy hydrocarbons masses detected respectively on activated carbon and XAD2 tubes placed at the outlet of environmental air treatment with Norit 1 mm, time length: 16 h.*

	MTBE	**C5 Aliphatics**	**C6-C8 Aliphatics**	**C9-C12 Aliphatics**	**C9 -C18 Aliphatics**	**C19 -C36 Aliphatics**	**C9 -C10 Aromatics**	**C11 -C22 Aromatics**	**Naphthalene**
	µg	**µg**	**µg**	**µg**	**µg**	**µg**	**µg**	**µg**	**µg**
Tube - sampling part a	<0.2	<0.3	<0.3	<0.3	<0.5	<0.5	<0.3	<0.3	<0.2

5.3.4.2 Mixing test

Tab. 5.26 and Fig. 5.61 show results of the mixing test (**test 17**). The chamber revealed poor vertical mixing through OUT, especially in the central part (13cm from the cover), as the sampled concentration was much lower than those in other points. This is probably due to the proximity of the sweep flow injection point.

Tab. 5.26*: ethanol concentration [mg l^{-1}] from OUT with tube inserted for different distance from the cover (test 17); s.d.: standard deviation.*

Sampling distance from the cover	**$C_{ethanol}$ OUT**
cm	**mg l^{-1}**
4	3.6
13	0.7
21	1.6
average ± s.d.	2 ± 1

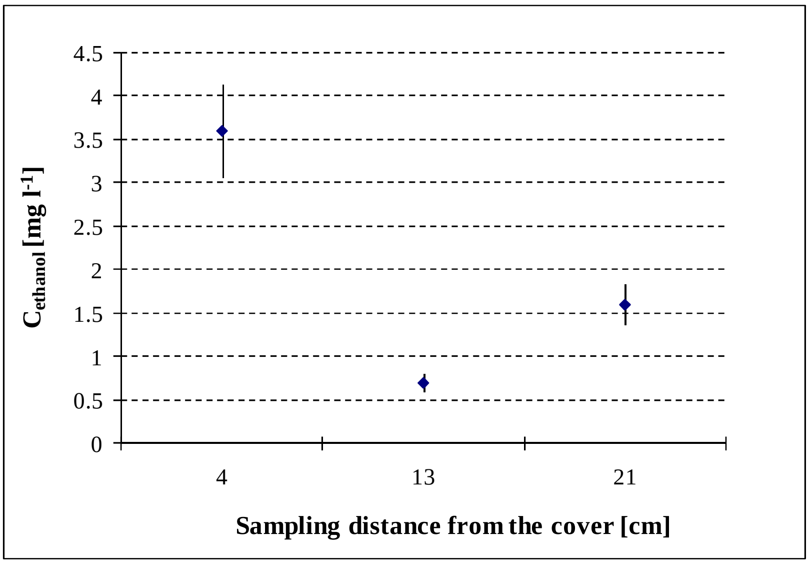

Fig. 5.61: *ethanol concentration [mg l^{-1}] in the FC from mixing test 17 (Tab. 5.26); in OUT; error bars indicate analytical error.*

ΔP measurements, taken half way up way up the cylinder during the test, gave positive values (average of 0.24 ± 0.06 Pa), also indicating that with this setup the chamber does not suck external air.

5.3.5 FC final setup

5.3.5.1 Mixing test

Tests 18 and **19** showed that the spiral allows complete vertical mixing inside the chamber at OUT position as, for both tests, the ethanol concentration levels sampled at different distances were all similar, as indicated in Tab. 5.27 and shown in Fig. 5.62.

Tab. 5.27: *ethanol concentration [mg l^{-1}] from OUT with tube inserted for different distance from the cover (tests 18 and 19); s.d.: standard deviation.*

Sampling distance from the cover	**$C_{ethanol}$ OUT**	
cm	**mg l^{-1}**	
4	2.3	1.7
13	1.9	1.6
21	2.3	1.6
average ± s.d.	2.1 ± 0.2	1.61± 0.03

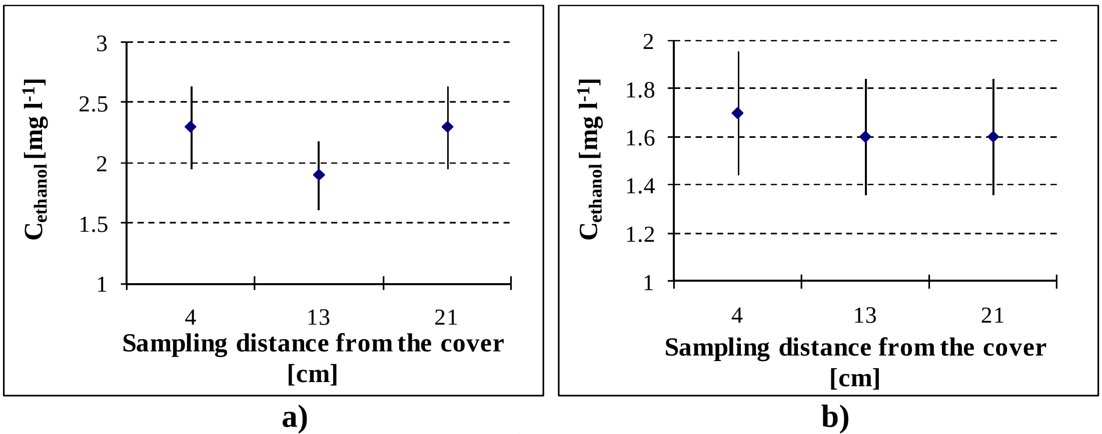

Fig. 5.62*: ethanol concentration [mg l^{-1}] in the FC from mixing test 18 (a) and test 19 (b) (Tab. 5.27); in OUT; error bars indicate analytical error.*

Fig. 5.63 shows average ΔP values (on 3 replicates) measured through both the VENTs at different flow rates, recorded at the end of test 18. There was a slight difference between ΔP measured in the two ports, probably due to different influence of sweeping gas on pressure probe, depending on its mutual position with holes on the spiral. As hypothesized ΔP became negative when exiting sucked flow rate was equal to sweep inflow rate (7.5 l min^{-1}).

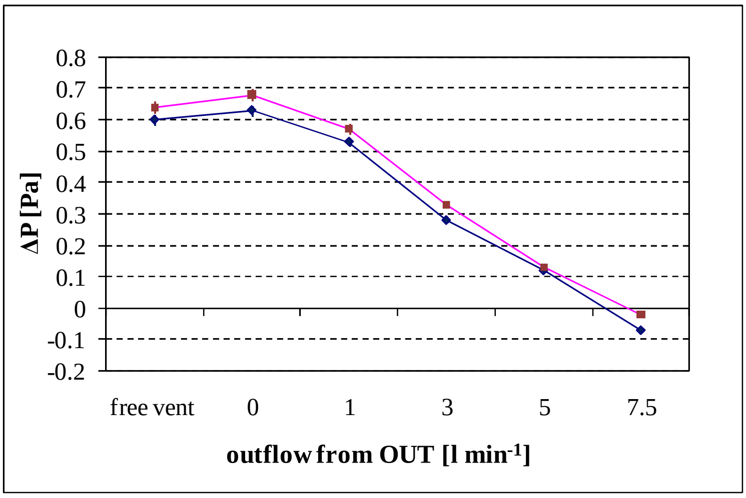

Fig. 5.63*:* average *pressure difference ΔP [Pa] as a function of sucking air flow rate measured in VENT 1 (blue lozenges) and VENT 2 (pink squares); error bars indicate standard deviation on three replicates.*

Fig. 5.64 shows average ΔP values observed at half way up the height of the cylinder, from both VENT 1 and 2, during test 19. Positive ΔP values show that the FC was slightly pressurized throughout the test and it is clear a good agreement between values obtained from the two VENTs.

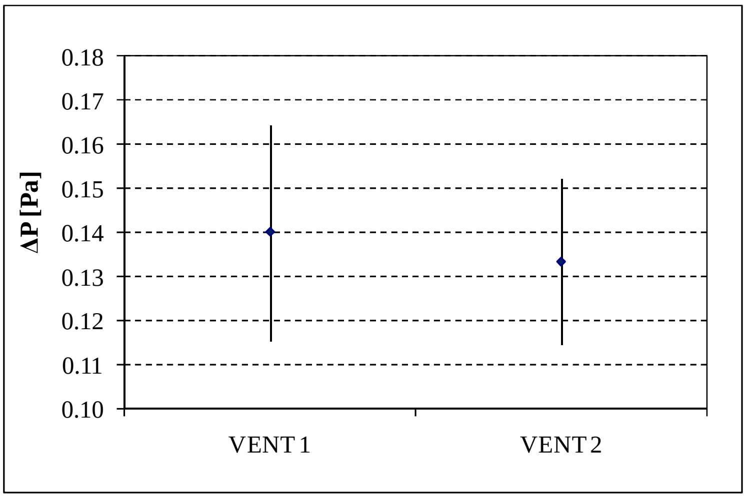

Fig. 5.64: average *pressure difference ΔP [Pa] measure at the cylinder half way up height in VENT 1 and VENT 2 during test 19; error bars indicate standard deviation on three replicates.*

Test 20 results, obtained by sampling from OUT as well as VENTs 1 and 2, are shown in Tab. 5.28 and Fig. 5.65. Comparing ethanol concentrations taken from different distances through all three ports, it emerged that the chamber was well mixed. Furthermore a good level of horizontal mixing was reached, since samples collected through OUT, VENT 1 and VENT 2, at the same distance, were similar.

Tab. 5.28: *ethanol concentration [mg l^{-1}] from OUT, VENTs 1 and 2, with tube inserted for different distance from the cover (tests 20); s.d.: standard deviation.*

Sampling distance from the cover	**$C_{ethanol}$**			
	OUT	**VENT 1**	**VENT 2**	**Average ± s.d. on horizontal position**
Cm	**mg l^{-1}**			
4	1.2	1.0	0.9	1.0± 0.1
13	1.0	1.1	1.0	1.00± 0.02
21	0.9	0.8	1.0	0.9± 0.1
average ± s.d. on vertical position	1.1±0.1	1.0±0.1	0.95±0.03	

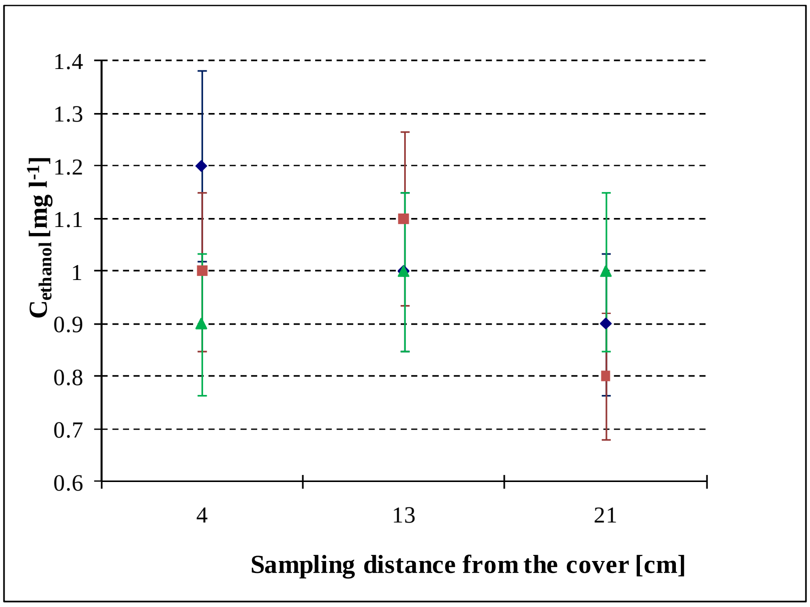

Fig. 5.65: *ethanol concentration [mg l^{-1}] in the FC from mixing test 20 (Tab. 5.28); in OUT (blue lozenges), VENT 1 (pink squares) and VENT 2 (green triangles); error bars indicate analytical error.*

Test 21 results, performed similarly to test 20, but by using other source features, and taking replicates for each sample, are presented in Tab. 5.29 and Fig. 5.66. From the results it was confirmed that the chamber was homogeneously mixed, both vertically and horizontally.

Test 22 results, with analysis performed by on-line FID, as indicated in Fig. 5.28, taking 8 replicates for each point, are shown in Tab. 5.30 and Fig. 5.67. From the results it was again confirmed that the chamber was well mixed, both vertically and horizontally, because standard deviation was lower than analytical error. Furthermore, it was clear that the sampling flow rate did not affect the results.

Tab. 5.29: *ethanol concentration [mg l^{-1}] from OUT, VENTs 1 and 2, with tube inserted for different distance from the cover (tests 21); s.d.: standard deviation, n: number of replicate for each sample.*

.

Sampling distance from the cover	**$C_{ethanol}$**			
	OUT	**VENT 1**	**VENT 2**	**Average ± s.d. on horizontal position**
Cm	**mg l^{-1}**			
4	2.0 ± 0.2 n = 3	2.15 ± 0.09 n = 2	2.143 ± 0.003 n = 2	2.11 ± 0.05
13	2.2 ± 0.1 n = 3	2.1 ± 0.2 n = 2	2.01 ± 0.04 n = 2	2.10 ± 0.09
21	2.0 ± 0.1 n = 3	1.8 ± 0.3 n = 2	2.18 ± 0.06 n = 2	2.0 ± 0.2
average ± s.d. on vertical position	2.10 ± 0.09	2.0 ± 0.1	2.11 ± 0.07	

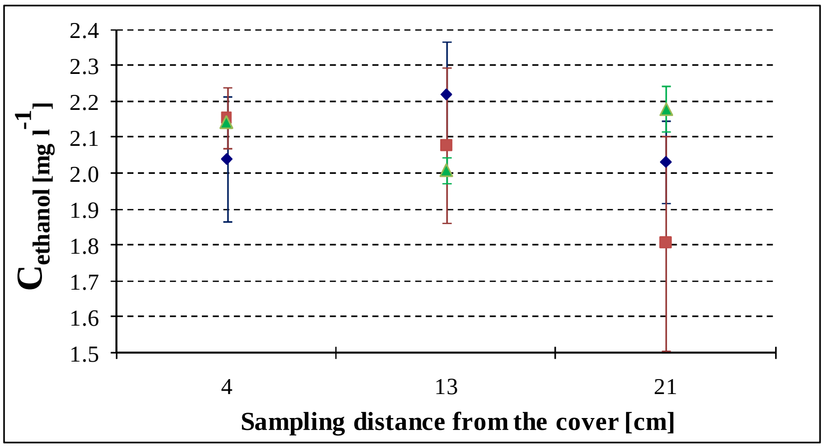

***Fig. 5.66**: ethanol concentration [mg l^{-1}] in the FC from mixing test 21 (Tab. 5.29); in OUT (blue lozenges), VENT 1 (pink squares) and VENT 2 (green triangles); error bars indicate deviation standard on replicates.*

***Tab. 5.30:** ethanol concentration [mg l^{-1}] from OUT, VENTs 1 and 2, with tube inserted for different distance from the cover (tests 22), for three different suction sampling flows: a) 3.0 ± 0.1 l min^{-1} , b) 1.5 ± 0.1 l min^{-1} and c) 0.22 ± 0.01 l min^{-1}; s.d.: standard deviation on 8 replicates for each sample.*

a)

Sampling distance from the cover	**$C_{ethanol}$ – Q_{out} = 3.0 ± 0.1 l min^{-1}**			
	OUT	**VENT 1**	**VENT 2**	**Average ± s.d. on horizontal position**
cm	**mg l^{-1}**			
4	3.06 ± 0.02	3.08 ± 0.07	3.2 ± 0.2	3.11 ± 0.06
13	3.068 ± 0.009	3.11 ± 0.03	3.13 ± 0.02	3.10 ± 0.03
21	3.08 ± 0.02	3.13 ± 0.01	3.13 ± 0.02	3.12 ± 0.02
average ± s.d. on vertical position	3.072 ± 0.009	3.10 ± 0.02	3.15 ± 0.03	

b)

Sampling distance from the cover	**$C_{ethanol}$ – Q_{out} = 1.5 ± 0.1 l min^{-1}**			
	OUT	**VENT 1**	**VENT 2**	**Average ± s.d. on horizontal position**
cm	**mg l^{-1}**			
4	3.23 ± 0.04	3.19 ± 0.03	3.16 ± 0.01	3.19 ± 0.03
13	3.24 ± 0.03	3.2 ± 0.1	3.18 ± 0.01	3.21 ± 0.03
21	3.20 ± 0.06	3.16 ± 0.04	3.18 ± 0.02	3.18 ± 0.02
average ± s.d. on vertical position	3.22 ± 0.02	3.19 ± 0.02	3.17 ± 0.01	

c)

Sampling distance from the cover	**$C_{ethanol}$ – Q_{out} = 0.22 ± 0.01 l min^{-1}**			
	OUT	**VENT 1**	**VENT 2**	**Average ± s.d. on horizontal position**
Cm	**mg l^{-1}**			
4	3.287 ± 0.007	3.294 ± 0.005	3.25 ± 0.04	3.28 ± 0.02
13	3.296 ± 0.003	3.30 ± 0.01	3.27 ± 0.03	3.29 ± 0.01
21	3.304 ± 0.006	3.31 ± 0.03	3.28 ± 0.03	3.30 ± 0.01
average ± s.d. on vertical position	3.296 ± 0.007	3.299 ± 0.005	3.27 ± 0.01	

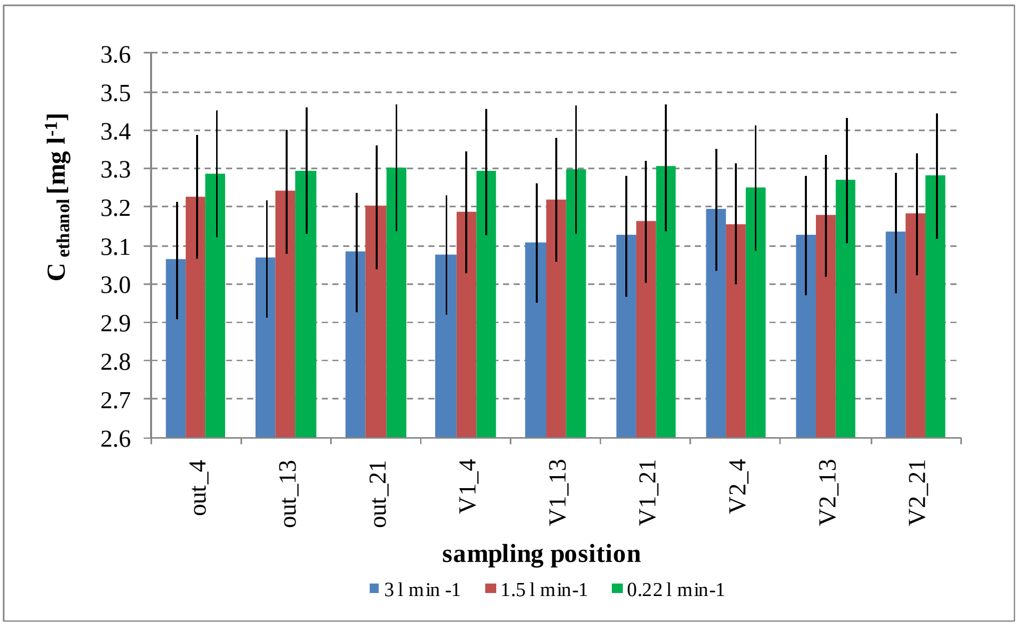

Fig. 5.67*: ethanol concentration [mg l^{-1}] in the FC from mixing test 22 (Tab. 5.30); in OUT, VENT 1and VENT 2 at different sampling flow rates; error bars indicate PID precision.*

5.3.5.2 Purge duration

Test 23 results indicated that with the new chamber setup, a purge duration of 2 h 30 min was enough to reach ethanol concentration level d.l. inside the FC (Fig. 5.68).

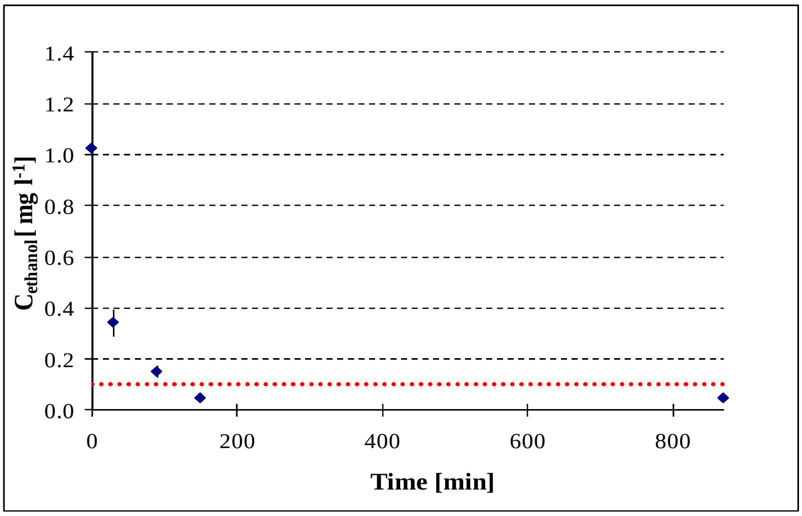

Fig. 5.68*: ethanol concentration [mg l^{-1}] in the FC from purge test 23, with samples taken at different times; values < d.l. where taken equal to 0.5 d.l.; red dotted line indicates d.l.; error bars indicate analytical error.*

Test 24 (performed by FID instrument) initial conditions, in terms of amount of in the FC before the source was switched on, are indicated in Tab. 31. Ethanol concentration trend over time, for the three replicates, is indicated in Fig. 5.69. Results confirmed that the purge duration was shorten than seen in previous tests, and that 1 h 30 min was long enough for ethanol concentrations to reach initial levels in the FC.

Tab. 5.31*: ethanol concentration [mg l^{-1}] in the FC before starting test 24*

$C_{ethanol}$ before test 24 beginning		
mg l^{-1}		
test 24.a	test 24.b	test 24.c
0.024 ± 0.001	0.026 ± 0.001	0.026 ± 0.001

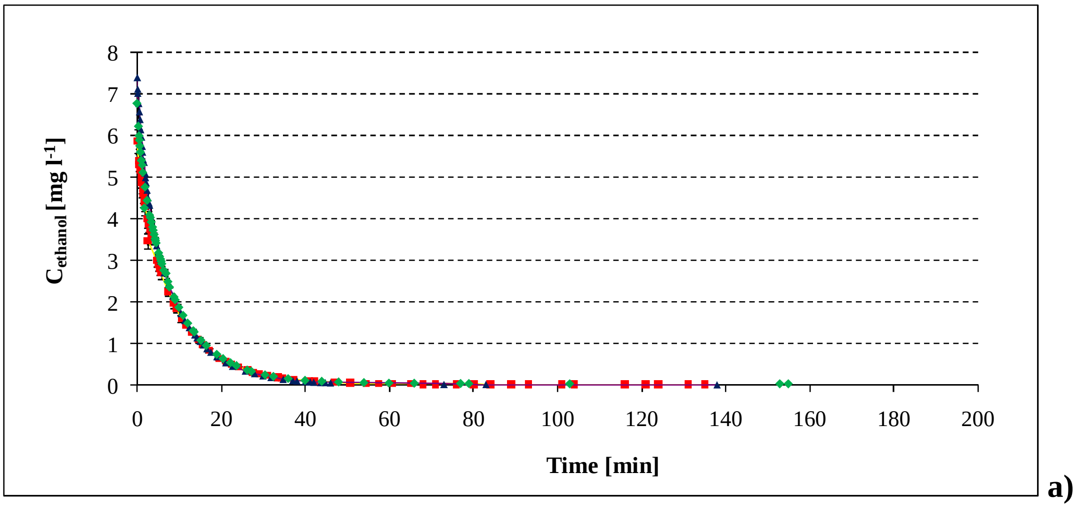

Fig. 5.69*: continue.*

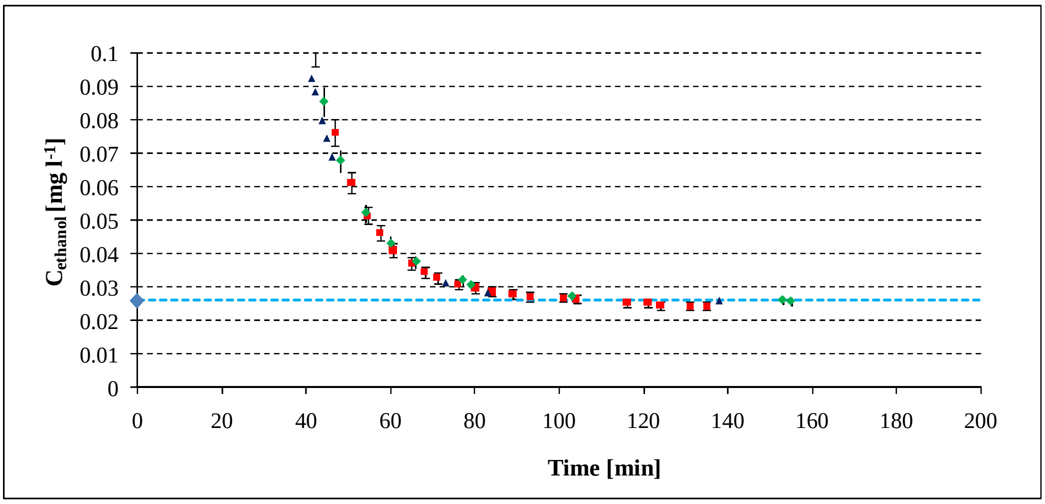

b)

Fig. 5.69*: ethanol concentration [mg l^{-1}] in the FC from purge test 24, with samples taken at different times; on three replicates. a) full test length; b) detail on final times, with dashed light blue line indicating initial ethanol concentration (before the source was injected into the FC; error bars indicate FID analytical error.*

5.4 Conclusions

Experimental tests carried out with the commercial FC (with both steel tube and rings as sweep air injection methods) showed that stationary conditions were reached within 2 h. The chamber however resulted badly mixed and purge duration needed more than 2 h 30 min. These results, unsatisfactory from monitoring device performance point of view, were caused by the sweep gas injection system, by the shape of the dome (which caused stagnation areas not involved in the inner mixing) and by the material constituting it (because it adsorbed organic compounds, therefore prolonging purge times).

To solve the previous highlighted problems, the Plexiglass dome was replaced by a flat PTFE cover, the silicone and the spongy gasket by a PTFE gasket and the air injection system by a Teflon spiral (since the tube had been proved inappropriate).

Tests carried out with this setup indicated that the chamber was homogeneously mixed, with purge duration shorter than 2h 30 min. This was due to both an increase in sweep gas flow rate and a reduction in the FC volume, therefore reducing the residence time HRT (because the complete volume exchanges inside the FC increased, in relation to the same length of time).

Since for field scale activity it is often difficult and expensive to use nitrogen tanks, mostly because of transport and storage safety problems, a new ambient air treatment system was set up; therefore, treated ambient air became suitable as sweep gas for FC applications.

Once a satisfactory setup was defined, field tests were carried out on a site potentially contaminated by petroleum products (§ 6).

6

FIELD APPLICATION: CASE STUDY

6.1 Introduction

Chapter 6 describes a field study application of the dynamic flux chamber (FC) with the setup defined in § 5.2.5, on an Italian site potentially contaminated by hydrocarbons. Due to dealing with sensible data (because public procedure on the site is still open) specific details cannot be reported here.

The site was characterized from the geological, hydrogeological and chemical points of view, in order to develop its conceptual model. Three different monitoring campaigns were performed in July 2009, December 2009 and July 2010, and the contaminants concerned included monoaromatic solvents and petroleum hydrocarbons (both light and polycyclic aromatic). Data of researched chemical concentrations in groundwater and soil gas, and ambient air measurements were provided by a local public environmental Agency thanks to a collaboration grant assigned to Politecnico di Milano. On the contrary FC monitoring was performed directly by Politecnico di Milano.

Different possible approaches to evaluate vapours emitted from soil, presented in § 1.3, were evaluated for this specific case study. Flux data obtained from FC measurements were compared to modelled fluxes resulting from geological information obtained from the conceptual site model and separately from groundwater and soil gas data by the use of Johnson and Ettinger (§ 3.4.2.2) model, loaded in RISC 4.05 software –SW- (RISC, 2010). Dispersion box model was applied to fluxes evaluated during the third campaign for a comparison with direct air measurements. As a precautionary measure RA (§ 1.2) was performed using maximum concentrations from each approach that was consistently carried out using RISC 4.05 SW.

6.2 Materials and methods

6.2.1 The site general information

The site, which is located in the North of Italy, extends over 19 ha and is used for recreational activities (legal boundaries of the site are indicated by dashed line in Fig. 6.1). An active industrial plant is located on north-East, where accidental spills of petroleum products have occurred in the past. A river bank bounds the site to the south/south-east.

The site is found on a plain constituted by fluvial sediments. A phreatic aquifer, hosted by a medium-coarse-grained sand layer, is isolated from the deeper aquifer by an uniform silty clay layer of low permeability (geological tests had indicated a hydraulic conductivity of 4.5 10^{-10} m s^{-1}), extending from 17 to 20 m below ground surface (b.g.s.). Groundwater flows south/south-west (Fig. 6.1), draining off towards the river, with an average hydraulic gradient equal to 0.5%. During the year, the water table fluctuates from approximately 5 to 8 m b.g.s., the depth also being affected by the water level in the river located down-gradient.

On the northern boundary of the site, groundwater in the phreatic aquifer exceeded the concentration screening values (residential/recreational CSCs of L.D. 152/06, as in § 1.2) for benzene, toluene, ethylbenzene, p-xylene (BTEX), naphthalene and MTBE (the last two exceeded ISS -§ 1.2- official judgement (ISS, 2010), since there is no CSC for these compounds) and total petroleum hydrocarbons. The fingerprinting carried out on light petroleum hydrocarbons (number of carbon atoms $\leq$ 12: C $\leq$ 12, according to definition in § 5.2.4) in groundwater samples resulted in C5-C8 aliphatics, C9-C12 aliphatics and C9-C10 aromatics, accounting for 30%, 15%, and 55% (on mass basis) of total petroleum hydrocarbons respectively.

Soil samples collected at smearing zone depth also showed potential pollution due to BTEX monoaromatic solvents and light petroleum hydrocarbons. The fingerprinting carried out on light petroleum hydrocarbons in soil resulted in 23%, 54% and 22% (on mass basis) of C5-C8 aliphatics, C9-C12 aliphatics, and C9-C10 aromatics respectively. This was due to transport of chemicals dissolved in groundwater as it oscillates over time in the capillary fringe.

6.2.2 Site characterization: specific contaminated part of the site

The part involved in groundwater contamination was identified by a rectangular (defined by a continuous line in Fig. 6.1) whose sides run parallel to the legal boundaries of the site (indicated by a dashed line in Fig. 6.1) containing all the Thiessen polygons (ET, 2010) centred in five wells where groundwater contamination was found; groundwater contamination in the south-west part of the site, near the river, was lower than CSCs (probably due to natural attenuation phenomena). The rectangular was located in a zone of greater permeability (seat of an ancient river bed), bounded on one side by the front of contamination in the neighbour’s property (210 m long) and, on the other side, by a line approximately half the total length of the site (60 m long). In all, it occupied an area of 12600 m^2. A sketch of the area, with positions of well and soil gas/FC monitoring points is indicated in Fig. 6.1.

From now on, therefore, the study will only focus on this part of the site.

6.2.2.1 Local geology and hydrogeology

The impermeable layer isolated above strata from deeper soil and therefore the potential contamination did not involve the second groundwater system. 10 soil cores investigations (in correspondence with soil gas stations A, …, L in Fig. 6.1) were taken in that zone, at different depths following L.D. 152/2006 definitions.

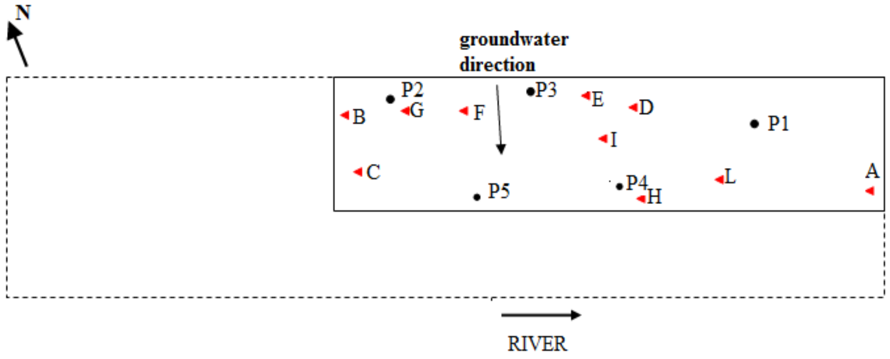

***Fig. 6.1**: sketch of the contaminated area with indications of well (black points) and soil gas/FC monitoring points (red triangles). Dashed lines indicate the legal boundaries of the site, whereas the continuous ones the potentially contaminated zone where monitoring took place; hydrological information is also provided by arrows.*

Results of soil texture classification (as per ASTM, 2006) performed on them (not directly by Politecnico di Milano) are indicated in Tab. 6.1.

***Tab. 6.1**: grain-size distribution classes for 10 soil cores taken in A,.., L points. Samples were all taken at several depths: shallow unsaturated soil "Shal. Uns." (from 0 to 1 m below ground surface –b.g.s.-), deep unsaturated soil "Deep Uns." (from 1m b.g.s. to the water level) and, only in some situations, deep saturated soil "Deep Sat." (from water level to 10 m b.g.s.). d.s.: dry soil. In bold type major grain-size ratios are highlighted.*

point	**depth**	**gravel**	**sand**	**loam**	**clay**	**f$_{oc}$**
	m b.g.s.	**% w/w d.s.**	**% w/w d.s.**	**% w/w d.s.**	**% w/w d.s.**	**% w/w d.s.**
A	Shal. Uns.	1.45	**48.92**	**48.52**	1.11	0.32
	Deep Uns	0.39	23.56	**75.61**	0.43	0.24
	Deep Sat.	0.06	**73.98**	25.88	0.08	0.41
B	Shal. Uns.	4.6	**53**	39	4.1	0.24
	Deep Uns	0.61	**63**	17.6	18.6	0.11
	Deep Sat.	0.43	**74**	25	0.22	0.41
C	Shal. Uns.	3.84	**77.39**	18.76	<0,01	0.89
	Deep Uns	24.14	**52.77**	23.09	<0,01	1.17
	Deep Sat.	0.03	**80.62**	19.36	<0,01	0.22
D	Shal. Uns.	0.48	**61.31**	37.48	0.73	0.79
	Deep Uns	0.27	41.68	**57.36**	0.7	1.08

***Tab. 6.1**: continued.*

E	Shal. Uns.	17.64	**57.14**	25.2	0.02	0.26
	Deep Uns	7.27	**57.95**	34.74	0.04	0.41
F	Shal. Uns.	3.19	**66.24**	30.36	0.21	0.57
	Deep Uns	1.07	34.59	**64.21**	0.14	0.67
G	Shal. Uns.	13.71	**60.04**	25.78	0.48	1.06
	Deep Uns	<0,01	**64.19**	35.72	0.09	0.81
H	Shal. Uns.	8.9	**54**	37	0.06	0.7
	Deep Uns	0.01	**64**	35	0.24	0.89
I	Shal. Uns.	9.2	**76**	14.7	0.3	0.61
	Deep Uns	4.1	**69**	27	0.44	0.23
L	Shal. Uns.	3.22	37.5	**59.22**	0.05	0.94
	Deep Uns	0.02	8.62	**91.26**	0.1	0.47

As for hydrological information, groundwater level was defined as the average between the values recorded in the 5 cited wells (§ 6.2.2) during each measuring campaign in which Politecnico di Milano was involved in FC monitoring. Data are reported in Tab. 6.2.

***Tab. 6.2**: average groundwater levels, during three FC monitoring sessions.*

	July 2009	**December 2009**	**July 2010**
Water table [m b.g.s.]	8.1±0.2	5.6±0.2	8.3±0.2

6.2.2.2 Contamination

During the above-mentioned three sessions, monitoring of groundwater, soil gas and open air were performed under the supervision of a local public environmental Agency, not directly Politecnico di Milano; indications about monitoring procedures and features of analytical methods are given in this paragraph.

Tab. 6.3 presents the physical properties of the researched compounds as they are reported in ISS/ISPESL Italian Institutes database (DB) (ISS/ISPESL, 2010, § 1.2), or for still absent compounds, from RISC 4.05 SW DB (RISC, 2010).

***Tab. 6.3**: physical properties of the researched compounds; sources: $^{\#}$: ISS/ISPESL DB (ISS/ISPESL, 2010); *: RISC 4.05 SW DB (RISC, 2010).*

	Organic matter partitioning coefficient	**Air diffusion**	**Water diffusion**	**Henry's law constant**
	K_{oc}	**D^g**	**D^w**	**H**
	$l\ kg^{-1}$	**$cm^2\ s^{-1}$**	**$cm^2\ s^{-1}$**	**-**
Benzene $^{\#}$	6.20E+01	8.80E-02	9.80E-06	2.28E-01
Toluene $^{\#}$	1.40E+02	8.70E-02	8.60E-06	2.72E-01
ethylbenzene $^{\#}$	2.04E+02	7.50E-02	7.80E-06	3.23E-01

***Tab. 6.3**: continued.*

p-xylene #	3.11E+02	7.69E-02	8.44E-06	3.14E-01
C5-C8 aliphatics #	2.27E+03	8.00E-02	1.00E-05	5.40E+01
C9-C12 aliphatics #	6.80E+05	7.00E-02	5.00E-06	6.90E+01
C13-C18 aliphatics #	6.80E+05	7.00E-02	5.00E-06	6.90E+01
C19-C36 aliphatics *	1.00E+09	1.00E-01	1.00E-05	4.60E+03
C9-C10 aromatics #	1.78E+03	7.00E-02	1.00E-05	3.30E-01
C11-C12 aromatics #	5.00E+03	6.00E-02	1.00E-05	3.00E-02
naphthalene *	2.00E+03	5.90E-02	7.50E-06	1.98E-02
MTBE #	1.20E+01	8.00E-02	9.41E-05	2.40E-02

6.2.2.2.1 Groundwater monitoring

Before starting each campaign of groundwater monitoring, purge operations were performed by pumping a volume of water at least equal to three times the volume contained inside the well column. Each sample was collected by a mono-use bailer and stored at 4°C in a glass vial, awaiting analysis on the analytes indicated in § 6.2.1.3.

BTEX and C9-C10 aromatics were analysed according to EPA 5030 C (2003) and EPA 8260 C (2006) methods, C5-C8 and C9-C18 aliphatics by MADEP EPH (2004), naphthalene EPA 3510 C (1996) and EPA 8270 D (2007) and MTBE by MP-1154-R1/03 ones.

In each monitoring session the weighed average of values coming from the 5 wells situated in the contaminated zone was calculated, using higher weights for P2, P3 and P4 located near to most of the soil gas/FC sampling points (to obtain a more representative comparison with results from other approaches).

Tab. 6.4 and Fig. 6.2 summarize average contaminant concentrations for each monitoring session.

***Tab. 6.4**: average groundwater pollutant content [µg l^{-1}].*

$C_{groundwater}$ [µg l^{-1}]	**benzene**	**toluene**	**ethylbenzene**	**p-xylene**	**C5-C8 aliphatics**	**C9-C12 aliphatics**	**C9-C10 aromatics**	**naphthalene**	**MTBE**
July 2009	6232	2191	4564	3212	11322	5661	20756	not determined	79
December 2009	3299	404	393	776	2955	1478	5418	36	52
July 2010	1616	486	1	686	2723	1361	4992	26	166

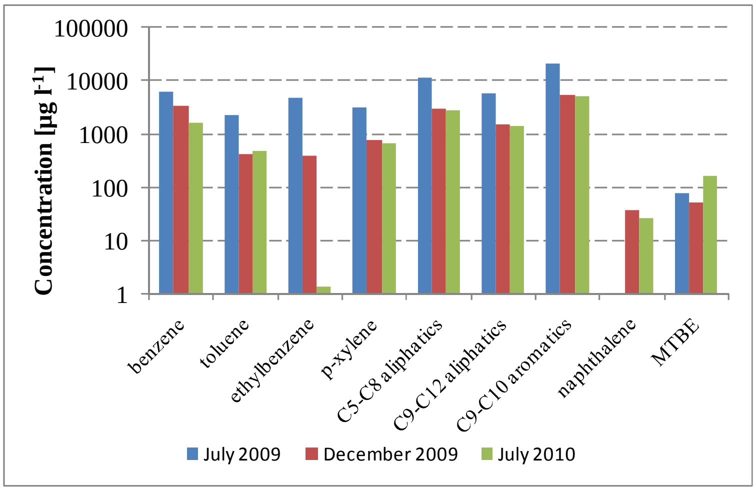

Fig. 6.2*: groundwater pollutant concentration [µg l^{1}] recorded during three FC monitoring sessions.*

6.2.2.2.2 Soil gas monitoring

10 permanent soil gas monitoring stations were installed in the potentially contaminated zone (at named points A, …, L, placed as in Fig. 6.1), to monitor vapour concentration in interstitial gas. With the exception of two points (G and I), all of them were double stations, with two independent gas probes screwed at different depths: collocation 1 "C1" equal to -0.8 m b.g.s. and collocation 2 "C2" equal to -3.0 m b.g.s.. G and I had only C1 sampling point.

The position of each soil gas station is summarised in Tab. 6.5.

Tab. 6.5*: details of soil gas positions; FC and outdoor air measurements were taken in their vicinity.*

A	far from contamination nucleus revealed by ground water concentrations
B	on gravel, in a car parking area
C	far from contamination nucleus revealed by ground water concentrations
D	on gravel
E	busy place, near to contamination nucleus revealed by ground water concentrations
F	near a contaminated well, about which information was unavailable
G	near an paved structure, poorly investigated area (only shallow soil gas)
H	shallow alloctone material, busy place
I	busy place, near to contamination nucleus revealed by ground water concentrations, poorly investigated area (only shallow soil gas)
L	near a concrete platform, busy place

Samples were taken at least 24 h after a meteorological event or irrigation, and after a purge equal to 3 times the dead volume in the probe.

BTEX, C5-C12 aliphatics and C9-C10 aromatics, naphthalene and MTBE sampling supports depended on their expected concentrations. A preliminary screening indication was given by a hand-held PID (§ 4.2.5.1), providing an overall concentration as voC (volatile organic Carbon). In the case of low concentration (voC < 5 ppm) they were sampled into a canister (§ 4.2.5.2, with sampling flow of 0.05 l min^{-1}, for 60 min), otherwise they were collected in a Tedlar bag (§ 4.2.5.2) (with the same sampling procedure). For heavy hydrocarbons, such as aliphatics ≥ C13 and aromatics ≥ C11, samples were collected on XAD2 tubes, after having passed through a PTFE filter. Tab. 6.6 summarizes analytical methods and detection limits for soil gas sampling. The variation coefficient for all the compounds is 15%.

Tab. 6.6*: analytical methods and reached detection limits (d.l.) for soil gas analysis.*

compound	analytical method	sampling medium	d.l. [µg m^{-3}]
benzene	MADEP APH (2000)	canister	2-20
	internal laboratory method	Tedlar bag	100
toluene	MADEP APH (2000)	canister	2-20
	internal laboratory method	Tedlar bag	100
ethylbenzene	MADEP APH (2000)	canister	2-20
	internal laboratory method	Tedlar bag	100
xylene	MADEP APH (2000)	canister	2-20
	internal laboratory method	Tedlar bag	100
C5-C8 aliphatics	MADEP APH (2000)	canister	25-100
	internal laboratory method	Tedlar bag	1000
C9-C12 aliphatics	MADEP APH (2000)	canister	25-100
	internal laboratory method	Tedlar bag	1000
C13-C18 aliphatics	NIOSH 5515 (1994)	XAD2	1000
C19-C36 aliphatics	NIOSH 5515 (1994)	XAD2	5000
C9-C10 aromatics	MADEP APH (2000)	canister	25-100
	internal laboratory method	Tedlar bag	1000
C11-C12 aromatics	NIOSH 5515 (1994)	XAD2	1000
naphthalene	MADEP APH (2000)	canister	2-20
	internal laboratory method	Tedlar bag	50-100
MTBE	MADEP APH (2000)	canister	2-20
	internal laboratory method	Tedlar bag	50-100

Tabs. 6.7, 6.8 and 6.9 and Fig. 6.3 present the results of soil gas concentrations sampled at A, …, L points, for each FC monitoring session. C13-C18 aliphatic, C19-C36 aliphatic and C11-C12 aromatic hydrocarbon classes were for all the points and all the sessions lower than detection limit (d.l.), equal to 1000, 5000 and 1000 µg m^{-3} respectively.

***Tab. 6.7**: analytical results [$\mu g\ m^{-3}$] from soil gas monitoring during the **July 2009** session; C1: shallow collocation at -0.8 m b.g.s., C2: deep collocation at -3.0 m b.g.s.. C13-C18 and C19-C36 aliphatics and C11-C12 aromatics were lower than d.l. (1000, 5000 and 1000 $\mu g\ m^{-3}$ respectively) for all the points.*

sampling point	Depth	benzene	toluene	ethylbenzene	xylene	C5-C8 aliphatics	C9-C12 aliphatics	C9-C10 aromatics	naphthalene	MTBE
A	C1	<5	8	<5	25	122	83	<50	<5	<5
	C2	<5	25	8	15	6689	103	<50	<5	<5
B	C1	<5	7	8	34	222	186	<50	<5	<5
	C2	50	1651	50	136	1385510	500	<500	<50	<50
C	C1	<5	<5	<5	<5	148	2485	125	<5	<5
	C2	<5	207	6	12	2682	<50	<50	<5	<5
D	C1	85	805	120	216	11038	555	<50	<5	<5
	C2	24	212	104	236	18816	2,411	76	<5	<5
E	C1	266	1396	366	1220	1984125	117249	338	<5	<5
	C2	115	479	600	378	2074329	74324	1258	<5	<5
F	C1	<5	10	7	16	243	269	<50	<5	<5
	C2	826300	998714	373642	984192	16924405	374789	115309	<50	<50
G	C1	142	734	85	141	91673	654	<50	<5	<5
H	C1	<5	<5	<5	<5	355	50	<50	<5	<5
	C2	2586	376	723	379	702986	16766	1023	<5	<5
I	C1	454	1632	558	1160	1453321	59658	870	<5	<5
L	C1	<5	42	6	10	4741	153	<50	<5	<5
	C2	60	46	11	30	108472	535	52	<5	<5

***Tab. 6.8**: analytical results [$\mu g\ m^{-3}$] from soil gas monitoring during the **December 2009** session; C1: shallow collocation at -0.8 m b.g.s., C2: deep collocation at -3.0 m b.g.s.. C13-C18 and C19-C36 aliphatics and C11-C12 aromatics were lower than d.l. (1000, 5000 and 1000 $\mu g\ m^{-3}$ respectively) for all the points.*

sampling point	depth	benzene	toluene	ethylbenzene	xylene	C5-C8 aliphatics	C9-C12 aliphatics	C9-C10 aromatics	naphthalene	MTBE
A	C1	<5	9	<5	10	123	286	<50	<5	<5
	C2	<5	9	6	15	179	134	<50	<5	<5
B	C1	<100	563	114	390	433295	34651	1268	<100	<100
	C2	<100	2440	<100	1175	16112410	156947	1738	<100	<100
C	C1	<5	27	21	52	248	2617	111	<5	<5
	C2	<5	22	15	51	202	891	<50	<5	<5

***Tab. 6.8**: continued.*

D	C1	<5	9	6	16	68	75	<50	<5	<5
	C2	<5	10	10	45	132	123	72	30	<5
E	C1	<100	2530	<100	840	9416327	115695	1159	<100	<100
F	C1	<5	9	<5	13	234	495	<50	<5	<5
	C2	2075260	226223	116861	253661	9023422	113812	22678	<100	<100
G	C1	738	990	332	858	2254015	28355	1976	<100	<100
H	C1	<5	8	<5	13	5461	318	<50	<5	<5
	C2	27762	3000	2648	<100	16652910	1170068	99113	<100	<100
I	C1	<100	1200	<100	1480	18669607	614389	1648	<100	<100
L	C1	791	8095	1170	39271200	747226	126864	7097	<100	<100
	C2	1019	1836	455	1953	1022664	163079	11009	<100	<100

***Tab. 6.9**: analytical results [$\mu g\ m^{-3}$] from soil gas monitoring during the **July 2010** session; C1: shallow collocation at -0.8 m b.g.s., C2: deep collocation at -3.0 m b.g.s.. C13-C18 and C19-C36 aliphatics and C11-C12 aromatics were lower than d.l. (1000, 5000 and 1000 $\mu g\ m^{-3}$ respectively) for all the points.*

sampling point	**depth**	**benzene**	**toluene**	**ethylbenzene**	**xylene**	**C5-C8 aliphatics**	**C9-C12 aliphatics**	**C9-C10 aromatics**	**naphthalene**	**MTBE**
A	C1	<5	12	15	41	<50	52	69	10	<5
	C2	<5	8	34	100	13909	7925	294	26	<5
B	C1	<5	9	50	102	1271	135	158	27	<5
	C2	4130	8051	2204	8367	9085762	500	5536	<50	<50
C	C1	<5	9	16	26	<50	256	50	16	<5
	C2	<5	22	26	51	159	485	61	<5	<5
D	C1	<5	13	25	58	71	112	85	<5	<5
	C2	<5	15	37	159	107	165	165	<5	<5
E	C1	1787	4265	1242	2510	6878111	500867	2015	1398	<50
	C2	1125	7392	1632	7175	13112822	850038	9822	<50	688
F	C1	<5	12	22	63	101	829	83	12	<5
	C2	37249	29916	8399	51803	369313	275904	20456	<50	<50
G	C1	3916	5831	1101	3362	1258995	7015	2412	1818	<50
H	C1	7	62	120	153	7284	9969	437	110	<5
	C2	765	8399	2735	5141	2976157	221876	3355	<50	<50
I	C1	1698	8205	1418	5448	7815631	322915	5160	<50	<50
L	C1	1704	2444	1137	2876	2313608	782521	2454	827	<50
	C2	922	1950	10357	10431	1011033	9398	15657	1381	<50

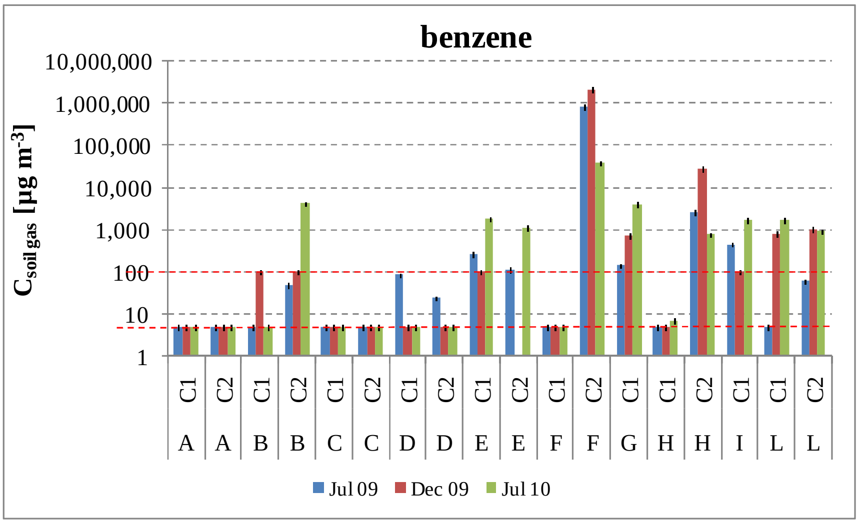

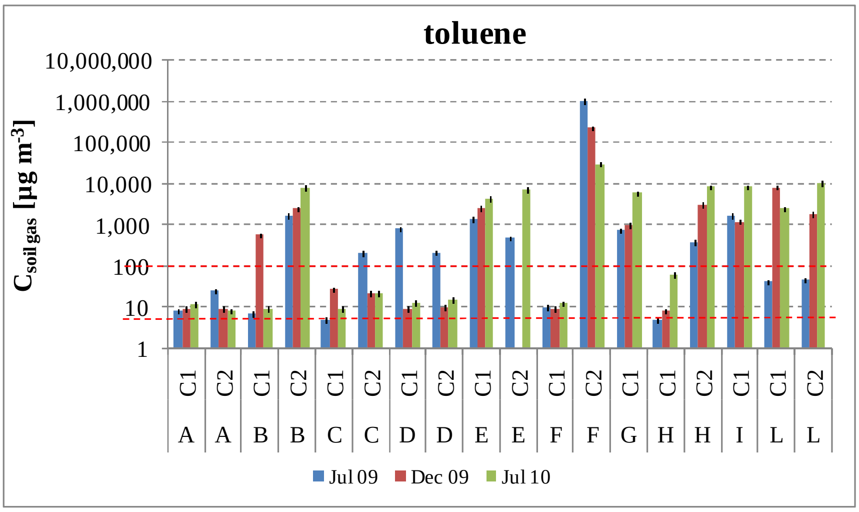

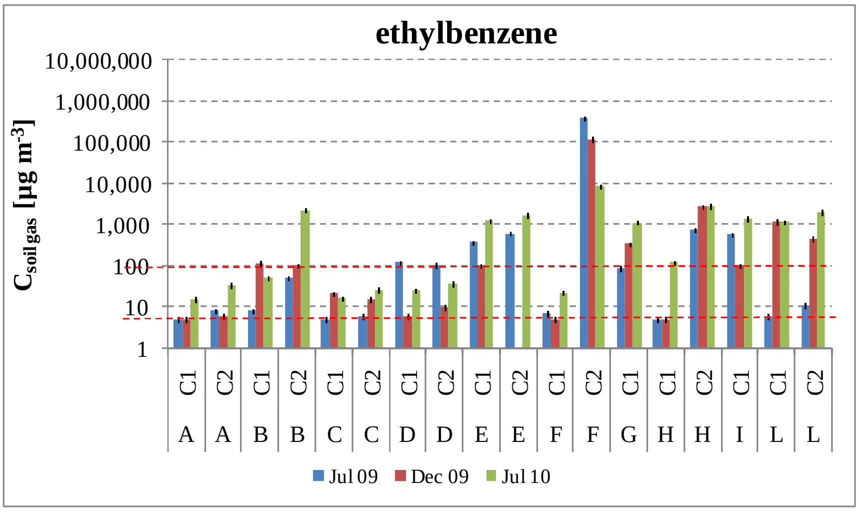

***Fig. 6.3**: continue*

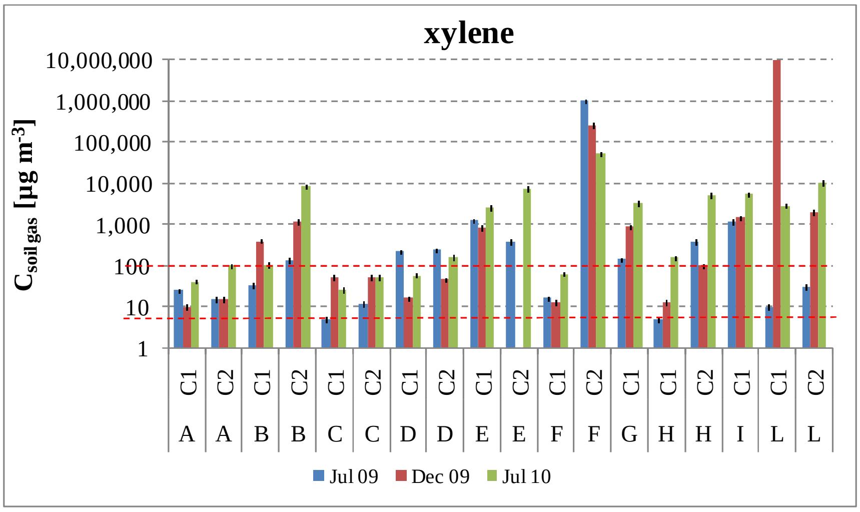

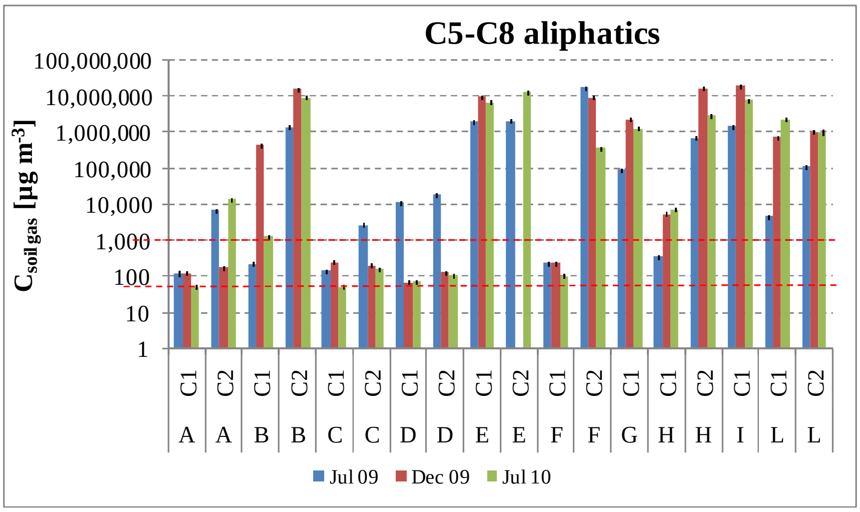

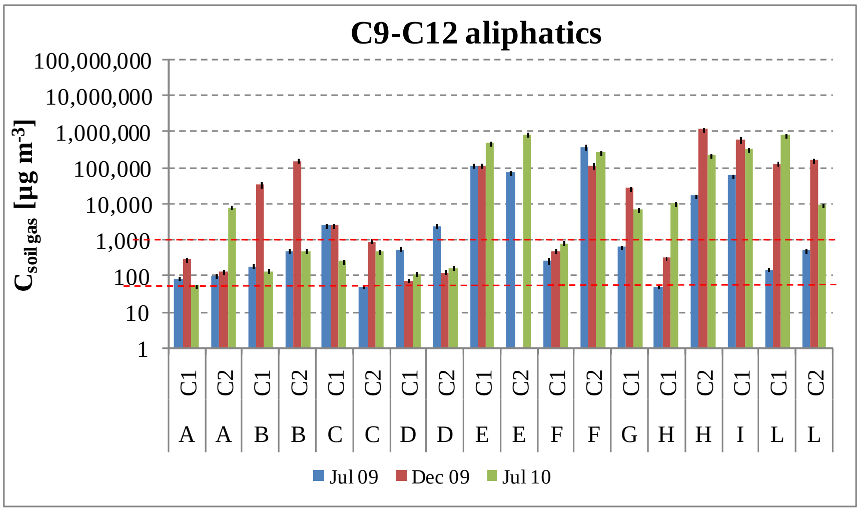

***Fig. 6.3**: continue.*

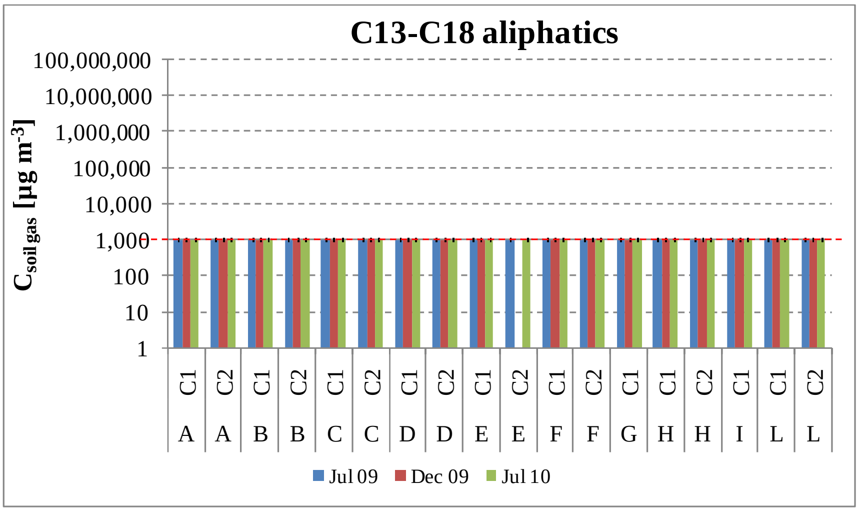

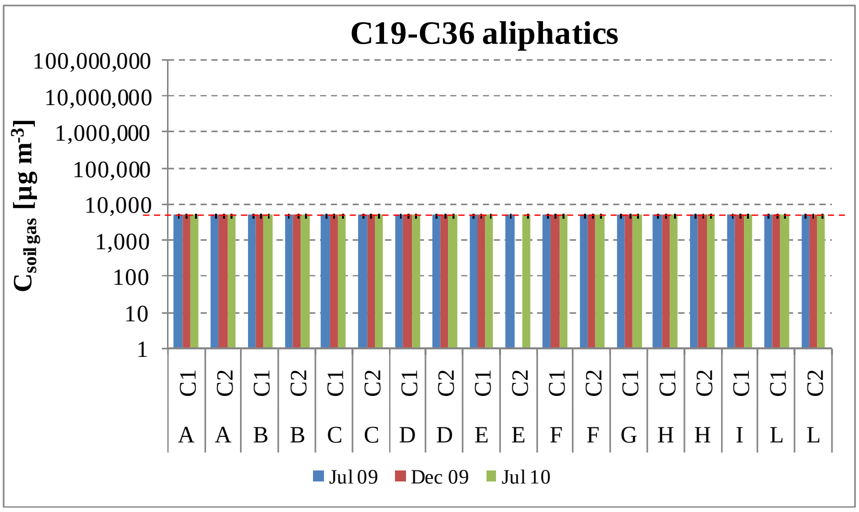

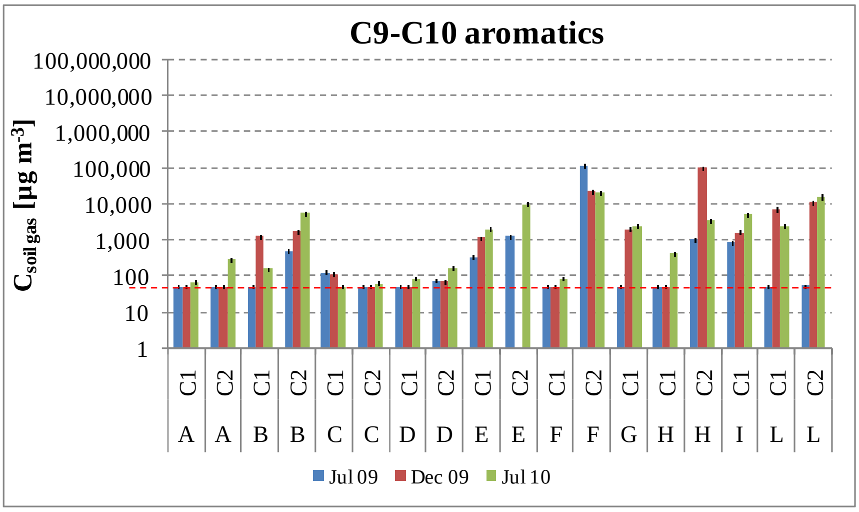

Fig. 6.3: *continue.*

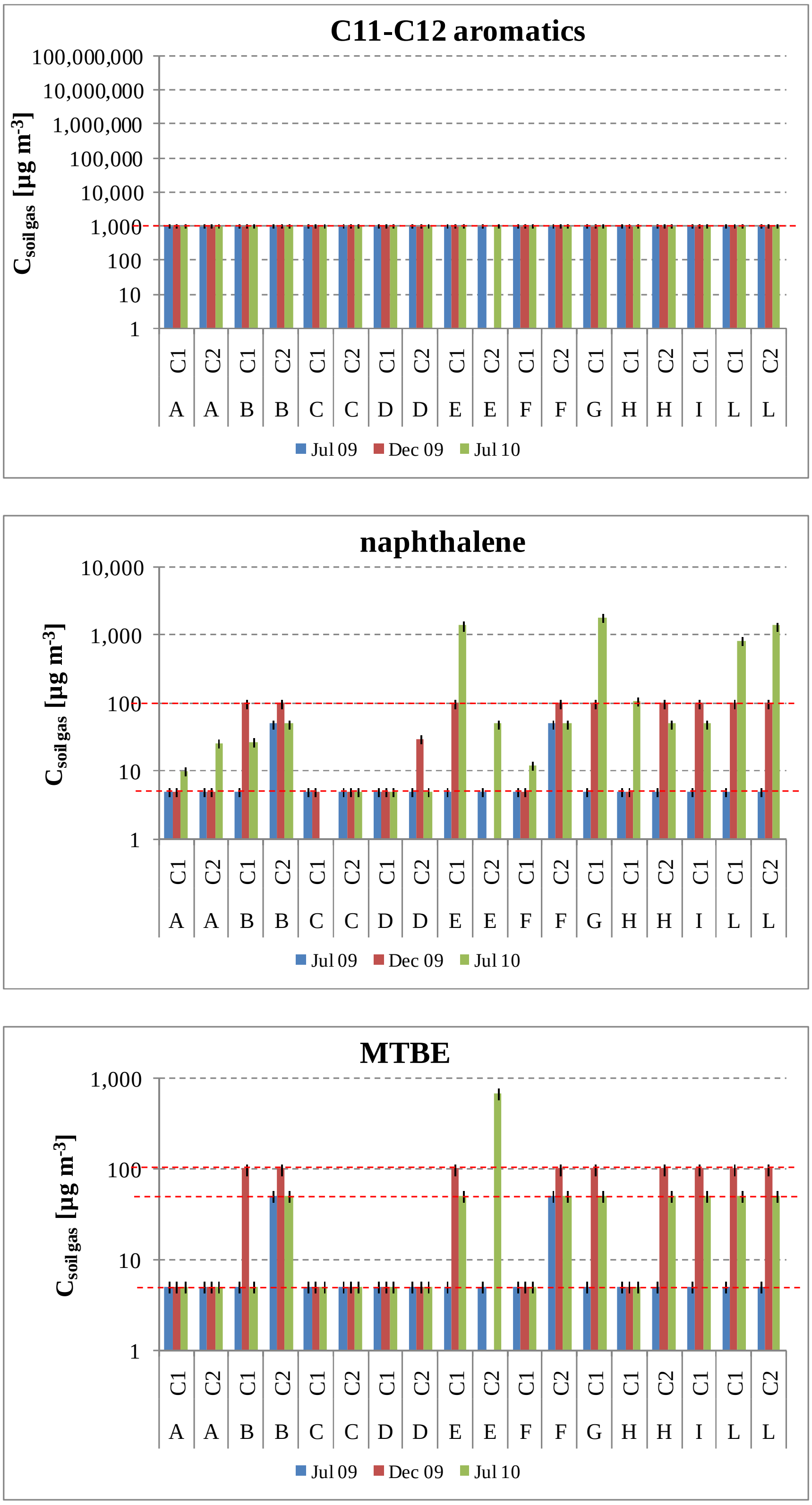

Fig. 6.3: *comparison (in logarithm scale) between soil gas concentrations [µg m^{-3}] at different points and during the 3 monitoring sessions (different colours), for each compound. C1: shallow point at -0.8 m b.g.s., C2: deep point at -3.0 m b.g.s.; error*

bars indicate analytical error whereas dashed red lines d.l. of different analytical techniques (Tab. 6.6).

As for BTEX, they seemed to behave in an overall similar way; it was however impossible to specify a trend over time or a correlation between the shallow (C1) and deep (C2) sampling depths: for some positions they seemed to change less than an order of magnitude (o.o.m.) with depth (such as A, D, E, and L with the exception, for this point, of the second sampling campaign), whereas for others they appeared to increase meaningfully (more than 1 o.o.m) with depth (B, F, H).

Point F, at depth C2, for all the sampling sessions, seemed however the most contaminated soil gas station by benzene, toluene, ethylbenzene and xylene: F was in fact placed near a contaminated well, about which information was unavailable (Tab. 6.5). As for xylene, however, during the winter 2009 campaign, L point, at C1 depth, revealed an anomalous maximum concentration over all the other samples.

As regards detected (> d.l.) hydrocarbons both the absence of a general correlation between C1 and C2 monitoring depths (relative to the same point) and of a trend over time were noticed. Point F was confirmed to be one of the highest contaminated locations, together with points B, E, G, H, I and L, for all light hydrocarbons. E, G, L presented presence of naphthalene vapours too. MTBE was detected with concentration higher than d.l. only at deep point E, and only during the summer 2010 campaign.

No further indication is possible to add about C13-C36 aliphatics and C11-12 aromatics, as they were always lower than d.l..

6.2.2.2.3 Open air monitoring

Only during the July 2010 sampling campaign, also outdoor air samples ($C_{out,meas}$) were taken at points A, B, E, G, I and L (Fig. 6.1), through collection into canister (not directly by Politecnico di Milano). BTEX, C5-C8 and C9-C12 aliphatics, C9-C10 aromatics, naphthalene and MTBE were detected by MADEP APH (2000) with d.l. equal to 50 $\mu g\ m^{-3}$ for hydrocarbon compounds and 2 $\mu g\ m^{-3}$ for the other analytes.

Maximum measured concentrations ($C_{out,meas,max}$) are reported too, by posing data lower than d.l. equal to d.l..Results are indicated in Tab. 6.10 and Fig. 6.4.

Of all the BTEX, xylene was found in all the sampled points with the highest concentrations, in good agreement with soil gas monitoring (Fig. 6.3). As for benzene, ethylbenzene and aliphatic hydrocarbons there was no direct correlation with samples of soil gas, for instance the particularly high value in B does not correspond to an exclusively higher concentration in soil gas (also G, I and L points presented concentrations of the same o.o.m.). As Tab. 6.5 indicates, B was placed in a car-parking area and measurements were probably affected by some local vehicle emissions; in fact fumes from gasoline combustion contain BTEX substances.

As far as toluene was concerned, on the contrary, a good correlation was noticed. As for aromatics, naphthalene and MTBE nothing was deduced because detected concentrations were lower than d.l.s.

***Tab. 6.10**: analytical results $C_{out,meas}$ [µg m^{-3}] for outdoor air monitoring in 6 points during the **July 2010** campaign. Maximum values are indicated $C_{out,meas,max}$ too, with values lower than d.l. highlighted in bold type.*

$C_{out,meas}$ [µg m^{-3}]	**benzene**	**toluene**	**ethylbenzene**	**xylene**	**C5-C8 aliphatics**	**C9-C12 aliphatics**	**C9-C10 aromatics**	**naphthalene**	**MTBE**
A	<2	<2	<2	9	91	<50	<50	<2	<2
B	6	5	4	20	100	104	<50	<2	<2
E	<2	4	2	12	69	<50	<50	<2	<2
G	<2	5	2	15	51	<50	<50	<2	<2
I	<2	5	2	11	75	<50	<50	<2	<2
L	<2	6	<2	11	110	60	<50	<2	<2
$C_{out,meas,max}$	6	6	4	20	110	104	**50**	**2**	**2**

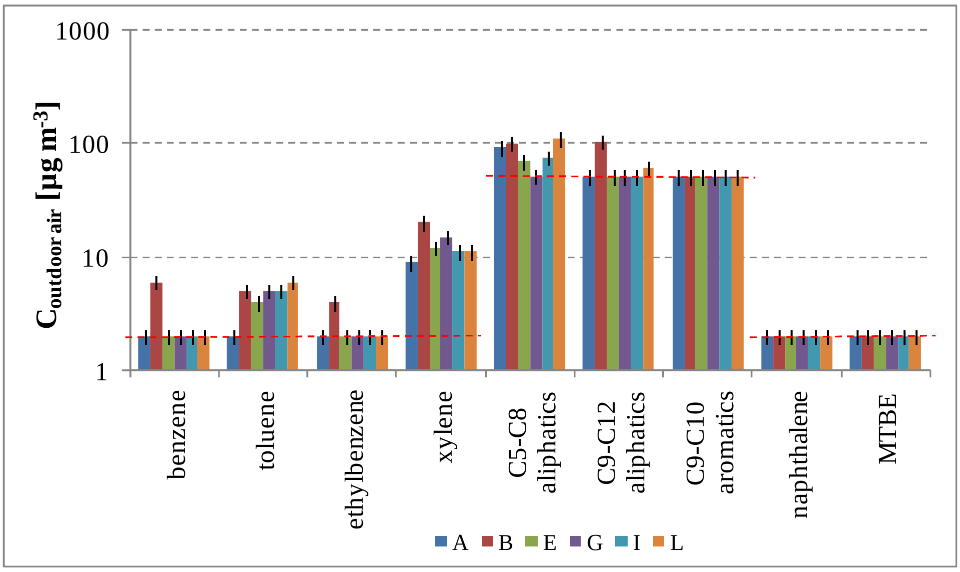

***Fig. 6.4**: analytical results [µg m^{-3}] for outdoor air monitoring in 6 points during the **July 2010** campaign. Segments of dashed red line, overlapping histogram groups for each compound, represent its d.l..*

6.2.3 Flux chamber monitoring

During the monitoring activities presented in § 6.2.2, three sampling campaigns with dynamic flux chamber (§ 4.2.1.2) were carried out by the author for Politecnico di Milano, to monitor the emitted flux at ground surface. Summer/winter 2009 campaigns were chosen as seasonal monitoring is suggested in literature (§

4.2.3) and the second summer campaign was useful to compare similar environmental context but with changed contaminant condition.

6.2.3.1 Field equipment

New tested FC setup (§ 5.2.5) was used and monitoring was carried out according to an inner developed protocol which considered the results of activities described in § 5.

In each monitoring point the chamber was sealed to the soil by using wet sand and dried treated air was used as the sweep flow, as described in § 5.2.4.

A sketch of the measuring system is indicated in Fig 6.5 and a picture of the same in Fig. 6.6.

It was composed by:

i. a tank with some granular silica gel (Carlo Erba) (2 in Fig 6.5) to absorb moisture of environmental air (1 in Fig 6.5) preceded by a PTFE filter to protect from environmental dust and stabilize the suction pump (point ii). When the gel was exhausted (it had changed colour) it was regenerated in an oven at 120°C for 24 h;

ii. a suction pump (KNF Laboport) (3 in Fig 6.5); since the outflow was overheated, pipeline from 3 to 4 was connected to a glass midget impinger (Sigma Aldrich, Fig. 6.7) placed in a cold water bath (with some ice packs) in order to cool it and further to create a compensation volume which stabilized the flow;

iii. U shaped container filled with activated carbon Norit 1 mm to purify environmental air from the compounds researched on sampling line (BTEX, C5-C8 aliphatics, C9-C18 aliphatics, C19-C36 aliphatics, C9-C10 aromatics, C11-C22 aromatics, naphthalene and methyl tert-butyl ether -MTBE-) similarly to what is indicated in § 5.2.4. Activated carbon (a.c.) was changed for each sampling point measurement and regenerated according to procedure in § 5.2.4;

iv. checking lines to verify purification of sweep air flowing into the FC, commonly constituted by two lines. One (Ck1) was constituted of an a.c. tube (Sigma Aldrich) (5 in Fig 6.5), followed by a rotameter (Zambelli, § A1.1.2.5) (6 in Fig 6.5) and a valve to regulate the airflow properly. It was used for analysis on BTEX, C6-C8 aliphatics, C9-C12 aliphatics and C9-C10 aromatics. The second line (Ck2) had a similar structure, and contained a XAD2 tube (Sigma Aldrich) (5’ in Fig 6.5) followed by an a.c. one and another system to regulate the flow (L80418/01, § A1.1.2.5). They were respectively used to adsorb C13-C18 aliphatics, C19-C36 aliphatics, C11-C22 aromatics and naphthalene on the first one, and C5 aliphatic and MTBE on the second one (because XAD2 does not retain them). Detailed reasons are given in § A2.2.4. As for the July 2009 campaign only Ck1 line was necessary to verify BTEX content;

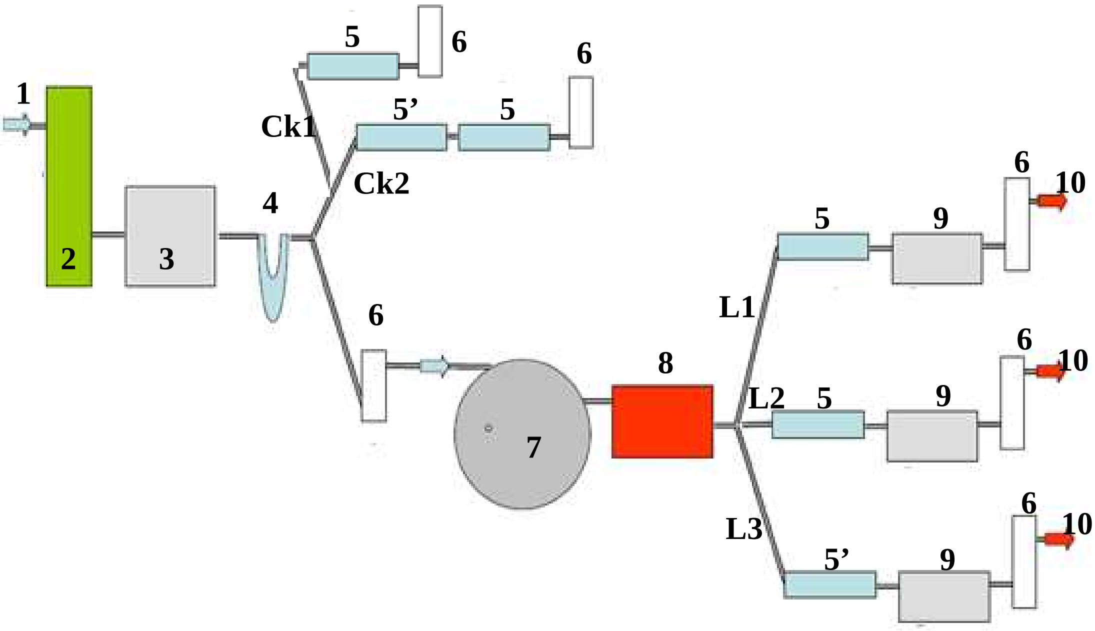

***Fig 6.5**: sketch FC system used for field activity. 1: ambient air, 2: silica gel tank, 3: PTFE suction pump, 4: activated carbon U shape reactor, 5: activated carbon tube, 5': XAD2 tube, 6: flow meter to regulate inflow (Q_{in}) into FC, 7: flux chamber, 8: impinger and cold bath, 9: suction pump, 10: flow Q_{sampl} flowing through each sampling line; Ck: check line to verify treated air pureness, L: sampling line.*

v. parallel line conducting the sweep gas into FC (7 in Fig 6.5). Another rotameter (Gilmont n° 13, § A1.1.2.5) and a valve regulated the air flow at the proper rate (Q_{in}) diverting the excess. Mass flow controller (§ 5.2.2) was no longer used because some electronic problems arose at the temperature in which the campaigns were performed (which was often outside the optimum range, § A1.1.2.3);

vi. two glass midget impingers in series (Sigma Aldrich, Fig. 6.7), located in a cold water bath (with some ice packs) (8 in Fig 6.5), were places to protect monitoring tubes from moisture contained the out-flow (§ 4.2.5.3) and to pick up condensed water for further analysis;

vii. sampling system that was generally constituted by three parallel lines (L1, L2 and L3 in Fig 6.5, each one needed for a different group of analytes. Each line was constituted by a sampling tube (Sigma Aldrich) and a constant flow pump (SKC AirCheck -§ A1.1.2.1- or Ego Plus TT, Zambelli -§ A1.1.2.2-) (9 in Fig 6.5), regulated at proper flow (Q_{sampl}). Flow was verified periodically by a flow meter (SKC, § A1.1.2.5) (6 in Fig 6.5) linked to the pump outflow. Tubes were respectively an a.c. one for BTEX, C6-C8 aliphatics, C9-C12 aliphatics and C9-C10 aromatics, another a.c. for C13-C18 aliphatics, C19-C36 aliphatics, C11-C22 aromatics and naphthalene and a XAD2 one for C5 aliphatic and MTBE (5' in Fig 6.5).

The difference between Q_{in} and Q_{sampl} escaped through the two open left vents (§ 4.2.4.7).

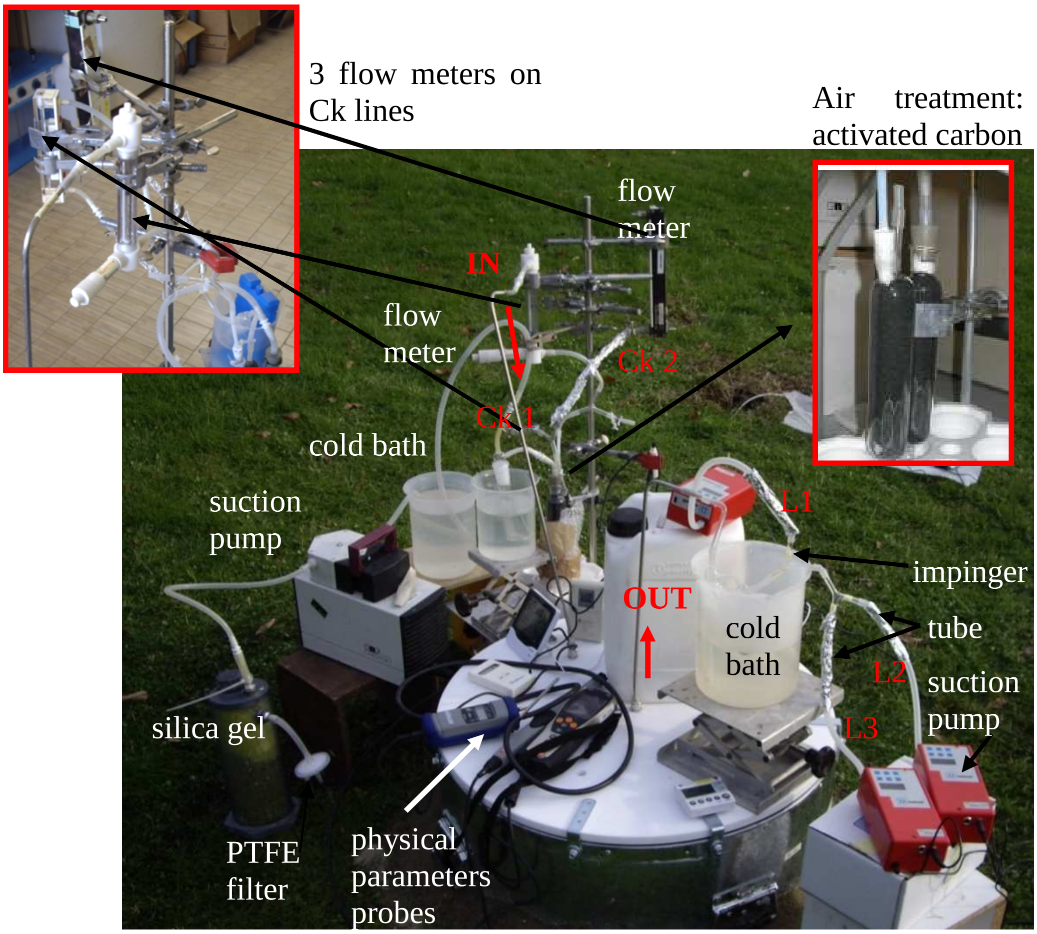

Fig 6.6*: picture of FC system used for field activity*

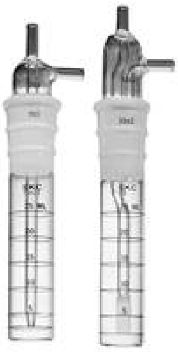

Fig. 6.7*: glass midget impingers used to cold air flow along sampling line.*

6.2.3.2 FC measurements

Before starting each measurement, purge of the environmental air initially trapped under the FC was performed, thus also reaching a pseudo-steady state inside the chamber; sweep air was switched on for 2 h, regulated at the same condition maintained during monitoring operations, without tubes connected on L1, L2 and L3 lines. On the contrary tubes were already fixed on Ck1 and Ck2 lines to verify the overall mass flowed through the system, therefore increasing the possibility to detect chemicals on the tubes (as their concentrations were potentially very low). Analytical results on tubes are, in fact, expressed as total mass adsorbed on the support (§ 4.2.5.3) and, when the monitoring duration increases, the volume passing through the tube increases too, with higher probability to detect a mass higher than d.l..

After 2 h, sampling tubes were connected to outflow-line on one side, and to a suction pump to the other. All the tubes were covered with some aluminium foil to protect them from direct sunlight that could have altered the absorbed molecules.

FC blanks (§ 4.2.3) were also performed at the beginning and end of each campaign (called FC-blank-t_{in} and FC-blank-t_{fin} respectively): FC was placed indoors over a PTFE sheet (§ 5.2.2) and usual protocol was followed.

3 field-blank tubes (2 of a.c. and 1 of XAD2) (§ 4.2.5.3) were opened for each sampling point and left open long enough (a few seconds) to connect the sampling tubes to lines. Then they were stored in the same way as samples, thus representing a reference for transport and storage conditions. They were analysed similarly to samples (§ A2.2), enabling any external interference not due to soil vapour emissions to be quantified.

At the end of measurement, tubes were closed with sealing caps, covered by aluminium foil and placed in closed glass pots (one for each sampling point) at - 4°C awaiting analyses. The pots were previously left in an oven at 105 °C for at least 8 h to make any VOC volatilize. Liquid samples were collected from impingers and placed in 5 ml glass vials (filled to the brim if the volume of water was enough) and stored similarly as tubes.

Tubes were analysed from DIIAR Laboratory at Politecnico di Milano, according to methods indicated in § A2.2.2 for BTEX (including all xylene forms, such as in § 2.1) and in § A2.2.3 for hydrocarbon compounds, giving results indicated as mass M_{sampl}. C5-C8 aliphatic results were calculated by adding C5 aliphatic to C6-C8 aliphatics; the d.l. of the new class was therefore defined as the sum of single d.l.. Both sampling part “a” and checking par “b” (§ 4.2.5.3) were analysed.

Moisture samples were analysed according to methods in § A2.2.4 to evaluate potential amounts of chemicals diluted in the aqueous phase.

Monitoring duration lasted approximately 5/6 h, with the aim of simulating the exposure of a potential receptor in the recreational area, as long as possible compatibly with remaining time available, which guaranteed a reliable assessment as far as RA is concerned (§ 4.2.5), and increased furthermore possibility of detecting low concentrations. Different sampling durations did not influence comparability of results because these were elaborated as indicated in § 6.2.4.2.

Each point measurement lasted 7/8 h in all, plus the time needed to mount the system setup, and that is why one point was taken a day.

Tab. 6.11 indicates the points monitored during the campaigns, for each of which FC was placed next to the respective soil gas station (to be compared directly with its results) on unpaved areas (§ 4.1.2). Locations were chosen according to time available with good weather conditions (as indicated in § 6.2.2.2.2), and insisting on more frequented places (points E, I and L).

***Tab. 6.11**: points of FC monitoring during different campaigns.*

	A	**B**	**C**	**D**	**E**	**F**	**G**	**H**	**I**	**L**
July 2009	x		x	x	x	x		x	x	x
December 2009				x	x	x		x	x	x
July 2010		x			x		x		x	x

Tabs. 6.12, 6.13 and 6.14 indicate the operative parameters for each FC measurement.

Only BTEX were monitored during the first campaign needing only one tube, overall requiring a lower Q_{sampl} than in later campaigns; a lower sweep flow rate was needed however guaranteeing FC internal pressure higher than outside (as was verified in § 6.3.1.1.3). During December 2009 and July 2010 all the above mentioned chemicals were analyzed and therefore all 3 sampling lines were active. During the last campaign the available suction pump sometimes gave lower flow rate (probably due to high temperature) and the operative conditions were regulated as a consequence.

***Tab. 6.12**: sampling points and operative parameters of the **July 2009** campaign.*

	air flow rate in FC	**air flow rate passing through sampling tube**	**sampling duration**
	$\mathbf{Q_{in}}$ [l min^{-1}]	$\mathbf{Q_{sampl}}$ [l min^{-1}]	**Δt** [min]
FC-A	6.3±0.1	1.9±0.1	300
FC-C	6.4±0.1	2.0±0.1	302
FC-D	6.3±0.1	2.0±0.1	305
FC-E	6.3±0.1	2.0±0.1	240
FC-F	6.2±0.1	2.0±0.1	307
FC-H	8.0±0.1	2.0±0.1	300
FC-I	6.3±0.1	2.0±0.1	312
FC-L	6.5±0.1	2.0±0.1	305
FC-blank-t_{in}	6.3±0.1	2.0±0.1	240
FC-blank-t_{fin}	6.4±0.1	2.0±0.1	300

***Tab. 6.13**: sampling points and operative parameters of the **December 2009** campaign.*

	air flow rate in FC	**air flow rate passing through sampling tube**	**sampling duration**
	$\mathbf{Q_{in}}$ [l min^{-1}]	$\mathbf{Q_{sampl}}$ [l min^{-1}]	**Δt** [min]
FC-D	7.5±0.1	1.5±0.1	313
FC-E	7.5±0.1	1.5±0.1	312
FC-F	7.5±0.1	1.5±0.1	313
FC-H	7.5±0.1	1.0±0.1	307
FC-I	7.5±0.1	1.5±0.1	310
FC-L	7.5±0.1	1.5±0.1	310
FC-blank-t_{in}	7.5±0.1	1.5±0.1	315
FC-blank-t_{fin}	7.5±0.1	1.5±0.1	330

***Tab. 6.14**: sampling points and operative parameters of the **July 2010** campaign.*

	air flow rate in FC	**air flow rate passing through sampling tube**	**sampling duration**
	$\mathbf{Q_{in}}$ [l min^{-1}]	$\mathbf{Q_{sampl}}$ [l min^{-1}]	**Δt** [min]
FC-B	6.3±0.1	1.2±0.1	350
FC-E	6.3±0.1	1.5±0.1	370
FC-G	7.0±0.1	1.5±0.1	336
FC-I	6.3±0.1	1.2±0.1	370
FC-L	7.0±0.1	1.5±0.1	373
FC-blank-t_{in}	7.3±0.1	1.5±0.1	299
FC-blank-t_{fin}	6.5±0.1	1.2±0.1	312

6.2.3.3 Recording physical parameters

Physical parameters (as measured during laboratory scale tests in § 5) were also recorded by inserting the probes inside the chamber through one of the two left open vents.

In detail, temperature and humidity both inside (T_{in} and H_{in}) and outside (T_{out} and H_{out}) the FC were taken by using a digital thermo-igrometer (TFA) (§ A1.1.1.4). The temperature difference $\Delta T = T_{out} - T_{in}$ and the averaged environmental temperature during the monitoring T_{envir} were calculated, too.

The pressure difference between the inside and the outside of the chamber ($\Delta P = P_{in} - P_{out}$) was also measured, by using Micro-manometer DC 100^{PRO} probe, half way up the cylinder and 2 cm over ground level (although not detected for all the points) and, only during the third campaign, 2 cm from the top, too.

During the December 2009 and the July 2010 campaigns, physical data of initial FC blanks were not recorded.

6.2.4 Fluxes from modelling

Available geological information showed a poor level of examination typical of investigations performed for characterization of potentially contaminated sites for RA purposes (§ 1.2). A simple conceptual site model sketch (§ 1.2) was therefore elaborated, resulting composed of an unsaturated layer made of loamy sand monolayer.

The physical features of the site, summarized in Tab. 6.15, were therefore defined following ex-APAT Agency indications according to the prevalent grain size ratio (APAT, 2008a).

An analytical model was chosen for transport modelling because it requires a low amount of input data (§ 3.4.2); the followed procedure is, also for this, in agreement with ex-APAT indications (APAT, 2008a) on which RA is based. Johnson and Ettinger (J&E) model (§ 3.4.2.2) (loaded into RISC 4.05 SW -RISC, 2010-) was preferred because it is the best-known reference model for vapour transport evaluation for risk analysis.

The results obtained were therefore in agreement with procedure commonly followed in compliance with Italian Law (L.D. 152/2006).

***Tab. 6.15**: physical properties of loamy sand soil* (APAT, 2008a).

parameter	inner reference	symbol	measuring unit	value
Soil density	§ 3.2.2.3	ρ_b	g cm^{-3}	1.7
Total porosity	§ 3.2.1	f	-	0.41
Effective porosity	§ 3.2.1	f_e	-	0.353
Water content	§ 3.2.1	θ_w	-	0.103
Residual water content	§ 3.2.1	θ_{wr}	-	0.057
Capillary fringe thickness	§ 3.2.1	h_{cap}	cm	18.8
Effective porosity at capillary fringe	§ 3.2.1	$f_{e,cap} = f_e$	-	0.353
Water content at capillary fringe	§ 3.2.1	$\theta_{w,cap}$	-	0.318
Air content at capillary fringe	§ 3.2.1	$\theta_{a,cap}$	-	0.035
Gaseous permeability	§ 3.2.2.2	k_r	cm^2	10^{-7}

6.2.4.1 Transport from groundwater

To simulate vapour from groundwater contamination (F_{GW}) the following data were used: geological information, concerning both capillary fringe and unsaturated soil (Tab. 6.15), contaminant physical properties (Tab. 6.3), and for each monitoring session, the proper water level depth (Tab. 6.2) and concentrations in groundwater (Tab. 6.4).

6.2.4.2 Transport from soil gas

To simulate vapour from soil gas (F_{SG}) the following data were used: geological information concerning unsaturated soil (Tab. 6.15), contaminant physical properties (Tab. 6.3), and for each monitoring session the proper monitoring depth (§ 6.2.2.2.2) and concentrations in soil gas (Tabs. 6.7, 6.8 and 6.9).

Maximum flux values ($F_{SG,max}$) are reported too, considering for concentrations lower than d.l., a value equal to d.l.. No average was calculated because of the presence of values lower than d.l..

6.2.5 Fluxes from flux chamber measurements

At each monitoring point, the average flux from the soil under the chamber, F_{FC}, was calculated by using equation (4.17), where A is FC area indicated in Tab. 5.6 and M_{sampl} is defined in § 6.2.3.2.

Maximum flux values ($F_{FC, max}$) are reported too, considering for M_{sampl} lower than d.l., a value equal to d.l.. No average was calculated because of the presence of values lower than d.l..

6.2.6 Ambient air measurements from modelling

To simulate dispersion of vapour flux from soil into atmosphere, the box model, commonly applied during RA for contaminated sites, was used. This approach complied with ex-APAT indications (APAT, 2008a). Concentration in air, C_{out}, due to the sole contribution of soil vapour, is considered to be spread in a box h high and L long, according to:

$$C_{out} = \frac{F*L}{v*h} \qquad (6.1)$$

where h, expressing the mixed layer height, was taken equal to 2 m as to default ex-APAT indication (APAT, 2008); L, indicating the length of the source along the prevalent wind direction, was taken as the diagonal of the contaminant part of the site (§ 6.2.2.1) equal to 220 m (according to a precautionary approach, independently of the direction of the wind); v is the wind velocity with a measured value of 1 m s^{-1}.

C_{out} was calculated with (6.1) from F_{GW}, F_{SG} (both two sampling depths) and $F_{FC,}$ referred to the July 2010 campaign, giving respectively $C_{out,GW}$, $C_{out,SG}$ and $C_{out,FC}$. Outdoor concentrations of each analyte, modelled from correspondent maximum fluxes of the July 2010 campaign ($F_{SG,\ C1,max}$, $F_{SG,C2,max}$ and $F_{FC,\ max}$) are called $C_{out,SG,C1,max}$, $C_{out,SG,C2,max}$ and $C_{out,FC,max}$.

6.2.7 Risk calculation

C_{out}, as indicated in § 1.3, is the chemical input datum which joined to toxicological and exposure parameters, is used in the estimation of risk due to vapour inhalation. Indications of ex-APAT Institute regarding RA execution (APAT, 2008a) were followed: from a statistical point of view, when the number of measures is lower than or equal to ten, the maximum value is to be used. As $C_{out,meas}$ were less than ten, $C_{out,meas,max}$ (of each compound) was used to calculate the risk due to inhalation. In particular cancer risk (R) for the carcinogenic compound (benzene), hazard index (HI) due separately to each analyte and Total HI as sum of single HI were evaluated. Results were compared with risks estimated from $C_{out,GW,max}$, $C_{out,SG,C1,max}$, $C_{out,SG,C2,max}$ and $C_{out,FC,max}$.

According to Italian law (L.D. 152/2006), maximum tolerable risks due to exposure to a potentially polluted site, are equal to $R_{tol} = 10^{-6}$ for R from a single substance and $HI_{tol} = 1$ both for HI and total HI (due to the overall exposure to non-carcinogenic compounds).

RISC 4.05 SW (RISC, 2010) was used in all cases. For the present case-history, toxicological data were taken from ISS-ISPESL database (ISS/ISPESL, 2010) (Tab. 6.16) and the exposure parameters were default ex-APAT values (APAT, 2008a), with the exception of site-specific established exposure frequency and time of permanence (indicated in Tab. 6.17 both for adult and child potential receptors).

***Tab. 6.16**: toxicological parameter values for analytes researched during outdoor air monitoring (source: ISS/ISPESL, 2010); SF: slope factor, RfD: reference dose.*

	inhalation SF $[mg\ (kg\text{-}d)^{-1}]^{-1}$	**inhalation RfD $[mg\ (kg\text{-}d)^{-1}]$**
benzene	2.73E-02	8.55E-03
toluene	-	1.43E+00
ethylbenzene	-	2.85E-01
p-xylene	-	2.00E-01
C5-C8 aliphatic	-	5.70E-02
C9 - C18 aliphatic	-	5.70E-02

***Tab. 6.16**: continued.*

C9 - C10 aromatic	-	1.43E-02
naphthalene	-	8.60E-04
MTBE	-	8.60E-01

***Tab. 6.17**: applied exposure parameters for child and adult receptors.*

	Adult	Child
Average lifetime (year)	70	70
Body weight (kg)	70	15
Exposure duration (year)	24	6
Exposure frequency (d year^{-1})	300	300
Time outdoors (h d^{-1})	16	16
Inhalation rate (m^3 h^{-1})	1,5	1
Lung retention factor (-)	1	1

6.3 Results

6.3.1 Flux chamber measurements

Tabs. 6.18, 6.20 and 6.22 indicate the mass of compounds adsorbed on tubes placed along check lines (Ck1 and Ck2 in Fig. 6.5) during each monitoring session. Tabs. 6.19, 6.21 and 6.23, on the other hand, summarize analytic results in terms of M_{sampl} found on each tube placed along sampling lines (L1, L2 and L3 in Fig. 6.5).

Analysis of moisture matrix collected during summer sessions (whose results are not reported in tables directly) revealed a negligible mass of each analyte (lower than d.l.) in each sample. During the winter session, due to low temperature, no moisture was collected in midget impingers. Results from tubes along outflow lines, therefore, did not have to be corrected by any additional amount.

All the “field and transport blank” tubes presented a mass lower than d.l. for all the analyzed compounds (data not directly indicated) and there were no artefacts due to incorrect technical handling or storage.

Sweep air flowing into the FC was properly treated by a.c. system, as it is indicated by values lower than d.l., both on part a and part b of tubes along check lines (Tabs. 6.19, 6.21 and 6.23).

None of the FC-blanks, performed at the beginning and end of each campaign, presented any trace of contamination (Tabs. 6.19, 6.21 and 6.23), and therefore memory effects had to be excluded.

The sampling tubes captured completely contaminant mass, without breakthrough phenomena, because their parts b were always lower than d.l..

Summing up, BTEX were detected just during the July 2009 campaign, in points I (toluene) and L (m-xylene). During the winter campaign C9-C12 aliphatics were detected in D and H, whereas lighter class (C5-C8 aliphatics) were found in I, confirmed also in July 2010. During the last monitoring campaign amounts > d.l. of different aliphatic compounds were recorded in B, E, G, I and L, and in G also C9-

C10 aromatics. Results cannot be compared directly as M_{sampl} had to be elaborated as in § 6.2.5.

***Tab. 6.18**: contaminant mass [μg] found on a.c. tubes along check Ck1 line (to control proper air treatment), during the **July 2009** campaign; part a: sampling part and part b: check part.*

	tube part	**benzene**	**toluene**	**ethylbenzene**	**o-xylene**	**m- xylene**	**p- xylene**
Air Ck - A	**a**	<0.9	<0.9	<0.9	<0.9	<0.9	<0.9
	b	<0.3	< 0.3	< 0.3	< 0.3	< 0.3	< 0.3
Air Ck -C	**a**	<0.9	<0.9	<0.9	<0.9	<0.9	<0.9
	b	<0.3	< 0.3	< 0.3	< 0.3	< 0.3	< 0.3
Air Ck -D	**a**	<0.9	<0.9	<0.9	<0.9	<0.9	<0.9
	b	<0.3	< 0.3	< 0.3	< 0.3	< 0.3	< 0.3
Air Ck -E	**a**	<0.9	<0.9	<0.9	<0.9	<0.9	<0.9
	b	<0.3	< 0.3	< 0.3	< 0.3	< 0.3	< 0.3
Air Ck -F	**a**	<0.9	<0.9	<0.9	<0.9	<0.9	<0.9
	b	<0.3	< 0.3	< 0.3	< 0.3	< 0.3	< 0.3
Air Ck -H	**a**	<0.9	<0.9	<0.9	<0.9	<0.9	<0.9
	b	<0.3	< 0.3	< 0.3	< 0.3	< 0.3	< 0.3
Air Ck -I	**a**	<0.9	<0.9	<0.9	<0.9	<0.9	<0.9
	b	<0.3	< 0.3	< 0.3	< 0.3	< 0.3	< 0.3
Air Ck -L	**a**	<0.9	<0.9	<0.9	<0.9	<0.9	<0.9
	b	<0.3	< 0.3	< 0.3	< 0.3	< 0.3	< 0.3
Air Ck blank-t_{in}	**a**	<0.9	<0.9	<0.9	<0.9	<0.9	<0.9
	b	<0.3	< 0.3	< 0.3	< 0.3	< 0.3	< 0.3
Air Ck blank.t_{fin}	**a**	<0.9	<0.9	<0.9	<0.9	<0.9	<0.9
	b	<0.3	< 0.3	< 0.3	< 0.3	< 0.3	< 0.3

***Tab. 6.19**: contaminant mass M_{sampl} [µg] found on a.c. tubes during the **July 2009** campaign; part a: sampling part and part b: check part. Values higher than d.l. are indicated in bold type.*

	tube part	**benzene**	**toluene**	**ethylbenzene**	**o-xylene**	**m- xylene**	**p- xylene**
FC-A	**a**	<0.9	<0.9	<0.9	<0.9	<0.9	<0.9
	b	<0.3	<0.3	<0.3	<0.3	<0.3	<0.3
FC-C	**a**	<0.9	<0.9	<0.9	<0.9	<0.9	<0.9
	b	<0.3	<0.3	<0.3	<0.3	<0.3	<0.3
FC-D	**a**	<0.9	<0.9	<0.9	<0.9	<0.9	<0.9
	b	<0.3	<0.3	<0.3	<0.3	<0.3	<0.3
FC-E	**a**	<0.9	<0.9	<0.9	<0.9	<0.9	<0.9
	b	<0.3	<0.3	<0.3	<0.3	<0.3	<0.3
FC-F	**a**	<0.9	<0.9	<0.9	<0.9	<0.9	<0.9
	b	<0.3	<0.3	<0.3	<0.3	<0.3	<0.3
FC-H	**a**	<0.9	<0.9	<0.9	<0.9	<0.9	<0.9
	b	<0.3	<0.3	<0.3	<0.3	<0.3	<0.3
FC-I	**a**	<0.9	<0.9	<0.9	<0.9	**0.92**	<0.9
	b	<0.3	<0.3	<0.3	<0.3	<0.3	<0.3
FC-L	**a**	<0.9	**0.97**	<0.9	<0.9	<0.9	<0.9
	b	<0.3	<0.3	<0.3	<0.3	<0.3	<0.3
FC-blank-t_{in}	**a**	<0.9	<0.9	<0.9	<0.9	<0.9	<0.9
	b	<0.3	<0.3	<0.3	<0.3	<0.3	<0.3
FC-blank-t_{fin}	**a**	<0.9	<0.9	<0.9	<0.9	<0.9	<0.9
	b	<0.3	<0.3	<0.3	<0.3	<0.3	<0.3

***Tab. 6.20**: contaminant mass [µg] found on tubes along check Ck1 and Ck2 lines (to control proper air treatment), during the **December 2009** campaign; part a: sampling part and part b: check part.*

	tube part	**benzene**	**toluene**	**ethylbenzene**	**o-xylene**	**m- xylene**	**p- xylene**	**C5-C8 aliphatics**	**C9-C12 aliphatics**	**C13-C18 aliphatics**	**C19-C36 aliphatics**	**C9-C10 aromatics**	**C11-C22 aromatics**	**naphthalene**	**MTBE**
Air Ck - D	**a**	<0.3	<0.3	<0.3	<0.3	<0.3	<0.3	<0.6	<0.3	<0.5	<0.5	<0.3	<0.5	<0.2	<0.2
	b	<0.1	<0.1	<0.1	<0.1	<0.1	<0.1	<0.2	<0.1	<0.18	<0.18	<0.1	<0.18	<0.07	<0.07
Air Ck -E	**a**	<0.3	<0.3	<0.3	<0.3	<0.3	<0.3	<0.6	<0.3	<0.5	<0.5	<0.3	<0.5	<0.2	<0.2
	b	<0.1	<0.1	<0.1	<0.1	<0.1	<0.1	<0.2	<0.1	<0.18	<0.18	<0.1	<0.18	<0.07	<0.07
Air Ck -F	**a**	<0.3	<0.3	<0.3	<0.3	<0.3	<0.3	<0.6	<0.3	<0.5	<0.5	<0.3	<0.5	<0.2	<0.2
	b	<0.1	<0.1	<0.1	<0.1	<0.1	<0.1	<0.2	<0.1	<0.18	<0.18	<0.1	<0.18	<0.07	<0.07
Air Ck -H	**a**	<0.3	<0.3	<0.3	<0.3	<0.3	<0.3	<0.6	<0.3	<0.5	<0.5	<0.3	<0.5	<0.2	<0.2
	b	<0.1	<0.1	<0.1	<0.1	<0.1	<0.1	<0.2	<0.1	<0.18	<0.18	<0.1	<0.18	<0.07	<0.07
Air Ck -I	**a**	<0.3	<0.3	<0.3	<0.3	<0.3	<0.3	<0.6	<0.3	<0.5	<0.5	<0.3	<0.5	<0.2	<0.2
	b	<0.1	<0.1	<0.1	<0.1	<0.1	<0.1	<0.2	<0.1	<0.18	<0.18	<0.1	<0.18	<0.07	<0.07
Air Ck -L	**a**	<0.3	<0.3	<0.3	<0.3	<0.3	<0.3	<0.6	<0.3	<0.5	<0.5	<0.3	<0.5	<0.2	<0.2
	b	<0.1	<0.1	<0.1	<0.1	<0.1	<0.1	<0.2	<0.1	<0.18	<0.18	<0.1	<0.18	<0.07	<0.07
Air Ck blank-t_{in}	**a**	<0.3	<0.3	<0.3	<0.3	<0.3	<0.3	<0.6	<0.3	<0.5	<0.5	<0.3	<0.5	<0.2	<0.2
	b	<0.1	<0.1	<0.1	<0.1	<0.1	<0.1	<0.2	<0.1	<0.18	<0.18	<0.1	<0.18	<0.07	<0.07
Air Ck blank-t_{fin}	**a**	<0.3	<0.3	<0.3	<0.3	<0.3	<0.3	<0.6	<0.3	<0.5	<0.5	<0.3	<0.5	<0.2	<0.2
	b	<0.1	<0.1	<0.1	<0.1	<0.1	<0.1	<0.2	<0.1	<0.18	<0.18	<0.1	<0.18	<0.07	<0.07

***Tab. 6.21**: contaminant mass M_{sampl} [µg] found on tubes during the December 2009 campaign; part a: sampling part and part b: check part. Values higher than d.l. are indicated in bold type.*

	tube part	**benzene**	**toluene**	**ethylbenzene**	**o-xylene**	**m- xylene**	**p- xylene**	**C5-C8 aliphatics**	**C9-C12 aliphatics**	**C13-C18 aliphatics**	**C19-C36 aliphatics**	**C9-C10 aromatics**	**C11-C22 aromatics**	**naphthalene**	**MTBE**
FC - D	**a**	<0.3	<0.3	<0.3	<0.3	<0.3	<0.3	<0.6	**0.38**	<0.5	<0.5	<0.3	<0.5	<0.2	<0.2
	b	<0.1	<0.1	<0.1	<0.1	<0.1	<0.1	<0.2	<0.1	<0.18	<0.18	<0.1	<0.18	<0.07	<0.07
FC -E	**a**	<0.3	<0.3	<0.3	<0.3	<0.3	<0.3	<0.6	<0.3	<0.5	<0.5	<0.3	<0.5	<0.2	<0.2
	b	<0.1	<0.1	<0.1	<0.1	<0.1	<0.1	<0.2	<0.1	<0.18	<0.18	<0.1	<0.18	<0.07	<0.07
FC -F	**a**	<0.3	<0.3	<0.3	<0.3	<0.3	<0.3	<0.6	<0.3	<0.5	<0.5	<0.3	<0.5	<0.2	<0.2
	b	<0.1	<0.1	<0.1	<0.1	<0.1	<0.1	<0.2	<0.1	<0.18	<0.18	<0.1	<0.18	<0.07	<0.07
FC -H	**a**	<0.3	<0.3	<0.3	<0.3	<0.3	<0.3	<0.6	**0.31**	<0.5	<0.5	<0.3	<0.5	<0.2	<0.2
	b	<0.1	<0.1	<0.1	<0.1	<0.1	<0.1	<0.2	<0.1	<0.18	<0.18	<0.1	<0.18	<0.07	<0.07
FC -I	**a**	<0.3	<0.3	<0.3	<0.3	<0.3	<0.3	**183**	<0.3	<0.5	<0.5	<0.3	<0.5	<0.2	<0.2
	b	<0.1	<0.1	<0.1	<0.1	<0.1	<0.1	<0.2	<0.1	<0.18	<0.18	<0.1	<0.18	<0.07	<0.07
FC -L	**a**	<0.3	<0.3	<0.3	<0.3	<0.3	<0.3	<0.6	<0.3	<0.5	<0.5	<0.3	<0.5	<0.2	<0.2
	b	<0.1	<0.1	<0.1	<0.1	<0.1	<0.1	<0.2	<0.1	<0.18	<0.18	<0.1	<0.18	<0.07	<0.07
FC blank-t_{in}	**a**	<0.3	<0.3	<0.3	<0.3	<0.3	<0.3	<0.6	<0.3	<0.5	<0.5	<0.3	<0.5	<0.2	<0.2
	b	<0.1	<0.1	<0.1	<0.1	<0.1	<0.1	<0.2	<0.1	<0.18	<0.18	<0.1	<0.18	<0.07	<0.07
FC blank-t_{fin}	**a**	<0.3	<0.3	<0.3	<0.3	<0.3	<0.3	<0.6	<0.3	<0.5	<0.5	<0.3	<0.5	<0.2	<0.2
	b	<0.1	<0.1	<0.1	<0.1	<0.1	<0.1	<0.2	<0.1	<0.18	<0.18	<0.1	<0.18	<0.07	<0.07

***Tab. 6.22**: contaminant mass [µg] found on tubes along check Ck1 and Ck2 lines (to control proper air treatment), during the **July 2010** campaign; part a: sampling part and part b: check part.*

	tube part	**benzene**	**toluene**	**ethylbenzene**	**o-xylene**	**m- xylene**	**p- xylene**	**C5-C8 aliphatics**	**C9-C12 aliphatics**	**C13-C18 aliphatics**	**C19-C36 aliphatics**	**C9-C10 aromatics**	**C11-C22 aromatics**	**naphthalene**	**MTBE**
Air Ck -B	**a**	<0.3	<0.3	<0.3	<0.3	<0.3	<0.3	<0.6	<0.3	<0.5	<0.5	<0.3	<0.5	<0.2	<0.2
	b	<0.1	<0.1	<0.1	<0.1	<0.1	<0.1	<0.2	<0.1	<0.18	<0.18	<0.1	<0.18	<0.07	<0.07
Air Ck -E	**a**	<0.3	<0.3	<0.3	<0.3	<0.3	<0.3	<0.6	<0.3	<0.5	<0.5	<0.3	<0.5	<0.2	<0.2
	b	<0.1	<0.1	<0.1	<0.1	<0.1	<0.1	<0.2	<0.1	<0.18	<0.18	<0.1	<0.18	<0.07	<0.07
Air Ck -G	**a**	<0.3	<0.3	<0.3	<0.3	<0.3	<0.3	<0.6	<0.3	<0.5	<0.5	<0.3	<0.5	<0.2	<0.2
	b	<0.1	<0.1	<0.1	<0.1	<0.1	<0.1	<0.2	<0.1	<0.18	<0.18	<0.1	<0.18	<0.07	<0.07
Air Ck -I	**a**	<0.3	<0.3	<0.3	<0.3	<0.3	<0.3	<0.6	<0.3	<0.5	<0.5	<0.3	<0.5	<0.2	<0.2
	b	<0.1	<0.1	<0.1	<0.1	<0.1	<0.1	<0.2	<0.1	<0.18	<0.18	<0.1	<0.18	<0.07	<0.07
Air Ck -L	**a**	<0.3	<0.3	<0.3	<0.3	<0.3	<0.3	<0.6	<0.3	<0.5	<0.5	<0.3	<0.5	<0.2	<0.2
	b	<0.1	<0.1	<0.1	<0.1	<0.1	<0.1	<0.2	<0.1	<0.18	<0.18	<0.1	<0.18	<0.07	<0.07
Air Ck blank-t_{in}	**a**	<0.3	<0.3	<0.3	<0.3	<0.3	<0.3	<0.6	<0.3	<0.5	<0.5	<0.3	<0.5	<0.2	<0.2
	b	<0.1	<0.1	<0.1	<0.1	<0.1	<0.1	<0.2	<0.1	<0.18	<0.18	<0.1	<0.18	<0.07	<0.07
Air Ck blank-t_{fin}	**a**	<0.3	<0.3	<0.3	<0.3	<0.3	<0.3	<0.6	<0.3	<0.5	<0.5	<0.3	<0.5	<0.2	<0.2
	b	<0.1	<0.1	<0.1	<0.1	<0.1	<0.1	<0.2	<0.1	<0.18	<0.18	<0.1	<0.18	<0.07	<0.07

***Tab. 6.23**: contaminant mass M_{sampl} [µg] found on tubes during the **July 2010** campaign; part a: sampling part and part b: check part. Values higher than d.l. are indicated in bold type.*

	tube part	**benzene**	**toluene**	**ethylbenzene**	**o-xylene**	**m- xylene**	**p- xylene**	**C5-C8 aliphatics**	**C9-C12 aliphatics**	**C13-C18 aliphatics**	**C19-C36 aliphatics**	**C9-C10 aromatics**	**C11-C22 aromatics**	**naphthalene**	**MTBE**
FC - B	**a**	<0.3	<0.3	<0.3	<0.3	<0.3	<0.3	**8.6**	<0.3	**9**	**4**	<0.3	<0.5	<0.2	<0.2
	b	<0.1	<0.1	<0.1	<0.1	<0.1	<0.1	<0.2	<0.1	<0.18	<0.18	<0.1	<0.18	<0.07	<0.07
FC - E	**a**	<0.3	<0.3	<0.3	<0.3	<0.3	<0.3	**3.5**	<0.3	**14**	**2**	<0.3	<0.5	<0.2	<0.2
	b	<0.1	<0.1	<0.1	<0.1	<0.1	<0.1	<0.2	<0.1	<0.18	<0.18	<0.1	<0.18	<0.07	<0.07
FC - G	**a**	<0.3	<0.3	<0.3	<0.3	<0.3	<0.3	**20.4**	<0.3	**30**	**6**	**0.3**	<0.5	<0.2	<0.2
	b	<0.1	<0.1	<0.1	<0.1	<0.1	<0.1	<0.2	<0.1	<0.18	<0.18	<0.1	<0.18	<0.07	<0.07
FC - I	**a**	<0.3	<0.3	<0.3	<0.3	<0.3	<0.3	**1.1**	**0.4**	**22**	**9**	<0.3	<0.5	<0.2	<0.2
	b	<0.1	<0.1	<0.1	<0.1	<0.1	<0.1	<0.2	<0.1	<0.18	<0.18	<0.1	<0.18	<0.07	<0.07
FC - L	**a**	<0.3	<0.3	<0.3	<0.3	<0.3	<0.3	<0.6	<0.3	**25**	**5**	<0.3	<0.5	<0.2	<0.2
	b	<0.1	<0.1	<0.1	<0.1	<0.1	<0.1	<0.2	<0.1	<0.18	<0.18	<0.1	<0.18	<0.07	<0.07
FC blank-t_{in}	**a**	<0.3	<0.3	<0.3	<0.3	<0.3	<0.3	<0.6	<0.3	<0.5	<0.5	<0.3	<0.5	<0.2	<0.2
	b	<0.1	<0.1	<0.1	<0.1	<0.1	<0.1	<0.2	<0.1	<0.18	<0.18	<0.1	<0.18	<0.07	<0.07
FC blank-t_{fin}	**a**	<0.3	<0.3	<0.3	<0.3	<0.3	<0.3	<0.6	<0.3	<0.5	<0.5	<0.3	<0.5	<0.2	<0.2
	b	<0.1	<0.1	<0.1	<0.1	<0.1	<0.1	<0.2	<0.1	<0.18	<0.18	<0.1	<0.18	<0.07	<0.07

6.3.1.1 Physical parameters recording

6.3.1.1.1 Temperature

Figs. 6.8, 6.10 and 6.12 indicate T_{in} (green squares), T_{out} (red triangles) and ΔT (blue lozenges) recorded during each monitoring campaign. The end of purge phase, coincident with the beginning of monitoring, is indicated by a black triangle on x-axis. Further, for a clear reading, y-axis was kept the same on each group of figures.

Separately for each monitoring campaign, Tabs. 6.24, 6.25 and 6.26 summarize the average of T_{out} and T_{in} during each sampling day, and also T_{envir} at the bottom of average T_{out} column. ΔT is added, too, separately for purge (ΔT_{purge}) and monitoring (ΔT_{monit}) phases, in order to highlight difference between them. For each average, its standard deviation (s.d.) and variation coefficient (VC) are specified. Figs. 6.9, 6.11 and 6.13 represent these data.

July 2009 campaign

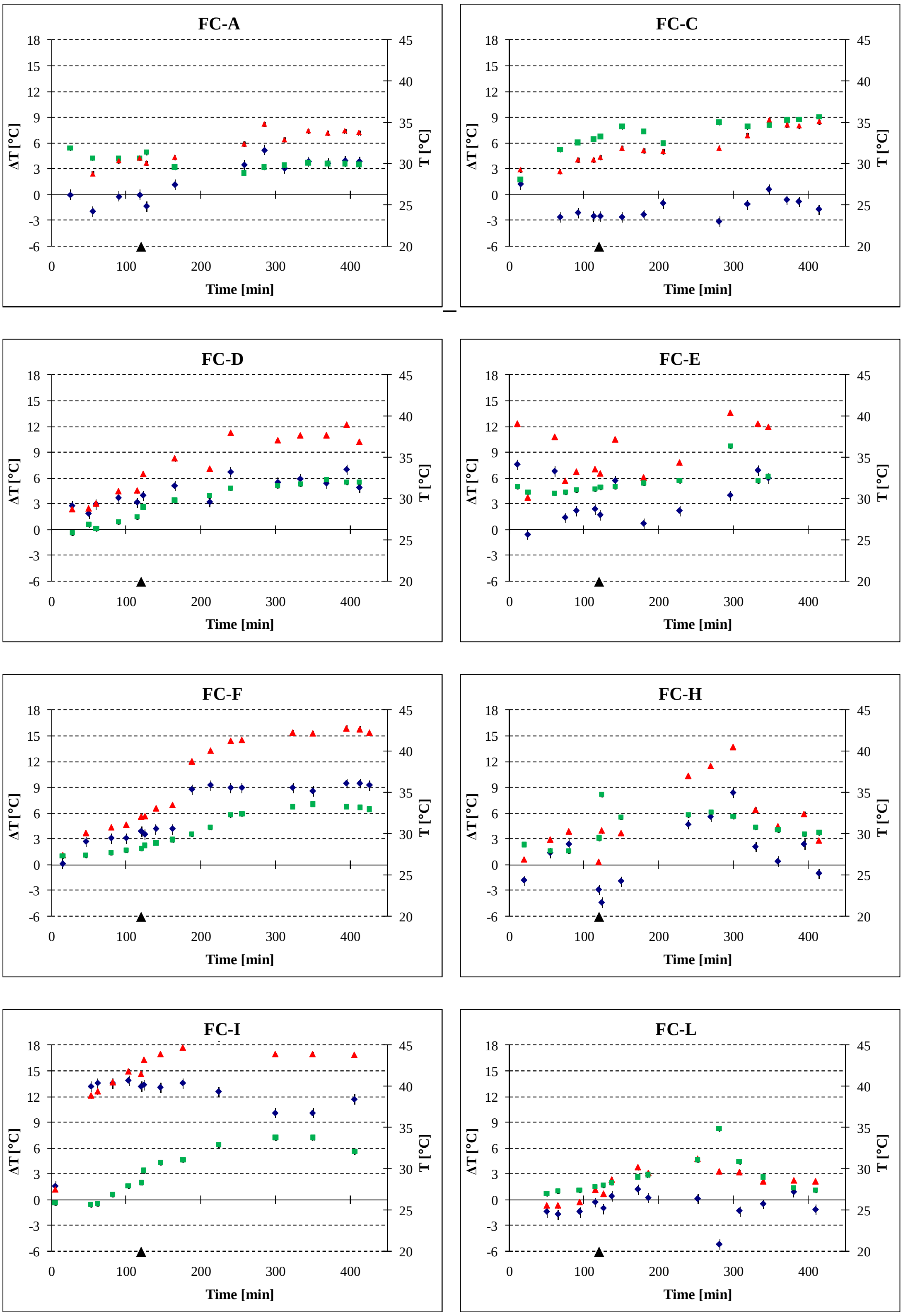

***Fig. 6.8**: continue*

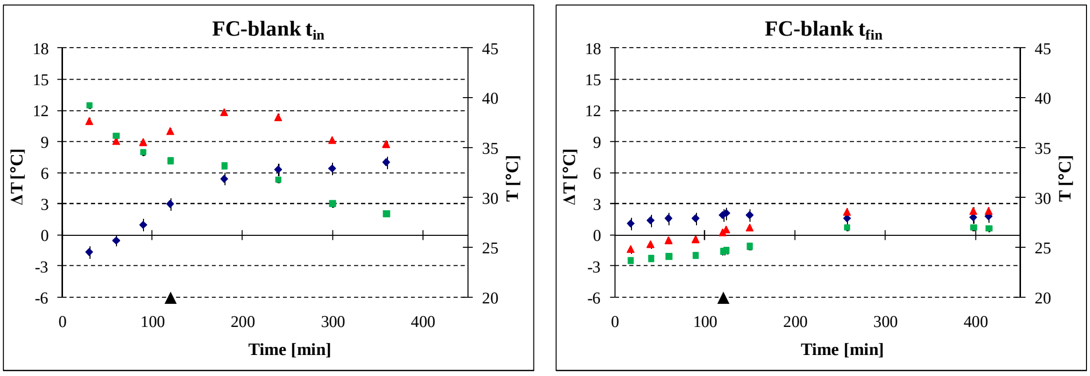

***Fig. 6.8**: temperature measured outside (red triangles) and inside the FC (green squares) (on right axis), and their difference (blue lozenges) (on left axis) recorded during the **July 2009** monitoring session. Black triangle on x-axis represents the end of purge phase and error bar indicates instrumental error or its propagation on temperature difference.*

***Tab. 6.24**: summary table for temperature during the **July 2009** campaign: average, standard deviation (s.d.) and variation coefficient (VC) for each point, of outside (T_{out}) and inside (T_{in}) the FC temperatures and ΔT, separately for purge (ΔT_{purge}) and monitoring (ΔT_{monit}) phases. Average temperature of the campaign (T_{envir}) and its statistics are indicated in bold type.*

	T_{out}			**T_{in}**			**ΔT_{purge}**			**ΔT_{monit}**		
	average	**s.d.**	**VC**	**average**	**s.d.**	**VC**	**average**	**s.d.**	**VC**	**average**	s.d.	VC
	°C	**°C**	**%**	**°C**	**°C**	**%**	**°C**	**°C**	**%**	**°C**	**°C**	**%**
A	32	2	6	30	1	3	-0.7	0.9	122	3	2	60
C	32	2	6	34	2	6	-2	2	105	-2	1	71
D	34	4	11	30	2	8	2.9	0.6	20	5	1	21
E	35	3	9	32	1	4	3	3	89	4	2	57
F	37	5	15	30	2	8	3	1	50	8	2	29
H	32	4	13	31	2	6	0	2	973	2	4	209
I	41	4	11	30	3	10	12	4	39	12	1	11
L	28	2	6	29	2	7	-1.2	0.5	44	-1	2	271
blank t_{in}	37	1	3	33	3	10	0	2	363	6.3	0.6	9
blank t_{fin}	27	1	5	25	1	5	1.5	0.3	17	1.8	0.2	9
T_{envir}	**34**	**4**	**11**									

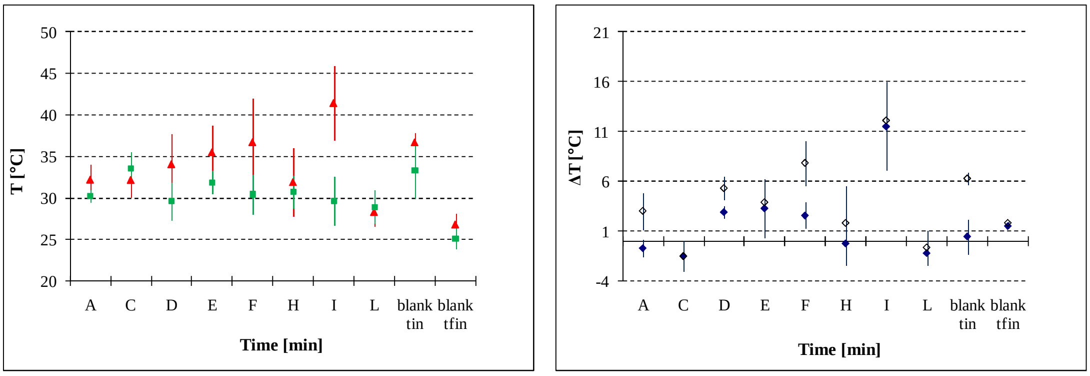

a) **b)**

Fig. 6.9*: the* ***July 2009*** *campaign: average temperature measured outside (red triangles) and inside (green squares) the FC (a), and ΔT separately for purge (full blue lozenges) and monitoring (empty black lozenges) phases (b); error bars indicate standard deviations.*

December 2009 campaign

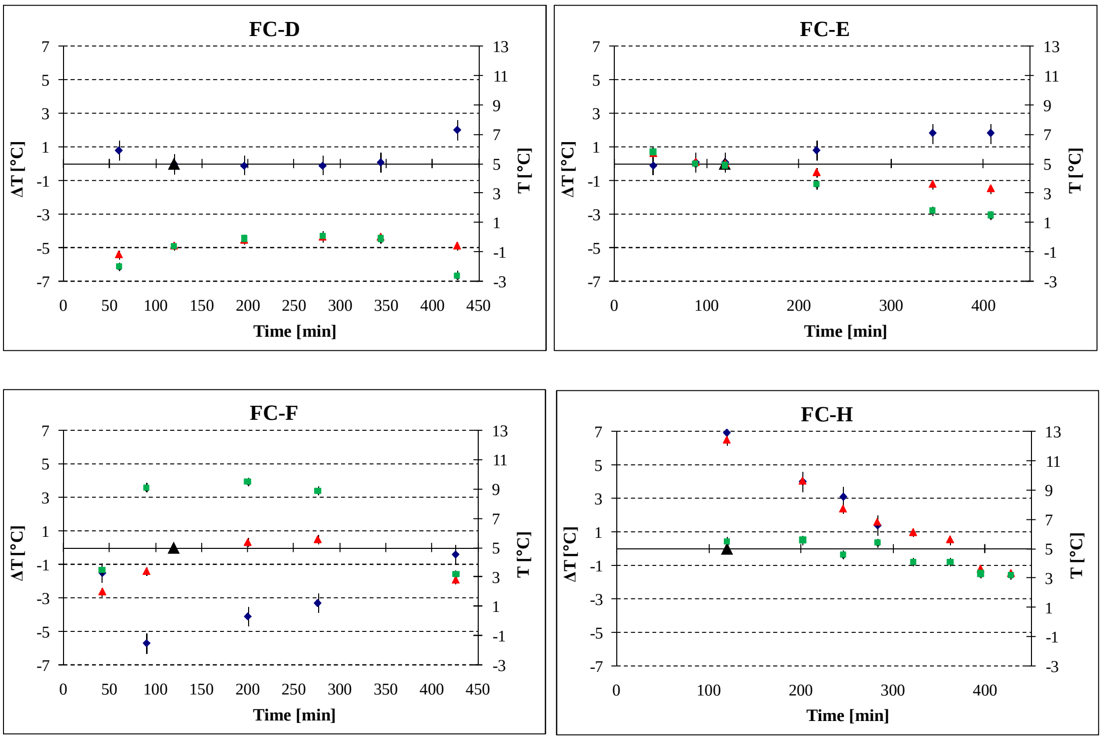

Fig. 6.10*: continue.*

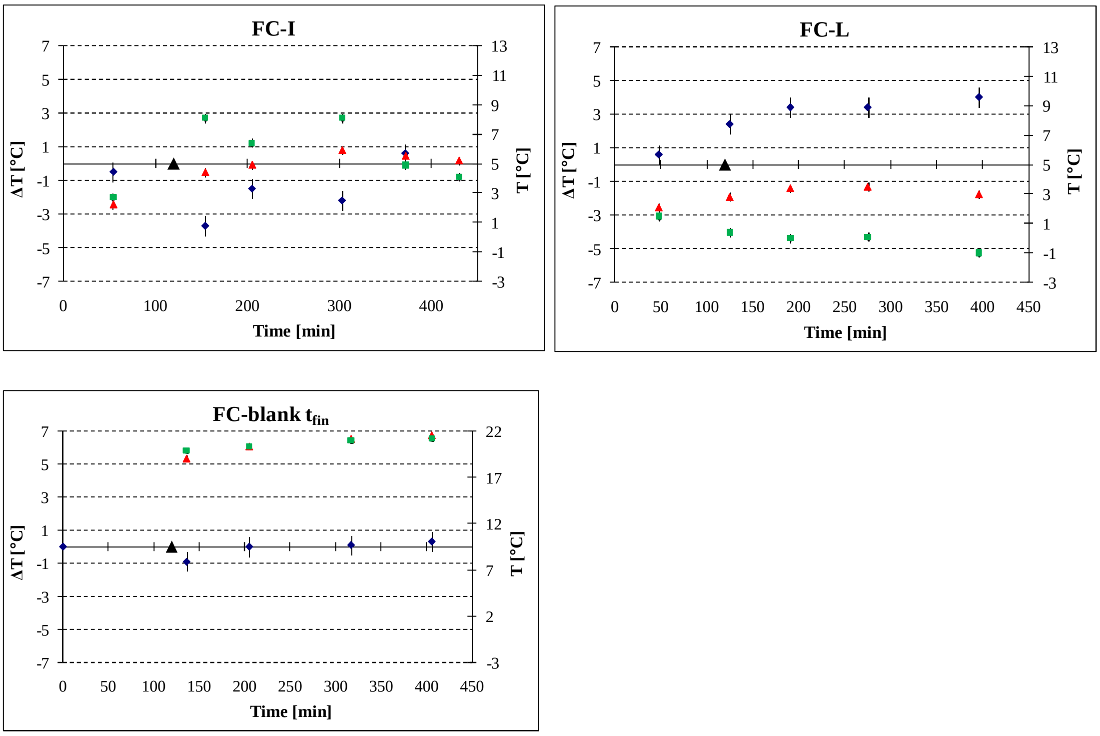

Fig. 6.10: *temperature measured outside (red triangles) and inside the FC (green squares) (on right axis), and their difference (blue lozenges) (on left axis) recorded during the* ***December 2009*** *monitoring session. Black triangle on x-axis represents the end of purge phase and error bar indicates instrumental error or its propagation on temperature difference.*

Tab. 6.25: *summary table for temperature during the* ***December 2009*** *campaign: average, standard deviation (s.d.) and variation coefficient (VC) for each point, of outside (T_{out}) and inside (T_{in}) the FC temperatures and ΔT, separately for purge (ΔT_{purge}) and monitoring (ΔT_{monit}) phases. Average temperature of the campaign (T_{envir}) and its statistics are indicated in bold type.*

	T_{out}			T_{in}			ΔT_{purge}			ΔT_{monit}		
	average	**s.d.**	**VC**	**average**	**s.d.**	**VC**	**average**	**s.d.**	**VC**	**average**	s.d.	VC
	°C	**°C**	**%**	**°C**	**°C**	**%**	**°C**	**°C**	**%**	**°C**	**°C**	**%**
D	-0.4	0.4	98	-0.9	1	118	0.8	-		0.4	0.8	214
E	4.5	0.8	19	4	2	43	0.0	0.1	-	1.1	0.7	64
F	4	1	37	7	3	42	-4	2	58	-3	2	61
H	2.5	0.5	24	3.4	0.4	13	-			4	2	52
I	5	1	26	6	2	35	-0.5	-		-2	2	91
L	3.0	0.5	17	0.2	0.8	401	0.6	-		3.3	0.6	17
blank t_{fin}	21	1	5	20.6	0.5	3	-			-0.1	0.5	368
T_{envir}	**3**	**2**	**445**									

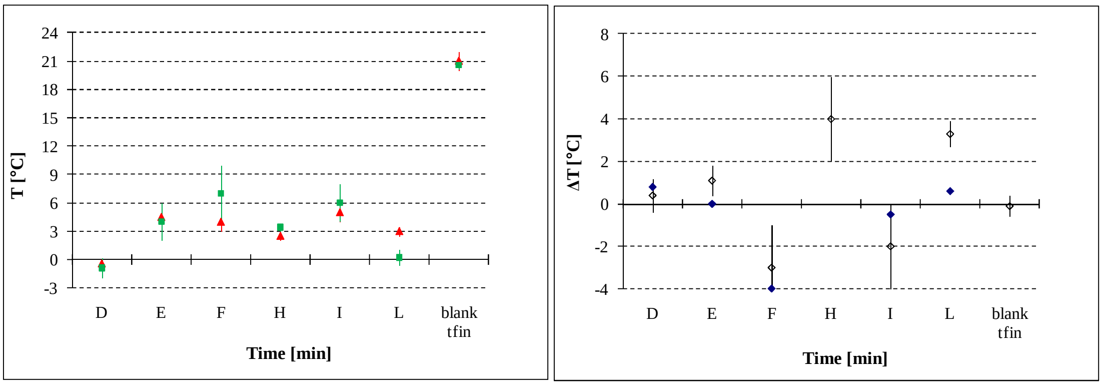

a) **b)**

***Fig. 6.11**: **December 2009** campaign: average temperature measured outside (red triangles) and inside (green squares) the FC (a), and ΔT separately for purge (full blue lozenges) and monitoring (empty black lozenges) phases (b); error bars indicate standard deviations.*

July 2010 campaign

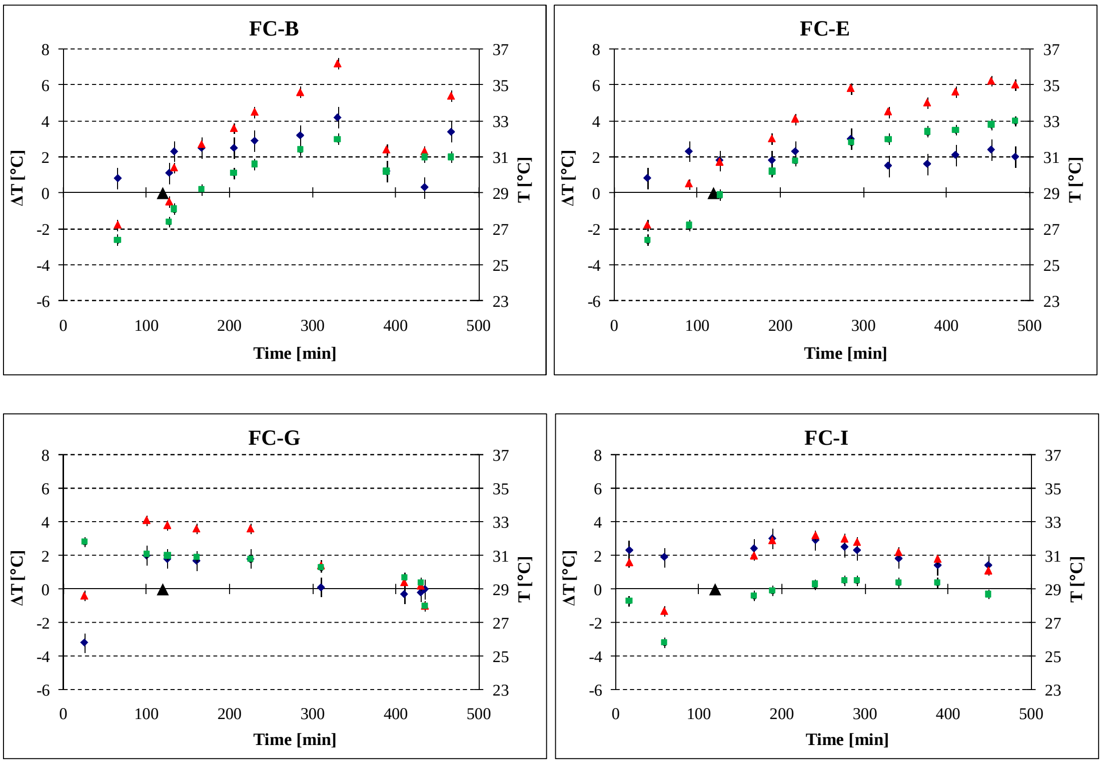

***Fig. 6.12**: continue.*

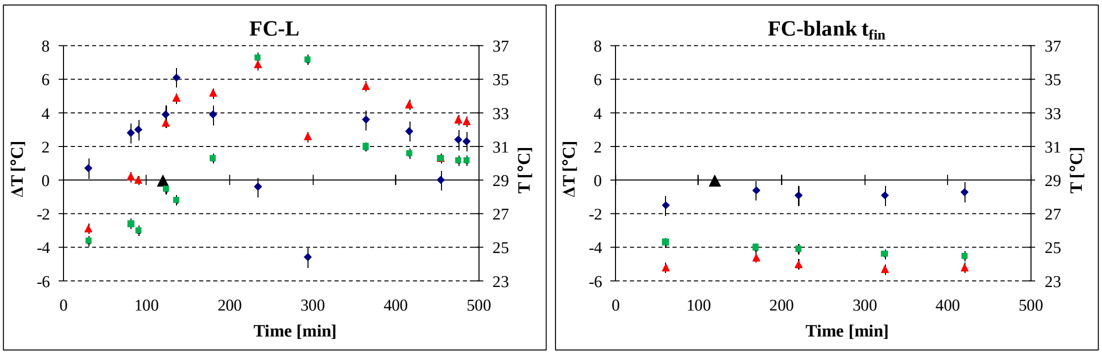

***Fig. 6.12**: temperature measured outside (red triangles) and inside the FC (green squares) (on right axis), and their difference (blue lozenges) (on left axis) recorded during the **July 2010** monitoring session. Black triangle on x-axis represents the end of purge phase and error bar indicates instrumental error or its propagation on temperature difference.*

***Tab. 6.26**: summary table for temperature during the **July 2010** campaign: average, standard deviation (s.d.) and variation coefficient (VC) for each point, of outside (T_{out}) and inside (T_{in}) the FC temperatures and ΔT, separately for purge (ΔT_{purge}) and monitoring (ΔT_{monit}) phases. Average temperature of the campaign (T_{envir}) and its statistics are indicated in bold type.*

	T_{out}			**T_{in}**			**ΔT_{purge}**			**ΔT_{monit}**		
	average	**s.d.**	**VC**	**average**	**s.d.**	**VC**	**average**	**s.d.**	**VC**	**average**	s.d.	VC
	°C	**°C**	**%**	**°C**	**°C**	**%**	**°C**	**°C**	**%**	**°C**	**°C**	**%**
B	32	3	8	30	2	6	1.0	0.2	16	3	1	44
E	33	3	8	31	2	7	1.6	0.8	48	2.1	0.4	21
G	31	2	6	30	1	4	-1	3	433	0.7	0.9	133
I	31	1	4	29	1	4	1.9	-		2.2	0.5	25
L	32	3	8	30	3	11	3	2	61	2	3	169
blank t_{fin}	24.0	0.3	1	24.8	0.2	1	-1.5	-		-0.8	0.1	17
T_{envir}	**31**	**3**	**10**									

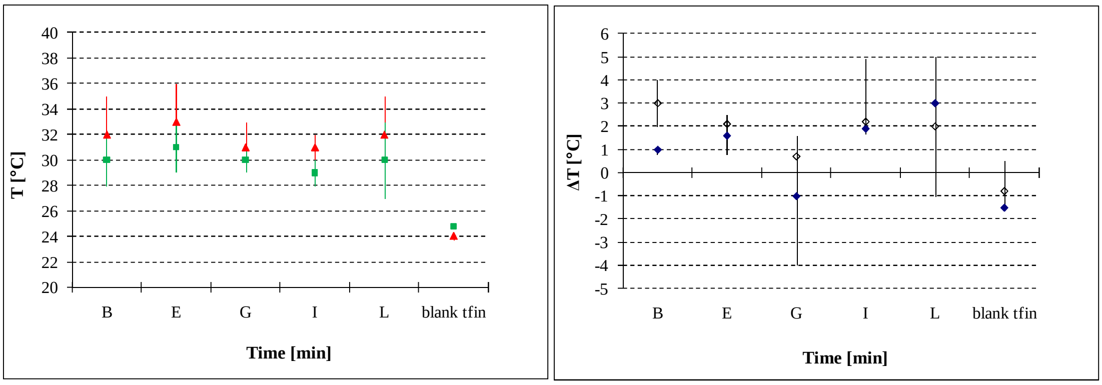

a) **b)**

***Fig. 6.13**: the **July 2010** campaign: average temperature measured outside (green squares) and inside (red triangles) the FC (a), and ΔT separately for purge (full blue lozenges) and monitoring (empty black lozenges) phases (b); error bars indicate standard deviations.*

The July 2009 campaign was performed at T_{envir} equal to 34±4 °C and the flux chamber had a fairly constant inner temperature during the campaign (Fig. 6.9.a). As for sampling points (Fig. 6.8), on hotter days (monitoring F and I) the temperature inside the FC was always lower than the external one and followed its increasing trend (due to different sun irradiation during the day); their average values where considerably different (Fig. 6.9.a). During less hot days, the two temperatures were more similar and generally T_{in} was slightly lower than T_{out} (A, D and E) or coincident (C and L), because the FC was placed under a sun umbrella.

The December 2009 campaign was performed at T_{envir} equal to 3±2 °C. With the exception of the day on which H was sampled, external temperature was generally constant during each monitoring. Apart from the indoor FC blank, points collected on warmer days (F and I in Fig. 6.10 and Fig. 6.11.a) presented T_{in} higher than T_{out}, whereas for the other days (E, H and L in Fig. 6.10 and Fig. 6.11.a) the opposite occurred or they coincided (D).

The third campaign was performed at T_{envir} equal to 31±3 °C. Internal temperature was generally lower than external one (Fig. 6.13.a) and followed its trend (Fig. 6.12); ΔT was therefore fairly constant during each point monitoring (Fig. 6.12).

During all three campaigns there was an insignificant difference between data recorded during purge phase and those recorded during monitoring (Figs. 6.9.b, 6.11.b and 6.13.b).

As regards FC blanks, temperature was generally different from monitoring places because they all took place indoors (§ 6.2.3.2).

6.3.1.1.2 Humidity

Figs. 6.14, 6.15 and 6.16 indicate internal (H_{in} in green squares) and external (H_{out} in red triangles) humidity recorded during each monitoring campaign. y-axis was maintained the same, on each group of figures, to favour a clearer reading.

July 2009 campaign

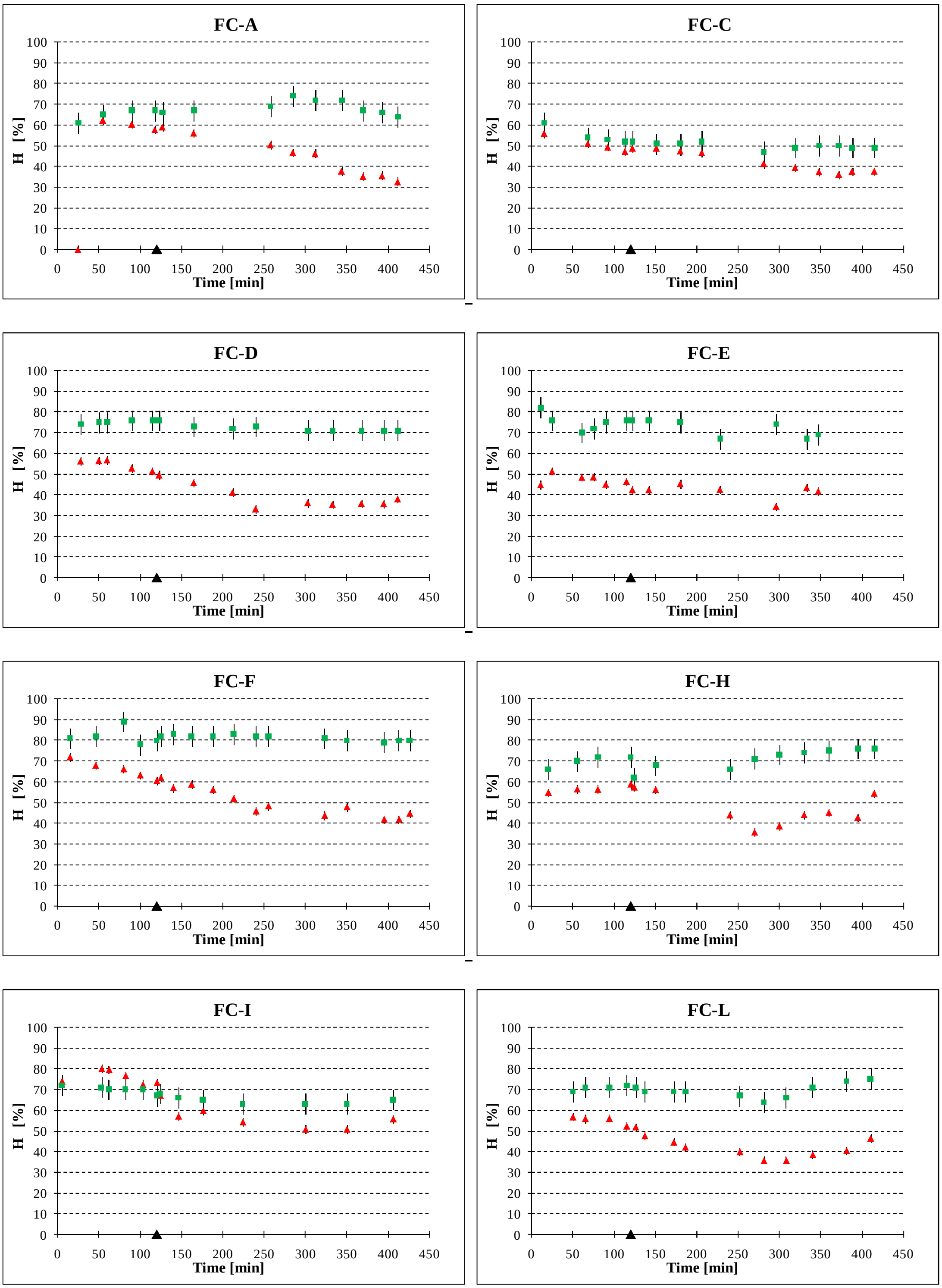

Fig. 6.14: *continue.*

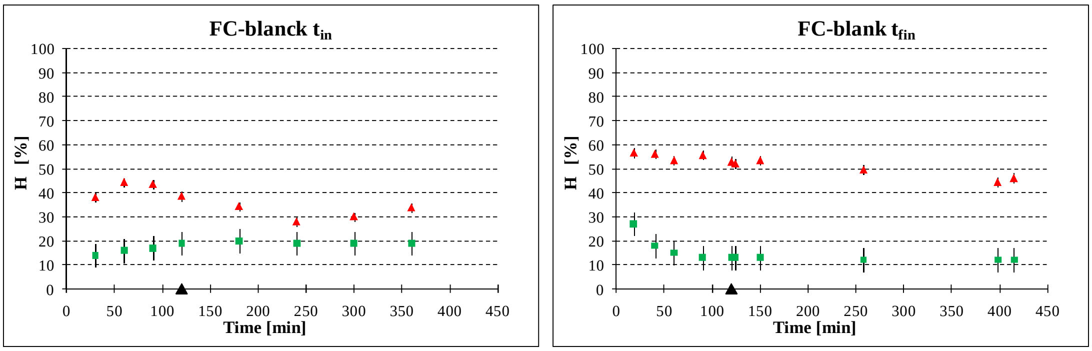

*Fig. 6.14: humidity measured outside (red triangles) and inside (green squares) the FC) recorded during the **July 2009** monitoring session. Black triangle on x-axis represents the end of purge phase and error bars indicate instrumental errors.*

December 2009 campaign

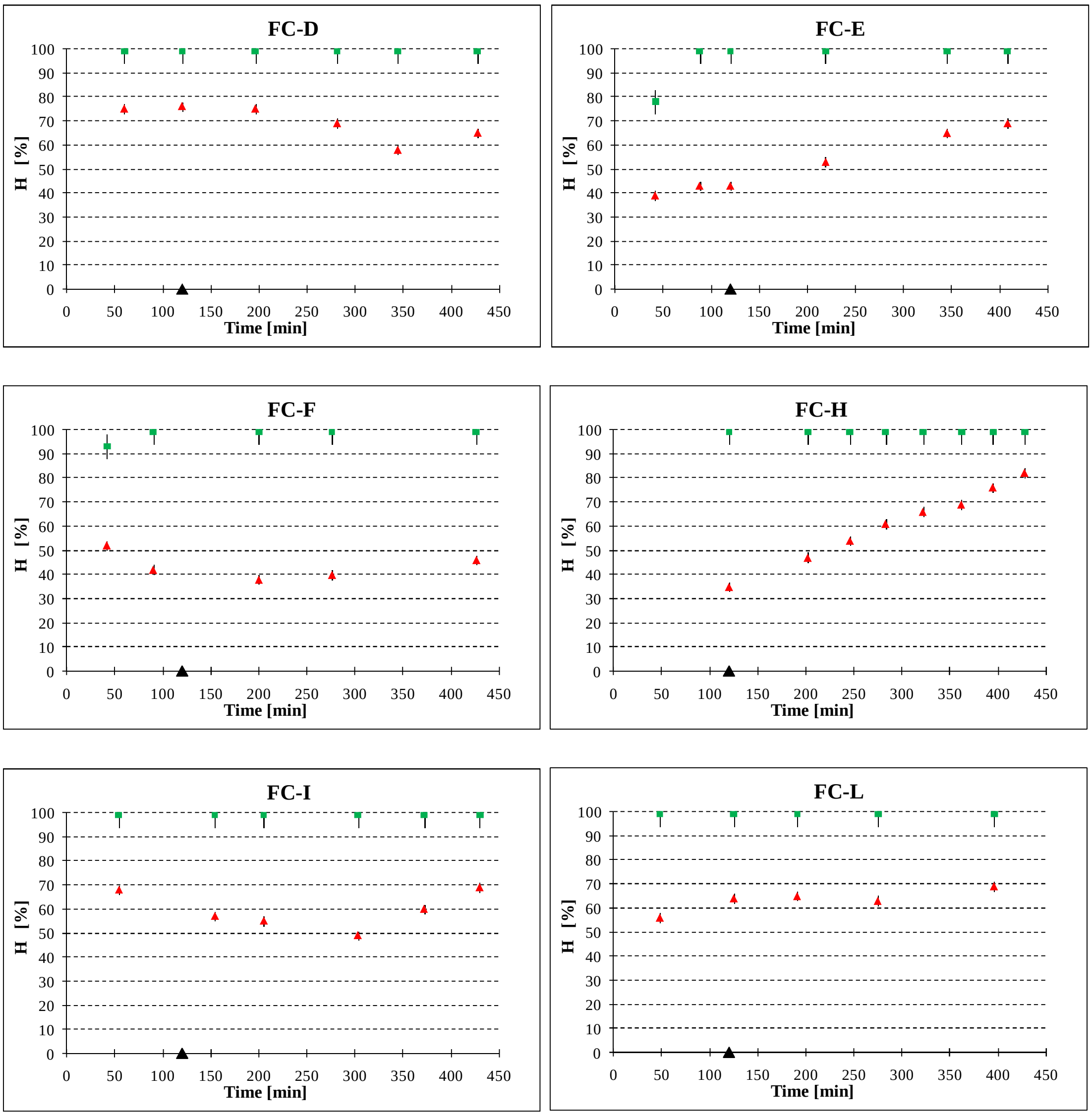

Fig. 6.15: continue.

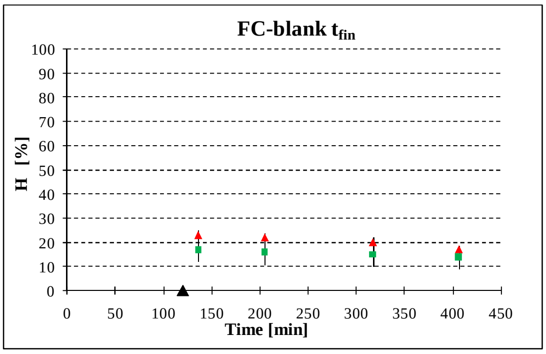

Fig. 6.15: *humidity measured outside (red triangles) and inside (green squares) the FC recorded during the* **December 2009** *monitoring session. Black triangle on x-axis represents the end of purge phase and error bars indicate instrumental errors.*

July 2010 campaign

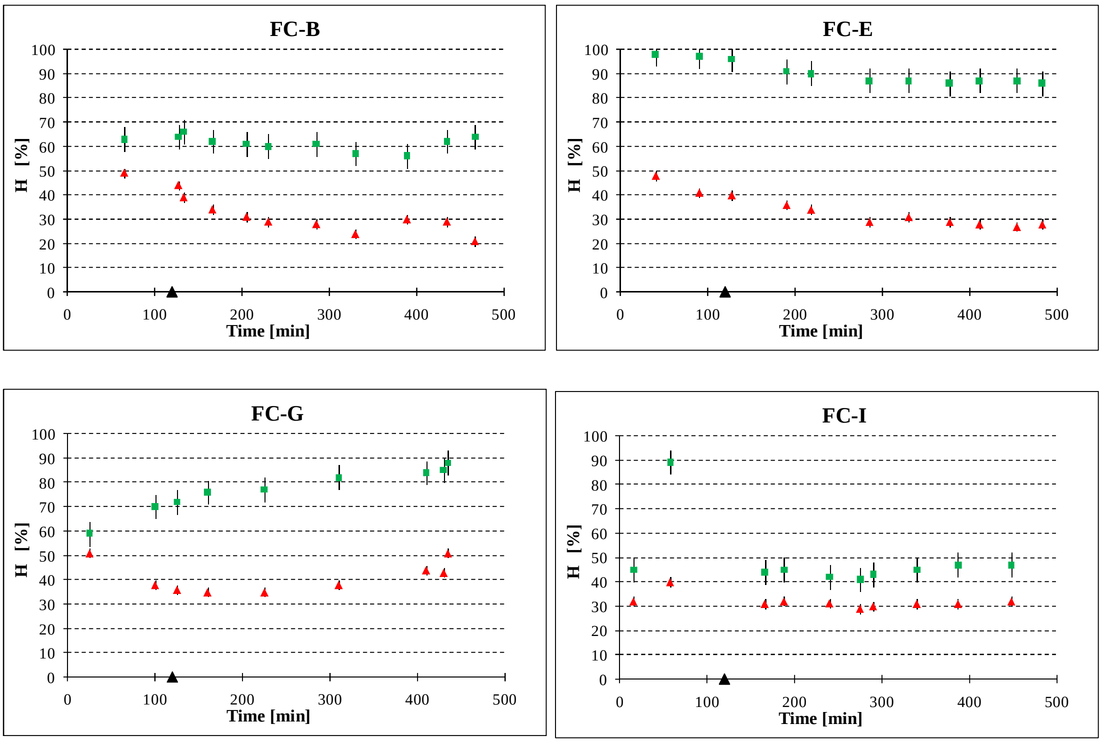

Fig. 6.16: *continue.*

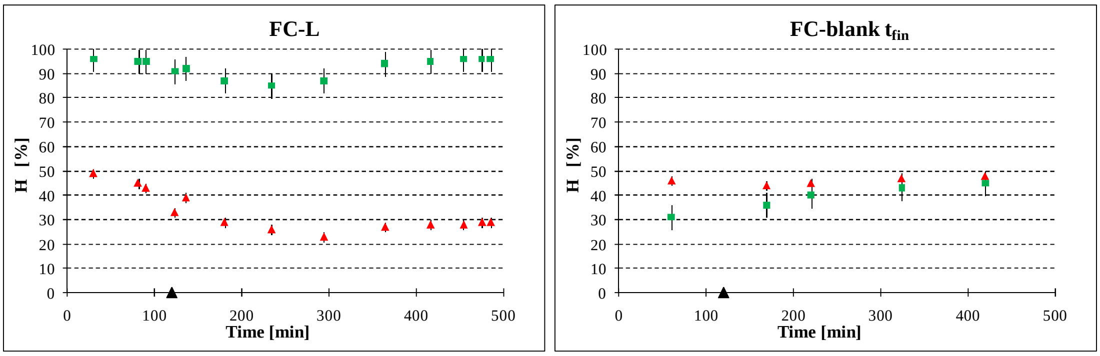

Fig. 6.16*: humidity measured outside (red triangles) and inside (green squares) the FC recorded during the* ***July 2010*** *monitoring session. Black triangle on x-axis represents the end of purge phase and error bars indicate instrumental errors.*

As far as the July 2009 campaign was concerned, internal humidity followed a constant trend and independent of external humidity during each sampling day (Fig. 6.14). It was further higher than H_{out} because monitoring took place on hot days and the major contribution was due to water evaporation from soil.

As for the December 2009, although the sampling took place at least 48 h after rain had stopped, low temperatures (§ 6.3.1.1.1) caused soil to be wet and even frosty in the morning. During monitoring water probably diffused from soil into the chamber due to a humidity gradient caused by dry sweep air, which gave H_{in} fixed at a value of 99%, independently of external value (Fig. 6.15).

As regards the third session (Fig. 6.16), humidity was quite constant throughout the monitoring of each point (apart from an anomalous datum in I) and independent of stable external one. During 2 measurements it was slightly higher than 90% (E and L) whereas in 3 other it was in the range 50 - 77 %.

In all the monitoring sessions, during FC blanks, recorded H_{in} was low, because the chamber was placed over a Teflon sheet.

6.3.1.1.3 Pressure difference

Figs. 6.17, 6.19 and 6.21 indicate internal ΔP half way up the cylinder (red triangles) at ground level (blue squares) and, only for the July 2010 session at the top of the cover (green lozenges) recorded during each monitoring campaign (as indicated in § 6.2.3.3). y-axis was maintained the same, in each group of figures, to favour clearer reading.

Figs. 6.18, 6.20 and 6.22 are summarizing pictures of average collected ΔP, separately for measured heights, for different sampling points.

July 2009 campaign

During the first campaign monitoring was not performed during initial FC blank and at H place, whereas at points E and F the probe was located only half way up the cylinder.

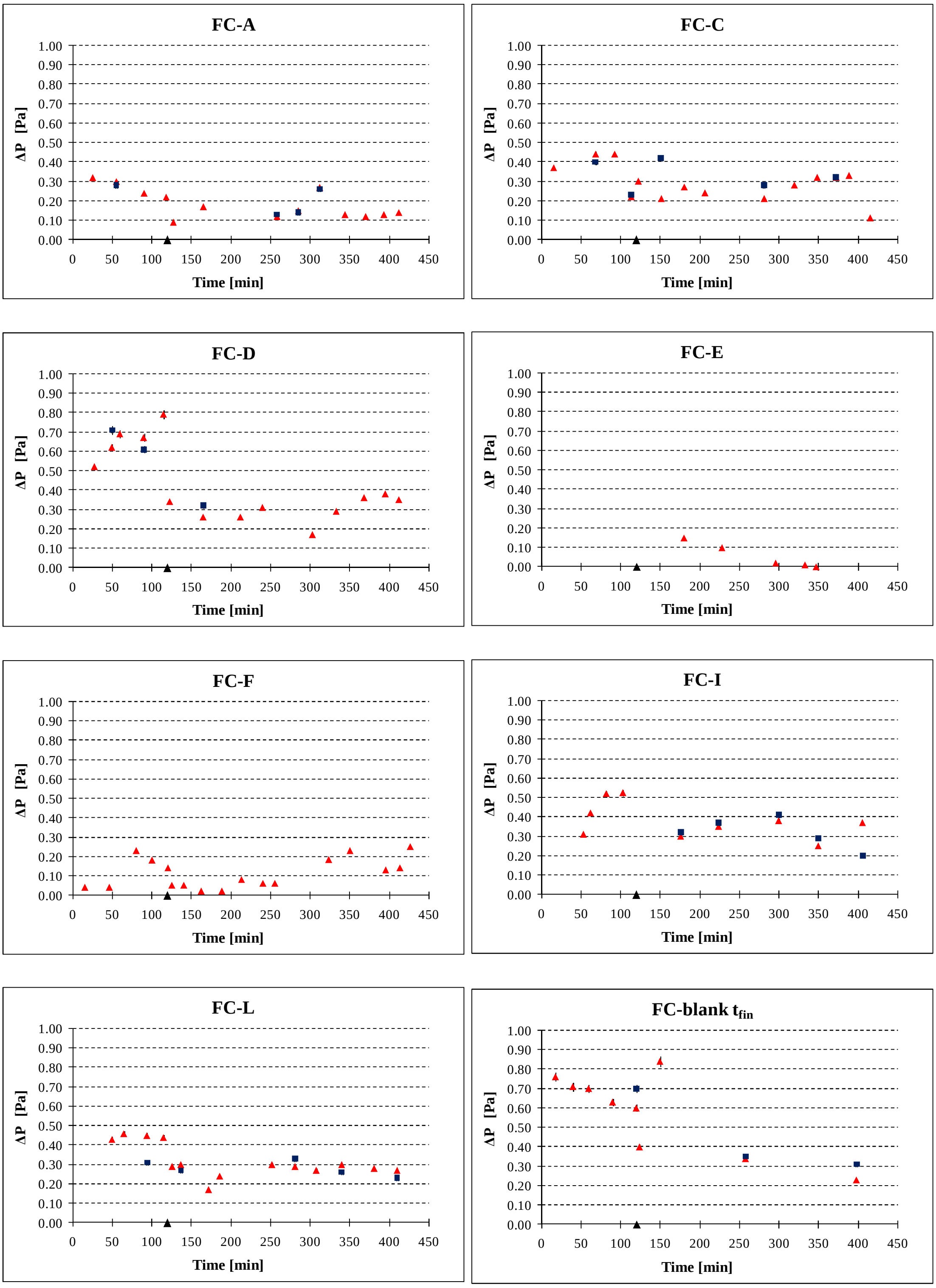

***Fig. 6.17**: pressure difference $\Delta P = P_{in} - P_{out}$ measured half way up the cylinder (red triangles) and at ground level (blue squares) recorded during the **July 2009** monitoring session. Black triangle on x-axis represents the end of purge phase and error bar indicates instrumental error.*

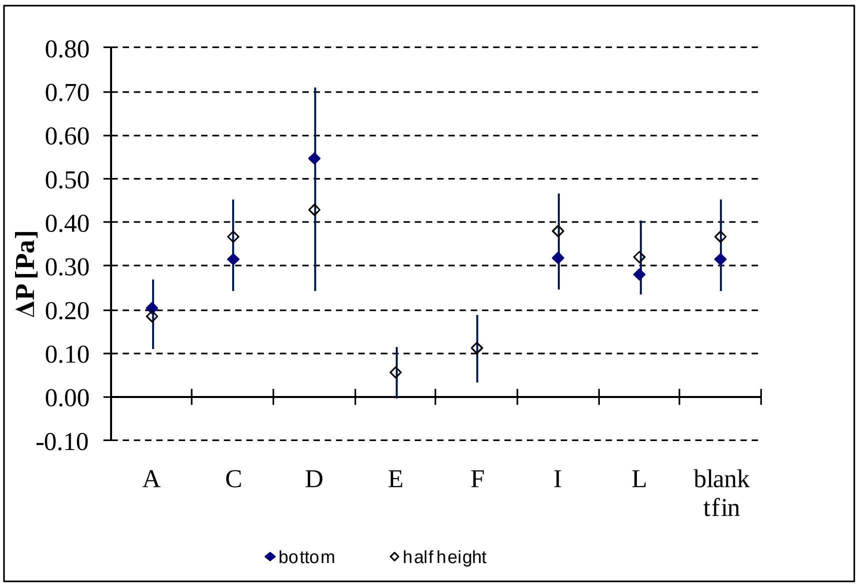

***Fig. 6.18**: average pressure difference $\Delta P = P_{in} - P_{out}$ measured half way up the cylinder (empty lozenges) and at ground level (full lozenges) recorded during the **July 2009** session, for different monitoring points; error bar indicates standard deviation of the average.*

<u>December 2009 campaign</u>

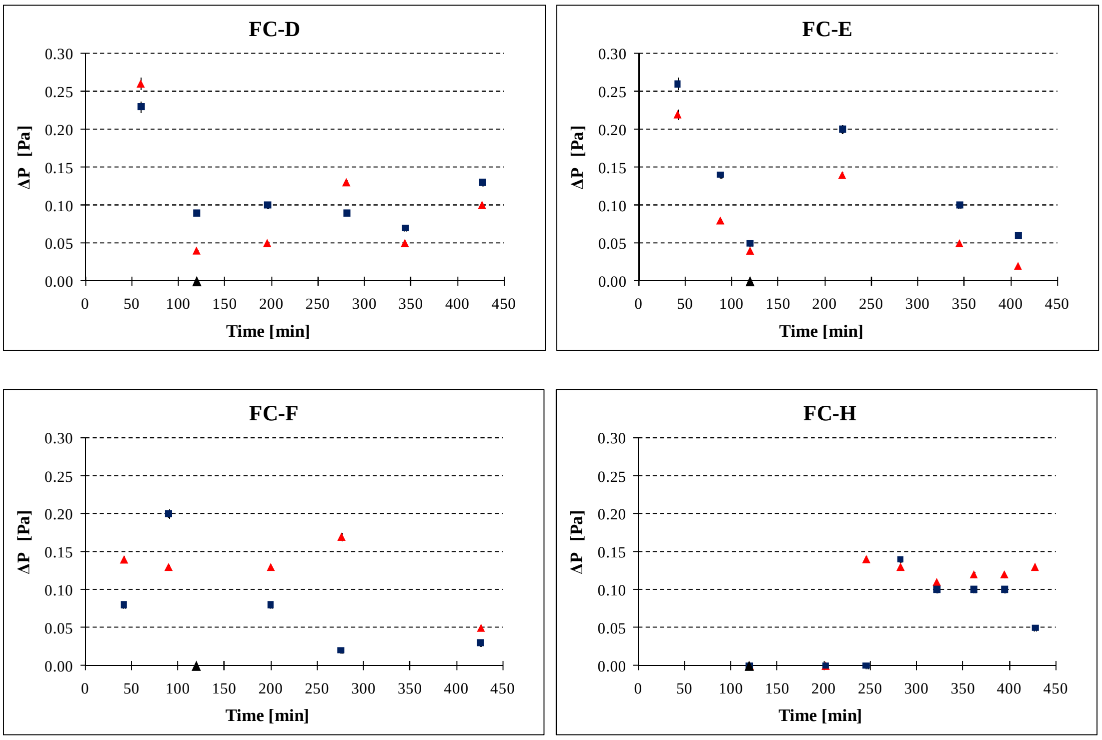

***Fig. 6.19**: continue.*

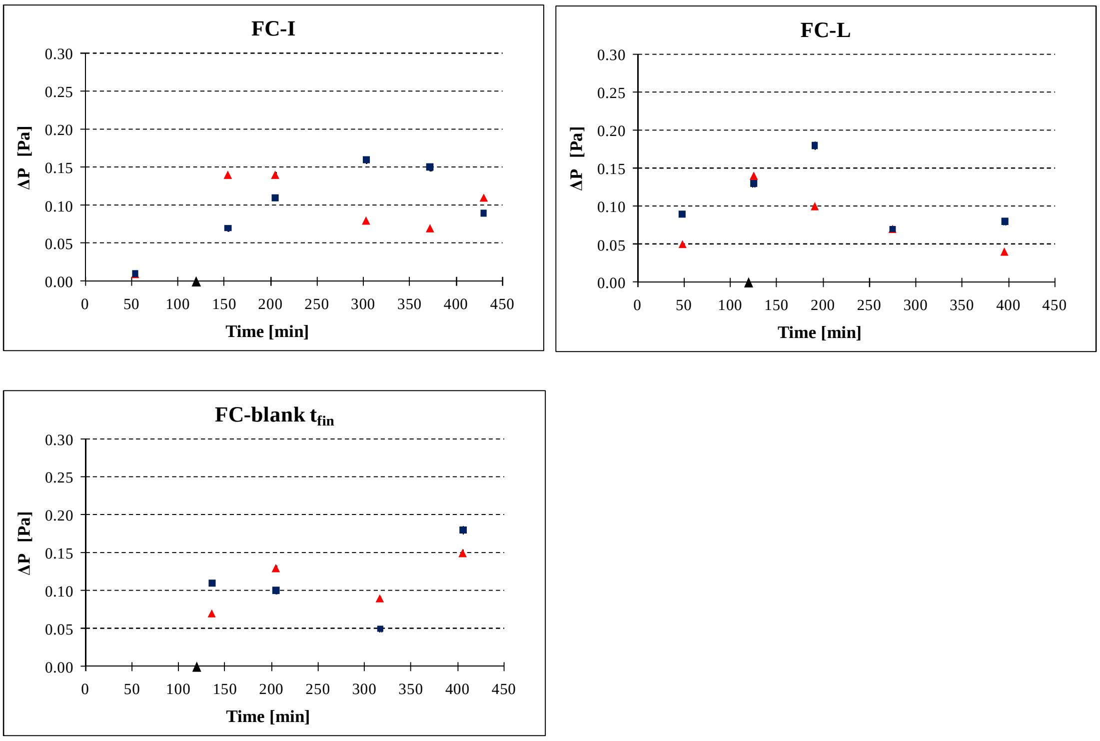

***Fig. 6.19**: pressure difference $\Delta P = P_{in} - P_{out}$ measured half way up the cylinder (red triangles) and at ground level (blue squares) recorded during the **December 2009** monitoring session. Black triangle on x-axis represents the end of purge phase and error bar indicates instrumental error.*

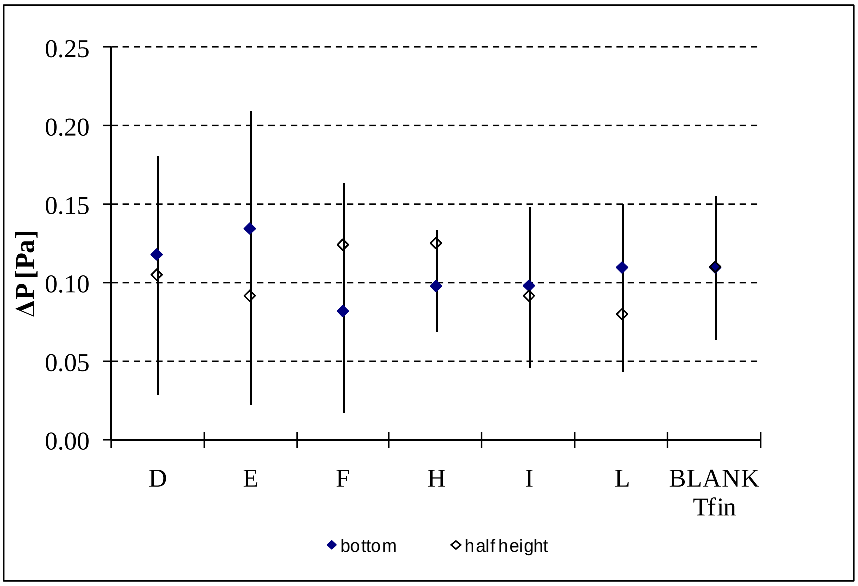

***Fig. 6.20**: average pressure difference $\Delta P = P_{in} - P_{out}$ measured half way up the cylinder (empty lozenges) and at ground level (full lozenges) recorded during the **December 2009** session, for different monitoring points; error bar indicates standard deviation of the average.*

July 2010 campaign

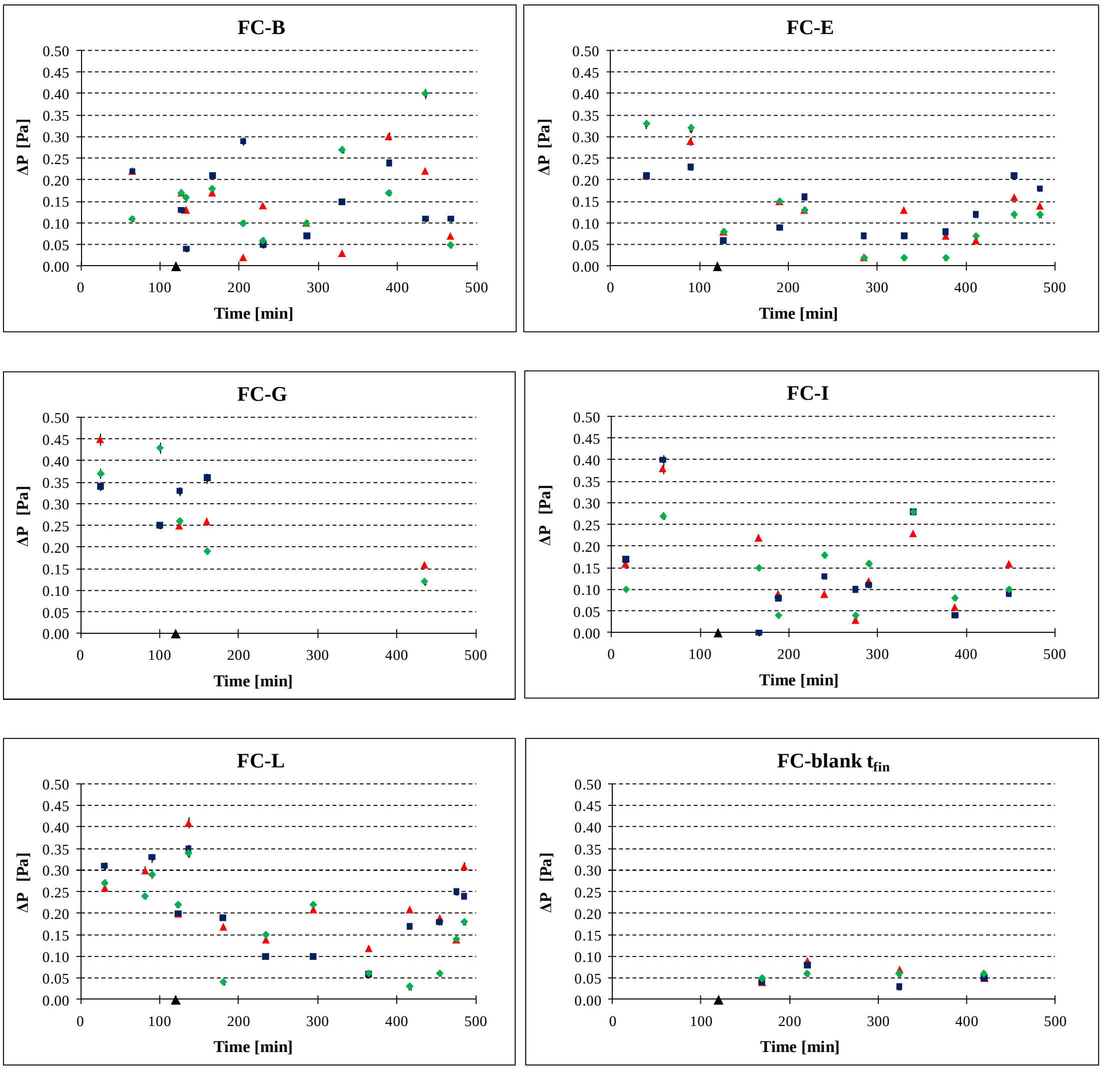

__Fig. 6.21__: pressure difference $\Delta P = P_{in} - P_{out}$ measured at ground level (blue squares), half way up the cylinder (red triangles) and at its top height (green lozenges) recorded during the __July 2010__ monitoring session. Black triangle on x-axis represents the end of purge phase and error bar indicates instrumental error.

All the measured values were positive, meaning that the chamber operated under proper conditions. For each position, in general, measurements taken at different heights at the same time were in good agreement, meaning that the chamber was really homogeneously mixed, whereas ΔP over time was irregular (probably also depending on temperature effects).

Average ΔPs during the first campaign, for both probe positions, were 0.3 ± 0.1 Pa; during the second one they were equal to 0.10 ± 0.02 and to 0.11 ± 0.01, respectively half way up the cylinder and at its bottom; whereas during the third session they were equal to 0.16 ± 0.04, 0.2 ± 0.1 and to 0.17 ± 0.03, respectively at the top, middle and bottom of the cylinder. These values perfectly satisfy the indications in § 4.2.4.8.2.

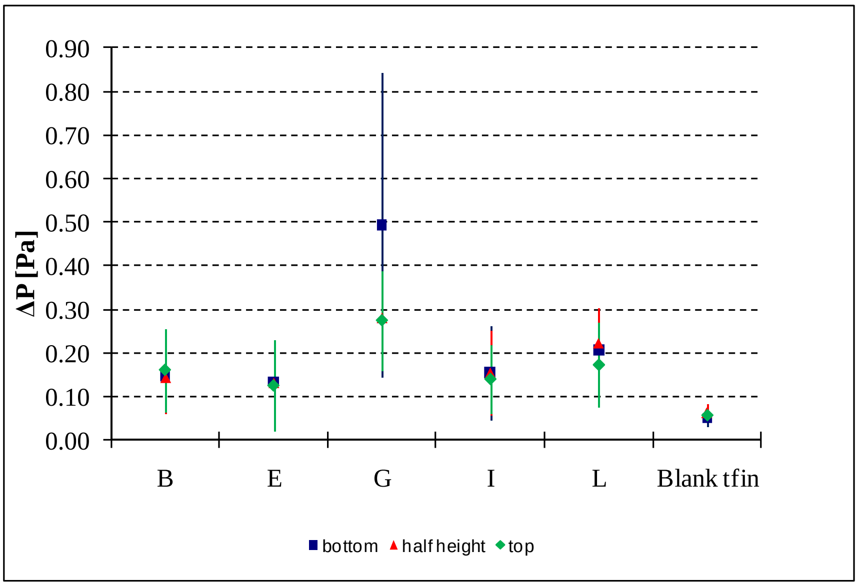

***Fig. 6.22**: average pressure difference $\Delta P = P_{in} - P_{out}$ measured at ground level (blue squares), half way up the cylinder (red triangles) and at its top height (green lozenges).*

6.3.2 Fluxes from modelling

6.3.2.1 Transport from groundwater

Results of simulated fluxes from groundwater chemical concentrations (according to § 6.2.4.1) at different monitoring sessions, are indicated in Tab. 6.27.

***Tab. 6.27**: modelled vapour flux F_{GW} [mg m^{-2} s^{-1}] from groundwater data.*

F_{GW} [mg m^{-2} s^{-1}]	**benzene**	**toluene**	**ethylbenzene**	**p-xylene**	**C5-C8 aliphatics**	**C9-C12 aliphatics**	**C9-C10 aromatics**	**naphthalene**	**MTBE**
July 2009	1.22E-05	4.56E-06	9.35E-06	6.73E-06	2.84E-03	1.58E-03	4.48E-05	-	1.28E-07
Dec. 2009	6.75E-06	8.73E-07	8.35E-07	1.69E-06	7.62E-04	4.25E-04	1.22E-05	1.98E-08	1.15E-07
July 2010	3.16E-06	1.01E-06	2.04E-09	1.43E-06	6.81E-04	3.80E-04	1.07E-05	1.22E-08	2.63E-07

6.3.2.2 Transport from soil gas

Results of simulated fluxes from soil gas chemical concentrations (according to § 6.2.4.2) are indicated in Tabs. 6.28, 6.29 and 6.30 respectively for the July 2009, December 2009 and July 2010 monitoring campaigns.

***Tab. 6.28**: modelled vapour flux F_{SG} [mg m^{-2} s^{-1}] from soil gas data collected in the **July 2009**; C1: shallow collocation at -0.8 m b.g.s., C2: deep collocation at -3.0 m b.g.s.. $F_{SG,max}$ is indicated too, with values higher than d.l. in bold type.*

F_{SG} [mg m^{-2}s^{-1}]	**Depth**	**benzene**	**toluene**	**ethylbenzene**	**p- xylene**	**C5-C8 aliphatics**	**C9-C12 aliphatics**	**C13-C18 aliphatics**	**C19-C36 aliphatics**	**C9-C10 aromatics**	**C11-C12 aromatics**	**naphthalene**	**MTBE**
A	C1	<4.34 E-09	6.87 E-09	<3.70 E-09	1.90 E-08	9.64 E-08	5.74 E-08	<6.91 E-07	<4.94 E-06	<3.46 E-08	<5.93 E-07	<2.91 E-09	<3.96 E-09
	C2	<1.16 E-09	5.73 E-09	1.58 E-09	3.04 E-09	1.41 E-06	1.90 E-08	<1.84 E-07	<1.32 E-06	<9.22 E-09	<1.58 E-07	<7.77 E-10	<1.06 E-09
B	C1	<4.34 E-09	6.01 E-09	5.92 E-09	2.58 E-08	1.75 E-07	1.29 E-07	<6.91 E-07	<4.94 E-06	<3.46 E-08	<5.93 E-07	<2.91 E-09	<3.96 E-09
	C2	1.16 E-08	3.78 E-07	9.87 E-09	2.75 E-08	2.92 E-04	9.22 E-08	<1.84 E-07	<1.32 E-06	<9.22 E-08	<1.58 E-07	<7.77 E-09	<1.06 E-08
C	C1	<4.34 E-09	<4.30 E-09	<3.70 E-09	<3.80 E-09	1.17 E-07	1.72 E-06	<6.91 E-07	<4.94 E-06	8.64 E-08	<5.93 E-07	<2.91 E-09	<3.96 E-09
	C2	<1.16 E-09	4.74 E-08	1.18 E-09	2.43 E-09	5.65 E-07	<9.22 E-09	<1.84 E-07	<1.32 E-06	<9.22 E-09	<1.58 E-07	<<7.77 E-10	1.06 E-09
D	C1	7.39 E-08	6.92 E-07	8.89 E-08	1.64 E-07	8.72 E-06	3.84 E-07	<6.91 E-07	<4.94 E-06	<3.46 E-08	<5.93 E-07	<2.91 E-09	<3.96 E-09
	C2	5.56 E-09	4.86 E-08	2.05 E-08	4.78 E-08	3.96 E-06	4.44 E-07	<1.84 E-07	<1.32 E-06	1.40 E-08	<1.58 E-07	<7.77 E-10	<1.06 E-09
E	C1	2.31 E-07	1.20 E-06	2.71 E-07	9.26 E-07	1.57 E-03	8.10 E-05	<6.91 E-07	<4.94 E-06	2.34 E-07	<5.93 E-07	<2.91 E-09	<3.96 E-09
	C2	2.66 E-08	1.10 E-07	1.18 E-07	7.65 E-08	4.37 E-04	1.37 E-05	<1.84 E-07	<1.32 E-06	2.32 E-07	<1.58 E-07	<7.77 E-10	<1.06 E-09
F	C1	<4.34 E-09	8.59 E-09	5.18 E-09	1.21 E-08	1.92 E-07	1.86 E-07	<6.91 E-07	<4.94 E-06	<3.46 E-08	<5.93 E-07	<2.91 E-09	<3.96 E-09
	C2	1.91 E-04	2.29 E-04	7.38 E-05	1.99 E-04	3.57 E-03	6.91 E-05	<1.84 E-07	<1.32 E-06	2.13 E-05	<1.58 E-07	<7.77 E-09	<1.06 E-08
G	C1	1.23 E-07	6.31 E-07	6.29 E-08	1.07 E-07	7.24 E-05	4.52 E-07	<6.91 E-07	<4.94 E-06	<3.46 E-08	<5.93 E-07	<2.91 E-09	<3.96 E-09
H	C1	<4.34 E-09	<4.30 E-09	<3.70 E-09	<3.80 E-09	2.80 E-07	3.46 E-08	<6.91 E-07	<4.94 E-06	<3.46 E-08	<5.93 E-07	<2.91 E-09	<3.96 E-09
	C2	5.99 E-07	8.61 E-08	1.43 E-07	7.67 E-08	1.48 E-04	3.09 E-06	<1.84 E-07	<1.32 E-06	1.89 E-07	<1.58 E-07	<7.77 E-10	<1.06 E-09

***Tab. 6.28**: continued.*

I	C1	3.94 E-07	1.40 E-06	4.13 E-07	8.81 E-07	1.15 E-03	4.12 E-05	<6.91 E-07	<4.94 E-06	6.01 E-07	<5.93 E-07	<2.91 E-09	<3.96 E-09
L	C1	<4.34 E-09	3.61 E-08	4.44 E-09	7.59 E-09	3.75 E-06	1.06 E-07	<6.91 E-07	<4.94 E-06	<3.46 E-08	<5.93 E-07	<2.91 E-09	<3.96 E-09
	C2	1.39 E-08	1.05 E-08	2.17 E-09	6.07 E-09	2.28 E-05	9.86 E-08	<1.84 E-07	<1.32 E-06	9.58 E-09	<1.58 E-07	<7.77 E-10	<1.06 E-09
$F_{SG,C1,max}$		**3.94 E-07**	**1.40 E-06**	**4.13E-07**	**9.26 E-07**	**1.57 E-03**	**8.10 E-05**	6.91 E-07	4.94 E-06	**6.01 E-07**	5.93 E-07	2.91 E-09	3.96 E-09
$F_{SG,C2,max}$		**1.91 E-04**	**2.29 E-04**	**7.38 E-05**	**1.99 E-04**	**3.57 E-03**	**6.91 E-05**	1.84 E-07	1.32 E-06	**2.13 E-05**	1.58 E-07	7.77 E-09	1.06 E-08

***Tab. 6.29**: modelled vapour flux F_{SG} [mg m^{-2} s^{-1}] from soil gas data collected in **December 2009**; C1: shallow collocation at -0.8 m b.g.s., C2: deep collocation at -3.0 m b.g.s.. $F_{SG,max}$ is indicated too, with values higher than d.l. in bold type.*

F_{SG} [mg m-2 s-1]	**Depth**	**benzene**	**toluene**	**ethylbenzene**	**p- xylene**	**C5-C8 aliphatics**	**C9-C12 aliphatics**	**C13-C18 aliphatics**	**C19-C36 aliphatics**	**C9-C10 aromatics**	**C11-C12 aromatics**	**naphthalene**	**MTBE**
A	C1	<4.34 E-09	7.73 E-09	<3.70 E-09	7.59 E-09	9.72 E-08	1.98 E-07	<6.91 E-07	<4.94 E-06	<3.46 E-08	<5.93 E-07	<2.91 E-09	<3.96 E-09
	C2	<1.16 E-09	2.06 E-09	1.18 E-09	3.04 E-09	3.77 E-08	2.47 E-08	<1.84 E-07	<1.32 E-06	<9.22 E-09	<1.58 E-07	<7.77 E-10	<1.06 E-09
B	C1	<8.69 E-08	4.84 E-07	8.44 E-08	2.96 E-07	3.42 E-04	2.40 E-05	<6.91 E-07	<4.94 E-06	8.76 E-07	<5.93 E-07	<5.83 E-08	<7.92 E-08
	C2	<2.32 E-08	5.59 E-07	<1.97 E-08	2.38 E-07	3.39 E-03	2.89 E-05	<1.84 E-07	<1.32 E-06	3.20 E-07	<1.58 E-07	<1.55 E-08	<2.11 E-08
C	C1	<4.34 E-09	2.32 E-08	1.56 E-08	3.95 E-08	1.96 E-07	1.81 E-06	<6.91 E-07	<4.94 E-06	7.67 E-08	<5.93 E-07	<2.91 E-09	<3.96 E-09
	C2	<1.16 E-09	5.04 E-09	2.96 E-09	1.03 E-08	4.26 E-08	1.64 E-07	<1.84 E-07	<1.32 E-06	<9.22 E-09	<1.58 E-07	<7.77 E-10	<1.06 E-09
D	C1	<4.34 E-09	7.73 E-09	4.44 E-09	1.21 E-08	5.37 E-08	5.18 E-08	<6.91 E-07	<4.94 E-06	<.46 E-08	<5.93 E-07	<2.91 E-09	<3.96 E-09
	C2	<1.16 E-09	2.29 E-09	1.97 E-09	9.11 E-09	2.78 E-08	2.27 E-08	<1.84 E-07	<1.32 E-06	1.33 E-08	<1.58 E-07	4.66 E-09	<1.06 E-09
E	C1	<8.69 E-08	2.17 E-06	<7.41 E-08	6.38 E-07	7.44 E-03	8.00 E-05	<6.91 E-07	<4.94 E-06	8.01 E-07	<5.93 E-07	<5.83 E-08	<7.92 E-08
F	C1	<4.34 E-09	7.73 E-09	<3.70 E-09	9.87 E-09	1.85 E-07	3.42 E-07	<6.91 E-07	<4.94 E-06	<3.46 E-08	<5.93 E-07	<2.91 E-09	<3.96 E-09
	C2	4.81 E-04	5.18 E-05	2.31 E-05	5.14 E-05	1.90 E-03	2.10 E-05	<1.84 E-07	<1.32 E-06	4.18 E-06	1<.58 E-07	<1.55 E-08	<2.11 E-08
G	C1	6.41 E-07	8.50 E-07	2.46 E-07	6.52 E-07	1.78 E-03	1.96 E-05	<6.91 E-07	<4.94 E-06	1.37 E-06	<5.93 E-07	<5.83 E-08	<7.92 E-08

***Tab. 6.29**: continued.*

H	C1	<4.34 E-09	6.87 E-09	<3.70 E-09	9.87 E-09	4.31 E-06	2.20 E-07	<6.91 E-07	<4.94 E-06	<3.46 E-08	<5.93 E-07	<2.91 E-09	<3.96 E-09
	C2	6.43 E-06	6.87 E-07	5.23 E-07	2.02 E-08	3.51 E-03	2.16 E-04	<1.84 E-07	<1.32 E-06	1.83 E-05	<1.58 E-07	<1.55 E-08	<2.11 E-08
I	C1	<8.69 E-08	1.03 E-06	<7.41 E-08	1.12 E-06	1.47 E-02	4.25 E-04	<6.91 E-07	<4.94 E-06	1.14 E-06	<5.93 E-07	<5.83 E-08	<7.92 E-08
L	C1	6.87 E-07	6.95 E-06	8.66 E-07	2.98 E-02	5.90 E-04	8.77 E-05	<6.91 E-07	<4.94 E-06	4.91 E-06	<5.93 E-07	<5.83 E-08	<7.92 E-08
	C2	2.36 E-07	4.21 E-07	8.99 E-08	3.95 E-07	2.15 E-04	3.01 E-05	<1.84 E-07	<1.32 E-06	2.03 E-06	<1.58 E-07	<1.55 E-08	<2.11 E-08
$F_{SG,C1,max}$		6.87 E-07	6.95 E-06	8.66 E-07	2.98 E-02	1.47 E-02	4.25 E-04	**6.91 E-07**	**4.94 E-06**	4.91 E-06	**5.93 E-07**	**5.83 E-08**	**7.92 E-08**
$F_{SG,C2,max}$		4.81 E-04	5.18 E-05	2.31 E-05	5.14 E-05	3.51 E-03	2.16 E-04	**1.84 E-07**	**1.32 E-06**	1.83 E-05	**1.58 E-07**	**1.55 E-08**	**2.11 E-08**

***Tab. 6.30**: modelled vapour flux F [mg m^{-2} s^{-1}] from soil gas data collected in the **July 2010**; C1: shallow collocation at -0.8 m b.g.s., C2: deep collocation at -3.0 m b.g.s.. $F_{SG,max}$ is indicated too, with values higher than d.l. in bold type.*

F_{SG} [mg m-2 s-1]	**Depth**	**benzene**	**toluene**	**ethylbenzene**	**p- xylene**	**C5-C8 aliphatics**	**C9-C12 aliphatics**	**C13-C18 aliphatics**	**C19-C36 aliphatics**	**C9-C10 aromatics**	**C11-C12 aromatics**	**naphthalene**	**MTBE**
A	C1	<4.35 E-09	1.031 E-08	1.111 E-08	3.113 E-08	<3.95 E-08	3.594 E-08	<6.912 E-07	<4.937 E-06	4.769 E-08	<5.926 E-07	5.828 E-09	<3.96 E-09
	C2	<1.16 E-09	1.833 E-09	6.714 E-09	2.025 E-08	2.93 E-06	1.461 E-06	<1.843 E-07	<1.317 E-06	5.419 E-08	<1.58 E-07	4.04 E-09	<1.056 E-09
B	C1	<4.35 E-09	7.732 E-09	3.703 E-08	7.745 E-08	1.004 E-06	9.331 E-08	<6.912 E-07	<4.937 E-06	1.092 E-07	<5.926 E-07	1.573 E-08	<3.96 E-09
	C2	9.57 E-07	1.844 E-06	4.353 E-07	1.694 E-06	1.91 E-03	9.216 E-08	<1.843 E-07	<1.317 E-06	1.02 E-06	<1.58 E-07	<7.77 E-09	<1.056 E-08
C	C1	<4.35 E-09	7.732 E-09	1.185 E-08	1.974 E-08	<3.95 E-08	1.769 E-07	<6.912 E-07	<4.937 E-06	3.456 E-08	<5.926 E-07	9.324 E-09	<3.96 E-09
	C2	<1.16 E-09	5.04 E-09	5.135 E-09	1.033 E-08	3.349 E-08	8.939 E-08	<1.843 E-07	<1.317 E-06	1.124 E-08	<1.58 E-07	<7.77 E-10	<1.056 E-09
D	C1	<4.35 E-09	1.117 E-08	1.851 E-08	4.404 E-08	5.608 E-08	7.741 E-08	<6.912 E-07	<4.937 E-06	5.875 E-08	<5.926 E-07	<2.914 E-09	<3.96 E-09
	C2	<1.16 E-09	3.436 E-09	7.307 E-09	3.22 E-08	2.254 E-08	3.041 E-08	<1.843 <E-07	<1.317 E-06	3.041 E-08	<1.58 E-07	<7.77 E-10	<1.056 E-09
E	C1	1.55 E-06	3.664 E-06	9.198 E-07	1.906 E-06	5.43 E-03	3.46 E-04	<6.912 E-07	<4.937 E-06	1.393 E-06	<5.926 E-07	8.147 E-07	<3.96 E-08
	C2	2.61 E-07	3.739 E-07	1.46 E-06	1.453 E-06	2.76 E-03	1.57 E-04	<1.843 E-07	<1.317 E-06	1.81 E-06	1.58 E-07	<7.77 E-09	1.453 E-07

***Tab. 6.30**: continued.*

F	C1	<4.35 E-09	1.916 E-08	9.183 E-09	4.791 E-08	7.98 E-08	5.73 E-07	<6.912 E-07	<4.937 E-06	5.737 E-08	<5.926 E-07	7.226 E-09	<3.96 E-09
	C2	8.631 E-06	1.924 E-06	5.908 E-06	1.049 E-05	7.78 E-05	5.09 E-05	<1.843 E-07	<1.317 E-06	3.77 E-06	<1.58 E-07	<7.77 E-09	<1.056 E-08
G	C1	3.403 E-06	9.458 E-07	4.318 E-06	2.553 E-06	9.95 E-04	4.85 E-06	<6.912 E-07	<4.937 E-06	1.667 E-06	<5.926 E-07	1.059 E-06	<3.96 E-08
H	C1	5.909 E-09	1.027 E-07	4.614 E-08	1.163 E-07	5.75 E-06	6.89 E-06	<6.912 E-07	<4.937 E-06	3.021 E-07	5.926 E-07	6.399 E-08	<3.96 E-09
	C2	1.773 E-07	6.265 E-07	1.659 E-06	1.041 E-06	6.27 E-04	4.09 E-05	<1.843 E-07	<1.317 E-06	6.184 E-07	<1.58 E-07	<7.77 E-09	<1.056 E-08
I	C1	1.475 E-06	1.218 E-06	6.076 E-06	4.137 E-06	6.17 E-03	2.23 E-04	<6.912 E-07	<4.937 E-06	3.567 E-06	<5.926 E-07	<2.914 E-08	<3.96 E-08
L	C1	1.481 E-06	9.767 E-07	1.81 E-06	2.184 E-06	1.83 E-03	5.41 E-04	<6.912 E-07	<4.937 E-06	1.696 E-06	<5.926 E-07	4.819 E-07	<3.96 E-08
	C2	2.136 E-07	4.467 E-07	2.045 E-06	2.112 E-06	2.13 E-04	1.73 E-06	<1.843 E-07	<1.317 E-06	2.886 E-06	<1.58 E-07	2.146 E-07	<1.056 E-08
$F_{SG,C1,max}$		3.40 E-06	3.66 E-06	6.08 E-06	4.14 E-06	6.17 E-03	5.41 E-04	**6.91 E-07**	**4.94 E-06**	3.57 E-06	**5.93 E-07**	1.06 E-06	**3.96 E-08**
$F_{SG,C2,max}$		8.63 E-06	1.92 E-06	5.91 E-06	1.05 E-05	2.76 E-03	1.57 E-04	**1.84 E-07**	**1.32 E-06**	3.77 E-06	**1.58 E-07**	2.15 E-07	1.45 E-07

6.3.3 Fluxes from flux chamber measurements

Vapours flux F and F_{max} of each compound and sampling point, for the three monitoring campaigns are indicated in Tabs. 6.31, 6.32, 6.33.

***Tab. 6.31**: vapour flux F_{FC} and $F_{FC,max}$ [mg m^{-2} s^{-1}] from the **July 2009** FC campaign; bold type indicates values higher than d.l..*

F_{FC} [mg m^{-2} s^{-1}]	**benzene**	**toluene**	**ethylbenzene**	**o-xylene**	**m-xylene**	**p- xylene**
FC-A	<5.62E-07	<5.62E-07	<5.62E-07	<5.62E-07	<5.62E-07	<5.62E-07
FC-C	<5.51E-07	<5.51E-07	<5.51E-07	<5.51E-07	<5.51E-07	<5.51E-07
FC-D	<5.33E-07	<5.33E-07	<5.33E-07	<5.33E-07	<5.33E-07	<5.33E-07
FC-E	<6.87E-07	<6.87E-07	<6.87E-07	<6.87E-07	<6.87E-07	<6.87E-07
FC-F	<5.23E-07	<5.23E-07	<5.23E-07	<5.23E-07	<5.23E-07	<5.23E-07
FC-H	<6.94E-07	<6.94E-07	<6.94E-07	<6.94E-07	<6.94E-07	<6.94E-07
FC-I	<5.21E-07	<5.21E-07	<5.21E-07	<5.21E-07	**5.33E-07**	<5.21E-07
FC-L	<5.54E-07	**5.98E-07**	<5.54E-07	<5.54E-07	<5.54E-07	<5.54E-07
$F_{FC, max}$	6.94E-07	6.94E-07	6.94E-07	6.94E-07	6.94E-07	6.94E-07

***Tab. 6.32**: vapour flux F_{FC} and $F_{FC,max}$ [mg m^{-2} s^{-1}] from the **December 2009** FC campaign; bold type indicates values higher than d.l..*

F_{FC} [mg $m^{-2}s^{-1}$]	benzene	toluene	ethylbenzene	o-xylene	m- xylene	p- xylene	C5-C8 aliphatics	C9-C12 aliphatics	C13-C18 aliphatics	C19-C36 aliphatics	C9-C10 aromatics	C11-C22 aromatics	naphthalene	MTBE
FC - D	<2.75 E-07	<2.75 E-07	<2.75 E-07	<2.75 E-07	<2.75 E-07	<2.75 E-07	<5.50 E-07	**2.75 E-07**	<4.59 E-07	<4.59 E-07	<2.75 E-07	<4.59 E-07	<1.83 E-07	<1.83 E-07
FC -E	<2.76 E-07	<2.76 E-07	<2.76 E-07	<2.76 E-07	<2.76 E-07	<2.76 E-07	<5.52 E-07	<2.76 E-07	<4.60 E-07	<4.60 E-07	<2.76 E-07	<4.60 E-07	<1.84 E-07	<1.84 E-07
FC -F	<2.75 E-07	<2.75 E-07	<2.75 E-07	<2.75 E-07	<2.75 E-07	<2.75 E-07	<5.50 E-07	<2.75 E-07	<4.59 E-07	<4.59 E-07	<2.75 E-07	<4.59 E-07	<1.83 E-07	<1.83 E-07
FC -H	<4.21 E-07	<4.21 E-07	<4.21 E-07	<4.21 E-07	<4.21 E-07	<4.21 E-07	<8.42 E-07	**4.35 E-07**	<7.02 E-07	<7.02 E-07	<4.21 E-07	<7.02 E-07	<2.81 E-07	<2.81 E-07
FC -I	<2.78 E-07	<2.78 E-07	<2.78 E-07	<2.78 E-07	<2.78 E-07	<2.78 E-07	**1.70 E-04**	<2.78 E-07	<4.63 E-07	<4.63 E-07	<2.78 E-07	<4.63 E-07	<1.85 E-07	<1.85 E-07
FC -L	<2.78 E-07	<2.78 E-07	<2.78 E-07	<2.78 E-07	<2.78 E-07	<2.78 E-07	<5.56 E-07	<2.78 E-07	<4.63 E-07	<4.63 E-07	<2.78 E-07	<4.63 E-07	<1.85 E-07	<1.85 E-07
$F_{FC, max}$	4.21 E-07	4.21 E-07	4.21 E-07	4.21 E-07	4.21 E-07	4.21 E-07	**1.70 E-04**	**4.35 E-07**	7.02 E-07	7.02 E-07	4.21 E-07	7.02 E-07	2.81 E-07	2.81 E-07

***Tab. 6.33**: vapour flux F_{FC} and $F_{FC,max}$ [mg m^{-2} s^{-1}] from the **July 2010** FC campaign; bold type indicates values higher than d.l. (continues on the next page).*

F_{FC} [mg m^{-2} s^{-1}]	benzene	toluene	ethylbenzene	o-xylene	m- xylene	p- xylene	C5-C8 aliphatics	C9-C12 aliphatics	C13-C18 aliphatics	C19-C36 aliphatics	C9-C10 aromatics	C11-C22 aromatics	naphthalene	MTBE
FC - B	<2.56 E-07	<2.56 E-07	<2.56 E-07	<2.56 E-07	<2.56 E-07	<2.56 E-07	**7.35 E-06**	<2.56 E-07	**7.69 E-06**	**3.42 E-06**	<2.56 E-07	<4.27 E-07	<1.71 E-07	<1.71 E-07
FC -E	<1.92 E-07	<1.92 E-07	<1.92 E-07	<1.92 E-07	<1.92 E-07	<1.92 E-07	**2.25 E-06**	<1.92 E-07	**8.98 E-06**	**1.28 E-06**	<1.92 E-07	<3.21 E-07	<1.28 E-07	<1.28 E-07
FC -G	<2.40 E-07	<2.40 E-07	<2.40 E-07	<2.40 E-07	<2.40 E-07	<2.40 E-07	**1.63 E-05**	<2.40 E-07	**2.40 E-05**	**4.80 E-06**	**2.40 E-07**	<4.00 E-07	<1.60 E-07	<1.60 E-07
FC -I	<2.46 E-07	<2.46 E-07	<2.46 E-07	<2.46 E-07	<2.46 E-07	<2.46 E-07	**9.01 E-07**	**3.28 E-07**	**1.80 E-05**	**7.37 E-06**	<2.46 E-07	<4.09 E-07	<1.64 E-07	<1.64 E-07
FC -L	<2.16 E-07	<2.16 E-07	<2.16 E-07	<2.16 E-07	<2.16 E-07	<2.16 E-07	<4.31 E-07	<2.16 E-07	**1.80 E-05**	**3.59 E-06**	<2.16 E-07	<3.59 E-07	<1.44 E-07	<1.44 E-07
$F_{FC, max}$	2.56 E-07	2.56 E-07	2.56 E-07	2.56 E-07	2.56 E-07	2.56 E-07	**1.63 E-05**	**3.28 E-07**	**2.40 E-05**	**7.37 E-06**	2.56 E-07	4.27 E-07	1.71 E-07	1.71 E-07

6.3.4 Comparison between modelled and calculated fluxes

Figs. 6.23, 6.24 and 6.25 present a direct comparison in each monitoring place, for each researched analyte, between F_{GW} (§ 6.3.2.1, in violet), $F_{SG,C1}$ and $F_{SG,C2}$ (§ 6.3.2.2, in red and green respectively), and F_{FC} (§ 6.3.3, in light blue colour), respectively during the July 2009, December 2009 and July 2010 monitoring sessions.

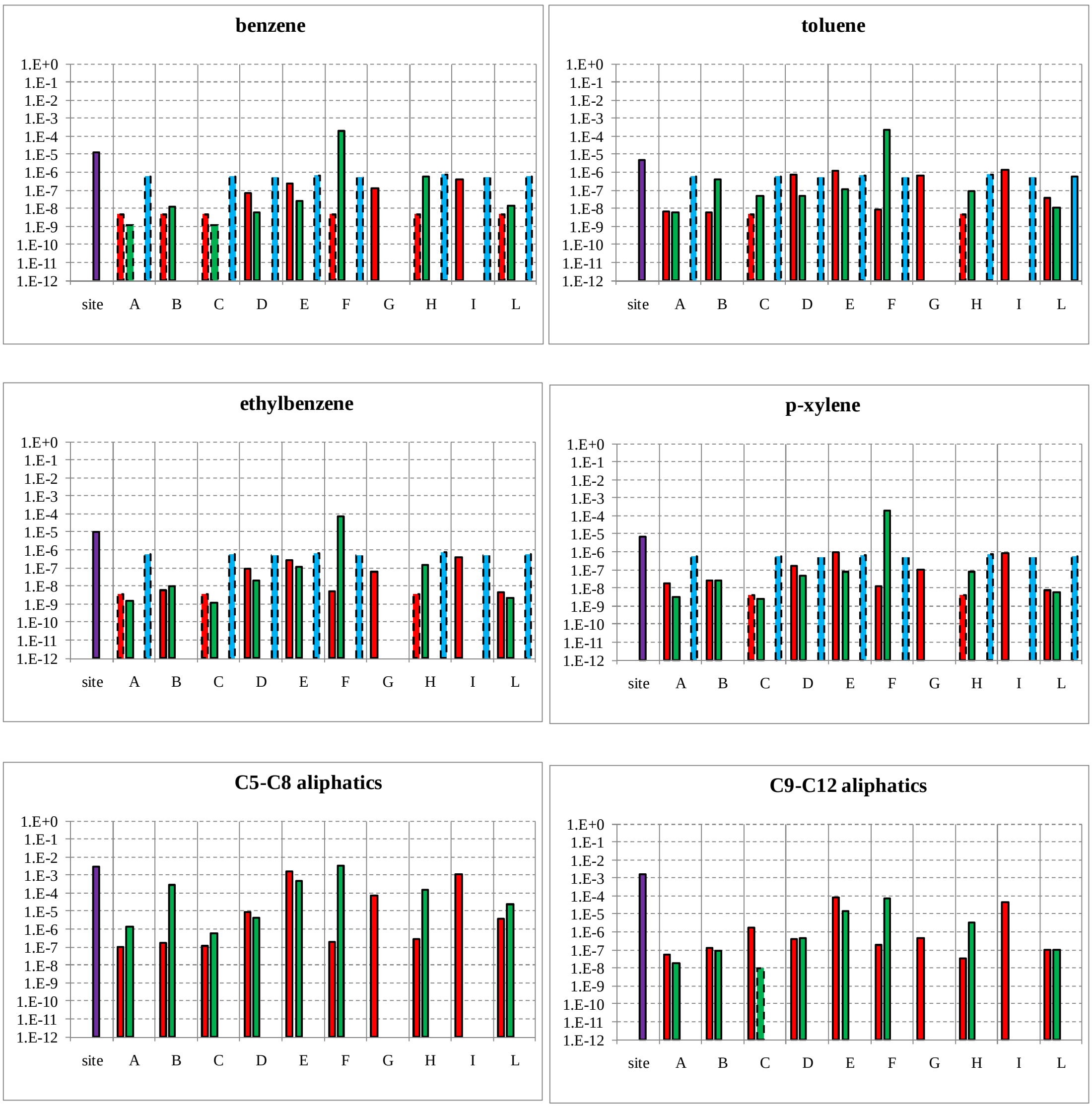

***Fig. 6.23**: continue.*

***Fig. 6.23**: modelled vapour flux F [mg m^{-2} s^{-1}] (in logarithm scale) from contaminant concentrations in groundwater (violet), shallow soil gas –C1- (red) and deep soil gas –C2- (green) and calculated ones from FC measurements (light blue), for each point monitored during the **July 2009** campaign; dashed boundaries indicate values lower than d.l. (F calculated by posing concentration or M_{samp} = d.l.).*

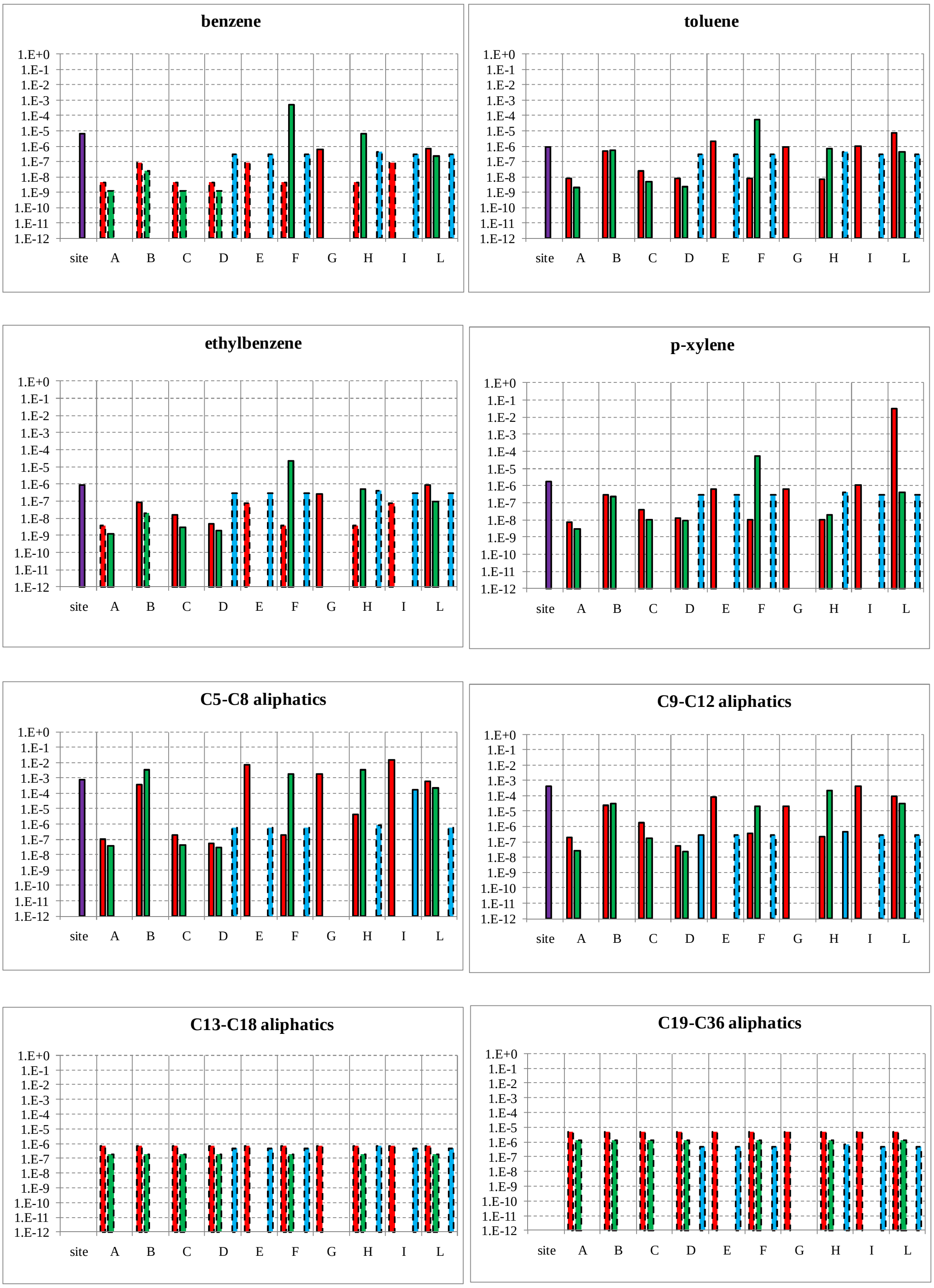

***Fig. 6.24**: continue.*

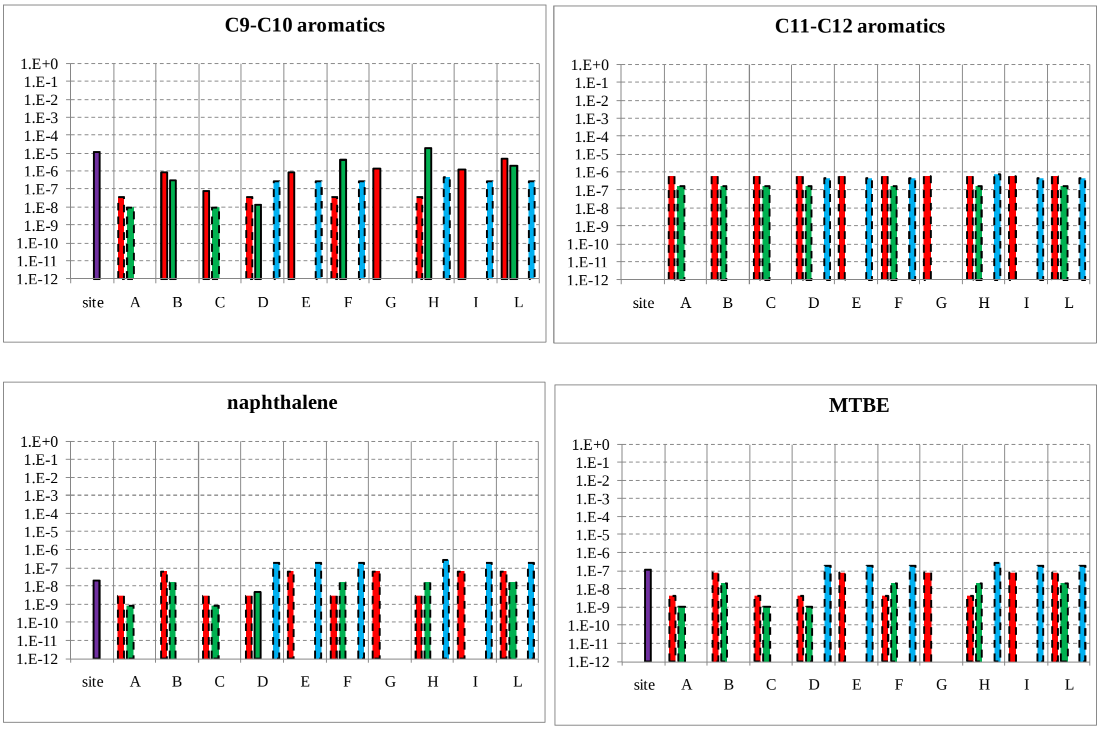

Fig. 6.24: *modelled vapour flux F [mg m^{-2} s^{-1}] (in logarithm scale) from contaminant concentrations in groundwater (violet), shallow soil gas –C1- (red) and deep soil gas –C2- (green) and calculated ones from FC measurements (light blue), for each point monitored during the* ***December 2009*** *campaign; dashed boundaries indicate values lower than d.l. (F calculated by posing concentration or M$_{samp}$ = d.l.).*

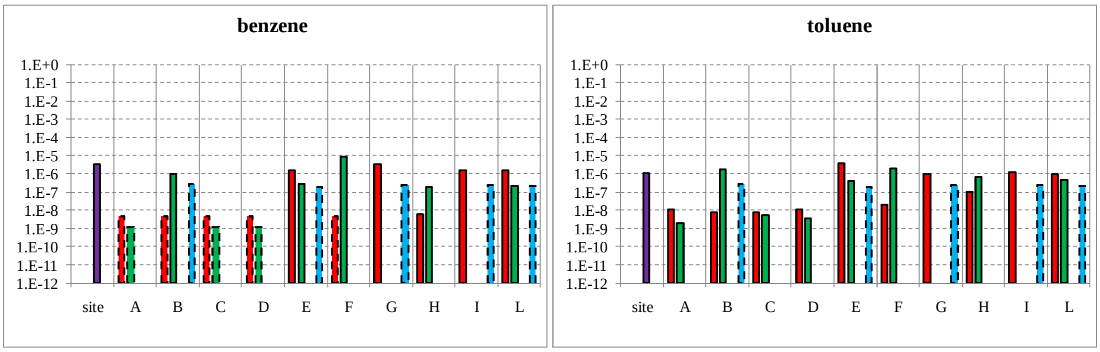

Fig. 6.25*: continue.*

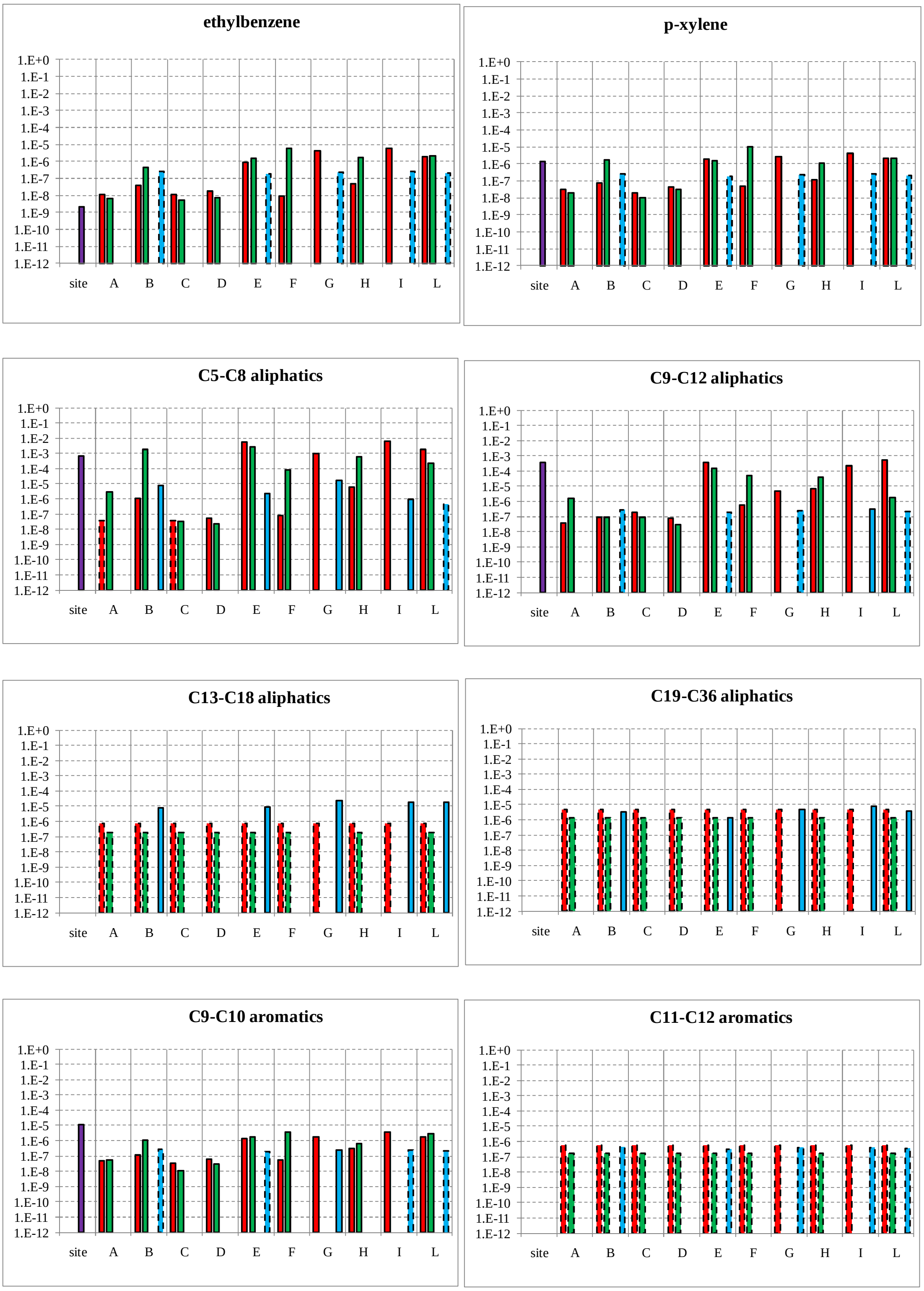
ethylbenzene

p-xylene

C5-C8 aliphatics

C9-C12 aliphatics

C13-C18 aliphatics

C19-C36 aliphatics

C9-C10 aromatics

C11-C12 aromatics

***Fig. 6.25**: continue.*

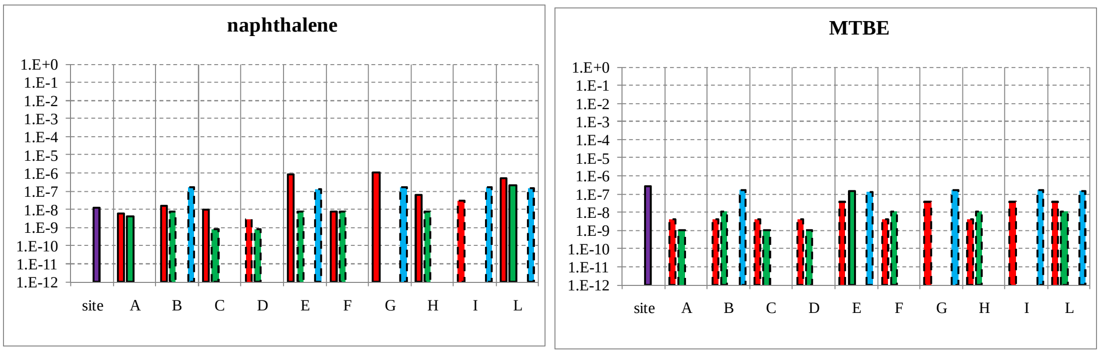

Fig. 6.25: *modelled vapour flux F [mg m^{-2} s^{-1}] (in logarithm scale) from contaminant concentrations in groundwater (violet), shallow soil gas –C1- (red) and deep soil gas –C2- (green) and calculated ones from FC measurements (light blue), for each point monitored during the* ***July 2010*** *campaign; dashed boundaries indicate values lower than d.l. (F calculated by posing concentration or M_{samp} = d.l.).*

Graphs in Figs. 6.23, 6.24 and 6.25 compare fluxes obtained from different sources.

As for the July 2009 campaign (Fig. 6.23), F_{GW} of all BTEX was higher than all the other fluxes, with the exception of $F_{SG,C2}$ in F which was the highest flux between modelled and calculated ones. Only for toluene the FC quantified a flux higher than d.l., which was 17 and 57 times respectively $F_{SG,C1}$ and $F_{SG,C2}$ in relation to the same point (L). L was in fact placed near to a concrete platform and construction works could have modified the structure of the soil, creating a preferential path that the model was not able to simulate (because of the simplified hypothesis used).

$F_{SG,C2}$ in F was the highest estimated flux also during the winter 2009 campaign (Fig. 6.24) for BTE, whereas for p-xylene, $F_{SG,C1}$ in L was revealed to be the maximum one because it came from anomalous detected concentration (see Fig 6.3). F_{GW} for BTEX during this campaign was lower than the summer one because concentrations were lower (Tab. 6.4) even if water table was higher (which means that the level of the water table does not affect the vapour flux much).

In the 2010 campaign (Fig. 6.25), detected (> d.l.) F_{SG}s were more in line with F_{GW}s than in previous campaigns as far as BTX fluxes were concerned (B and H at C2 depth, E, G, I, L) or, with the exception of F, lower. Regarding ethylbenzene, they were generally higher than F_{GW}.

As for December 2009 and July 2010, F_{FC}s were, for all the BTEX, lower than d.l.s For the majority of points d.l.s were higher than F_{SG}s, not providing any meaningful comparison; however for others they were lower, indicating that modelled F were overestimated as compared to measured ones.

In all the three campaigns point F showed the highest $F_{SG,C2}$, but during July 2010 they were comparable to other points because it considerably decreased. This point was placed next to a well which had been found to be contaminated in 2008 (Tab. 6.5); no further information is available, but it is possible that groundwater contamination tended to decrease over time because of natural attenuation (as can be seen in Fig. 6.2).

As for hydrocarbons, they were not researched during the first FC campaign. For the lightest ones (C5-C12 aliphatics), in summer 2009, F_{GW} was higher than the value defined from soil gas; regarding C5-C8 aliphatics, they corresponded with each-other in some points (E, I, B and F, the last two of which only at C2 depth, in Fig. 6.23).

As regards the winter 2009 campaign, F_{GW} was in line with the highest F_{SG} (B, E, G, I, F and H, the last two of which only at C2 depth, in Fig. 6.24). Quantified F_{FC} (involving C9-C12 aliphatics measured in points D and H) were in good agreement with $F_{SG,C1}$, absolutely different from $F_{SG,C2}$ (F_{FC} was higher than it in D and lower in H), and lower than G_{GW}.

During the July 2010 campaign F_{GW} and F_{SG} showed the same values as the previous campaign (slightly lower for points F and H). As for C5-C8 aliphatics measured by FC, detected (> d.l.) F_{FC}s were lower than F_{SG} detected in the same points, and always lower than F_{GW} (from 42 to 756 times, as a reference to points G and I respectively), with the exception of $F_{SG,C1}$ in B (Fig. 6.25). In this case, shallow soil stratum composed of gravel (Tab. 6.5) probably made vapours move easily in soil; this heterogeneity was not considered in simplified model hypothesis (§ 6.2.4). As for C9-C12 aliphatics, F_{GW} and F_{SG} gave roughly the same indications and FC revealed a contaminant (higher than d.l.) vapour flux in I.

As for C9-C10 aromatic hydrocarbons, F_{GW} was constant and always higher than F_{SG} during all campaigns in all the points, with the exception of point H in the December 2009 session. Estimated values seemed to increase over time, with higher values in summer 2010. During that campaign F_{FC} in G was quantified, with a value lower than F_{SG}.

Heavier aliphatics (C13-C18 and C19-C36) and C11-C12 aromatics, in the detected matrices (soil gas and, with the exception of July 2009, also by flux chamber) always resulted lower than d.l.s.

As far as naphthalene is concerned, during the July 2009 campaign it was not collected either from groundwater or by FC. F_{SG}s were lower than d.l. (with the exception of deep soil gas in D) in both campaigns performed in 2009. F_{GW}s modelled from the December 2009 and July 2010 results were similar. In the first session, comparison with F_{FC}s was not meaningful because these last were lower than d.l.s having values higher than F_{GW}s.

As for July 2010, several F_{SG}s were quantified and in some points they were higher than F_{GW}s, even if no quantifiable flux was verified with the FC.

In the first two campaigns MTBE was quantified (> d.l.) only in flux modelled from groundwater; in the third session it was quantified in deep soil gas placed in point E, too.

To sum up, modelling flux directly from groundwater concentration always performed an overestimation of fluxes probably because it does not take into account biological aspects happening in the soil.

As far as F_{SG} was concerned, fluxes from the two monitored depths, considering only quantified points (>d.l.), often gave contrasting information. This was true for all the campaigns. During the July 2009 session, in some cases they were in good agreement (such as point A for toluene, points B and L for ethylbenzene, p-xylene and C9-C12 aliphatics), sometimes the shallower depth gave higher fluxes (points D and E for all BTEX) or lower (F and H for all BTEX and hydrocarbons, and B for benzene, toluene and C5-C8 aliphatics). During the December 2009 campaign the estimated flux from the two depths of each point, with exception of F and H, seemed more lined up and in general with $F_{SG,C1}$ higher than $F_{SG,C2}$ (for BTEX, C5-C8 aliphatics, C9-C12 aliphatics and C9-C10 aromatics, with the exception of point D). During July 2010 a greater difference was seen for point B, where $F_{SG,C1}$ was lower than $F_{SG,C2}$ for BTEX and C5-C8 aliphatics (also for points A and L for this class); F and H confirmed their trend and the other points had similar modelled fluxes from the two depths.

As a general note, it seemed that reciprocal relationships between F_{SG} at two depths, in each point and for all the compounds, followed the same behaviour of soil gas concentrations, meaning that soil gas concentration weighs more than depth as for flux estimation.

If fluxes from the two depths coincided, it would mean that the biodegradation on the site was poor, probably due to high concentrations. Modelled fluxes, in fact, were affected only by diffusion (as hypothesis in J&E model) using both C1 and C2 data; however concentration in C2 should be affected by the biological depletion which occurred along C2-C1 distance; thus $F_{SG,C1}$ should be similar to $F_{SG,C2}$ minus the biodegraded amount along 2.2 m of the distance between them.

Low temperature can affect biological activity and winter conditions generally slow down the rate of biodegradation. This could justify higher soil gas concentration in C1 in winter (Fig. 6.3) that caused higher $F_{SG,C1}$ at point B as for C5-C8 aliphatics detected during the December 2009 session.

Evaluation from soil gas is therefore difficult to define. Natural attenuation phenomena or some small heterogeneities in soil may heavily influence vertical profile of interstitial gas concentrations along soil. Therefore it is impossible to provide a recommendation as to which depth it is better to sample from and use to define the flux properly, due to insufficient information collected by a cost-acceptable characterization and the lack of biological parameters (such as CO_2, O_2 or oxidation / reduction potential) that should be monitored during soil gas monitoring. These data might be used, for example, in a deeper level of modelling, also considering biodegradation, that is loaded in another version of the J&E model (§ 3.4.2.2). Governmental Agencies, relatively to RA, are however still sceptical about considering natural attenuation and impose a more conservative approach without consider it (§1.3; APAT, 2008a)

Figs. 6.26, 6.27 and 6.28 present a summarising comparison between F_{GW} $F_{SG,C1,max}$, $F_{SG,C2,max}$ and $F_{FC,\ max}$ of each monitoring session, respectively for BTEX, aliphatic hydrocarbons and aromatic ones including MTBE.

As for benzene, $F_{SG,C2,max}$ was the maximum value in all three campaigns (higher in winter), followed by F_{GW} (decreasing over time), whereas $F_{SG,C1,max}$ slightly increased over time. Toluene, ethylbenzene and p-xylene showed a behaviour similar to the previous compound, but as regards toluene, in summer 2010, $F_{SG,C1,max}$ was higher than $F_{SG,C2,max}$; ethylbenzene in F_{GW} sharply decreased in July 2010, whereas p-xylene revealed anomalous $F_{SG,C1,max}$ in December (coming from point L), of about 4 o.o.m. higher than same flux in other sessions.

For all the BTEX, in general $F_{FC,max}$, always minor than d.l., was lower than all the other modelled fluxes; it was slightly higher than $F_{SG,C1,max}$ in July 2009 as regards to benzene and ethylbenzene, and in the case of the latter, two o.o.m. higher than F_{GW}, but no quantitative comparison may be drawn.

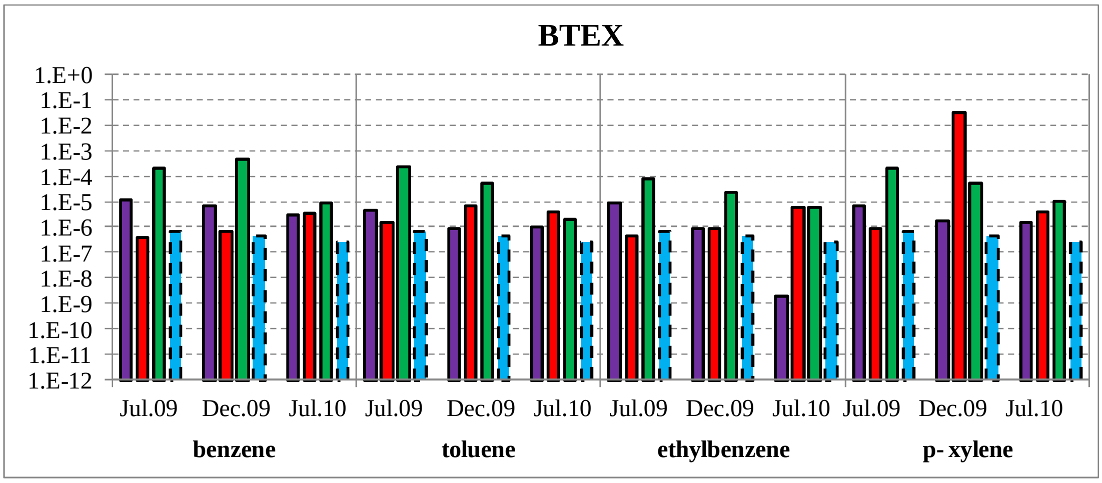

***Fig. 6.26**: vapour flux [mg m^{-2} s^{-1}] (in logarithm scale) derived from contaminant concentrations in groundwater -F_{GW}- (violet), maximum flux from shallow -$F_{SG,C1,max}$- (red) and deep soil gas -$F_{SG,C2,max}$- (green) and from FC measurements -$F_{FC,\ max}$- (light blue), for each monitoring session, regarding BTEX compounds; dashed boundaries indicate values lower than d.l..*

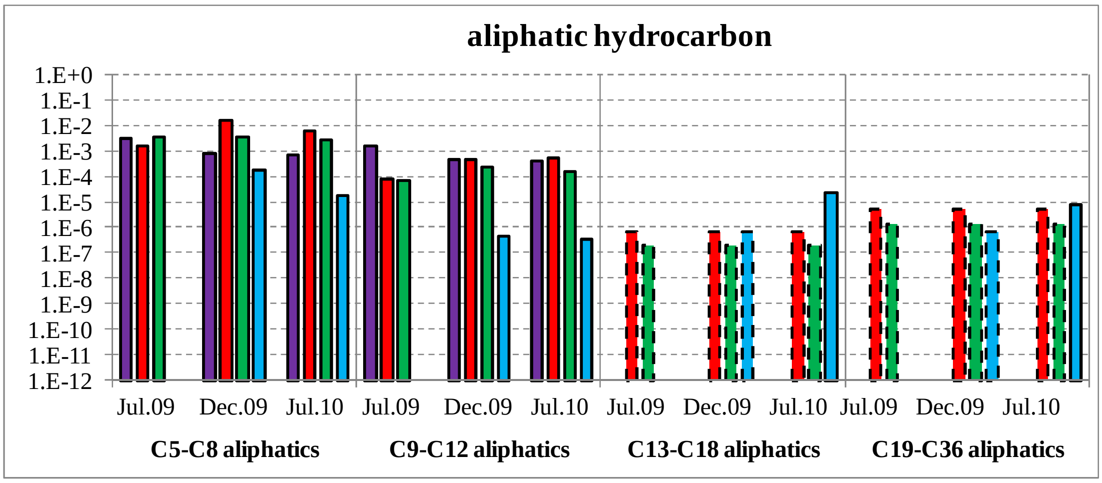

***Fig. 6.27**: vapour flux [mg m^{-2} s^{-1}] (in logarithm scale) derived from contaminant concentrations in groundwater -F_{GW}- (violet), maximum flux from shallow -$F_{SG,C1,max}$- (red) and deep soil gas -$F_{SG,C2,max}$- (green) and from FC measurements -$F_{FC,\ max}$- (light blue), for each monitoring session, regarding aliphatic hydrocarbons; dashed boundaries indicate values lower than d.l..*

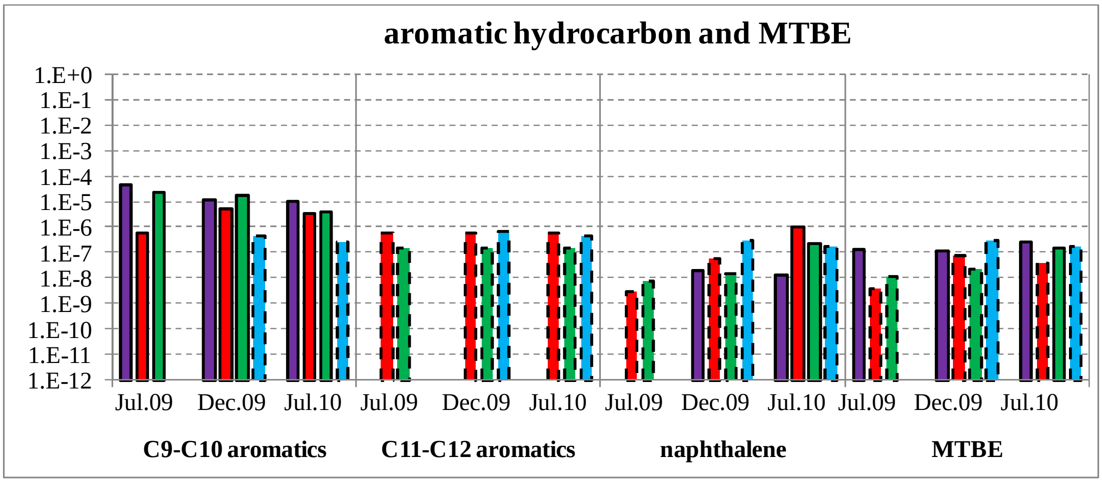

***Fig. 6.28**: vapour flux [mg m^{-2} s^{-1}] (in logarithm scale) derived from contaminant concentrations in groundwater -F_{GW}- (violet), maximum flux from shallow -$F_{SG,C1,max}$- (red) and deep soil gas -$F_{SG,C2,max}$- (green) and from FC measurements -$F_{FC,\ max}$- (light blue), for each monitoring session, regarding aromatic hydrocarbons; dashed boundaries indicate values lower than d.l..*

Lighter aliphatic hydrocarbons were all quantified. Maximum fluxes of C5-C8 aliphatics were all modelled from soil gas data, whereas F_{GW} showed a slightly decreasing trend over time. Calculated $F_{FC,max}$ was lower than all other maximum fluxes. F_{GW} and $F_{SG,max}$ were in good agreement as for C9-C12 aliphatics. For this class, too, $F_{FC,\ max}$ was up to two o.o.m. lower than the predicted values.

C13-C18 and C19-C36 aliphatic hydrocarbons were not detected in the groundwater because they are insoluble. Their concentrations were lower d.l. in soil gas samples and, on the contrary, in July 2010, in all the 5 FC monitored points, their fluxes were higher than d.l., with average values of respectively $15 \cdot 10^{-6} \pm 6 \cdot 10^{-6}$ mg m^{-2} s^{-1} and $4 \cdot 10^{-6} \pm 2 \cdot 10^{-6}$ mg m^{-2} s^{-1} (as standard deviation), and with a minimum value of $8 \cdot 10^{-6}$ mg m^{-2} s^{-1} and $1 \cdot 10^{-6}$ mg m^{-2} s^{-1}. This is a meaningful discovery because FC was revealed able to detect also contributions due to hotspot or heterogeneity that conventional methods may not detect.

As far as C9-C10 aromatic compounds were concerned, F_{GW}s were in good agreement with $F_{SG,max}$s with the exception of low $F_{SG,C1,max}$ monitored during the first campaign. $F_{FC,max}$ was an undetectable value lower than modelled fluxes, but in July 2010, in point G, F_{FC} was quantified at $2 \cdot 10^{-7}$ mg m^{-2} s^{-1} not too far from the maximum one. C11-C12 aromatic compounds were not researched in groundwater and with the other two techniques undetectable values were found.

F_{GW} of naphthalene was the not comparable with other fluxes along winter session, because they had too high d.l.s. During July 2010 it was lower than $F_{SG,C1,max}$ (found in point G, followed by points E and L) and $F_{SG,C2,max}$ (found in L). Not quantifiable F_{FC}s were found, but the d.l. was comparable with $F_{SG,C2,max}$ and higher than F_{GW}.

MTBE was quantified only in groundwater and in deep soil gas, during summer 2010 campaign at point E. Values under d.l. were found by FC, however d.l.s were comparable with detected fluxes.

6.3.5 Ambient air measurements from modelling

Fig. 6.29 presents modelled concentrations [µg m^{-3}] from F_{GW} (yellow), $F_{SG,C1,max}$ (red), $F_{SG,C2,max}$ (green) and from $F_{FC,max}$ (light blue), calculated as indicated in § 6.2.6, in comparison with results from air measurements (violet, taken from Tab. 6.10).

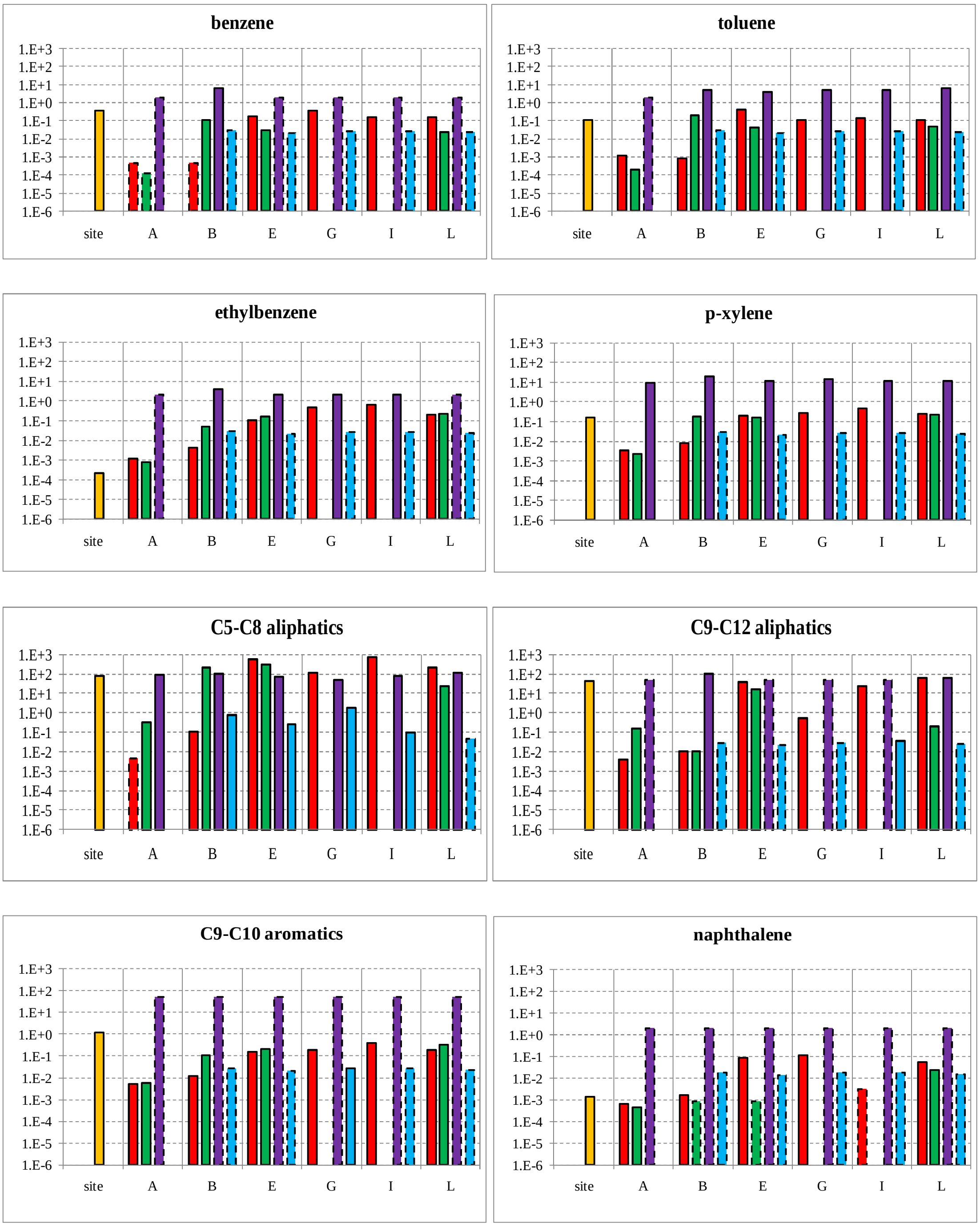

***Fig. 6.29**: continue.*

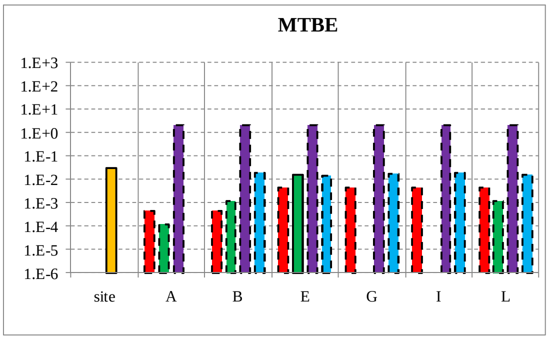

***Fig. 6.29**: comparison between outdoor air concentrations [µg m^{-3}] (in logarithm scale) during the **July 2010 campaign**, for each point where direct measurements (violet) were taken. Modelled concentrations from F_{GW} (yellow), F_{SG} from shallow soil gas –C1- (red) and deep soil gas –C2- (green) and from F_{FC} (light blue) are represented; dashed boundaries indicate values from F lower than d.l..Note: F_{GW}: flux from concentrations in groundwater; F_{SG}: flux from concentrations in soil gas; F_{FC}: flux from FC measurements.*

The comparison between $C_{out,meas}$ and estimated values underlines the added contribution included in directly measured values, depending on sources external to vapours flowed from soil. As for the relationships between estimated values from groundwater, soil gas and flux chamber, they were the same as those between respective fluxes (§ 6.3.4), because of their direct proportionality to flux due to (6.1).

As far as benzene was concerned, $C_{out,GW}$s were higher than all the other estimated values. $C_{out,meas}$s were lower than d.l. for the majority of monitored points, with d.l. higher than $C_{out,GW}$; $C_{out,meas}$ was, however, quantified at point B, resulting the highest of all the other values.

Most of $C_{out,meas}$ for TEX were quantified with values higher than all the other estimated outdoor air concentrations.

As for C5-C8 aliphatics, $C_{out,meas}$ were comparable between the measured points, independently of their position, in good agreement with $C_{out,GW}$ and in general also with $C_{out,SG}$, with the exception of point A; quantified $C_{out,FC}$ were always lower than $C_{out,meas}$. No correspondence was noticed between higher $C_{out,meas}$ and $C_{out,SG}$ probably because $C_{out,meas}$ were affected by the environmental air background; further measurements, taken in a similar context far from the potential contaminated site, should have been taken.

$C_{out,GW}$ and quantified $C_{out,meas}$ as regards to C9-C12 aliphatics were comparable and higher at least for up than 3 o.o.m. than $C_{out,FC}$ (< d.l.). At points B and L (only C2 depth), they were in poor agreement with $C_{out,SG}$. In point I $C_{out,FC}$ was quantified with a value of 0.03 µg m^{-3} lower than $C_{out,SG}$ and not directly comparable to not quantified $C_{out,meas}$ (with d.l. > $C_{out,FC}$).

As for C9-C10 aromatic hydrocarbons a similar situation was noticed for point G. Relatively to the other points, $C_{out,GW}$ was higher than $C_{out,SG}$. The d.l.s of $C_{out,meas}$ were too high to be meaningfully compared with other estimates, whereas $C_{out,FC}$s (< d.l.) were however compatible with them.

As regards naphthalene and MTBE $C_{out,meas}$ and $C_{out,FC}$ followed the same trend, but $C_{out,GW}$ was lower than $C_{out,SG}$ in three points for the first compound and comparable to $C_{out,SG}$ in the only detected point for MTBE (E).

Fig. 6.30 presents a comparison, for the 9 compounds researched during outdoor air measuring, between $C_{out,meas,\ max}$ (on the x-axis) and estimated $C_{out,GW,max}$, $C_{out,SG,C1,max}$, $C_{out,SG,C2,max}$ and $C_{out,FC,max}$ (on the y-axis).

As a general trend, almost all the estimated values were lower than measured ones. In particular, as for $C_{out,FC,max}$, with the exception of C5-C8 aliphatic hydrocarbons (equal to a value 61 times lower than $C_{out,meas,\ max}$), all the estimates were more than 2 o.o.m. lower than measures.

$C_{out,GW,max}$ was always lower than $C_{out,meas,\ max}$ from less than 1 o.o.m. for C9-C12 aliphatic and C9-C10 aromatic hydrocarbons, to more than 3 o.o.m. for ethylbenezene and naphthalene.

$C_{out,SG,C1,max}$ and $C_{out,SG,C2,max}$ were generally more than 1 o.o.m. lower than maximum measured values (generally between 1 and 2 o.o.m. for deep soil gas and more variable for shallow points), with the exception of a few points less than 1 o.o.m. (C9-C12 aliphatic for both and ethylbenezene for C1); as for C5-C8 aliphatic hydrocarbons, they were higher than $C_{out,meas,\ max}$ (at point I for C1 -in good agreement with values of points E, G and L too- and at point E for C2 -in good agreement with values of points B and L too-).

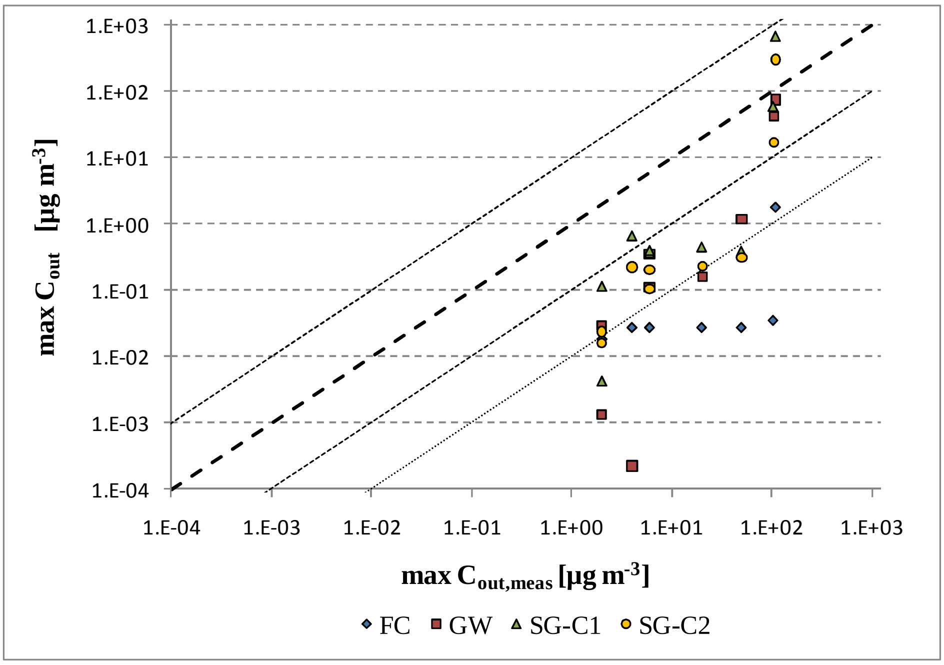

Fig. 6.30*: comparison between maximum outdoor air concentrations [μg m^{-3}] for each analyte, concerning the* ***July 2010*** *campaign, in x-y graph with logarithm scale. On x-axis:* $C_{out,meas,max}$*; on y-axis:* $C_{out,FC,max}$ *(blue lozenges),* $C_{out,GW,max}$ *(red squares),* $C_{out,SG,C1,max}$ *(green triangles),* $C_{out,SG,C2,max}$ *(yellow circles); symbols explained in § 6.2.4.3. Thick dashed line indicates x=y values, thin small dashed line y=10 or* 10^{-1}*x and thin pointed dashed line y=*100^{-1}*x value.*

6.3.6 Risk calculation

Results of RA performed according to § 6.2.7 are indicated in Tab. 6.34.

R_{tol} was exceeded by calculating R just from $C_{out,meas,max}$ for both receptors. HI due to inhalation just of C5-C8 aliphatic hydrocarbon vapours is higher than HI_{tol} from $C_{out,meas,max}$ and $C_{out,meas,max}$ just for child receptor and from $C_{out,SG,max}$ for both receptors. HI_{tol} was exceeded for C9-C12 aliphatic, C9-C10 aromatic and naphthalene, for child receptor, just from $C_{out,meas,max}$. For all the estimations the most sensitive receptor was the child. Total HI was maximum from $C_{out,SG,C1,max}$ followed by $C_{out,meas,max}$, $C_{out,SG,C2,max}$ and $C_{out,GW,max}$. On the contrary, assessments from $C_{out,FC,max}$, gave a total HI lower than HI_{tol}.

Tab. 6.34*: calculated risk (R), hazard index (HI) for different analytes, and total HI on from* $C_{out,meas,max}$, $C_{out,FC,max}$, $C_{out,GW,max}$, $C_{out,SG,C1,max}$ *and* $C_{out,SG,C2,max}$, *for both potential receptor of the sites. Values higher than maximum tolerable risks are indicated by bold types.*

		$C_{out,meas,max}$		$C_{out,FC,max}$		$C_{out,GW,max}$		$C_{out,SG,C1,max}$		$C_{out,SG,C2,max}$	
		adult	**child**	**adult**	**child**	**adult**	**child**	**adult**	**child**	**adult**	**child**
benzene	R	**1.6 E-05**	**1.2 E-05**	7.4 E-08	5.8 E-08	9.2 E-07	7.1 E-07	9.9 E-07	7.7 E-07	2.8 E-07	2.5 E-07
	HI	2.0 E-01	6.2 E-01	9.3 E-04	2.9 E-03	1.1 E-02	3.6 E-02	1.2 E-02	3.8 E-02	3.5 E-03	1.1 E-02
toluene	HI	1.2 E-03	3.7 E-03	5.6 E-06	1.7 E-05	2.2 E-05	6.8 E-05	7.9 E-05	2.5 E-04	4.0 E-05	1.2 E-04
ethyl-benzene	HI	4.0 E-03	1.2 E-02	2.8 E-05	8.7 E-05	2.2 E-07	6.9 E-07	6.6 E-04	2.1 E-03	2.2 E-04	6.9 E-04
p-xylene	HI	2.8 E-02	8.8 E-02	4.0 E-05	1.2 E-04	2.2 E-04	6.9 E-04	6.4 E-04	2.0 E-03	3.3 E-04	1.0 E-03
C5-C8 aliphatic	HI	5.4 E-01	**1.7 E+00**	8.9 E-03	2.8 E-02	3.7 E-01	**1.2 E+00**	**3.4 E+00**	**1.0 E+01**	**1.5 E+00**	**4.7 E+00**
C9-C12 aliphatic	HI	5.1 E-01	**1.6 E+00**	1.8 E-04	5.5 E-04	2.1 E-01	6.4 E-01	2.9 E-01	9.2 E-01	8.5 E-02	2.6 E-01
C9-C10 aromatic	HI	9.9 E-01	**3.1 E+00**	5.6 E-04	1.7 E-03	2.3 E-02	7.2 E-02	7.7 E-03	2.4 E-02	6.2 E-03	1.9 E-02
naphthalene	HI	6.6 E-01	**2.0 E+00**	6.2 E-03	1.9 E-02	4.4 E-04	1.4 E-03	3.8 E-02	1.2 E-01	7.7 E-03	2.4 E-02
MTBE	HI	6.6 E-04	2.0 E-03	6.2 E-06	1.9 E-05	9.5 E-06	2.9 E-05	1.4 E-06	4.4 E-06	5.2 E-06	1.6 E-05
Total HI		**2.9 E+00**	**9.1 E+00**	1.7 E-02	5.2 E-02	6.1 E-01	**1.9 E+00**	**4.5 E+00**	**1.2 E+01**	**1.6 E+00**	**5.0 E+00**

6.4 Conclusions

This chapter presented the comparison between results of different approaches used to improve site-specific risk assessment due to inhalation of volatile organic contaminants.

Fluxes resulting from modelled estimation (by Johnson and Ettinger model) using groundwater and soil gas concentrations were compared to results of the flux chamber measurement with the setup defined in previous chapter.

As a general trend, the applied model tends to overestimate compared to the observed values, probably because it does not take into account the biodegradation in the soil or lateral air movements, since it is 1-D (§ 3.4). A good agreement or a slight underestimation (such as toluene detected in point L during the July 2009 campaign or C13-C18 aliphatic hydrocarbons detected during the July 2010 campaign) was however found for some pollutants, indicating that models offer a slightly unreliable assessment of vapour transport, that is not always the most precautionary one, because they are based on simplified hypotheses, rigid conceptual site models, not considering therefore either natural attenuation or small heterogeneities (in agreement with § 1.3). It is therefore impossible to provide a recommendation as to which depth it is better to sample from and use to define the flux properly; any further information on the season to choose for monitoring to have precautionary assessment may be extracted, too.

Maximum fluxes were also used to calculate outdoor concentrations to compare with direct measurements. It emerged that air measurement overestimated the contribution of risk due to vapour inhalation of contaminated vapours from soil, as a reference to all the other approaches, because they are also affected by environmental pollutant background. FC technique, on the contrary, considering only soil vapours, gave a completely acceptable risk.

7

A REMEDIATION TECHNIQUE: BIOCHAR-AMENDED SOIL

7.1 Introduction

VOCs are a wide spread, well-known cause of soil and groundwater contamination. Conventional techniques used to remediate soils affected by them are generally in situ or on site techniques which vary according to the level and kind of contamination. Next to more complex techniques, based on physical-chemical or biological principles, such as Bioventing/Soil Vapour Extraction (in unsaturated soil) or Biosparging/Air Sparging (for impacted groundwater systems), simpler biological techniques are also suggested.

The level of human and technical involvement in the procedure is variable. The simplest approach is monitoring of in situ natural attenuation (MNA) consisting in regular checking over time of the decrease of mass, concentration, mobility or toxicity of pollutants in soil and groundwater, due to natural physical, chemical and biological mechanisms that occur in soil (Bonomo, 2005). If treatment time has to be reduced, also ex situ biological technologies for unsaturated soil such as landfarming or more engineered biopiles may be applied.

The aim of the experimental tests presented in this chapter is to evaluate the effects of an innovative, little known low-cost in situ landfarming treatment, consisting of soil amendment with biochar.

All the tests presented in this chapter were performed at Civil and Environmental Laboratory of Newcastle University (UK).

7.1.1 Biochar

Biochar is a high-carbon, fine-grained residue which was produced in centuries-old techniques by smouldering biomass, differing from charcoal only because its primary use is not for fuel, but for agricultural and environmental gain (IBI, 2010). Today it is produced by a slow (Fig. 7.1a) or fast (Fig. 7.1b) pyrolysis process, consisting in heating biomass in a kiln in the absence of oxygen (Lehmann, 2007), producing an exothermic reaction whose byproducts are a black liquid, tar, and a mixture of CO and H_2, called syngas, both useful as biofuels.

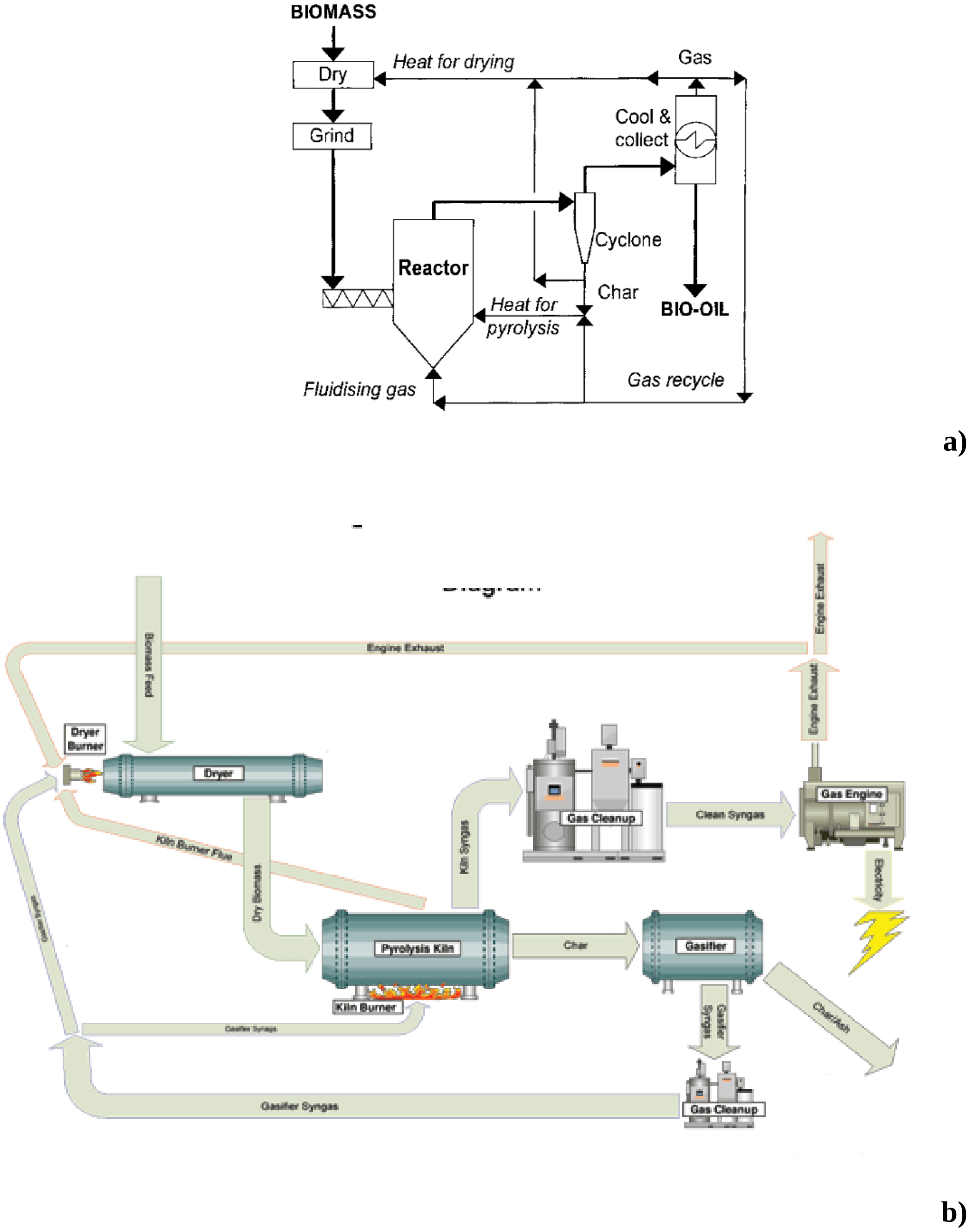

***Fig. 7.1:** sketch of a) fast (Bridwager et al., 2000) and b) slow (Best Energies, 2010) pyrolysis process applied for biochar production*

Biomass pyrolysis is a well established technique for the production of biofuel, but the commercial exploitation of biochar by-products as soil amendments is still undeveloped. In Japan, which has the largest market for such products, approximately 14000 t yr^{-1} are traded annually for soil use (Okimori et al., 2003). The other more common uses are gasification to extract the residual energy, or the production of high value products such as activated carbon (Sohi et al., 2009). The biochar market is, in fact, still in its infancy, but there are several small product sellers and local research groups (Regional Biochar groups) supporting local research and projects in the countries indicated in Fig. 7.2.

Fig.7.2: *map with Regional Biochar Groups seats (IBI, 2010).*

Biochar is mainly used in some practices to lock carbon in the soil and represents a biosequestration technique able to capture and store atmospheric CO_2 (Novak et al., 2009; Zimmerman, 2010); Fig. 7.3 shows the complexity of potentially beneficial interactions of biochar in the context of natural cycles and anthropogenic interventions.

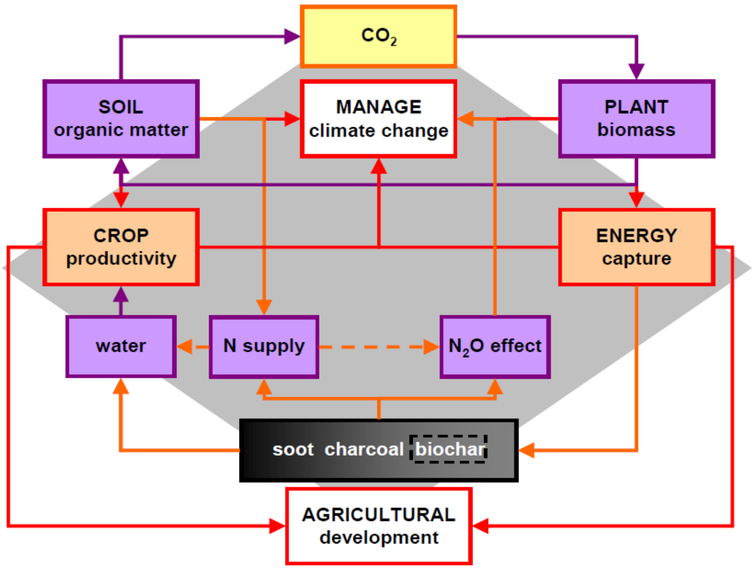

Fig. 7.3: *interactions of biochar in the environment, involving physical (purple arrows), natural (orange arrows) and anthropogenic (red arrows) interactions (Sohi et al., 2009).*

The CO_2 sequester in biochar is different than the natural carbon cycle according to plants, whose matter decomposes rapidly after their deaths, emitting CO_2 again in an overall neutral carbon cycle (Fig. 7.4a). The process of pyrolysis produces, instead, a much more stable material, not subject to normal microbial decay, representing therefore a soil carbon pool and making it a carbon-negative process (Fig. 7.4b) (Lehmann et al., 2007). Additionally, it has been shown to decrease nitrous oxide and methane emissions from soil, thus further reducing greenhouse gas emissions.

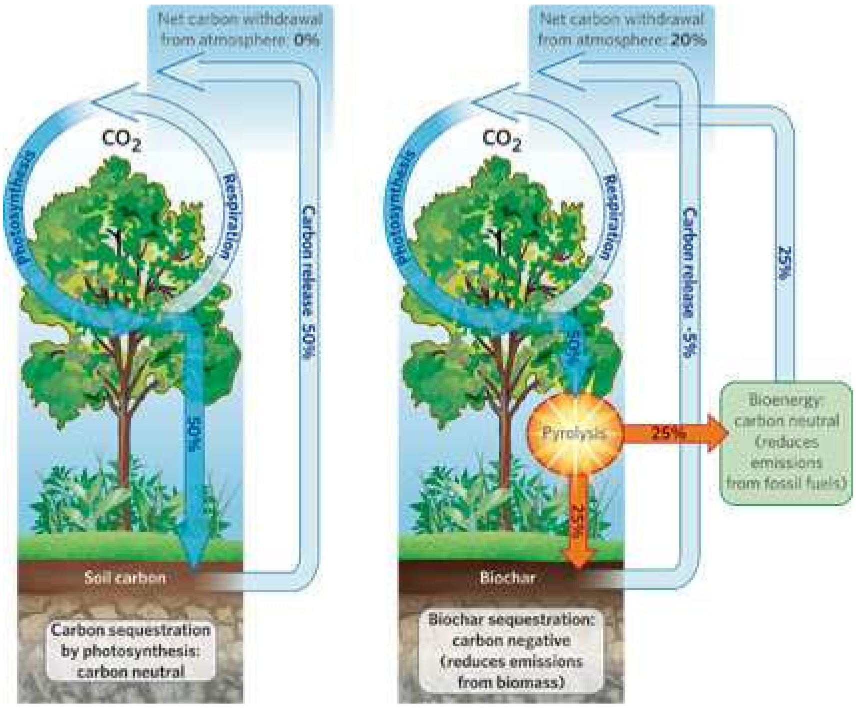

a) **b)**

***Fig. 7.4**: interactions CO_2 mass balance due to plants (a) and to biochar sequestration (b) (Lehmann et al., 2007).*

The stability of carbon that is the length of time biochar will remain in the soil, depends on the feedstock material, the pyrolysis conditions, the particle surface-volume ratio and soil conditions, ranging from 100 to 10,000 years, with 5,000 being a common estimate (Cheng et al., 2008).

Charcoal is applied to soils by currently used tillage machinery or equipment used to spread fertilizer; given the variability in biochar materials and soils there are no indications about the amount to add to soil, although it has been shown that rates between 0.5 and 5 kg m^{-2} have often been used successfully (IBI, 2010).

In general its behaviour depends on its physical and chemical properties, due to different production techniques (Fig. 7.5) (Gaskin et al., 2007; Lehmann et al., 2007), principally connected with temperature and furnace residence time parameters (Sohi et al., 2009). As for soil advantages, it lends high organic matter that is slowly oxygenated and transformed into physically stable but chemically reactive humus, therefore increasing its fertility (Glaser et al., 2002), as such as what happened on anthropogenic soils (Terra Preta) in central Amazonia. It influences cation exchange capacity (Liang et al., 2006; Brodowski et al, 2007; Steiner et al., 2007), buffers soil acidification, allows greater availability of phosphorus and less phytotoxic aluminium leaching, and, in some cases, it increases water retention (only where large amounts of biochar are added, in the range 4 to 45% in weight) (Novak et al., 2009). Its pH is basic due the presence of cations, among which calcium and potassium are important for biological activity (Chan et al., 2007 in Miglietta et al., 2010), however, due to surface oxidation, new acid functional groups are formed and pH may decrease releasing aluminium. It works as a bulking agent too, useful for really fine soils. Regarding nutrients, its addition to soils seems not to provide them directly, but to reduce significantly leaching of applied nitrogen fertilizers, related to the higher exchange capacity and the increased surface area (Glaser et al., 2002); however the carbon to nitrogen ratio is too high (around 200) to sustain biological activity alone (Novak et al., 2009).

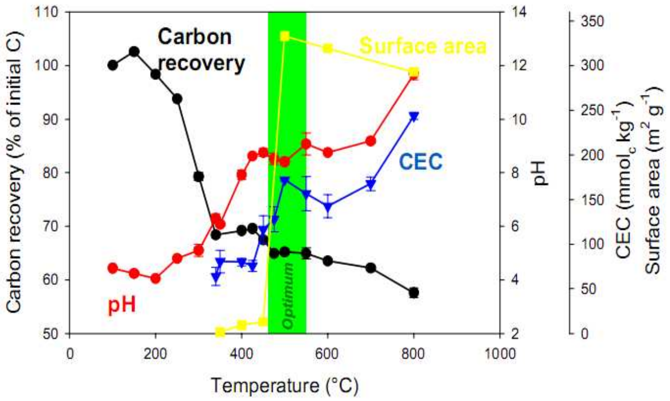

***Fig. 7.5**: influence of furnace temperature on carbon recovery availability (in black line) on the left y axis; pH (in red), cation exchange capacity, CEC (in blue) and specific biochar area (in yellow), all indicated on right y axis (Lehmann et al., 2007).*

The effects on soil biology seem relevant, because biochar has the potential to alter the microbial biomass and composition (Steiner, 2009). The majority of conducted experiments show that biochar amendments result in enhancement of beneficial fungi (Warnock et al., 2007) and nitrogen fixing microbes (Rondon et al., 2007); however, the physical, biological and chemical processes that it may exert on microbial communities are not completely understood (Sohi et al., 2009).

Biochar may be produced from a wide range of biomass materials, from forest residues and consumer waste to purpose-grown crops (Rutherford et al., 2009).

It is an amorphous form of graphite formed when biomass, reaching the ignition temperature of 275°C, spontaneously converts to the more stable amorphous graphitic bonds (Fig. 7.6), gas and liquids. Graphite is composed of two dimensional sheets of strongly bonded carbon held together by Van der Waals forces, being therefore able to absorb other molecules (Reed et al., 2009).

Biochar obtained by pyrolyzing organic feedstock at low temperatures (250 to 400ºC) includes aliphatic and cellulose type; it is highly absorbent and almost amorphous, contains C=O and C-H functional groups working as nutrient exchange sites. Biochar produced at higher temperatures (400 to 700ºC) has a diversified organic character: it contains poly-condensed aromatic structures, more regular graphite islands, fewer oxygen functional groups and, having stood dehydration and decarboxylation processes, lower ion-exchange functional, potentially limiting its usefulness in retaining soil nutrients (Novak et al., 2009). Its structure has to be well analysed, because it may contain constituents toxic to both humans and animals. Those of special concern are (i) crystalline silica that may be produced at high temperatures from rice husk, (ii) organic compounds, such as PAH and dioxins, derived from certain waste sources and (iii) heavy metals using contaminated biomass feedstock.

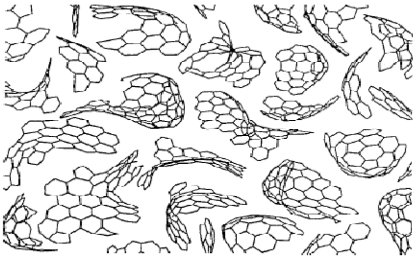

Fig. 7.6*: amorphous graphitic bonds constituting biochar structure (Reed et al., 2009).*

Its application is useful also to treat contaminated soil and sediment. It has a proved capacity to adsorb persistent and high-weight compounds, such as polycyclic aromatic hydrocarbons (PAHs) (Cornelissen et al., 2006; Brandli et al., 2008; Hale et al., 2010a), polychlorinated biphenyls (Sun et al., 2009) and pesticides (Yu et al., 2010), and its capacity to retain metals (Beesley et al., 2010), because of its ion exchange capability, thus limiting their bioaccumulation and potentially toxic effects on biological organisms. In particular some studies have shown the positive effect of adding strong sorbents during biodegradation of organic pollutants, especially on heavily contaminated sites, thus reducing treatment time of conventional biostimulation techniques (Hale et al, 2010b). However, the impact of strong sorbents on the biodegradation of more readily available and biodegradable organic pollutants such as VOCs has so far not been fully investigated.

This chapter deals with the effect of biochar on behaviour of volatile petroleum hydrocarbons, which are among the most common environmental pollutants in soils and are often present at PAH contaminated sites.

7.2 Materials and methods

7.2.1 Pollutant mixture

A mixture of 12 typical constituents of gasoline or kerosene was prepared from high purity chemicals obtained from Sigma-Aldrich (Dorset, UK). Their weight percentage was chosen according to typical fuel compositions analogously to what was performed in other previous tests in literature (Pasteris et al., 2002). They may be divided into four family groups: straight chain, branched and cyclic alkanes and aromatic. The list of the compounds, including their physical and chemical properties, is summarized in Tab. 7.1.

It comprises:

- their chemical structure;
- the used percentages in volume in the mixture (V%) [%];
- the level of purity of the used chemicals (Sigma- Aldrich) (P) [-];
- their molecular weight MW [g mol^{-1}];
- the maximum saturation vapour pressure $P^0_{v,\ sat}$ (§ 2.2.2) at 20°C (§ 7.2.4 and 7.2.5), as a pure liquid phase [atm], reached from MPBPWIN, belonging to Estimations Programs Interface for Windows (EPI Suite) (http://www.epa.gov/opptintr/exposure/pubs/episuitedl.htm);
- their chemical density (ρ) at 20°C (Sigma- Aldrich) [g ml^{-1}];
- the calculated mole fraction (X) in the mixture [-] according to (2.2), where

$$\mathrm{n_i} = \frac{\rho_i * V\%_i * P_i}{MW_i} \tag{7.1}$$

- the derived saturation vapour pressure $P_{v,sat}$ in a mixture as from (2.1) and perfect gases law, at 20°C, expressed as saturated gas concentration in the head phase of a closed system $C_{g,sat}$ [g m^{-3} = µg ml^{-1}]

$$\mathrm{C_{g,sat,i}} = \frac{X_i * MW_i * P^0{}_{v,sat,i} * 10^3}{R * T} \tag{7.2}$$

where R = 0.0821 l atm mol^{-1} K^{-1} and T = 293.15 K.

Sulfur hexafluoride (SF_6) (Sigma –Aldrich, Steinheim, D) was used as a volatile recalcitrant tracer under aerobic conditions.

In Tab. 7.2 other physical-chemical properties (§ 2.2) (referred to 25°C, which is the common reference temperature are indicated, with the aim of making a relative comparison of their behaviour in the environment.

***Tab. 7.1**: Composition of the petroleum hydrocarbon mixture. V%: volume percentage in the mixture; P: chemical purity; MW: molecular weight; $P^0_{v,\,sat}$: NAPL vapour pressure as a pure liquid phase from MPBPWIN Software; X: molar ratio; $C_{g,sat}$: saturated gas concentration in the mixture.*

Molecule	**Brutal Structure**	**CAS number**	**Chemical Structure**	**V%**	**P**	**MW**	**$P^0_{v,\,sat}$ @ 20 °C**	**ρ @ 20 °C**	**X**	**$C_{g,sat}$**
Measure unit				**%**	**%**	**g mol^{-1}**	**atm**	**g ml^{-1}**	**-**	**µg ml^{-1}**
n-pentane	C_5H_{12}	109-66-0	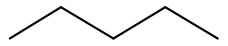	5	99.0	72	0.55806	0.626	0.061	101.88
n-hexane	C_6H_{14}	110-54-3	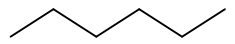	9	95.0	86	0.1703	0.660	0.093	56.62
methylcyclopentane	C_6H_{12}	96-37-7	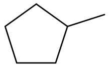	8	99.8	84	0.1834	0.749	0.101	64.62
cyclohexane	C_6H_{12}	110-82-7	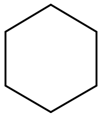	8	99.8	84	0.12445	0.779	0.105	45.60
Isooctane (2,2,4-trimethylpentane)	C_8H_{18}	540-84-1	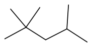	15	99.0	114	0.05371	0.692	0.128	32.52
methylcyclohexane	C_7H_{14}	108-87-2	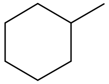	12	99.0	98	0.04847	0.770	0.132	26.12
toluene	C_7H_8	108-88-3	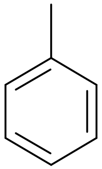	4.0	99.8	92	0.02882	0.865	0.053	5.86

***Tab. 7.1**: continued.*

n-octane	C_8H_{18}	111-65-9	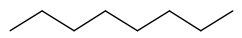	8.0	99.0	114	0.01441	0.703	0.069	4.73
m-xylene	C_8H_{10}	108-38-3	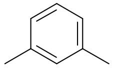	5.0	99.0	106	0.01179	0.868	0.057	2.98
1,2,4,TMB (1,2,4-trimethylbenzene)	C_9H_{12}	29222-48-8	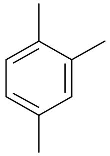	6.0	98.0	120	0.0019	0.889	0.061	0.59
n-decane	$C_{10}H_{22}$	124-18-5	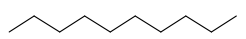	14.0	99.0	142	0.001572	0.730	0.101	0.94
n-dodecane	$C_{12}H_{26}$	112-40-3	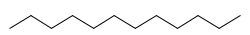	6.0	99.0	170	0.000393	0.748	0.037	0.10

Tab. 7.2*: Summary of different physical-chemical properties (calculated at 25°C) of the compounds which are the object of the present research; (a): Pasteris et al. (2002) - addendum; (b) experimental data from Estimations Programs Interface for Windows (EPI Suite) (http://www.epa.gov/opptintr/exposure/pubs/episuitedl.htm); (c): Schwarzenbach et al., 1993; (d): calculated according to the method of Fuller for organic material (Schwarzenbach et al., 1993, eq.9-22);(e):* Sander, 2010; *(f): Wilhelm et al., 1972. #: constants referred as [atm m^3 mol^{-1}] and transformed in indicated unites using perfect gases law.*

Molecule	**Henry's law constant @ 25 °C**	**Octanol-water partitioning coefficient**	**Water solubility**	**Air diffusion coefficient**
Symbol	**H**	**log K_{ow}**	**S**	**D^g**
Measure unit	**- = mol l_{gas}^{-1} (mol l_{water}^{-1}) $^{-1}$**	**log (l kg^{-1})**	**mg l^{-1}**	**cm^2 s^{-1}**
n-pentane	50.67 (a) 51.91 (b, #)	3.62 (c) 3.39 (b)	22.52 (b)	0.0822 (d)
n-hexane	68.38 (a) 73.54 (b, #)	4.11 (c) 3.90 (b)	7.81 (b)	0.0744 (d)
methylcyclopentane	14.65 (a) 14.83 (b, #)	3.10 (c) 3.37 (b)	31.62 (b)	0.0785 (d)
cyclohexane	7.33 (a) 6.13 (b, #)	3.44 (c, b)	48.76 (b)	0.0794 (d)
Isooctane	132.35 (a) 124.20 (b, #)	4.09 (c, b)	3.61 (b)	0.0641 (d)
methylcyclohexane	4.23 (a) 17.57 (b, #)	3.61 (c, b)	17.22 (b)	0.0725 (d)
toluene	0.26 (a) 0.27 (b, #)	2.69 (c) 2.73 (b)	471.12 (b)	0.0780 (d)
n-octane	120.67 (a) 131.14 (b, #)	5.18 (c, b)	0.87 (b)	0.0638 (d)
m-xylene	0.26 (a) 0.29 (b, #)	3.15 (c) 3.20 (b)	161.92 (b)	0.0714 (d)
1,2,4,TMB	0.27 (a) 27.53 (b, #)	3.65 (c) 3.94 (b)	3.86 (b)	0.0662 (d)
n-decane	293.05 (a) 210.39 (b, #)	5.01 (c, b)	0.09 (b)	0.0566 (d)
n-dodecane	293.05 (a) 334.18 (b, #)	6.1 (c, b)	0.01 (b)	0.0514 (c)
Sulfur hexafluoride	125.82 (b, #)	1.68 (b)	0.02 (f)	0.093
Carbon dioxide	0.75 (e)	0	1450 (b)	0.17

7.2.2 Material Characterization

7.2.2.1 Material Origin

Two different matrices were used during the tests. One was used as a reference material, a sandy soil obtained from the King Gate Building construction site on the Newcastle University campus at the UK. The other one was biochar type NBN 010 obtained from EPi-Energy (Environmental Power international, UK) and produced by fast pirolysis (Fig. 7.1a) from wood chips in a fixed bed reactor at high temperature (800 ºC) and heating rate, in the presence of an inert gas.

7.2.2.2 Biochar petrography and screening carbon fingerprint

Biochar structure was analysed by Dr Elisa Lopez-Capel at Sir Joseph Swan Institute of Newcastle University. Both an optical mineralogy/petrography technique and a thermogravimetric (TG) applied to a quadrupole mass spectrometer (QMS) were performed.

Polarized light microscopy (PLM) is generally used to identify minerals in thin sections. In the case of biochar, the sample was mounted in an epoxy resin, immersed in oil and placed under white incident light and blue light excitation (fluorescence mode). Polarized light with the addition of λ retarder plate was also used in order to check the anisotropy of the materials. The total magnification was 500 times.

The TG analysis is based on pyrolysis and vaporisation processes according to a thermal protocol and the lost mass is recorded through a thermo-balance. When it is coupled to QMS, different components may be identified according to the mass to charge (m/z) ratio due to ionization effect. In this specific case the TG data was processed by targeting the carbon dioxide (m/z 44) traces from the QMS, and using ‘Grams’ software to estimate the stability of the carbon present in each of the samples. Thus the proportion of the four main carbon pools in biochar (labile, recalcitrant, resistant, inorganic) was estimated. The proportion of labile carbon provides an indication of how rapidly biochar may decay, and therefore the availability of organic carbon for microorganisms (Thies et al., 2009). At the same time the C:N:S content was defined.

7.2.2.3 Grain size distribution

Soil grain distribution curve was obtained on nr. 2 samples of 500 g of wet soil, dried at 105°C to reach constant weight (according to ASTM, 2006). Each sample was poured into the top of a stake of 7 nested square mesh sieves (conforming to ASTM, 2009), where the sieves having larger screen openings were placed above the ones with smaller openings (4 mm, 2 mm, 1 mm, 600 μm, 425 μm, 212 μm and 63 μm). At the base there was a round pan, called the receiver; the column was placed over a mechanical sieve shaker working for 15 minutes.

Retained soil on each sieve M_j is a ratio of total dried mass M_{dried_t}.
In order to calculate weight percentages of soil with grains lower than i-sieve (passing it), P_i, this relation was applied (Scesi et al., 1997):

$$P_i = \frac{M_{dried\_t} - \sum_{j=1}^{i} M_j}{M_{dried\_t}} * 100 \tag{7.3}$$

The results were compared with the data provided by Derwentside Environmental Testing Services (DETs) geology laboratory (Co Durham, UK) according to BS 1377-2:1990 method (British Standard, 1990).

Biochar was ground and sieved to a particle size of 163 μm.

7.2.2.4 Soil porosity

Soil porosity f was calculated on a volume principle technique. A known volume V of dry sample was poured into a graduated cylinder; then a volume V' of deionised water was poured (measured by weight in order to achieve greater accuracy) and the new volume V'' was measured. Porosity was given by (Scesi et al., 1997):

$$f = \frac{V' - (V'' - V)}{V} \tag{7.4}$$

Porosity was calculated on 3 equal parts of dry soil sample and V' was chosen in order to reach V'' = V.

7.2.2.5 Soil and biochar density

Particle or solid density ρ_s was calculated according to ASTM F1815-97 (ASTM, 1997), on 6 parts of soil sample and for biochar on 3 parts. Different glass pycometers (with proper tips) were used, each tared (T) and then filled with deionised water and weighed again (WT) to define the net volume. Each part was poured into a pycometer and weighed (ST), and then filled with deionised water, shaken to send the air out in order to fill the vessel to the brim, and finally weighed (WST). All the weights are expressed in grams. Particle density [g ml^{-1}] was calculated as:

$$\rho_s = \frac{ST - T}{WT - [WST - (ST - T)]} \tag{7.5}$$

ρ_s for biochar-amended soil was calculated using a weighed averaged of biochar and soil solid density.

Bulk density ρ_b was calculated from f (§7.2.2.4) and ρ_s:

$$\rho_b = \rho_s * (1 - f) \tag{7.6}$$

7.2.2.6 Moisture

For each water content w determination 3 parts of matrix sample were used (weight among 15 and 25 g). Previously dried at 105°C and tared glass/ceramic crucible vessels were used. Matrix samples were left in them in an oven (at 105°C), for 24 h, then placed in a desiccator and finally weighed. Moisture is expressed as the percentage of the ratio of water to dry soil content.

Biochar contained no water.

7.2.2.7 Organic carbon content

Organic carbon content was determined according to a modified method C in ASTM D2974-07a (ASTM, 2000) and Karam (1993). 3 parts of dried soil sample were placed in ceramic crucibles (tared at 550°C) and left in muffle at 550°C for 2 hours, then they were left to cool in a desiccator to ambient temperature and then weighed to obtain a measure of soil content without volatile solids (VS). Organic content ratio f_{oc} was estimated as 58% of VS content (Wiedemeier et al., 1999; Schumacher, 2002) and referred to dry soil. The results were compared with the data provided by Derwentside Environmental Testing Services (DETs) geology laboratory (Co Durham, UK) following a documented in-house Method nr. DETSC 2084 by combustion and infra red detection.

7.2.2.8 pH

The pH was measured according to Method D 4972-95a (ASTM, 1995). A solution in deionised water with $CaCl_2$ 0.01 M was prepared. Wet soil was added to the solution according to 1:1 solid to liquid ratio (20 g of soil: 20 ml of solution), whereas biochar, due to its bulk, to a 1:3 solid to liquid ratio. 3 independent parts were prepared for each analysed sample. The mixtures were shaken for 1 h at 100 rpm, then solid-liquid phases were separated in a centrifuge for 13 minutes, at 4000 rpm, and at the end pH was measured by an electronic pH-meter and the values read 20 seconds after continuous stable value was reached.

7.2.2.9 Nutrient content

Soil nutrients content, in terms of a) phosphorus and specifying nitrogen species [b) nitrite, c) nitrate and d) ammoniacal nitrogen] was determined by Derwentside Environmental Testing Services (DETs) geology laboratory (Co Durham, UK) by a documented in-house method; in particular for a) DETS 042 by ICP-OES (inductively coupled plasma optical emission spectrometry), for b) and c) DETS 055 by ion chromatography and for d) DETS 019.

7.2.2.10 Microbiological analysis

Several matrix samples were stored for future microbiological analysis, such as cell counts or denaturing gradient gel electrophoresis (DGGE) for DNA analysis. For each sample 3 independent parts were poured into sterilised glass bottles and covered with a 1:1 solution of ethanol and sterile deionised water (autoclaved), and then left in a freezer at -20°C, as indicated in literature (Frantzen et al., 1998; Brown, 2006).

7.2.3 Chemical analysis

Analyses were performed directly at Civil and Environmental Engineering laboratory of Newcastle University. As for the gas phase, VOC identification and quantification followed the method described in Pasteris et al. (2002), in GC-FID, whereas CO_2, O_2, and SF_6 analyses were performed in GC-MS, as detailed in § A2.3.

Daily gas standards were used to calibrate instrument outputs given as peak areas. For VOCs, 0.5 ml[5] of the head space of a vial containing the same composition of pollutant mixture used for tests (§ 7.2.1), where injected into a 60 ml vial. Different volumes V_{ST} (20, 40, 60, 80, 100 µl) of this gas phase mixture were injected in GC-FID. Theoretic gas concentrations $C_{g,sat}$ in Tab. 7.1 and proper dilution factor were used for calibration.

---

[5] 0.5 ml of head space were diluted into 9.5 ml of air inside the syringe in order to avoid sorption on syringe Teflon flange during injection. 0.5 volume was chosen among different attempts.

Since the instrument was quite stable over time, average standards were used: for each i-compound, and each V_{ST}, the average of the areas recorded during test time length was calculated. Linear regression was used to interpolate them:

$$\text{Mass} = a * \text{Area} + b \tag{7.7}$$

Two different sets of standards were applied, because, during the break between the two column tests involving different matrices, maintaining operations were executed on GC, which therefore needed a new calibration set.

Three heavy compounds, 1,2,3,TMB, n-decane and n-dodecane were hard to detect in the presence of more volatile compounds. For each of them, 3 ml of single pure compound were poured in a vial, and 0.5 ml of head phase were taken via an airtight syringe. This amount was diluted in a 60 ml vial following the same procedure used for the mixture.

As for GC-MS analysis, since the instrument used was quite unstable over time, for each analysis run, one starting and one ending standard set were performed, in order to check no variations in detection during the same run. Environmental air, taken at 20 ± 2°C, was used as standard for oxygen and carbon dioxide. 1 ml of pure SF_6 gas (Sigma –Aldrich, Steinheim, D) was injected by a gastight glass syringe directly into the vial containing air [closed with Teflon Mininert valves (Supelco, Bellefonte, USA)]. Outputs (in terms of areas) from injection of 5 different V_{ST} of the air mixing (such as for VOCs) were interpolated by linear regression for CO_2 and O_2, and by a power function for SF_6.

For all the analytes, areas from 60 µl standard injections (the same volume used for test samples) were transformed into concentration values using the calculated calibration parameters. The ratio percentage between their standard deviation and average, for each i-compound, was used as analytical variation, $VC_{analysis}$ [%].

NAPL analysis on VOC mixture was performed by technicians of inner Environmental Chemistry Laboratory at Newcastle University. Samples were prepared by diluting each 5 µl of NAPL in 10 ml of dichloromethane (DCM) (Sigma –Aldrich, Steinheim, D), with a dilution factor of 2020. They were analysed in GC and different i-VOCs were recognised on the basis of their characteristic retention time on the used column.

To prepare liquid standards, pure VOC mixture was diluted in DCM as VOC: DCM in volume = $1{:}10^3$. From this diluted VOC solution 7 different standards were prepared with different dilution factors, with volume ratio of diluted VOC on DCM equal to 32.3, 9.0, 2.3, 1.5, 1.0, 0.7 and 0.4. Data were interpolated by using linear regression as similar to (7.7).

n-pentane could not be detected because of the coincidence with the detection time of DCM used as solvent. Some problems were also found on n-hexane when delay mode analysis was erroneously performed by the laboratory. To define analytical variability, 1 ml of initial pure VOC mixture was analysed in triplicate according to previous procedure. Areas were transformed into concentration values using the calculated calibration parameters, and the ratio between their standard deviation and average, for each i-compound, was used as analytical variation, $VC_{analysis}$ [%].

Details about the analytical technique, average standards and detection limits for VOC analysis and $VC_{analysis}$ for all the analytes are indicated in Appendix 2.

7.2.4 Laboratory batch microcosm experiments

Microcosms tests were performed to define adsorption and biodegradation kinetics. In both the cases, tests were performed in dark (to avoid photoxidation reactions) glass vials of ~ 63 ml (H×Ø = 9.5 cm×1.2 cm) closed with Teflon Mininert valves (Supelco, Bellefonte, USA) at room temperature (20 ± 2 ^oC) (Fig. 7.7).

Tests were performed on three different matrices: a) wet soil, b) wet soil amended with biochar in 2% w. biochar/w. dry soil, c) biochar (just for sorption tests), in triplicate for each test.

Each microcosm vial was filled with an indicated (details in § 7.2.4.2 and 7.2.4.3) amount of matrix, stored for 24 hours at room temperature, and then a 2 μl of NAPL pollutant mixture was injected by glass syringe on the empty high glass wall of the vial in order to avoid direct contact with a part of the sample; in a few minutes (2-3 minutes) no liquid drop could be seen on the vial, because the volatile compounds has evaporated into the gas phase. The liquid phase was chosen in order to avoid errors linked to gas injection, especially for less volatile compounds that could be adsorbed on syringe flange; this would have given low repeatability to the process and, therefore, not representative results (as seen in preliminary tests). Counts were performed to assure that the gas concentration of each compound in the gas volume inside the vial (due to completely volatilisation of the introduced NAPL) was less than the maximum calculated gas concentration due to $C_{g,sat}$ as from (7.2).

Soon after the screw tips were closed, 2 ml of inert SF_6 gas tracer were injected by a gas tight syringe through Mininert Valve, in order to monitor possible gas phase leaks.

After the bottle was shared, initial conditions were monitored: 60 μl of gas head space were collected via a gas tight syringe for VOC analyses (in GC) and soon after the same procedure was repeated to monitor SF_6 (in GC-MS). Using the same method, gas samples were taken every day and directly analysed to monitor microcosm gas phase concentration changes. For VOCs, II standard set was used for data elaborations (§ A2.3).

Real vial volume (V_{vial}) was evaluated for each vial by filling it with water and weighing it; water volume (V_{water}) was evaluated according to §7.2.2.6 on 3 replicates for each matrix; solid volume V_{solid} was calculated as dry mass M_{solid} divided by solid density (§7.2.2.5) and real air volume V_{gas}, by using:

$$V_{gas} = V_{vial} - V_{water} - V_{solid} \tag{7.8}$$

***Fig. 7.7**: microcosms for sorption and biodegradation tests.*

7.2.4.1 Blank vials

Blank controls were performed to account for sorption on glass and lids. Two empty vials were autoclaved at 120 °C for 30 min, to destroy any biological activity, as in preparation for sorption tests.

Blank vials were considered as reference to know the gas concentration really present in the gas phase of vials. For each i-VOC, the average and the standard deviation of the daily sampled gas concentrations were calculated for each sample. The mean between the two replicates gave the calculated starting condition for microcosms tests: $C_{blank,i}$. Error on $C_{blank,i}$ ($\sigma C_{blank,i}$) was calculated as the maximum between the standard deviation on 2 replicates and the propagation of variables' uncertainties (§ A3); the considered errors were both $VC_{analysis}$ and standard variation of each duplicate average concentration.

The blank tests lasted 8 days.

7.2.4.2 Sorption tests

Filled microcosm vials were autoclaved at 120 °C for 30 min to destroy any biological activity. Aluminium foil and screwed plastic caps were used to close the vials during treatment, but they had to be left slightly open in order to prevent vial breaking due to pressure conditions in the autoclave. Losses in weight after this treatment were measured and original moisture content was therefore replaced by sterilised demineralised water.

Vials were filled with: a) 30 g of wet soil, with $w = 0.111 \pm 0.007\ g_{water}\ g_{dry\ soil}^{-1}$ (as standard deviation), b) 3 g and b') 15g of biochar-amended soil (in duplicate), with $w = 0.126 \pm 0.003\ g_{water}\ g_{dry\ amend\ soil}^{-1}$ (as standard deviation), c) 0.25 g of dry biochar.). Material amount was chosen in order to assure that gas phase concentrations were above the detection limit and to observe the effect of compound/adsorbent material ratio. Details are indicated in Tab. 7.3. The tests lasted for a period of 12 days.

For each j-triplicate of each k-matrix, only stationary concentrations (starting at t_{stat}) were chosen, in order to define adsorption at equilibrium conditions. t_{stat} was established excluding the initial concentrations that, included in average $C_{gas\_stat,i,j,k,}$ would have given a standard deviation higher than the analytical variation. For each i-VOC, the average on the stationary sampled gas concentrations were calculated, giving $C_{gas\_stat,i,j,k}$ [μg ml_{gas}^{-1}].

The amount in the water phase $C_{water,i,j,k}$ was calculated as [μg ml_{water}^{-1}]:

$$C_{water,i,j,k} = C_{gas\_stat,i,j,k} / H_i \tag{7.9}$$

for H_i see values in Tab. 7.2.

The mass adsorbed on k-matrix $M_{i,j,k}$ [μg] was given by:

$$M_{i,j,k} = (C_{blank,i} - C_{gas\_stat,i,j,k)}* V_{gas,j,k} - C_{water,i,j,k}* V_{water,j,k} \tag{7.10}$$

It was assumed a linear simple relationship between dissolved and solid phases as indicated in (2.7) and therefore each $Kd_{i,j,k}$ [(μg g_{solid}^{-1})*(μg $ml_{gas}^{-1})^{-1}$ = ml_{gas} g_{solid}^{-1}] was evaluated as:

$$Kd_{i,j,k} = C_{solid,i,j,k} * C_{water,i,j,k}^{-1} \tag{7.11}$$

where $C_{solid,i,j,k}$ is the concentration of i-adsorbed on k-solid:

$$C_{solid,i,j,k} = M_{i,j,k} * M_{solid,j,k}^{-1} \tag{7.12}$$

For each matrix and each compound, average adsorption constants were calculated, considering the effective j-replicates (J_k):

$$Kd_{i,k} = \frac{\sum_{j=1}^{Ji,k} Kd_{i,j,k}}{J_k} \tag{7.13}$$

Error on $Kd_{i,k}$, $\sigma Kd_{i,k}$, was calculated as standard deviation among J_i replicates.

Kd_i from soil tests (a) where compared with theoretical values ($Kd_{est,i,soil}$) got from an analytical relationship (Wiedemeier et al., 1999), function of sing f_{oc} (§ 7.2.2.7) and K_{ow} (they were used average values of in Tab. 7.2):

$$Kd_{est,i,soil} = 1.72 * f_{oc} * 10^{0.82*\log K_{ow}+0.14} \tag{7.14}$$

For b and b' tests, in order to choose the more representative Kd_i, their estimated values $Kd_{est,i,soil+biochar}$ were calculated on a weighed average basis:

$$Kd_{est,i,soil+biochar} = 2\% * Kd_{i,biochar} + 98\% * Kd_{i,soil} \tag{7.15}$$

and they were compared with experimental ones.

7.2.4.3 Biodegradation tests

Vials were filled with: a) 30 g of wet soil, with w = 0.107 ± 0.003 g_{water} $g_{dry\ soil}^{-1}$ (as standard deviation), b) 15g of biochar-amended soil, with w = 0.126 ± 0.003 g_{water} $g_{dry\ amend\ soil}^{-1}$ (as standard deviation). Details are indicated in Tab. 7.3. The tests lasted for a period of 6-10 days according to vial performance.

During tests CO_2 and O_2 were also monitored i) to exclude potential risk of oxygen limitation available just in the vial head space volume and ii) monitor evolution of biological activity. Results were expressed as percentages in volume (equal to mole ratio percentages) from perfect gas law (7.2).

They were used first order degradation rates in gas phase, $K_{deg,gas,\ i,j,k}$ [s^{-1}], according to (3.27), as it was suggested in other similar evaluations (Pasteris et al., 2002; Hoener et al., 2003).

The solution of (3.27) is:

$$\ln \frac{C_{gas,i,j,k}}{C_{0gas,i,j,k}} = -K_{deg,gas,i,j,k}(t - t_0) \tag{7.16}$$

$$\ln C_{gas\_i,j,k} = -K_{deg,gas,i,j,k}\, t + K_{deg,gas,i,j,k}\, t_0 + \ln C_{0gas,i,j,k} \tag{7.17}$$

where 0 subscript indicates initial condition.

(7.17) shows that $K_{deg,gas,i,j,k}$ is the slope of a $\ln(C_{gas,z,i,j,k})$-t line, and therefore linear regression was used for modelling the relationship between these two variables, applying minimum square theory by the use of excel (Microsoft). This function returned also standard error of the estimation, $\sigma K_{deg,gas,i,j,k}$. For compounds it was evidenced an initial lag time, lasting from till t*, due to volatilisation from liquid phase and reaching equilibrium with adsorption. Initial data (before t*) were therefore excluded; undetectable values (lower than detection limit, d.l., indicated in § A2.3) were disregarded too. For highly degradable compounds, for which concentrations at second sampling time were already lower than the d.l., that concentration was set equal to d.l.. It was then supposed that they had reached d.l. exactly when the second sample was taken, and therefore for those compounds $K_{deg,gas,i,j,k}$ may be underestimated. No further intermediate sampling times could have been taken because of technical GC run length.

Since microorganisms use substrates dissolved in water, the first-order degradation rate was referred to the aqueous phase; passage from gas-phase to water-phase first order degradation rate, $K_{deg,water,i,j,k}$ [s^{-1}], was calculated on the basis of the following relationships:

$$\frac{d(V_{gas,j,k} * C_{gas,i,j,k} + V_{water,j,k} * C_{water,i,j,k} + M_{solid,j,k} C_{solid,i,j,k})}{dt} = -K_{\deg,wat,i,j,k} * V_{water,j,k} * C_{water,i,j,k} \tag{7.18}$$

where $V_{gas,k}$, $V_{water,k}$ and $M_{solid,k}$ are the averages of $V_{gas,j,k}$, $V_{water,j,k}$ and $M_{solid,j,k}$ on the 3 replicates. Eq.7.18 becomes:

$$\frac{d\left(V_{gas,j,k} * C_{gas,i,j,k} + V_{water,j,k} * C_{gas,i,j,k} / H_i + M_{solid,j,k} * Kd_{i,k} * C_{gas,i,j,k} / H_i\right)}{dt} =$$

$$= -K_{deg,wat,i,j,k} * V_{water,j,k} * C_{gas,i,j,k} / H_i \tag{7.19}$$

$$\frac{dC_{gas,i,j,k}}{dt} = -K_{deg,wat,i,j,k} * \frac{V_{water,j,k} / H_i}{V_{gas,j,k} + V_{water,j,k} / H_i + M_{solid,j,k} * Kd_{i,k} / H_i} * C_{gas,i,j,k} \tag{7.20}$$

and calling $f_{water,i,j,k}$ the mass fraction of each compound in the aqueous phase:

$$f_{water,i,k} = \frac{V_{water,j,k} * C_{gas,i,j,k}}{V_{gas,j,k} * C_{gas,i,j,k} + V_{water,j,k} * C_{water,i,j,k} + M_{solid,j,k} * C_{solid,i,j,k}} =$$

$$= \frac{1}{\frac{V_{gas,j,k} * H_i}{V_{water,j,k}} + 1 + \frac{M_{solid,j,k} * Kd_{i,k}}{V_{water,j,k}}} \tag{7.21}$$

(7.20) becomes

$$\frac{dC_{gas,i,j,k}}{dt} = -K_{deg,wat,i,j,k} * f_{water,i,j,k} * C_{gas,i,j,k} = -K_{deg,gas,i,j,k} * C_{gas,i,j,k} \tag{7.22}$$

and therefore

$$K_{deg,water,i,j,k} * f_{water,i,j,k} = K_{deg,gas,i,j,k} \tag{7.23}$$

finally giving

$$K_{deg,water,i,j,k} = \frac{K_{deg,gas,i,j,k}}{f_{water,i,j,k}} \tag{7.24}$$

For each matrix and each compound, average $K_{deg,water,i,k}$ on replicates was calculated. $K_{deg,water,i,k}$ errors, $\sigma K_{deg,water,i,k}$, were estimated as the maximum between standard deviation and error propagation in the average from $\sigma K_{deg,gas,i,j,k}$ and measures uncertainties in $f_{i,j,k}$ (according to error theory in Appendix 3).

***Tab. 7.3**: summary of composition of microcosm tests.*

	Vial	**Weight (W) of wet solid matrix**	**W of dried matrix**	**V of water**	**V of gas in vial**
			$M_{solid,j,k}$	$V_{water,j,k}$	$V_{gas,j,k}$
		g	**g**	**ml**	**ml**
blank tests	**B1**	0	0	0.000	64.200
	B2	0	0	0.000	64.000
sorption tests	**a1**	30	26.995	3.005	50.203
	a2	30	26.995	3.005	50.503
	a3	30	26.995	3.005	50.703
	b1	3	2.665	0.335	62.702
	b2	3	2.665	0.335	62.352
	b3	3	2.665	0.335	62.602
	b'1	15	13.372	1.678	56.686
	b'2	15	13.283	1.667	56.436
	c1	0.28	0.2510	0.03	63.375
	c2	0.28	0.2516	0.03	63.473
biodegradation tests	**a1**	30	27.092	2.908	50.562
	a2	30	27.092	2.908	50.162
	a3	30	27.092	2.908	50.262
	b1	15	13.327	1.673	56.811
	b2	15	13.327	1.673	56.711
	b3	15	13.327	1.673	55.711

7.2.5 Laboratory column experiments

7.2.5.1 Experimental apparatus

After batch tests, column experiments were performed using the same glass column for each test, with the geometry indicated in Fig. 7.8, placed in vertical position.

The column shape changed along vertical axis z; at the bottom there was a neck connected to a funnel, and then a cylinder 45 cm long, and with a 9.4 cm inner diameter. The column had 4 different lateral sampling ports each placed 7 cm from the top of funnel shape (z_0). Each port was sealed with inert GC septa (injection rubber plugs, Thermogreen LB-2, Supelco, Bellefonte, USA) and the empty volume between the column core and the septum was filled with glass wool in order to avoid dead volumes.

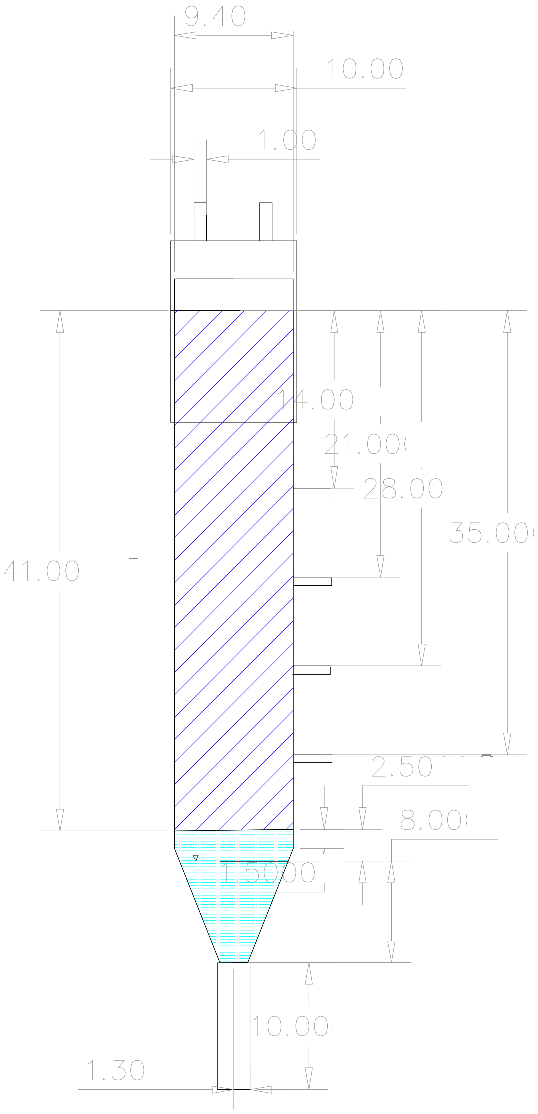

Fig. 7.8: *column geometry details.*

Tests with two different matrices were performed in the fume cupboard at 20 ± 2 °C. The first tested matrix was soil, and the other soil amended with 2% biochar on a dry weight basis. For each column two different boundary conditions (b.c.) were posed (Fig. 7.9): the first with column top left open, and, the other with a beaker placed on it. This covering had an inner diameter slightly bigger than the external one of the column, so that a certain gap remained between these two elements (Figs. 7.8 and 7.9.b). The beaker worked as a sort of static non stationary chamber (§ 4.2.2.1) and was used to determine flux emitted from the column; it had, in fact, two sampling ports on it, closed by the same GC septa as the lateral ones. A picture of the two column conditions may be seen in Fig. 7.10.

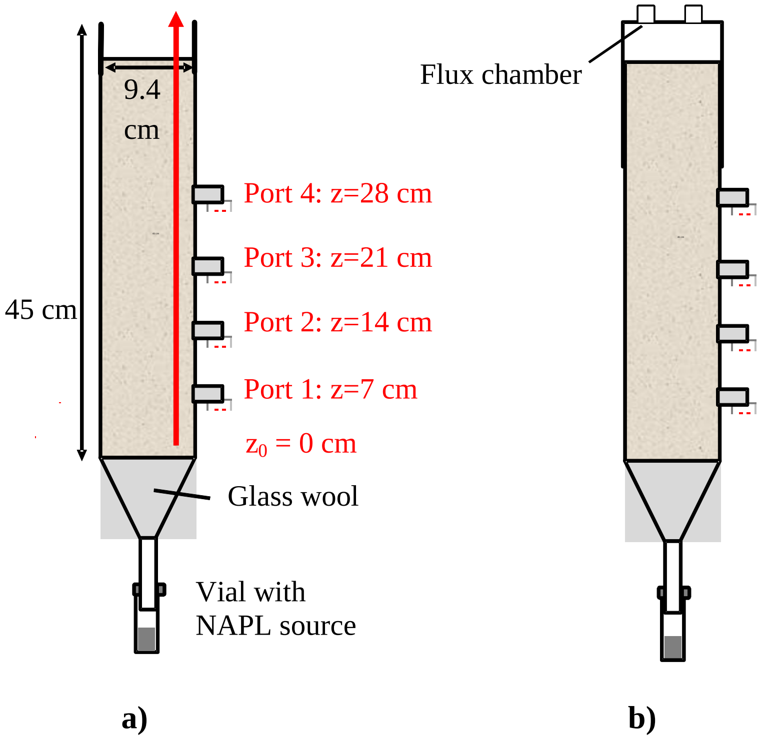

Fig. 7.9: *schematic drawing of the column experimental apparatus, with both open (a) and closed by a beaker (b) boundary conditions.*

7.2.5.1 Filling up

Before filling up the column, the funnel was packed with glass wool to separate the matrix from the contaminative source (§ 7.2.5.3), then, for both matrices, the core was homogeneously packed up to 42.7 cm from z_0, to a total volume of 2.96 l.

For tests with soil, the column was filled with 4051.2 kg of wet soil, reaching a soil bulk density $\rho_{b,soil\ col}$ of 1.367 kg d.w. m^{-3}, with the water content indicated in § 7.3.1.5, being 21.6% ($S_{w,\ soil\ col}$) of the total porosity (0.48 $m^3\ m^{-3}$) which was calculated from (7.6) and knowing $\rho_{b,soil\ col}$ and ρ_s indicated in § 7.3.1.4.

For tests with biochar-amended soil, the column was filled with 4273.2 kg of wet amended soil, achieving a soil bulk density $\rho_{b,soil+biochar\ col}$ of 1.442 kg d.w. m^{-3}, with the water content indicated in § 7.3.1.5, being 35.4% ($S_{w,\ soil+biochar\ col}$) of the total porosity (0.44 $m^3\ m^{-3}$).

After packing, the soil column was left undisturbed for 6 days to monitor the background respiration. At the end of open b.c. the source vial was removed and column behaviour was monitored for 2 days before starting with closed b.c..

a) **b)**

Fig. 7.10: *pictures of column apparatus for both open (a) and closed by a beaker (b) boundary conditions.*

a) **b)**

Fig. 7.11: *pictures of some details of column apparatus: VOC source at the bottom of the column (a) and beaker with two sampling ports to impose closed boundary conditions (b).*

7.2.5.2 VOC Source

After initial condition monitoring (§ 7.2.5.4), on day 0, a vial containing 10 ml of the pollutant mixture (§ 7.2.1) was tightly connected to the bottom of the funnel shaped end of the column using a Teflon-lined rubber seal (Fig. 7.11.a).

Before changing boundary conditions or starting a new matrix test, the source was replaced in order to assure that the initial conditions of each experiment were similar; to check the availability of all the compounds in the LNAPL phase of the source, before source positioning and soon after its removal, a 1 ml NAPL sample of it was taken, and analysed in three replicates according to § 7.2.3.

7.2.5.3 Column monitoring

Tracer tests

At the end of soil closed column experiment, tracer tests were performed: a vial with 5 ml of SF_6 was tightly connected to the bottom of the column similarly to § 7.2.5.3 and, with high frequency, gas samples were taken from different ports. SF_6 experiments were used to verify analytical function used to define tortuosity and calibrate the gap area between column and beaker, both set into the numerical code.

For both the matrices, still with closed column, a similar test was repeated in duplicate, with a vial, at the bottom, containing CO_2 gas. The exact volume of gas is unknown, because the vial had to be left open to connect it to the column, which thus made the tests independent of each other. These tests were used to verify CO_2 transport model hypothesis (§ 7.2.5.5).

Background conditions

At first, after packing, the soil column was left undisturbed for 5 days and just biological parameters (O_2 and CO_2) were monitored, in each port, to record the background respiration. Closed b.c. was imposed for 3.2 days, then the beaker was taken off and open boundary condition was monitored too.

Soil gas sampling

After background monitoring, both biologic parameters and the 12 chemical compounds began to be monitored daily.

The reactive transport of VOC vapours was studied by taking air samples from interstice gas through a 100 µL gastight glass syringe (Hamilton) (Fig. 7.12.a). Volumes varied from 20 to 60 µl in order to collect a mass included inside the analytical range. Samples were collected from each port and, relatively to closed column, from top beaker too (Fig. 7.12.b). The material of GC septa was elastic enough to guarantee perfect gas tightness for the duration of the test, also without changing them after sampling punctures, as shown by previously experiences (conducted by Dr. David Werner). They were analysed according to the procedure indicated in § 7.2.3. To avoid perturbation of VOCs measurements due to adsorption on sampling medium, good gas sampling behaviour was followed, such as dilution of sample gas with clean air inside the same sampling syringe, or let syringe components split between one sampling and the next.

Similarly, other gas samplings were taken for analyses of CO_2 and O_2 in another instrument (§ 7.2.3).

Soil open b.c. lasted 13 days, closed b.c. 14 days, and for biochar-amended soil they lasted respectively 14 and 15 days. In order to avoid cross contamination, each day sampling started from higher ports, with lower VOC gas concentrations, to lower ones.

Matrix final condition

At the end of each matrix column test, when the column content was emptied, matrix samples were taken in correspondence with different sampling ports, in order to check its final conditions. In particular pH analysis (according to § 7.2.2.8) and moisture content (§ 7.2.2.6) were performed), and samples for possible future microbiological analyses (§ 7.2.2.10) were stored.

a) **b)**

Fig. 7.12*: gas sampling with 100 μL gastight glass syringe from later ports (a) and one port of beaker on column top for closed boundary conditions (b).*

7.2.5.4 Modelling code

The transport of VOC vapours inside soil and biochar-amended soil was modelled by a transport code to understand column results better.

In the code the matrix is described as a porous medium consisting of soil air, soil water and the solid matrix, in agreement with soil description of § 3.2.1, and all the solid surfaces are hypothesized as being wetted (as in Mendoza et al., 1990). The VOC partitioning among these phases may be described by an instantaneous, reversible linear equilibrium, as described in (3.14). This is affected by matrix properties too and, as it is shown in Fig. 7.13.

As described in § 3.3.2, for this case transport mechanism is due to diffusion in the gas phase and there is a net loss due to degradation occurring as (3.27) just in the water phase where substrates are available for biomass. The addition of biochar, increasing sorption capacity, reduces the VOCs concentrations in both soil air and soil water, retarding in this way the spreading of VOC vapours and potentially the VOC biodegradation.

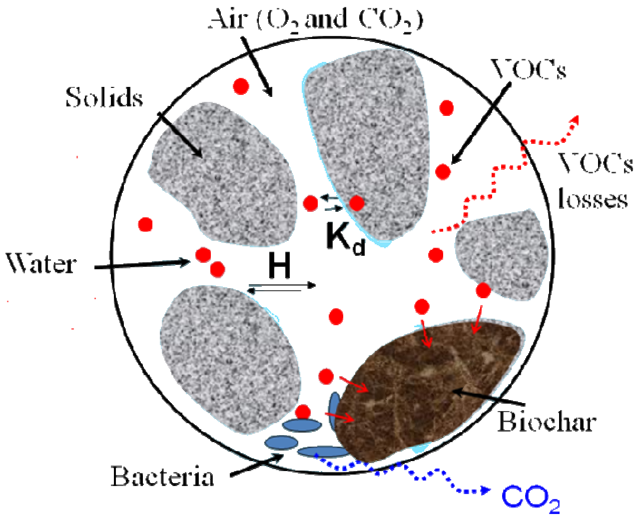

Fig. 7.13*: conceptual representation of soil constituents and processes affecting the fate of VOCs in soils, also considering the effects of biochar.*

It was supposed that the amount of degraded VOCs was completely mineralized, without giving subproducts. Just 60% of degraded carbon became CO_2; 40% were hypothesized becoming transformed in new biomass (as revealed from previous studies performed at Newcastle University). CO_2 and also SF_6 transport was simulated in a way analogous to VOCs, considering for the latter just diffusion phenomenon, whereas for the former also carbon equilibrium with other water phases. In particular the amount of CO_2 in equilibrium with carbon anionic forms was taken into account:

$$CO_{2(gas)} + H_2O \leftrightarrow H_2CO_3 \quad (7.25)$$

$$H_2CO_3 \leftrightarrow H^+ + HCO_3^- \quad (7.26)$$

$$HCO_3^- \leftrightarrow H^+ + CO_3^{2-} \quad (7.27)$$

K_1 and K_2 constants described the equilibrium between molar concentrations (indicated with [ ]) respectively in (7.26) and (7.27), as:

$$K_1 = [H^+][HCO_3^-]\,[H_2CO_3]^{-1} \quad (7.28)$$

$$K_2 = [H^+][CO_3^{2-}]\,[HCO_3^-]^{-1} \quad (7.29)$$

where $pK_1= 6.3$ and $pK_2= 10.25$.

From (7.28) and (7.29) respectively they were derived:

$$[HCO_3^-] = H_{CO2}*C_{gas,CO2} * \theta_g / \theta_w * 10^{pH-pK_1} \quad (7.30)$$

$$[CO_3^{2-}] = [HCO_3^-] * 10^{pH-pK_2} \quad (7.31)$$

The total mass of CO_2 was therefore the sum of the mass as $CO_{2(gas)}$, H_2CO_3, HCO_3^-, CO_3^{2-} (all these last three forms stay in aqueous phase); to find just the free volatile amount of the total mass of CO_2, this had to be divided for retardation factor due to repartition, R:

$$R= \theta_g+ \theta_w /H_{CO2}*(1+10^{(pH-pK1)+}10^{(2*pH- pK1-pK2)}) \quad (7.32)$$

Eventual precipitation or dissolution of solid phase $CaCO_3$ was neglected.

SF_6 and CO_2 physical parameters used in model are indicated in Tab. 7.2.

A monodimensional (function of z coordinate) finite difference model was developed to simulate the VOC concentration in the column study as a function of time. Numerical procedure to solve ordinary differential equations was an explicit procedure based on Euler method (Cheever, 2010), using central differencing for the first and second derivative terms. As for geometry, the column was divided in 70 z nods, with a grid-spacing (the distance between two contiguous z) of 1 cm, and it was assumed constant in diameter over the whole column length; however, the "extra volume" in the funnel neck (z from 1 to 12) was modelled as filled by an inert solid medium, whose θ_a (-) was equal to 0.0191, θ_w (-) was equal to 0, θ_s (-) was equal to 0 and τ_a (-) was equal to 1. Funnel part (z from 13 to 21), partially fill by glass wool, was considered in a similar way; real porosity was derived by the amount of water necessary to fill it (similarly to § 7.2.2.4), equal to 0.6. Its different shape in z was modelled at each j step as an inert porous solid medium, whose θ_a (-) changed with z. The other parameters were the same of funnel neck part. The τ_g value was estimated from the total and air-filled porosities according to the relationship (3.23) and verified by data from tracer tests (§ 7.2.5.4).

As far as b.c. were concerned, at the bottom, z =1:2, a no flow condition was posed to simulate the bottom of source vial. Then, z =2:21, the vial and funnel boundary condition was determined by the VOC gas phase concentration in the gas space under the matrix filled column, which was calculated according to (2.1). For each time step the amount of pollutants in the non-aqueous phase liquid (NAPL) source was recalculated based on the volatilization flux at the bottom of the column. The open upper b.c. was determined by assuming constant zero VOC concentration at the top of the column (for z from 65 to 70), because it was kept under the fume hood. As for the closed b.c., the beaker created two different compartments at the top of the column. The top one was hypothesized as well-mixed volume (due to its small height); the other was a slice between column and beaker through which some gases were lost. The section of this cavity wall, called gap area, was quantified from the SF_6 tracer experiments y a trial and error process. Over the column, for z from 65 to 69, the concentration was calculated from mass balance among vapours coming from the source, tapped by the beaker basis (simulated by a no flow condition at z = 70) and what was lost. Leaking flux was simulated as the results of diffusion transport in air (without solid matrix), from the well-mixed volume toward outside the column, along a distance equal to the length of the cavity wall, by using (3.18). VOCs concentrations outside the gap volume were posed zero since it indicated a position under the fume hood.

Gas concentration, tortuosity and each phase content were therefore functions of space (z coordinate). For the performed tests the governing equation for transport (3.29) and (3.30) became therefore:

$$\left(\theta_g(z)+\frac{\theta_w(z)}{H_i}+\frac{Kd_i\rho_s\theta_s(z)}{H_i}\right)\frac{dC_{ig}(z,t)}{dt}=$$

$$=\frac{d\left(\theta_g(z)\,\tau_g(z)D^{g}{}_{i}\,\frac{dC_{ig}(z,t)}{dz}\right)}{dz}-k_{deg,water}\theta_w(z)\frac{C_{ig}(z,t)}{H_i} \qquad (7.33)$$

where θ_s is

$$\theta_s = V_s\, V_{tot}^{-1} = \rho_b * \rho_s^{-1} \qquad (7.34)$$

and other symbols have been already introduced in Chapter 3.

Parameters used in model were defined as follows: H_i and D_i^g from literature indications (Tab. 7.2); θ_a from characterization data (§ 7.2.5.2) and (3.3); θ_w from relation in Fig. 3.1 and θ_a; θ_s from (7.34), ρ_b in § 7.2.5.2 and ρ_s (§ 7.3.1.4), and finally batch test results for Kd (Tab. 7.14) and $K_{deg,water}$ (Tab. 7.17).

Switching from one matrix setting to another was made by removing or adding % signs at the appropriate lines for the Kd (lines 42-45), $k_{deg,water}$ (lines 48-52) or initial moles (lines 118-121).

7.3 Results

7.3.1 Material Characterization

7.3.1.1 Biochar petrography and screening carbon fingerprint

The petrography microscopy research revealed a very brittle material, where the dominating particles were isotropic networks (Figs. 7.14.a and 7.14.b), similar to Fig. 7.6, typically deriving from the combustion of woody tissues, surrounded by char fragments. Tar- (Fig. 7.14.c) and coke-like (Fig. 7.14.d) particles, due to heating in poor oxygen conditions, displayed in fine mosaic and anisotropic structures, were also present. Some mineral grains (Fig. 7.14.e-f-h), unfused/partially fused thermally altered wood particles (Fig. 7.14.g), and coal particles resembling sapropelic-type (Fig. 7.14.h), were also identified inside the matrix of network fragments.

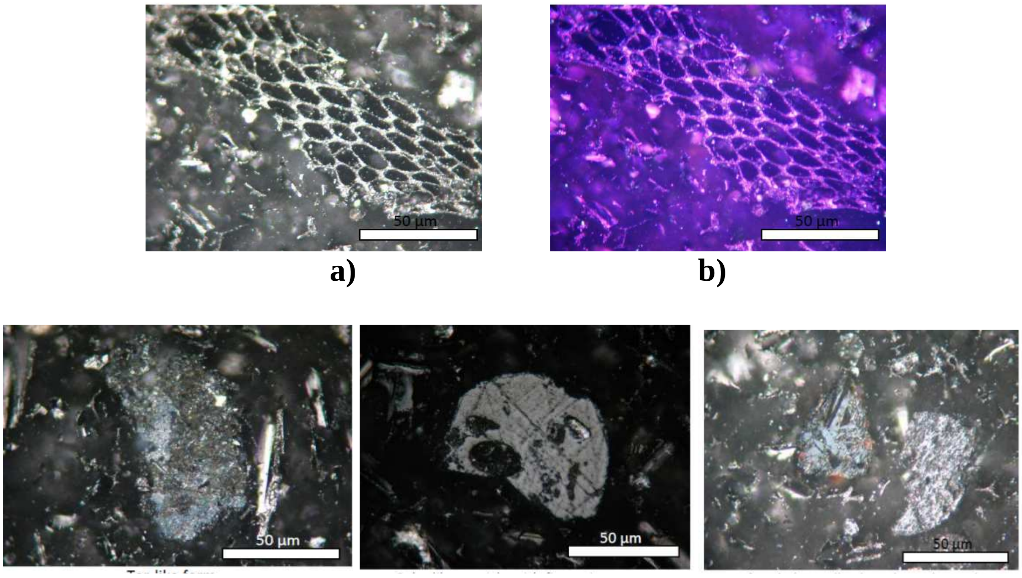

a) **b)**

c) **d)** **e)**

***Fig. 7.14**: continue.*

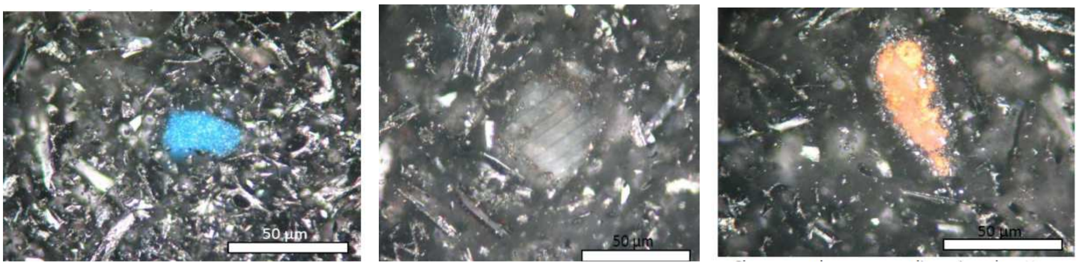

f) **g)** **h)**

Fig. 7.14: *results of biochar petrography microscopy: a) wood derived char network; b) same as a) but analysed on λ retarder plate; c) tar-like form; d) coke-like anisotropic particle; e) mineral grain in groundmass of chars; f) mineral crystal (calcite); g) unfused thermally altered wood; h) mineral matter surrounded by sapropelic-type coal.*

TG-QMS analysis, processed by Gram's software (Fig. 7.15), revealed that resistant carbon was the dominant form, present at 68% (typical in high temperature pyrolysis), recalcitrant C was present at 21%, the labile content was very low (3%), no inorganic matrix was found and 8% of the content was not identified.

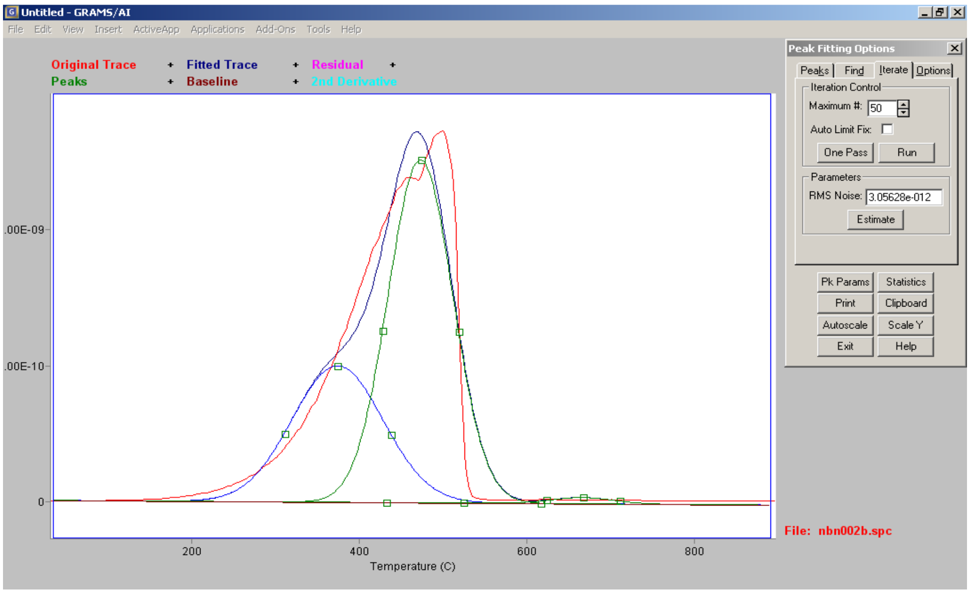

Maximum #: 50

Auto Limit Fix: ☐

RMS Noise: 3.05628e-012

File: nbn002b.spc

Fig. 7.15: *Grams software results to interpret TG_QMS analysis.*

C: N: S was found to be 288:4:1, therefore indicating a very high C/N ratio, 76.82 and a poor nutrient supply.

7.3.1.2 Soil grain size distribution

Tab. 7.4 shows the results of soil grain size distribution tests indicating for each granular range net weight M_j retained on the smaller opening size sieve. Tab. 7.5 indicates passing percentages P_i as described in § 7.2.2.3, as average [%], standard deviation [%] and variation coefficient [%] on the 2 replicates. Fig. 7.16 shows grain size distribution curves, in semi-logarithm scale, where on x-axis there is sieve mesh size and on y-axis P_i.

Tab. 7.4: *results of soil grain size distribution with indication of net weight M_j [g] retained on the smaller sieve mesh size of each indicated range.*

	> 2000 µm	**2000 - 1000 µm**	**1000 - 600 µm**	**600 - 425 µm**	**425 - 212 µm**	**212 - 63 µm**	**< 63 µm**	**total**
Sample A	105.2120	77.2820	78.7546	46.2190	97.4422	43.3234	6.7239	454.9571
Sample B	121.6609	80.0776	84.3753	40.0772	91.6022	32.9342	4.6777	455.4051

Tab. 7.5: *weight percentages of soil P_i and its statistics (average, standard deviation and variation coefficient – VC-) with grains lower than i-sieve.*

	< 4000 µm	**< 2000 µm**	**< 1000 µm**	**< 600 µm**	**< 425 µm**	**< 212 µm**	**< 63 µm**
Sample A [%]	100	77	60	43	32	11	1.5
Sample B [%]	100	73	56	37	28	8	0.9
Average [%]	100	75	58	40	30	10	1.2
Standard deviation [%]	0	2	2	3	2	1	0.3
VC [%]	0	2	4	7	7	15	23

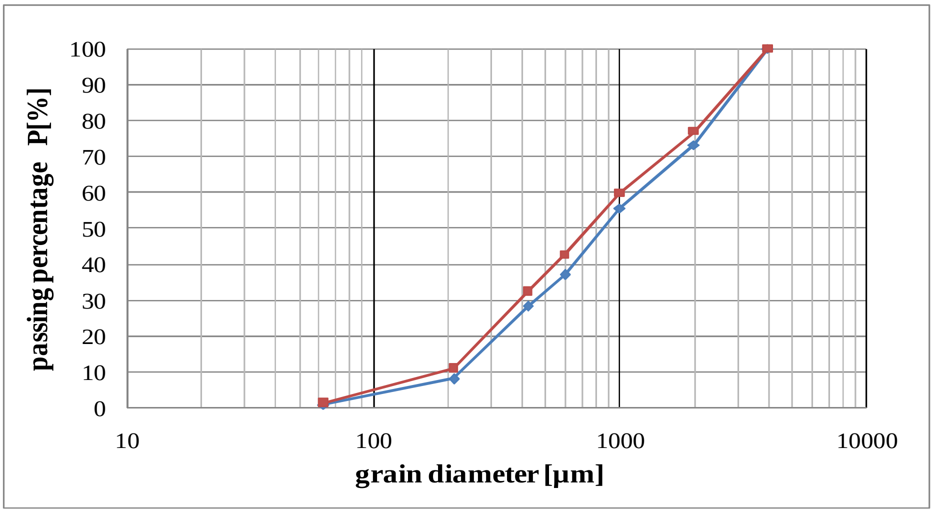

Fig. 7.16: *grain size distribution curves for tested soil.*

Analyzed soil was composed mainly of fine gravel (25% as dry weight -d.w.), sand (74 % divided in 17% of very coarse sand, 27 % of coarse sand, 21% of middle sand and 8% of fine one) and 1% of silt.

From grain size distribution graph, 60% of passing grains (P_i = 60%) had diameter equal to 1140 µm (D_{60}) and for P_i = 10% (D_{10}) equal to 220 µm. Uniformity coefficient $U = D_{60}/D_{10}$ resulted in 5.18 at the range between uniform and less uniform soils.

The results from DETs geology laboratory reported a soil composed of sand 93%, silt 6% and 1% clay. The poor correspondence with our results confirmed lack of uniformity in soil used.

7.3.1.3 Soil porosity

Results of tests on soil samples, made as indicated in § 7.2.2.4, are indicated in Tab. 7.6.

Tab. 7.6: *results of tests for soil porosity; symbols according to § 7.2.2.4.*

Sample	**V (ml)**	**V' (ml)**	**f (-)**
A	12.3	3.55	0,290
B	21.0	6.70	0,319
C	17.5	6.40	0,366

Average soil porosity value was 0.32 ± 0.03 (as standard deviation), with a variability of 9.6%.

7.3.1.4 Soil and biochar density

Results for tests on different soil and biochar samples, made as indicated in § 7.2.2.5, are indicated in Tab. 7.7.

Tab. 7.7: *results for soil and biochar solid density; symbols according to § 7.2.2.5.*

matrix	**sample**	**T**	**ST**	**WT**	**WST**	**ρ_s**
		g	**g**	**g**	**g**	**g ml^{-1}**
soil	**A**	32.1	42.2	81.3	87.5	2.589
	B	31.2	41.2	81.1	87.2	2.564
	C	34.1	44.1	82.9	89	2.564
	D	33	43.1	82.3	88.6	2.657
	E	27.1	37.1	76.7	82.8	2.564
	F	32.6	42.6	82.6	88.8	2.631
biochar	**A**	34.6	35.3	84.4	83.2	0.368
	B	25.4	25.8	75.4	74.3	0.266
	C	25.4	26.7	74.6	73.0	0.448

For soil, average solid density was 2.62 ± 0.04 kg l^{-1}(as standard deviation), with a variability of 1.4%. According to (7.6), using data in § 7.3.1.3, bulk density was 1.77 ± 0.09 kg l^{-1} (due to error propagation, as in Appendix 3), with a variation coefficient 4.8%. For biochar, just solid density was determined, equal to 0.36 ± 0.07 kg l^{-1} (as standard deviation), with a variability of 20.6%.

For soil with 2% biochar ρ_s was calculated according to a weighed average to 2.57 ± 0.04 kg l^{-1} (as error propagation from error on the two materials ρ_s), with a variability of 1.4%.

7.3.1.5 Soil and amended soil moisture

Test results to define initial water content of soil and biochar-amended soil, according to method in § 7.2.2.6, are indicated in Tab. 7.8.

Initial soil moisture was 8.2 % ± 0,2% (g_{water} $g^{-1}{}_{dry\ soil}$ %) as standard deviation, corresponding to a variation coefficient of 2.4%; that one of soil amended with 2% biochar was 12.11% ± 0,2% (g_{water} $g^{-1}{}_{dry\ soil}$ %) as standard deviation, corresponding to a very low variation coefficient, 0.13%

7.3.1.6 Soil organic carbon content

Results of soil organic content ratio (f_{oc}), made as indicated in § 7.2.2.7, are indicated in Tab. 7.9.

Soil organic carbon content was equal to 1.18% ± 0.03% (g_{oc} $g^{-1}{}_{dry\ soil}$ %) as standard deviation, with a percentage variability of 2.8%. Results from DETs geology laboratory (0.8%) gave an underestimation of 32% as a reference to inner evaluation.

***Tab. 7.8**: results of soil and biochar-amended soil initial moisture determination.*

	Sample	**Wet soil**	**Dry Soil**	**Water content**	**w**
		g	**g**	**g**	**%**
soil	**A**	54.99	25.21	1.99	7.89
	B	42.99	25.11	2.09	8.32
	C	50.09	25.11	2.09	8.32
	D	54.99	25.21	1.99	7.89
Soil + 2% biochar	**A**	20.4	18.2	2.2	12.09
	B	18.5	16.5	2.0	12.12
	C	18.5	16.5	2.0	12.12

***Tab. 7.9**: results of soil organic content ratio determination; symbols according to § 7.2.2.7.*

Sample	Dry soil	Muffled soil	VS	f_{OC}
	g	g	g	%
A	45.2363	44.3328	0.9035	1.158
B	45.1038	44.1493	0.9545	1.227
C	45.1537	44.2533	0.9004	1.156

7.3.1.7 Natural/amended soil and biochar pH

Results for tests on soil, soil with 2% of biochar and pure biochar samples, made as indicated in § 7.2.2.8, are indicated in Tab. 7.10.

***Tab. 7.10**: pH test results for soil, soil with 2% of biochar and pure biochar; A, B, C: 3 replicates, SD: standard deviation, VC: variation coefficient [%].*

	A	B	C	average	SD	VC
	-	-	-	-	-	%
soil	8.01	7.94	7.92	7.96	0.04	0.48
soil + biochar	8.12	8.10	8.06	8.09	0.02	0.31
biochar	9.20	9.32	9.02	9.2	0.1	1.3

Soil had a slightly basic pH whereas biochar had a higher one that could impede biological activity. Soil with 2% of biochar still has got a pH similar to soil, even if it is higher than results from mass balance.

7.3.1.8 Nutrient content

The soil nutrient content is indicated in Tab. 7.11 as it was reported on DETs geology laboratory’s certificates of Analysis.

***Tab. 7.11**: soil nutrient content (from DETs geology laboratory) as mg $kg^{-1}_{dry\ soil}$ (d.s.).*

Phosphorus	Nitrite	Nitrate	Ammonial Nitrogen	Total oxidised nitrogen
P	NO_2^-	NO_3^-	$N\text{-}NH_4^+$	Oxidized N
mg $kg^{-1}_{d.s.}$	mg $kg^{-1}_{d.s.}$	mg $kg^{-1}_{d.s.}$	mg $kg^{-1}_{d.s.}$	mg $kg^{-1}_{d.s.}$
490	< 1.00	3.9	6.7	3.9

Total nitrogen content was lower than 7.89 mg N $kg^{-1}_{dry\ soil}$ (equal to 0.00079% of dry soil weight), corresponding (by using f_{oc} in § 7.3.1.6) to 0.067% of organic content weight. As for phosphorus, its total content was 0.049% of dry soil weight, consistent with common sandy soil (INEA, 2010), corresponding to 4.1% of organic content weight and it was 62 times higher than total nitrogen content. Therefore, the used soil seemed really poor especially in nitrogen content, because literature indicates an optimum ponderal ratio between organic biodegradable carbon, nitrogen and phosphorus, C:N:P, of 100:10:1 (Bonomo et al., 2005), with extreme values of 350:10:1. Nitrogen content was 2.3% of the minimum suggested content.

7.3.2 Laboratory batch microcosm experiments

7.3.2.1 Blank vials

Fig. 7.17 indicates C_{gas} in blank vials for each i-compound.

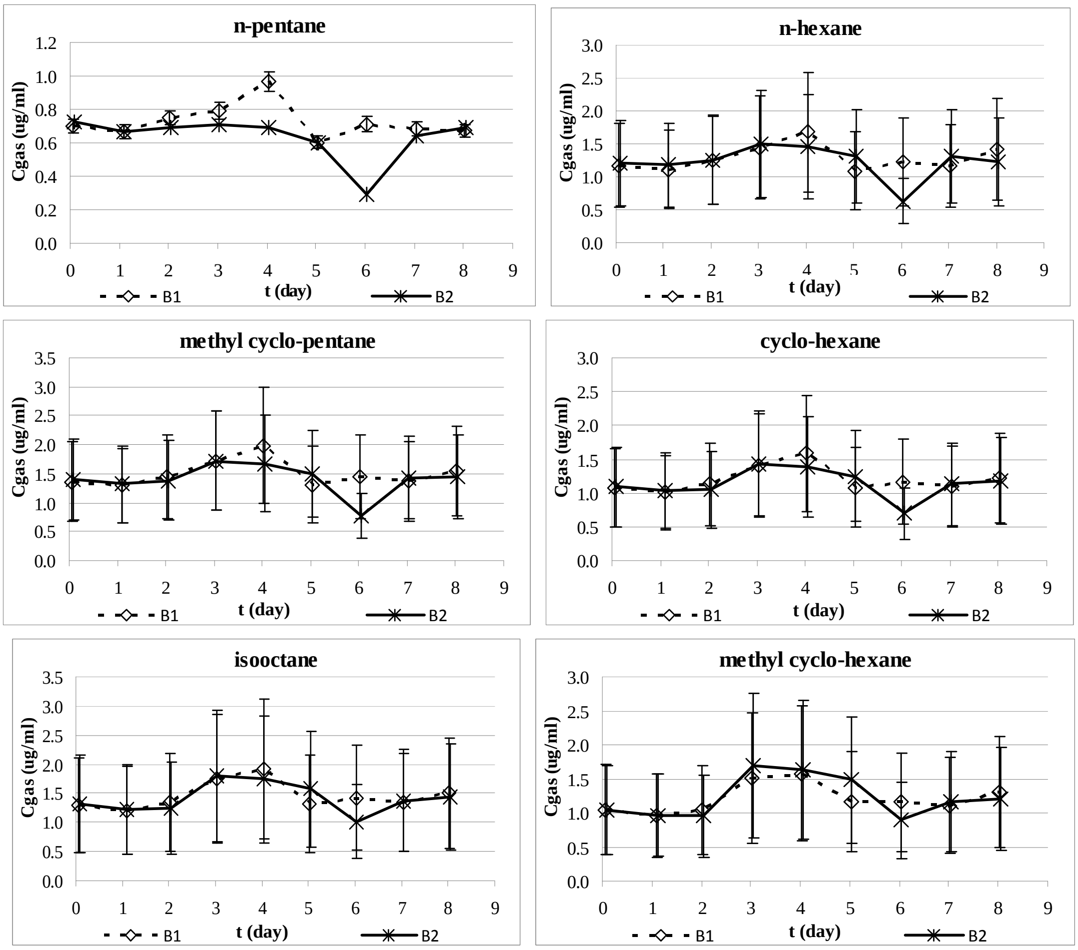

***Fig. 7.17**: continue.*

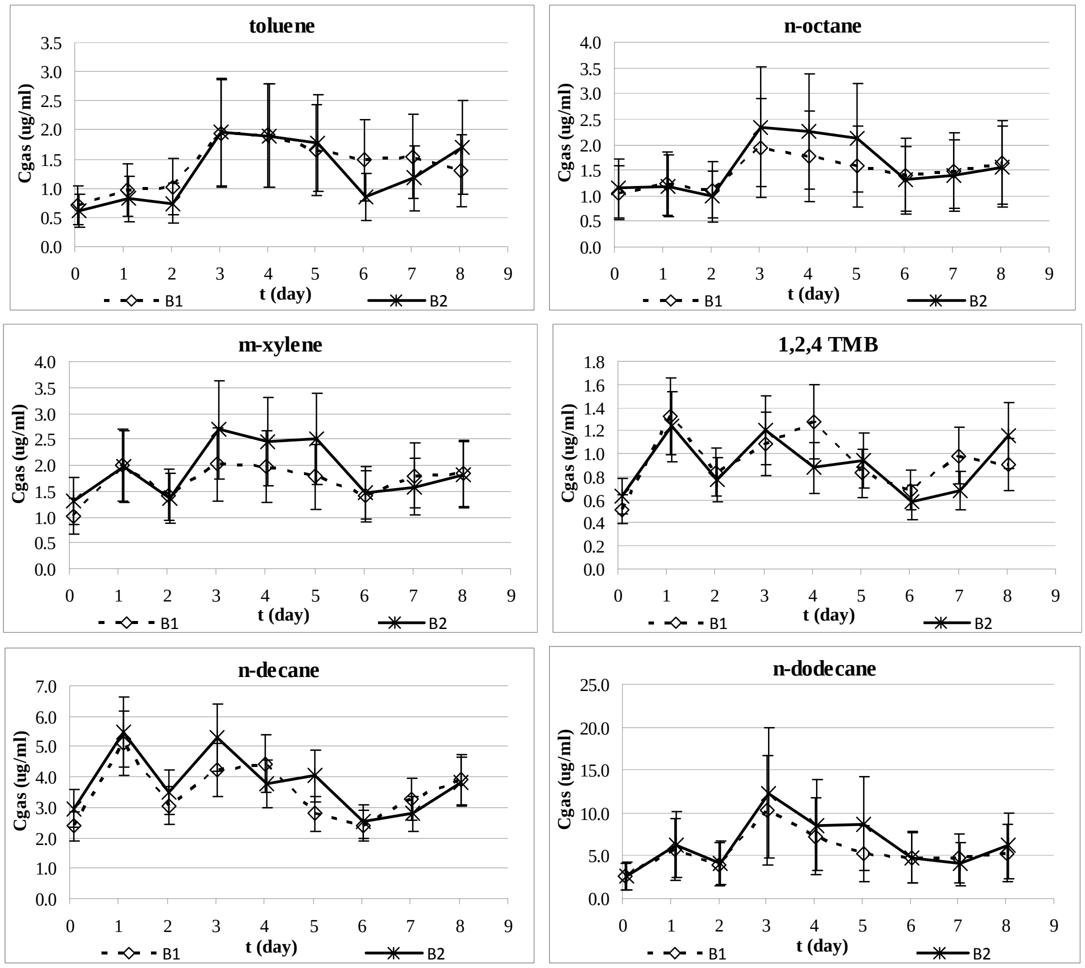

Fig. 7.17: *C_{gas} in 2 replicates (B1 and B2) of blank vials. Error bars indicate analytical variance (Tab. A2.3).*

In Tab. 7.12 $C_{blank,i}$ and its statistical evaluation are reported.

Tab. 7.12: $C_{blank,i}$ (§ 7.2.4.1) (mean between all gas concentrations taken at different times into the 2 blank replicates) used as reference starting condition for microcosms tests.

	n-pentane	**n-hexane**	**methyl cyclo-pentane**	**cyclo-hexane**	**isooctane**	**methyl cyclo-hexane**	**Toluene**	**n-octane**	**m-xylene**	**1,2,4 TMB**	**n-decane**	**n-dodecane**
$C_{blank,i}$ (μg ml^{-1})	0.63	1.2	1.4	1.1	1.4	1.2	1.3	1.5	1.8	0.9	3.5	6
$\sigma C_{blank,i}$ **(μg ml^{-1})**	0.08	0.4	0.5	0.4	0.6	0.5	0.4	0.5	0.4	0.2	0.6	3
VC (%)	12	38	35	38	44	44	33	36	25	18	17	44

7.3.2.2 Sorption test

SF_6 average concentrations in each of the j,k-vials with the exception of a1 flask (that was therefore not considered during the data elaboration), had a standard deviation lower than analytical variation, and therefore no leaks were considered in those test vials.

Fig. 7.18 indicates $C_{gas,i,j,k}$ at different times for three different researched matrices: a) soil, b) amended soil and c) biochar. Sample a1 confirmed leaks of the most volatile compounds. Furthermore gas concentrations at stationary conditions for n-decane and n-dodecane were higher than $C_{g,sat}$ in Tab. 7.1. Thus was because the gas phase composition due to evaporation of a limited quantity of NAPL was different from head space over an infinite source. In particular, very volatile compounds were suddenly moved to gas phases, achieving concentrations much lower than the saturated ones; thus allowed semi-volatile compounds to reach their maximum saturation gas concentration.

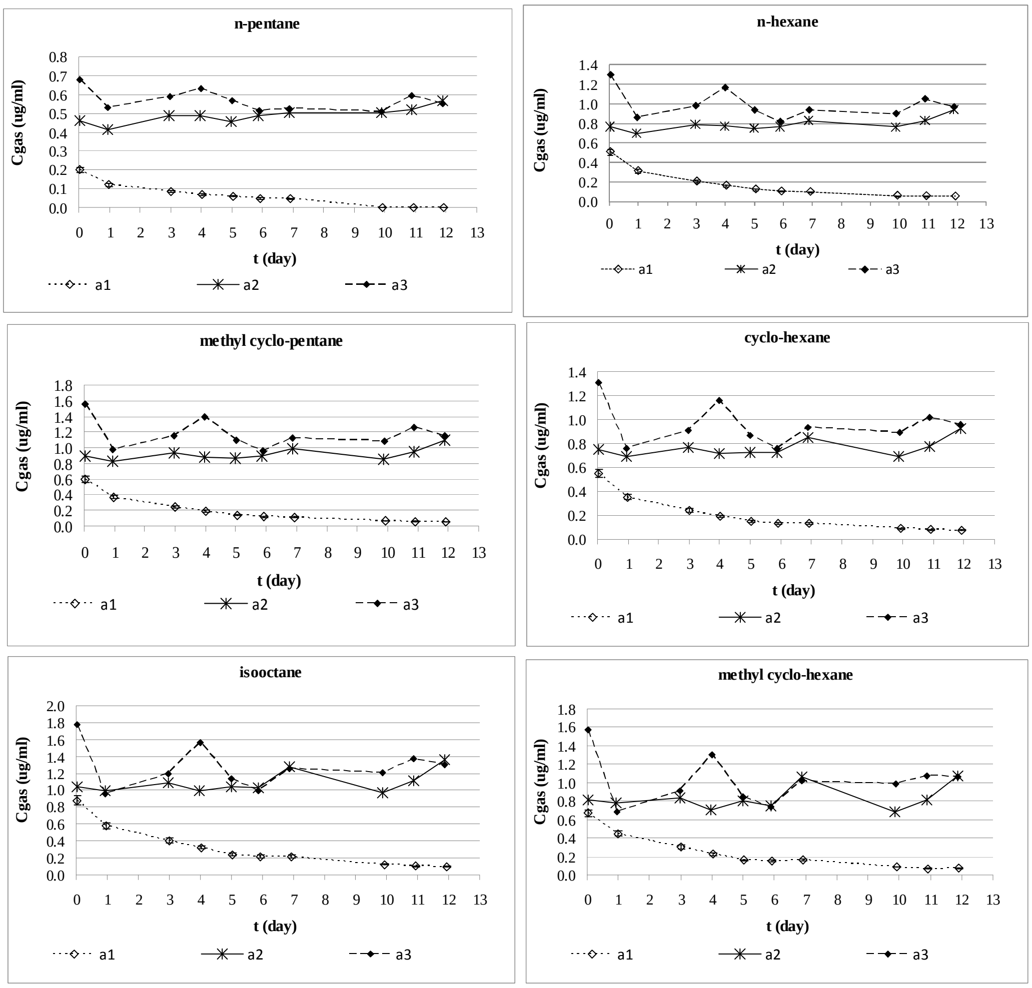

***Fig. 7.18**: continue.*

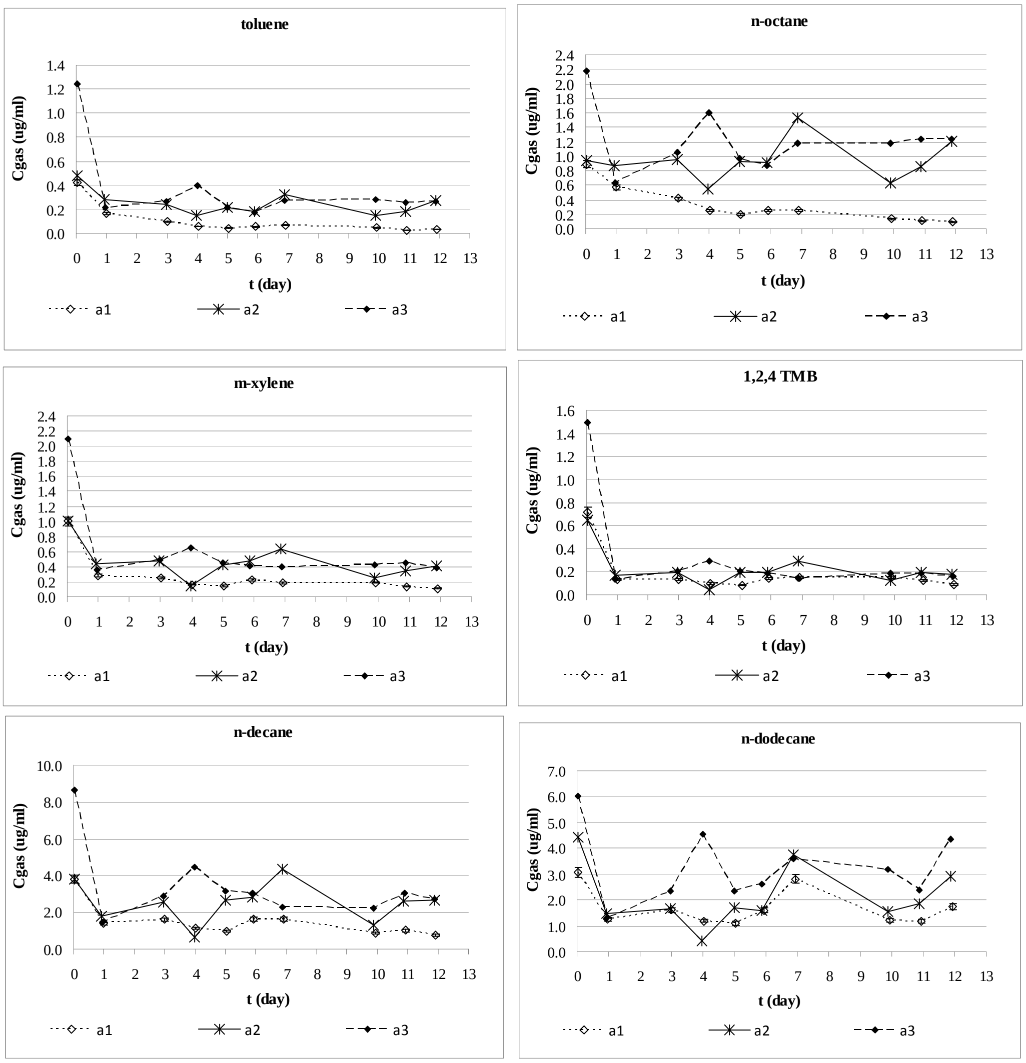

a)

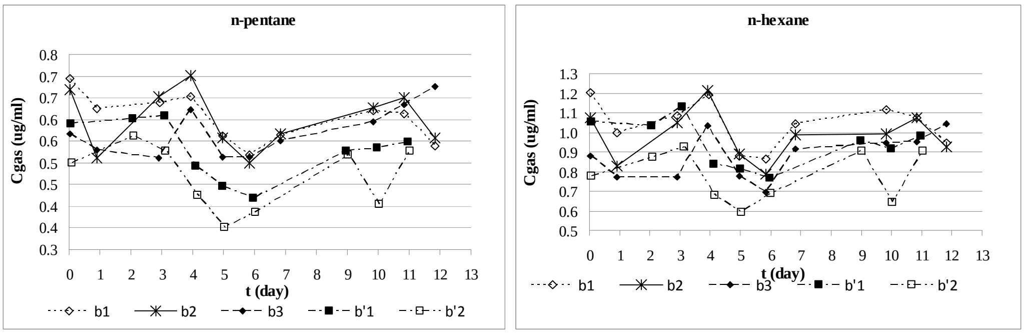

***Fig. 7.18**: continue.*

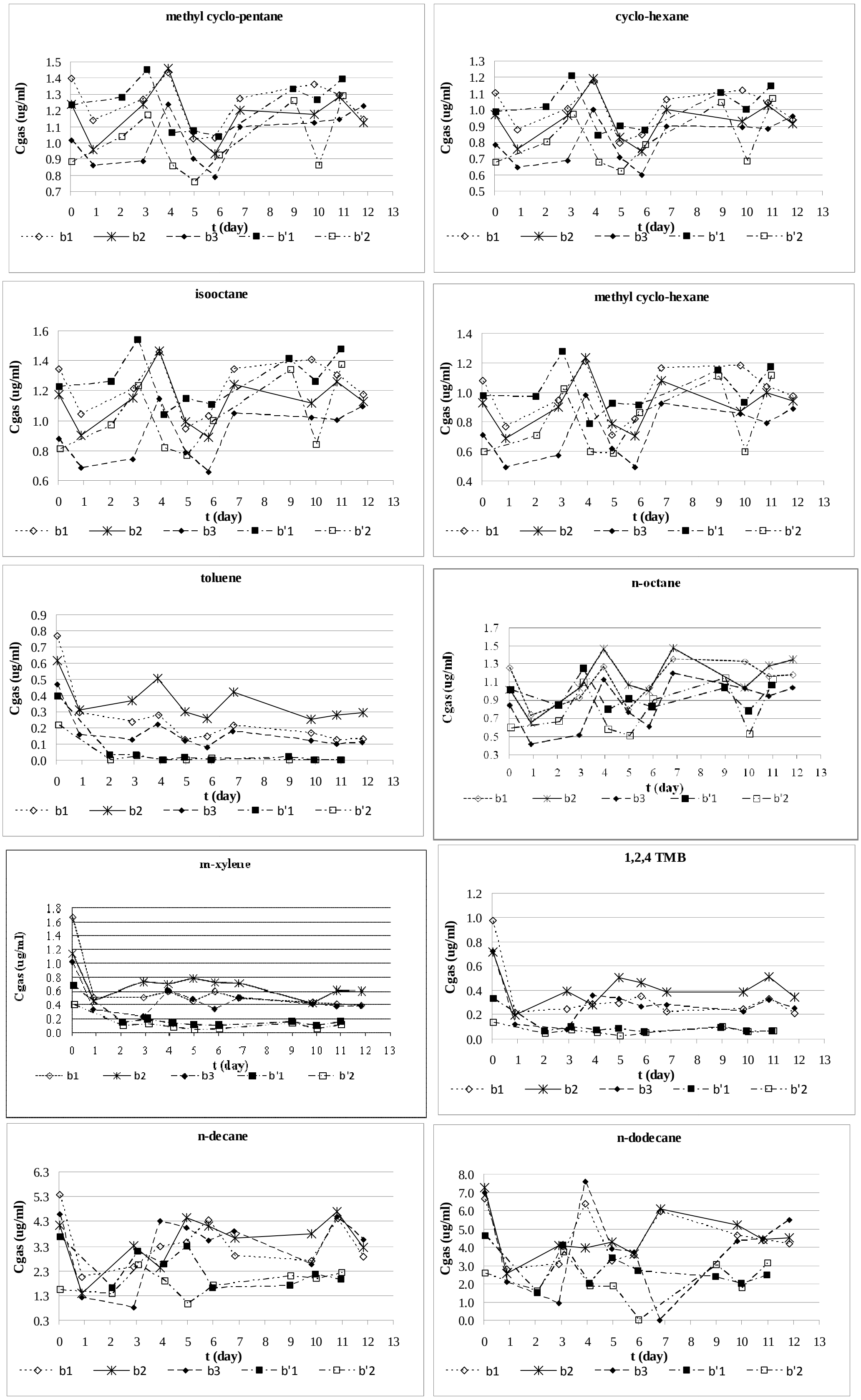

b)

***Fig. 7.18**: continue.*

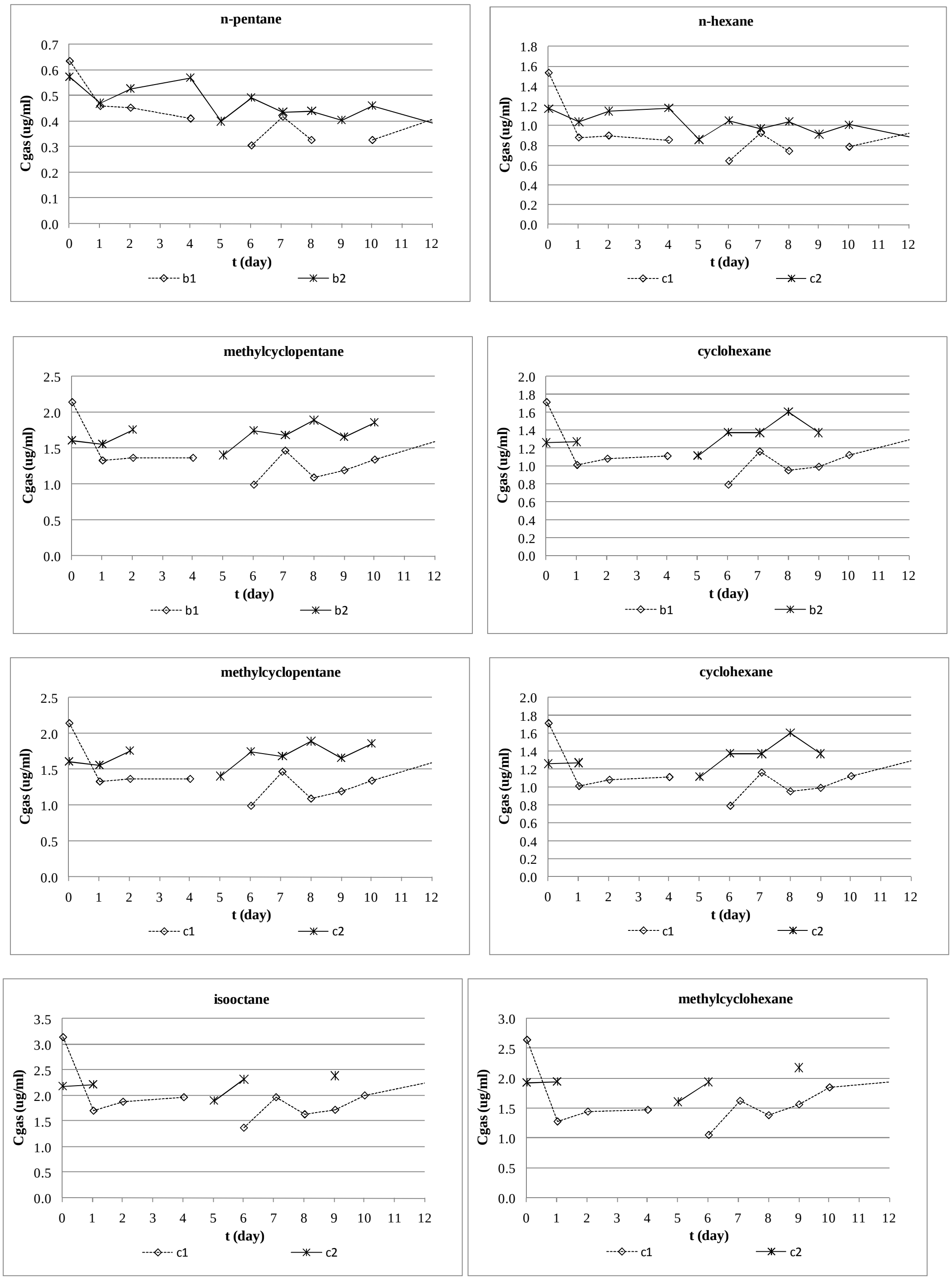

Fig. 7.18*: continue.*

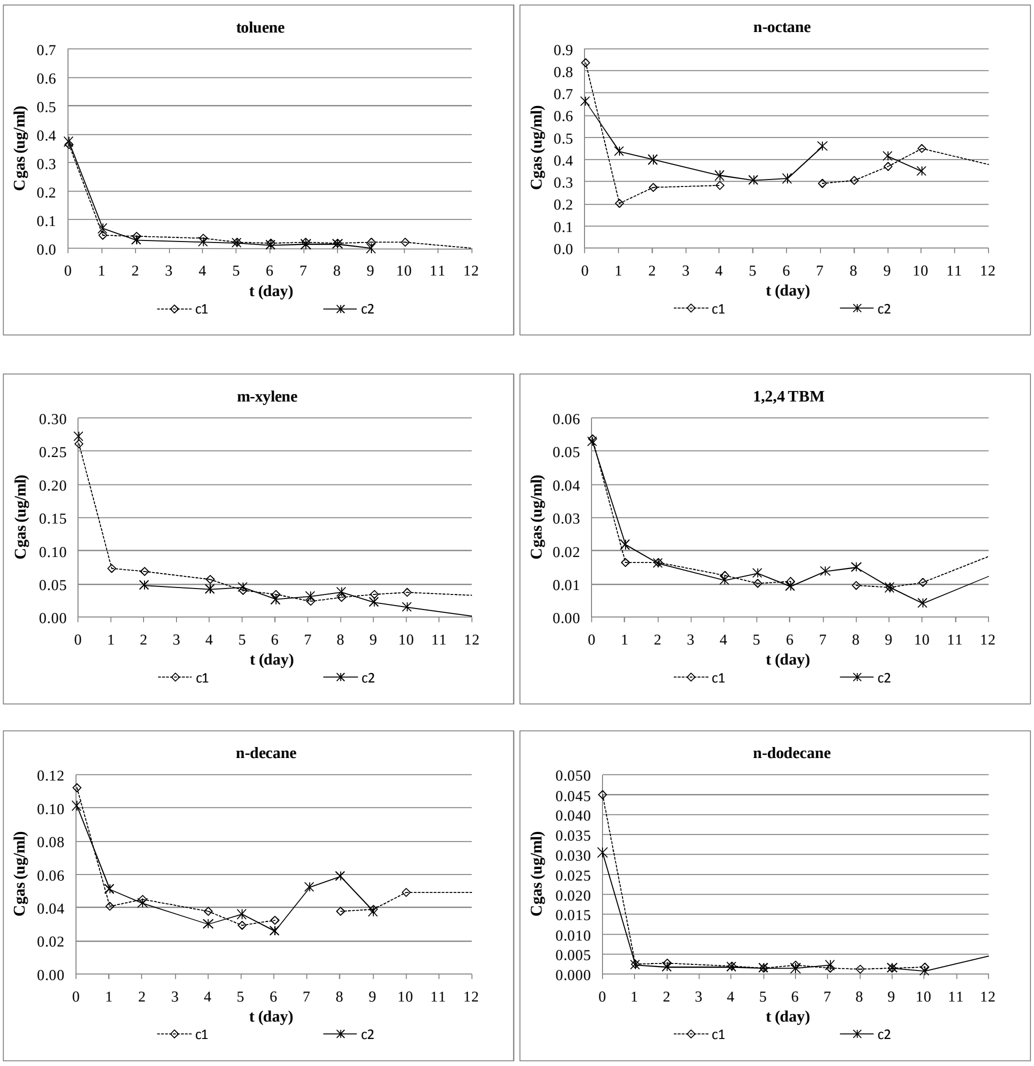

c)

Fig. 7.18*: time behaviour of VOC air concentrations in different prepared replicates and for each observed matrix, $C_{gas,z,i,j,k}$, for sorption tests with a) soil, b) amended soil and c) biochar matrices. No error bars, indicating analytical variance are reported for clearer reading.*

As it is possible to see from Fig. 7.18.b the concentrations in gas phase, for almost all the compounds, were quite similar for the 2 amounts of tested amended soil, but for aromatic compounds (toluene, m-xylene and 1,2,4 TMB) they were consistently lower for the two 15 g replicates.

Evaluated initial times of stationary conditions are reported in Tab. 7.13; Tab. 7.14 shows calculated $Kd_{i,k}$ values [$ml_{gas}\ g_{solid}^{-1}$] with error and variation coefficient indications, as indicated in § 7.2.4.2.

As for adsorption on soil, $Kd_{est,i,soil}$ values (7.14) are indicated in Tab. 7.15 along with the logarithm of the ratio between the experimental data values (“a” tests in Tab. 7.14,) and them. Experimental values are all slightly lower than the estimated ones. In general the difference is lower than an order of magnitude, and a little higher for methylcyclohexane and 1,2,4,TMB, without revealing any particular correlation with any chemical or physical property.

Tab. 7.13*: times from which, for each i-compound in each j,k-vial, stationary conditions were maintained stable (t_{stat}); *: sample not considered due to proven leaks.*

t_{stat} **(min)**	**n-pentane**	**n-hexane**	**methyl cyclo-pentane**	**cyclo-hexane**	**isooctane**	**methyl cyclo-hexane**	**toluene**	**n-octane**	**m-xylene**	**1,2,4 TMB**	**n-decane**	**n-dodecane**
a1	*	*	*	*	*	*	*	*	*	*	*	*
a2	30	30	30	30	30	30	30	30	30	30	30	30
a3	1364	1364	1364	1364	1364	1364	1364	1364	1364	1364	1364	1364
b1	1289	1289	1289	1289	1289	1289	1289	1289	1289	1289	1289	1289
b2	1290	1290	1290	1290	1290	1290	1290	1290	1290	1290	1290	1290
b3	1289	1289	1289	1289	1289	1289	1289	1289	1289	1289	1289	1289
b'1	90	90	90	90	90	90	2986	90	2986	2986	90	90
b'2	119	119	119	119	119	119	3015	119	3015	119	119	119
c1	7229	7229	5789	1469	1469	1469	7229	1469	10196	7228	1469	1469
c2	7229	7229	5789	1469	1469	1469	7229	1469	10196	7228	1469	1469

Tab. 7.14*: adsorption coefficient values Kd [ml g^{-1}] for each i-compound and each k-matrix analysed, according to § 7.2.4.2. $\sigma Kd_{i,k}$ [ml g^{-1}] indicates error on calculated $Kd_{i,k}$ and VC is the percentage of the variation coefficient [%].*

Matrix		**n-pentane**	**n-hexane**	**methyl cyclo-pentane**	**cyclo-hexane**	**isooctane**	**methyl cyclo-hexane**	**Toluene**	**n-octane**	**m-xylene**	**1,2,4 TMB**	**n-decane**	**n-dodecane**
Soil (a vials)	Kd	20	47	9	4	43.7	2.3	1.9	104	1.3	1.6	123	774
	σKd	7	17	4	2	16.0	0.7	0.1	27	0.0	0.2	27	211
Amended soil (15 g matrix) (b' vials)	Kd	43	90	10	5	73	4	69	314	14	13.0	520	1630
	σKd	16	36	7	4	70	3	16	69	3	0.8	190	352
Biochar (c vials)	Kd	3993	6039	265	114	2271	267	2834	20283	718	862	207795	1097264
	σKd	920	986	43	33	775	136	432	4541	130	149	20294	137358

***Tab. 7.15**: theoretical adsorption coefficient values $Kd_{est,i,soil}$ [ml g^{-1}] from (7.14) and logarithm of the ratio among the experimental data values and them.*

	n-pentane	n-hexane	methyl cyclo-pentane	cyclohexane	isooctane	methyl cyclo-hexane	toluene	n-octane	m-xylene	1,2,4 TMB	n-decane	n-dodecane
$Kd_{est,i,soil}$	21	54	13	19	63	26	5	496	11	36	359	2815
$\log\left(\frac{Kd_{i,soil}}{Kd_{est,i,soil}}\right)$	0.0	-0.1	-0.1	-0.6	-0.2	-1.1	-0.4	-0.7	-0.9	-1.3	-0.5	-0.6

The ratio between Kd_i reached from b) and b') is reported in Tab.7.16: it seems that distribution coefficient depended on the amount of tested matrix. With the exception of aromatics, Kd for lower matrix content were higher, and since $C_{gas,i}$ were similar, it means that $C_{solid,i}$ were higher, and therefore that more M_i was adsorbed for unit of M_{solid}. As for aromatics, for which C_{gas} were lower in b') vials, Kd had the same magnitude, and for toluene it was even higher, meaning that the sorption capacity was proportional, for this compound, to biochar-amended soil presence.

***Tab. 7.16**: ratio between experimental Kd values (Tab. 7.14) from b (with 3 g of amended soil) and b' (with 15 g of amended soil) tests.*

	n-pentane	n-hexane	methyl cyclo-pentane	cyclo-hexane	isooctane	methyl cyclo-hexane	toluene	n-octane	m-xylene	1,2,4 TMB	n-decane	n-dodecane
$\frac{Kd_i \text{ in } 3g \text{ b tests}}{Kd_i \text{ in } 15g \text{ b' tests}}$	3.48	5.25	8.94	10.08	13.74	10.06	0.55	4.72	1.13	1.08	1.19	2.03

From Fig. 7.19 in which $Kd_{est,i,soil+biochar}$ from (7.15) and experimental Kd from b and b' tests are compared, it appears that b' test results fitted estimated values better, and they were therefore used as representative of biochar-amended soil.

Fig. 7.20 presents a comparison between Kd values for soil and amended-soil matrix, split for different chemical families. The addition of 2% biochar increased the K_d values of the straight chain, cyclic and branched alkanes approximately by a factor F of 1.1 to 4.2, since

$$F = \frac{Kd_{i,\,biochar}}{Kd_{i,\,soil}} = 10^{\log Kd_{i,\,biochar} - \log Kd_{i,soil}} \quad (7.35)$$

This is consistent with the increase by a factor 2.4 in the total organic carbon content (TOC) (from 1.18% to 2.89 % of the dry solid mass) due to biochar amendment.

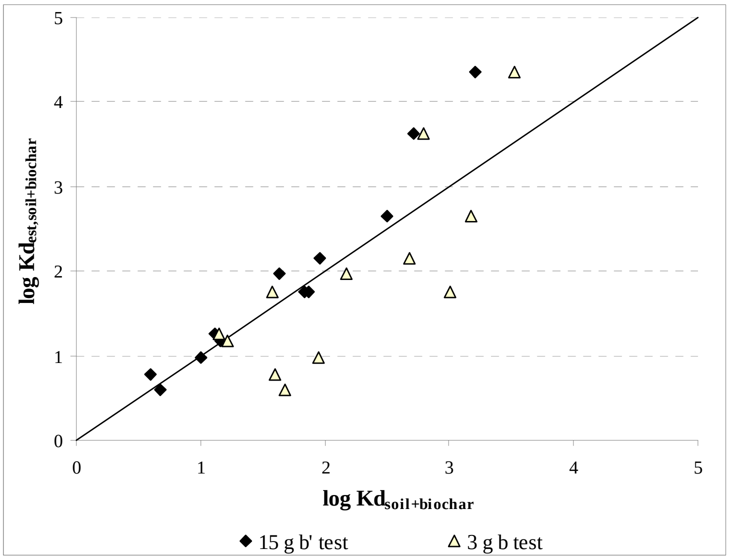

Fig. 7.19*: comparison, for biochar-amended soil, between logarithm of estimated value* $Kd_{est,i,soil+biochar}$ *and experimental* $Kd_{soil+biochar}$ *(from Tab. 7.14) from b and b' tests.*

As far as aromatic behaviour was concerned, F was generally higher, in particular for toluene for which it was 35.6, because of the ability of these compounds to interact with the aromatic surface of the biochar (Fig. 7.6). m-xylene and 1,2,4-TMB showed lower F probably due to methyl-groups on the aromatic ring interfering with these interatomic interactions.

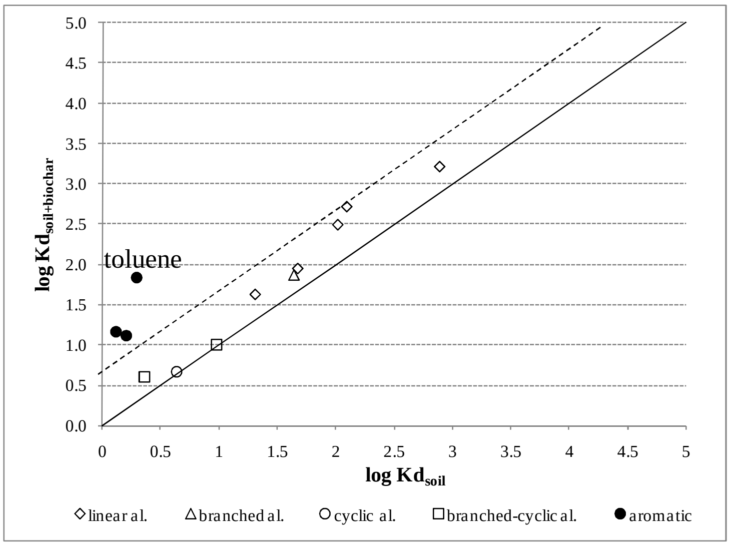

Fig. 7.20*: Comparison between log* K_d *(ml* g^{-1}*) in soil and soil amended with 2% biochar soil, split for different chemical families. The continuous line is the bisectrix,*

whereas the dotted one indicates Y values higher than X values by about 0.6 log units.

7.3.2.3 Biodegradation test

SF_6 average concentrations in each of the j,k-vial had a standard deviation lower than analytical variation, and therefore no leaks were considered in test vials.

In Fig. 7.21 $C_{gas,i,j,k}$ are indicated at different times for three different researched matrices: a) soil and b) amended soil.

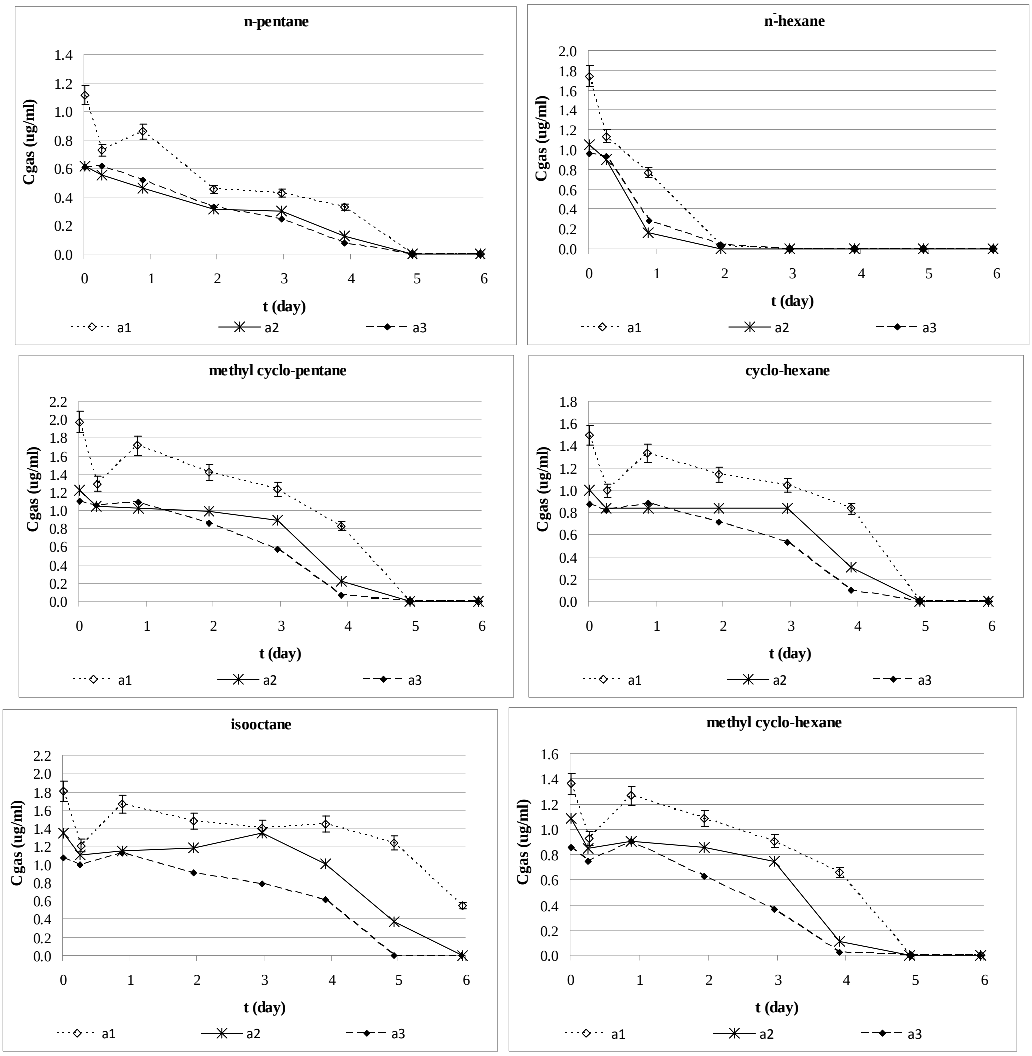

Fig. 7.21*: continue.*

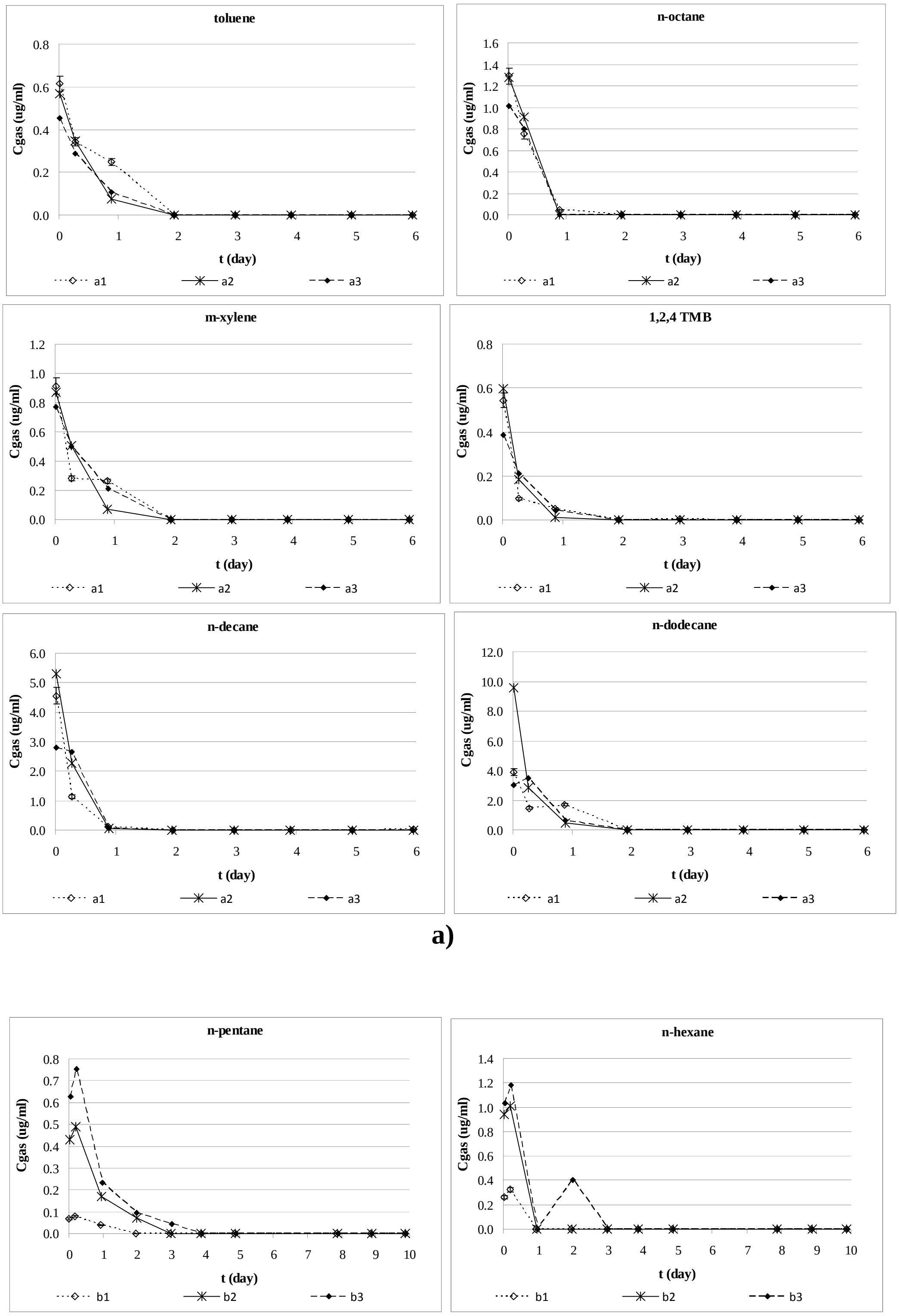

Fig. 7.21*: continue.*

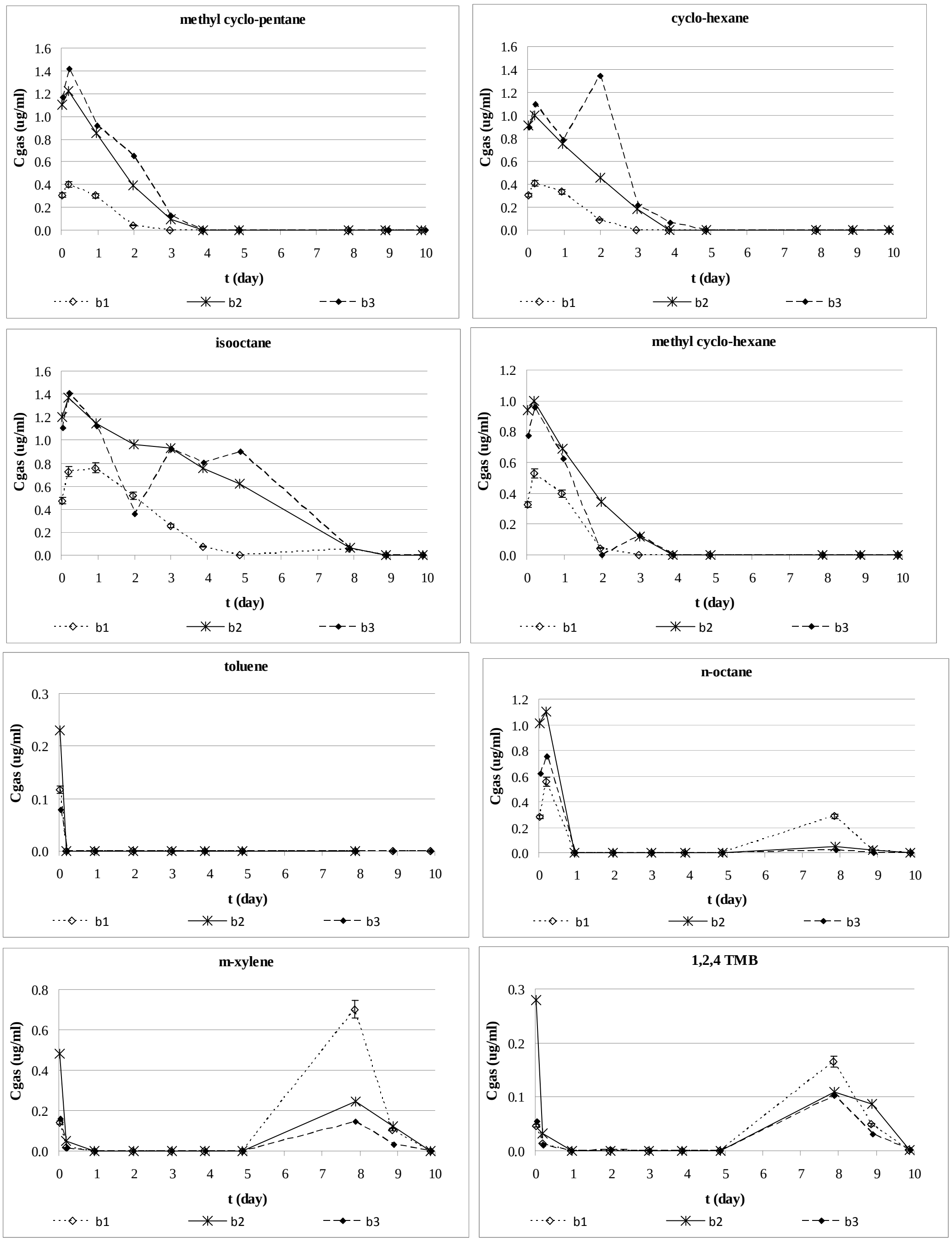

Fig. 7.21: *continue.*

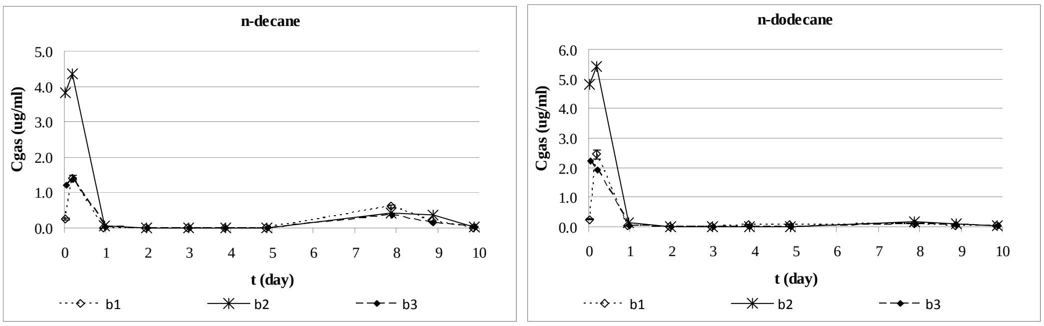

b)

Fig. 7.21*: behaviour over time of VOC air concentrations for different replicates and for each observed matrix, $C_{gas,z,i,j,k}$, for biodegradation tests with a) soil and b) amended soil. No error bars indicating analytical variance are reported for clearer reading.*

In all the performed tests oxygen concentrations were always higher than 251.28 µg ml^{-1}, equivalent to 18.6 % as volume percentage in the vial head space.

In detail, average and standard deviation of oxygen content during test period were: 20 ± 2 %, 22± 2 %, 23± 2 % in respectively a1), a2), a3) vials with soil; 21 ± 3 %, 21 ± 4 % and 23± 3 % in respectively b1), b2), b3) vials with biochar-amended soil.

CO_2 initial content had an average and standard deviation of 0.7 ± 0.1 µg ml^{-1}, equivalent to 0.038 ± 0.006 %, and therefore similar to atmospheric one.

CO_2 increased by 2097± 8%, 1090± 5% and 1416± 6% respectively in a1), a2), a3) vials with soil, where the error expresses the propagation of variables' uncertainties due to analysis uncertainty (§ A3); in vials with biochar-amended soil it increased by 426 ± 2 %, 417 ± 2 % and 647± 3 % respectively in b1), b2), b3).

Tab.7.16 present t* , the time since which $C_{gas,z,i,j,k}$ were used to define degradation rates, and Tab. 7.18 and Fig. 7.22 show average $K_{deg,water,i,,k}$ and their $K_{deg,water,i,,k}$ errors.

Tab. 7.16*: t*[min] from which gas concentrations are used in regression analyses to define degradation constants.*

t (min)	n-pentane	n-hexane	methyl cyclo-pentane	cyclo-hexane	Isooctane	methyl cyclo-hexane	toluene	n-octane	m-xylene	1,2,4 TMB	n-decane	n-dodecane
a1	30	1742	1271	1271	5635	1271	30	30	30	389	30	30
a2	30	30	387	1279	4275	1273	30	30	30	387	30	30
a3	30	387	1279	1279	4275	1279	30	30	30	387	1279	30
b1	269	269	269	269	2826	269	18	269	18	18	269	269
b2	294	294	294	294	294	294	45	294	45	45	294	294
b3	319	319	319	319	4343	319	73	319	73	73	319	319

Tab. 7.17: *average water-phase first order degradation rates, $K_{deg,water,i,k}$ [s^{-1}], their errors $\sigma K_{deg,water,i,j,k}$ [s^{-1}] and variation coefficients (VC) [%]; *: possible underestimated rates.*

		n-pentane	**n-hexane**	**methyl cyclo-pentane**	**cyclo-hexane**	**Isooctane**	**methyl cyclo-hexane**	**toluene**	**n-octane**	**m-xylene**	**1,2,4 TMB**	**n-decane**	**n-dodecane**
soil	***$K_{deg,water}$***	3.7 e-3	2.9 e-2	1.2 e-3	6.4 e-4	1.6 e-2	4.1 e-4	8.9 e-4	1.7 e-1	7.3 e-4	1.8 e-3	1.7 e-1	1.6 e-1
	$\sigma K_{deg,water}$	1.2 e-3	0.3 e-2	1.1 e-3	0.6 e-4	0.2 e-2	4.0 e-4	3.1 e-4	0.5 e-1	3.0 e-4	0.4 e-3	1.0 e-1	0.4 e-1
	VC	32	10	92	9	13	98	35	29	0	22	59	25
Soil+bioch	***$K_{deg,water}$***	2.1 e-2	5.7 e-2	5.6 e-3	1.1 e-3	1.8 e-2	1.6 e-3	1.5 e-2*	2.1 e-1*	5.1 e-3	5.0 e-3	3.7 e-1	3.1 e-1
	$\sigma K_{deg,water}$	0.4 e-2	2.6 e-2	0.9 e-3	0.2 e-3	0.7 e-e	0.3 e-3	0.1 e-2	0.09 e-1	0.4 e-3	1.1 e-3	0.4 e-1	0.3 e-1
	VC	19	46	16	18	39	19	7	4	8	22	11	10

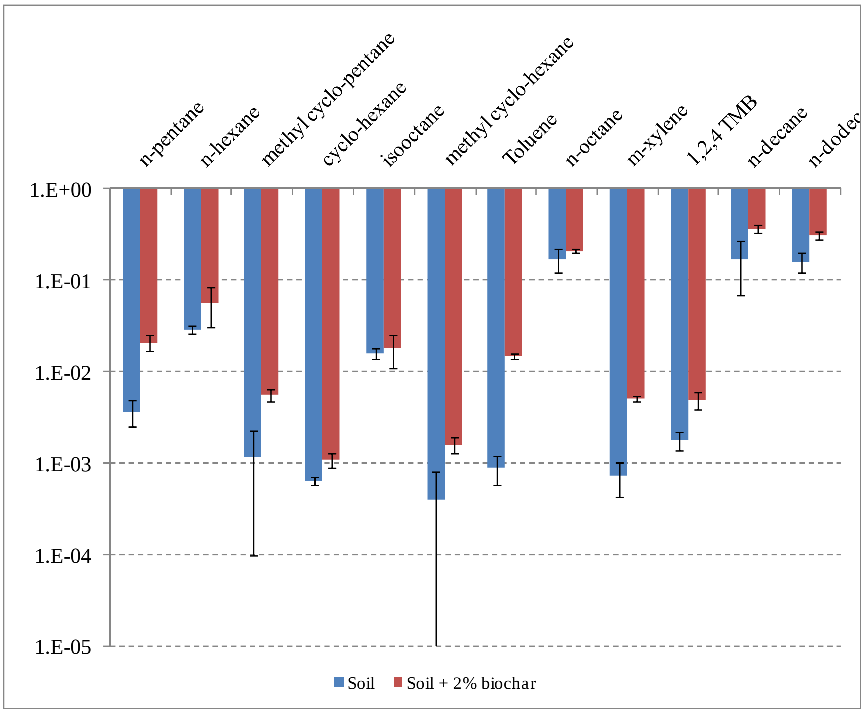

Fig. 7.22: *comparison, in logarithm scale, between degradation rates $K_{deg,water,i,k}$ [s^{-1}] in soil and biochar-amended soil; error bars indicate $\sigma K_{deg,water,i,j,k}$ [s^{-1}].*

As it is possible to deduce from Fig. 7.22, biochar presence increased biodegradation rates also considering $\sigma K_{deg,water,i,j,k}$; the ratio between degradation constants in soil and in amended soil varied from 1.1 for isooctane to 16.9 for toluene. Higher degradation rates were observed for biochar that did not correspond to lower CO_2 increases; this might be due to biochar capacity of absorbing CO_2 gas (§ 7.1.1).

High $K_{deg,water,i,j,k}$ values were obtained for straight-chain alkanes (*Tab. 7.17*), equivalent to a half-life of only a few seconds for the dissolved portion of these compounds in the batches. Such a short half-life may indicate that the solubility of these compounds may have been greater than predicted based on Henry's constant, for instance because of the presence of microbial surfactants or other dissolved organic matter in soil pore water.

7.3.2.4 Conclusions

The difference between abiotic and biotic tests for both soil and amended soil matrices is more clearly presented in Fig. 7.23, where the average behaviour over time of $C_{gas,i,k}$ on the J_k replicates is indicated.

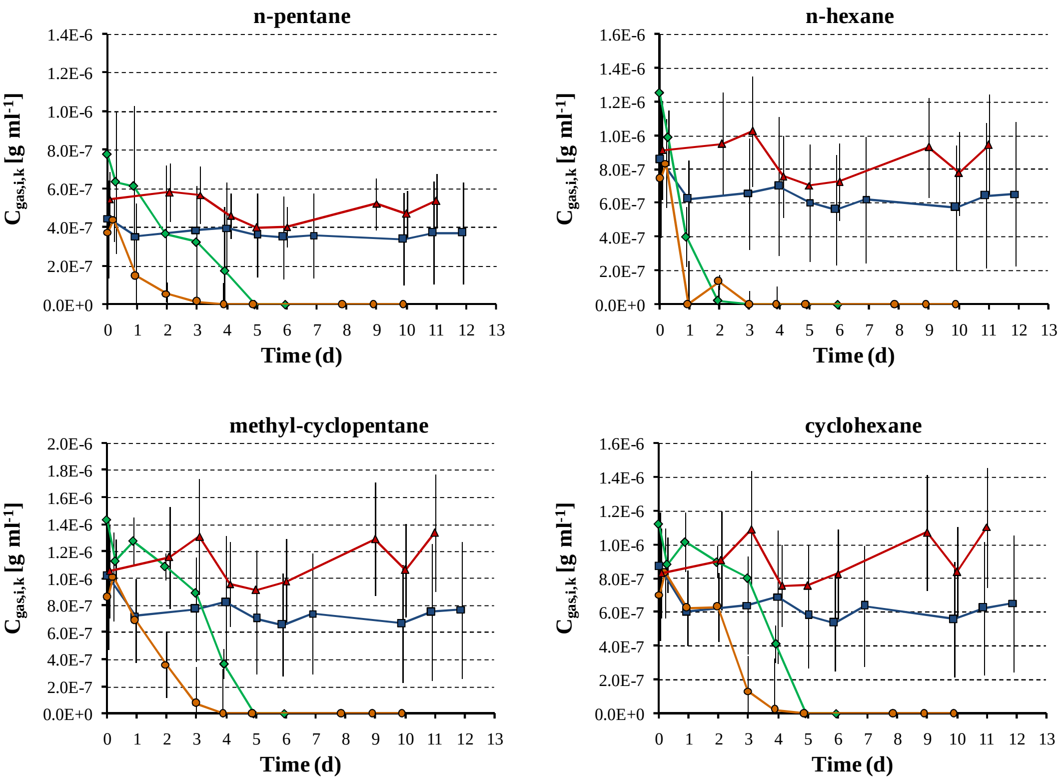

***Fig. 7.23**: continue.*

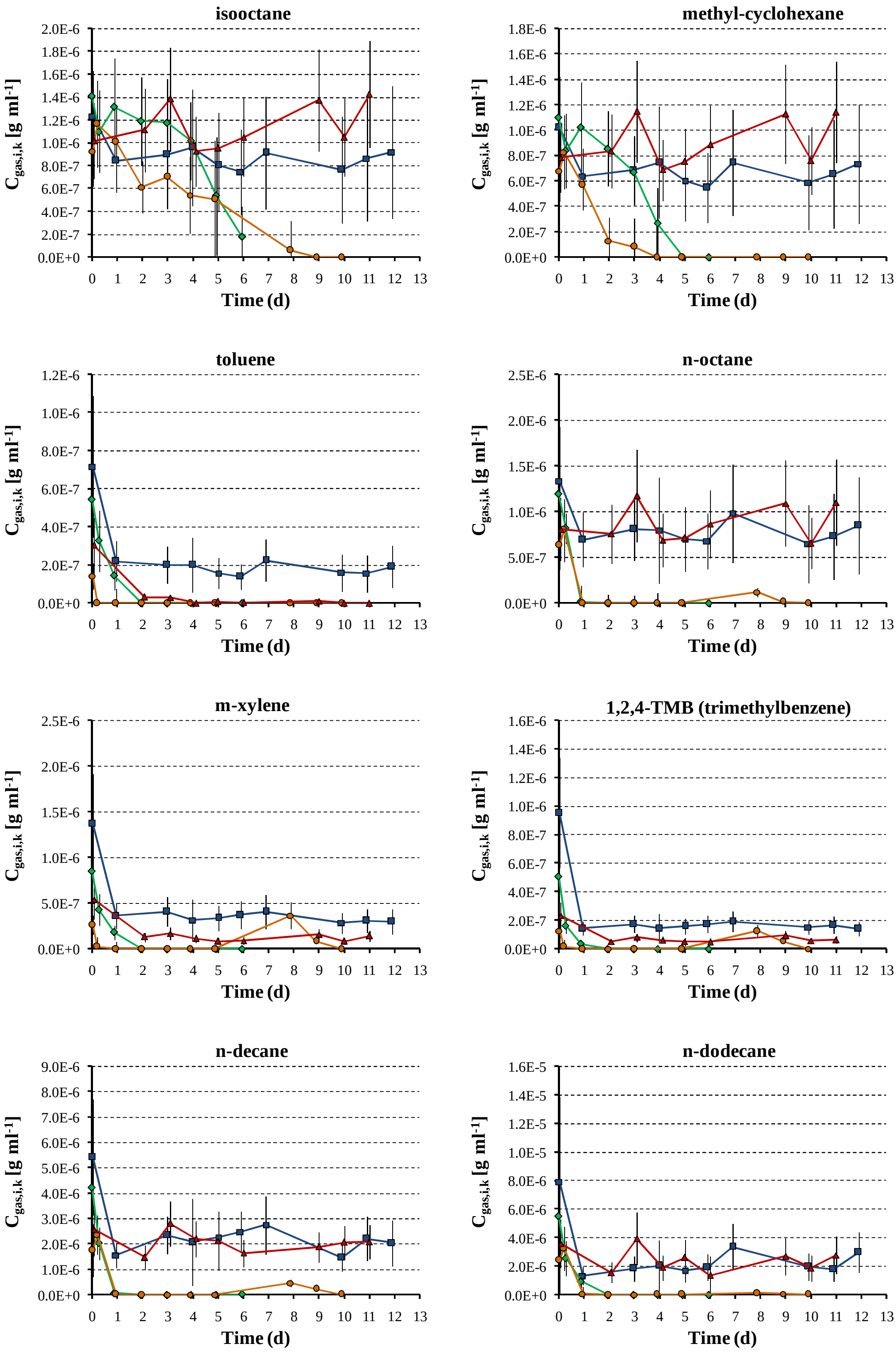

Fig. 7.23: *VOC soil gas concentration $C_{gas,i,k}$ in batches containing either 30 g of soil (■ abiotic test, ◆ live soil) or 15 g of soil amended with 2% biochar (▲*

abiotic test, —●— live test). Error bars represent the maximum between standard deviation and error propagation due to analysis uncertainty.

It is possible to see that in the non-sterile soil without biochar (green rhombi in Fig. 7.23), straight-chain alkanes and monoaromatic hydrocarbons were rapidly biodegraded, whereas the biodegradation of cyclic and branched alkanes (cyclohexane, isooctane, methylcyclopentane, methylcyclohexane) was characterized by a lag phase before the its onset, roughly consistent with the time needed to degrade the straight-chain alkanes (n-pentane, n-esane, n-octane, n-decane and n-octane) and monoaromatic hydrocarbons (toluene, m-xylene and 1,2,4-TMB).

In the soil amended with biochar a lag phase was not detected even for branched and cyclic alkanes.

7.3.3 Laboratory column experiments

7.3.3.1 VOC Source

Results on VOC source at the beginning and end of open and closed b.c. for soil and biochar-amended soil column tests are reported in Fig. 7.24 and Fig. 7.25 respectively.

n-pentane and in some cases n-hexane are not indicated because of analytical problems with solvent peak that arose at the same retention time as these compounds, overlapping them (§ 7.2.3).

In Fig. 7.26 it is indicated the chemical composition of the pollutant mixture (as molar ratio) at different source sampling times. All the analysed compounds are present in all the final samples taken, which means that there was always an amount of each VOC in NAPL source, and that therefore there was a continuous release of vapours of each VOC during the performed tests: eventual absences of any VOC in interstitial gas were just due to transport phenomena.

For open boundary conditions it is possible to see that compounds were depleted with different behaviours according to their vapour pressure: those with higher P_v decreased more than those with lower P_v. This is why the NAPL composition varied during the tests, and the final mixture resulted richer in heavier compounds.

With a few exceptions (cyclohexane in biochar-amended soil), it seems that the initial concentrations of each VOC at the beginning of two different boundary conditions, for each matrix, were comparable, considering the analytical uncertainty. The general initial composition of the source, for the two matrices, was also similar, and therefore column tests results were comparable, too.

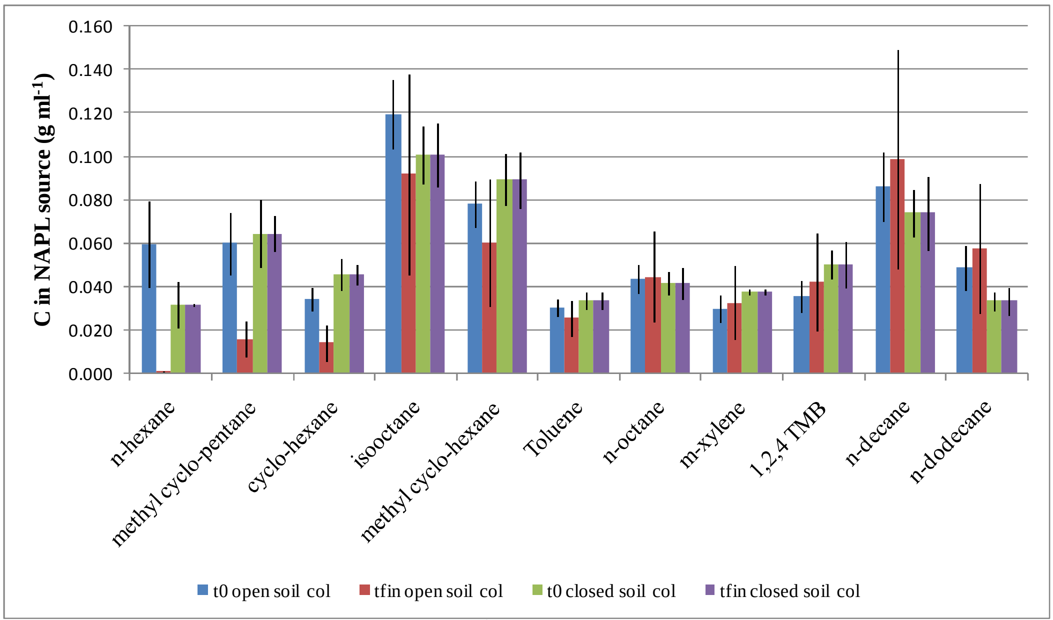

Fig. 7.24: *VOCs concentration [g ml^{-1}] in NAPL of source taken at the beginning (t0) and end (tfin) of open and closed b.c. for soil column test. Error bars indicate the maximum between standard deviation on 3 replicates and analytical variation coefficient. n-pentane is not indicated because of analytical impossibility to determine them, as indicated in § A2.3.*

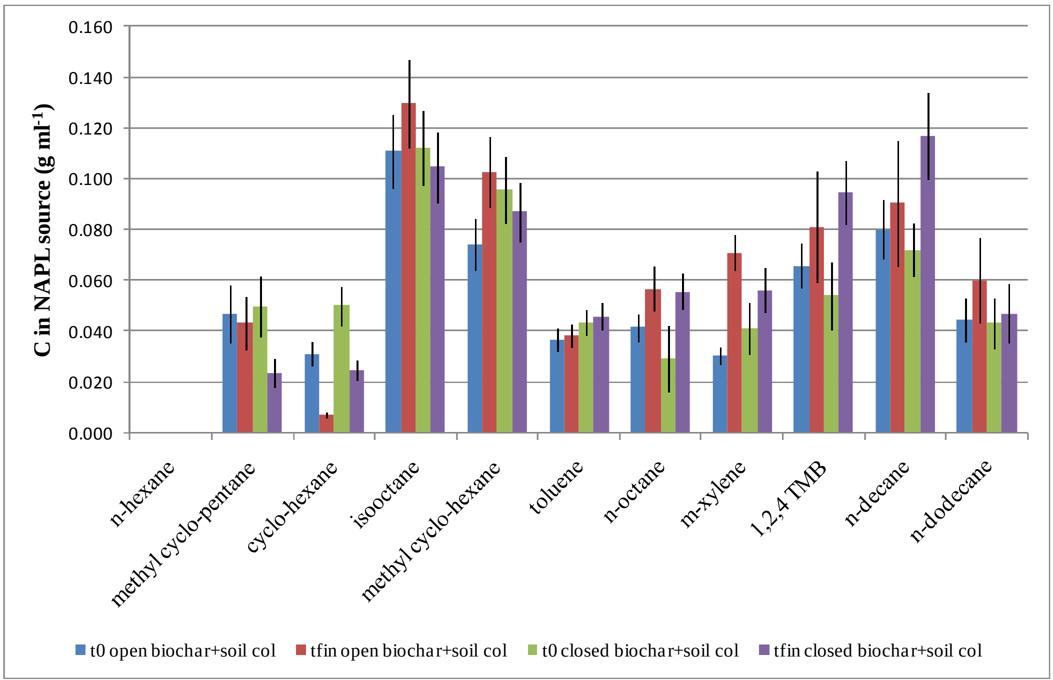

Fig. 7.25: *VOCs concentration [g ml^{-1}] in NAPL of source taken at the beginning (t0) and end (tfin) of open and closed b.c. for column test with soil amended with 2% of biochar. Error bars indicate the maximum among standard deviation on 3 replicates and analytical variation coefficient. n-pentane and 3 data on n-hexane are not indicated because of analytical impossibility to determine them, as indicated in § A2.3.*

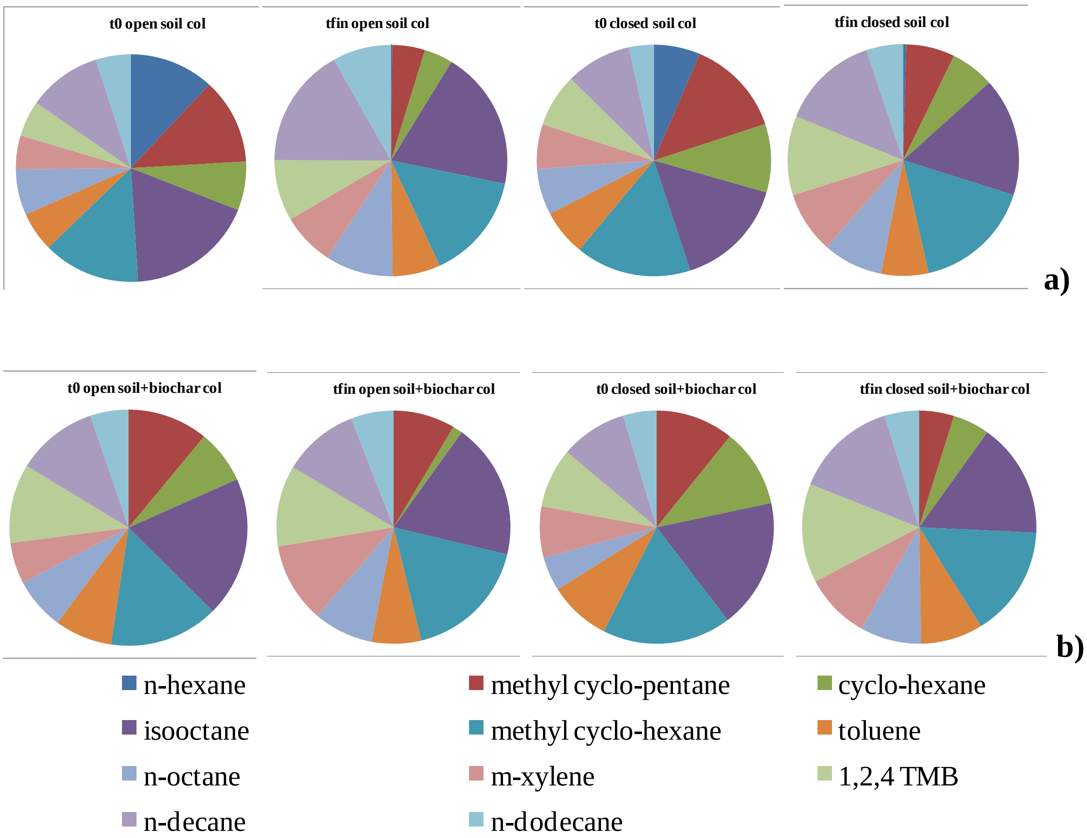

Fig. 7.26*: chemical composition of the pollutant mixture (as molar ratio) at different source sampling times, for soil (a) and biochar-amended soil (b). n-pentane (for both the matrices) and n-hexane (just for soil plus biochar) are not indicated because of analytical impossibility to determine them (§ 7.2.3).*

7.3.3.2 Tracer tests

Results for SF_6 text on soil column are indicated in Fig. 7.27.

The trial-and-error procedure made it possible to quantify the gap area between the flux chamber and the soil column equivalent to 1.5 cm^2. Diffusion from (3.23) was verified by the good coincidence between measured (symbols) and simulated (continuous line) results in all five ports.

Results of CO_2 tests, as described in § 7.2.5.4, are indicated in Fig. 7.28; for soil (a1 and a2) and biochar-amended soil (b1 and b2) the experimental data, in the two replicates, and relative simulations, are presented.

The general trend in each port of each test seems to represent experimental data qualitatively, but suitability is still to be improved, probably because carbon equilibrium is more complex than was assumed, depending on pH changes (§ 7.3.3.5.3) during the test in each port, microbiological activity and any subproducts released during biodegradation process.

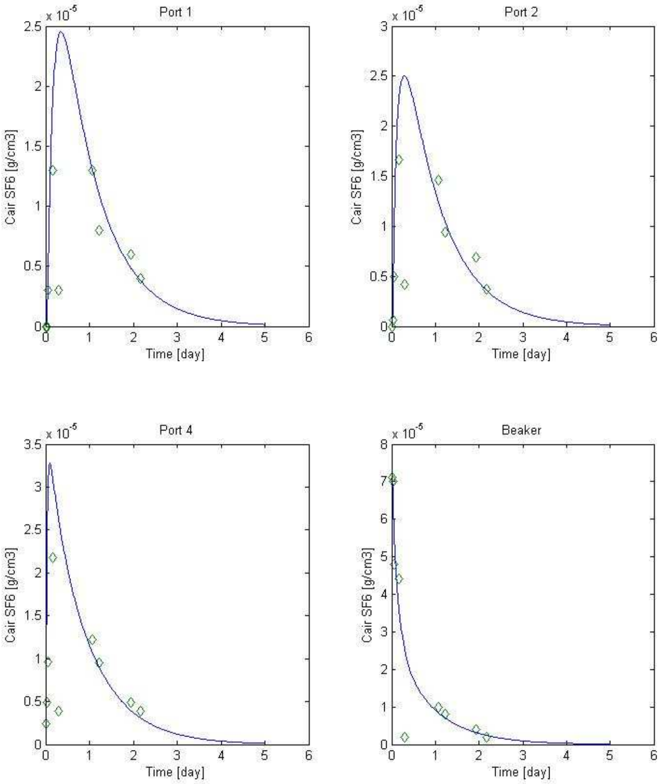

Fig. 7.27*: SF_6 tracer test used to determine the size of the gap area between the flux chamber and the soil column.*

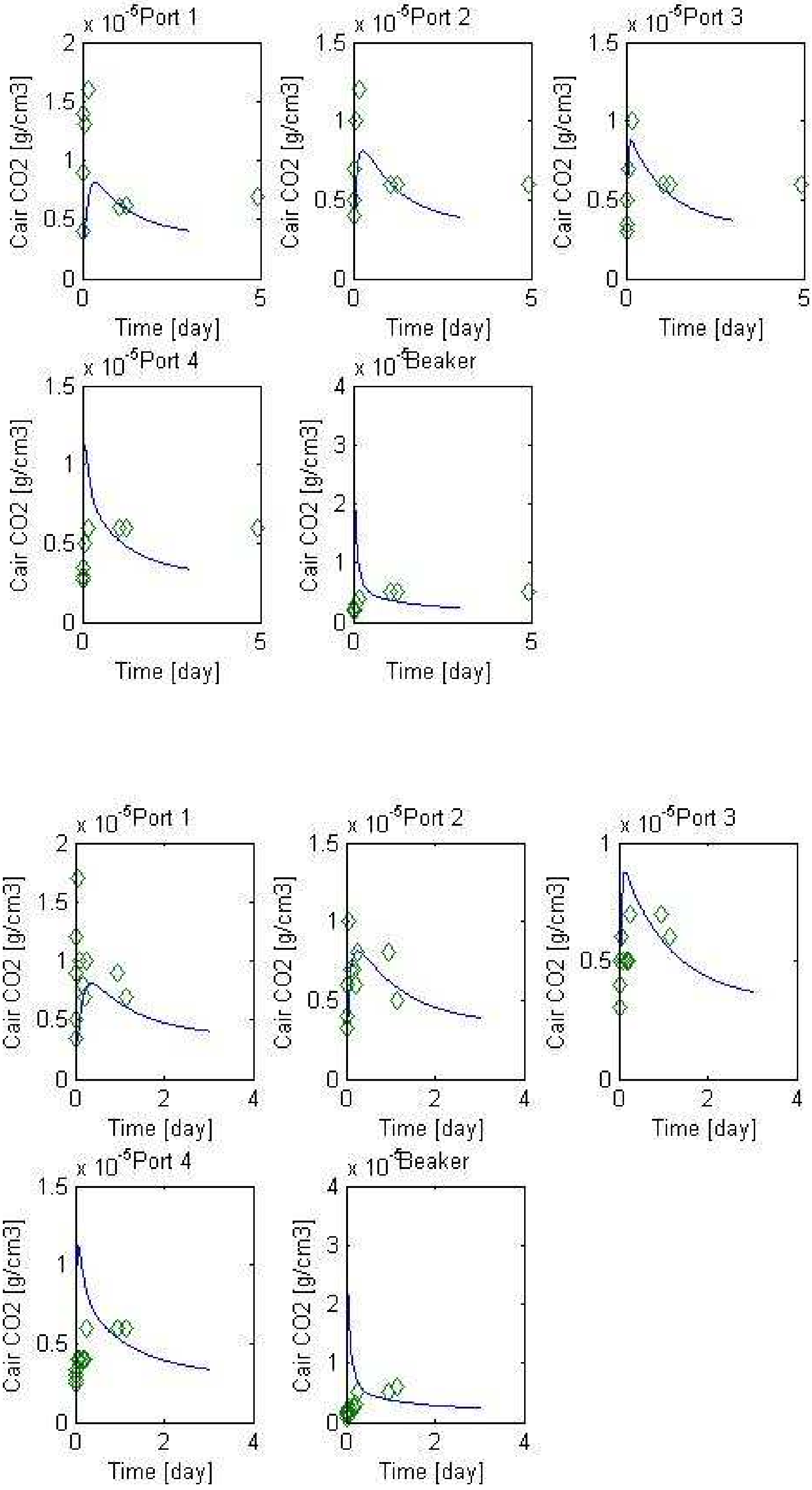

a1)

a2)

Fig. 7.28: *continue.*

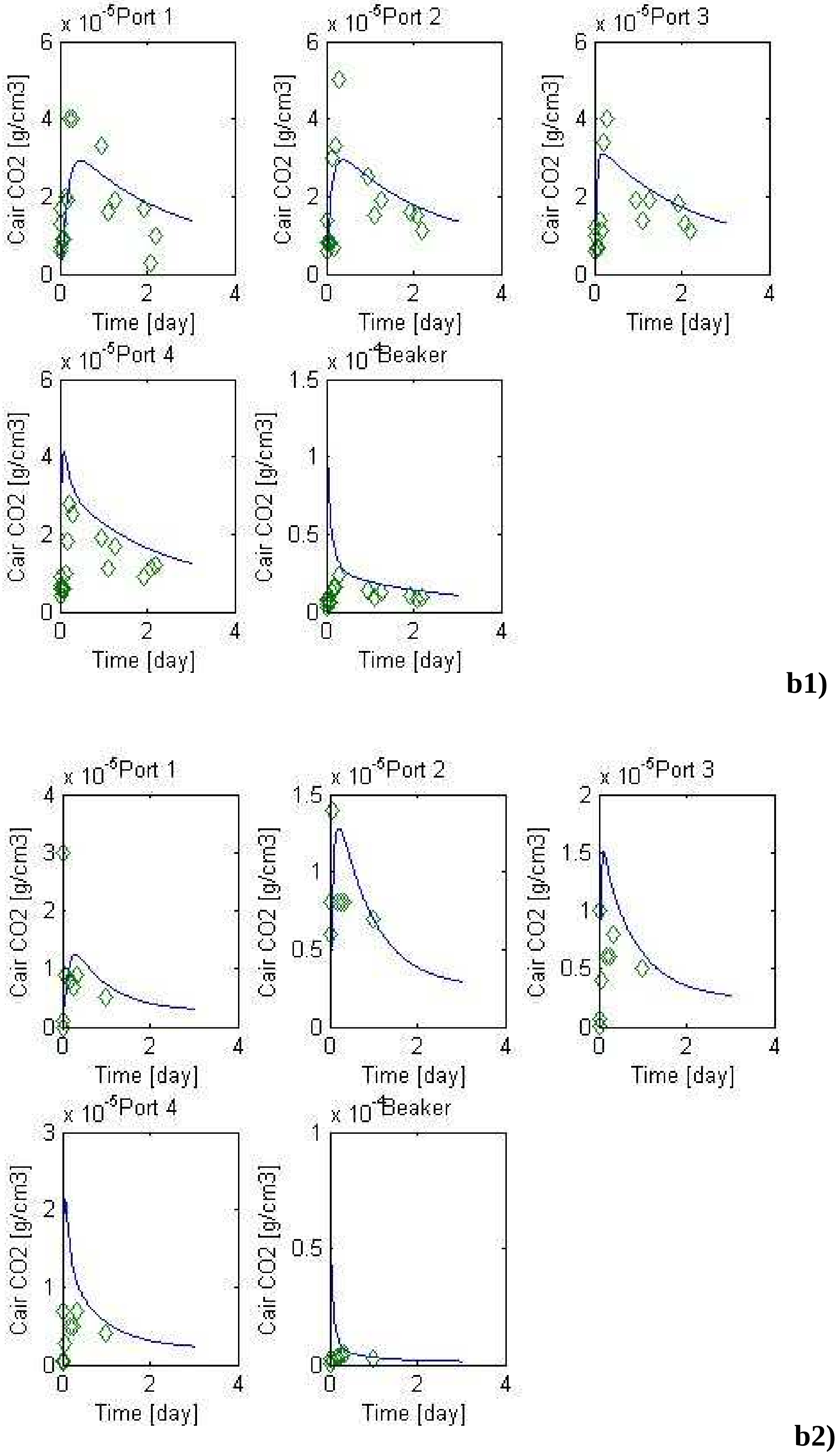

***Fig. 7.28**: results of duplicates of CO_2 tests, as described in § 7.2.5.4, in each of five sampling ports, for soil (a1 and a2) and biochar-amended soil (b1 and b2) closed column. Experimental data are indicated by green symbols, whereas simulations by black continuous line.*

7.3.3.3 Background conditions

Fig. 7.29 indicates the results from O_2 and CO_2 monitoring that took place soon after filling up with soil, as described in § 7.2.5.4. The arrow in graphs indicates the moment in which the beaker was taken off.

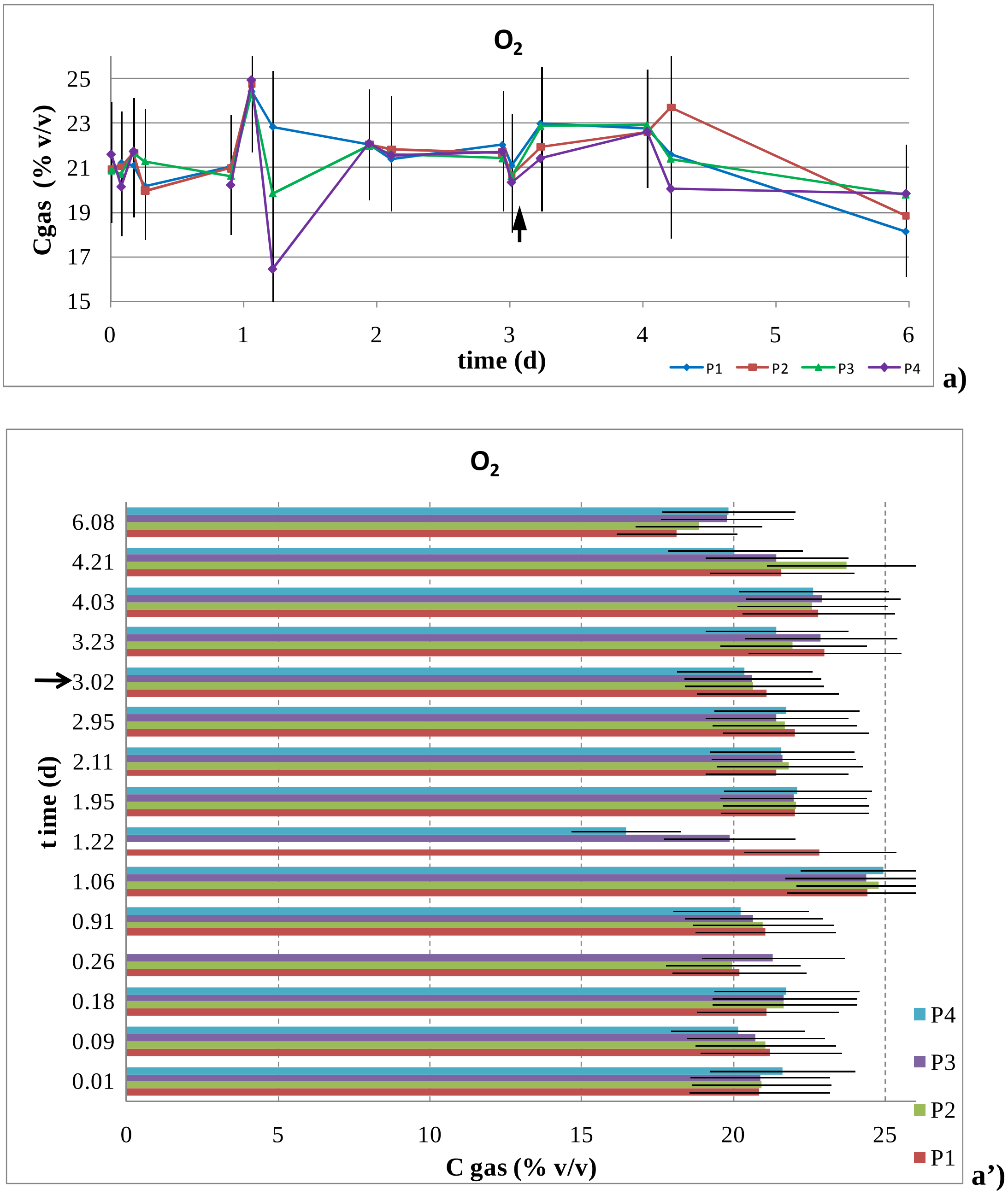

***Fig. 7.29**: continue.*

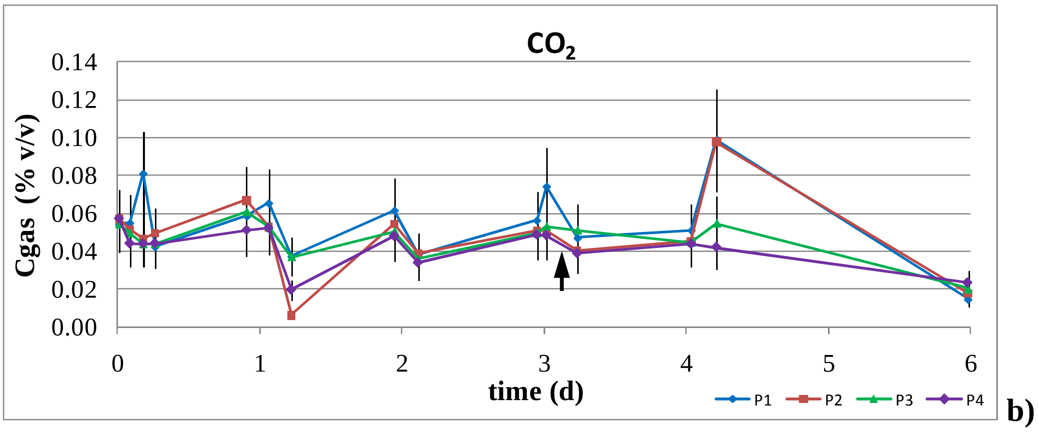

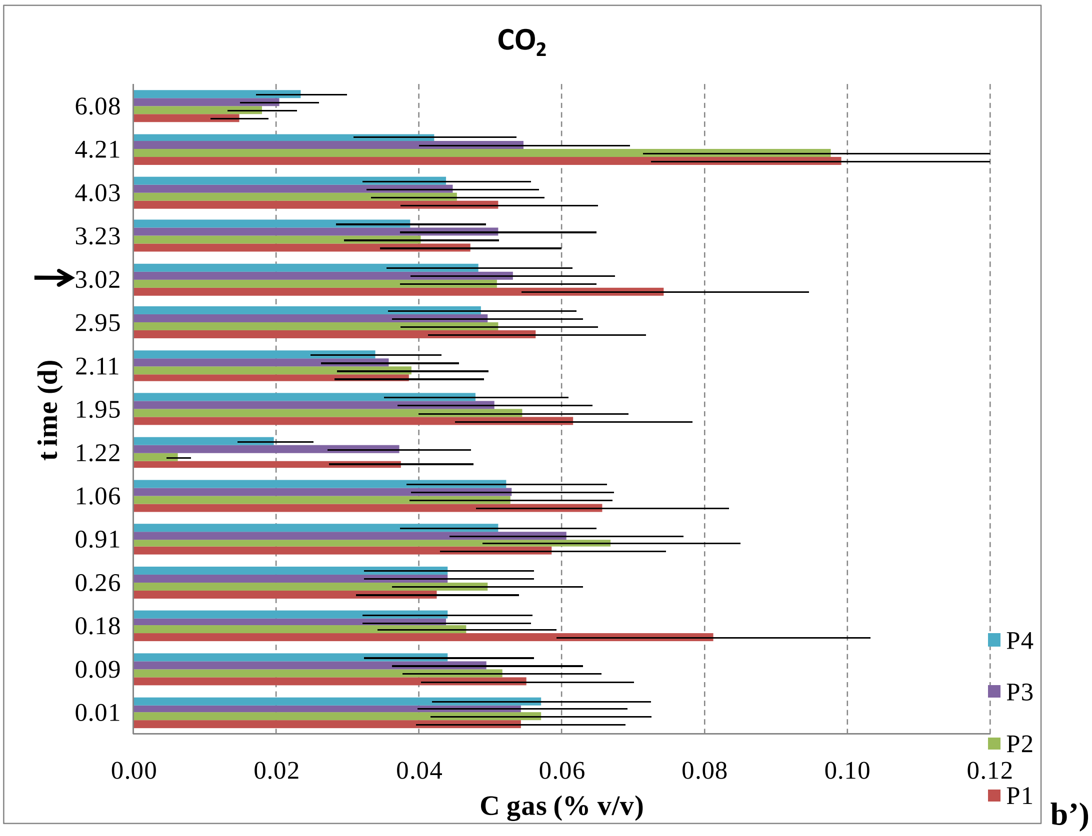

Fig. 7.29: *O_2 (a, a') and CO_2 (b, b') percentages in soil gas, at different sampling ports of soil column soon after the filling up (in § 7.2.5.4). Arrow indicates the moment in which the beaker covering the top was taken off, leaving open boundary conditions. Graphs a and b describe gas percentage behaviour over time, whereas a' and b' underline comparison between different ports. Error bars indicate analytical uncertainty (§ A2.3).*

As it possible to deduce, initial oxygen content in the soil column was, in all the sampling ports, near to atmospheric levels, with an average value on the sampling period of 21±1% (as standard error). CO_2 was near to natural atmospheric content, with an average value of 0.05±0.02%. An increase in this gas was not noted during closed boundary conditions, meaning that the natural biological activity was low. Small values on 6th day were probably due to GC-MS analytical problems because the same behaviour was observable in oxygen.

7.3.3.4 Open boundary conditions

7.3.3.4.1 Biological parameters

The behaviours of O_2 and CO_2 (as volume percentages) during column tests with open boundary conditions, are indicated in Figs. 7.30 and 7.31 respectively, both for soil (Fig. 7.30.a and 7.31.a) and for biochar-amended soil (Fig. 7.30.b and 7.31.b).

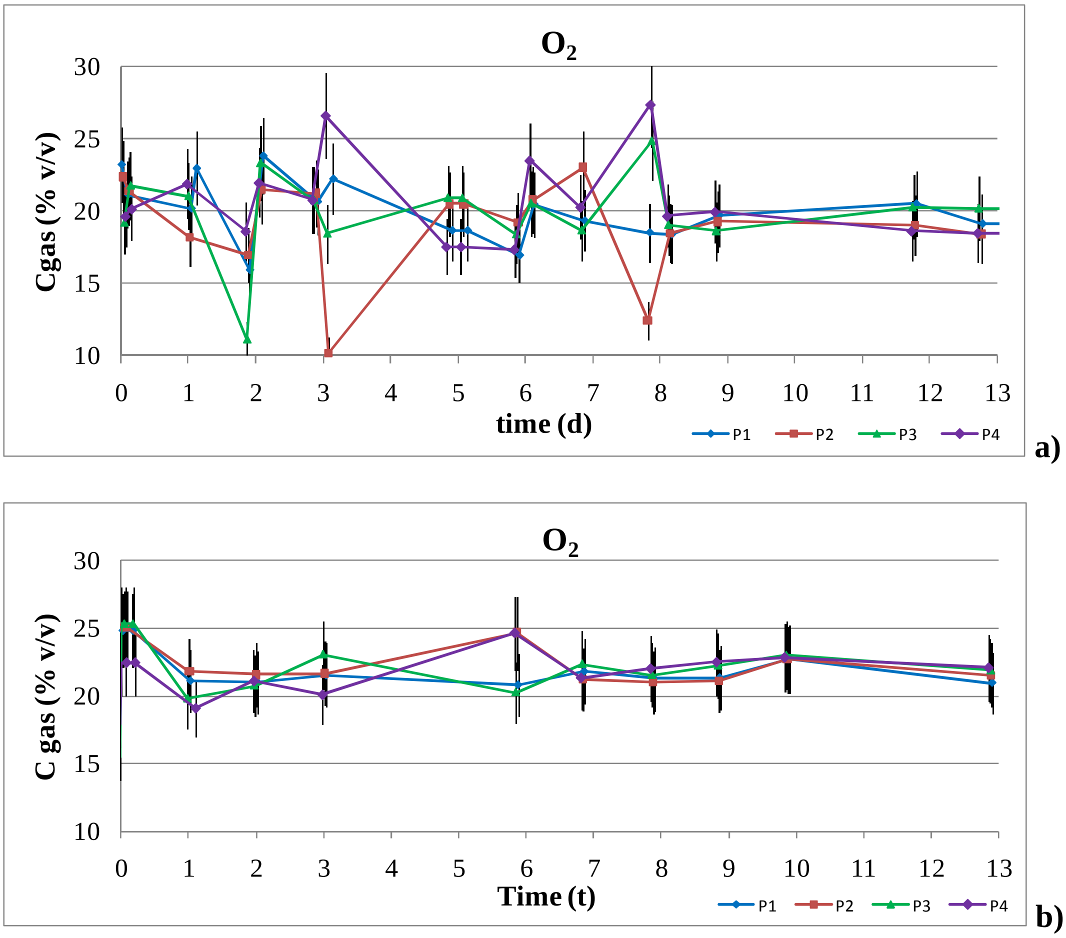

Fig. 7.30: *O_2 volume percentages behaviour along soil (a), and biochar-amended soil (b) column tests with open boundary conditions. Error bars indicate analytical uncertainty (§ A2.3).*

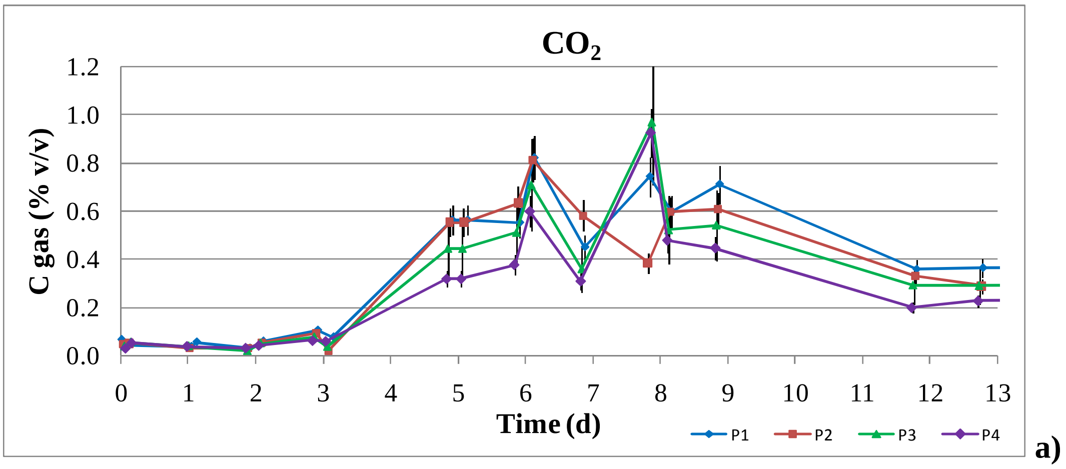

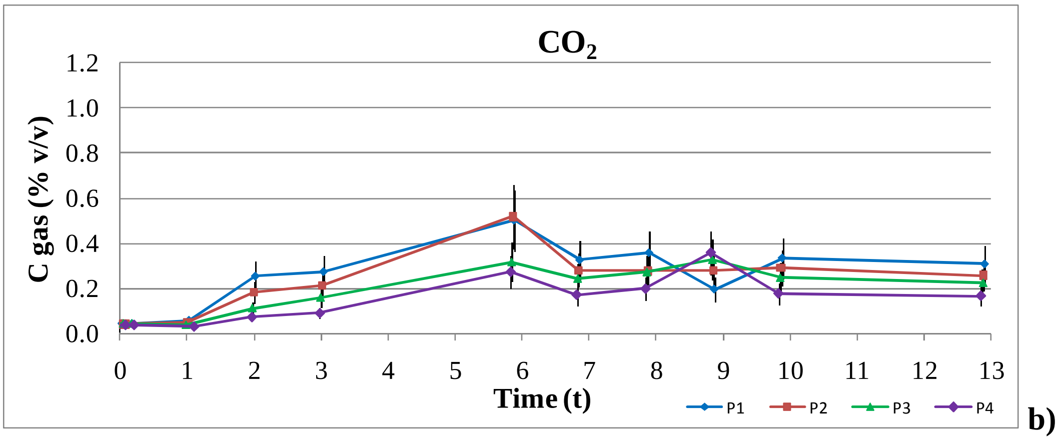

***Fig. 7.31**: CO_2 volume percentages behaviour along soil (a), and biochar-amended soil (b) column tests with open boundary conditions. Error bars indicate analytical uncertainty (§ A2.3).*

With the exception of some outlier points, due to analytical problems with GC-MS, it is clear that the two columns were conducted in aerobic condition, with an average oxygen content of 20±3% for soil and 22±2% for biochar-amended soil (errors indicate standard deviation on all sampling points).

As for CO_2, in soil an increase was seen from initial values reported in § 7.3.3.3 till 6th-8th day, of about 2599±1031%, 3995±1563%, 4860±1894%, 2773±1097% (with uncertainty due to analytical error propagation on ratio computation, equivalent to VC = 39 %), as a reference to initial values, respectively in ports 1, 2, 3 and 4. After that time a slow decrease began till 0.30±0.05% (as standard deviation of final time concentration for the four ports).

As for biochar-amended soil, it followed a similar trend, but with a less sharp increase, equivalent to 3554±1357%, 4017±1572%, 3120±1230%, 3134±1235% (uncertainty calculated as previously, equal to 39%), reaching 0.24±0.07% (as standard deviation of final time concentration for the four ports). These behaviours could be associated to a first phase of faster degradation of VOCs followed by a slower one, where substrates were less degraded and mineralized to CO_2.

Simulations of CO_2 trend from modelling, only for a representative intermediate port (port 2), are shown in Fig. 7.32. Behaviours of CO_2 in presence or absence of microbial activity are indicated, for both soil and biochar-amended soil. The model concentration outputs, expressed as [g ml^{-1}], were transformed into volume percentages through the inversion of (7.2). Results from simulation present the same increasing followed by decreasing trend seen during experiments, but in both cases the maximum concentration was reached earlier than in tests. Simulation seems to suit soil better than amended soil column, because the ratio among maximum concentrations values from model and test, in port 2, is respectively 1.9 and 4.4.

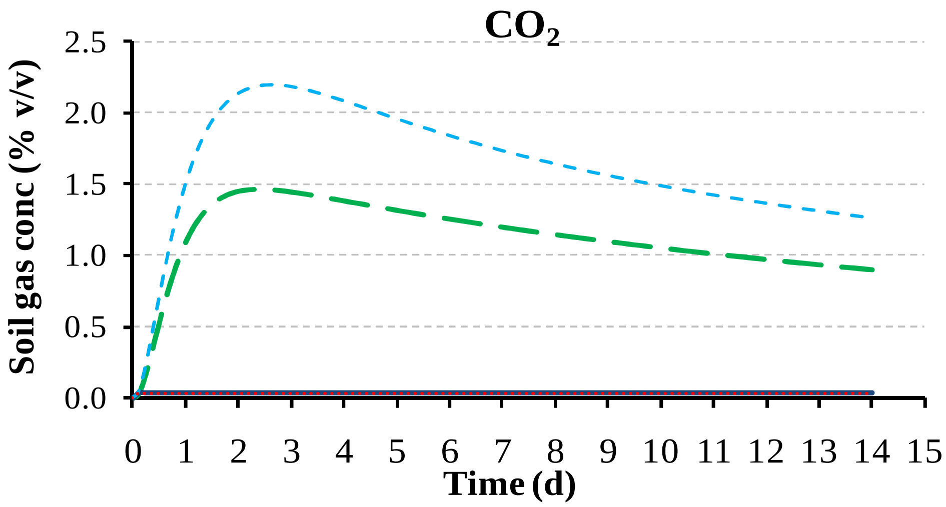

Fig. 7.32: *CO_2 modelled volume percentages over time, in port 2, for soil and biochar-amended soil open column tests. Visible lines indicate biodegradation simulation: thick green long dashed lines indicate trend in soil and thin light blue short dashed line trend in biochar-amended soil column. Faint blue continuous line, and red dotted line indicate respectively soil and biochar-amended soil without biodegradation.*

It seems that biodegradation in column tests involved a lag time that was not considered in model formulation; furthermore biodegradation activity is lower than behaviours in batch tests, and there were probably some CO_2 absorption phenomena that were not considered. In biochar-amended column, in fact, in view of higher degradation rate (Tab.7.17), lower CO_2 concentrations were found.

7.3.3.4.2 VOC monitoring

Fig. 7.33 indicates the behaviour, for each i-VOC, of gas concentration over time, recorded during soil and biochar-amended soil column tests with open boundary conditions, in each sampling port (port 1 (a), port 2 (b), port 3 (c), port 4 (d)).

For port 2 only the concentrations predicted by assuming either no degradation ($k_{deg,water} = 0$) or using the $k_{deg,water}$ data (Tab. 7.17) are illustrated next to them. Only one port is indicated because of similar behaviour of modelled curve in each port, changing just in maximum concentration reached (as it is possible to deduce also from experimental data and Fig. 7.34).

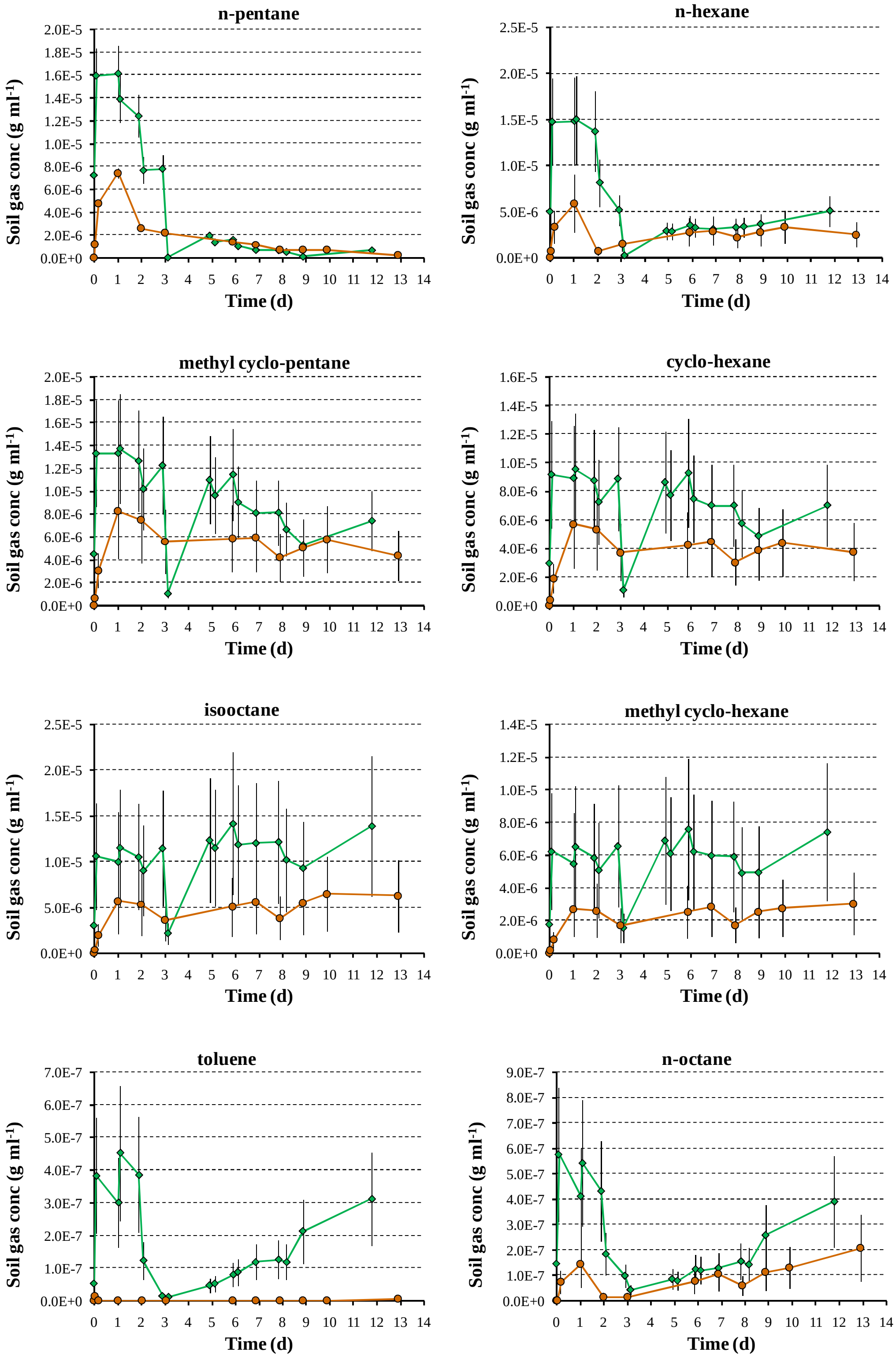

***Fig. 7.33**: continue.*

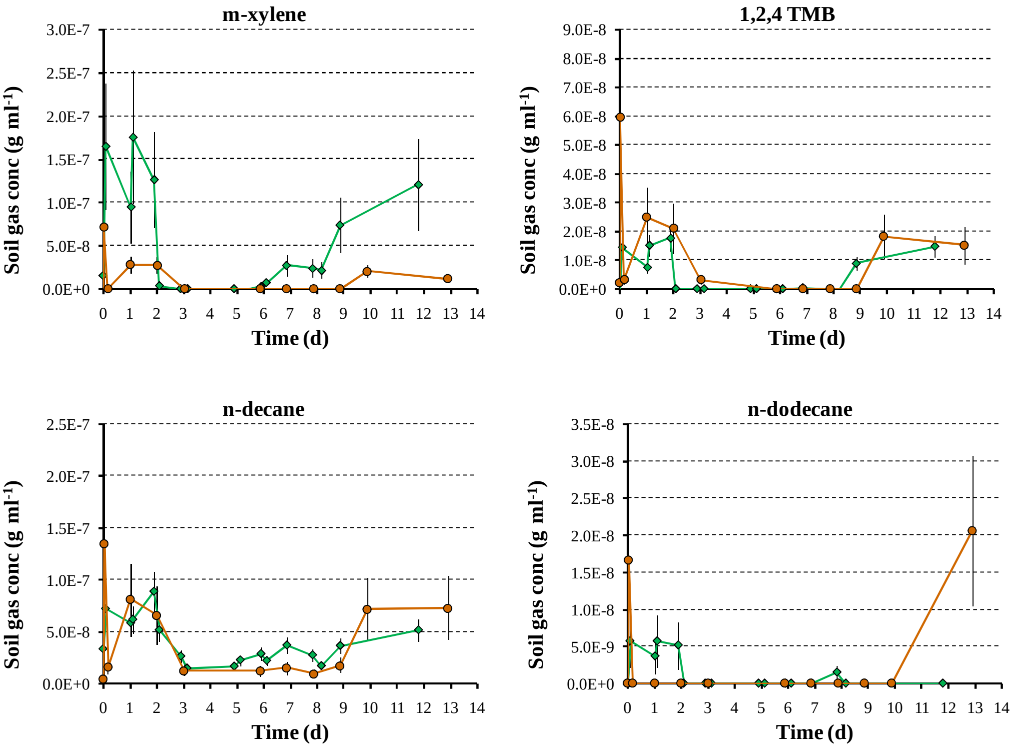

a)

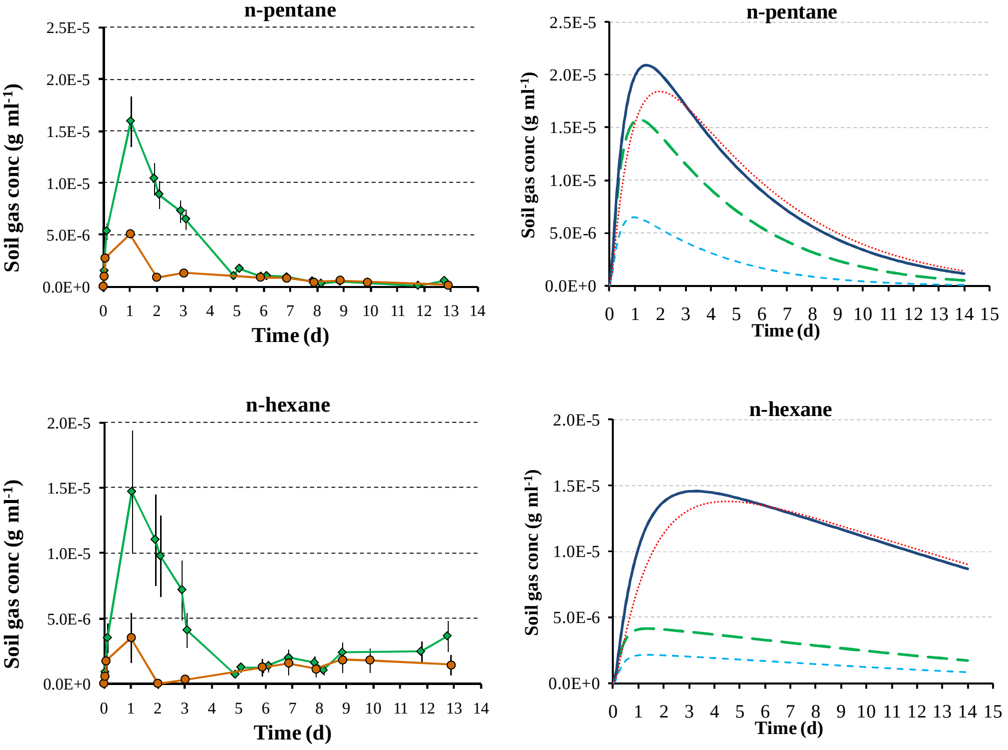

Fig. 7.33: *continue.*

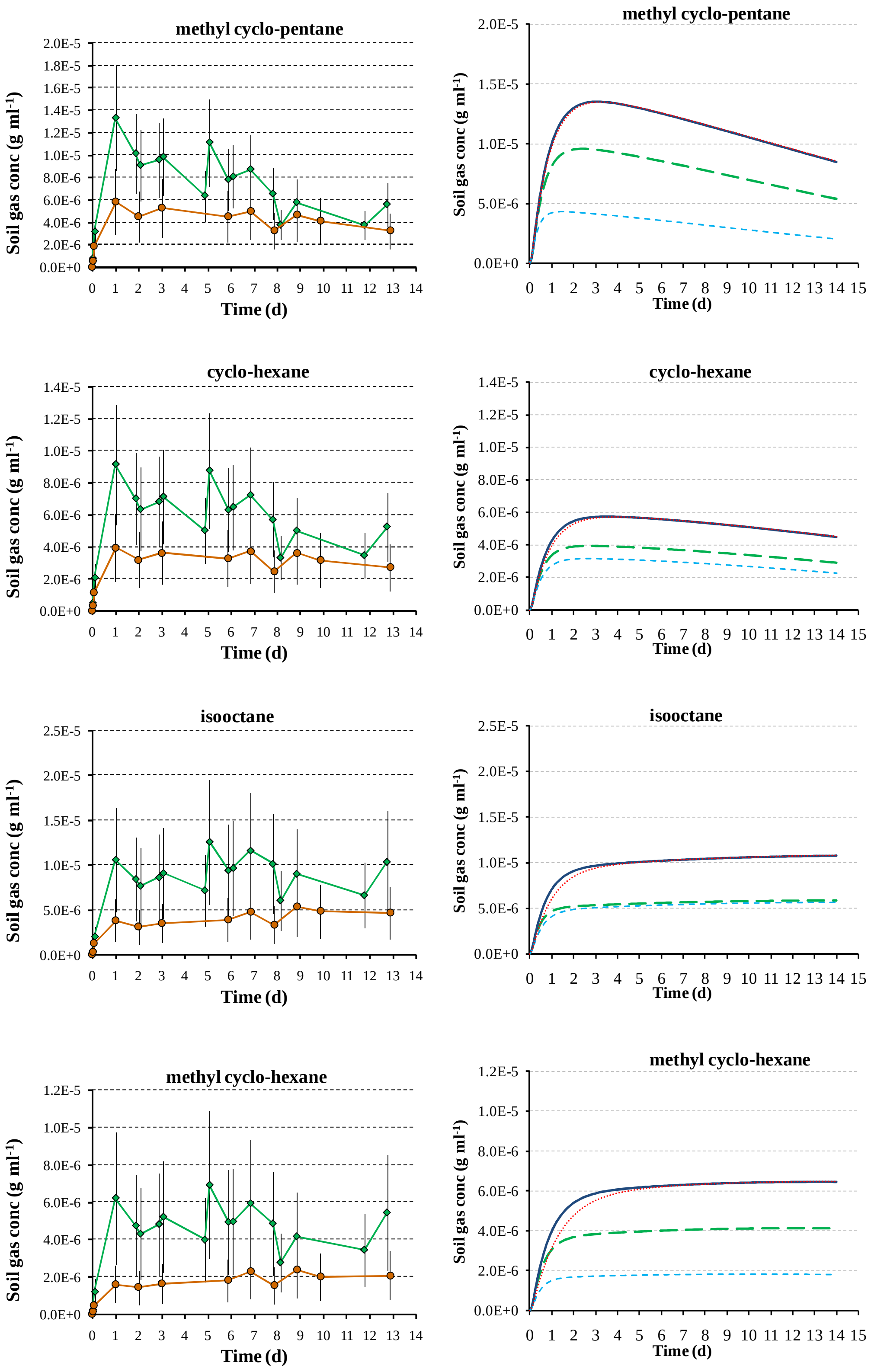

***Fig. 7.33**: continue.*

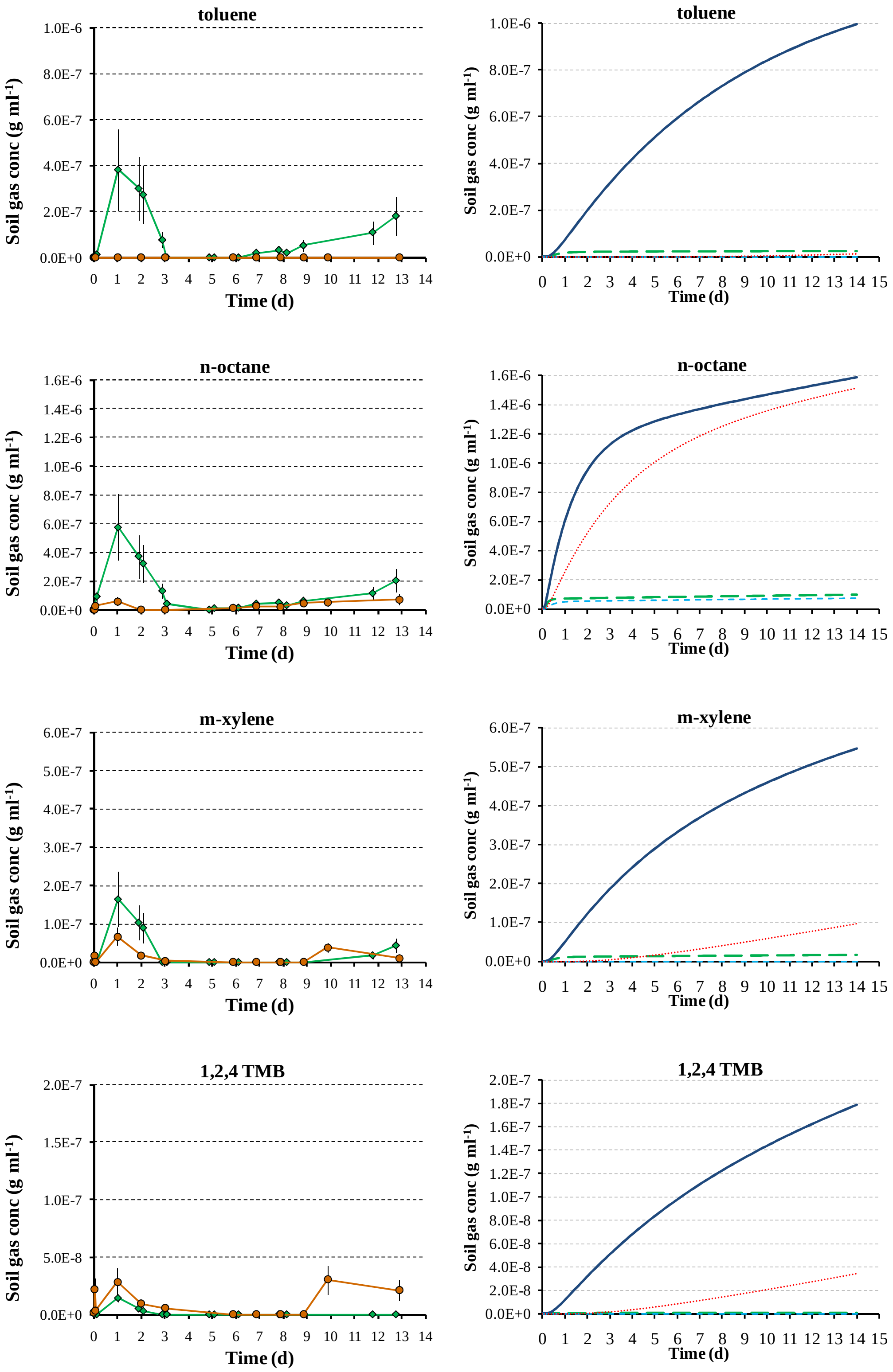

***Fig. 7.33**: continue.*

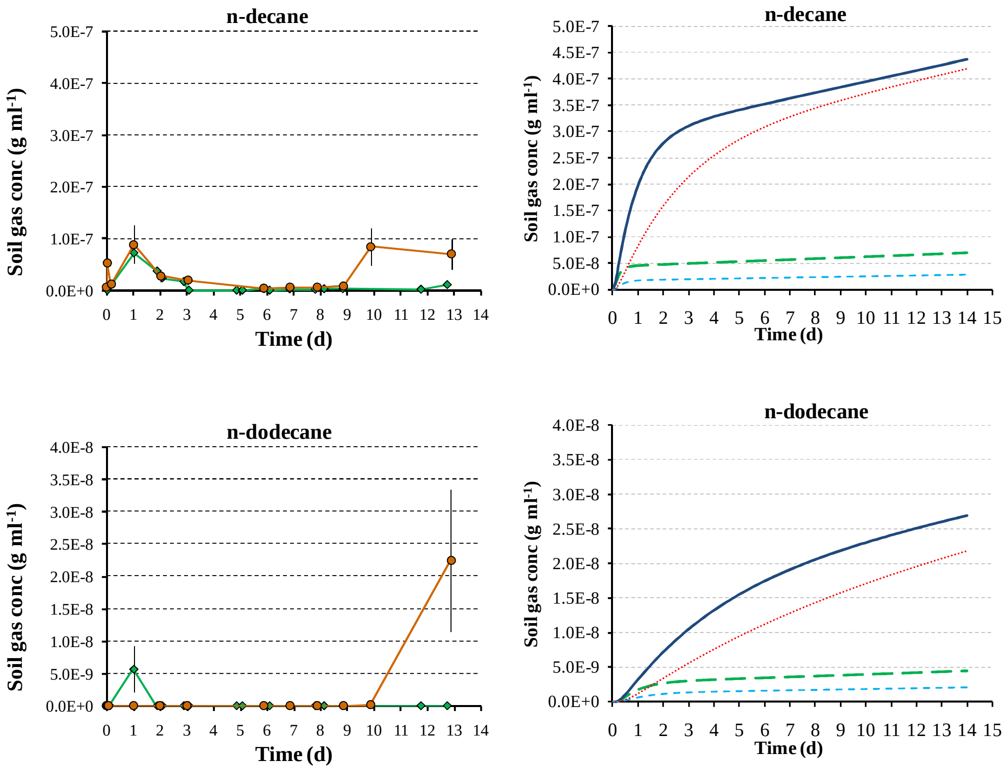

b) **b')**

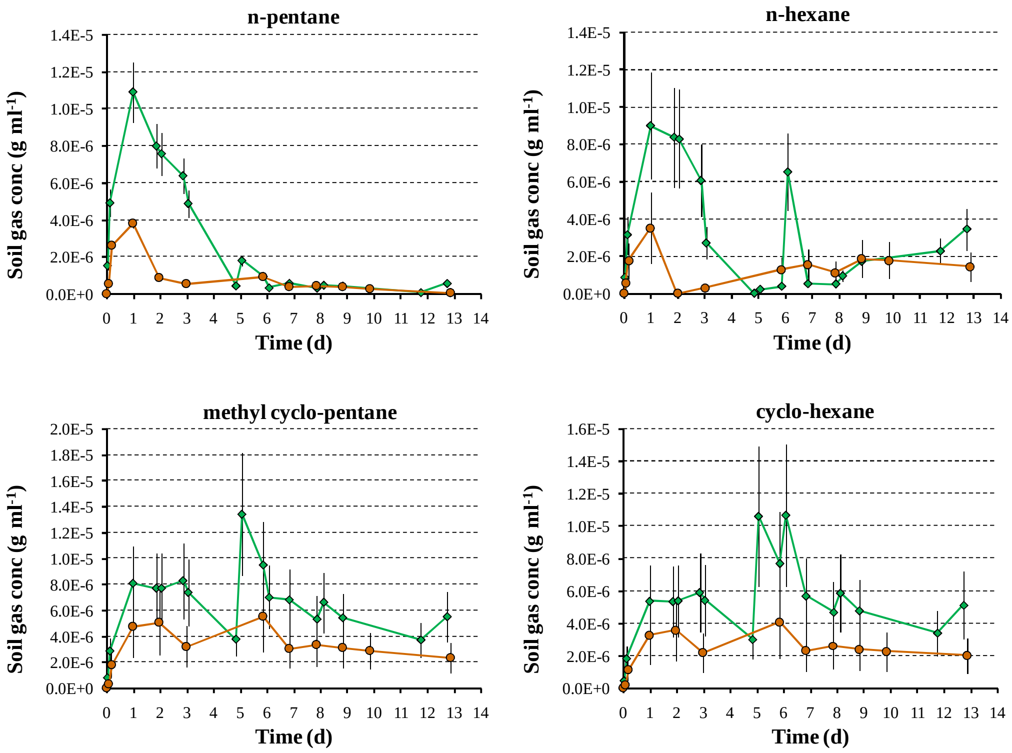

***Fig. 7.33**: continue.*

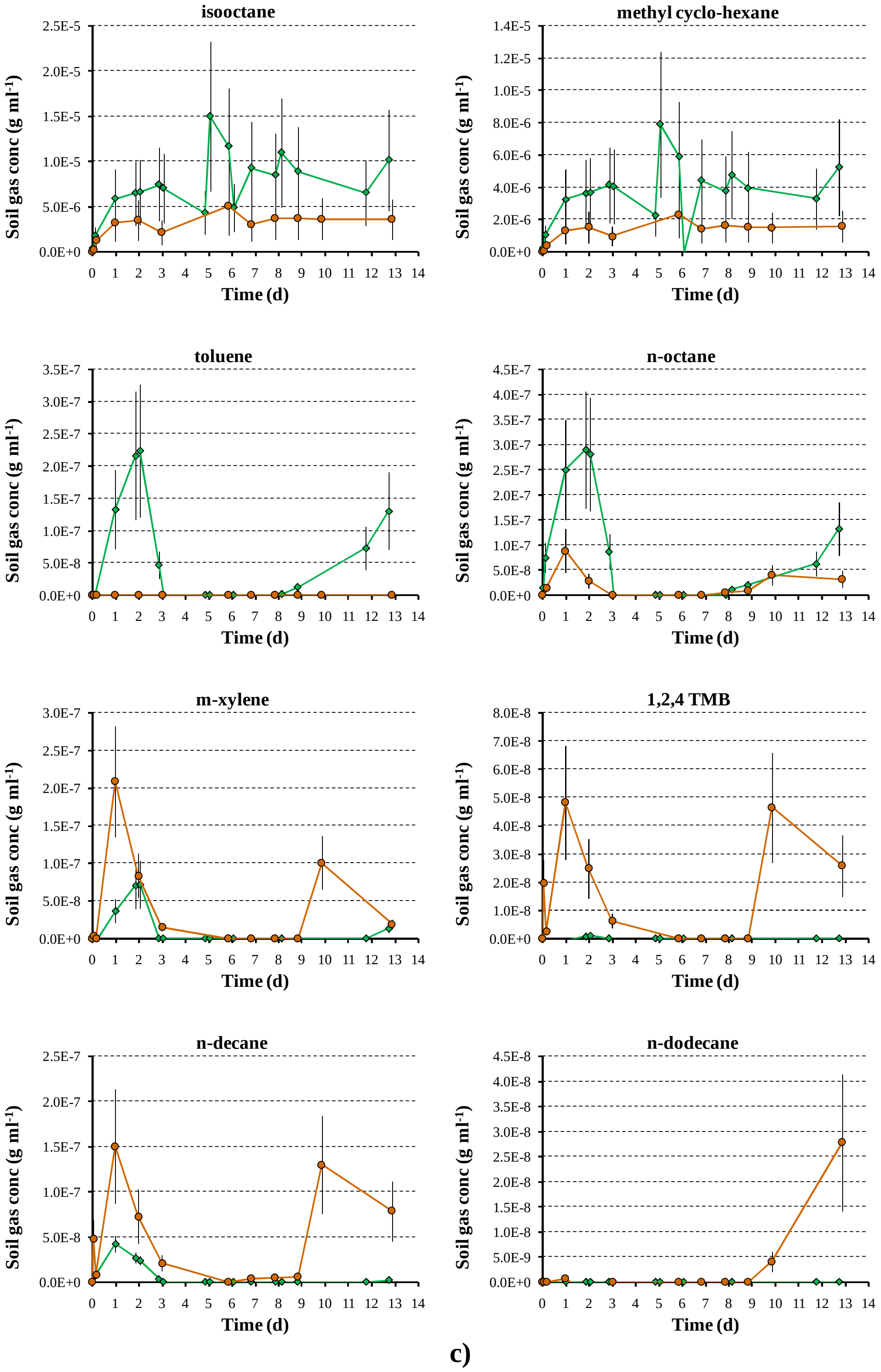

***Fig. 7.33**: continue.*

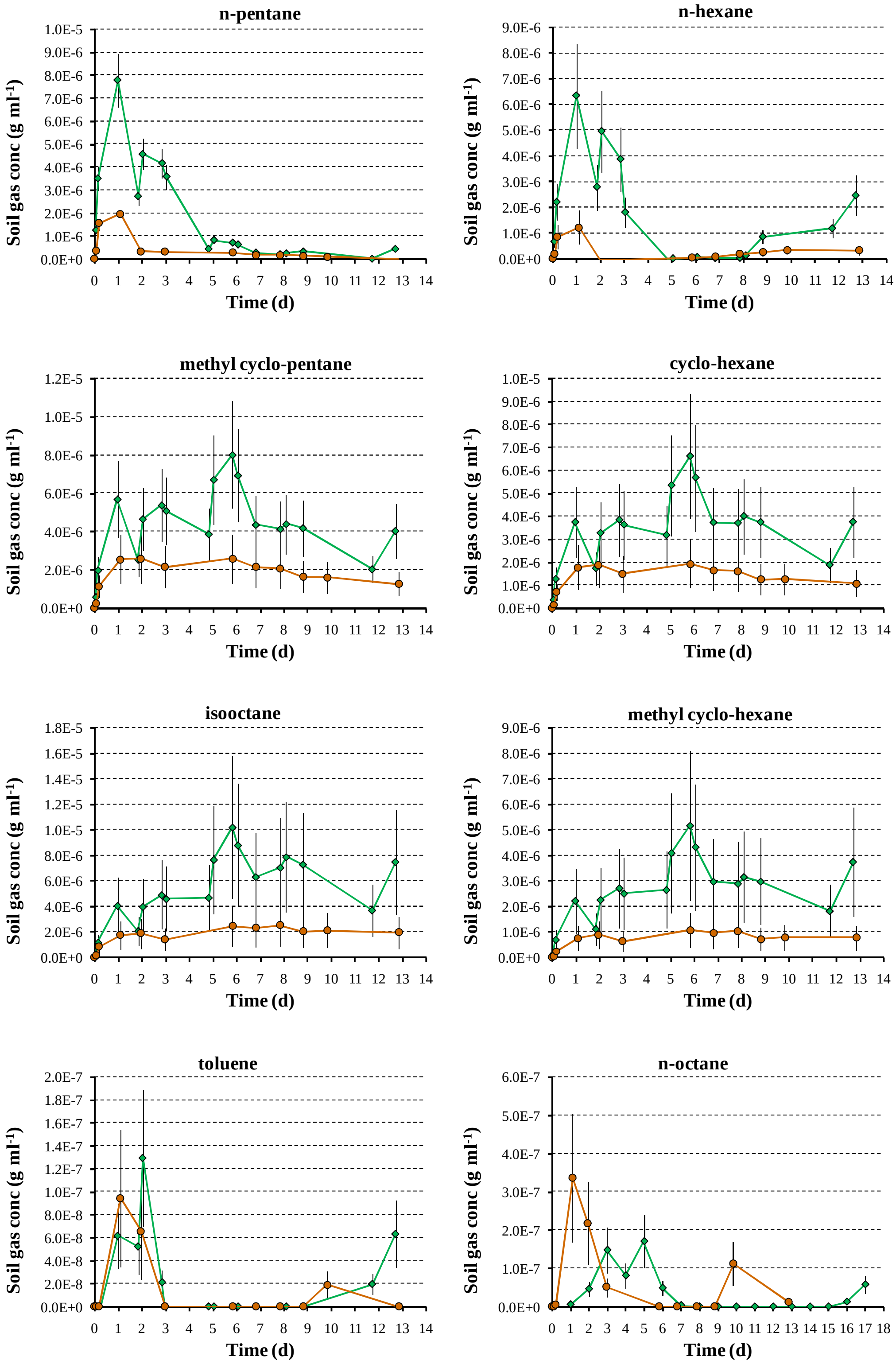

***Fig. 7.33**: continue.*

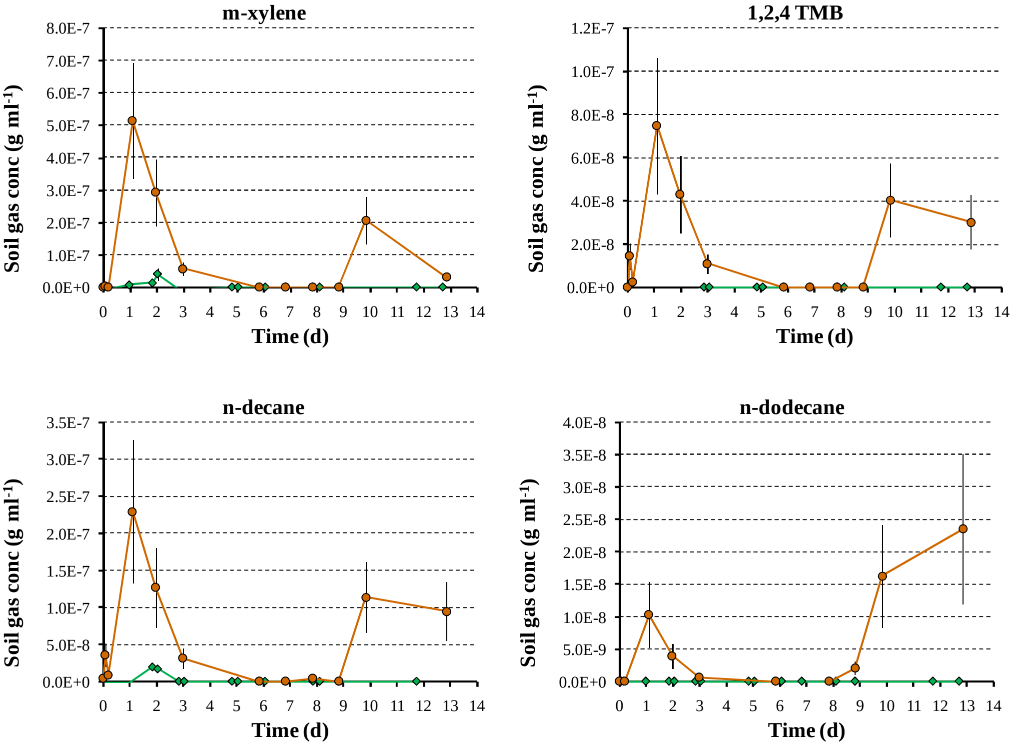

d)

Fig. 7.33*: gas concentration [g ml^{-1}] for each i-VOC versus time, for open column tests, for each VOC in each sampling port (port 1 (a), port 2 (b), port 3 (c), port 4 (d)). Soil data are indicated by green lozenges (—◆—), biochar-amended soil by orange circles (—●—). Error bars indicate analytical variance. As for b', thick lines indicate soil column and dashed lines simulation with biodegradation. In detail simulations for SOIL: continuous blue line (———) without biodegradation, long dashed green line (— —) with biodegradation; for biochar-amended soil: thin dotted red line (········) without biodegradation, short dashed light blue line (- - -) with biodegradation.*

Simulations of some representative compounds for each port are attached, too (Fig. 7.34); four molecules were chosen, three of different chemical and biodegradability behaviour (n-pentane, cyclohexane and toluene), and the fourth one chemically similar to toluene (xylene) in order to verify the model easily. It is clear that for each compound the difference between one port and another is just in the numerical amount of the concentrations, and not into their trend shape over time.

From the benchmark between Figs.7.33.b and 7.33.b', behaviours of 12 studied VOCs may be divided in chemical family groups. All the n-alkanes initially presented huge increase in concentration, and then a smoother decrease, for both soil and biochar-amended soil. The final behaviour changed for specific compounds. At the end of the test, n-pentane, n-dodecane and n-decane (with the exception of the last sampled points) reached values similar to the results of simulation considering biodegradation. As for n-hexane and n-octane, their concentrations initially increased in line with the predictions for a system without biodegradation. Then after 1 day concentrations decreased rapidly in both soil and soil with biochar and became more consistent with simulations in which the $k_{deg,water}$ values determined in the batch study were used. In particular for the soil without biochar, n-octane concentrations increased again after 10 days above the levels predicted based on the $k_{deg,water}$ in Tab. 7.17, indicating a decreased microbial degradation rate. In general the modelled transport curve did not suit properly the behaviour of this compound.

	Soil: C_g [g ml^{-1}]	**Biochar-amended soil: C_g [g ml^{-1}]**
Port 1	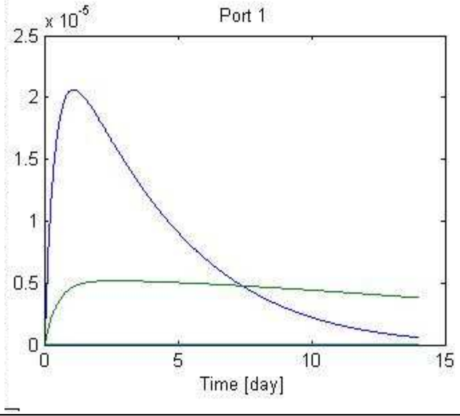	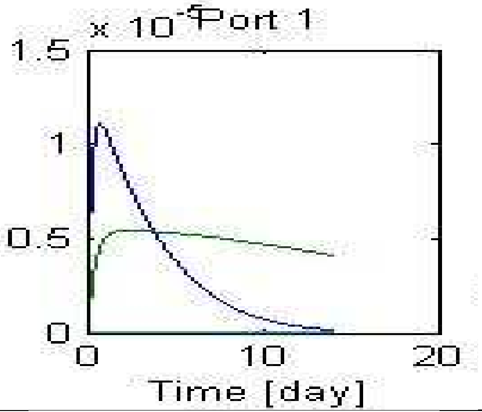
Port 2	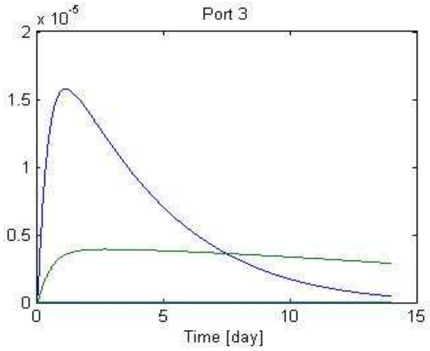	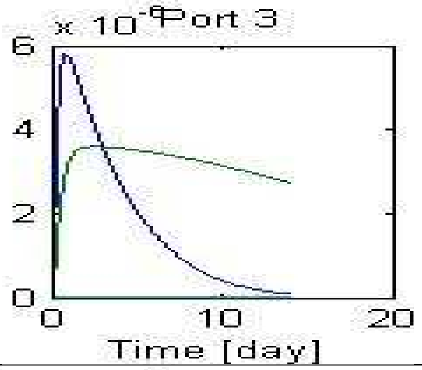
Port 3	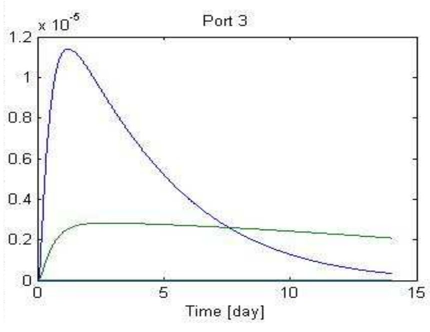	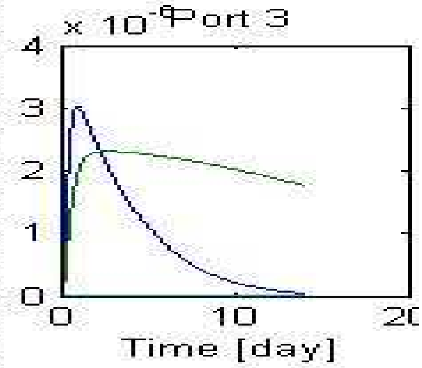

***Fig. 7.34**: continue.*

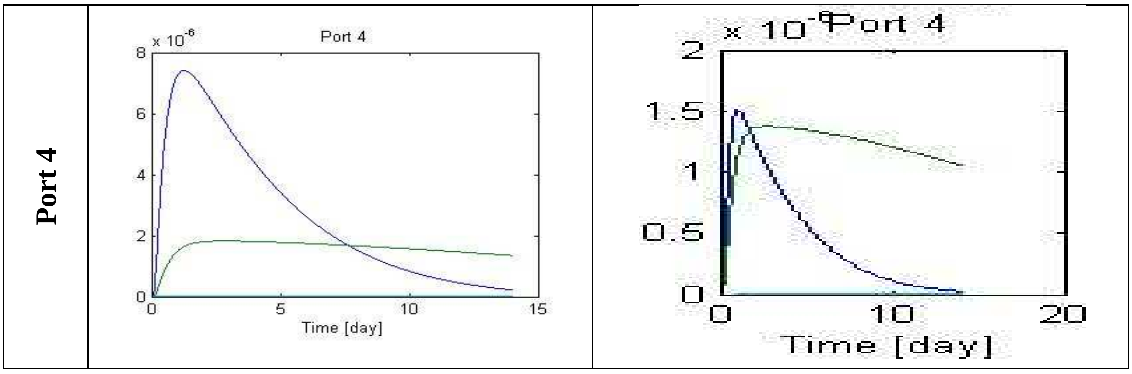

***Fig. 7.34**: results of simulations, at different ports, for soil column and biochar-amended column, considering microbiological activity with degradation rates resulting from batch tests. Gas concentrations [g ml^{-1}] for n-pentane (with blue line), cyclohexane (with green line), toluene (with light blue line) and xylene (with yellow line) are presented.*

As far as cyclic compounds were concerned, cyclohexane followed the same trend of concentration versus time reached by the model, however maintaining concentration values between levels from simulation with and without biodegradation, for both natural and amended soil; further details cannot be added because of great analytical uncertainty.

Branched alkanes (isooctane) in soil seemed to degrade badly, because experimental data were well fitted with no-degradation curve. The presence of biochar favoured biodegradation, in fact the degradation model suited experimental data well.

Branched-cyclic compounds were well degraded, both in soil and in biochar, where experimental data followed the same trend as modelled ones; for methyl cyclo-hexane the behaviour on soil was hardly observable because of high analytical uncertainty and low $k_{deg,water}$ value.

As for toluene, concentrations at port 2 in the column without biochar initially increased in line with the simulation assuming no biodegradation, intermittently decreased to very low levels consistent with the prediction based on the $k_{deg,water}$ value from the batch study, then started to rise again. For the soil amended with biochar toluene concentrations remained below the detection limit (§ A2.3). Even at the lowest port 1 (Fig. 7.33) toluene could only once be detected in soil amended with biochar 33 min after the start of the experiment with a measured concentration of 1.4 10^{-8} (g cm^{-3}).

m-xylene and 1,2,4-TMB concentrations followed, in soil, a trend similar to n-octane and n-decane respectively; the first compound, in fact, after a period of good agreement with simulations considering biodegradations, showed gradual increasing of concentrations. In biochar-amended soil this same trend was noticed for both molecules. They quickly spiked in biochar-amended soil towards the end of the experiment, indicating a temporary decrease in the microbial degradation of these compounds.

7.3.3.5 Closed boundary conditions

7.3.3.5.1 Biological parameters

As for soil column, during sampling just before starting with new b.c., value concentrations of 23.2 ± 0.3% v/v (VC = 1%) of O_2 and 0.219 ± 0.007% v/v (VC = 3%) of CO_2 were recorded. Regards biochar-amended soil, at the same time, initial values of O_2 and CO_2 were 21 ± 1% v/v (VC = 6%) and 0.06 ± 0.01% v/v (VC = 25%); in both cases data were the average and standard deviation on the four lateral ports, lower than what had been detected at the end of the first b.c. tests (§ 7.3.3.4.1).

The behaviours of O_2 and CO_2 (as volume percentages) during column tests with closed boundary conditions, are indicated in Fig. 7.35 and Fig. 7.36 respectively, both for soil (Fig. 7.35.a and 7.36.a) and biochar-amended soil (Fig. 7.35.b and 7.36.b).

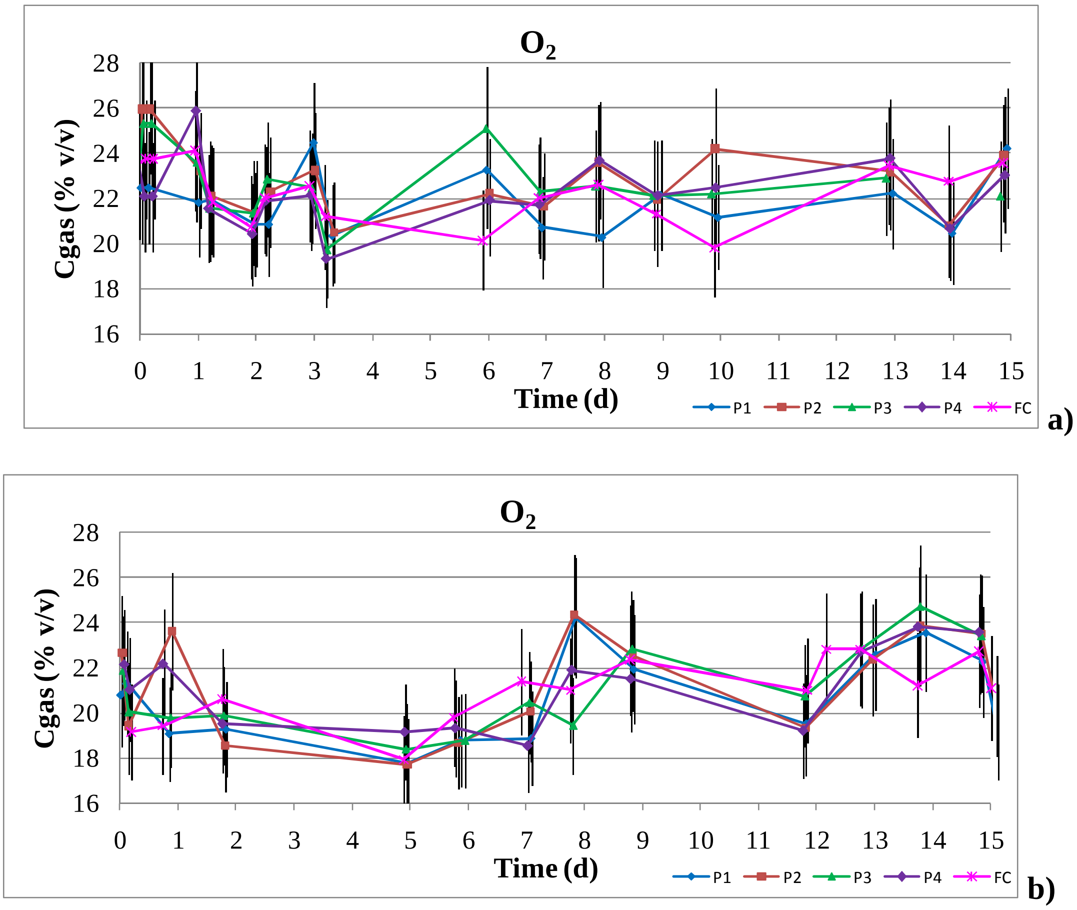

Fig. 7.35: *O_2 volume percentages behaviour over time in soil (a), and biochar-amended soil (b) column tests with closed boundary condition, at the height of sampling ports. Error bars indicate analytical uncertainty (§ A2.3).*

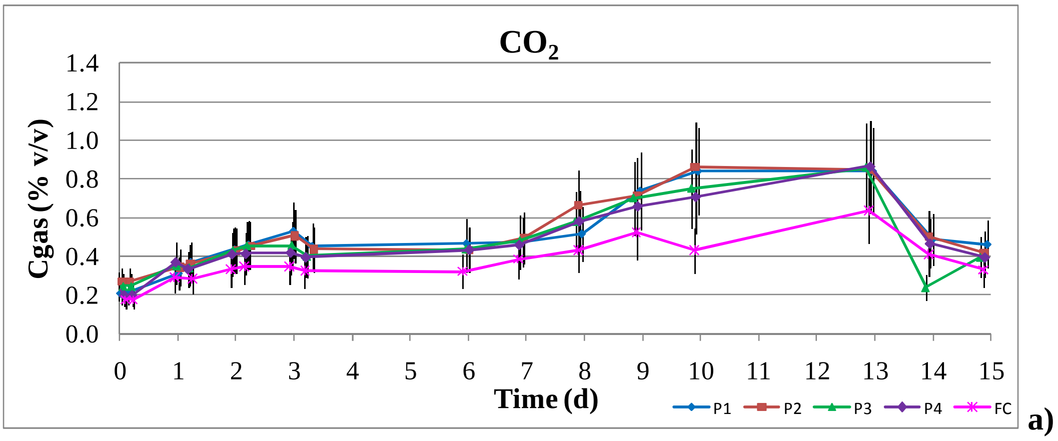

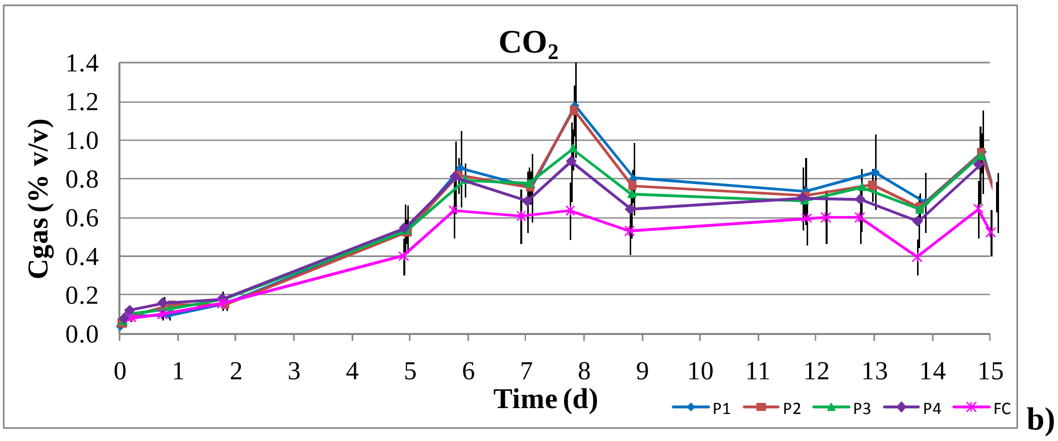

Fig. 7.36: *CO_2 volume percentages behaviour in soil (a), and biochar-amended soil (b) column tests with closed boundary conditions, at the height of sampling ports. Error bars indicate analytical uncertainty (§ A2.3).*

Experiments conducted with closed boundary conditions were also performed under aerobic condition: with an average oxygen content of 22±2% for soil and 21±2% for biochar-amended soil (errors indicate standard deviation on all sampling points). All the concentration variations were within analytical errors.

In soil column CO_2 increased till 10th -13th day, of about 299±153%, 243±131%, 259±137%, 331±164% and 263±138% (with uncertainty due to analytical error propagation on ratio computation), as a reference to initial values, respectively in port 1, 2, 3, 4 and inside the beaker on the column top. The maximum values were similar to one checked for open b.c. (Fig. 7.31.a). After that time a slow decrease began till 0.37±0.03% (as standard deviation of final time concentration for the four ports), equivalent to 1.7 times the initial value.

As for biochar-amended soil, it reached its maximum concentration on 8th day, equivalent to 1142±474%, 1218±504%, 817±350%, 645±285% and 978±412% (uncertainty calculated as previously, equal to maximum 42%), reaching, at the end of the test a value of 0.8±0.1% (as average on 5 sampling ports), equivalent to 12 times the initial concentration.

Simulations of CO_2 trend from modelling, just for a representative intermediate port (port 2) are indicated in Fig. 7.37. For both soil and biochar-amended soil, trends of this gas are indicated, in presence or absence of microbial activity, similarly to Fig. 7.32. Results from simulation presented the same increasing followed by decreasing trend seen during experiments, but in both cases the maximum concentration was reached earlier than in tests (huge difference for soil matrix) as previously seen for open column conditions, too. The ratio between maximum concentrations values from model and test, for the considered port, is 1.4 soil and 1.8 for biochar-amended soil column.

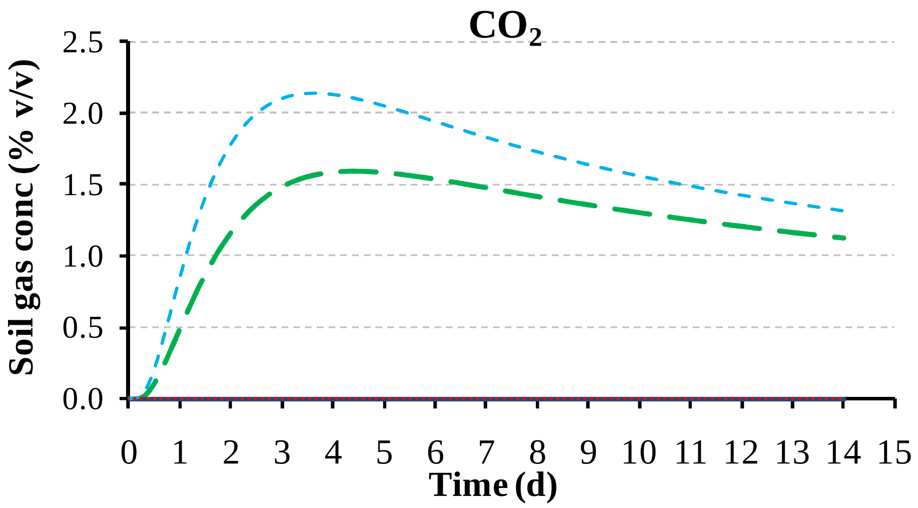

Fig. 7.37: *CO_2 modelled volume percentages over time, in port 2, for soil and biochar-amended soil closed column tests. Visible lines indicate biodegradation simulation: thick green long-dashed line indicate in soil and thin light-blue short dashed line in biochar-amended soil column. Faint continuous blue line, and red pointed line indicate respectively soil and biochar-amended soil without biodegradation.*

Comparison between experimented and simulated data for closed boundary conditions column tests confirm the observations made for open column in §7.3.3.4.1.

7.3.3.5.2 VOC monitoring

Fig. 7.38 indicates the behaviour, for each i-VOC, of gas concentration in time recorded during soil and biochar-amended soil column tests with open boundary conditions, in each sampling port (port 1 (a), port 2 (b), port 3 (c), port 4 (d), flux chamber (e)).

For the top port only, placed on static flux chamber closing the column, the predicted concentrations are indicated by assuming either no degradation or using the $k_{deg,water}$ data (Tab. 7.38.e'). Only this port was indicated because it was considered the most meaningful one of the closed b.c. tests.

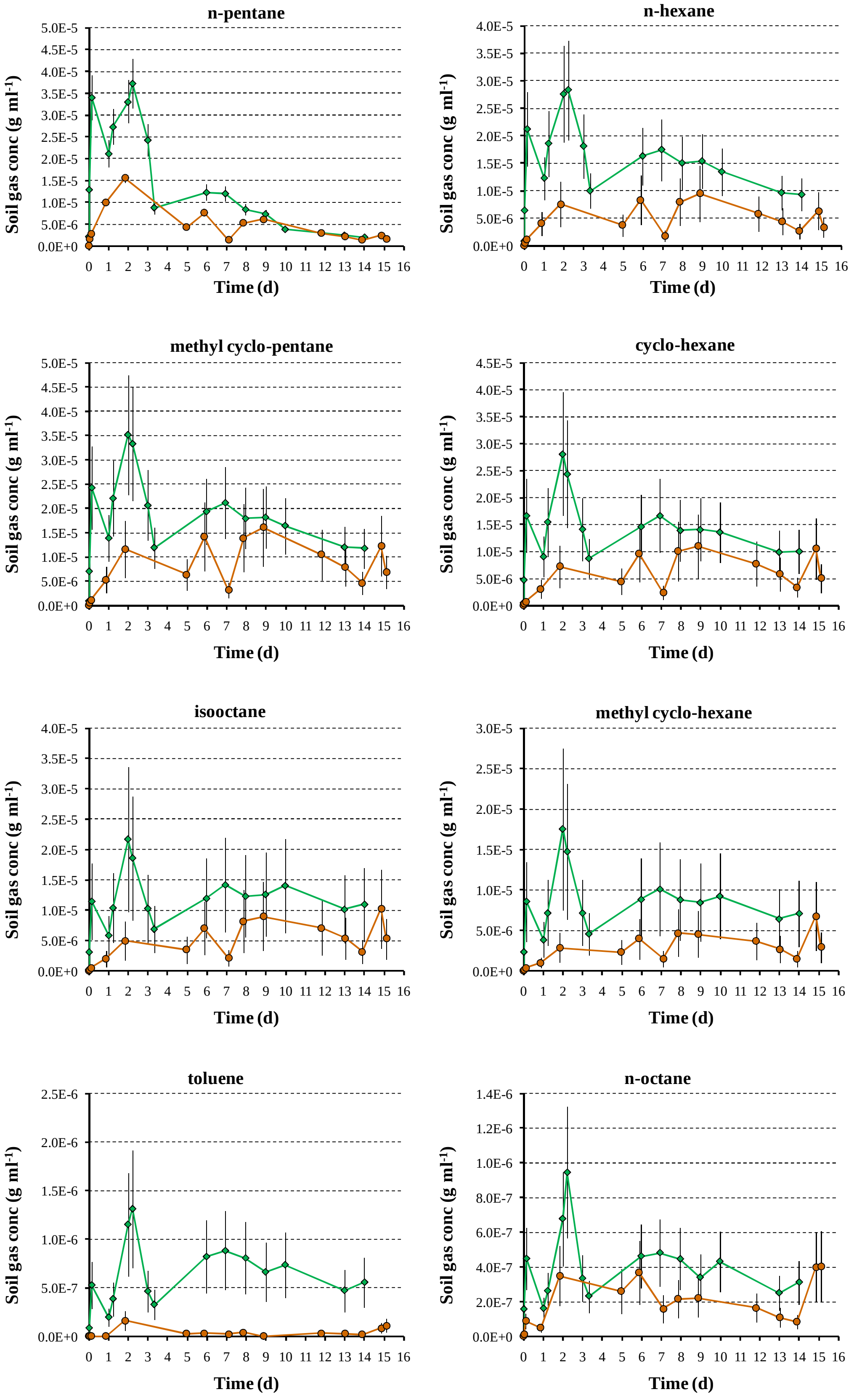

Fig. 7.38: *continue.*

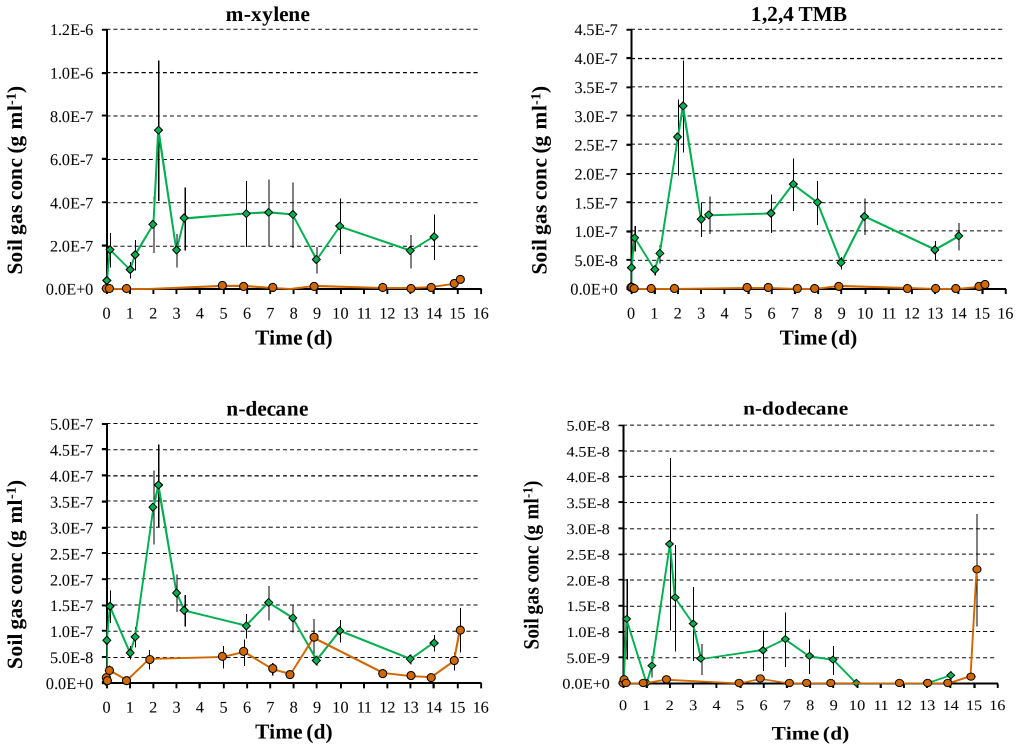

a)

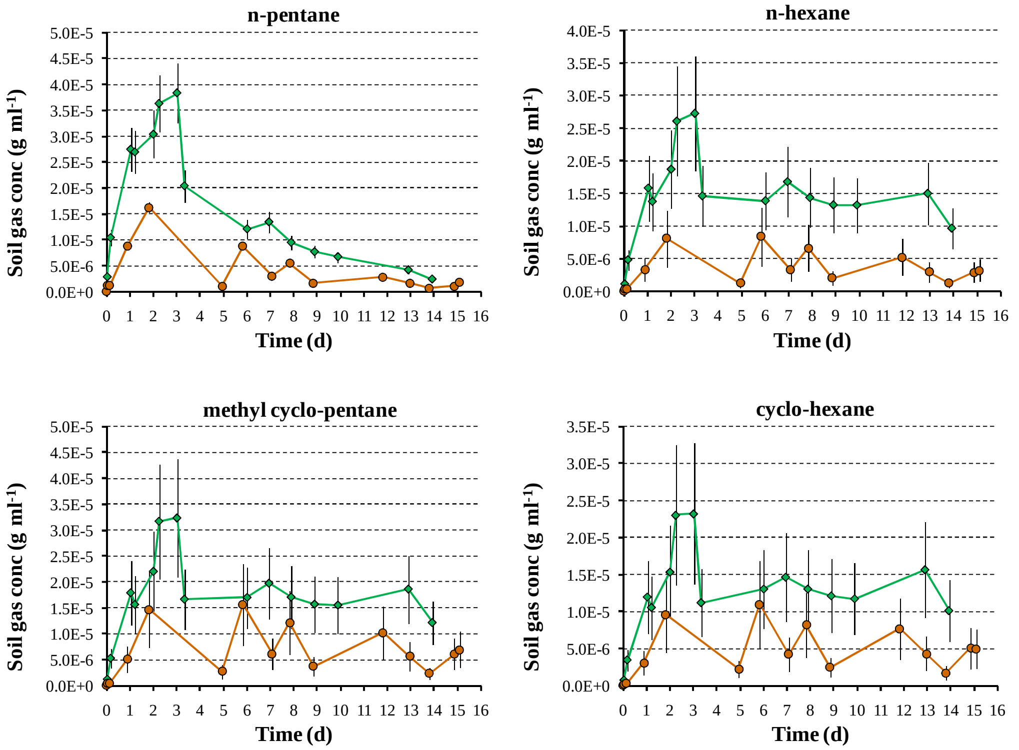

***Fig. 7.38**: continue.*

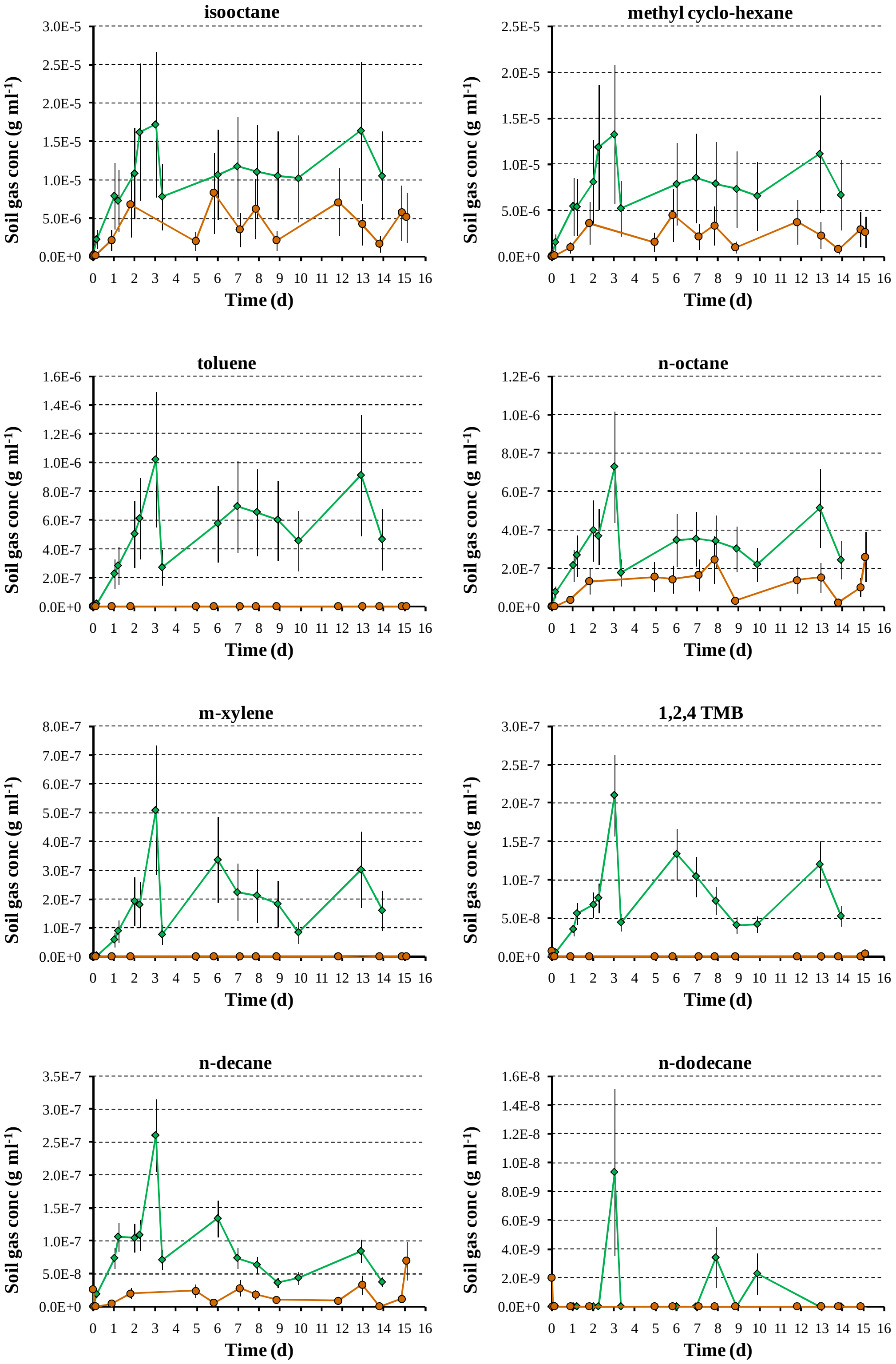

b)

***Fig. 7.38**: continue.*

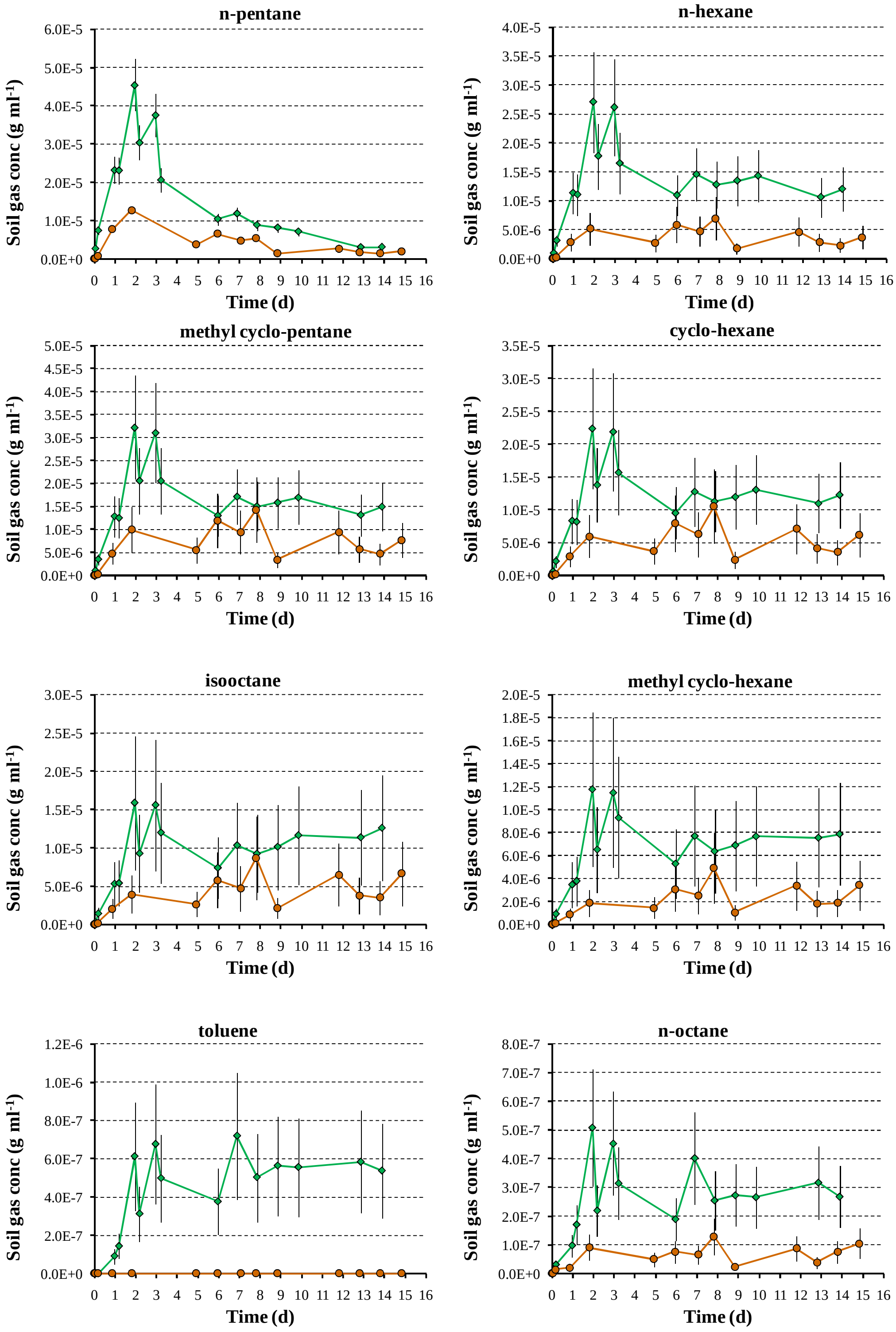

***Fig. 7.38**: continue.*

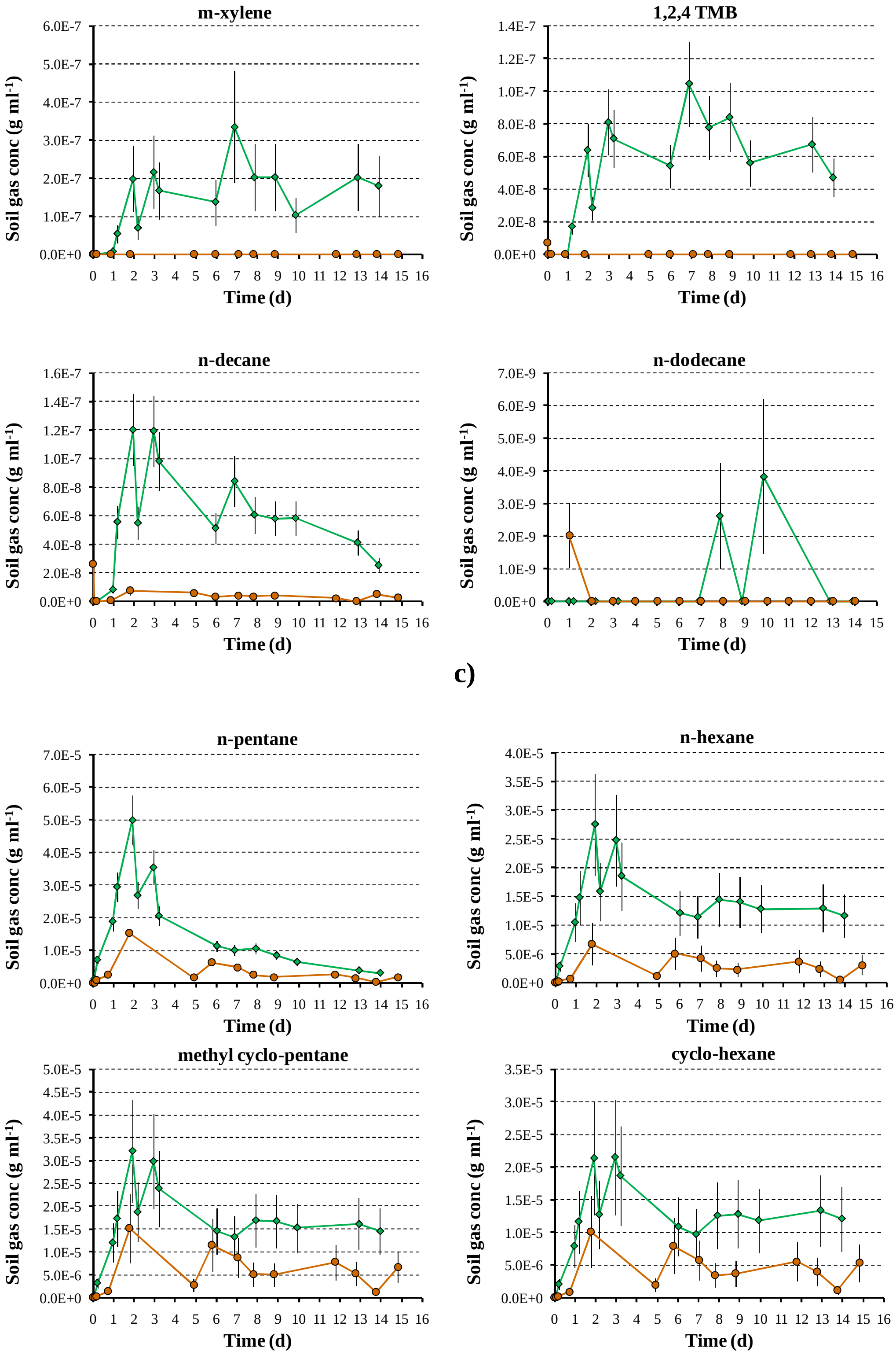

Fig. 7.38: *continue.*

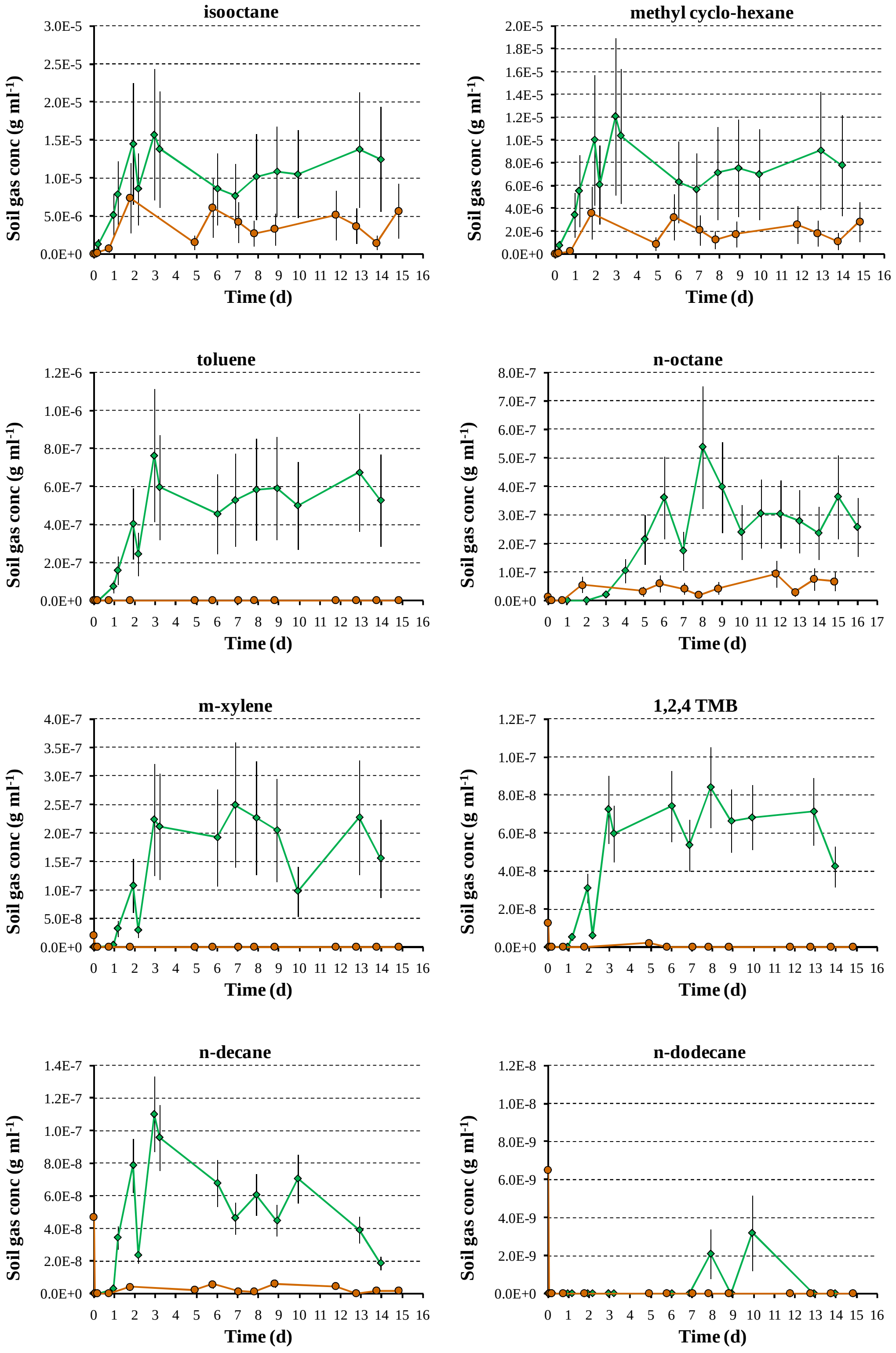

d)

***Fig. 7.38**: continue.*

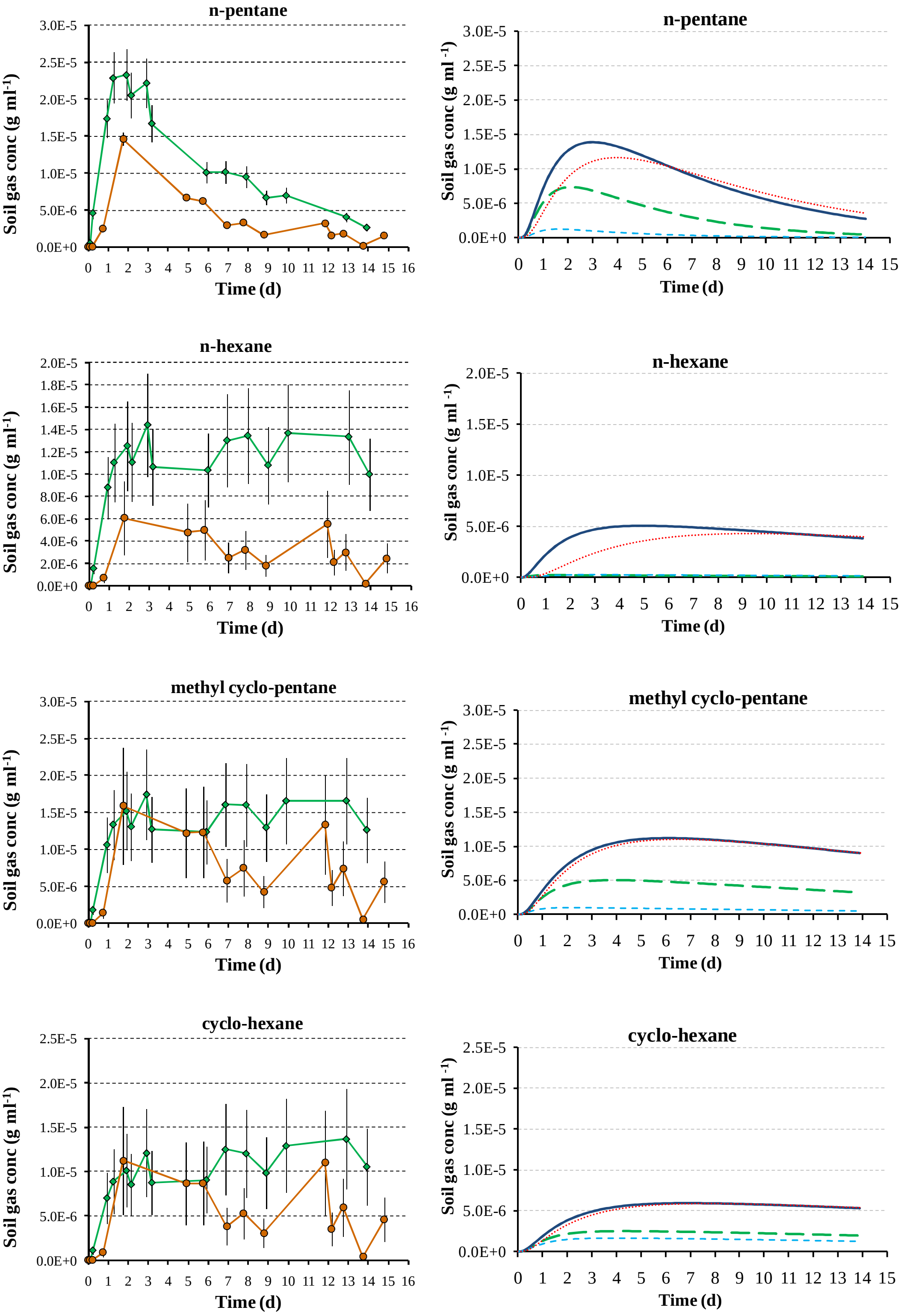

***Fig. 7.38**: continue.*

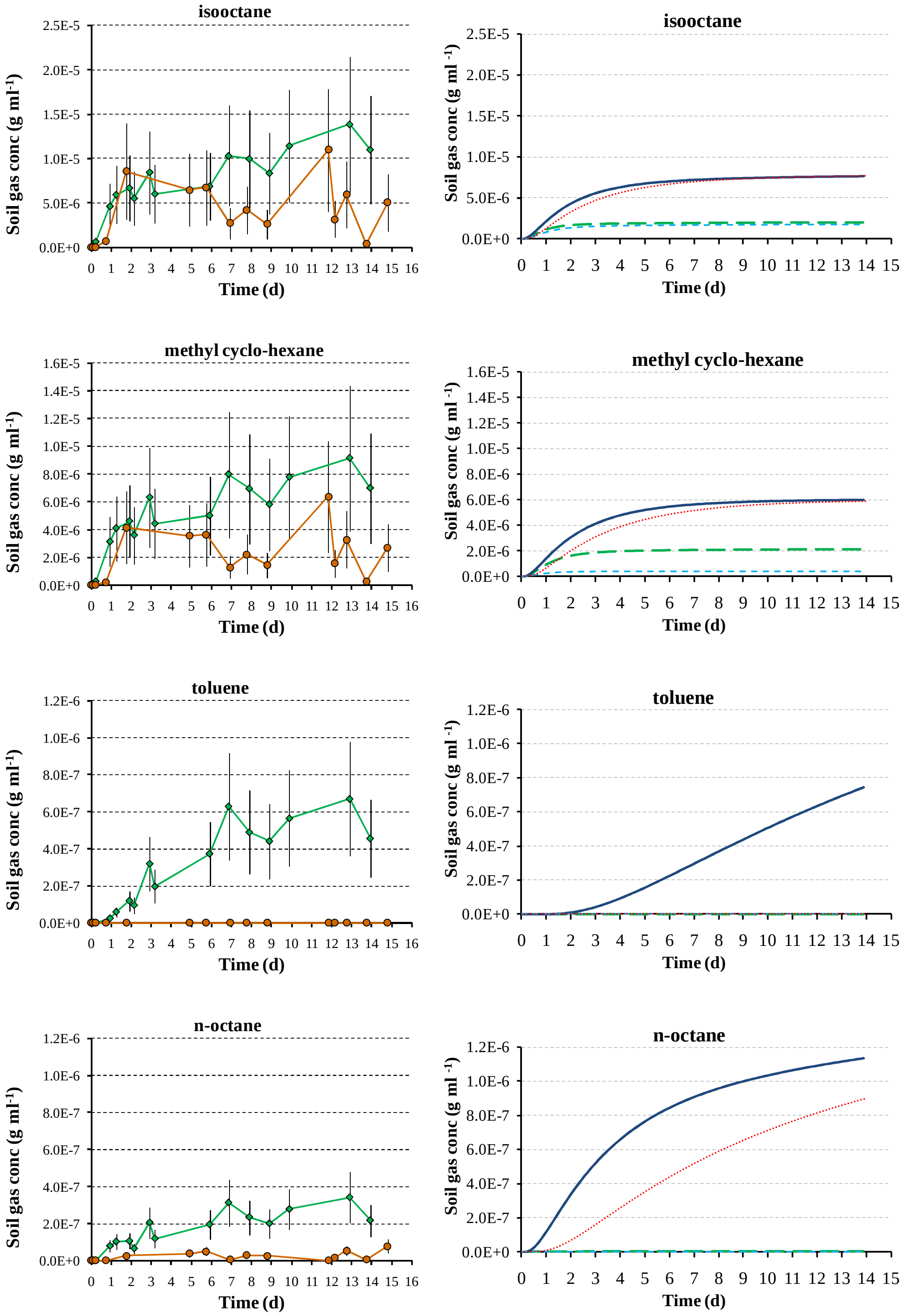

***Fig. 7.38**: continue.*

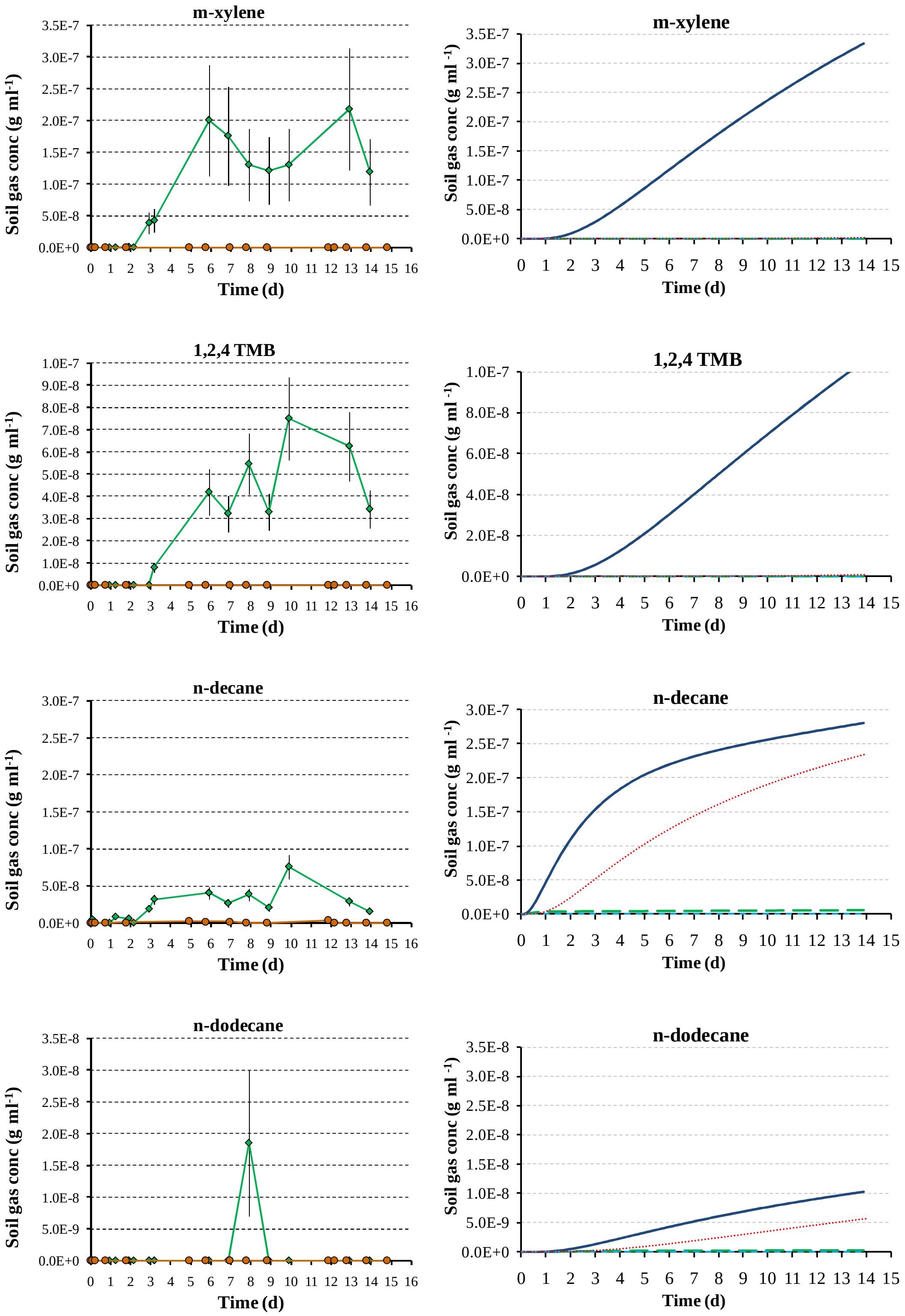

e) **e’)**

Fig. 7.38*: gas concentration [g ml^{-1}] for each i-VOC versus time, for open column tests, for each VOC in each sampling port (port 1 (a), port 2 (b), port 3 (c), port 4 (d), beaker (e)). Soil data are indicated by green lozenges (—◆—), biochar-amended*

soil by orange circles (—●—). Error bars indicate analytical variance. As for e', thick lines indicate soil column and dashed lines simulation with biodegradation. In detail simulations for soil: continuous blue line (━━) without biodegradation, long-dashed green line (▬ ▬) with biodegradation; for biochar-amended soil: thin dotted red line (·········) without biodegradation, short dashed light blue line (- - -) with biodegradation.

Simulations for the same representative compounds as Fig. 7.34 (n-pentane, cyclohexane, toluene and xylene) are indicated in Fig. 7.39.

Comparison between experimental data and modelled trend in the port located in the beaker closing the column is shown in Figs. 7.38.e and 7.38.e'.

As far as n-alkanes were concerned, a compound specific behaviour was observed: n-pentane and n-hexane followed, for soil column, a trend similar to transport without biodegradation; whereas in biochar-amended soil, at the end of the test, a behaviour intermediate between simulated situations with and without degradation. n-octane and n-decane gaseous concentrations quickly decreased in biochar- amended soil, in good agreement with simulation trends, whereas for natural soil, they presented an increasing trend over time (followed for n-decane by a decreasing stretch) reaching values inside the range between two simulated scenarios; n-dodecane was always lower than the detection limits for both the matrices, with the exception of a point that could have been caused by a sampling error (such as polluted syringe).

	Soil: C_g [g ml^{-1}]	**Biochar-amended soil: C_g [g ml^{-1}]**
Port 1	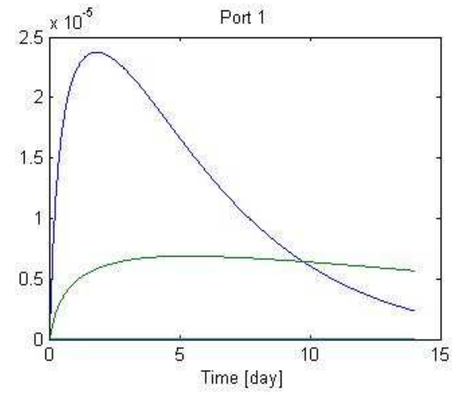	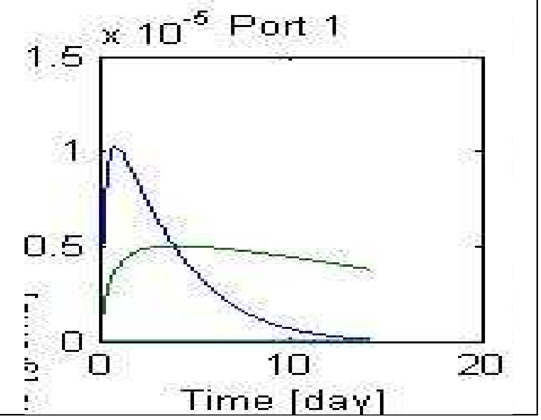

***Fig. 7.39** results of simulations, at different ports, for soil column and biochar-amended column, considering microbiological activity with degradation rates resulting from batch tests. Gas concentrations [g ml^{-1}] for n-pentane (with blue line), cyclohexane (with green line), toluene (with light blue line and xylene (with yellow line) are presented.*

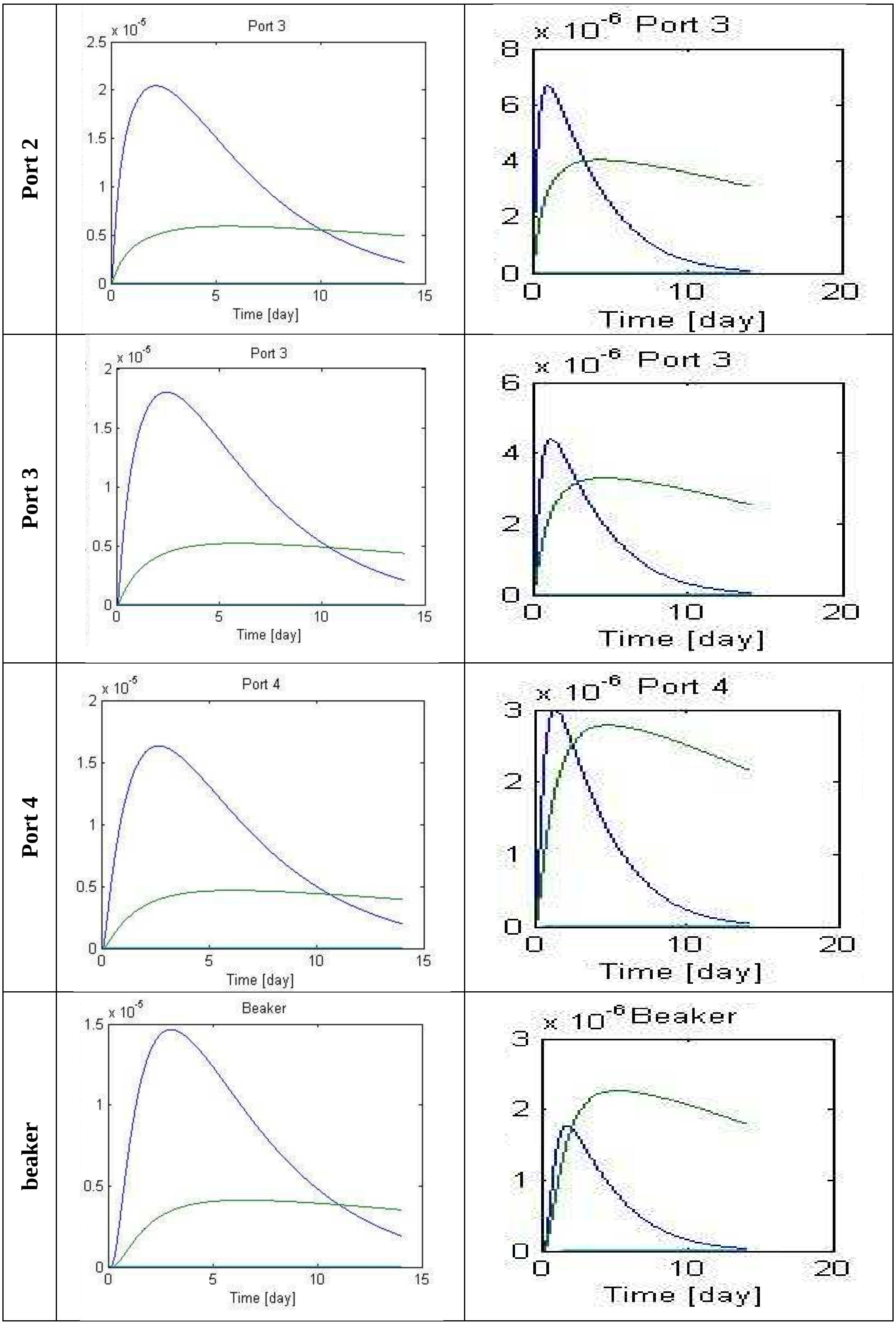

***Fig. 7.39**: continued.*

Cyclo-hexane, isooctane and the branched forms of cyclic compounds (methyl cyclo-pentane and methyl cyclo-hexane), during soil column, showed concentrations similar to the model without considering biodegradation. Towards the end of biochar-amended soil test, however, they all presented a behaviour intermediate between simulated situations with and without degradation.

For all three aromatic compounds (toluene, m-xylene and 1,2,4 TMB) with unamended soil, a constant increasing trend in good agreement with the model without biodegradation was noticed, whereas for amended soil gas concentrations were always lower than the detection limits (§ A2.3).

It is important to remember that closed boundary conditions were performed after the open ones, that is after 15 days of biodegradation had been performed, and some discrepancies with notes of § 7.3.3.4.2 could be due to the depletion of the less available nutrients (no oxygen deficiency could have affected biodegradation, because of results from biologic parameters monitoring, § 7.3.3.5.1).

7.3.3.5.3 Matrix final conditions

Results for pH (following procedure in §7.2.2.8) and moisture content (following indications in §7.2.2.6), measured at the end of both matrix columns, for different sampling ports positions, are indicated in Tab. 7.18.

***Tab. 7.18**: pH and moisture content tests results from soil and soil with 2% of biochar samples, taken at the end of closed boundary conditions. Samples were taken at different sampling ports heights: from the lower one (port1) to the top of the column. Each pH datum was calculated on 3 replicates, whereas for moisture an only one datum was taken per port; uncertainty is given by standard deviation on three replicates; VC: variation coefficient [%].*

		Port 1	**Port 2**	**Port 3**	**Port 4**	**Top column**	**average**	**VC [%]**
soil	**pH**	7.5±0.5	7.85±0.00	7.87±0.02	7.89±0.01	7.93±0.00	7.8±0.3	3.5
	W [g_{water} $g^{-1}_{dry\ soil}$ %]	9.46	9.01	8.33	7.46	6.98	8.2±0.9	11
Soil + biochar	**pH**	7.94±0.03	7.96±0.01	7.95±0.02	7.99±0.04	7.92±0.05	7.95±0.04	0.45
	W [g_{water} $g^{-1}_{dry\ soil}$ %]	12.45	11.98	12.12	12.18	11.95	12.1±0.2	1.5

The average pH inside both the columns was the same, near 7.9, that is a low basic condition not inhibiting biological activity. In soil column considering data variation, pH was kept equal to initial condition (Tab. 7.10), whereas for biochar-amended soil it was lightly decreased.

Regarding moisture, the average values in both columns had similar water content, as a reference to initial values in Tab. 7.8.

7.4 Conclusions

The petroleum hydrocarbon flux emitted from the top of the soil column may be viewed as the measure of the amount of compound that was not attenuated within the soil.

Conceptualization of the soil processes, illustrated in § 7.2.5.5, was based on the assumption that the first-order degradation rates for the dissolved VOCs, $k_{deg,water}$, were constant over time and not affected negatively by the biochar addition. From preliminary batch tests, biochar would be expected to affect, above all, the emissions of strongly sorbable compounds such as aromatic ones.

The results of this study suggest, however, that the biodegradation rate of petroleum hydrocarbons in soil is not constant over time, but appears to fluctuate quite significantly, leading to intermittent spikes and reductions in the gas-phase concentrations of these pollutants. To add further complexity, the degradation rates of different compounds appear to be interdependent. Overall, the results of the performed experiments are most consistent with the concept that the reduction of the dissolved aromatic compounds concentrations, due to strong sorption to the biochar, may have allowed for the increase in the degradation of the dissolved cyclic and branched alkanes, which were only poorly degraded in soil without biochar. This observation is likely explained by a critical factor such as low nitrogen availability (§ 7.3.1.8) that may have occurred in the soil investigated, limiting the overall amount of petroleum hydrocarbon degradation. Consequently, the amount of CO_2 produced was comparable for the soil with and without biochar (Fig. 7.36).

Clearly, the interactions between soil, biochar and the intrinsic soil microbial communities are more complex than stated in the original modelling assumptions. Moreover, the impact of biochar on the fate of VOCs needs to be further investigated for different soil types and also under field conditions.

Nevertheless, it is encouraging to note that no detrimental effect of the biochar addition on the natural attenuation of the more readily biodegradable and more volatile petroleum hydrocarbons was observed in this study.

CONCLUSIONS

Flux chamber technique is useful to measure vapour fluxes at soil surface, isolating environmental background contribution that has not to be considered for Risk Analysis at contaminated sites. In Italy and in most part of Europe, its use is still limited to analyse greenhouse gases emitted from landfills and even less for application to contaminated sites. Thanks to the collaboration between the Soil Remediation Group of Politecnico di Milano and some local Environmental and Health Agencies, it is being recommended as a useful tool in the guidelines that are being assessed by the Region of Lombardy (Politecnico di Milano et al., 2010).

The results of the present research revealed that dynamic flux chamber setup has to be designed considering results of purge and mixing tests, built of inert material and used according to proper protocols. Tests performed on the commercial chamber, in fact, resulted unsatisfactory since it was not homogeneously mixed due to the inappropriate sweep gas injection system and the dome shape. Purge duration, also, took more than 2 h 30 min because the material it was made of (Plexiglass) adsorbed organic compounds. A new setup was defined, which replaced the dome with a flat PTFE cover, old inappropriate gasket with a PTFE one and changed the inflow gas injection system for a Teflon spiral. This new chamber resulted homogeneously mixed, with purge duration shorter than 2 h. An ambient air treatment system was set up to be used as sweep gas and monitoring procedure was drawn up. In particular, sampling line details and analytical protocol were defined. The importance of recording physical parameters, such as temperature, humidity and pressure difference between outside and inside the FC, was affirmed as a recommended monitoring rule. Thanks to the results of this work, a new research contract between Politecnico di Milano and an Italian private company is forthcoming. The aim of the work will be to develop a smaller chamber, in order to reduce purge time and allow shortening field activities. A fluidodynamic model will be developed to optimize chamber geometry and sweep air injection device.

As for field scale tests, flux data from FC measurements were compared to modelled fluxes (Johnson and Ettinger model in RISC 4.05 software). As a general trend, the applied model tended to overestimate, even if a good agreement or a slight underestimation was found for some pollutants at some sampling locations, suggesting models to offer an unreliable and not always precautionary assessment of vapour transport in soil. Dispersion box model was applied to calculate air concentrations from each approach to compare with the measured air concentrations. This information was used for Risk Analysis. Air concentration measurements resulted to overestimate risk in comparison with all the other approaches because of the pollutant environmental background. New dynamic flux chamber campaigns have been already planned to perform monitoring at other contaminated sites. The aim will be to compare results between traditional techniques and flux chamber results, also for different pollutants (chlorinated compounds) and conceptual models.

As biochar-amendment tests, results performed at Newcastle University showed that the biodegradation of petroleum hydrocarbons was not constant over time and was interdependent of the presence of other compounds, leading to sudden rises and falls in the gas-phase concentrations. Their behaviour was probably more complex than stated in the original modelling assumptions. It appeared, however, that biochar increased sorption of aromatic compounds without having negative effects on microbial activity. In particular, toluene vapours were effectively adsorbed on the amended matrix allowing increase in the degradation of cyclic and branched alkanes, which were only poorly degraded in soil without biochar. In general, in both column tests, biodegradation rates were lower than those simulated using data from batch results, probably because soil nutrients, in particular nitrogen, were not sufficient to support a long-term biodegradation activity. Nevertheless, it is encouraging to note that no detrimental effect of the biochar on the natural attenuation of the more readily biodegradable and more volatile petroleum hydrocarbons was observed in this study. Further investigations, however, need to be performed to evaluate biochar amendment for different soil types (potentially less poor in nutrients) and for different biochar types, too. Future work will require more detailed biological analyses to observe the effects on biomass composition over time. Finally, tests at field scale for long periods are suggested too.

BIBLIOGRAPHY

Abreu L.D.V., Johnson P.C. (2005). Effect of Vapor Source−Building Separation and Building Construction on Soil Vapor Intrusion as Studied with a Three-Dimensional Numerical Model. *Environ. Sci. Technol.*, 39, 4550-4561.

Abreu L.D.V., Johnson P.C. (2006). Simulating the Effect of Aerobic Biodegradation on Soil Vapor Intrusion into Buildings: Influence of Degradation Rate, Source Concentration, and Depth. *Environ. Sci. Technol.*, 40, 2304-2315.

Allaire S.E., Yates S.R., Ernst F.F., Gan J. (2002). A dynamic two-dimensional system for measuring volatile organic compound volatilization and Movement in Soils. *J. Environ. Qual.*, 31, 1079-1087.

APAT (2008a), Criteri metodologici per l'applicazione dell'analisi assoluta di rischio ai siti contaminate, Revisione 2, Marzo.

APAT (2008b), Appendice P - presenza di prodotto libero (NAPL), Revisione 2, Marzo.

Argonne (2010). Porosity. http://web.ead.anl.gov/resrad/datacoll/porosity.htm (November 2010).

ASTM (1995). Standard Test Method for pH of Soils; D4972-95a.

ASTM (1997). Standard Test Method for Saturated Hydraulic Conducitivity, Water Retention, Porosity, Particle Density, and Bulk Density of Putting Green and Sports Turf Root Zones (Withdrawn 2006); ASTM F1815-97.

ASTM (1998). RBCA fate and transport models: compendium and selection guidance. ASTM Technical & Professional training.

ASTM (2000). Standard Test Methods for Moisture, Ash, and Organic Matter of Peat and Other Organic Soils; ASTM D2974 - 07a.

ASTM (2002). Standard Guide for Risk-Based Corrective Action Applied at Petroleum Release Sites.; E1739.

ASTM (2004). Standard guide for risk-based corrective action; E2081.

ASTM (2006). Standard Test Method for Sieve Analysis of Fine and Coarse Aggregates; C136 – 06.

ASTM (2009). Standard Specifications for Wire-Cloth and Sieves for Testing Purposes; ASTM E11-09e1

Baehr A. (1987) Selective Transport of Hydrocarbons in the Unsaturated Zone Due to Aqueous and Vapor Phase Partitioning. *Water Resour. Res.*, 23, 1926-1938.

Bahlman E., Ebinghaus R., Ruck W. (2006): Development and Application of a Laboratory Flux Measurement System (LFMS) for the Investigation of the Kinetics of Mercury Emissions from Soils. *J. Environ. Manage.*, 81, 114-125.

Baldocchi D.D., Meyers T.P. (1991). Trace Gas Exchange Above the Floor of a Deciduous Forest 1. Evaporation and CO_2 Efflux. *J. Geophys. Res.,* 96 (D4), 7271-7285.

Balfour W.D., Schmidt C.E., Eklund B.M. (1987). Sampling approaches for the measurement of volatile compounds at hazardous waste sites. *J. Hazard. Mater.*, 14, 135-148.

Batterman S.A., McQuown B.C., Murthy P.N., McFarland A.R. (1992). Design and evaluation of a long-term soil gas flux sampler. *Environ. Sci. Technol*., 26, 709-714.

Batterman S., Kulshreastha A.K., Cheng H.-Y. (1995). Hydrocarbon vapor transport in low moisture soils. *Environ. Sci. Technol.*, 29, 171-180.

Beesley L., Moreno-Jiménez E., Gomez-Eyles J.L. (2010). Effects of biochar and greenwaste compost amendments on mobility, bioavailability and toxicity of inorganic and organic contaminants in a multi-element polluted soil. *Environmental Pollution*, 2158, 2282-2287.

Benson D.A. (1994). User’s Manual to VENT2D: A multi-compound vapor transport and phase distribution model, DAB/524, Claremont St., Reno, NV.

Berkowitz, B. ; Silliman, S. E.; Dunn, A. M. (2004). Impact of the capillary fringe on local flow, chemical migration, and microbiology. Vad. Zone J., 3, 534-548.

BEST Energies (2010). BEST Pyrolysis, Inc. http://www.bestenergies.com/companies/bestpyrolysis.html (December 2010).

Bird R. B., Stewart W. E., Lightfoot E. N. (1960). Transport Phenomena, Wiley.

Böhme F., Rinklebe J., Stärk H.J., Wennrich R., Mothes S., Neue H.U. (2005). A simple field method to determine mercury volatilization from soils. *Environ Sci Pollut Res Int.*,12, 133-135.

Bonomo L., 2005. Bonifica di siti contaminati. Caratterizzazione e tecnologie di risanamento. McGraw-Hill.

Bozkurt O., Pennell K.G., Suuberg E. M. (2009). Simulation of the Vapor Intrusion Process for Nonhomogeneous Soils Using a Three-Dimensional Numerical Model. Ground Water Monit. Remed., 29, 92–104.

Brandli R.C., Hartnik T., Henriksen T., Cornelissen G. (2008). Sorption of native polyaromatic hydrocarbons (PAH) to black carbon and amended activated carbon in soil. *Chemosphere*, 73, 1805-1810.

Bridgwater A.V., Peacocke G.V.C. (2000). Fast pyrolysis processes for biomass. *Ren. Sust. Energy Rev.*, 4, 1-73.

British Standard (1990). Methods of test for soils for civil engineering purposes. Classification tests; BS 1377-2:1990.

Brodowski S., Amelung W., Haumaier L., Zech W. (2007). Black carbon contribution to stable humus in German arable soils. *Geoderma*, 139, 220-228.

Brown A. (2006). Microbiology sample storage (guidelines). Personal communication.

Brown R.H. (1993). The use of diffusive samplers for monitoring of ambient air. *Pure & Appl. Chem*., 65, 1859-1874.

Brown R.H. (2002). Monitoring volatile organic compounds in air - the development of ISO standards and a critical appraisal of the methods. *J. Environ. Monit.*, 4, 112N-118N.

Byrnes A. P. (2008). Issues with gas and water relative permeability in low-permeability sandstones http://www.searchanddiscovery.net/documents/abstracts/2005hedberg_vail/abstracts/extended/byrnes/byrnes.htm (August, 2010)

Capelli L., Sironi S., Del Rosso R., Centola P. (2009). Design and validation of a wind tunnel system for odour sampling on liquid area sources. Water Science & Technology. 59.8. 1611-1620.

Carlsen T.M., Martins S.A., McNeel P. (2010). Emission Isolation Flux Chambers and Risk Assessments: Applications for Cost-Effective Risk Assessment and Risk Management. http://www-erd.llnl.gov/library/spec/122294.html (November 2010).

Carpi A., Lindberg S. (1998). Application of a Teflon^{TM} dynamic flux chamber for quantifying soil mercury flux: tests and results over background soil. Armospheric Environment, 32, 873-882.

Castro M.S., Galloway J.N. (1991). A Comparison of Sulfur-Free and Ambient Air Enclosure Techniques for Measuring the Exchange of Reduced Sulfur Gases Between Soils and the Atmosphere. *J. Geophys. Res*. 96, 15427-15437.

CECOM (2006). Directive of the European Parliament and the Council. Establishing a framework for the protection of soil and amending. Directive 2004/35/EC. Brussels, 22 September.

Cheever E. (2010). Euler's Method for First Order Differential Equations. http://www.swarthmore.edu/NatSci/echeeve1/Ref/NumericInt/Euler1.html (December 2010).

Chen C., Green R.E., Thomas D. M., Knuteson J.A. (1995). Modeling 1,3-D fumigant volatilization with vapor-phase advection in the soil profile. *Environ. Sci. Technol*., 29, 1816–1821.

Cheng C.-H., Lehmann J., Engelhard M.H. (2008). Natural oxidation of black carbon in soils: Changes in molecular form and surface charge along a climosequence. *Geochemica et Cosmochemica ACTA*, 72, 1598-1610.

Choi J.W., Tillman F.D., Smith J.A. (2002). Relative Importance of Gas-Phase Diffusive and Advective Trichloroethene (TCE) Fluxes in the Unsaturated Zone under Natural Conditions. *Environ. Sci. Technol*., 36, 3157-3164.

COMEOEA (2002). Indoor air sampling and evaluation guide. Commonwealth of Massachussetts. Executive. Office of Environmental Affairs – Department of environmental protection. WSC POLICY #02-430.

Cooper C.D., Reinhart D.R.,Seligman D.R.H. (1994). Apparatus for measuring gas emission rate from soil. *United states Patent* 5,355,739.

Conen F., Smith K.A. (1998). A re-examination of closed flux chamber methods for the measurement of trace gas emissions from soils to the atmosphere. *Eur. J. Soil Sci*., 49, 701-707.

Corey A. T. (1986). Mechanisms of immiscible fluids in porous media; 86-50589; Water resources publications, Littleton. CO.

Cornelis W. M.; Khlosi M.; Hartmann R.; van Meirvenne M., De Vos B. (2005). Comparison of unimodal analytical expressions for the soil-water retention curve. Soil Sci. Soc. Am. J., 69, 1902-1911.

Cornelissen G., Breedveld G.D., Kristoffer N., Oen A.M.P., Ruus A. (2006). Bioaccumulation of native polycyclic aromatic hydrocarbons from sediment by a polychaete and a gastropod: Freely dissolved concentrations and activated carbon amendment. *Environ. Toxicol. Chem*., 25, 2349–2355.

Crank, J (1970) The Mathematics of Diffusion. London, Oxford University Press, 45-47.

Cropper W.P. Jr., Ewel K.C., Raich J.W. (1985). The measurement of soil CO_2 evolution in situ. *Pedobiologia*, 28, 35-40.

D'Aprile L., Scozza, E. (2008). Application of environmental risk analysis at contaminated sites. Ann. Ist. Super. Sanità. 44, 244-251.

Davidson E.A., Savage K., Verchot L. V., Navarro R. (2002). Minimizing artifacts and biases in chamber-based measurements of soil respiration. *Agric. and Forest Meteor.*, 113, 21-37.

Davis, R. (2006). Vapor attenuation in the subsurface from petroleum hydrocarbon sources: an update and discussion on the ramifications of the vapor-intrusion risk pathway, LUSTLine Bulletin 52, May, New England Interstate Water Pollution Control Commission, Massachusetts, 22-25.

Davis, R. (2009) Bioattenuation of petroleum hydrocarbon vapors in the subsurface update on recent studies and proposed screening: criteria for the vapor-intrusion pathway, LUSTLine Bulletin 61, May, New England Interstate Water Pollution Control Commission, Massachusetts,11-14.

Davis G. B., Trefry M. G., Patterson B. M. (2009). Petroleum vapour model comparison. Technical Report Number 9, March. CRC for Contamination Assessment and Remediation of the Environment.

De Bortoli M., Ghezzi E., Knöppel H., Vissers H. (1999). A New Test Chamber To Measure Material Emissions under Controlled Air Velocity. *Environ. Sci. Technol*., 33, 1760-1765.

De Mello W.Z., Hines M.E. (1994). Application of static and dynamic enclosures for determining dimethyl sulfide and carbonyl sulfide exchange in Sphagnum peatlands:Implications for the magnitude and direction of flux. *J. Geophys. Res*., 99, 14601-14607.

Denmead O.T. (1979). Chamber Systems for Measuring Nitrous Oxide Emission from Soils in the Field. *Soil Sci. Soc. Am. J.,*48, 89-95.

DeVaull G., Ettinger R., Gustafson J. (2002). Chemical Vapor Intrusion from Soil or Groundwater to Indoor Air: Significance of Unsaturated Zone Biodegradation of Aromatic Hydrocarbons. *Soil and Sedim. Contam*, 11, 625-641.

DeVaull G. (2007). Indoor Vapor Intrusion with Oxygen-Limited Biodegradation for a Subsurface Gasoline Source. *Environ. Sci. Technol.*, 41, 3241-3248.

Di Francesco F., Ferrara R., Mazzolai B. (1998). Two ways of using a chamber for mercury flux measurement – A simple mathematical approach. *Sci. Total Environ.*, 213, 33-41.

DTSC (2004). Guidance for the Evaluation and Mitigation of Subsurface Vapor Intrusion to Indoor Air. Department of Toxic Substances Control California Environmental Protection Agency.

Dullien, F. A. L. (1979) *Porous media: fluid transport and pore structure*. Academic Press, New York, N.Y., 200-209.

Dupont R.R., Reineman J.A. (1986). Evaluation of Volatilization of Hazardous Constituents at Hazardous Waste Land Treatment Sites. Research and Development Report EPA/600/S2-86/07.

Eklund B. M., Balfour W. D., Schmidt C. E. (1985).Measurement of fugitive volatile organic emission rates. *Environ. Prog.*, 4, 199-202.

Eklund B. (1992). Practical Guidance for Flux Chamber Measurements of Fugitive Volatile Organic Emission Rates. *JAPCA J. Air Waste Ma.*, 42, 1583-1591.

Eklund B., Anderson E.P., Walker B.L., Burrows D.B. (1998). Characterization of Landfill Gas Composition at the Fresh Kills Municipal Solid-Waste Landfill. *Environ. Sci. Technol*., 32, 2233-2237.

EOLBNL (1999). Tough2 User's Guide - Version 2.0, LBNL-43134, Ernest Orlando Lawrence Berkeley National Laboratory, Berkeley, CA.

Evans D., Hers I, Wolters R. M., Boddington R. T .B., Hall D. H. (2002). Vapour transfer of soil contaminants. *R&D Technical Report P5-018/TR*, Environment Agency, United Kingdom.

ET (2010). Build Thiessen Polygons Wizard. http://www.ian-ko.com/ET_GeoWizards/UserGuide/thiessenPolygons.htm (December 2010)

Falta, R. W., Pruess I. J., Witherspoon K. P. (1989) Density Driven Flow of Gas in the Unsaturated Zone Due to the Evaporation of Volatile Organic Compounds *Water Resour. Res.* , 25, 2159-2169.

Fang C., Moncrieff J.B. (1998). An open-top chamber for measuring soil respiration and the influence of pressure difference on CO_2 efflux measurement. *Funct. Ecol*. 12, 319-325.

Farmer W. J., Yang M. S., Letey J., Spencer W. F. (1980). Hexachlorobenzene: Its Vapor Pressure and Vapor Phase Diffusion in Soil. *Soil Sci Soc Am J,* 44, 676-680.

Farrell J., Reinhard M. (1994), Desorption of Halogenated Organics from Model Solids, Sediments, and Soil under Unsaturated Conditions. 1. Isotherms. *Environ. Sci. Technol.,* 28, 53-62.

Ferguson C.C., Krylov V.V., McGrath P.T. (1995). Contamination of indoor air by toxic vapours: a screening risk assessment model. *Building and Environment*, 30, 375-383.

Ferguson C., Darmendrail D., Freier K., Jensen B.K., Jensen J., Kasamas H., Urzelai A., Vegter, J. (1998). Risk Assessment for Contaminated Sites in Europe. Volume 1. Scientific Basis. LQM Press, Nottingham.

Fisher M. L., Bentley A. J., Dunkin K. A., Hodgson A. T., Nazaroff W. W., Sextro R. G., Daisey J. M., (1996). Factors Affecting Indoor Air Concentrations of Volatile Organic Compounds at a Site of Subsurface Gasoline Contamination. *Environ. Sci. Technol.*, 30, 2948–2957.

Fitzpatrick N. A.; Fitzgerald J. J. (2002). An Evaluation of Vapor Intrusion Into Buildings Through a Study of Field Data. *Soil Sed Contam*, 11, 603-623.

Focht, D. D. (1992). Diffusional Constraints on Microbial Processes in Soil. *Soil Science*, 154, 300-307.

Folkes D., Wertz W., Kurtz J., Kuehster (2009). Observed Spatial and Temporal Distributions of CVOCs at Colorado and New York Vapor Intrusion Sites. *Ground. Water Monit. & R.*, 29,70-80.

Frantzen M.A.J., Silk J.B., Ferguson J.W.H., Wayne R.K., Kohn M.H. (1998). Empirical evaluation of preservation methods for faecal DNA. *Mol. Ecol.*, 7, 1423-1428.

Frez W.A., Tolbert J.N., Hartaman B., Kline T. R. (1998). Determining Risk Based Remediation Requirements Using Rapid Flux Chamber Technology. http://tegncal.com/documents/hartman/RapidfluxChamberTechnology.pdf (November 2010).

Fried A., Klinger L.F., Erickson III D.J. (1993). Atmospheric Carbonyl Sulfide Exchange in Bog Microcosms. *Geophy. Res. Lett.*, 20, 129-132.

Fuel Cell Knowledge (2010). Free molecule (Knudsen) Flow in porous media, http://www.fuelcellknowledge.org/research_and_analysis/heat_and_mass_transfer/index.html (April 2010).

Gan J., Yates S.R., Wang D., Spencer W.F. (1996). Effect of Soil Factors on Methyl Bromide Volatilization after Soil Application. *Environ. Sci. Technol.*, 30, 1629-1636.

Gao F., Yates S.R., Yates M.V., Gan J., Ernst F.F. (1997). Design, Fabrication, and Application of a Dynamic Chamber for Measuring Gas Emissions from Soil. *Environ. Sci. Technol.*,31, 148-153.

Gao F., Yates S.R. (1998). Laboratory study of closed and dynamic flux chambers: Experimental results and implications for field application. *J. Geophys. Res*, 103, 26115-26125.

Garbesi K., Sextro R.G. (1989) Modeling and Field Evidence of Pressure-Driven Entry of Soil Gas into a House through Permeable Below-Grade Walls. *Environ. Sci. Technol.*, 23, 1481-1487.

Gaskin J.W., Speir A., Morris L.M., Ogden L., Harris K., Lee D., Das K.C. (2007). Potential for pyrolysis char to affect soil moisture and nutrient status of a loamy sand soil. Proceedings of the 2007 Georgia Water Resources Conference (27–29 March), University of Georgia.

Gholson A.R., Albritton J.R., Jayanty R.K.M. (1991). Evaluation of an Enclosure Method for Measuring Emissions of Volatile Organic Compounds from Quiescent Liquid Surfaces. *Environ. Sci. Technol.*, 25, 519-524.

Glaser B., Lehmann J., Zech W., (2002). Ameliorating physical and chemical properties of highly weathered soils in the tropics with charcoal – a review. *Biol Fertil Soils*, 35:219- 230.

Glotfelty D. E., Taylor A.W., Turner B. C., Zoller W. H. (1984). Volatilization of surface-applied pesticides from fallow soil. *J. Agric. Food Chem.*, 32, 638-643.

Guarnaccia J.F., Pinder G., Fishman M. (1997). NAPL: Simulator Documentation. EPA/600/R-97/102.

Gustin M.S., Rasmussen P., Edwards G., Schroeder W., Kemp J. (1999). Application of a laboratory gas exchange chamber for assessment of in situ mercury emissions. *J. Geophys. Res*, 104, D17, 21873-21878.

Hale S.E., Werner D. (2010a). Modeling the mass transfer of hydrophobic organic pollutants in briefly and continuously mixed sediment after amendment with activated carbon. *Environ. Sci. Technol.*, 44, 3381-3387.

Hale S.E., Meynet P., Davenport R.J., Martin Jones D., Werner, D. (2010b). Changes in polycyclic aromatic hydrocarbon availability in River Tyne sediment following bioremediation treatments or activated carbon amendment. *Water Research*, 44, 4529-4536.

Hartman B. (2002). How to Collect Reliable Soil-Gas Data for Risk-Based Applications. Part 1: Active Soil-Gas Method. *LUSTLine Bulletin*, 42, 17-22.

Hartman B. (2003). How to Collect Reliable Soil-Gas Data for Upward Risk Assessments. Part 2: Surface Flux – Chamber Method. *LUSTLine Bulletin*, 44, 14-18 e 34.

Hartman B. (2004). How to Collect Reliable Soil-Gas Data for Risk-Based Applications - Specifically Vapor Intrusion. Part 3 – Answers to Frequently Asked Questions. *LUSTLine Bulletin*, 48, 12-17.

Hartman B. (2006). How to Collect Reliable Soil-Gas Data for Risk-Based Applications-Specifically Vapor Intrusion Part 4 - Updates on Soil-Gas Collection and Analytical Procedures. *LUSTLine Bulletin*, 53, 14-19.

Hers I., Zapf-Gilje R. (2001). The use of indoor air measurements to evaluate intrusion of subsurface VOC vapors into buildings. *Journal of the JAPCA J. Air Waste Ma.*, 51, 1318-1331.

Hers I., Reidar Z.-G., Dyfed E., Li L. (2002). Comparison, Validation, and Use of Models for Predicting Indoor Air Quality from Soil and Groundwater Contamination. *Soil and Sedim. Contam*, 11, 491-527.

Hers I., Reidar Z.-G., Johnson P.C., Li L. (2003). Evaluation of the Johnson and Ettinger Model for Prediction of Indoor Air Quality. *Ground Water Monit. Remed.*, 23, 119-133.

Hohener P., Duwig1 C., Pasteris G., Kaufmann K., Dakhel N., Harms H. (2003). Biodegradation of petroleum hydrocarbon vapors: laboratory studies on rates and kinetics in unsaturated alluvial sand. *J. Contam. Hydrol.*, 66, 93-115.

Hutchinson G.L., Mosier A.R. (1981). Improved Soil Cover Method for Field Measurement of Nitrous Oxide Fluxes. *Soil Science Society of America*, 45, 311-316.

Hutchinson, G. L., Brams E. A. (1992), NO Versus N_2O Emissions From an NH_4^+ - Amended Bermuda Grass Pasture, *J. Geophys. Res.*, 97(D9), 9889-9896.

Hutchinson G.L., Livingston G.P. (1993). Use of Chamber Systems to Measure Trace Gas Fluxes. Proceedings of *Agricultural Ecosystem Effects on Trace Gases and GlobalClimate Change* Symposium, 63-78. ASA Special Publication 55, Wisconsin, USA.

Hutchinson G.L., Livingston G.P., Healy R.W., Striegl R.G. (2000). Chamber measurement of surface–atmosphere trace gas exchange: numerical evaluation of dependence on soil, interfacial layer, and source/sink properties. *J. Geophys. Res.*,105, 8865-8875.

Hutchinson G.L., Livingston G.P. (2001). Vents and seals in non-steady state chambers used for measuring gas exchange between soil and the atmosphere. Eur J. Soil Sci, 52, 675-682.

Hutchinson G.L., Livingston G.P. (2002). Soil-Atmosphere Gas Exchange. In Dane J.H., Topp G.C. Eds., Methods of soil analysis. Part 4. 1159–1182. SSSA Book Ser. 5. SSSA, Madison, WI.

Hutchinson G.L., Rochette P. (2003). Non-Flow-Through Steady state Chambers for Measuring Soil Respiration: Numerical Evaluation of Their Performance. *Soil Sci. Soc. Am. J.*, 67, 166-180.

IBI (2010). International Biochar Initiative. http://www.biochar-international.org/biochar (December, 2010)

INEA (2010). Pedologia delle cinque aree. http://www1.inea.it/otris/file/pedologia_txt.htm (December, 2010)

IPCS (2004). Report of the first meeting of the IPCS Working Group on Uncertainty in Exposure Assessment in conjunction with a Scoping Discussion on Exposure Data Quality. WHO Headquarters, Geneva, 19-20 August.

Iritz Z, Lindroth A., Gärdenäs A. (1997). Open ventilated chamber system formeasurements of H_2O and CO_2 fluxes from the soil surface. *Soil Technology*, 10, 169-184.

ISS (2010). Banca dati bonifiche. http://www.iss.it/site/BancaDatiBonifiche/index.aspx (December, 2010)

ISS/ISPESL (2010). Criteri metodologici per l'applicazione dell'Analisi assoluta di Rischio e la Banca Dati ISS/ISPESL "Proprietà chimico-fisiche e tossicologiche dei contaminanti". http://www.iss.it/suol/docu/cont.php?id=96&tipo=13&lang=1 (August 2010).

ITRC (2007). Vapor Intrusion Pathway: A Practical Guideline. Washington D.C. The Interstate Technology and Regulatory Council, Vapor Intrusion Team, January.

ITRC (2008). Use of Risk Assessment in Management of Contaminated Sites.Interstate Technology & Regulatory Council. RISK-2. Washington, D.C. The Interstate Technology & and Regulatory Council, Risk Assessment Resources Team, August.

Jeffries J., Martin I. (2008). Science Report - Updated technical background to the CLEA model. Environmental Agency, Bristol, SC050021/SR3.

Jellali S., Benremita H., Muntzer P., Razakarisoa O., Schafer G. (2003). A large-scale experiment on mass transfer of trichloroethylene from the unsaturated zone of a sandy aquifer to its interfaces. *J. Contam. Hydrol.*, 60, 31-53.

Jiang K., Kaye R. (1996). Comparison study on portable wind tunnel system and isolation chamber for determination of VOCs from areal sources. *Wat. Sci. Tech.*, 34, 583-589.

Johnson P.C., Ettinger R.A. (1991). Heuristic Model for Predicting the Intrusion Rate of Contaminant Vapors into Buildings. *Environ. Sci. Technol.*, 25, 1445-1452.

Johnson P.C., Johnson R.L., Kemblowski M.W. (1998). Assessing the Significance of Subsurface Contaminant Migration to Enclosed Spaces: Site-Specific Alternatives to Generic Estimates. *API American Petroleum Institute Publication*, nr. 4674, December.

Johnson P.C., Ettinger R.A., Kurtz J., Bruan R., Kester J.E. (2002a). Migration of Soil Gas Vapors to Indoor Air: An Empirical Assessment of Subsurface Vapor-to-Indoor Air Attenuation Factors Using Data from the CDOT-MTL

Denver, Colorado Site. *API Soil and Groundwater Research Bulletin*, nr. 16, April.

Johnson P.C. (2002b). Identification Of Critical Parameters For The Johnson And Ettinger (1991) Vapor Intrusion Model. *API Soil and Groundwater Research Bulletin*, nr. 17, May.

Johnson P.C. (2005). Identification of Application-Specific Critical Inputs for the 1991 Johnson and Ettinger Vapor Intrusion Algorithm. *Ground Water Monit. R.*, 25, 63-78.

Jury W.A., Grover R., Spencer W.F., Farmer W.J. (1980). Modeling Vapor Losses of Soil-lncorporated Triallate. *Soil Sci.Soc.Am. J.*, 44, 445-450.

Jury W.A., Letey J., Collins T. (1982). Analysis of chamber methods used for measuring nitrous oxide fluxes. *Soil Sci. Soc. Am. J.*, 46, 250-256.

Jury, W. A., Spencer, W. F., Farmer, W. J. (1983). Behavior Assessment Model for Trace Organics in Soil: I. Model Description. *J. Environ. Qual.*, 12, 558-564.

Jury, W. A., Farmer, W. J., Spencer, W. F., (1984). Behavior Assessment Model for Trace Organics in Soil: II. Chemical Classification and Parameter Sensitivity. *J. Environ. Qual.*, 13, 567-572.

Jury, W. A., Farmer, W. J., Spencer, W. F., (1984b). Behavior Assessment Model for Trace Organics in Soil: IV. Review of experimental evidence. *J. Environ. Qual.*, 13, 580-586.

Jury W. A., Russo D., Streile G., El Abd H. (1990). Evaluation of Volatilization by Organic Chemicals Residing Below the Soil Surface. *Water Resour. Res.* , 26, 13-20.

Kanemasu E.T., Powers W.L., Sij J.W. (1974). Field Chamber Measurements of CO_2 Flux from Soil Surface. *Soil Science*, 118, 233-237.

Karam A. (1993). Chemical properties of organic soils. Soil sampling and methods of analysis, Carter M.R. ed., 459-471. Lewis Publ., Boca Raton, FL.

Katyal, A.K., Kaluarachchi, J.J., Parker, J.C., Cho, J.S., Swaby, L.G. (1991). MOFAT: A two dimensional finite element program for multiphase flow and multicomponent transport, EPA/600/2-91/020.

Karapanagioti H.K., Gaganis P., Burganos V.N. (2003). Modeling attenuation of volatile organic mixtures in the unsaturated zone: codes and usage. *Environ. Modell. Softw.*, 18, 329-337.

Kim K., Lindberg S.E. (1995). Design and Initial Tests of a Dynamic Enclosure Chamber for Measurements of Vapor-Phase Mercury Fluxes over Soils. *Water Air Soil Poll.*, 80, 1059-1068.

Kliest J., Fast T., Boley J.S.M., Van de Wiel H., Bloemen H. (1989). The relationship between soil contaminated with volatile organic compounds and indoor air pollution. *Environ. Int.*, 15, 419-425.

Klinger, L. F., Zimmerman P. R., Greenberg J. P., Heidt L. E., Guenther A. B. (1994). Carbon trace gas fluxes along a successional gradient in the Hudson Bay lowland. *J. Geophys. Res.*, 99(D1), 1469-1494.

Koblizková M., Růzicková P., Cupr P., Komprda J., Holoubek I., Klánová J. (2009). Soil burdens of persistent organic pollutants: their levels, fate, and risks. Part iv. Quantification of volatilization fluxes of organochlorine pesticides and polychlorinated biphenyls from contaminated soil surfaces. *Environ Sci Technol.*43, 3588-3595.

Kreamer D. K., Weeks E. P., Thompson G. M. (1988). A field technique to measure the tortuosity and sorption-affected porosity for gaseous diffusion of materials in the unsaturated zone with experimental results from near Barnwell, South Carolina. *Water Resour. Res.*, 24, 331-341.

Krylov V. V., Ferguson C. C. (1998). Contamination of indoor air by toxic soil vapours: the effects of subfloor ventilation and other protective measures. *Build. Environ.* 33, 331-347.

Labieniec P. A., Dzombak D. A., Siegrist R. L. (1996). SoilRisk: Risk assessment model for organic contaminants in soil. J. Environ. Eng., 122, 388-398.

Lahvis M.A., Baehr A.L. (1998). Documentation of R-UNSAT, a computer model for the simulation of reactive, multispecies transport in the unsaturated zone. *US Geological Survey (USGS).* Report 97-630USGS.

Lahvis M. (2010). Vapour transport from soil and groundwater to indoor air: analytical modelling approach. In Vapor Emission to Outdoor Air and Enclosed Spaces for Human Health Risk Assessment: Site Characterization, Monitoring and Modeling. Saponaro S., Sezenna E., Bonomo L. Eds., Nova Science Publishers, Hauppauge NY, Chapter 5 (at press).

Lehmann, J., Da Silva Jr. J.P., Steiner C., Nehls T., Zech W., Glaser B. (2003). Nutrient availability and leaching in an archaeological Anthrosol and a Ferralsol of the Central Amazon basin: fertilizer, manure and charcoal amendments. *Plant and Soil*, 249, 343-357.

Lehmann J. (2007). A handful of carbon. *Nature*, 447, 143-144.

Lehmann J., Gaunt J., Hanley K. (2007). Mitigation of Ecosystem Degradation by Bioenergy with Biochar. Poster at Environmental Monitoring, Evaluation, and Protection in New York: linking science and policy (15-16 November), Albany, NY.

Liang B., Lehmann J., Solomon D., Kinyangia J., Grossman J., O'Neill B., Skjemstad J.O., Thies J., Luizão F.J., Petersen J., Neves E.G. (2006). Black Carbon Increases Cation Exchange Capacity in Soils. *Soil Sci. Soc. Am. J.*, 70, 1719–1730.

Lin J.-S., Hildemann L.M. (1995). A nonsteady state analytical model to predict gaseous emissions of volatile organic compounds from landfills. *J. Hazard. Mater.*, 40, 271-295.

Lin T.F., Su Y.Y., Su M.C. (2003). Performance of Gas Mixing in a Flux Chamber. *Energ. Sourc.*, 25, 597-605.

Lindberg S. E., Kim K.-H., Meyers T. P., Owens J. G. (1995). Micrometeorological gradient approach for quantifying air surface exchange of mercury vapor: tests over contaminated soils. *Environ. Sci. Technol.*, 29, 126–135.

Lindberg S.E., Zhang H., Gustin M., Vette A., Marsik F., Owens J., Casimir A., Ebinghaus R., Edwards G., Fitzgerald C., Kemp J., Kock H.H., London J., Majewski M., Poissant L., Pilote M., Rasmussen P., Schaedlich F., Schneeberger D., Sommar J., Turner R., Wallschläger D., Xiao Z. (1999). Increases in mercury emissions from desert soils in response to rainfall and irrigation. J. *Geophys. Res.*, 104, 21879-21888.

Lindberg S.E., Zhang H., Vette A.F., Gustin M.S., Barnett M.O., Kuiken T. (2002) Dynamic flux chamber measurement of gaseous mercury emission fluxes over soils: Part 2 – effect of flushing flow rate and verification of a two-resistance exchange interface simulation model. *Atmos. Environ.*, 36, 847-859.

Little, J. C., Daisy, J. M., Nazaroff, W. W. (1992). Transport of subsurface contaminants into buildings. *Environ. Sci. Technol.*, 26, 2058-2066.

Liptak J. F., Lomardo G. (1996). The Development of Chemical-Specific, Risk-Based Soil Cleanup Guidelines Results in Timely and Cost-Effective Remediation. *J. S. Contam.*, 5, 1-12.

Livingston G.P., Hutchinson G.L. (1995). Enclosure-based measurement of trace gas exchange: applications and sources of error. In Matson P.A. Harriss and R.C. (eds.), *Methods in Ecology: Biogenic Trace Gases: Measuring Emissions from Soil and Water*, Blackwell Science Ltd., Oxford, 14-51.

Livingston G.P., Hutchinson G.L., Spartalian K. (2006). Trace Gas Emission in Chambers: A Non-Steady- state Diffusion Model. *Soil Science Society of America Journal*, 70: 1459-1469.

Lonati G. (2010). Vapor transport in atmospheric air. In Vapor Emission to Outdoor Air and Enclosed Spaces for Human Health Risk Assessment: Site Characterization, Monitoring and Modeling. Saponaro S., Sezenna E., Bonomo L. Eds., Nova Science Publishers, Hauppauge NY, Chapter 2 (at press).

Loureiro C.O., Abriola L.M., Martin J.E., Sextro R.G. (1990) Three-Dimensional Simulation of Radon Transport into Houses with Basements under Constant Negative Pressure. *Environ. Sci. Technol.*, 24, 1938-1948.

Lowell P.S., Eklund B. (2004). VOC Emission Fluxes as a Function of Lateral Distance from the Source. *Environ. Prog.*, 23, 52-58.

Luckner L.; van Genuchten M. Th.; Nielsen D.R. (1989). A consistent set of parametric models for the two-phase flow of immiscible fluids in the subsurface. Water Resour. Res., 25, 2187-2193.

Lund C.P., Riley W.J., Pierce L.L., Field C.B., (1999). The effects of chamber pressurization on soil-surface CO2 flux and the implications for NEE measurements under elevated CO_2. *Glob. Change Biol.*, 5, 269-281.

MADEP (2002). Characterizing Risks Posed by Petroleum Contaminated Sites: Implementation of the MADEP VPH/EPH Approach. Final Policy, Department of Environmental Protection, Boston. WSC-02-411 (31 October).

MADEP (2004). Method for the determination of extractable petroleum hydrocarbons (EPH), Department of Environmental Protection, Division of Environmental Analysis (May).

MADEP (2009). Updated Vapor Intrusion Guidance Document. Investigative Approach to Assess Vapor Intrusion. Massachusetts Department of Environmental Protection. DRAFT dated 3/27/09 http://indoorairproject.files.wordpress.com/2009/03/assessment-text-draft-3-27-093.doc (May 2010)

MADEP (2009b). Method for the determination of air-phase petroleum hydrocarbons (APH), Department of Environmental Protection, Office of Research and Standards (December).

Magarelli G., Fostier A.E. (2005). Influence of deforestation on the mercury air/soil exchange in the Negro River Basin, Amazon. *Atmos. Environ.*, 39, 7518-7528.

Majewski M.S., Glotfelty D.E., Paw U T.P., Seiber J.N. (1990). A Field Comparison of Several Methods for Measuring Pesticide Evaporation Rates from Soil. *Environ. Sci. Technol.*, 24, 1490-1497.

Martins S. (2010). Lawrence Livermore National Laboratory (LLNL) Flux Chamber Modifications. http://www-erd.llnl.gov/library/JC-137682.pdf (November 2010).

Massmann J.W. (1989) Applying groundwater flow models in vapor extraction system. *J. Environ. Eng.*, 129-149.

Massmann J.; Farrier D. F. (1992), Effects of Atmospheric Pressures on Gas Transport in the Vadose Zone. *Water Resour. Res.*, 2, 777-791.

Matthews T.G. (1987). Environmental chamber test methodology for characterizing organic vapors from solid emission sources. *Atmos. Environ.*, 21, 321-329.

Matthias A.D., Blackmer A.M., Bremner J.M. (1980). A Simple Chamber Technique for Field Measurement of Emissions of Nitrous Oxide from Soils. *J. Environ. Qual.*, 9, 251-256.

McCarthy J. H. (1972). Mercury vapor and other volatile components in the air as guides to ore deposits. *J. Geochem. Explor.*, 1, 143-162.

McCarthy K.A., Johnson, R.L. (1993). Transport of volatile organic compounds across the capillary fringe. *Water Resour. Res*, 29, 1675-1683.

McHugh T.E., Connor J.A., Farrukh A. (2004). An Empirical Analysis of the Groundwater-to-Indoor-Air Exposure Pathway: The Role of Background Concentrations in Indoor Air Environmental Forensics 5: 33-44.

McKay D., Matsuga R. S. (1973) Evaporation Rates of Liquid Hydrocarbon Spills on Land and Water. *Can. J. Chem. Eng.*, 51, 434-439.

MDNR (2005). Missouri Risk-Based Corrective Action (MRBCA) for petroleum storage tanks - Soil gas sampling protocol, Missouri Department of Natural Resources, April 21.

Mei C.C., Cheng Z., Ng C.O. (2002). A model for flow induced by steady air venting and air sparging. *Applied Mathematical Modeling.*, 26, 727-750

Mendoza C. A., Frind E. O. (1990). Advective-Dispersive Transport of Dense Organic Vapors in the Unsaturated Zone- 1. Model Development. *Water Resour. Res.*, 26, 379-387.

Meyers T.P., Hall M.E., Lindberg S.E., Kim K. (1996). Use of the modified bowen-ratio technique to measure fluxes of trace gases. *Atmos. Environ.*, 30, 3321-3329.IBIMET- CNR, Istituto di Biometeorologia del Consigilio Nazionale delle Ricerche

Miglietta F., Baronti S., Grasso V., Magno R., Di Gennaro F., Genesio L., Vaccari F. (2010). Biochar background. http://www.ichar.org/biochar_background.pdf (December 2010).

Millington, R. J., Quirk, J. P. (1961) Permeability of porous solids. *Trans.Faraday Soc.*, 57, 1200-1207.

Mills W.B., Liu S., Rigby M.C., Brenner D. (2007). Time-Variable Simulation of Soil Vapor Intrusion into a Building with a Combined Crawl Space and Basement. *Environ. Sci. Technol.*, 41, 4993-5001.

Morrison M.C., Hines M.E. (1990). The variability of biogenic sulfur flux from a temperate salt marsh on short time and space scales. *Atmos. Environ.*, 24A, 1771-1779.

Moseley W. A., Dhir V. K. (1996). Capillary pressure-saturation relations in porous media including the effect of wettability. *J. Hydrolo*., 178, 33-53.

Mosier A., Schimel D., Valentine D., Bronson K., Parton W. (1991). Methane and nitrous oxide fluxes in native, fertilized and cultivated grasslands. *Nature*, 350, 330-332.

Narasimhan T.N., Witherspoon P.A. (1977). Numerical model for saturated-unsaturated flow in deformable porous media, I. theory. *Wat. Resours. Res*., 13, 657-664.

Nay S.M., Mattson K.G., Bormann B.T. (1994). Biases of Chamber Methods for Measuring Soil CO_2 Efflux Demonstrated with a Laboratory Apparatus. *Ecology*, 75, 2460-2463.

Nazaroff W.W., Feustel H., Nero, A. V., Revzan,K. L., Grimsrud D. T. (1985). Radon transport into a detached one-story house with a basement. *Atmos. Environ*., 19, 31-46.

Nazaroff W.W., Lewis S.R., Doyle S. M., Moed B. A., Nero A.V. (1987). Experiments on Pollutant Transport from Soil into Residential Basements by Pressure-Driven Airflow. Environ. Sci. Technol., 21, 459-466.

NJDEP (2005). Vapor Intrusion Guidance. New Jersey Department of Environmental Protection.

NJDEP (2009). What's New for the SRP Vapor Intrusion Guidance Documents. Revisions to indoor air and sub slab soil gas sampling requirements at vapor intrusion investigations. New Jersey Department of Environmental Protection. http://www.nj.gov/dep/srp/guidance/vaporintrusion/whatsnew.htm (May 2010).

Norman J.M., Gracia R., Verma S.B. (1992). Soil Surface CO_2 Fluxes and the Carbon Budget of a Grassland. *J. Geophys. Res.,* 97, D17, 18845-18853.

Norman J. M., Kucharik C.J., Gower S.T., Baldocchi D.D., Crill P.M., Rayment M., Savage K., Striegl R.G. (1997). A comparison of six methods for measuring soilsurface carbon dioxide fluxes. *J. Geophys. Res*., 102, D24, 28771-28777.

Novak J.M., Lima I., Xing B., Gaskin G. W., Steiner C., Das K.C., Ahmedna M., Rehrah D., Watts D.W. (2009). Characterization of designer biochar produced at differenty temperatures and their effects on a loamy sand. Annals of Environmental Science, 3, 195-206.

NPI (2006). NPI volatile organic compound definition and information, Version 2.5, National Pollutant Inventory. September, 1-4. http://www.envirofloors.com.au/PDF%20Doc/npi%20voc%20info.pdf (August 2010).

NRC (1983). Risk Assessment in the FederalGovernment: Managing the Process. National Research Council National Academy Press, Washington, D.C. http://books.nap.edu/openbook.php?record_id=366&page=R1

NYSDOH (2006). Final guidance for evaluating soil vapor intrusion in the state of New York. New York state Department of Health, Center for Environmental Health, Bureau of Environmental Exposure Investigation, Troy, New York, October.

OEHHA (2004). Human-Exposure-Based Screening Numbers Developed to Aid Estimation of Cleanup Costs for Contaminated Soil. Integrated Risk

Assessment Section, Office of Environmental Health Hazard Assessment, California Environmental Protection Agency, November.

Okimori, Y., Ogawa, M., Takahashi, F. (2003). Potential of CO_2 emission reductions by carbonizing biomass waste from industrial tree plantation in south Sumatra, Indonesia. *Mitigation and adaptation strategies for global change*, 8, 261-280.

Olson D. A., Corsi R. L. (2001). Characterizing exposure to chemicals from soil vapor intrusion using a two-compartment model. *Atmos. Environ.*, 35, 4201-4209.

Olson D. A., Corsi R. L. (2002). Fate and Transport of Contaminants in Indoor Air. *Soil and Sedim. Contam.*, 11, 583-601.

Park H. S. (1999). A method for assessing soil vapor intrusion from petroleum release sites: multi-phase/multi-fraction partitioning. *Global Nest: the Int. J.*, 1,195-204.

Parker J. C. (2003). Modeling volatile chemical transport, biodecay, and emission to indoor air. *Ground Water Monitor. Remediat.*, 23, 107-120.

Parkin T., Mosier A., Smith J., Venterea R., Johnson J., Reicosky D., Doyle G., McCarty G., Baker J. (2003). Chamber-based Trace Gas Flux Measurement Protocol. *USDA-ARS GRACEnet*. http://amazonpire.org/PDF/FC2010/Volume%202/Baker%20et%20al_2003_GRACEnet_analyses_protocol.pdf (November 2010).

Pasteris G., Werner D., Kaufmann K., Hohener P. (2002). Vapor phase transport and biodegradation of volatile fuel compounds in the unsaturated zone: a large scale lysimeter experiment. *Environ. Sci. Technol*., 36, 30-39.

Pedersen A.R. (2000). Estimating the Nitrous Oxide Emission Rate from the Soil Surface by Means of a Diffusion Model. *Scand. J. Stat.*, 27, 385-403.

Pennell K. G., Bozkurt O., Suuberg E. M. (2009). Development and Application of a Three-Dimensional Finite Element Vapor Intrusion Model. *J.Air Waste Manag. Assoc.* 59, 447-460.

Pennell K. G., Suuberg E.M.(2010). Vapor transport from soil and groundwater: numerical modeling approach. In Vapor Emission to Outdoor Air and Enclosed Spaces for Human Health Risk Assessment: Site Characterization, Monitoring and Modeling. Saponaro S., Sezenna E., Bonomo L. Eds., Nova Science Publishers, Hauppauge NY, Chapter 4 (at press).

Poe S. H., Valsaraj K.T., Thibodeaux, L. J., Springer C.J. (1988) Equilibrium vapor phase on dry soils. *Hazard. Mater.*, 19, 17-32.

Poissant L., Casimir A. (1998). Water-Air and Soil-Air Exchange Rate of Total Gaseous Mercury Measured at Background Sites. *Atmos. Env.*, 32, 883-893.

Poissant L., Pilote M., Casimir A. (1999). Mercury flux measurements in a naturally enriched area: correlation with environmental conditions during the Nevada Study and Tests of the Release of Mercury From Soils (STORMS). *J. Geophys. Res.*, 104, D17, 21845-21857.

Politecnico di Milano (Puricelli S., Romele L., Saponaro S., Sezenna E.), ARPA (Bellaria l., Bosticco L., Narducci C., Racciatti R., Ughini S.), ASL (Colombo L.), Municipality of Milan (Visani M.) (2010) . Linee guida vapori - Technical document for local environmental Agencies to treat vapours from polluted sites for Risk Assessment - submitted.

Provoost J., Reijnders L., Swartjes F., Bronders J., Seuntjens P., Lijzen J. (2009a). Accuracy of seven vapour intrusion algorithms for VOC in groundwater. *J Soils Sed.,* 9, 62-73.

Provoost J., Bsman A., Reijnders L., Bronders J., Touchant K., Swartjes F. (2009b). Vapour intrusion from the vadose zone-seven algorithms compared. *J. Soils Sed*., published on line 20 August.

Pumpanen J., Kolari P., Ilvesniemi H., Minkkinen K., Vesala T., Niinistö S., Lohila A., Larmola T., Morero M., Pihlatie M., Janssens I., Yuste J.C., Grünzweig J.M., Reth S., Subke J.A., Savage K., Kutsch W., Ostreng G., Ziegler W., Anthoni P., Lindroth A., Hari P. (2004). Comparison of different chamber techniques formeasuring soil CO_2 efflux. *Agr. Forest Meteorol.*, 123, 159-176.

Puricelli S, Saponaro S., Sezenna E. (2010). Vapor emission at polluted sites: comparison between model predictions and field data. CONSOIL-11th International UFZ- Deltares/TNO Conference on Management of Soil, Groundwater and Sediment. Salzburg, 22-24 September.

Rabideau C.G., Comey III K.R. (1996). Estimating VOC Emissions from Waste Water Treatment Units Using a Flow-Through Flux Chamber and Chemdat7. *Volatile organic compounds (VOCs) in the environment*. Wang W., Schnoor J.L., Doi J. Eds., ASTM special technical publication 1261, 147-155.

Rayment M.B., Jarvis P.G. (1997). An improved open chamber system for measuring soil CO_2 effluxes in the field. In: *J. Geophys. Res.*, 102, D24, 28779-28784.

Rayment M. B. (2000). Closed chamber systems underestimate soil CO2 efflux. *Eur J. Soil Sci*, 51, 107-110.

Rannaud D., Cabral A., Allaire S.E. (2009). Modeling Methane Migration and Oxidation in Landfill Cover Materials with TOUGH2-LGM. *Water Air Soil Pollut*, 198, 253-267.

Ravi V., Johnson J.A. (1997). VLEACH: A one-dimensional finite difference vadose zone leaching model, Version 2.2, Center for Subsurface Modeling Support, USEPA RSKERL, Ada, OK.

Reed T, McLaughlin H. (2009). Bonding and Structure in BioChar. North American Biochar Conference 2009, Biochar Characterization session.

Reiche N., Lorenz W., Borsdorf H. (2010). Development and application of dynamic air chambers for measurement of volatilization fluxes of benzene and MTBE from constructed wetlands planted with common reed. *Chemosphere*, 79, 162-168.

Reichman R., Rolston D.E. (2002). Design and Performance of a Dynamic Gas Flux Chamber. J. Environ. Qual., 31, 1774–1781.

Reinhart D.R., Cooper D.C. (1992). Flux Chamber Design and Operation for the Measurement of Municipal Solid Waste Landfill Gas Emission Rates. *Air Waste Manage. Assoc.*, 42, 1067-1070.

Revzan K. L., Fisk W. J., Gadgil A. J. (1991). Modeling Radon Entry into Houses with Basements: Model Description and Verification. Lawrence Berkeley National Laboratory - LBL-27742, January.

Rinklebe J., During A., Overesch M., Wennrich R., Stark H.-J., Mothes S., Neue H.-U. (2009). Optimization of a simple field method to determine mercury volatilization from soils--Examples of 13 sites in floodplain ecosystems at the Elbe River (Germany). *Ecol. Eng.*, 35, 319-328.

Rinklebe J., During A., Overesch M., Du Laing G., Wennrich R., Stärk H.J., Mothes S. (2009b). Dynamics of mercury fluxes and their controlling factors in large Hg-polluted floodplain areas. *Environ Pollut.*, 158, 308-318.

Rikken M.G.J., Lijzen J.P.A., Cornelese A.A. (2001). Evaluation of model concepts on human exposure. Proposals for updating the most relevant exposure routes of CSOIL). National Institute of Public Health and Environmental Protection, Bilthoven. Report n. 711701022.

Ririe G. T., Sweeney R. E., Daugherty S. J. (2002). A Comparison of Hydrocarbon Vapor Attenuation in the Field with Predictions from Vapor Diffusion Models. *Soil and Sedim. Contam.*, 11, 529-554.

RISC (2010). RISC: The New Standard for Human Health Risk Assessment for Contaminated Sites. http://www.groundwatersoftware.com/risc.htm (May 2010)

Robinson N. I., Turczynowicz L., (2005). One- and Three-Dimensional Soil Transportation Models for Volatiles Migrating from Soils to House Interiors. Transp. Porous. Med., 59, 301–323.

Roffman A., Macoskey K., Shervill R.P. (1995). Assessing the Effect of Mercury Emissions from Contaminated Soil at Natural Gas Gate Stations. J. appl. Meteorol. , 34, 594-602.

Roggemans S., Bruce C. L., Johnson P. C., Johnson, R. L. (2001). Vadose Zone Natural Attenuation Of Hydrocarbon Vapors: An Empirical Assessment Of Soil Gas Vertical Profile Data. *API Soil and Groundwater Research Bulletin*, nr. 15, December.

Romele L., Sezenna E. (2010). Indoor and outdoor air sampling techniques. In Vapor Emission to Outdoor Air and Enclosed Spaces for Human Health Risk Assessment: Site Characterization, Monitoring and Modeling. Saponaro S., Sezenna E., Bonomo L. Eds., Nova Science Publishers, Hauppauge NY, Chapter 8 (at press).

Rondon M. A., Lehmann J., Ramirez J., Hurtado M. (2007). Biological nitrogen fixation by common beans (Phaseolus vulgaris L.) increases with bio-char additions. *Biol. Fert. Soils*, 43, 699-708.

Rutherford D.W., Rostad C.E., Wershaw R.L. (2010). The adsorption and absorption of water by wood and grass chars.Pyrogenic Black Carbon, or Biochar, in Soils and Sediments, Its Characterization and Fate - Effects On the Carbon Cycle and Carbon Sequestration, and Its Effects on Soil Properties. Proceedings of 2010 GSA Denver Annual Meeting (31 October - 3 November 2010), Geological Society of America Eds, 42, n° 5, 159.

Sadek S.E., Lee T.C., Smith J.D., Gebel R. (1998). Flux Chamber Measurements of Mass Transfer Rates. *J. Environ. Eng.-ASCE*, 124, 111-121.

Sander R. (2010). Henry's Law Constants. http://www.mpch-mainz.mpg.de/~sander/res/henry.html (December 2010).

Sanders P.F., McChesney M.M., Seiber J.N. (1985). Measuring Pesticide Volatilization from Small Surface Areas in the Field. *Bull. Environ. Contam. Toxicol.*, 35, 569-575.

Sanders P. F., Stern A. H. (1994). Calculation of soil cleanup criteria for carcinogenic volatile organic compounds as controlled by the soil-to-indoor air exposure pathway. *Environ. Toxicol. Chem.* 13, 1367-1373.

Sanders P. F., Talimcioglu N. M. (1997). Soil-to-indoor air exposure models for volatile organic compounds: The effect of soil moisture. *Environ. Toxicol. Chem.*, 16, 2597-2604.

Sartin J.H.; Halsall C.J., Davison B., Owen S., Hewitt C.N. (2000). Determination of biogenic volatile organic compounds (C8-C16) in the coastal atmosphere at Mace Head, Ireland. *Anal. Chim. Acta*, 428, 61-72.

Sbaffoni S. (2007). "Bonifica dei siti contaminati – soil remediation-" course. Università Sapienza di Roma, Dipartimento di Idraulica, Trasporti e Strade (DITS) - Idraulic, Transport and Street Department-. (August, 2010).

Scesi L., Papini M. (1997). Il rilevamento geologico-tecnico. Città Studi Edizioni.

Schmidt C.E., Balfour W.D. (1983). Direct Gas Emission Measurement Techniques and the Utilization of Emissions Data from Hazardous Waste Sites. Proceedings of national Conference on Environmetal Engineering, ASCE.

Schmidt C.E. (1991).Evaaluation of volatile organic compound emission control of rusmar AC-900L and AC-900 foam using the surface emission isolation flux chamber. Technical Memorandum. http://www.aquafoam.com/papers/voc.pdf (November 2010).

Schmidt C.E., Zdeb T.F. (1998a). Direct measurement of indoor infiltration through a concrete slab using the US EPA flux chamber. Proceeding of Air and Waste Management Association's 91st Annual Meeting & Exhibition, 98-TA9C.01, June 14-18, San Diego, California.

Schmidt C.E., Copeland T.L., Pesin R. (1998b). Comparison Of Measured And Modeled Emissions From Subsurface Contamination At An Industrial Site In A Residential Neighborhood. Proceeding of Air and Waste Management Association's 91st Annual Meeting & Exhibition, 98-WPC.01P, June 14-18, San Diego, California.

Schroeder W. H. (1995). Environmental measurements and results of mercury volatilization rates ("fluxes") from soil and lake surfaces. Proceedings of Canadian Mercury network workshop.

Schumacher B.A. (2002). Methods for the determination of total organic carbon (TOC) in soils and sediments. Ecologicval Risk Assessment Support center, Offfice of Researrch and Development, US. Environmental Protection Agency.

Schwarzenbach R.P, Gschwend P.M, Imboden D.M. (1993). Environmental Organic Chemistry. Wiley-Interscience, New Jersey, USA.

Schwartzkopf S.H. (1978). An Open Chamber Technique for the Measurement of Carbon Dioxide Evolution from Soils. *Ecology*, 59, 1062-1068.

Sleep B. E., Sykes J. F. (1989). Modeling the Transport of Volatile Organics in Variably Saturated Media, *Water Resour. Res.*, 25, 81-92.

Sleep B. E. (1998). Modeling transient organic vapor transport in porous media with the dusty gas model. *Adv. Water Resour.*, 22, 247-256.

Smith J.A., Tisdale A.K., Cho H.J. (1996). Quantification of Natural Vapor Fluxes of Trichloroethene in the Unsaturated Zone at Picatinny Arsenal, New Jersey. *Environ. Sci. Technol.*, 30, 2243–2250.

Sohi S., Lopez-Capel E., Krull E., Bol R., (2009). Biochar, climate change and soil: A review to guide future research. CSIRO Land and Water Science Report 05/09.

Song X., Heyst B.V. (2005). Volatilization of mercury from soils in response to simulated precipitation. *Atmos. Environ.*, 39, 7494-7505.

Steinberg, S.M. Kreamer D.K. (1993). Evaluation of the sorption of volatile organic compounds by unsaturated calcareous soil from Southern Nevada using inverse gas chromatography. *Environ. Sci. Technol.*, 27, 883-888.

Steiner C., Teixeira W.G., Lehmann J., Nehls T., De Macêdo J. L. V., Blum W. E. H., Zech W. (2007). Long term effects of manure, charcoal and mineral fertilization on crop production and fertility on a highly weathered Central Amazonian upland soil. *Plant Soil*, 291, 275- 290.

Steiner C. (2009). Biochar Carbon Sequestration. Green ThinDisc, An Interactive Multimedia Book, Chapter 17, The United Nations Commission on Sustainable Develoment Partnership in New Technologies for Small Island Developing states Pubs. http://www.biochar.org/joomla/images/stories/Steiner%20Chapter%2017%202009.pdf (December 2010)

Sun X., Werner D., Ghosh U. (2009). Modeling PCB Mass Transfer and Bioaccumulation in a Freshwater Oligochaete Before and After Amendment of Sediment with Activated Carbon. *Environ. Sci. Technol.*, 43, 115-1121.

Taylor J.R. (2000). Introduzione all'analisi degli errori. Lo studio delle incertezze nelle misure fisiche. Zanichelli.

Teggi S. (2008). "Bonifica dei siti contaminati – soil remediation-" course. Università degli studi di Modena e Reggio Emilia, Dip. Ingegneria Meccanica e Civile - Mechanical and Civic Department-. http://cdm.unimo.it/home/dimec/teggi.sergio/Proprieta%20chimicofisiche%20degli%20inquinanti.pdf (August 2010).

Thies J. E., Rillig M.C. (2009). Characteristics of Biochar: Biological Properties. In Characteristics of Biochar: Biological Properties. Lehmann J., Joseph S. Eds., Earthscan, London, UK.

Tillman F. D.; Choi J.-W., Katchmark W.; Smith J. A., Wood H. G (2001). Unsaturated-zone airflow: implications for natural remediation of ground water by contaminant transport through the subsurface. Chapter 14, 307-339. In Smith J. A., Burns S.E., Physicochemical Groundwater Remediation, Kluwer Academic/Plenum Publishing, New York (http://books.google.com/books?hl=en&lr=&id=N8vId2rjIwgC&oi=fnd&pg=PA1&sig=ez5o6GuuF3GyjqUQRkbmod9X030&dq=%22Smith%22+%22Physicochemical+Groundwater+Remediation%22+#v=onepage&q&f=false) (August 2010).

Tillman F.D., Choi J.W., Smith J.A. (2003). A comparison of direct measurement and model simulation of total flux of volatile organic compounds from the subsurface to the atmosphere under natural field conditions. *Water Resour. Res.*, 39, 5-11.

Tillman F.D., Smith J.A. (2004). Design and laboratory testing of a chamber device to measure total flux of volatile organic compounds from the unsaturated zone under natural conditions. *J. Contam. Hydrol.*, 75, 71-90.

Tillman F.D., Weaver J.W. (2005). Review of Recent Research on Vapor Intrusion, U. S. Environmental Protection Agency - Office of Research and Development, Washington, DC, EPA/600/R-05/106.

Thorstenson, D. C., Pollock D. W. (1989) Gas Transport in Unsaturated Zones: Multicomponent Systems and the Adequacy of Fick's Laws. *Water Resour. Res*., 25, 477-507.

Trevitt A. C. F., Freney J. R., Denmead O. T., Zhu Zhao-Liang, Cai Gui-Xin, Simpson J. R. (1988). Water-air transfer resistance for ammonia from flooded rice. *J. Atmos. Chem*., 6, 133-147.

TOXNET (2010). Toxicology Data Network. http://toxnet.nlm.nih.gov/index.html (August 2010)

Turczynowicz L., Robinson N. I. (2007). Exposure Assessment Modeling for Volatiles—Towards an Australian Indoor Vapor Intrusion Model. *J. Toxicol. Env. Health,* Part A, 70, 1619-1634.

USEPA (1986). Measurement of Gaseous Emission Rates from Land Surfaces Using an Emission Isolation Flux Chamber, Users Guide; Environmental Monitoring Systems Laboratory, US. Environmental Protection Agency: Washington, DC. EPA/ 600/8-86/008.

USEPA (1994). Air emissions models for waste and wastewater, US. Environmental Protection Agency, EPA-453/R-94-080A, cap 7- land Treatment, 7-1, 7-57.

USEPA (1996a). Soil Screening Guidance: Technical Background Document. Limited Validation of the Jury Infinite Source and Jury Finite Source Models. Office of Solid Waste and Emergency Response: Washington, DC. EPA/540/R95/128

USEPA (1996b). Soil Screening Guidance: User's guide. U.S. Environmental Protection Agency - Office of Emergency and Remedial Response: Washington, DC. EPA/540/R-96/018.

USEPA (1999). Compendium of Methods for the Determination of Toxic Organic Compounds in Ambient. U.S. Environmental Protection Agency- Office of Research and Development - Center for Environmental Research Information: Cincinnati. EPA/625/R-96/010b

USEPA (2002a) OSWER Draft Guidance for Evaluating the Vapor Intrusion to Indoor Air Pathway from Groundwater and Soils (Subsurface Vapor Intrusion Guidance), US. Environmental Protection Agency.

USEPA (2002b). User`s guide for evaluating subsurface vapor intrusion into buildings, US. Environmental Protection Agency.

USEPA (2004). User's guide for evaluating subsurface vapor intrusion into buildings. US. Environmental Protection Agency: Office of Emergency and Remedial Response, Washington, D.C., Contract No. 68-W-02-33.

Valente R.J., Thronton F.C., Williams E.J. (1995). Field comparison of static and flow-through chamber techniques for measurement of soil NO emission. *J. Geophys. Res.*, Vol. 100, D10, 21147-21152.

Van Den Berg R. (1994). Human exposure to soil contamination: a qualitative and quantitative analysis towards proposals for human toxicological intervention values (partly revised edition). National Institute of Public Health and Environmental Protection, Bilthoven. Report n. 755201011.

Van Dijke M.I.J., Van der Zee S.E.A.T.M., Van Duijn C.J. (1995). Multi-phase flow modeling of air sparging. *Adv. Water Resour.* 18, 319-333.

Van Genuchten M. Th. (1980). A Closed-form Equation for Predicting the Hydraulic Conductivity of Unsaturated Soils. Soil Sci. Soc. Am. J., 44, 892-898.

Van Wijnen H. J., Lijzen J.P.A. (2006). Validation of the VOLASOIL model using air measurements from Dutch contaminated sites - Concentrations of four chlorinated compounds. National Institute for Public Health and the Environment (RIVM), Bilthoven. Report n. 711701041/2006.

VHBC (2010). RISC-HUMAN 3.2. Van Hall Business Centre http://www.risc-site.nl/index.html?riscmainFrame=sw_risc_uk.htm (May 2010).

Waitz M.F.W., Freijer J.I., Kreule P., Swartjes F.A. (1996). The VOLASOIL risk assessment model based on CSOIL for soils contaminated with volatile compounds. National Institute of Public Health and the Environment (RIVM), Bilthoven. Report n. 715810014.

Walden T. (2005). Risk assessment in soil pollution: comparison study. *Rev Environ Sci Biotechnol*, 4, 87-113.

Wallschläger D., Turner R.R., London J., Ebinghaus R., Kock H.H., Sommar J., Xiao Z. (1999). Factors affecting the measurement of mercury emissions from soils with flux chambers. *J. Geophys. Res.*, 104, D17, 21859-21871.

Wallschläger D., Kock H.H., Schroeder W.H., Lindberg S.E., Ebinghaus R., Wilken R.D. (2002). Estimating Gaseous Mercury Emissions from Contaminated Floodplain Soils to the Atmosphere with Simple Field Measurement Techniques. *Water Air Soil Poll.*, 135, 39-54.

Wang D., Yates S.R., Ernst F.F. (1997). Calibration and Testing of a Dynamic Flowthrough Chamber for Field Determination of Methyl Bromide Volatilization Flux. *Atmos. Environ.*, 31, 4119-4123.

Wang F., Ward, I.C. (2002). Radon entry, migration and reduction in houses with cellars. *Build. Environ.* 37, 1153-1165.

Warnock D. D., Lehmann J., Kuyper T. W., Rillig M. C. (2007). Mycorrhizal responses to biochar in soil concepts and mechanisms. *Plant Soil*, 300, 9-20.

Webb S., Pruess K., (2003) The Use of Fick's Law for Modeling Trace Gas Diffusion in Porous. *Transport Porous Med.*, 51, 327–341.

Werner D., Grathwohl P., Höhener P. (2004), Review of Field Methods for the Determination of the Tortuosity and Effective Gas-Phase Diffusivity in the Vadose Zone. *Vadose Zone Journal*, 3, 1240–1248.

Widén B., Lindroth A. (2003). A Calibration System for Soil Carbon Dioxide-Efflux Measurement Chambers: Description and Application. *Soil Sci. Soc. Am. J.*, 67, 327-334.

Wiedemeier, T. H., Rifai H., Newell C., Wilson J.T. (1999). Natural attenuation of fuels and chlorinated solvents in the subsurface. Wiley J. and Sons Eds, New York.

Wilhelm E., Battino R., Wilcock R.J. (1977). Low-pressure solubility of gases in liquid water. Chem. Rev., 77, 219–262.

Woodrow J.E., Seiber J.N. (1991). Two Chamber Methods for the Determination of Pesticide Flux from Contaminated Soil and Water. *Chemosphere*, 23, 291-304.

Xiao Z.F., Munthe J., Schroeder W.H., Lindqvist O. (1991). Vertical fluxes of volatile mercury over forest soil and lake surfaces in Sweden. *Tellus*, 43B, 267-279.

Yates S.R., Gan J., Ernst F.F., Wang D. (1996). Methyl Bromide Emissions from a Covered Field: III. Correcting Chamber Flux for Temperature. *J.Environ. Qual.*, 25, 892-898.

Yates S.R., Wang D., Ernst F.F., Gan J. (1997). Methyl Bromide Emissions from Agricultural Fields: Bare-Soil, Deep Injection. *Environ. Sci. Technol.*, 31, 1136-1143.

Yaron B., Calvet R., Prost R. (1996). Soil pollution, processes and dynamics. Springer, Berlin.

Yu X., Pan, L., Ying G., Kookana R.S. (2010). Enhanced and irreversible sorption of pesticide pyrimethanil by soil amended with biochars. *J. Environ. Sci.*, 22, 615-620.

Zhang H., Lindberg S.E., Barnett M.O., Vette A.F., Gustin M.S. (2002). Dynamic flux chamber measurement of gaseous mercury emission fluxes over soils. Part 1: simulation of gaseous mercury emissions from soils using a two-resistance exchange interface model. *Atmos. Environ.*, 36, 835-846.

Zimmerman A.R. (2010). Abiotic and Microbial Oxidation of Laboratory-Produced Black Carbon (Biochar). *Environ. Sci. Technol.*, 44, 1295-1301.

APPENDIX 1

MEASURING INSTRUMENTS

In this Appendix technical features of instruments used during the experiments described at Chapter 5, 6 and 7. It is divided in two sections: one containing information about instruments used to measure physical parameters and control or/and check air flow meters during tests with the flux chamber (at DIIAR laboratory of Politecnico di Milano or on site); the second one about what was used to define physical properties of the matrices used at Civil Engineering and Geosciences, Laboratory, of Newcastle University.

A1.1 Instruments used for experimentation at Politecnico di Milano and for FC field activity (§ 5 and § 6)

A1.1.1 Instruments for physical parameter determination

A1.1.1.1 Multifunction digital micro manometer DC 100^{PRO} (WÖHLER)

Working temperature: from -5 to 40 °C

***Tab. A1.1**: technical features of micro pressure gauge DC 100^{PRO}.*

	pressure	**inner temperature probe**	**external temperature probe**	**Inner humidity probe**
Measuring unit	hPa, Pa, mbar, mm_{H2O}, PSI	°C and °F	°C and °F	%
Measuring range	± 100 hPa	from -20.0 to 60.0 °C	from - 20.0 to 60.0 °C	from 0 to 100 %
precision	± 0.3 Pa or 3% measured value	± 2 °C	± 2 °C	± 2% for 0-90% range; ± 3% for 91-100% range
resolution	0.1 Pa or 0.01 Pa till 1100 Pa and 1 Pa for values higher than 1100 Pa	± 0.1 °C	± 0.1 °C	1%

A1.1.1.2 Multifunction measuring instrument Testo – 435. IAQ (Indoor Air Quality) Probe

***Tab. A1.2**: technical features of micro Testo-435 probe.*

	Absolute pressure	**temperature**	**humidity**
Measuring unit	hPa, inch$_{H2O}$	°C and °F	% (relative humidity - RH)
Measuring range	From 600 to 1150 hPa	from 0 to 50 °C	from 0 to 100 % RH
precision	± 5 hPa	± 0.3 °C	± 2 % RH (2 - 98 % RH)

A1.1.1.3 Temperature probe Checktemp-1 (Hanna Instruments)

***Tab. A1.3**: technical features of Checktemp-1 temperature probe.*

	temperature	
Measuring unit	°C	°F
Measuring range	from -50.0 to 150.0 °C	from -58.0 to 302 °F
precision	± 0.3 °C (from -20 to 90 °C) ± 0.5 °C (outside that range)	± 0.5 °F (from -2 to 194 °F) ± 1 °F (outside that range)

A1.1.1.4 Digital thermo-igrometer (TFA)

***Tab. A1.4**: technical features of digital thermo-igrometer.*

	temperature	**humidity**
Measuring unit	°C	% Relative Humidity (RH)
Measuring range	from -10.0 to 60.0 °C	from 10 to 99 % RH
precision	± 0.8 °C (from 10 to 30 °C) ± 1 °C (outside that range)	± 3.5 % RH (from 30 to 80 % RH) ± 5 % RH (outside that range)

A1.1.2 Instruments for air flow regulation

A1.1.2.1 SKC AirCheck XR 5000 Sample Pump

Working temperature: from 0 to 45 °C

***Tab. A1.5**: technical features of SKC pump.*

	pressure
Measuring unit	ml min^{-1}
Measuring range	from 1000 to 5000 ml min^{-1}
precision	± 5 % of set-point after proper calibration phase

A1.1.2.2 Ego Plus TT (Zambelli) Sample Pump

Working temperature: from 5 to 40 °C (with relative humidity in the range 30-90 %)

***Tab. A1.6**: technical features of Ego Plus TT pump.*

	pressure
Measuring unit	ml min^{-1}
Measuring range	from 20 to 7500 ml min^{-1}
precision	± 2 %

A1.1.2.3 Thermal mass flow controller Model 80D-10 (McMillan Company)

Recommended working temperature: from 10 to 40 °C

***Tab. A1.7**: technical features of Mass Flow Controller (80D-10).*

	pressure
Measuring unit	l min^{-1}
Measuring range	from 0 to 10 l min^{-1}
precision	± 1.5 %
Suitable gases	Clean, dry, non corrosive gases

A1.1.2.4 Mass flow controller (ALBORG)

***Tab. A1.8**: technical features of Mass Flow Controller (AALBORG).*

	pressure
Measuring unit	l min^{-1}
Measuring range	from 0 to 10 l min^{-1}
precision	± 1.5 %
Suitable gases	Clean gases

A1.1.2.5 Rotameters

***Tab. A1.9**: technical features of used rotameters; *: to convert in l min^{-1} by using its calibration table*

Type	**Measuring unit**	**Range**	**Precision**
Gilmont n. 13	l min^{-1}	0.2 - 14	± 0.2 (from 0 to 0.2 l min^{-1}) ± 0.5 (from 1 to 14 l min^{-1})
Gilmont n. 14	l min^{-1}	1 - 39	± 1
SKC	l min^{-1}	0.4 - 5	± 0.1
Zambelli	l min^{-1}	0.3 - 4	± 0.1
T45787	mm *	0 - 150	± 1
L80418/01	mm *	0 - 150	± 1

A1.1.3 Other used instruments

PID: Phocheck Plus

Tab. A1.10*: technical features of Phocheck Plus.*

	pressure
Measuring unit	mg m^{-3} of TPH equivalent
Measuring range	0.001 – 10000 mg m^{-3}
precision	± 5 %
Suction flow	220 ml min^{-1}
Working temperature	From -20 to 60 °C

Suction pumps:	DYMAX 30, Charles Austen Pumps (Cellai); KNF Neuberger Laboport.
Muffle:	Nabertherm L9/11/C6.
Oven:	Heraeus UT 6060; G®-Therm 075.

A1.2 Instruments used for experimentation at Newcastle University (§ 7)

A1.1.1 Instruments used for matrices characterization

Sieves	Endecotte Ltd, London , UK
Oven:	UM500, Memmert, Germany
Muffle:	Gallenhampe Muffle Furnace - Size 1
Centrifuge :	Eppendorf- centrifuge 5810, Scientific laboratory supplies, UK
pH-meter	3020 pH-meter, Jenway, UK

APPENDIX 2

ANALYTICAL METHODS

This Appendix presents the analytical methods performed to analyse chemical compounds involved in the presented experiments.

It is divided in three sections: § A2.1 a general introduction about GC features; § A2.2 about inner methods used at DIIAR Laboratory (Politecnico di Milano) to analyse i) ethanol sampled in glass balloon during flux chamber setup definition (§ 5), ii) BTEX sampled on activated carbon (a.c.) tubes during air treatment verification (§ 5) and field measurements (§ 6), iii) features of methods for air hydrocarbon compounds analyses, sampled on tubes, according to MADEP indications (§ 5 and § 6) and iv) BTEX and hydrocarbons on condensation; § A2.3 on methods performed at Newcastle University, directly by the author, for i) VOCs and ii) O_2, CO_2 and SF_6 compounds in air phase or, by the inner environmental laboratory, for iii) VOCs as pure NAPL phase.

A2.1 Gas chromatography

This section presents further details to what was already presented in § 4.2.5.3. Gas chromatography (GC), is type of chromatography used for separating and analyzing compounds that may be vaporized without decomposition. It is based on a repartition technique among a moving (or mobile) phase and a stationary one. The first one is a carrier gas whereas the second one is a layer of liquid or polymer on an inert solid support called a column. The sample (initially having either gaseous, liquid or solid phase) has to be transformed in gaseous phase and being analyzed interacts with the walls of the column, which is coated with different stationary phases. In this way each compound is eluted at a different time, called the retention time of the compound.

The basic elements to characterize each different GC analysis are:

- column inlet (or injector) providing the means to introduce a sample into a continuous flow of carrier gas. Generally the sample is introduced into a heated small chamber via a GC syringe through a septum. It may be used in Splitless or Split way, where respectively the complete sample or a portion is swept by the carrier gas into the column, according to analyte concentration (respectively for low and high one). Programmed Temperature Vaporising (PTV) injector is on the other hand used when low-boiling solvent are involved: the detector temperature is chosen slightly below the boiling point of the solvent and the sample is continuously evaporated and vented through the split line;

- carrier gases that are usually inert such as helium, nitrogen, argon, hydrogen and air, depending on the detector being used;
- GC columns that are divided in packed and capillary columns. The first one (with length, L, from 1.5 to 10 m and an internal diameter, ∅, of 2- 4 mm) are made of stainless steel or glass and contain a packing of finely divided, inert, solid support material (e.g. diatomaceous earth) that is coated with a liquid or solid stationary phase, influencing what type of materials will be most strongly adsorbed. The second ones have a very small internal diameter (∅ = a few tenths of mm) and are longer (L=25 ÷ 60 m), they are made of fused-silica and coated with the active materials;
- thermal program, which is the temperature range needed to make the compound volatilize into the GC;
- detector, which is generally a flame ionization detector (FID) or a thermal conductivity detector (TCD). FID is sensitive primarily to hydrocarbons: it contains a small hydrogen-air flame that burns the chemical compound giving an ion current directly proportional to analyte concentration;
- chromatogram, which is instrument output to electron current produced by the detector, through which analyte concentration is deduced via a calibration curve (prepared with some known analyte concentration).

A2.2 Chemical analysis performed at DIIAR laboratory (Politecnico di Milano)

A2.2.1 GC configuration for Ethanol determination

GC Model: DANI 8610;
injector: split mode, at temperature equal to 200 °C;
carrier gas: nitrogen;
GC column: SUPEL-Q PLOT, capillary column, coated by a porous polimer for gases with low molecule weight (L=30 m; ∅ = 0.32 mm);
thermal program: 35 °C for 5 min, 10 °C min^{-1} till 150 °C, then 150 °C for 10 min;
detector: FID (T = 240°C);
detection limit (d.l.): 0.07 mg l^{-1};
variation coefficient ($VC_{analysis}$): ± 15 %.

A2.2.2 GC configuration for BTEX measures

BTEX, sampled on a.c. tube, were chemically desorbed separately from sampling part a and backup part b (§ 4.2.5.3) using carbon disulfide (CS_2) as a solvent, and analyzing it through ISO 16200-1:2001 method.

According to the amount of solvent that the operating chemical technician had to use to dissolve contaminant from the adsorbent matrix, different detection limit may be reach. Three different volumes were used, as indicated in Tab. A2.1.

GC Model:	TRACE GC;
injector:	PTV (Programmed Temperature Vaporising injector) used in splitless mode, at temperature equal to 35 °C;
carrier gas:	nitrogen;
GC column:	NUKOL, capillary column idoneous for solvents (L=30 m; ∅ = 0.32 mm; stationary phase thick = 1 μm);
thermal program:	35 °C for 3 min, 6 °C min^{-1} till 120 °C, then 12°C min^{-1} till 200 °C, finally 200 °C for 10 min;
detector:	FID;
variation coefficient ($VC_{analysis}$):	± 15 %.

Tab. A2.1: *amounts of carbon disulfide (CS_2) [ml] used to desorbe a.c. tubes (according to the ability of the chemical technician who performed the analysis) and corresponding detection limit (d.l.)[μg].*

Part a		**Part b**	
Volume CS_2 [ml]	**d.l. [μg]**	**Volume CS_2 [ml]**	**d.l. [μg]**
6	0.9	2	0.3
3	0.45	1	0.15
2	0.3	0.66	0.1

A2.2.3 air hydrocarbon analysis

Hydrocarbon compounds (detected for §5 and § 6 tests) were sampled on a.c. or XAD2 tubes according to the chemical affinity of each analyte, following the indications in Tab. 4.6. The followed analytical procedure were were a modified MADEP APH (MADEP, 2009b) and MADEP EPH (MADEP, 2004) methods.

In Tab. A2.2 they are indicated, for each analyzed hydrocarbon compound, i) type of sampling tube, ii) the type and amount of used solvent to extract the analyte from the adsorbing matrix, iii) the detection limit and iv) the analytical variation coefficient.

A2.2.4 analysis for BTEX and hydrocarbon in moisture phase

The analysis of all the interested analytes in moisture phase were performer according to UNICHIM MU 1210/1997 method. It happened by extraction on a micro-fiber through SPME (Solid Phase Micro-Extraction) technique and analysis in GC-FID.

Reached detection limits (d.l.) are: 8 ng for Benzene, 5 ng TEX and 10 ng for all the other researched compounds. Analytical variation coefficients ($VC_{analysis}$) are: ± 15 %.

***Tab. A2.2**: details about air hydrocarbon analysis: type of sampling tube, kind and amount (V)[ml] of used solvent to extract the analyte from the adsorbing matrix, the detection limit (d.l.)[μg] and analytical variation coefficient ($VC_{analysis}$) [%]. CS_2: carbon disulfide; DCD: dichloromethane.*

	MTBE	**C5 Aliphatics**	**C6-C8 Aliphatics**	**C9-C12 Aliphatics**	**C13 -C18 Aliphatics**	**C19 -C36 Aliphatics**	**C9 -C10 Aromatics**	**C11 -C22 Aromatics**	**Naphthalene**
tube	a.c.	a.c.	a.c.	a.c.	XAD2	XAD2	a.c.	XAD2	XAD2
solvent	CS_2	CS_2	CS_2	CS_2	DCM	DCM	CS_2	DCM	DCM
solvent V part a [ml]	2	2	2	2	3	3	2	3	3
solvent V part b [ml]	0.66	0.66	0.66	0.66	1	1	0.66	1	1
d.l. part a [μg]	<0.2	<0.3	<0.3	<0.3	<0.5	<0.5	<0.3	<0.5	<0.2
d.l. part b [μg]	<0.07	<0.1	<0.1	<0.1	<0.18	<0.18	<0.1	<0.18	<0.07
$VC_{analysis}$ [%]	15	15	15	15	15	15	15	15	15

A2.3 Chemical analysis performed at Civil and Geotechnical laboratory (Newcastle University)

A2.3.1 air VOC analyses

GC Model: HP-7890 Series GC, Agilent Technologies, Palo Alto, USA;
injector: split mode, split ratio = 10, at temperature equal to 200 °C;
carrier gas: hydrogen at a flow rate of 2 ml min^{-1};
GC column: HP-5 capillary column (L= 30 m; ∅ =0.249 mm; stationary phase thick = 0.25 μm)
thermal program: 30 °C for 5 min, 10 °C min^{-1} till 120 °C, then 120 °C for 6 min;
detector: FID.

Each sample run took about 30 min.
Parameters of regression analysis according to (7.7), $VC_{analysis}$ and detection limits (d.l.) are indicated in Tab. A2.3, for both the two performed standard sets.

A2.3.2 CO_2, O_2 and SF_6 analyses

CO_2, O_2, and SF_6 analysis were performed by GC-MS, on a Fisons 8060 GC, linked to a Fisons MD800 MS (electron voltage 70 eV, filament current 4 A, source current 800 µA, source temperature 200 °C, multiplier voltage 500 V, interface temperature 150 °C).

injector:	split mode (at 100 ml min^{-1}), at temperature equal to 150 °C;
carrier gas:	helium (flow rate of 1 ml min^{-1}, pressure 65 kPa);
GC column:	HP-PLOT-Q capillary column (L= 30 m; ∅ =0.32 mm; stationary Q phase thick = 20 µm);
thermal program:	held isothermally at 35°C.

Analytical variation coefficients ($VC_{analysis}$) for CO_2, O_2, and SF_6 are respectively 27%, 11% and 32%.

A2.3.2 Liquid VOCs analyses

Liquid VOC mixture analysis was performed by GC-MS, on an Agilent 7890 AC Gas Chromatography system, linked to a MS Agilent 5975 C, in scan mode acquisition, according to the following way: no considered solvent delay, electron voltage 2000 eV, filament current 2 A, source temperature 230 °C.

injector:	split mode (split ratio 10:1), at temperature equal to 280 °C;
carrier gas:	helium (flow rate of 12.044 ml min^{-1}, pressure 45 kPa);
GC column:	Agilent 19091S-433 capillary column (L= 30 m; ∅ =0.25 mm; stationary phase thick = 0.25 µm); stationary phase: HP-5MS 5% of phenyl methyl silox: 1105.57187 (Agilent Technologies, Palo Alto, USA).
thermal program:	30 °C for 5 min, 5 °C min^{-1} till 300 °C, then 300 °C for 1 min;

Parameters of regression analysis according to (7.7), VOCs $VC_{analysis}$ and detection limits (d.l.) are indicated in Tab. A2.3. Detection limits are calculated from the minimum area detectable from GC (0.02), transformed in mass using standard line. If the found d.l. mass was negative, all resulting negative values obtained from analysis were considered equal to 0.

***Tab. A2.3**: a and b regression analysis parameters (according to (7.7)), variation coefficient of analysis (VC) and detection limit for I and II gas standard analysis sets and for liquid phase analysis; A: areal units from GC outputs; #: not detectable; *: d.l., using the indicated regression parameters, is negative, and therefore all negative calculated mass were considerate equal to 0.*

.

		n-pentane	**n-hexane**	**methyl cyclo-pentane**	**cyclo-hexane**	**isooctane**	**methyl cyclo-hexane**	**Toluene**	**n-octane**	**m-xylene**	**1,2,4 TMB**	**n-decane**	**n-dodecane**
I gas standard	**a (µg/A)**	2693.8829	2531.8886	2110.9816	2326.8842	2568.8969	2535.4643	2821.9297	1616.534	1586.3294	1805.3051	1223.02282	5323.96
	b (µg)	0.0680675	-4.874155	-4.947129	-4.284804	-0.251282	-0.769112	7.3353782	7.917246	3.5424684	1.28724837	0.750558824	0
	VC (%)	15	32	35	41	55	57	46	40	44	42	42	49
	d.l. (µg)	*	*	0.002	0.002	0.0001	0.0003	*	*	*	*	*	0.000004
II gas standard	**a (µg/A)**	2660.4948	2470.799	2057.416	2248.0411	2440.3901	2413.8497	2997.8005	1849.4387	1657.4711	1327.30612	956.9410043	5323.96
	b (µg)	11.986701	10.368858	11.487132	11.970794	17.640298	13.489011	8.9694021	6.9406595	3.6874746	2.17475	1.521293137	0
	VC (%)	6	54	50	54	63	63	47	50	35	25	21	62
	d.l. (µg)	*	*	*	*	*	*	*	*	*	*	*	0.000004
liquid standard	**a (µg/A)**	#	6941439	18313788	20346077	30488687	26658174	28013043	28518312	36723691	33473920	34888183	4178220
	b (µg)		576471.6	75404.3	11640.3	42003.0	29460.1	-12463.6	20817.3	-45873.3	19909.7	47178.4	27251.2
	VC (%)		33	24	16	13	14	12	13	2	13	15	13

APPENDIX 3

MEASURING UNCERTAINTY

In Appendix 3 it is described the propagation of error which is the effect of variables' uncertainties (or errors) on the uncertainty of a function based on them. In particular since the treated variables are the values of experimental measurements they have uncertainties due to measurement limitations (such as instrument precision) which propagate to the combination of variables in the function.

Calling δx,…, δz the uncertainties of x,…, z variables used to calculate a function q(x,…,z), if they are independent and casual, uncertainty in q is therefore (Taylor, 2000):

$$\delta q = \sqrt{\left(\frac{\delta q}{\delta x}\delta x\right)^2 + ... + \left(\frac{\delta q}{\delta z}\delta z\right)^2} \tag{A3.1}$$

That however is always lower than ordinary sum:

$$\delta q = \left|\frac{\delta q}{\delta x}\right|\delta x + ... + \left|\frac{\delta q}{\delta z}\right|\delta z \tag{A3.2}$$

APPENDIX 4

NUMERICAL CODE DESCRIBING VOC VAPOURS TRANSPORT IN COLUMN TEST

It is here copied the monodimensional finite difference model written in Matlab to describe transport of VOCs vapours in column tests, as it was described in § 7.2.4.6. For an easier interpretation of the code a legend is proposed in Tab. A4.1. It indicates, for each variable, the kind of information it describes, a short definition, and the measuring units and kind of data it has.

Only code for soil matrix is here indicated; for biochar-amended soil they were simply changed physical parameters describing the medium (§ 7.2.5.5). With this code version open b.c. is active, but there is included also closed b.c.: they may be switched by respectively posing and removing “%” sign from the head of command scribing top boundary conditions.

```
tic

% Soil core properties

% Length soil core [cm]
soillength = 42.7;
% Radius soil core [cm]
soilradius = 4.7;
% Solid density [g/cm3]
ds = 2.62;
% Soil pH [-]
pH = 7.2

% Column properties

% MOD Length headspace [cm]
headspacelength = 5.5;
% Length beaker [cm]
beakerlength = 15;
% MOD Gap area [cm2]
gaparea = 1.5;
% MOD Radius becker [cm]
beakerradius = 4.9;
```

```
% MOD Vial properties

% Length Vial [cm]
Viallength = 9.5;
% MOD Gap area [cm2]
Vialgaparea = 0.1;
% Radius Vial [cm]
Vialradius = 1.2;

% Compound properties (order: Pentane, Hexane, Octane, Decane,
Dodecane, Methylcyclopentane, Methylcyclohexane,
% Cyclohexane, Isooctane, Toluene, Xylene, TMB, CO2)

% Number of compounds
compounds = 13;
% Molecular diffusion coefficients [cm2/s]
D =
[0.082;0.074;0.064;0.057;0.051;0.079;0.073;0.080;0.064;0.078;0.072;0
.066;0.17]
% Soil solid-water partitioning coefficient [cm3/g]
Kd = [20;47;104;123;774;9;2.3;4;43.7;1.9;1.3;1.6;0]
% Soil with biochar solid-water partitioning coefficient [cm3/g]
% Kd = [43;90;314;520;1630;10;4;5;73;69;14;13]
% Dimensionless Henry's law constant [-]
H = [50;70;120;293;293;15;4.2;7.3;132;0.26;0.26;0.27;0.75]
% Soil first order biodegradation rate [1/s]
% kdeg =
[0.0037;0.029;0.17;0.17;0.16;0.0012;0.00041;0.00064;0.016;0.00089;0.
00073;0.0018]
% Soil with biochar first order biodegradation rate [1/s]
% kdeg =
[0.021;0.057;0.21;0.37;0.31;0.0056;0.0016;0.0011;0.018;0.015;0.0051;
0.0050]
kdeg = [0;0;0;0;0;0;0;0;0;0;0;0]
% Molecular weights [g/mol]
MW = [72;82;114;142;170;84;89;84;114;92;106;120;44]
% Pure liquid vapor pressure [g/cm3]
VP =
[0.00197;0.000685;0.000089;0.000014;0.000002;0.0006;0.00021;0.00042;
0.00027;0.00014;0.000047;0.000015]
% Mass fraction of carbon in each compoudnd [-]
Carbon =
[5*12/72;6*12/82;8*12/114;10*12/142;12*12/170;6*12/84;7*12/89;6*12/8
4;8*12/114;7*12/92;8*12/106;9*12/120]
% Yield (ratio of carbon transformed into biomass)
yield = 0.4
% Duration of the simulation [s]
duration = 14*24*3600;
% Factor of data reduction for storage [-]
reduction = 2.5*2000;

% Numerical parameters

% Nods (must be an uneven number)
nodsz = 68;
```

```
% Gridspacing [cm]
dz = 1;
% Timestep [s]
dt = 2;
% Number of timesteps [-]
n = round(duration/dt);
% Number of storage timesteps [-]
nstore = round(n/reduction);


% Data storage
Pentane  = zeros(nstore+1,nodsz+2);
Hexane  = zeros(nstore+1,nodsz+2);
Octane  = zeros(nstore+1,nodsz+2);
Decane  = zeros(nstore+1,nodsz+2);
Dodecane  = zeros(nstore+1,nodsz+2);
Methylcyclopentane  = zeros(nstore+1,nodsz+2);
Methylcyclohexane  = zeros(nstore+1,nodsz+2);
Cyclohexane  = zeros(nstore+1,nodsz+2);
Isooctane  = zeros(nstore+1,nodsz+2);
Toluene  = zeros(nstore+1,nodsz+2);
Xylene  = zeros(nstore+1,nodsz+2);
TMB = zeros(nstore+1,nodsz+2);
CO2 = zeros(nstore+1,nodsz+2);
Mdeg = zeros(nstore+1,compounds);
Msoil = zeros(nstore+1,compounds);
mfstorage = zeros(nstore+1,compounds);
mvolstorage1 = zeros(nstore+1,compounds);
mvolstorage2 = zeros(nstore+1,compounds);
mvolstorage3 = zeros(nstore+1,compounds);
mvolstorage4 = zeros(nstore+1,compounds);
timestorage = zeros(nstore+1,1);
R = zeros(compounds,nodsz+2);

% Interim Data storage
Profile = zeros(compounds,nodsz+2);
NextProfile = zeros(compounds,nodsz+2);
moles = zeros(compounds,1);
nextmoles = zeros(compounds,1);
nexttotmoles = zeros(compounds,1);
mdeg = zeros(nodsz+2,compounds);
msoil = zeros(nodsz+2,compounds);
mCO2 = zeros(nodsz+2,compounds);
mf = zeros(compounds,1);
nextmf = zeros(compounds,1);

% Initial condition

% Initial moles open boundary condition
% moles0 =
[0.0042;0.0069;0.0038;0.0061;0.0029;0.0071;0.0080;0.0041;0.010;0.002
1;0.0028;0.0030;0];
% Initial moles closed boundary condition
moles0 =
[0.0042;0.0037;0.0036;0.0052;0.0020;0.0077;0.0091;0.0054;0.0088;0.00
36;0.0035;0.0042;0];
% moles0 = [0.31;0;0;0;0;0;0;0;0;0;0;0;0];
```

```
totmoles0 = sum(moles0');
% Initial mole fraction
mf0 = moles0./totmoles0;
Profile(1:12,1) = mf0(1:12,1).*VP;
Profile(13,1) = 0;
mvol1 = zeros(1,compounds);
mvol2 = zeros(1,compounds);
mvol3 = zeros(1,compounds);
mvol4 = zeros(1,compounds);

% MOD Initial concentration at bottom of column [g/cm3]

Pentane(1,1)  = mf0(1,1).*VP(1,1);
Hexane(1,1)  = mf0(2,1).*VP(2,1);
Octane(1,1)  = mf0(3,1).*VP(3,1);
Decane(1,1)  = mf0(4,1).*VP(4,1);
Dodecane(1,1)  = mf0(5,1).*VP(5,1);
Methylcyclopentane(1,1)  = mf0(6,1).*VP(6,1);
Methylcyclohexane(1,1)  = mf0(7,1).*VP(7,1);
Cyclohexane(1,1)  = mf0(8,1).*VP(8,1);
Isooctane(1,1)  = mf0(9,1).*VP(9,1);
Toluene(1,1)  = mf0(10,1).*VP(10,1);
Xylene(1,1)  = mf0(11,1).*VP(11,1);
TMB(1,1) = mf0(12,1).*VP(12,1);
mfstorage(1,:)= mf0';
timestorage(1,1) = 0;
moles = moles0;

% Define the porosities, tortuosity and capacity factor as a
function of depth

Vfw = zeros(1,nodsz+2);
Vfa = zeros(1,nodsz+2);
Vfs = zeros(1,nodsz+2);
tort = zeros(1,nodsz+2);

% For the funnel neck
for j = 1:12
        Vfa(1,j)=pi*0.65^2/(pi*4.7^2);
        Vfw(1,j)=0;
        Vfs(1,j)=0;
        tort(1,j)= 1;
        for l = 1:12
        R(l,j)=(Vfa(1,j)+
Vfw(1,j)/H(l,1)+Vfs(1,j)*ds*Kd(l,1)/H(l,1));
        end
        R(13,j)=Vfa(1,j)+ Vfw(1,j)/H(13,1)*(1+10^(pH-6.3)+10^(2*pH-
6.3-10.25));
end

% For the funnel
for j = 13:21
        Vfa(1,j)=pi*(0.65+(j-12)*4.05/9)^2*0.6/(pi*4.7^2);
        Vfw(1,j)=0;
        Vfs(1,j)=0;
        tort(1,j)= 1;
```

```
        for l = 1:12
        R(l,j)=(Vfa(1,j)+
Vfw(1,j)/H(l,1)+Vfs(1,j)*ds*Kd(l,1)/H(l,1));
        end
        R(13,j)=Vfa(1,j)+ Vfw(1,j)/H(13,1)*(1+10^(pH-6.3)+10^(2*pH-
6.3-10.25));
end

% For the column

for j = 22:64
        Vfa(1,j)=0.33;
        Vfw(1,j)=0.10;
        Vfs(1,j)=1-Vfa(1,j)-Vfw(1,j);
        tort(1,j)= Vfa(1,j)^1.5/(1-Vfs(1,j));
        for l = 1:12
        R(l,j)=(Vfa(1,j)+
Vfw(1,j)/H(l,1)+Vfs(1,j)*ds*Kd(l,1)/H(l,1));
        end
        R(13,j)=Vfa(1,j)+ Vfw(1,j)/H(13,1)*(1+10^(pH-6.3)+10^(2*pH-
6.3-10.25));
end

% For the headspace
for j = 65:70
        Vfa(1,j)=1;
        Vfw(1,j)=0;
        Vfs(1,j)=0;
        tort(1,j)= 1;
        for l = 1:12
        R(l,j)=(Vfa(1,j)+
Vfw(1,j)/H(l,1)+Vfs(1,j)*ds*Kd(l,1)/H(l,1));
        end
        R(13,j)=Vfa(1,j)+ Vfw(1,j)/H(13,1)*(1+10^(pH-6.3)+10^(2*pH-
6.3-10.25));
end

% Timestep loop

for i = 2:(nstore+1)
    for k = 1:reduction
    for l = 1:12
    for j = 2:21
        NextProfile(l,j) =
Profile(l,j)+dt*D(l,1)/R(l,j)*((Profile(l,j+1)-Profile(l,j-
1))/2/dz*(tort(1,j)*(Vfa(1,j+1)-Vfa(1,j-
1))/2/dz+Vfa(1,j)*(tort(1,j+1)-tort(1,j-
1))/2/dz)+Vfa(1,j)*tort(1,j)*(Profile(l,j-1)-
2*Profile(l,j)+Profile(l,j+1))/dz^2);
    end
    for j = 22:64
        NextProfile(l,j) =
Profile(l,j)+dt*D(l,1)/R(l,j)*((Profile(l,j+1)-Profile(l,j-
1))/2/dz*(tort(1,j)*(Vfa(1,j+1)-Vfa(1,j-
1))/2/dz+Vfa(1,j)*(tort(1,j+1)-tort(1,j-
1))/2/dz)+Vfa(1,j)*tort(1,j)*(Profile(l,j-1)-
```

```
2*Profile(l,j)+Profile(l,j+1))/dz^2)-
dt*kdeg(l,1)*Vfw(1,j)/H(l,1)/R(l,j)*Profile(l,j);
        % Calculating the degradation
        mdeg(j,l) =
mdeg(j,l)+dt*kdeg(l,1)*pi*soilradius^2*dz*Vfw(1,j)/H(l,1)*Profile(l,
j);
        msoil(j,l) = pi*soilradius^2*dz*R(l,j)*Profile(l,j);
        % Calculating the amount of CO2 produced
        mCO2(j,l) = (1-
yield)*Carbon(l,1)*44/12*dt*kdeg(l,1)*pi*soilradius^2*dz*Vfw(1,j)/H(
l,1)*Profile(l,j);
    end
    for j = 65:(nodsz+1)
        NextProfile(l,j) =
Profile(l,j)+dt*D(l,1)/R(l,j)*((Profile(l,j+1)-Profile(l,j-
1))/2/dz*(tort(1,j)*(Vfa(1,j+1)-Vfa(1,j-
1))/2/dz+Vfa(1,j)*(tort(1,j+1)-tort(1,j-
1))/2/dz)+Vfa(1,j)*tort(1,j)*(Profile(l,j-1)-
2*Profile(l,j)+Profile(l,j+1))/dz^2);
    end
    nextmoles(l,1) =
max(0,moles(l,1)+dt*pi*soilradius^2*D(l,1)*tort(1,2)*Vfa(1,2)/dz*(Pr
ofile(l,2)-Profile(l,1))/MW(l,1));
    % Top of the column no flux
    NextProfile(l,nodsz+2) = Profile(l,nodsz);
    % Additional loss though beaker gap
    NextProfile(l,66) = NextProfile(l,66)-
dt*D(l,1)*gaparea/(beakerlength-
3)/pi/soilradius^2/dz/R(l,66)*Profile(l,66);
    % NextProfile(l,66) = 0;
    % Resetting profiles and moles compound in the source for the
next loop
    Profile(l,:) = NextProfile(l,:);
    moles(l,1) = nextmoles(l,1);
    mvol1(1,l) =
mvol1(1,l)+dt*pi*soilradius^2*D(l,1)*tort(1,2)*Vfa(1,2)/dz*(Profile(
l,1)-Profile(l,2));
    mvol2(1,l) =
mvol2(1,l)+dt*pi*soilradius^2*D(l,1)*tort(1,11)*Vfa(1,11)/dz*(Profil
e(l,11)-Profile(l,12));
    mvol3(1,l) =
mvol3(1,l)+dt*pi*soilradius^2*D(l,1)*tort(1,22)*Vfa(1,22)/dz*(Profil
e(l,22)-Profile(l,23));
    mvol4(1,l) =
mvol4(1,l)+dt*pi*soilradius^2*D(l,1)*tort(1,63)*Vfa(1,63)/dz*(Profil
e(l,63)-Profile(l,64));
    end
    for l = 13:compounds
            for j = 2:21
            NextProfile(l,j) =
Profile(l,j)+dt*D(l,1)/R(l,j)*((Profile(l,j+1)-Profile(l,j-
1))/2/dz*(tort(1,j)*(Vfa(1,j+1)-Vfa(1,j-
1))/2/dz+Vfa(1,j)*(tort(1,j+1)-tort(1,j-
1))/2/dz)+Vfa(1,j)*tort(1,j)*(Profile(l,j-1)-
2*Profile(l,j)+Profile(l,j+1))/dz^2);
            end
            for j = 22:64
```

```
            NextProfile(l,j) =
Profile(l,j)+dt*D(l,1)/R(l,j)*((Profile(l,j+1)-Profile(l,j-
1))/2/dz*(tort(1,j)*(Vfa(1,j+1)-Vfa(1,j-
1))/2/dz+Vfa(1,j)*(tort(1,j+1)-tort(1,j-
1))/2/dz)+Vfa(1,j)*tort(1,j)*(Profile(l,j-1)-
2*Profile(l,j)+Profile(l,j+1))/dz^2)+sum(mCO2(j,:))/R(l,j)/pi/soilra
dius^2/dz;
            end
            for j = 65:(nodsz+1)
            NextProfile(l,j) =
Profile(l,j)+dt*D(l,1)/R(l,j)*((Profile(l,j+1)-Profile(l,j-
1))/2/dz*(tort(1,j)*(Vfa(1,j+1)-Vfa(1,j-
1))/2/dz+Vfa(1,j)*(tort(1,j+1)-tort(1,j-
1))/2/dz)+Vfa(1,j)*tort(1,j)*(Profile(l,j-1)-
2*Profile(l,j)+Profile(l,j+1))/dz^2);
            end
        % Top of the column no flux
        NextProfile(l,nodsz+2) = Profile(l,nodsz+1);
        % Additional loss though beaker gap
        NextProfile(l,66) = NextProfile(l,66)-
dt*D(l,1)*gaparea/(beakerlength-
3)/pi/soilradius^2/dz/R(l,66)*Profile(l,66);
        % NextProfile(l,66) = 0;
    end
    % Change in NAPL moles
    nextmolestot = sum(nextmoles');
    nextmf = nextmoles./nextmolestot;
    NextProfile(1:12,1) = nextmf(1:12,1).*VP;
    Profile(:,:) = NextProfile(:,:);
    end

    mvolstorage1(i+1,:)  = mvol1(1,:);
    mvolstorage2(i+1,:)  = mvol2(1,:);
    mvolstorage3(i+1,:)  = mvol3(1,:);
    mvolstorage4(i+1,:)  = mvol4(1,:);

    Pentane(i,:)  = NextProfile(1,:);
    Hexane(i,:)  = NextProfile(2,:);
    Octane(i,:)  = NextProfile(3,:);
    Decane(i,:)  = NextProfile(4,:);
    Dodecane(i,:)  = NextProfile(5,:);
    Methylcyclopentane(i,:)  = NextProfile(6,:);
    Methylcyclohexane(i,:)  = NextProfile(7,:);
    Cyclohexane(i,:)  = NextProfile(8,:);
    Isooctane(i,:)  = NextProfile(9,:);
    Toluene(i,:)  = NextProfile(10,:);
    Xylene(i,:)  = NextProfile(11,:);
    TMB(i,:)  = NextProfile(12,:);
    CO2(i,:) = NextProfile(13,:);
    mfstorage(i,:)= nextmf(:,1)';
    timestorage(i,1) = timestorage(i-1,1)+dt*reduction;
    Mdeg(i,:) = sum(mdeg);
    Msoil(i,:) = sum(msoil);
end

toc
```

```
% Plotting
subplot(2,3,1);plot(timestorage,Pentane(:,29),timestorage,Cyclohexan
e(:,29),timestorage,Toluene(:,29),timestorage,Xylene(:,29));title('P
ort 1');xlabel('Time [day]');ylabel('Cair Pentane, Cyclohexane,
Toluene, Xylene [g/cm3]');
subplot(2,3,2);plot(timestorage,Pentane(:,36),timestorage,Cyclohexan
e(:,36),timestorage,Toluene(:,36),timestorage,Xylene(:,36));title('P
ort 3');xlabel('Time [day]');ylabel('Cair Pentane, Cyclohexane,
Toluene, Xylene [g/cm3]');
subplot(2,3,3);plot(timestorage,Pentane(:,43),timestorage,Cyclohexan
e(:,43),timestorage,Toluene(:,43),timestorage,Xylene(:,43));title('P
ort 3');xlabel('Time [day]');ylabel('Cair Pentane, Cyclohexane,
Toluene, Xylene [g/cm3]');
subplot(2,3,4);plot(timestorage,Pentane(:,50),timestorage,Cyclohexan
e(:,50),timestorage,Toluene(:,50),timestorage,Xylene(:,50));title('P
ort 4');xlabel('Time [day]');ylabel('Cair Pentane, Cyclohexane,
Toluene, Xylene [g/cm3]');
subplot(2,3,5);plot(timestorage,Pentane(:,66),timestorage,Cyclohexan
e(:,66),timestorage,Toluene(:,66),timestorage,Xylene(:,66));title('B
eaker');xlabel('Time [day]');ylabel('Cair Pentane, Cyclohexane,
Toluene, Xylene [g/cm3]');

% Mass balance
Massbalance = (Mdeg(nstore+1,:)+ Msoil(nstore+1,:)+
mvolstorage4(nstore+1,:)+ (moles(:,1).*MW(:,1))')'./(moles0.*MW)

% save Pentane5KdDegCB.txt Pentane -ASCII;
% save Hexane5KdDegCB.txt Hexane -ASCII;
% save Octane5KdDegCB.txt Octane -ASCII;
% save Decane5KdDegCB.txt Decane -ASCII;
% save Dodecane5KdDegCB.txt Dodecane -ASCII;
% save Methylcyclopentane5KdDegCB.txt Methylcyclopentane -ASCII;
% save Methylcyclohexane5KdDegCB.txt Methylcyclohexane -ASCII;
% save Cyclohexane5KdDegCB.txt Cyclohexane -ASCII;
% save Isooctane5KdDegCB.txt Isooctane -ASCII;
% save Toluene5KdDegCB.txt Toluene -ASCII;
% save Xylene5KdDegCB.txt Xylene -ASCII;
% save TMB5KdDegCB.txt TMB -ASCII;
% save Massfractions5KdDegCB.txt mfstorage -ASCII;
% save time5KdDegCB.txt timestorage -ASCII;
```

Tab. A4.1: *legend with explanations of all the symbols introduced into Matlab numerical code.*

variable name	**type of information**	**description**	**m. u.**	**kind of datum**
alfa	CO_2 analysis	ratio of Carbon used for biomass anabolism	-	scalar
beakerlength	geometry	length of FC	cm	scalar
beakerradius	geometry	radius of FC	cm	scalar
C	*inner note*	*concentration*		
Carbon	CO_2 analysis	number of C atoms in each VOC compound	-	vector (compounds x 1)

Tab. A4.1: *continued.*

CO$_2$ (i,j)	CO$_2$ analysis	CO$_2$ produced at different t and z from all the compounds	g cm^{-3}	vector (t step x z nodes)
CO$_2$ storage	CO$_2$ data storage	CO$_2$ storage = zeros(nstore+1,nodsz+2);	g cm^{-3}	vector (t step x z nodes)
Comp CO$_2$	CO$_2$ analysis	CO$_2$ produced at different z for each compound	g cm^{-3}	vector (compounds x z nodes)
compounds	VOCs property	number of VOCs compounds	-	scalar
Cyclohexane	data storage	gas C of cyclohexane at different t and z	g cm^{-3}	vector (t step x z nodes)
D	VOCs property	Molecular diffusion coefficients	cm^2 s^{-1}	vector (compounds x 1)
Decane	data storage	gas C of decane at different t and z	g cm^{-3}	vector (t step x z nodes)
Dodecane	data storage	gas C of dodecane at different t and z	g cm^{-3}	vector (t step x z nodes)
ds	soil property	Solid density	g cm^{-3}	scalar
dt	run parameter	t step	s	scalar
duration	run parameter	duration of the simulation	s	scalar
dz	domain	grid spacing alomg z direction	cm	scalar
FC	*inner note*	*flux chamber*		
gaparea	geometry	gap area between FC and column	cm^2	scalar
H	VOCs property	Dimensionless Henry's law constant (Cg/Cw)	-	vector (compounds x 1)
headspacelength	geometry	head space over the column, below FC	cm	scalar
Hexane	data storage	gas C of hexane at different t and z	g cm^{-3}	vector (t step x z nodes)
i	inner parameter	t step index	-	scalar
Isooctane	data storage	gas C of isooctane at different t and z	g cm^{-3}	vector (t step x z nodes)
j	inner parameter	space index	-	scalar
k	inner parameter	storage t step index	-	scalar
Kd	VOCs property	Solid-water partitioning coefficient	cm^3 g^{-1}	vector (compounds x 1)
kdeg	VOCs property	First order biodegradation rate	s^{-1}	vector (compounds x 1)
l	inner parameter	compound index	-	scalar
Methylcyclohexane	data storage	gas C of cethylcyclohexane at different t and z	g cm^{-3}	vector (t step x z nodes)
Methylcyclopentane	data storage	gas C of methtlcyclopentane at different t and z	g cm^{-3}	vector (t step x z nodes)

Tab. A4.1: *continued.*

mf	interim data storage	molar ratio	-	vector (compounds x 1)
mf0	derived VOCs comp	initial molar ratio in VOCs source (t=0)	-	scalar
mfstorage	data storage	molar ratios in VOCs source at different t	-	vector (t step x compounds)
moles	interim data storage	moles in VOCs source (for a specfic t)	mol	vector (compounds x 1)
moles0	VOC composition	initial moles in VOCs source (t=0)	-	vector (compounds x 1)
MW	VOCs property	Molecular weights	g mol^{-1}	vector (compounds x 1)
n	derived run parameter	number of t steps	-	scalar
nextmf	derived data storage	molar ratio (for t=t previous + dt)	-	vector (compounds x 1)
nextmoles	derived data storage	moles in VOCs source (for t=t previous + dt)	mol	vector (compounds x 1)
nextmolestot	derived data storage	sum of nextmoles	mol	vector (compounds x 1)
NextProfile	derived data storage	gas C of VOC at different z (for t=t previous + dt)	g cm^{-3}	vector (compounds x z nodes)
nodsz	domain	number of nods along z direction	-	scalar
nstore	derived run parameter	number of storage t steps	-	scalar
Octane	data storage	gas C of octane at different t and z	g cm^{-3}	vector (t step x z nodes)
Pentane	data storage	gas C of pentane at different t and z	g cm^{-3}	vector (t step x z nodes)
Profile	interim data storage	gas C of VOC at different z (for a specfic t)	g cm^{-3}	vector (compounds x z nodes)
R	derived matrix and VOC property	retardation factor	-	vector (compounds x z nodes)
reduction	run parameter	factor of temporal data reduction for storage	-	scalar
soillength	geometry	Length soil core	cm	scalar
soilradius	geometry	Radius soil core	cm	scalar
t	*inner note*	*Time*		
timestorage	data storage	temporal step	-	vector (t step x 1)
TMB	data storage	gas C of TMB at different t and z	g cm^{-3}	vector (t step x z nodes)
Toluene	data storage	gas C oftoluene at different t and z	g cm^{-3}	vector (t step x z nodes)

Tab. A4.1: *continued.*

tort	derived matrix property	tortuosity	-	vector (1 x z nodes)
totmoles0	derived VOCs comp	total initial moles in VOCs source (t=0)	-	scalar
Vfa	matrix property	fraction of volume filled with air f(z)	cm^3 cm^{-3}	vector (1 x z nodes)
Vfs	matrix property	fraction of volume filled with solids f(z)	cm^3 cm^{-3}	vector (1 x z nodes)
Vfw	matrix property	fraction of volume filled with water f(z)	cm^3 cm^{-3}	vector (1 x z nodes)
Vialgaparea	geometry	gap area between vial and column	cm^2	scalar
Viallength	geometry	VOCs source vial length	cm	scalar
Vialradius	geometry	VOCs source vial radius	cm	scalar
VP	VOCs property	Pure liquid vapor pressure	g cm^{-3}	vector (compounds x 1)
Xylene	data storage	gas C of xylene at different t and z	g cm^{-3}	vector (t step x z nodes)